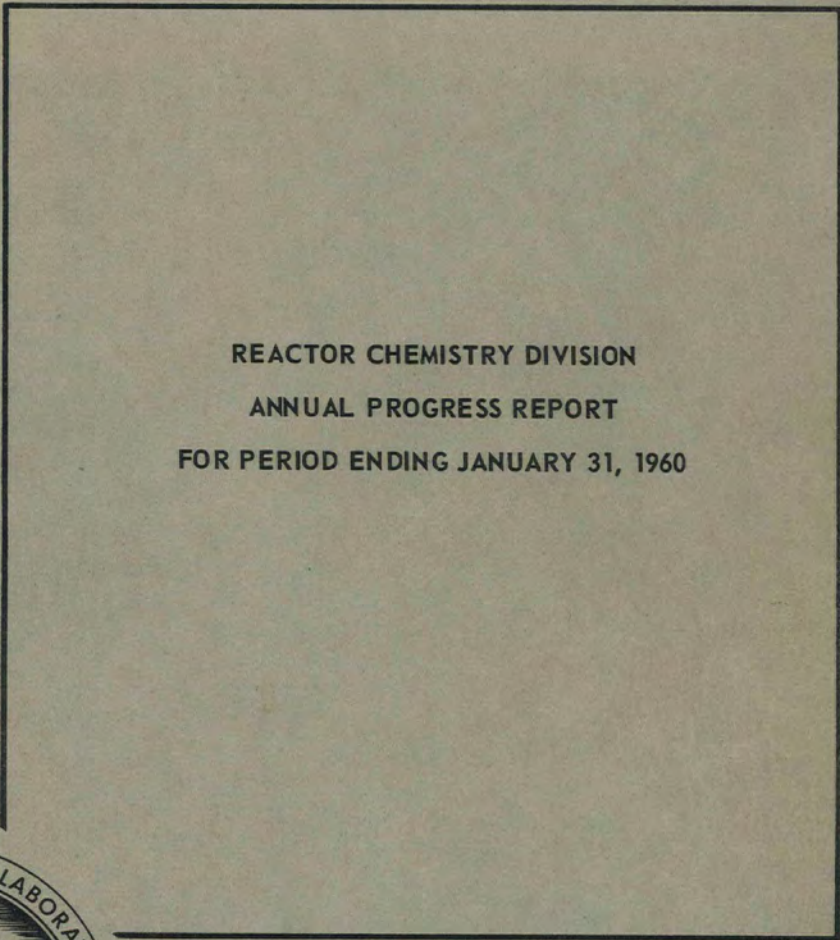
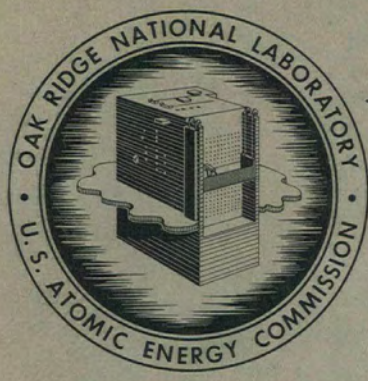


69

ORNL-2931  
UC-4 - Chemistry-General  
TID-4500 (15th ed.)



REACTOR CHEMISTRY DIVISION  
ANNUAL PROGRESS REPORT  
FOR PERIOD ENDING JANUARY 31, 1960



**OAK RIDGE NATIONAL LABORATORY**  
operated by  
UNION CARBIDE CORPORATION  
for the  
U.S. ATOMIC ENERGY COMMISSION

Printed in USA. Price \$3.50. Available from the  
Office of Technical Services  
Department of Commerce  
Washington 25, D. C.

LEGAL NOTICE

This report was prepared as an account of Government sponsored work. Neither the United States, nor the Commission, nor any person acting on behalf of the Commission:

- A. Makes any warranty or representation, expressed or implied, with respect to the accuracy, completeness, or usefulness of the information contained in this report, or that the use of any information, apparatus, method, or process disclosed in this report may not infringe privately owned rights; or
- B. Assumes any liabilities with respect to the use of, or for damages resulting from the use of any information, apparatus, method, or process disclosed in this report.

As used in the above, "person acting on behalf of the Commission" includes any employee or contractor of the Commission, or employee of such contractor, to the extent that such employee or contractor of the Commission, or employee of such contractor prepares, disseminates, or provides access to, any information pursuant to his employment or contract with the Commission, or his employment with such contractor.

ORNL-2931  
UC-4 - Chemistry-General  
TID-4500 (15th ed.)

Contract No. W-7405-eng-26

**REACTOR CHEMISTRY DIVISION ANNUAL PROGRESS REPORT**

**For Period Ending January 31, 1960**

W. R. Grimes, Director  
H. F. McDuffie, Assistant Director

DATE ISSUED

APR 29 1960

OAK RIDGE NATIONAL LABORATORY  
Oak Ridge, Tennessee  
operated by  
UNION CARBIDE CORPORATION  
for the  
U. S. ATOMIC ENERGY COMMISSION



# REACTOR CHEMISTRY DIVISION ANNUAL PROGRESS REPORT

## SUMMARY

### PART I. MOLTEN-SALT REACTOR PROGRAM

#### 1. High-Temperature Phase Equilibrium Studies

Phase diagrams for many fluoride systems of interest as fuels, blankets, or coolants for nuclear reactors or as fuel reprocessing media have been prepared from data obtained by a variety of techniques. Most of the emphasis has been given to systems involving LiF and BeF<sub>2</sub> with UF<sub>4</sub> or ThF<sub>4</sub>, since these materials offer the most promise in thermal breeder reactors.

The new compounds discovered in the course of molten-salt phase studies include 21 binary and ternary fluoride compounds whose compositions, optical properties, and x-ray diffraction patterns are presented. Systematization of the crystallographic properties of the 3:1 compounds of the alkali fluorides with ZrF<sub>4</sub>, HfF<sub>4</sub>, ThF<sub>4</sub>, and UF<sub>4</sub>, and of the 7:6 compounds in these systems has confirmed the importance of the M<sup>+</sup>/X<sup>4+</sup> ion radius ratio and a structural proposal previously made at this Laboratory.

Plutonium was shown to exhibit sufficient solubility in molten fluoride systems to be of interest as a potential reactor fuel. Portions of the systems LiF-PuF<sub>3</sub>, PuF<sub>3</sub>-LiF-BeF<sub>2</sub>, PuF<sub>3</sub>-NaF-BeF<sub>2</sub>, PuF<sub>3</sub>-NaF-LiF-BeF<sub>2</sub>, and PuF<sub>3</sub>-LiF-BeF<sub>2</sub>-UF<sub>4</sub> were studied in the temperature range 550 to 650°C. The addition of ThF<sub>4</sub>, in one case, had little effect on the solubility of PuF<sub>3</sub>, but the addition of BaF<sub>2</sub> or CeF<sub>3</sub> reduced the solubility. A preliminary phase diagram was constructed for the system NaF-PuF<sub>3</sub>.

#### 2. Gas Solubilities in Molten Salts

A systematic study of the solubilities of the noble gases in molten salts was undertaken because of the occurrence of these gases as fission products of high neutron-absorption cross section. The results have been published, together with a theory relating the solubility of such gases to their atomic radii and the surface tensions of the molten-salt solvents. The solubility of HF in molten fluoride mixtures containing NaF and BeF<sub>2</sub> or ZrF<sub>4</sub> was found to be related to the composition of the molten fluoride solvent when expressed as NaF plus Na<sub>2</sub>BeF<sub>4</sub> or Na<sub>3</sub>ZrF<sub>7</sub>; low solubility was noted when there was a "deficiency" of NaF, but high solubility was noted when the NaF

was in "excess." The solubility of CO<sub>2</sub> (an essentially unreactive nonspherical molecule) in an NaF-BeF<sub>2</sub> solvent was found to resemble that of the noble gases at temperatures of 600 to 800°C, but that of HF at temperatures below 600°C. The low solubility of xenon in molten salts and the relatively small effect of xenon diffusion through graphite formed a basis for a reactor system design in which Xe<sup>135</sup> would decay in a gas space outside the reactor core.

#### 3. Thermodynamic Studies in Molten-Salt Systems

Studies of the thermodynamic behavior of structural-metal corrosion products in fluoride melts have been extended to include CrF<sub>2</sub> in NaF-ZrF<sub>4</sub> and NiF<sub>2</sub> in LiF-BeF<sub>2</sub>. Published estimates of the standard free energy of reaction and the entropy of fusion for NiF<sub>2</sub> appeared to be questionable, and more consistent values were suggested.

Theoretical calculations based on a quasi-lattice model for molten reciprocal salt systems were compared with emf measurements, at several temperatures, of the activities of AgNO<sub>3</sub> in the two molten solvents NaNO<sub>3</sub> and KNO<sub>3</sub> dilute in Ag<sup>+</sup> and Cl<sup>-</sup> ions. The theory correctly predicts the temperature coefficients of the first association constant of Ag<sup>+</sup> and Cl<sup>-</sup> ions.

A new generalized calculation based on the model includes some of the higher associations in a more realistic manner and provides a separation of configurational or statistical factors and the factors containing "bond strength" for some of the successive association constants. The generalized calculation provides an insight into the interpretation of association constants and into the effects of the directionality of "bonds" on association constants.

The depressions of the freezing point of NaF upon the addition of alkali-metal fluorides, alkali-earth fluorides, and transition-metal difluorides were measured and correlated with theories of molten-salt behavior.

The vapor pressure of liquid UF<sub>4</sub> over the temperature interval 1018 to 1302°C was measured; the results suggested the absence of associated molecules in the vapor phase. Incomplete studies

of the vapor pressure of molten  $\text{UCl}_4$  and of  $\text{LiF-UF}_4$  mixtures are reported.

#### 4. Self-Diffusion of Chromium in Inconel Exposed to Molten Salts

Self-diffusion of chromium in nickel-based alloys in contact with molten fluorides has been studied by use of radiotracer  $\text{Cr}^{51}$ . Rates of diffusion are evaluated (1) from rates of depletion of radioactive  $\text{CrF}_2$  from the melt during exposure, (2) by counting the metal specimens after exposure, and (3) by counting the  $\text{Cr}^{51}$  removed in successive layers by electropolishing techniques.

#### 5. Purification and Handling of Molten Salts in Quantity

Molten mixtures of  $\text{LiF}$  and  $\text{BeF}_2$  with  $\text{ThF}_4$  and  $\text{UF}_4$  were purified by treatment in the molten state at  $800^\circ\text{C}$  with  $\text{H}_2$  to reduce  $\text{SO}_4^{--}$  and higher valence states of uranium, with anhydrous  $\text{HF}$  to remove  $\text{Cl}^-$  and  $\text{S}^{--}$  and to convert oxides and oxyfluorides to fluorides, and with  $\text{H}_2$  again to reduce  $\text{Fe}^{++}$ ,  $\text{Ni}^{++}$ , or  $\text{Cu}^{++}$  to the metallic state. These operations, performed in equipment of nickel or copper-lined stainless steel, have been demonstrated in batches as large as 250 lb. The purified materials are transferred in closed metal systems to clean containers of nickel and are stored at room temperature without exposure to the atmosphere.

#### 6. Graphite Compatibility

Molten fluorides containing  $\text{LiF-BeF}_2\text{-UF}_4\text{-ThF}_4$  do not react chemically with graphite.

Graphite is not wetted by molten  $\text{LiF-BeF}_2\text{-ThF}_4\text{-UF}_4$  mixtures. Although graphite is permeated by such salts to varying extents which depend on the temperature, pressure, surface tension of the salt, and permeability of the graphite used, several graphites are available which show weight gains of less than 0.5% under exposure at reactor temperature and pressure. Samples of GT-123-82 graphite showed a weight loss of 0.02% on exposure to an  $\text{LiF-BeF}_2\text{-UF}_4$  mixture at  $1300^\circ\text{F}$  for one year in a forced-circulation test loop. Adsorption of xenon on graphite has been measured over the temperature interval from  $-79$  to  $+80^\circ\text{C}$ ; extrapolations of the data suggest that less than  $1 \times 10^{-5} \text{ cm}^3$  (STP) of xenon per gram of graphite could be adsorbed at  $500^\circ\text{C}$  and a xenon pressure of 1 mm.

#### 7. Effect of Radiation on Static Corrosion of Structural Materials by Fused-Salt Fuels

The irradiation of molten salts in contact with graphite or Inconel has not revealed any substantial corrosion or damage attributable to the effect of radiation. In one set of tests, irradiated molten salt appeared to have flowed through small holes previously drilled in the bottom of a graphite cup, although unirradiated controls showed no evidence of flow. These results suggest either that the irradiated salt may have wetted the graphite or that initially high temperatures in the irradiated salt may have increased its fluidity.

#### 8. Reactions in Molten Salts

Nuclearly harmful rare-earth fission products such as  $\text{Sm}^{+++}$  can be selectively removed from molten fluoride solution by exchange with a solid bed of  $\text{CeF}_3$ ; the solubility of  $\text{CeF}_3$  in the molten fluoride is sufficiently low to permit use of such a process for removal of rare earths from an operating reactor. Selective precipitation of oxides by use of reagents such as  $\text{H}_2\text{O}$ ,  $\text{BeO}$ ,  $\text{CaO}$ , or possibly  $\text{ThO}_2$  from molten fluoride reactor fuels has been demonstrated. Studies of recovery of uranium and protactinium by precipitation with  $\text{BeO}$  or  $\text{ThO}_2$  are in progress.

### PART II. AQUEOUS HOMOGENEOUS REACTOR PROGRAM

#### 9. Phase Equilibria in Aqueous Systems at Elevated Temperature

A general description of the solid-liquid equilibria at  $300^\circ\text{C}$  for the  $\text{UO}_3\text{-CuO-NiO-SO}_3\text{-H}_2\text{O}$  system and its included four- and three-component systems was obtained by determining solubilities as functions of  $\text{SO}_3$  concentration under conditions in which one, two, or three solid phases were in equilibrium with the solution. The analogous  $\text{D}_2\text{O}$  systems were shown to be very similar. In this investigation a new compound,  $\text{CuO}\cdot\text{UO}_3$ , was discovered and characterized.

Compositions of light and heavy phases in the system  $\text{UO}_3\text{-SO}_3\text{-H}_2\text{O}$  and its  $\text{D}_2\text{O}$  counterpart were established at  $300$  and  $350^\circ\text{C}$ . Compositions in the heavy phase are very similar in  $\text{H}_2\text{O}$  and  $\text{D}_2\text{O}$ , but appreciable differences are observed in the water-rich phases. Temperature of formation

of two liquid phases has been shown to increase as the mole ratio  $\text{UO}_3/\text{SO}_3$  decreases; at sufficiently low values of this ratio the  $\text{UO}_3$  component is soluble in the supercritical fluid. The heavy phase from synthetic HRE-2 fuel solutions redissolves very slowly at temperatures slightly below the immiscibility temperature unless good mixing is provided.

Temperatures of formation of two liquid phases were determined in the system  $\text{UO}_3\text{-SO}_3\text{-N}_2\text{O}_5\text{-H}_2\text{O}$ . The system  $\text{UO}_3\text{-N}_2\text{O}_5\text{-H}_2\text{O}$  was investigated at 25°C and from 150 to 350°C. The mole ratio  $\text{UO}_3/\text{HNO}_3$  was found to decrease from saturation values of 0.6 to 1.1 at 25°C to values of 0.15 to 0.45 at 350°C. An exploratory investigation at 300°C of the system  $\text{UO}_3\text{-CuO-NiO-N}_2\text{O}_5\text{-H}_2\text{O}$  indicated no markedly lowered solubilities which might adversely effect its use as a reactor fuel.

Efforts to find thorium solutions that would be stable at 300°C and suitable for consideration as breeder blankets were unsuccessful.

#### 10. Reactions in Aqueous Solutions

The effectiveness of cupric nitrate as a soluble homogeneous catalyst for the recombination of radiolytic gas in uranyl nitrate solutions was measured and found to be about 40% of that of cupric sulfate in sulfate-based aqueous homogeneous reactor fuel solutions. The effects of acidity, temperature, copper concentration, and isotopic choice ( $\text{H}_2$  or  $\text{D}_2$ ,  $\text{H}_2\text{O}$  or  $\text{D}_2\text{O}$ ) on the catalytic activity of cupric perchlorate were determined in connection with studies of the mechanism of the recombination reaction.

Factors affecting the concentration of peroxide in uranyl solutions at incipient precipitation were determined experimentally and related to the solubility of uranium peroxide, the equilibrium between dissolved uranium peroxide and hydrogen peroxide, and the rate of peroxide decomposition. The decomposition of peroxide in nitrate solution was found to be similar to that in sulfate systems. Two crystalline forms of uranium peroxide were differentiated on the basis of their method of preparation, analytical composition, x-ray diffraction pattern, and chemical reactivity.

A simple ion exchange method was developed for the determination of free acid in solutions containing easily hydrolyzable cations and was applied to aqueous homogeneous reactor fuel solutions.

#### 11. Thermodynamic Studies in Aqueous Systems

In connection with studies of the hydrolysis of U(VI) and sulfate ions, an experimental program was initiated to measure acidity in aqueous solutions at elevated temperatures. The procedure is a well-established one – potentiometric titration using hydrogen-ion-responding electrodes in concentration cells with transference. A novel arrangement of two glass electrodes is being used in this study; this arrangement has an advantage in that the solutions measured are in contact only with the relatively inert glass electrodes and the containing vessel. Measurements of emf at 94°C have been made with a precision of 0.1 mv, and promising preliminary measurements have been made at 150°C. The results indicate that stoichiometric 0.01 *m* solutions of uranyl nitrate and perchlorate are about 17% hydrolyzed at 94°C, compared with reported values of 5 to 8% at temperatures of 20 to 40°C.

The isopiestic method for the study of electrolyte solutions at elevated temperature has been extended to seven representative 1-1, 1-2, 2-2, and 2-1 solutes at 99.6°C at reference NaCl concentrations above 1 *m*. Comparison with the published values for 25°C revealed, for 1-1 electrolytes, small systematic changes in the expected directions, with lithium chloride exhibiting unique behavior; the pronounced effect of the lithium ion on the structure of water at 25°C appeared to be considerably decreased at higher temperatures. The 2-1, 1-2, and 2-2 electrolytes showed considerably larger deviations from ideal behavior as the temperature was elevated.

### PART III. GAS-COOLED REACTOR PROGRAM

#### 12. Gas Evolution from Graphite

The volumes and compositions of the gases evolved from six reactor grades of graphite have been determined by outgassing techniques which included two methods of heating the graphite (external resistance or internal induction) and the use of temperatures as high as 2000°C. Of the gases recovered by external resistance heating, water vapor was universally released most easily at the lowest temperatures, CO was released throughout the whole temperature range, and the

volatile hydrocarbons were substantially removed below 1000°C. It was possible to distinguish between thermally purified graphite and gas-purified graphite on the basis of the type and rate of gas evolution. At 1000°C the volume of gas evolved by induction heating was always greater than that evolved by external resistance heating; induction heating to 1800 or 2000°C evolved twice the volume of gas obtained by external resistance heating to 1000°C. Correlation of outgassing behavior of graphite with measurable properties of the graphite specimens themselves appears less likely to be appropriate than correlation with the choice of raw materials and the conditions of graphitization.

### 13. Transport of Gases Through Ceramic Materials

The expectation that the transport of reactor coolant gases and fission product poison gases through ceramic fuel elements and graphite moderator bodies will become important for the development of high-performance reactors led to the initiation of a program of theoretical and experimental study of porosity, forced gas flow, and diffusion. The transition velocities (from viscous to turbulent flow) in porous media were found to extend through a wide range and to depend on the pore-size distribution. Measurements of the permeability of selected graphite specimens revealed that viscous flow became less important than Knudsen diffusion as the pressure and pore size were decreased. Constant-pressure-diffusion experiments with helium and argon as the diffusing gases gave results which suggest that both classical diffusion and Knudsen diffusion contributed to the observed transport. The open-pore porosities of several graphites were determined by the helium-gas-penetration technique with good reproducibility. Only a small increase in porosity resulted from outgassing the samples at 1000°C.

### 14. Importance of Alkali-Metal Fission Products in EGCR Fuel Capsules

Thermodynamic calculations suggested that cesium and rubidium (long-lived fission products formed in high yield) would appear in the EGCR fuel-element capsules both as free metals at moderate partial pressures and as compounds with the nonmetals (Br, I, Se, Te). Possible evidence for a slight penetration of stainless steel by cesium vapor at 850°C was observed. Tin and bismuth, both of which alloy readily with cesium, may

be useful for scavenging cesium in EGCR fuel-element capsules.

### 15. Effect of Reactor Irradiation on Beryllium Oxide

The irradiation of cylindrical specimens of BeO in the ETR at neutron fluxes (thermal and fast) of about  $5 \times 10^{14}$  under conditions of thermal stress has not so far revealed any noticeable mechanical damage to this moderator material.

### 16. Gaseous Aluminum Chloride as a Thermodynamic Working Fluid and Heat Transfer Medium

Dissociating gases have been proposed for possible use as reactor heat transfer media and thermodynamic working fluids. Calculations indicated that aluminum chloride has an equilibrium (monomer  $\rightleftharpoons$  dimer) which is suitable for use within the temperature and pressure limitations currently associated with gas-cooled reactors. A program of calculations and experiments is developing further information on aluminum chloride and other related compounds.

### 17. Measurement of Temperature in Reactor Environments

Corrections for thermocouples used to measure the temperatures of gas-cooled surfaces were determined experimentally and correlated with the flow characteristics of the cooling gas by means of a theoretical analysis and computations on the Oracle. In-pile measurements of specimen surface temperatures under similar conditions of gas flow have given satisfactory results.

The effects of changes in the chemical environment upon the readings of Chromel-Alumel thermocouples at 1000°C have been studied to provide understanding of the causes of drifts reported to occur over periods of time which are short compared with the times required for reactor operation. Rhenium-tungsten thermocouples were found to be stable over test periods of 64 hr at a temperature of 1800°C in a helium atmosphere. Small high-temperature furnaces containing electrically heated tungsten rod elements have been developed and were tested to above 2800°C for use in further experiments.

The effects of impurities produced by transmutation of thermocouple materials have been calculated for use in evaluating the results of in-pile long-term tests.

## 18. Removal of Radioactive Gaseous Fission Products from Other Gases

A review was prepared of all previous studies of the removal of radioactive gaseous fission products from other gases. An improved method was developed for evaluating the number of theoretical plates in an adsorber bed. The effect of carrier gas velocity on this number was measured; for the system oxygen-Columbia G charcoal, the optimum superficial linear velocity was found to be about 0.5 fpm. Changes in the composition of the carrier gas were found to affect the retention of krypton on adsorbents. Dynamic adsorption coefficients,  $k$ , for krypton and xenon with oxygen or helium as the carrier gas were determined for many samples of charcoal, molecular sieve material, and other possible adsorbents. The thermal conductivities of selected adsorbents, important for removal of heat from radioactive adsorbed gases, were measured by direct and indirect methods. Parameters affecting the ignition and combustion of charcoal in oxygen carrier gas or oxygen-hydrogen gas mixtures were studied experimentally and the results used to explain an observed ignition of the HRE-2 charcoal bed. The very dangerous consequences of the presence of even low concentrations of oxygen in gas streams passing over low-temperature charcoal beds were evaluated and called to the attention of the designers for the NS "Savannah."

The removal of radioiodine vapor from air streams was studied extensively. Transport of iodine adsorbed on tiny dust particles was found to provide a mechanism for bypassing an otherwise effective charcoal adsorber bed; filtration upstream of the adsorber eliminated this difficulty. Finer grades of charcoal, as expected, were found to be more efficient adsorbents. Moisture in the air did not interfere with adsorption, and iodine, once adsorbed, was *very* firmly held. A silver-plated copper ribbon mesh was found to be comparable to copper ribbon at room temperature but superior at elevated temperature. Charcoal is much superior to either but introduces a much larger pressure drop.

A number of proposed fission-gas or iodine adsorption systems were reviewed for technical feasibility and safety.

## PART IV. PREPARATION OF REACTOR-GRADE MATERIALS

### 19. Preparation of Oxygen-Free Yttrium

As part of a joint chemical-metallurgical program, preliminary laboratory-scale and intermediate-scale demonstrations were made of a process for removing oxygen from yttrium-bearing fluoride salts by hydrofluorination in the liquid state. Study of the phase behavior of the system  $YF_3$ - $LiF$ - $MgF_2$  revealed the existence of mixtures which melted below 800°C. Further work showed that, after purification, these melts could be reduced with metallic lithium to produce a low-melting Y-Mg alloy and essentially pure LiF, both of which melt below 1000°C, thus facilitating phase separation and metal recovery. Oxygen concentrations of the purified molten salt mixture before reduction were as low as 200 ppm in small (5-lb batch) experiments; in larger scale equipment some runs produced material having as little as 500 ppm oxygen.

### 20. Preparation of Inorganic Fluorides

A number of fluorides of chromium were prepared as a consequence of interest in the corrosion of chromium alloy containers by molten-fluoride reactor fluids. Anhydrous ammonium hexafluorochromate was synthesized and used as a starting material to prepare  $CrF_3$ ,  $CrF_2$ , and chromium(II,III) fluoride. New methods were developed for the production of anhydrous  $CrF_2$ ; the reaction of  $SnF_2$  with  $Cr^0$  in impervious graphite proved most convenient, and a good separation of molten  $Sn^0$  from  $CrF_2$  was readily obtained at 1100°C. Stannous fluoride was also found to be useful for the preparation of other fluorides and fluocomplexes, including  $MnF_2$ ,  $ZnF_2$ ,  $AlF_3$ ,  $FeF_2$ ,  $VF_3$ , and  $UF_4$ . Contrary to expectations, molten  $SnF_2$  produced the free metals Cu, Bi, and Sb from  $CuF_2$ ,  $BiF_3$ , and  $SbF_3$ . The reactions of molten  $NH_4HF_2$  were studied extensively for possible application in the conversion of metal oxides to fluorides.

### 21. Preparation and Properties of Inorganic Oxides

The chemistry of high-temperature oxide systems of interest to reactor programs has been approached initially by a study of the limits of

precision and accuracy available in chemical methods for ascertaining the oxygen/uranium ratios in uranium oxides. These ratios are being related to optical and x-ray diffraction measurements on uranium oxides and  $\text{UO}_2\text{-ThO}_2$  solid solutions. The optical properties of several oxides which are significant as nuclear reactor

materials have been measured and are reported for the first time.

Improvements were made in processes for preparing beryllium oxide of high purity; the sintering characteristics of the product were found to depend on the method of preparation and the calcium and silica content.

## CONTENTS

SUMMARY .....	iii
PART I. MOLTEN-SALT REACTOR PROGRAM	
1. HIGH-TEMPERATURE PHASE EQUILIBRIUM STUDIES .....	3
Systems for Use as Nuclear Reactor Fluids .....	3
The System LiF-BeF <sub>2</sub> -ThF <sub>4</sub> -UF <sub>4</sub> .....	3
The System NaF-BeF <sub>2</sub> -ThF <sub>4</sub> -UF <sub>4</sub> .....	5
The System NaF-BeF <sub>2</sub> -ThF <sub>4</sub> .....	7
The System NaF-BeF <sub>2</sub> -UF <sub>4</sub> .....	9
The System NaF-UF <sub>4</sub> -ThF <sub>4</sub> .....	9
Phase Relations in the System LiF-PuF <sub>3</sub> .....	11
Solubility of PuF <sub>3</sub> in Fused Alkali Fluoride-Beryllium Fluoride Mixtures .....	12
Phase Equilibria in the Systems NaF-PuF <sub>3</sub> and NaF-CeF <sub>3</sub> .....	14
Effect of Thermal Cycling on Molten-Salt Segregation .....	17
Dehydration of LiF-BeF <sub>2</sub> -UF <sub>4</sub> and LiF-BeF <sub>2</sub> -ThF <sub>4</sub> -UF <sub>4</sub> Mixtures .....	20
Volatility Process Solvents .....	20
The System NaF-FeF <sub>2</sub> -ZrF <sub>4</sub> .....	20
The System NaF-BeF <sub>2</sub> -ZrF <sub>4</sub> .....	20
Crystal Properties and Crystal Structure .....	21
Optical and X-Ray Data of New Fluoride Components .....	21
Crystal Structures of 3:1 Compounds of the Alkali Fluorides with ZrF <sub>4</sub> , HfF <sub>4</sub> , ThF <sub>4</sub> , and UF <sub>4</sub> .....	22
Some Properties of 7:6 Compounds .....	22
Investigation of Other Fused-Salt Systems .....	25
The System LiF-YF <sub>3</sub> .....	25
The System CsF-ThF <sub>4</sub> .....	25
The System LiF-UF <sub>3</sub> -UF <sub>4</sub> .....	26
2. GAS SOLUBILITIES IN MOLTEN SALTS .....	28
Solubility of Noble Gases in Molten LiF-BeF <sub>2</sub> .....	28
Solubility of Noble Gases in Molten NaF-BeF <sub>2</sub> .....	29
Solubility of HF in Molten Fluoride Mixtures .....	31
An Empirical Correlation for the Solubility of HF in Mixtures of NaF-BeF <sub>2</sub> and NaF-ZrF <sub>4</sub> .....	32
Solubility of CO <sub>2</sub> in Molten NaF-BeF <sub>2</sub> .....	35
Xenon Poisoning Control in Fused-Salt Reactors .....	37
3. THERMODYNAMIC STUDIES IN MOLTEN-SALT SYSTEMS .....	39
Thermodynamic Behavior of Structural-Metal Corrosion Products in Fluoride Melts .....	39
Theory of Molten-Salt Systems .....	43
A Quasi-Lattice Model of Molten Reciprocal Salt Systems .....	43
Electromotive Force Measurements in the System AgNO <sub>3</sub> -NaCl-NaNO <sub>3</sub> and Their Comparison to the Quasi-Lattice Theory .....	46
A Generalized Calculation Based on the Quasi-Lattice Model .....	47

Freezing-Point Depressions in Sodium Fluoride.....	48
Vapor Pressures of Systems Containing Uranium Halides.....	50
Uranium Tetrafluoride.....	50
Uranium Tetrachloride .....	51
Vapor Pressures of LiF-UF <sub>4</sub> Mixtures.....	51
4. SELF-DIFFUSION OF CHROMIUM IN INCONEL EXPOSED TO MOLTEN SALTS.....	52
Over-All Diffusion Coefficients.....	52
Wall Exchange Reaction.....	52
Depletion Method.....	53
Constant-Potential Method.....	53
Results .....	54
Discussion and Conclusions .....	56
Chromium-51 Diffusion Coefficients from Electropolishing Experiments .....	58
Experimental Approach.....	58
Results .....	59
Discussion .....	60
Interpretation of the Chromium-51 Diffusion Data.....	60
5. PURIFICATION AND HANDLING OF MOLTEN SALTS IN QUANTITY.....	64
Purification of LiF-BeF <sub>2</sub> -UF <sub>4</sub> Molten Salts .....	64
Techniques for Sampling and Enriching Molten-Salt Compositions .....	67
Service Work for Other Programs .....	68
6. GRAPHITE COMPATIBILITY .....	69
Permeation of Graphite by Molten Salts .....	69
Intercalation of Fission Products with Graphite.....	70
Adsorption of Xenon on Graphite.....	70
Extrapolation to Reactor Temperatures .....	72
Heat of Adsorption .....	73
7. EFFECT OF RADIATION ON STATIC CORROSION OF STRUCTURAL MATERIALS BY FUSED-SALT FUELS .....	74
Tests of Graphite Compatibility with Fused Salts under Irradiation .....	74
In-Pile Static Corrosion Tests.....	75
8. REACTIONS IN MOLTEN SALTS.....	77
Rare-Earth Fluoride Solubilities and Exchange Reactions .....	77
Exchange Rate Studies with Rare Earths.....	80
Exchange Reactions with Oxides and Carbides in Molten Fluorides.....	82
Chemical Reprocessing of Reactor Fuels by Oxide Precipitations .....	84
Extraction of Uranium by Surface Precipitation on Beryllium Oxide.....	84
The Reactions of Beryllium Oxide in Molten Fluorides .....	86
Extraction of Uranium by Reaction with Water Vapor .....	87
Reactions of the Alkaline Earth Oxides in Molten Fluorides .....	89
Cold-Zone Deposition of Solutes.....	90

PART II. AQUEOUS HOMOGENEOUS REACTOR PROGRAM

9. PHASE EQUILIBRIA IN AQUEOUS SYSTEMS AT ELEVATED TEMPERATURE.....	93
Solid-Liquid Equilibria in the System $UO_3-CuO-NiO-SO_3-H_2O$ and Its $D_2O$ Analog at $300^\circ C$ .....	93
New Solids of Special Interest: Laboratory Preparation of Solids .....	95
Solubilities in $D_2O$ Media .....	95
Application of Multicomponent Solubility Data to Aqueous Homogeneous Reactors.....	95
Boundary Curves Between Liquid-Solids and Liquid-Liquid-Solids Equilibria.....	97
Liquid-Liquid Equilibria in the System $UO_3-SO_3-H_2O$ , Its $D_2O$ Analog, and Similar Systems Containing $CuO$ and $NiO$ Components.....	98
The Compositions of the Two Liquid Phases of the Systems .....	98
Effect of the Mole Ratio, $UO_3/SO_3$ , on Immiscibility Temperatures of 0.02, 0.05, 0.10, and 0.20 <i>m</i> Sulfate Solutions.....	100
Aqueous Homogeneous Reactor Fuel Studies .....	103
Phase Stability of Synthetic HRE-2 Fuel Solutions and Their Concentrates.....	103
Phase Stability of Radioactive HRE-2 Fuel Solutions .....	105
Effect of Increased Temperature on the Heavy-Liquid Phase .....	105
Observations on Rate of Solution of Heavy Phase.....	105
Liquid-Liquid Equilibria in the System $UO_3-SO_3-N_2O_5-H_2O$ .....	106
Solid-Liquid Equilibria in the Systems $UO_3-N_2O_5-H_2O$ , 25 to $350^\circ C$ , and $UO_3-CuO-NiO-N_2O_5-H_2O$ , $300^\circ C$ .....	108
The System $UO_3-N_2O_5-H_2O$ .....	108
The System $UO_3-CuO-NiO-N_2O_5-H_2O$ and Its Relation to Homogeneous Reactors.....	110
Investigation of Thorium-Containing Nitrate and Fluoride Solutions for Breeder-Blanket Use.....	110
Liquid-Salt Bath for High-Temperature Aqueous Studies.....	111
10. REACTIONS IN AQUEOUS SOLUTIONS.....	113
Recombination of Hydrogen and Oxygen.....	113
Cupric Ion as a Homogeneous Catalyst in Nitrate Solutions .....	113
Rate of Oxidation of Dissolved Hydrogen or Deuterium Catalyzed by $Cu(ClO_4)_2$ in Light and Heavy Water .....	115
Peroxide Studies .....	116
The Concentration of Peroxide in Uranyl Sulfate Solutions at Incipient Precipitation .....	116
Peroxide Decomposition in Homogeneous Reactor Fuels – Nitrate System.....	123
Uranium Peroxide Precipitation and Structure .....	125
The Use of Cation Exchange Resins in the Determination of Free Acid .....	127
11. THERMODYNAMIC STUDIES IN AQUEOUS SYSTEMS.....	130
A High-Temperature EMF Cell for Acidity Measurements; the Hydrolysis of Uranium(VI) at $94^\circ C$ .....	130
The Osmotic Behavior of Representative Aqueous Salt Solutions at $100^\circ C$ .....	133

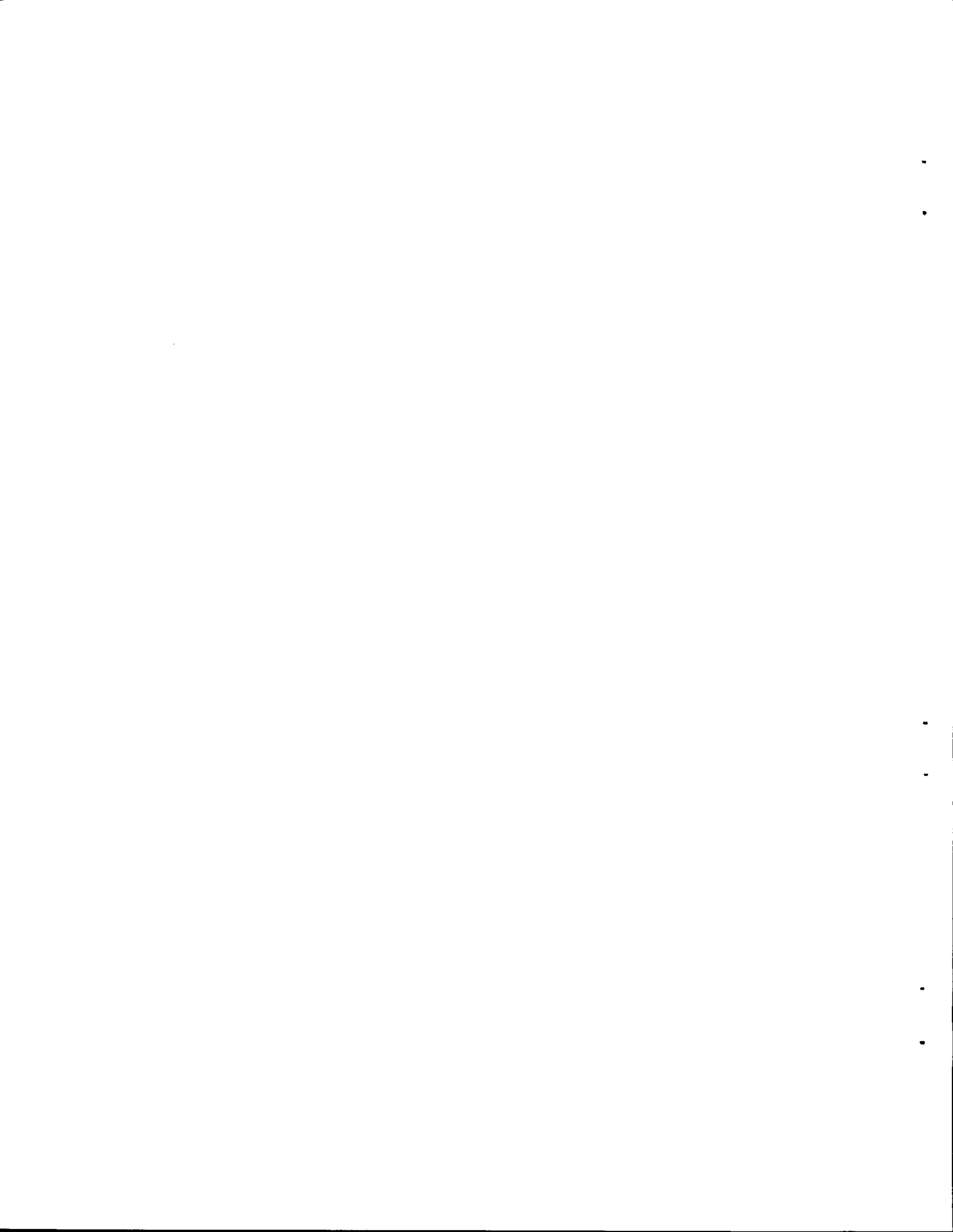
PART III. GAS-COOLED REACTOR PROGRAM

12. GAS EVOLUTION FROM GRAPHITE .....	139
13. TRANSPORT OF GASES THROUGH CERAMIC MATERIALS.....	149
Permeability .....	149

Diffusion of Gases.....	152
Porosity.....	153
14. IMPORTANCE OF ALKALI-METAL FISSION PRODUCTS IN EGCR FUEL CAPSULES.....	156
15. EFFECT OF REACTOR IRRADIATION ON BERYLLIUM OXIDE.....	157
16. GASEOUS ALUMINUM CHLORIDE AS A THERMODYNAMIC WORKING FLUID AND HEAT TRANSFER MEDIUM.....	158
17. MEASUREMENT OF TEMPERATURE IN REACTOR ENVIRONMENTS.....	159
Thermocouples for Measurement of Temperature of Gas-Cooled Surfaces.....	159
Development of Thermocouples for Use in a Thin Annulus.....	163
Drift Studies on Chromel-Alumel Thermocouples in Unusual Atmospheres.....	166
Development of High-Temperature Furnace for Thermocouple Studies.....	167
Stability of Rhenium-Tungsten Thermocouples.....	168
Effects of Radiation upon Thermocouples.....	168
18. REMOVAL OF RADIOACTIVE GASEOUS FISSION PRODUCTS FROM OTHER GASES.....	170
Removal of Noble Gases.....	170
Introduction.....	170
Improved Methods for Evaluating the Number of Theoretical Plates.....	171
Effect of Carrier Gas Velocity on <i>N</i> .....	171
Effect of Carrier Gas Composition and Pressure on Dynamic Adsorption.....	172
Krypton and Xenon Holdup Measurements on Various Adsorbents.....	173
Thermal Conductivity of Columbia G Activated Carbon in the Presence of Various Carrier Gases.....	173
Experiments Related to Ignition and Combustion of Charcoal in HRT Adsorber System.....	175
Potential Hazard Resulting from Oxygen Adsorption on Charcoal.....	175
Removal of Radioiodine Vapor.....	176
Activated Charcoal.....	177
Silver-Plated Copper Ribbon.....	177
Comparison of Charcoal and Silver-Copper Ribbon.....	179
Applications to Reactor Systems.....	179
Fission Gas Adsorption System for the NS "Savannah".....	179
Iodine Adsorption System at the Puerto Rico Nuclear Center (PRNC).....	181
Fission Gas-Iodine Vapor Adsorption Systems for In-Pile Experiments.....	181
PART IV. PREPARATION OF REACTOR-GRADE MATERIALS	
19. PREPARATION OF OXYGEN-FREE YTTRIUM.....	185
20. PREPARATION OF INORGANIC FLUORIDES.....	186
Synthesis of Fluorides of Chromium.....	186
Ammonium Hexafluochromate(III).....	186
Chromous Fluoride.....	186
Chromium(II,III) Fluoride.....	186
Disproportionation of Chromous Fluoride.....	186
Stannous Fluoride as a Preparative Reagent.....	186

Reactions of Ammonium Bifluoride .....	187
21. PREPARATION AND PROPERTIES OF INORGANIC OXIDES .....	188
High-Temperature Oxide Systems .....	188
Optical Properties of $UO_2$ - $ThO_2$ Solid Solutions .....	188
Preparation of High-Purity Beryllium Oxide .....	189
PUBLICATIONS .....	191
PAPERS PRESENTED AT SCIENTIFIC AND TECHNICAL MEETINGS .....	193

Part I  
MOLTEN-SALT REACTOR PROGRAM



## 1. HIGH-TEMPERATURE PHASE EQUILIBRIUM STUDIES

C. J. Barton                      H. A. Friedman                      H. Insley                      J. D. Redman  
R. A. Strehlow                      R. E. Thoma                      C. F. Weaver

The phase behavior of fused-salt materials which may be used to form fuels, heat transfer agents, converter/breeder blankets, and fuel reprocessing media for high-temperature nuclear reactors is directly related to the design, construction, and operation of those reactors. Relatively few materials have thermal neutron absorption cross sections so low that they can be considered for these uses. Until recently, almost no reports existed concerning the phase relationships in the condensed systems of fused salts suitable for these reactor uses. Accordingly, the principal effort of these studies has been to arrive at a good understanding of the phase behavior in such systems.<sup>1</sup>

Two general categories of high-temperature phase investigations have been involved. These are (1) studies directly related to the development of reactor fuels, heat transfer agents, etc., and (2) fundamental studies of reactor materials and of materials chemically similar to such substances.

The experimental data from which phase diagrams of fused-salt systems have been derived were obtained from thermal gradient quenching experiments, thermal analysis of heating and cooling effects occurring in melts, visual observation of phase changes occurring during heating and cooling, and filtration at high temperatures. Phases in samples from all these types of experiments were identified by the use of the petrographic microscope and with the x-ray diffractometer. Materials used have been, in each case, the commercially pure chemicals. These materials have been given further purification by alternate sparging in the molten state with HF and H<sub>2</sub> or by addition of NH<sub>4</sub>HF<sub>2</sub> before fusion. All handling of purified materials, prior to final examination, has been accomplished in dry boxes or under inert atmospheres.

The use of thermal gradient quenching combined with the complementary identification techniques of microscopic and x-ray diffraction analysis has developed in the Reactor Chemistry Division as a unique and peculiarly effective method in inorganic salt phase equilibrium studies. Except

<sup>1</sup>Phase diagrams of many of such systems previously investigated at this Laboratory have been reported in *Phase Diagrams of Nuclear Reactor Materials* (ed. by R. E. Thoma), ORNL-2548 (Nov. 2, 1959).

for BeF<sub>2</sub>-containing materials, high-temperature liquids of fluoride salt mixtures do not quench to true glasses. The occurrence of incipient crystals in the quenched materials generally precludes the use of x-ray diffraction techniques as a means of determining the liquidus or transitions where liquids appear or disappear. However, the combined techniques are definitive in cases of determining some solid state transitions, analyzing mixtures containing optically similar solids, and distinguishing between monophasic and polyphasic solid solutions. The optical technique is, of course, unmatched in its capability to detect traces of contaminants where these occur in concentrations below the detection limit of x-ray diffraction methods.

### SYSTEMS FOR USE AS NUCLEAR REACTOR FLUIDS

#### The System LiF-BeF<sub>2</sub>-ThF<sub>4</sub>-UF<sub>4</sub>

It has been demonstrated that LiF-BeF<sub>2</sub> mixtures can dissolve sufficient UF<sub>4</sub> and ThF<sub>4</sub> to provide a fuel solution for a U<sup>233</sup> molten-salt converter reactor.<sup>2</sup> The system LiF-BeF<sub>2</sub>-ThF<sub>4</sub>-UF<sub>4</sub> is, accordingly, of considerable potential importance. Efforts since the inception of this Division have included examination of all of the binary and ternary systems which are incorporated as limiting systems in this quaternary system, as well as examination of the composition regions of principal interest as core fluids for the converter reactor. Phase diagrams of eight of the ten limiting systems have been determined at ORNL. Polythermal projections of the four ternary limiting systems<sup>3-6</sup>

<sup>2</sup>C. F. Weaver *et al.*, *Phase Equilibria in Molten Salt Breeder Reactor Fuels. I. The System LiF-BeF<sub>2</sub>-UF<sub>4</sub>-ThF<sub>4</sub>*, ORNL-2892 (to be published).

<sup>3</sup>G. V. Jones *et al.*, *Phase Equilibria in the LiF-BeF<sub>2</sub>-UF<sub>4</sub> Fused Salt System*, MLM-1080 (Aug. 24, 1959).

<sup>4</sup>R. E. Thoma *et al.*, "Phase Equilibria in the Systems BeF<sub>2</sub>-ThF<sub>4</sub> and LiF-BeF<sub>2</sub>-ThF<sub>4</sub>," *J. Phys. Chem.*, in press.

<sup>5</sup>C. F. Weaver *et al.*, *Phase Equilibria in the Systems UF<sub>4</sub>-ThF<sub>4</sub> and LiF-UF<sub>4</sub>-ThF<sub>4</sub>*, ORNL-2719 (Aug. 17, 1959); *J. Am. Ceram. Soc.* **43**, 213 (1960).

<sup>6</sup>C. F. Weaver *et al.*, "The System BeF<sub>2</sub>-UF<sub>4</sub>-ThF<sub>4</sub>," unpublished work.

are shown in Figs. 1.1-1.4. Invariant equilibria in these systems are listed in reports elsewhere.<sup>1</sup> The marked similarity of the liquidus surfaces of the systems  $\text{LiF}-\text{BeF}_2-\text{ThF}_4$  and  $\text{LiF}-\text{BeF}_2-\text{UF}_4$  permits the inference that  $\text{UF}_4-\text{ThF}_4$  mixtures may be dissolved in  $\text{LiF}-\text{BeF}_2$  solvent mixtures in a wide variety of concentration ratios with little effect on the liquidus temperature. This inference is confirmed by the results of experiments shown in Figs. 1.5 and 1.6. The polythermal phase diagram of the system  $\text{LiF}-\text{ThF}_4-\text{UF}_4$  (Fig. 1.1) shows that the precipitating phases from most liquids contain both  $\text{UF}_4$  and  $\text{ThF}_4$  in relative concentrations nearly the same as those in the

liquids from which they were formed. An extensive report of the phase equilibria in this condensed system<sup>5</sup> shows that very little separation in the  $\text{ThF}_4-\text{UF}_4$  concentration ratio occurs on cooling solutions of these materials in  $\text{LiF}$ -containing solvents.

The marked similarity of the phase diagrams of the simple systems  $\text{BeF}_2-\text{UF}_4$  (ref 7) and  $\text{BeF}_2-\text{ThF}_4$  (ref 4) indicates that the ternary system  $\text{BeF}_2-\text{UF}_4-\text{ThF}_4$  should display only the primary

<sup>7</sup>T. B. Rhinehammer, P. A. Tucker, and E. F. Joy, *Phase Equilibria in the System  $\text{BeF}_2-\text{UF}_4$* , MLM-1082 (to be published).

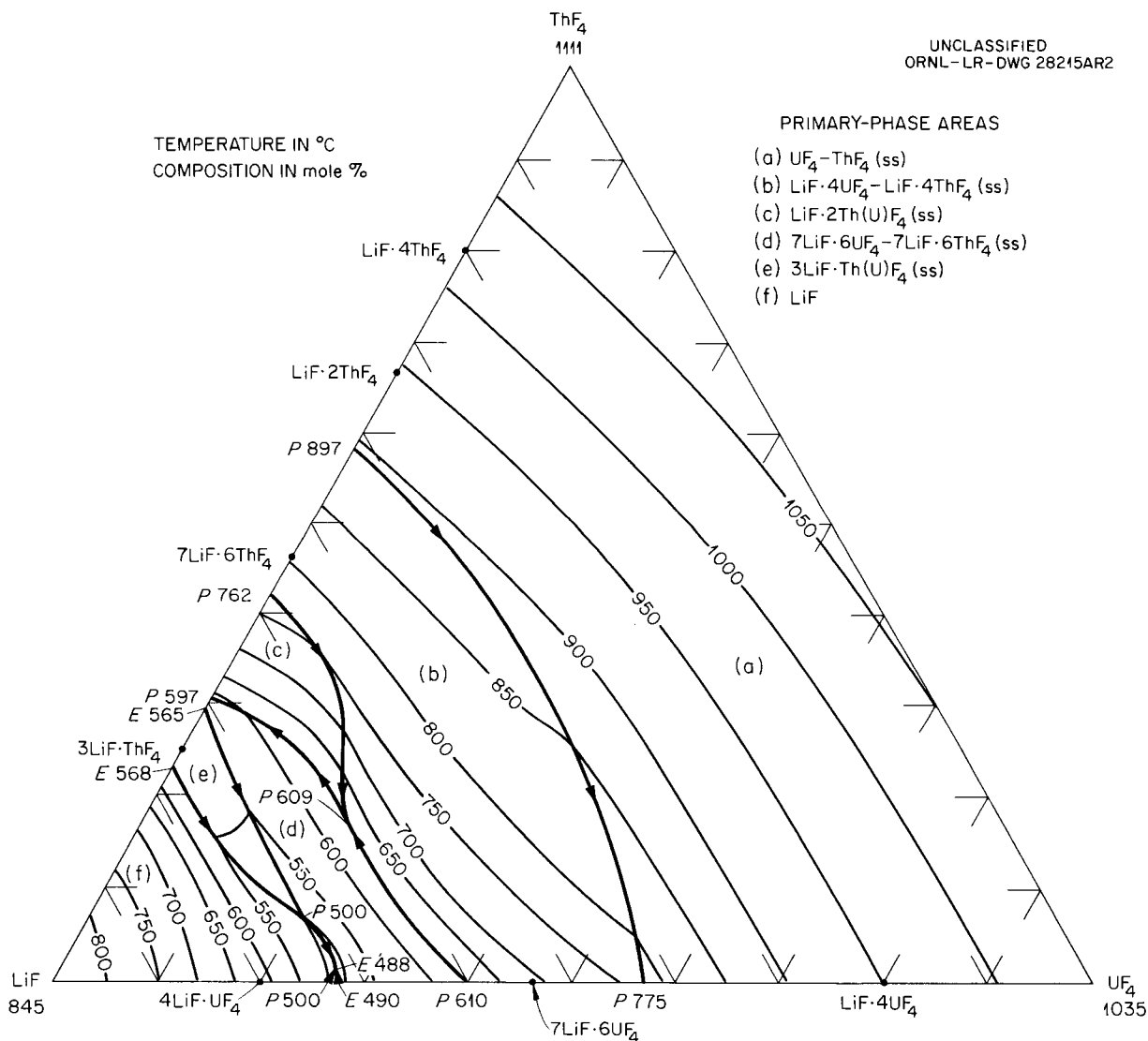


Fig. 1.1. The System  $\text{LiF}-\text{UF}_4-\text{ThF}_4$ .

UNCLASSIFIED  
ORNL-LR-DWG 37420AR2

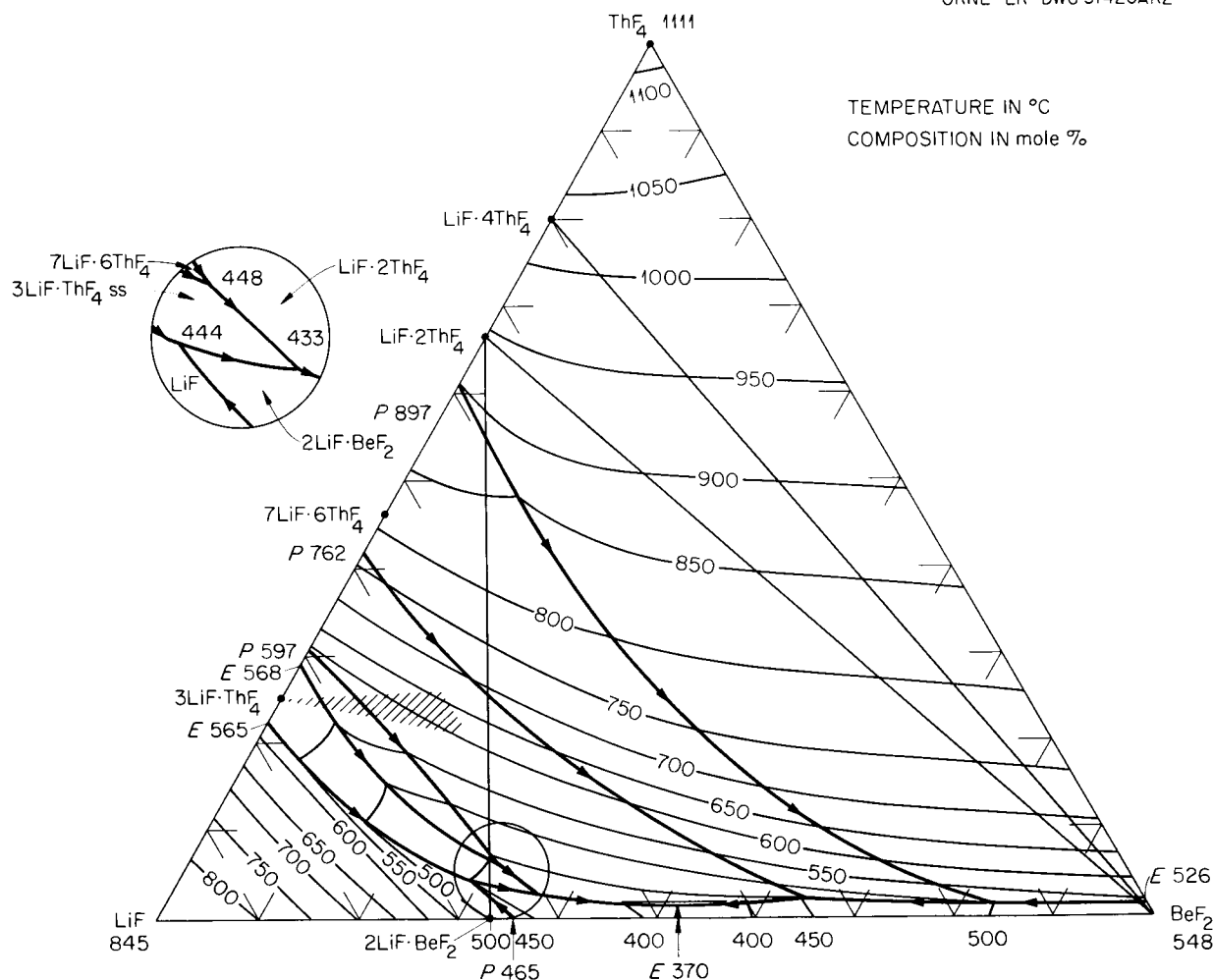


Fig. 1.2. The System LiF-BeF<sub>2</sub>-ThF<sub>4</sub>.

phase fields of UF<sub>4</sub>-ThF<sub>4</sub> solid solution and BeF<sub>2</sub>, and the even reaction boundary path between these primary phase fields. Experimental work is in progress to determine the validity of this hypothesis. Results of those experiments are shown in the preliminary phase diagram (Fig. 1.4).

#### The System NaF-BeF<sub>2</sub>-ThF<sub>4</sub>-UF<sub>4</sub>

Studies of the phase equilibria in the systems limiting the quaternary system NaF-BeF<sub>2</sub>-ThF<sub>4</sub>-UF<sub>4</sub> have been in progress for some time. These studies were undertaken in the expectancy that the physical properties of combinations of these materials may prove adequate for the demonstration that NaF-BeF<sub>2</sub> based fluids will serve as suitable

reactor core materials. Reports have been published concerning the phase equilibria in the limiting systems NaF-ThF<sub>4</sub> (ref 8), NaF-BeF<sub>2</sub> (ref 9), BeF<sub>2</sub>-ThF<sub>4</sub> (ref 4), ThF<sub>4</sub>-UF<sub>4</sub> (ref 5), and NaF-UF<sub>4</sub> (ref 10). Phase diagrams of the systems BeF<sub>2</sub>-UF<sub>4</sub> and NaF-BeF<sub>2</sub>-UF<sub>4</sub> have been constructed by other workers.<sup>7,11</sup> Studies in

<sup>8</sup>R. E. Thoma et al., *J. Phys. Chem.* **63**, 1266 (1959).

<sup>9</sup>D. M. Roy, R. Roy, and E. F. Osborn, *J. Am. Ceram. Soc.* **36**, 185 (1953).

<sup>10</sup>C. J. Barton et al., *J. Am. Ceram. Soc.* **41**, 63 (1958).

<sup>11</sup>J. F. Eichelberger et al., "The System NaF-BeF<sub>2</sub>-UF<sub>4</sub>," p 110 in *Phase Diagrams of Nuclear Reactor Materials* (ed. by R. E. Thoma), ORNL-2548 (Nov. 2, 1959).



UNCLASSIFIED  
ORNL-LR-DWG 45510

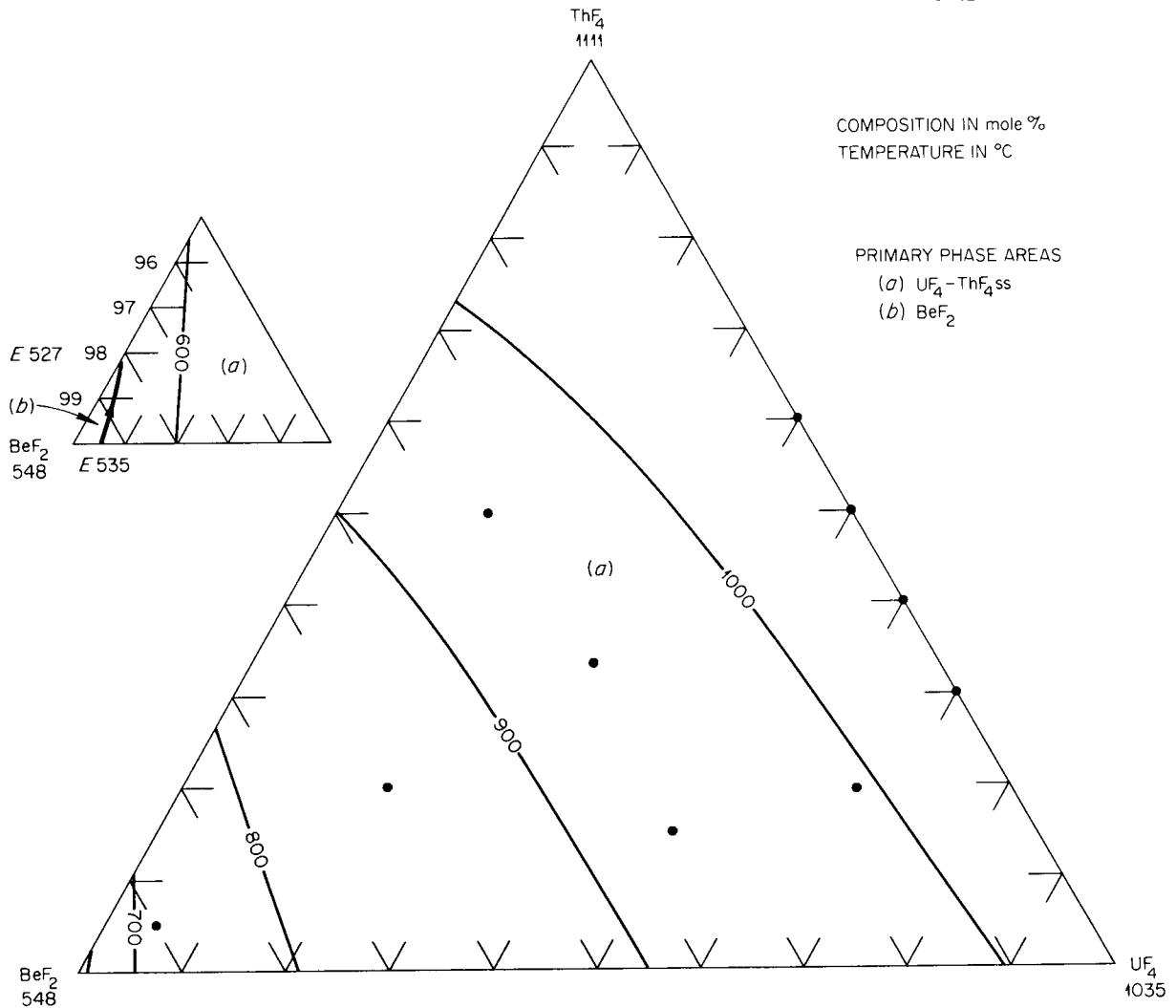


Fig. 1.4. The System  $BeF_2-ThF_4-UF_4$ .

progress at this Laboratory of the systems  $NaF-BeF_2-ThF_4$  and  $NaF-ThF_4-UF_4$  have progressed well enough that nearly completed phase diagrams of the systems can be constructed. These are shown in Figs. 1.7 and 1.8.

#### The System $NaF-BeF_2-ThF_4$

Continuing studies of the phase equilibria in the system  $NaF-BeF_2-ThF_4$  have established that this system involves 12 invariant equilibrium points. Of these, ten have been established to within

1 mole % and 5°C. A list of the established invariant equilibria is shown in Table 1.1.

The system contains a ternary compound  $NaF \cdot BeF_2 \cdot 3ThF_4$ , which melts to liquid and  $ThF_4$  solid solution (ss). Consequently, the join  $NaF \cdot BeF_2-ThF_4$  does not represent a true binary system. The maximum temperature on the boundary between the primary phase fields of  $ThF_4$  ss and  $NaF \cdot BeF_2 \cdot 3ThF_4$  is shifted from the  $NaF \cdot BeF_2-ThF_4$  join to a higher NaF concentration. This maximum temperature actually occurs at the  $ThF_4$  ss,  $NaF \cdot 2ThF_4$ ,  $NaF \cdot BeF_2 \cdot 3ThF_4$  invariant point.

REACTOR CHEMISTRY PROGRESS REPORT

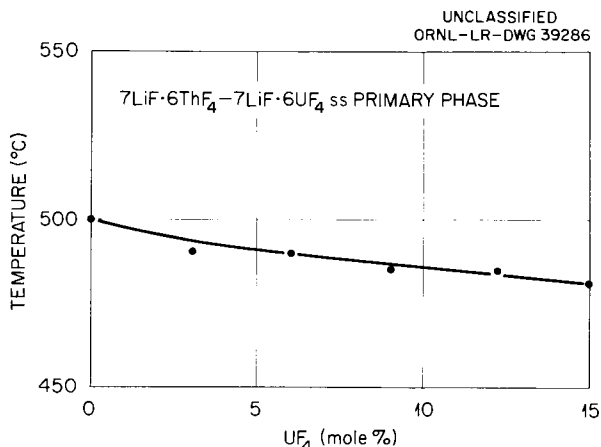


Fig. 1.5. The Join LiF-BeF<sub>2</sub>-ThF<sub>4</sub> (67.5-17.5-15)-LiF-BeF<sub>2</sub>-UF<sub>4</sub> (67.5-17.5-15) in the Quaternary System LiF-BeF<sub>2</sub>-ThF<sub>4</sub>-UF<sub>4</sub>.

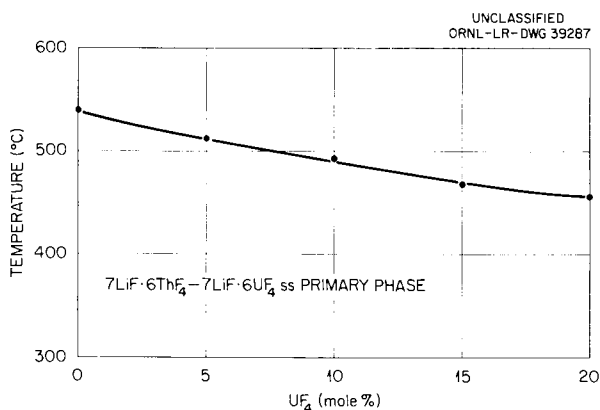


Fig. 1.6. The Join LiF-BeF<sub>2</sub>-ThF<sub>4</sub> (70-10-20)-LiF-BeF<sub>2</sub>-UF<sub>4</sub> (70-10-20) in the Quaternary System LiF-BeF<sub>2</sub>-ThF<sub>4</sub>-UF<sub>4</sub>.

Table 1.1. Invariant Equilibria in the System NaF-BeF<sub>2</sub>-ThF<sub>4</sub>

Composition of Liquid (mole %)			Invariant Temperature (°C)	Type of Equilibrium	Solid Phases Present
NaF	BeF	ThF <sub>4</sub>			
2	96	2	527		ThF <sub>4</sub> ss, BeF <sub>2</sub> , and NaF·BeF <sub>2</sub> ·3ThF <sub>4</sub>
43	55	2	365	Eutectic	NaF·BeF <sub>2</sub> , BeF <sub>2</sub> , and NaF·BeF <sub>2</sub> ·3ThF <sub>4</sub>
49	49	2	375		NaF·BeF <sub>2</sub> , NaF·2ThF <sub>4</sub> , and NaF·BeF <sub>2</sub> ·3ThF <sub>4</sub>
47	51	2	375	Peritectic	NaF·BeF <sub>2</sub> , NaF·2ThF <sub>4</sub> , and β-NaF·ThF <sub>4</sub>
56	42	2	320	Eutectic	NaF·BeF <sub>2</sub> , 2NaF·BeF <sub>2</sub> , and β-NaF·ThF <sub>4</sub>
57	41	2	415	Peritectic	β <sub>2</sub> -2NaF·ThF <sub>4</sub> , 2NaF·BeF <sub>2</sub> , and β-NaF·ThF <sub>4</sub>
72	22	6	510	Eutectic	β <sub>2</sub> -2NaF·ThF <sub>4</sub> , 2NaF·BeF <sub>2</sub> , and NaF
76	11	13	540	Peritectic	β <sub>2</sub> -2NaF·ThF <sub>4</sub> , β-4NaF·ThF <sub>4</sub> , and NaF
62	2	36	683	Peritectic	β <sub>2</sub> -2NaF·ThF <sub>4</sub> , 3NaF·2ThF <sub>4</sub> , and β-NaF·ThF <sub>4</sub>
42	31	27	740	Peritectic	NaF·2ThF <sub>4</sub> , ThF <sub>4</sub> ss, and NaF·BeF <sub>2</sub> ·3ThF <sub>4</sub>

UNCLASSIFIED  
ORNL-LR-DWG 38155R

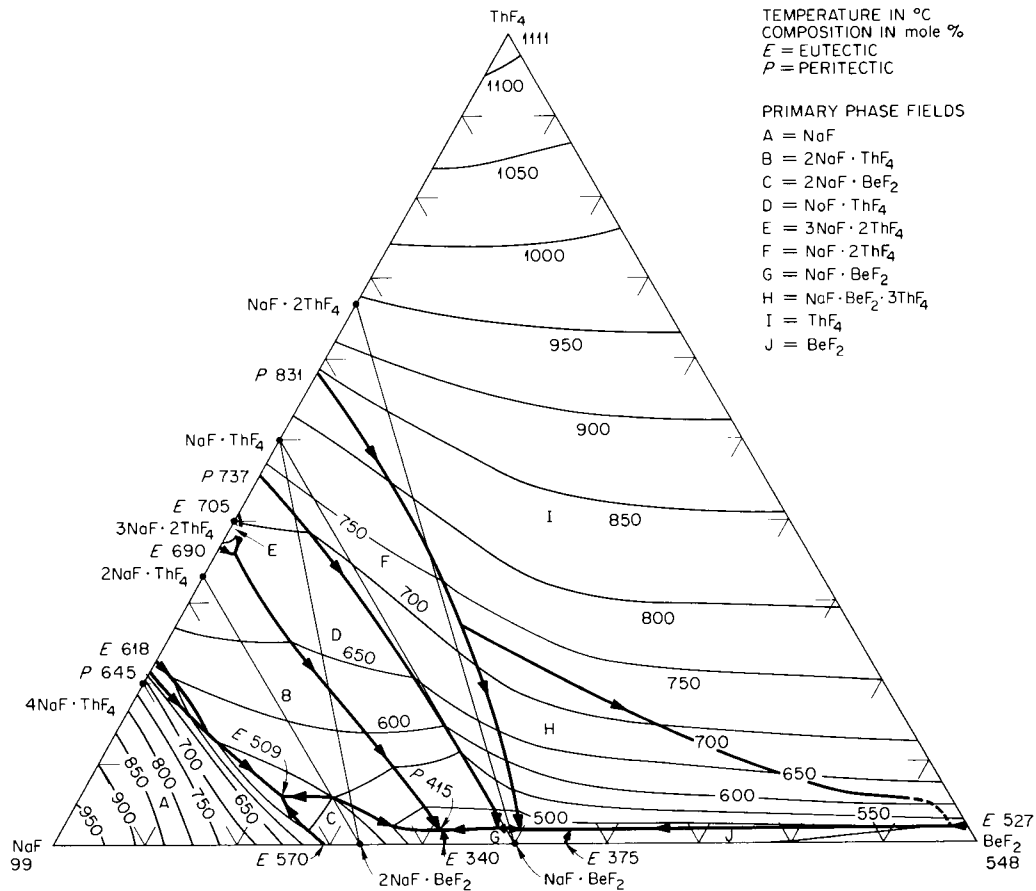


Fig. 1.7. The System NaF-BeF<sub>2</sub>-ThF<sub>4</sub>.

### The System NaF-BeF<sub>2</sub>-UF<sub>4</sub>

Studies by Barton *et al.*<sup>10</sup> on the system NaF-UF<sub>4</sub> and more recent attempts in this Laboratory to synthesize the compound NaF·4UF<sub>4</sub> by thermal gradient quenches of a substance with the composition 20 mole % NaF-80 mole % UF<sub>4</sub> have failed to confirm the existence of a compound having this composition reported by Eichelberger *et al.*<sup>11</sup> in their investigation of the system NaF-BeF<sub>2</sub>-UF<sub>4</sub>. Moreover, studies at this Laboratory in the system NaF-BeF<sub>2</sub>-ThF<sub>4</sub> have shown that a primary phase field exists corresponding to the "NaF·4UF<sub>4</sub>" primary phase field in the system NaF-BeF<sub>2</sub>-UF<sub>4</sub> and that the primary phase in this case is NaF·BeF<sub>2</sub>·3ThF<sub>4</sub>. This compound is analogous in optical properties to the so-called "NaF·4UF<sub>4</sub>" as reported by the Mound Laboratory. Quenched

samples at the composition 20 mole % NaF, 20 mole % BeF<sub>2</sub>, and 60 mole % UF<sub>4</sub> have shown that the compound NaF·BeF<sub>2</sub>·3UF<sub>4</sub> exists as a single solid phase at its composition. Optical properties and x-ray diffraction data for the NaF·BeF<sub>2</sub>·3UF<sub>4</sub> indicate that the compounds NaF·BeF<sub>2</sub>·3ThF<sub>4</sub> and NaF·BeF<sub>2</sub>·3UF<sub>4</sub> are isostructural. These data are listed separately in Table 1.6.

### The System NaF-UF<sub>4</sub>-ThF<sub>4</sub>

Sufficient experimental work has been done on the phase relationships in the condensed system NaF-UF<sub>4</sub>-ThF<sub>4</sub> that the primary phase fields and the temperatures and compositions of the invariant points can be described with a fair degree of confidence.

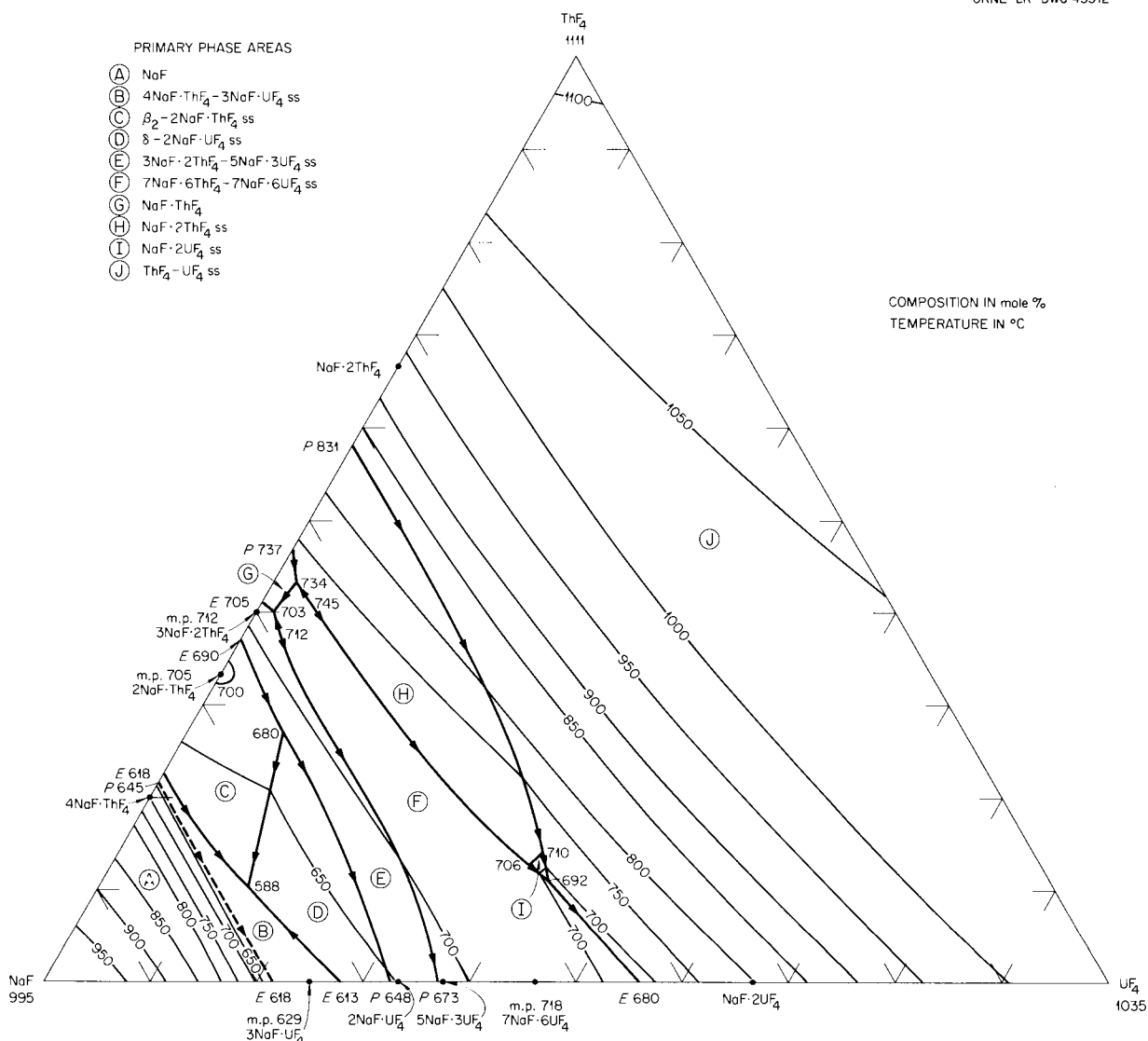


Fig. 1.8. The System NaF-ThF<sub>4</sub>-UF<sub>4</sub>.

Previous work on the binary systems NaF-UF<sub>4</sub> (ref 10) and NaF-ThF<sub>4</sub> (ref 8) has shown that the two systems are by no means completely analogous in spite of the fact that the binary system UF<sub>4</sub>-ThF<sub>4</sub> is composed of a complete series of solid solutions.<sup>5</sup>

The compound NaF·2ThF<sub>4</sub> is cubic and has a considerable range of primary crystallization in the binary system, whereas the compound NaF·2UF<sub>4</sub> possesses a lower, undetermined symmetry - orthorhombic, monoclinic, or triclinic - and is only stable at subsolidus temperatures in the

system NaF-UF<sub>4</sub>. The join between these compounds in the binary systems shows extensive mutual solid solution with a narrow miscibility gap. Indeed, the temperature of stability of the NaF·2UF<sub>4</sub> compound is raised so much (more than 60°) by the solution of NaF·2ThF<sub>4</sub> that this compound has a small primary phase field in the ternary system.

There is an NaF·ThF<sub>4</sub> compound with a small range of primary phase crystallization in the binary system. There is no corresponding compound in the NaF-UF<sub>4</sub> system, and the compound

$7\text{NaF}\cdot 6\text{UF}_4$ , which is congruently melting with a large primary phase range in the binary system  $\text{NaF}\text{-}\text{UF}_4$ , has only a metastable analog in the  $\text{NaF}\text{-}\text{ThF}_4$  system. Only about 2 mole %  $\text{UF}_4$  is required, however, to stabilize the 7:6 compound in the ternary system with a complete series of isostructural solid solutions to the  $\text{NaF}\text{-}\text{UF}_4$  boundary.

Apparently structurally similar cubic compounds exist in the  $\text{NaF}\text{-}\text{ThF}_4$  and  $\text{NaF}\text{-}\text{UF}_4$  systems,  $3\text{NaF}\cdot 2\text{ThF}_4$  and  $5\text{NaF}\cdot 3\text{UF}_4$ . In spite of the unmistakably different molecular ratios these two compounds form a complete series of solid solutions and have a continuous primary phase field across the ternary liquidus surface.

There are two isomorphous forms of  $2\text{NaF}\cdot\text{ThF}_4$  and  $2\text{NaF}\cdot\text{UF}_4$ , designated respectively as  $\beta_2$  and  $\alpha$ . Of pure  $2\text{NaF}\cdot\text{ThF}_4$  the  $\beta_2$  form is stable and the  $\alpha$  form metastable. Of pure  $2\text{NaF}\cdot\text{UF}_4$  the  $\alpha$  form is stable and the  $\beta_2$  form metastable. In the ternary system these two compounds form extensive solid solutions with a small miscibility gap (Fig. 1.9).

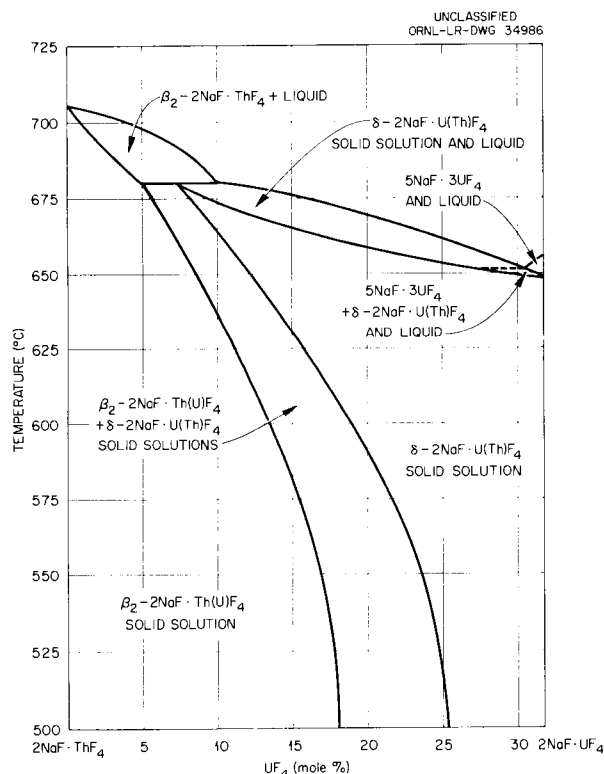


Fig. 1.9. The Section  $2\text{NaF}\cdot\text{ThF}_4\text{-}2\text{NaF}\cdot\text{UF}_4$ .

The compounds  $4\text{NaF}\cdot\text{ThF}_4$  and  $3\text{NaF}\cdot\text{UF}_4$  have some structural similarities, and quenching experiments have shown that they possess some mutual solid solubility, but sufficient detailed work to show quantitative relationships is still lacking.

### Phase Relations in the System $\text{LiF}\text{-}\text{PuF}_3$ <sup>12</sup>

Phase equilibrium relations in the system  $\text{LiF}\text{-}\text{PuF}_3$  were determined because of interest in the possible use of mixtures in the system  $\text{LiF}\text{-}\text{BeF}_2\text{-}\text{PuF}_3$  to fuel a plutonium-burning molten-fluoride power reactor. Thermal analysis apparatus developed for this study, shown in Fig. 1.10,

<sup>12</sup>Paper No. 27 presented in the Division of Physical Chemistry at the 135th National Meeting of the American Chemical Society, Boston, April 1959.

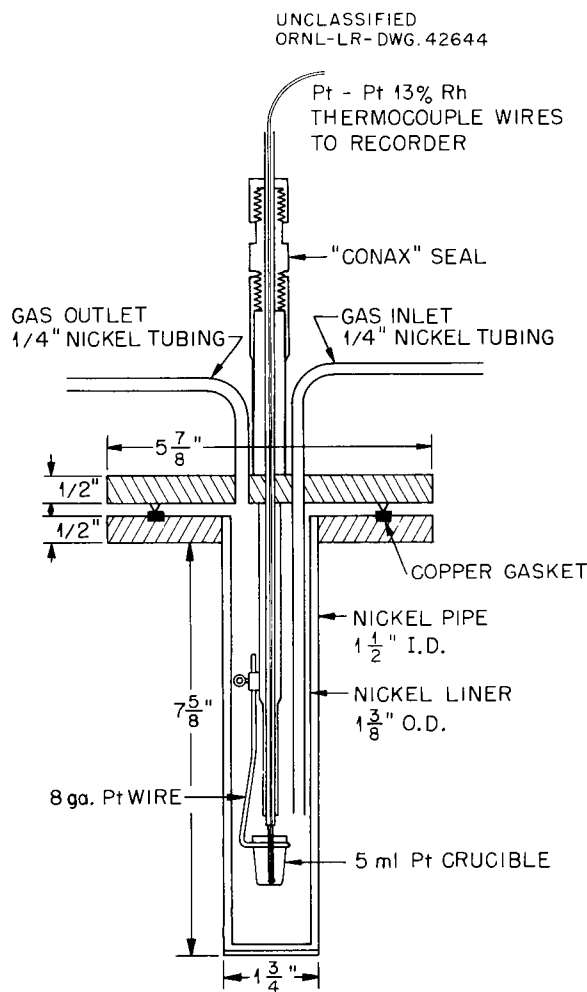


Fig. 1.10. Thermal Analysis Apparatus.

was capable of detecting thermal effects with 1- to 3-g quantities of materials. High sensitivity was achieved by supporting the platinum crucible at the top, providing a minimum amount of heat-conducting material in contact with the sample, and by immersing the unshielded thermocouple junction in the melt. Argon which had a very low oxygen content was used to provide an inert atmosphere in the apparatus while it was above room temperature. The lower part of the apparatus was surrounded by a 600-w uninsulated heater consisting of a ceramic cylinder 3 in. in diameter and 8 in. high wound with Nichrome wire. This heater and the apparatus were placed in a stainless steel glove box which had a heating well on the bottom heated externally by a 2700-w, 5-in. tube furnace. This combination of furnaces heated the contents of the crucible to a maximum temperature of about 1000°C. Temperature control was achieved by manual adjustment of variable transformers connected to the furnaces.

The following technique was used to obtain thermal analysis data. Weighed quantities of optical-grade LiF and high-purity PuF<sub>3</sub> were mixed in a 5-ml platinum crucible previously positioned in the thermal analysis apparatus as shown in Fig. 1.10. The apparatus was sealed, evacuated, and filled with argon which was allowed to flow through the apparatus at a pressure slightly above the pressure within the glove box. The mixture was heated slowly until the ammonium bifluoride decomposed and the resulting ammonium fluoride volatilized and then more rapidly to a temperature 25 to 150°C above the liquidus temperature of the mixture under test. Cooling rates of 1 or 2 deg/min were maintained through the temperature range of expected thermal effects, and two or more cooling curves were obtained with most of the compositions tested. Whenever thermal effects were noted on the recorded cooling curves, the temperature was checked by connecting the thermocouple to a portable potentiometer. The maximum difference between the recorder and potentiometer temperatures was 5° and the average difference was 2.8°. After thermal data were obtained, the mixtures were allowed to cool to room temperature and crushed to separate them from the thermocouple junction. The crushed samples were first weighed, then ground and submitted for chemical analysis and for identification of the crystalline components by means of a polarizing microscope mounted

in a glove box connected to the stainless steel box in which the material was heated.

Thermal analysis data obtained with mixtures containing 5 to 38 mole % PuF<sub>3</sub> are shown in Fig. 1.11. The diagram shows that LiF and PuF<sub>3</sub> form a simple eutectic system, with the eutectic mixture containing approximately 19.5 mole % PuF<sub>3</sub> and melting at 743 ± 2°C. Confirmation of the thermal indication of the nature of the system and the composition of the eutectic mixture was

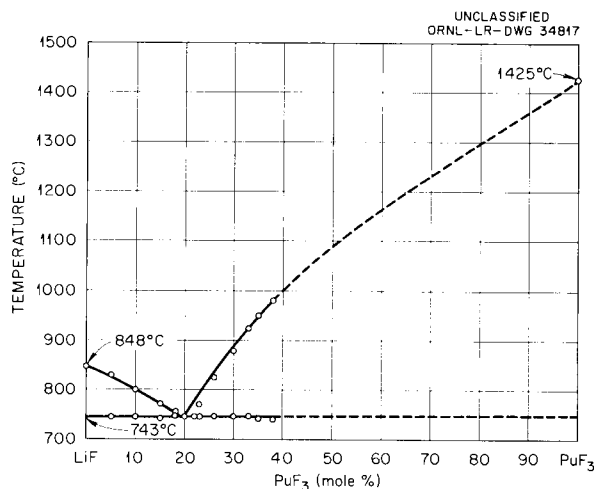


Fig. 1.11. The System LiF-PuF<sub>3</sub>.

obtained by microscopic examination of the fused mixtures. Only the pure, crystalline components were present, and no evidence of solid solution formation was observed. The presence of well-crystallized LiF, along with eutectic aggregates of LiF and PuF<sub>3</sub>, indicated that LiF was the first phase to separate from the melt on cooling the mixture containing 19 mole % PuF<sub>3</sub>. Similarly, the presence of well-crystallized PuF<sub>3</sub> in the mixture containing 20 mole % PuF<sub>3</sub> showed that PuF<sub>3</sub> was the primary phase of this composition, thus establishing the location of the eutectic composition between these limits.

#### Solubility of PuF<sub>3</sub> in Fused Alkali Fluoride-Beryllium Fluoride Mixtures<sup>13</sup>

The solubility of PuF<sub>3</sub> in five LiF-BeF<sub>2</sub> mixtures, three NaF-BeF<sub>2</sub> mixtures, two NaF-LiF-BeF<sub>2</sub> mixtures, and one LiF-BeF<sub>2</sub>-UF<sub>4</sub> mixture

<sup>13</sup>In press, *J. Phys. Chem.*; paper No. 106 presented at the symposium on High Temperature of the Division of Inorganic Chemistry at the 135th National Meeting of the American Chemical Society, Boston, April 1959.

was determined at temperatures ranging from about 550 to 650°C because of interest in the possibility of fueling fused-salt power reactors with plutonium. Solubility determinations were made in nickel filter apparatus by forcing liquid salt mixtures saturated with  $\text{PuF}_3$  through sintered nickel filters, cooling the filtrates, and analyzing them chemically to determine their plutonium content. The data obtained appeared to follow a linear relationship within the experimental accuracy of the measurements when plotted as molar concentration of  $\text{PuF}_3$  vs  $1/T$  (°K). The solubility of  $\text{PuF}_3$  in these solvents was found to be rather low, varying from about 0.4 to 2.5 mole % at 650°C and from 0.16 to 1.2 mole % at 550°C. The observed solubilities are believed to be adequate for some types of fused-salt reactors. Typical data obtained in this investigation are shown graphically in Fig. 1.12, which shows the data

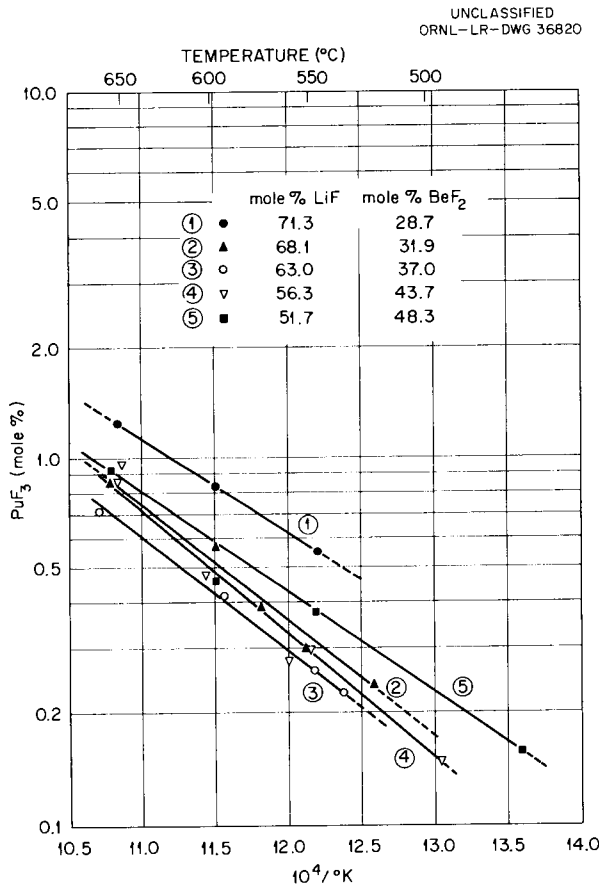


Fig. 1.12. Solubility of  $\text{PuF}_3$  as a Function of Temperature for  $\text{LiF-BeF}_2$  Solvents.

obtained with  $\text{LiF-BeF}_2$  mixtures. It was interesting to find that the solubility of  $\text{PuF}_3$  in the mixture 70  $\text{LiF-10 BeF}_2-20 \text{UF}_4$  (mole %) was higher than that in the  $\text{LiF-BeF}_2$  mixture having about the same  $\text{LiF}$  concentration. This observation is of some importance because it points to the possibility of converting  $\text{U}^{238}$  to  $\text{Pu}^{239}$  in a molten-salt reactor. Figure 1.13 shows how the solubility of  $\text{PuF}_3$  varies with the concentration of  $\text{BeF}_2$  in  $\text{LiF-BeF}_2$  and  $\text{NaF-BeF}_2$  mixtures.

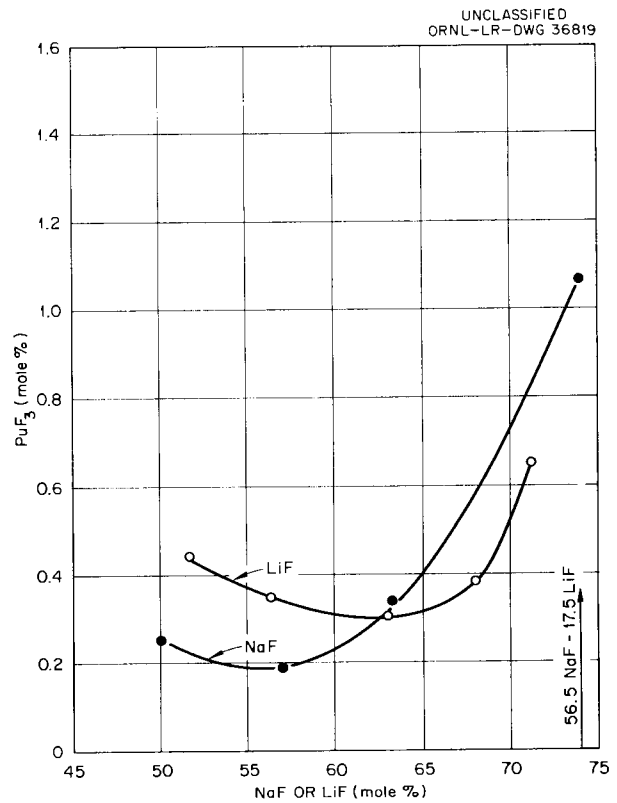


Fig. 1.13. Solubility of  $\text{PuF}_3$  in  $\text{LiF-BeF}_2$  and  $\text{NaF-BeF}_2$  at 565°C.

In addition to  $\text{UF}_4$  mentioned above, the effect of several other added ions on the solubility of  $\text{PuF}_3$  in one of the  $\text{LiF-BeF}_2$  mixtures was examined. The addition of one mole %  $\text{ThF}_4$  to the mixture  $\text{LiF-BeF}_2$  (63-37 mole %) had little effect on the solubility of  $\text{PuF}_3$  in this solvent, indicating that it might be feasible, from the solubility standpoint, to convert  $\text{Th}^{232}$  to  $\text{U}^{233}$  in a plutonium-fueled reactor. The addition of  $\text{BaF}_2$  to this mixture appeared to reduce the solubility of  $\text{PuF}_3$  in a manner not clearly understood, but

the data indicate that the buildup of divalent fission products in an operating power reactor should not seriously affect the solubility of  $\text{PuF}_3$ . Cerium trifluoride reduced the solubility of  $\text{PuF}_3$  in the same solvent in direct proportion to the molar ratio of  $\text{CeF}_3$  to  $\text{PuF}_3$  in the mixture. This indicates that it would be possible to precipitate  $\text{PuF}_3$  from solvents of this type, along with some other trivalent ions, by "salting" it out with  $\text{CeF}_3$ .

**Phase Equilibria in the Systems  
NaF-PuF<sub>3</sub> and NaF-CeF<sub>3</sub>**

Phase equilibrium relations in the system NaF-PuF<sub>3</sub> were investigated because of interest in possible use of mixtures in the system NaF-BeF<sub>2</sub>-PuF<sub>3</sub> or the system NaF-LiF-BeF<sub>2</sub>-PuF<sub>3</sub> to fuel a plutonium-burning molten-fluoride power reactor. Other studies<sup>14</sup> had shown that the solubility of  $\text{PuF}_3$  in these systems is adequate for some proposed reactors. This investigation also represented a logical extension of the previously completed study of the LiF-PuF<sub>3</sub> system, summarized elsewhere in this report. A study of a part of the NaF-CeF<sub>3</sub> system was performed at about the same time because of its suspected similarity to the NaF-PuF<sub>3</sub> system and because of the desirability of having suitable materials to test new high-temperature thermal analysis apparatus before it was used in the plutonium glove box. An earlier unpublished study of this system in this Laboratory failed to produce a complete phase diagram chiefly due to lack of liquidus temperatures in the  $\text{CeF}_3$  primary phase field. Some data obtained in that study are included in this report.

Thermal analysis data were obtained with NaF-PuF<sub>3</sub> mixtures containing 5 to 50 mole %  $\text{PuF}_3$  in the same type of thermal analysis apparatus used for investigation of the LiF-PuF<sub>3</sub> system described elsewhere in this report, and essentially the same technique was used except that the cooling rate was controlled by means of a Brown controller rather than manually. The data obtained to date are included in Table 1.2. The slowly cooled mixtures obtained in the thermal analysis study were examined by means of a polarizing microscope mounted in a glove box.

Facilities for x-ray examination of plutonium-containing mixtures and for quenching experiments with these materials were not available.

A preliminary phase diagram for the NaF-PuF<sub>3</sub> system based upon the available thermal analysis data contained in Table 1.2 and the results of microscopic identification of crystalline compounds in the slowly cooled melts is shown in Fig. 1.14. The absence of a liquidus thermal effect in the cooling curves obtained with the 50 mole %  $\text{PuF}_3$  mixture was undoubtedly due to the fact that the apparatus in use at that time was limited to a maximum temperature of 1000°C, about 40° below the estimated liquidus temperature. The eutectic between NaF and NaF·PuF<sub>3</sub> contains approximately 23 mole %  $\text{PuF}_3$  and melts at 727 ± 3°C. Insufficient data were obtained to locate the peritectic composition accurately, but it appears to contain approximately 40 mole %  $\text{PuF}_3$ . The observation of arrests at 842°C in the cooling curves obtained with mixtures containing 40 and 50 mole %  $\text{PuF}_3$  indicates that this is probably the incongruent melting temperature of the compound NaF·PuF<sub>3</sub>. The absence of an arrest at the eutectic temperature in cooling curves obtained with the 50 mole %  $\text{PuF}_3$  mixture and the observation of essentially single-phase material in the slowly cooled sample appear to confirm the identity of the binary compound formed by NaF and  $\text{PuF}_3$ . The optical properties of this compound formed in binary mixtures were the same as those of the compound formed in NaF-BeF<sub>2</sub>-PuF<sub>3</sub> and

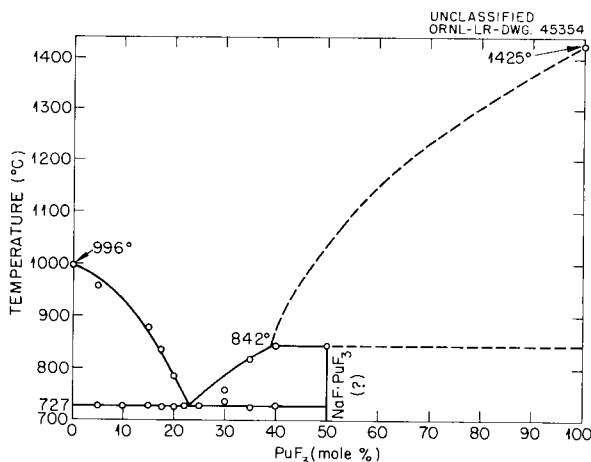


Fig. 1.14. The System NaF-PuF<sub>3</sub> (Preliminary Diagram). Data from thermal analysis experiments.

<sup>14</sup>C. J. Barton, *J. Phys. Chem.*, in press.

Table 1.2. Thermal Analysis Data Obtained with NaF·PuF<sub>3</sub> Mixtures

Composition (mole % PuF <sub>3</sub> )	Liquidus Temperature (°C)		Peritectic Temperature (°C)		Solidus Temperature (°C)		Microscopic Observations
	Recorder	Potentiometer	Recorder	Potentiometer	Recorder	Potentiometer	
0					996H	996	NaF
5	955				722H	728	NaF + eutectic aggregates
10					724UC	726	NaF + eutectic aggregates
15	875				723UC	728	NaF + eutectic aggregates
15	875H	877			728H	728	NaF + eutectic aggregates
17.5					720CS	721	NaF + eutectic aggregates
17.5	833CS	835			724H	725	NaF + eutectic aggregates
20	785H				723H	725	NaF + eutectic aggregates
22					724UC	726	eutectic aggregates
25					727H	728	NaF·PuF <sub>3</sub> + eutectic aggregates
30	756H	758			733CS	735	NaF·PuF <sub>3</sub> + eutectic aggregates
35	818H	818			722H	723	NaF·PuF <sub>3</sub> + eutectic aggregates
40			841UC	841	727H	727	NaF·PuF <sub>3</sub> + eutectic aggregates
50			842UC	842			Almost all NaF·PuF <sub>3</sub>

H = halt; CS = change of slope; UC = undercooled.

LiF-NaF-PuF<sub>3</sub> mixtures, indicating that there is little, if any, solubility of LiF, NaF, or BeF<sub>2</sub> in NaF·PuF<sub>3</sub>. The optical properties of NaF·PuF<sub>3</sub>, NaF·CeF<sub>3</sub>, and NaF·UF<sub>3</sub> were compared in an earlier report.<sup>15</sup>

The apparatus used to obtain thermal analysis data with NaF-PuF<sub>3</sub> and LiF-PuF<sub>3</sub> mixtures was limited to a maximum temperature of about 1000°C, as was mentioned above. In order to attain higher temperatures, this apparatus was modified in several ways. A photograph of the modified apparatus is shown in Fig. 1.15. Two 1250-w

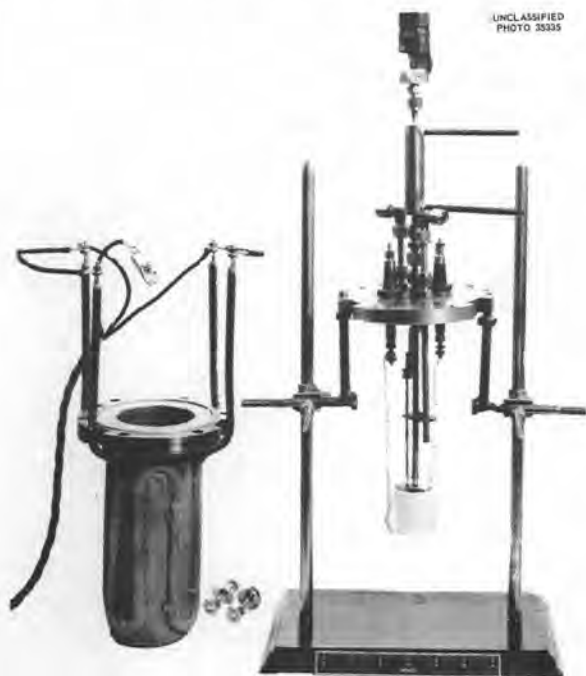


Fig. 1.15. Thermal Analysis Apparatus for Temperatures up to 1350°C.

Calrod heaters were first tack-welded to the outside of 3-in.-dia nickel containers and then spray-welded with 3 to 5 lb of nickel powder to provide a more uniform heating surface. The ends of the heaters were brought up through notches in the flanged top of the container and connected in parallel to a 115-v line through a variable transformer. A small platinum resistance furnace fabricated locally provided a source of heat quite

<sup>15</sup>C. J. Barton, W. R. Grimes, and R. A. Strehlow, *Solubility and Stability of PuF<sub>3</sub> in Fused Alkali Fluoride Mixtures*, Appendix B, ORNL-2530 (June 11, 1958).

close to the platinum crucible sample container. An alumina cylinder (Norton Co. RA 139), 1½ in. high, 1½ in. OD, and 1 in. ID, was internally grooved with a spiral of 10 to 12 turns in which 18-gage platinum wire was inserted. The interior of the cylinder was coated with alumina cement (Norton Co. RA-1139), air-dried, and then cured at 1300°C before use. The ends of the platinum wire were insulated with alumina spaghetti and fastened to the lower ends of spark-plug-type connectors in the cover plate of the apparatus. Other openings in the cover plate were occupied by gastight Swagelok fittings through which ¼-in. nickel tubing passed for the inlet and outlet gas lines and for the thermocouple insulator. The latter tube extended 10 in. above the cover plate and was water-jacketed near the top to prevent heating of the thermocouple junction located at the top end of the tube. Thermocouple lead wires from this junction connected the platinum vs platinum-13% rhodium thermocouple to a recording potentiometer having a 700 to 1500°C temperature range or to a portable potentiometer. Platinum disks above and below the crucible and a platinum cylinder around the alumina furnace core served as heat reflectors. The performance of this apparatus with additional heat supplied by a 5-in. tube furnace was tested by heating pure NaF, recrystallized from melted material, and, at the same time, the thermocouple was calibrated by checking the known freezing point of NaF. Halts of 3 to 9 min duration were observed in the NaF cooling curves at 996°C, in good agreement with the recent literature value of 995°C.<sup>16</sup> The maximum temperature reached was about 1300°C. The principal problems encountered in the operation of this apparatus were short life of the platinum resistance wire at the maximum temperature, embrittlement of the platinum support and crucible, and poor control of the cooling rate at high temperatures. The poor high-temperature performance of platinum in the apparatus is believed to be due to maintenance of an inert (argon) atmosphere within the apparatus and the consequent lack of a protective oxide film on the platinum at high temperatures. An inert atmosphere is considered desirable for work with CeF<sub>3</sub> and PuF<sub>3</sub> at high temperatures because both metals have higher valence states. A satisfactory solution

<sup>16</sup>M. A. Bredig, J. W. Johnson, and W. T. Smith, *J. Am. Chem. Soc.* **77**, 307 (1955).

to the materials problem has not been found thus far. The temperature control problem resulted from lack of insulating material around the platinum resistance furnace. A decrease in the voltage applied to this furnace caused an immediate drop in the temperature of the platinum wire and a consequent decrease in the temperature of the material heated by the furnace. This undesirable condition could be alleviated by careful manual manipulation of the variable transformer or by use of a controller activated by signals from a thermocouple placed quite close to the resistance wire.

In spite of the limitations mentioned above, thermal analysis data were obtained using the modified thermal analysis apparatus with NaF-CeF<sub>3</sub> mixtures containing 35 to 70 mole % CeF<sub>3</sub> at temperatures up to 1285°C, and the results are recorded in Table 1.3. Gradient quenching data provided by other workers in this Laboratory<sup>17</sup> were helpful in defining invariant equilibrium temperatures in this system and are included in Table 1.3. Thermal analysis data obtained earlier in this Laboratory<sup>18</sup> were considered sufficiently accurate to define the phase diagram in the region from 0 to 32.5 mole % CeF<sub>3</sub>, and the data are contained in Table 1.4. The proposed phase diagram is shown in Fig. 1.16. The eutectic between NaF and the compound NaF·CeF<sub>3</sub> contains

<sup>17</sup>H. A. Friedman, C. F. Weaver, and R. E. Thoma, personal communication.

<sup>18</sup>C. J. Borton and L. M. Bratcher, unpublished work performed in 1956.

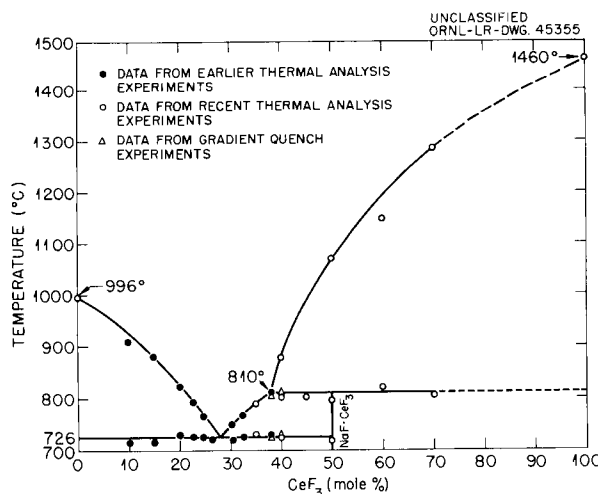


Fig. 1.16. The System NaF-CeF<sub>3</sub>.

28.0 ± 0.5 mole % CeF<sub>3</sub> and melts at 726 ± 5°C. The compound NaF·CeF<sub>3</sub> melts incongruently at 810 ± 5°C. Its identity was established by observation of essentially single-phase material in samples containing 50 mole % CeF<sub>3</sub> equilibrated and quenched at temperatures below 810°C. No evidence of a solid-phase inversion of this compound was observed. The thermal analysis data indicate that the peritectic composition contains approximately 38 mole % CeF<sub>3</sub>. The melting point of CeF<sub>3</sub> was obtained from the literature.<sup>19</sup> The low liquidus values obtained with the mixtures containing 10 and 60 mole % CeF<sub>3</sub> were probably due to undercooling. The thermal arrest at the eutectic temperature observed with the 50% CeF<sub>3</sub> mixture was undoubtedly due to incomplete reaction of liquid with solid CeF<sub>3</sub> at the peritectic temperature resulting from too rapid cooling of the mixture.

### Effect of Thermal Cycling on Molten-Salt Segregation

G. J. Nessel      J. Truitt

In the early stages of the engineering test program for the Molten-Salt Reactor a few instances of anomalous behavior of beryllium fluoride-containing mixtures, with regard to compositional stability, made it desirable to determine salt stability under drastic thermal cycling conditions.

During a building power failure, some pump-loop corrosion test units cooled to the extent of freezing the circulating salt in place. Attempts to restart these loops, by careful heating of the entire system, required temperatures of 100 to 300°F higher than the equilibrium liquidus temperature of the contained charge salt. At that time, it was assumed that cold spots, not monitored by thermocouples, existed somewhere in the system. In other instances, liquids which were transferred into engineering loops at a temperature of 1350°F were determined to contain a lower concentration of uranium than the nominal concentration of the over-all mixture.

In order to establish the conditions required to ensure the minimization of these effects, engineering tests were devised in which static samples in closed containers were repeatedly

<sup>19</sup>H. von Wartenberg, *Z. anorg. u. allgem. Chem.* **244**, 337 (1940).

Table 1.3. Recent Thermal Analysis Data and Gradient Quenching Data Obtained with NaF-CeF<sub>3</sub> Mixtures

Composition (mole % CeF <sub>3</sub> )	Liquidus Temperature (°C)			Peritectic Temperature (°C)			Solidus Temperature (°C)		
	Recorder	Potentiometer	Quenching Study	Recorder	Potentiometer	Quenching Study	Recorder	Potentiometer	Quenching Study
35	788UC	786					730H	726	
35	779H	782					723UC	723	
38	808UC	806	804 ± 3				730H	728	725 ± 2
40	876H	877		800H	800	810 ± 4	725H	726	728 ± 4
45				798UC	800				
50	1070H	1068		795UC	794		720CS	718	
60	1150H	1146		822UC	817				
60	1135UC	1130							
70	1285CS			803UC	803				

H = halt; UC = undercooled; CS = change of slope.

Table 1.4. Thermal Analysis Data from Earlier Unpublished Experiments with NaF-CeF<sub>3</sub> Mixtures

Composition (mole % CeF <sub>3</sub> )	Liquidus Temperature (°C)	Solidus Temperature (°C)
10	910	715
15	880	712UC
20	822	730
22.5	792	725
24.5	765	725
25	753	730
26.5		720
30.5	750	720
32.5	775	722

UC = undercooled.

frozen and melted. The three mixtures used in these tests were (1) LiF-BeF<sub>2</sub>-ThF<sub>4</sub> (71.0-16.0-13.0 mole %), liquidus temperature 932°F; (2) LiF-BeF<sub>2</sub>-UF<sub>4</sub> (62.0-37.0-1.0 mole %), liquidus temperature 824°F; and (3) LiF-BeF<sub>2</sub>-ThF<sub>4</sub>-UF<sub>4</sub> (62.0-36.5-1.0-0.5 mole %), liquidus temperature 824°F. Chemically analyzed samples of these mixtures were loaded in dry, inert atmospheres into 1/2-in.-OD nickel tubes, 18 in. long. Sufficient charge material was used to fill approximately 2/3 the volume

of the tubes. The tubes were then connected to a vacuum-helium system and placed in a vertical position in a tube furnace. After careful degassing by alternate vacuum and helium purge, the tubes were heated to predesignated temperatures, held at these temperatures for 30 min, and then cooled to 400°F. This cycle was repeated five times for each selected maximum temperature, and each salt was run in duplicate. The temperatures investigated were 850, 1200, and 1400°F.

At the conclusion of the experiments the salts were frozen in place and the tubes cut in 1-in. sections starting at the bottom. These sections were submitted for chemical analysis of the salt for uranium, beryllium, and thorium. From the analytical results it was evident that a definite phase separation had occurred, being most pronounced on those experiments at the 1200°F level. Similar tubes filled with these salts and held at 1200°F for periods of 25, 100, and 500 hr without thermal cycling showed no separation. The thermal-cycled tube sections showed definite increases in the uranium and/or thorium in the bottom sections with a corresponding decrease in lithium and beryllium. Examples of phase separation are given in Table 1.5.

The phase equilibrium diagrams of the fluoride systems enable one to identify the phases formed during cooling of these mixtures. By identification

Table 1.5. Effect of Thermal Cycling on Fused Salt Composition

Thermal cycle, 400 to 1200°F

Original salt batch analysis: Salt 1, U = 5.02%

Salt 2, Th = 46.5%

Salt 3, U = 2.97%, Th = 5.86%

Tube Section	Analysis of Salt for Fuel Constituents			
	Salt 1, Per Cent U	Salt 2, Per Cent Th	Salt 3	
			Per Cent U	Per Cent Th
1 (bottom)	7.16	50.5	4.15	9.02
2	5.45	49.5	2.77	6.58
5 (middle)	4.56	48.0	2.73	5.91
6	3.95	46.6	2.06	5.84
9	3.95	45.3	2.65	5.74
10 (top)	3.95	44.0	2.20	5.60

of phases which occur in cooled melts, one can deduce whether equilibrium was established or not. The first solids to form on cooling liquid mixtures of  $\text{LiF}\cdot\text{BeF}_2\text{-ThF}_4$ ,  $\text{LiF}\cdot\text{BeF}_2\text{-UF}_4$ , and  $\text{LiF}\cdot\text{BeF}_2\text{-ThF}_4\text{-UF}_4$  differ appreciably in density from the accompanying liquid phase, and can be expected to segregate from the liquid. It has been observed in phase equilibrium studies that variations in the rates of heating and cooling mixtures of  $\text{LiF}\cdot\text{BeF}_2\text{-ThF}_4$  and  $\text{LiF}\cdot\text{BeF}_2\text{-UF}_4$  can produce metastable phase combinations.<sup>20</sup> Such metastable phase combinations have been observed in the cooled samples from these tests. Therefore, the failure to achieve complete equilibrium on cooling and heating the materials tested here has obviously been the cause of the segregation of the uranium- and thorium-containing phases.

#### Dehydration of $\text{LiF}\cdot\text{BeF}_2\text{-UF}_4$ and $\text{LiF}\cdot\text{BeF}_2\text{-ThF}_4\text{-UF}_4$ Mixtures

A series of experiments has been completed for the purpose of developing a method for removing adsorbed water from  $\text{LiF}\cdot\text{BeF}_2\text{-UF}_4$  and  $\text{LiF}\cdot\text{BeF}_2\text{-ThF}_4\text{-UF}_4$  fuel mixtures during the course of reactor maintenance operations. The mixtures used were  $\text{LiF}\cdot\text{BeF}_2\text{-UF}_4$  (62-37-1 mole %) and  $\text{LiF}\cdot\text{BeF}_2\text{-ThF}_4\text{-UF}_4$  (62-36.5-1-0.5 mole %). Purified samples of these materials obtained from cooled melts were permitted to become nearly saturated with water by exposure to water-saturated air at room temperature, were then vacuum dried at 135°C and melted under vacuum. The cooled melts were 0.6 to 1.0% lower weight than the beginning materials, and contained appreciable amounts of  $\text{UO}_2$  as detected by petrographic analysis. These results indicate that hydrolysis of  $\text{UF}_4$  to  $\text{UO}_2$  in these crystallized fluoride mixtures occurs even at temperatures which are low relative to their liquidus temperatures, and that additional measures will need to be taken to protect exposed reactor fuels of  $\text{LiF}\cdot\text{BeF}_2\text{-UF}_4$  and  $\text{LiF}\cdot\text{BeF}_2\text{-ThF}_4\text{-UF}_4$  in reactor maintenance operations.

#### VOLATILITY PROCESS SOLVENTS

A knowledge of the system  $\text{LiF}\cdot\text{NaF}\cdot\text{ZrF}_4$  is important practically because mixtures of  $\text{LiF}$  and

$\text{LiF}\cdot\text{NaF}\cdot\text{ZrF}_4$  are now being used as solvents for Zircaloy in the volatility process for uranium recovery.<sup>21</sup> Studies of the phase equilibria in this system are nearly completed, and the results are summarized in the phase diagram shown in Fig. 1.17. A detailed understanding of the phase relationships in two areas in the system has been delayed because of the deliquescence of the compounds  $3\text{LiF}\cdot 4\text{ZrF}_4$  and  $3\text{NaF}\cdot 4\text{ZrF}_4$  and because of the inability to quench adequately preparations that involve the  $2\text{NaF}\cdot\text{ZrF}_4$  and  $5\text{NaF}\cdot 2\text{ZrF}_4$  solid solutions.

#### The System $\text{NaF}\cdot\text{FeF}_2\text{-ZrF}_4$

Few polycomponent salt systems of iron exist in which both low vapor pressures and 500 to 600°C liquidus surfaces occur with useful composition latitude. However, preliminary examination of the phase equilibria in the system  $\text{NaF}\cdot\text{FeF}_2\text{-ZrF}_4$  indicates that liquidus surfaces in the temperature range 500 to 600°C exist near the  $\text{NaF}\cdot\text{ZrF}_4$  binary system of compositions containing as much as 15 to 20 mole %  $\text{FeF}_2$ . The solubility of  $\text{FeF}_2$  in  $\text{NaF}\cdot\text{ZrF}_4$  solvents at temperatures between 500 and 600°C appears to be strongly composition dependent. The high melting temperatures of  $\text{FeF}_2$ ,  $\text{NaF}\cdot\text{FeF}_2$ , and of  $\text{NaF}\cdot\text{FeF}_2\cdot 2\text{ZrF}_4$  fields restrict the composition area having liquidus values below 600°C to a rather small region within a few mole per cent of the composition line between  $\text{NaF}\cdot\text{ZrF}_4$  (61-39 mole %) and  $\text{NaF}\cdot\text{FeF}_2\text{-ZrF}_4$  (45-25-30 mole %). Investigations of the phase equilibria in this system are continuing.

#### The System $\text{NaF}\cdot\text{BeF}_2\text{-ZrF}_4$

In the systems  $\text{LiF}\cdot\text{BeF}_2$  and  $\text{NaF}\cdot\text{BeF}_2$ , liquidus temperatures in the alkali-rich regions of the systems are low enough that ternary combinations of these materials with  $\text{ZrF}_4$  should afford large liquidus surfaces having temperatures below 500°C. Preliminary studies of the phase equilibria in the system  $\text{NaF}\cdot\text{BeF}_2\text{-ZrF}_4$  show that the composition  $\text{NaF}\cdot\text{BeF}_2$  (70.5-29.5 mole %) will form compositions with  $\text{ZrF}_4$  whose liquidus temperatures are generally lowered from 575°C to a minimum of 470°C at 30 mole %  $\text{ZrF}_4$  and rise to no higher than 500°C at 50 mole %  $\text{ZrF}_4$ . This sort of tie line has

<sup>20</sup>C. F. Weaver *et al.*, *Phase Equilibria in Molten Salt Breeder Reactor Fuels. I. The System  $\text{LiF}\cdot\text{BeF}_2\text{-UF}_4\text{-ThF}_4$* , ORNL-2896 (in preparation).

<sup>21</sup>G. I. Cathers *et al.*, *Proc. U.N. Intern. Conf. Peaceful Uses Atomic Energy 2nd, Geneva, 1958* 17, 473-79 (1958).

UNCLASSIFIED  
ORNL-LR-DWG 38115

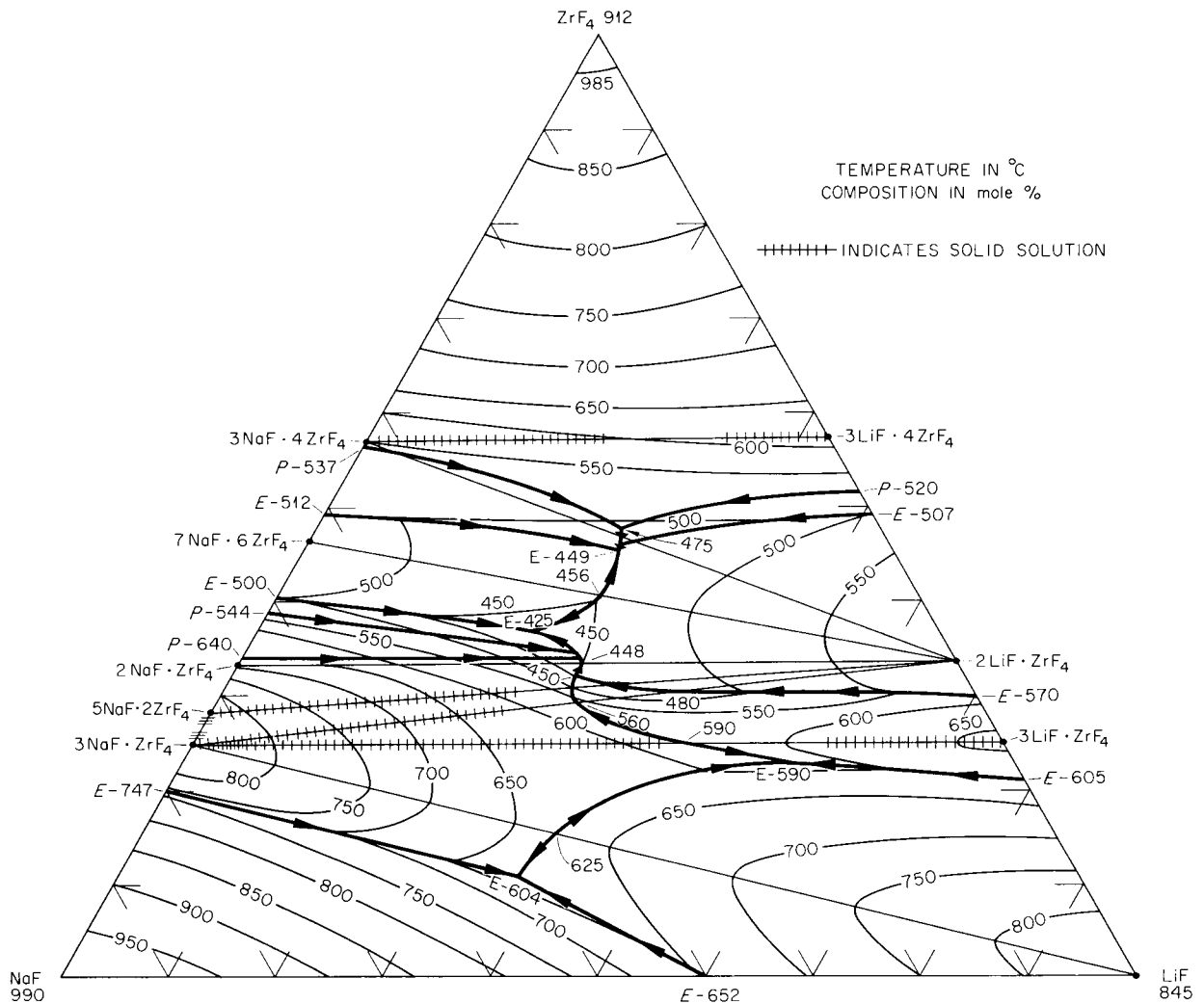


Fig. 1.17. The System LiF-NaF-ZrF<sub>4</sub>.

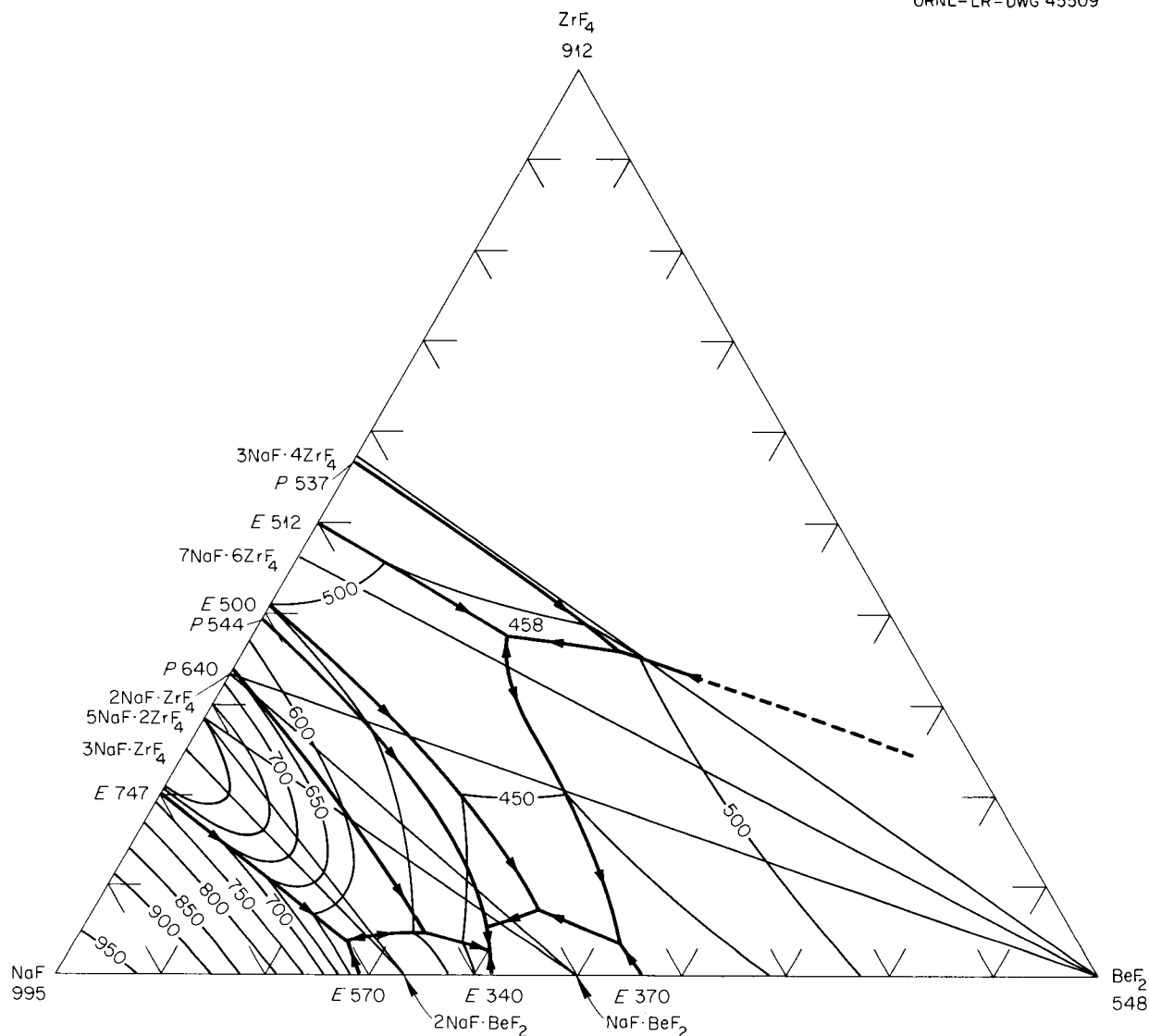
distinct advantages over those required in the use of the LiF-NaF eutectic as a solvent for ZrF<sub>4</sub> because use of this lower melting liquid tie line should effect a lower corrosion rate of the metal container vessel used in Zircaloy dissolution. A preliminary phase diagram of the system NaF-BeF<sub>2</sub>-ZrF<sub>4</sub> is shown in Fig. 1.18.

Investigations of the system LiF-BeF<sub>2</sub>-ZrF<sub>4</sub> are in an early stage and do not, as yet, permit estimates of the ZrF<sub>4</sub> solubilities in LiF-BeF<sub>2</sub>. It is expected that ZrF<sub>4</sub> solubility in this solvent will be comparable to that in NaF-BeF<sub>2</sub>.

### CRYSTAL PROPERTIES AND CRYSTAL STRUCTURE

#### Optical and X-Ray Data of New Fluoride Components

In the course of investigations in this Laboratory concerning the phase equilibria of fluoride salt systems the existence of many new compounds has been discovered. Within the last year the compositions, melting relationships, optical properties, and x-ray diffraction data have been established for 21 binary and ternary fluoride compounds.


 Fig. 1.18. The System NaF-BeF<sub>2</sub>-ZrF<sub>4</sub> (Preliminary Diagram).

The optical properties and the three most intense x-ray diffraction maxima of these compounds are given in Table 1.6.

#### Crystal Structures of 3:1 Compounds of the Alkali Fluorides with ZrF<sub>4</sub>, HfF<sub>4</sub>, ThF<sub>4</sub>, and UF<sub>4</sub>

Studies of the phase equilibria in the binary systems of alkali fluorides with ZrF<sub>4</sub>, HfF<sub>4</sub>, ThF<sub>4</sub>, and UF<sub>4</sub> have shown that the 3:1 compounds formed in these systems are generally cubic or tetragonal. Efforts to systematize the crystal and optical properties of these compounds are in

progress. Preliminary results of powder diffraction studies of these compounds are listed in Table 1.7 along with previously reported crystal data.

#### Some Properties of 7:6 Compounds

In the systems of alkali fluorides with ZrF<sub>4</sub>, HfF<sub>4</sub>, ThF<sub>4</sub>, and UF<sub>4</sub>, at least ten 7MF·6XF<sub>4</sub> compounds (where M is Li, Na, K, Rb, or Cs and X is Zr, Hf, Th, or U) are known to exist. Of these, eight are members of the rhombohedral (hexagonal)

Table 1.6. Optical and X-Ray Data on Some Fluoride Compounds

Compound	Optical Properties	X-Ray Lines	$I/I_1$
$\text{LiF} \cdot 4\text{ZrF}_4$	Uniaxial positive, $N_\omega = 1.582$ , $N_\epsilon = 1.588$	3.88, 1.92, 1.717	100, 90, 65
$\text{LiF} \cdot \text{YF}_3$	Uniaxial positive, $N_\omega = 1.454$ , $N_\epsilon = 1.472$	4.67, 3.025, 1.943	100, 100, 75
$\beta\text{-NaF} \cdot \text{ThF}_4$	Biaxial negative, $2V = 60^\circ$ , $N_\alpha = 1.500$ , $N_\gamma = 1.534$	6.11, 3.34, 3.24	70, 60, 100
$7\text{NaF} \cdot 6\text{ThF}_4$	Uniaxial negative, $N_\omega = 1.474$ , $N_\epsilon = 1.468$	4.39, 3.38, 3.26	100, 60, 65
$7\text{KF} \cdot 6\text{ThF}_4$	Uniaxial negative, $N_\omega = 1.474$ , $N_\epsilon = 1.470$	4.53, 3.48, 1.819	50, 100, 45
$7\text{RbF} \cdot 6\text{ThF}_4$	Uniaxial negative, $N_\omega = 1.486$ , $N_\epsilon = 1.482$	3.53, 3.071, 2.155	100, 55, 60
$3\text{CsF} \cdot \text{ZrF}_4$	Isotropic, $N = 1.471$	3.44, 1.985, 1.552	100, 30, 15
$3\text{RbF} \cdot \text{ThF}_4$	Isotropic, $N = 1.426$	3.37, 1.951, 1.509	100, 30, 15
$3\text{CsF} \cdot \text{UF}_4$	Isotropic, $N = 1.478$	3.53, 2.029, 1.56	100, 30, 10
$3\text{CsF} \cdot \text{ThF}_4$	Isotropic, $N = 1.464$	3.56, 2.049, 1.588	100, 30, 15
$2\text{CsF} \cdot \text{ThF}_4$	Biaxial, highly twinned, $N_\alpha = 1.500$ , $N_\gamma = 1.506$	6.32, 3.67, 2.112	30, 100, 60
$\text{CsF} \cdot \text{ThF}_4$	Biaxial negative, $2V = 20^\circ$ , $N_\alpha = 1.528$ , $N_\gamma = 1.544$	7.37, 3.67, 3.56	55, 100, 85
$2\text{CsF} \cdot 3\text{ThF}_4$	Biaxial positive, $2V = 15^\circ$ , $N_\alpha = 1.518$ , $N_\gamma = 1.526$	6.15, 3.70, 1.843	15, 100, 15
$\text{CsF} \cdot 2\text{ThF}_4$	Uniaxial negative, $N_\omega = 1.532$ , $N_\epsilon = 1.524$	3.86, 3.76, 1.840	45, 100, 45
$\text{CsF} \cdot 3\text{ThF}_4$	Biaxial positive, $2V = 35^\circ$ , $N_\alpha = 1.554$ , $N_\gamma = 1.558$	3.61, 3.48, 2.047	100, 90, 55
$\text{CsF} \cdot 6\text{ThF}_4$	Uniaxial negative, $N_\omega = 1.540$ , $N_\epsilon = 1.534$	4.23, 3.59, 2.087	100, 60, 50
$\text{LiF} \cdot \text{KF} \cdot \text{BeF}_2$	Biaxial, $2V = 15^\circ$ , $N \sim 1.321$ , birefringence very low	3.06, 2.421, 2.140	100, 100, 55
$\text{LiF} \cdot \text{KF} \cdot \text{ZrF}_4$	Uniaxial negative, polysynthetically twinned, $N_\omega = 1.403$ , $N_\epsilon = 1.407$	4.47, 3.79, 3.195	100, 40, 65
$\text{NaF} \cdot \text{BeF}_2 \cdot 3\text{ThF}_4$	Uniaxial positive, $N_\omega = 1.544$ , $N_\epsilon = 1.552$	4.19, 3.93, 2.092	100, 60, 45
$\text{NaF} \cdot \text{BeF}_2 \cdot 3\text{UF}_4$	Uniaxial positive, $N_\omega = 1.598$ , $N_\epsilon = 1.608$	4.12, 3.87, 2.056	100, 60, 30
$\delta\text{-NaF} \cdot \text{KF} \cdot \text{UF}_4$	Uniaxial negative, $N_\omega = 1.476$ , $N_\epsilon = 1.470$	7.79, 3.16, 2.220	100, 90, 50

crystal system and two are members of the tetragonal system. The radius ratio of the alkali ion/quadrivalent cation can serve as a criterion for predicting in which of the two crystal systems the 7:6 compound will occur, and whether the 7:6 compound will occur. However, no deductions concerning the relative equilibrium stability of these compounds appear possible at present. It is readily evident that while the ion radius ratio

$M^+/X^{4+}$  may serve as a criterion for these predictions, the factors involved in the formation of the compounds are not directly related, for similar cases involving these ratios are not found in either the chloride systems or in the  $U^{+++}$  systems.

The 7:6 compound occurs in all cases where the radius ratio  $M^+/X^{4+}$  lies between 0.99 and 1.65. At  $M^+/X^{4+}$  ratios larger than 1.65, no 7:6 compounds occur. According to the structure proposal

## REACTOR CHEMISTRY PROGRESS REPORT

 Table 1.7. Crystal Structures of 3:1 Compounds of the Alkali Fluorides with  $ZrF_4$ ,  $HfF_4$ ,  $UF_4$ , and  $ThF_4$ 

	Li	Na	K	Rb	Cs
Zr	<i>a</i>	Tetragonal, <sup>b</sup> $a_0 = 5.488$ , $c_0 = 10.917$	Cubic, <sup>c</sup> $a = 8.94$	Cubic, <sup>c</sup> $a = 9.30$	Cubic, <sup>c</sup> $a = 10.32$
Hf	<i>d</i>	Tetragonal, <sup>b</sup> $a_0 = 5.458$ , $c_0 = 10.917$	<i>d</i>	<i>d</i>	<i>d</i>
U	Tetragonal, <sup>e</sup> $a_0 = 6.12$ , $c_0 = 6.40$	Tetragonal <sup>f</sup> (alpha form), $a_0 = 5.448$ , $c_0 = 10.896$	Cubic <sup>f</sup> (alpha form), $a_0 = 9.21$ ; tetrago- nal <sup>f</sup> (beta form), $a_0 = 9.20$ , $c_0 = 18.40$	Cubic, <sup>g</sup> $a = 9.58$	Cubic, <sup>c</sup> $a = 10.62$
Th	Tetragonal, <sup>g</sup> $a_0 =$ $6.206$ , $c_0 = 6.470$	No compound occurs	Cubic, <sup>c</sup> $a = 9.91$	Cubic, <sup>c</sup> $a = 10.10$	Cubic, <sup>c</sup> $a = 10.65$

<sup>a</sup>Crystal system not determined.

<sup>b</sup>L. A. Harris, *Acta Cryst.* 12, 172 (1959).

<sup>c</sup>R. E. Thoma, unpublished work.

<sup>d</sup>Not investigated.

<sup>e</sup>L. A. Harris, G. D. White, and R. E. Thoma, *J. Phys. Chem.* 63, 1974 (1959).

<sup>f</sup>W. H. Zachariasen, *J. Am. Chem. Soc.* 70, 2147 (1948).

<sup>g</sup>L. A. Harris, unpublished work.

of Agron and Ellison<sup>22</sup> the 7:6 compound symmetry is described by the  $R_3-(C_{3i}^2)$  space group. These compounds contain six molecules per unit cell. They consider it significant that this space group, assigned to the compound previously described as  $NaUF_5$ , can accommodate an additional  $M^+$  cation into the vacant special position, (000), without changing the space group. The absence of 7:6 compounds in systems where  $M^+/X^{4+}$  is high appears, according to the above hypothesis, to be related to the absence of adequate space for the seventh alkali cation in the rhombohedral unit cell. Where this 7:6 compound exists at radius ratios below 0.99, the crystal system is tetragonal ( $I4_1/a$ ) rather than rhombohedral. Just below 0.99 ( $Li^+/Zr^{4+}$ ), neither the 7:6 nor 1:1 compound has been observed, a unique case in the group of systems. A list of the presently known  $MF_4 \cdot 6XF_4$  and  $7MF_4 \cdot 6XF_4$  compounds is shown in Table 1.8.

Each of the  $MF_4 \cdot XF_4$  compounds reported by Zachariasen<sup>23</sup> to be rhombohedral has been shown

to be  $7MF_4 \cdot 6XF_4$  at this Laboratory. If the generalization can be extended to include all 1:1 compounds reported as rhombohedral, the three compounds he reported as  $NaF \cdot PuF_4$ ,  $KF \cdot PuF_4$ , and  $RbF \cdot PuF_4$  are actually  $7NaF \cdot 6PuF_4$ ,  $7KF \cdot 6PuF_4$ , and  $7RbF \cdot 6PuF_4$ .

Americium tetrafluoride has been reported<sup>24</sup> to be monoclinic,  $a_0 = 12.49 \text{ \AA}$ ,  $b_0 = 10.47 \text{ \AA}$ ,  $c_0 = 8.20 \text{ \AA}$ ,  $\beta = 126 \pm 1^\circ$ . The same investigator<sup>24</sup> reported that  $KF \cdot AmF_4$  is rhombohedral,  $a_0 = 9.29 \text{ \AA}$ ,  $\alpha = 107.6^\circ$ . The close similarity of the crystal structures of these compounds with their  $UF_4$  analogs indicates that  $KF \cdot AmF_4$  is actually  $7KF \cdot 6AmF_4$ . These examples and the very nearly identical parameters of the unit cells of several known  $MF_4$  compounds of the actinides lead to the inference that 7:6 compounds will be routinely observed in the  $M^{4+}$  fluoride chemistry of the actinides.

<sup>23</sup>W. H. Zachariasen, *J. Am. Chem. Soc.* 70, 2147 (1948).

<sup>24</sup>L. B. Asprey, *J. Am. Chem. Soc.* 76, 2019 (1954).

<sup>22</sup>P. A. Agron and R. D. Ellison, *J. Phys. Chem.* 63, 2076 (1959).

Table 1.8. 7:6 and 1:1 Compounds of Alkali Fluorides with ZrF<sub>4</sub>, HfF<sub>4</sub>, UF<sub>4</sub>, and ThF<sub>4</sub>

U indicates that no compound of this formula was observed; S indicates that this is an equilibrium compound; M indicates metastable compound; T indicates tetragonal symmetry

	Li	Na	K	Rb	Cs	
Zr	0.88	1.27	1.72	1.92	2.16	M <sup>+</sup> /X <sup>4+</sup> **
	7:6U	7:6S	7:6U	7:6U	7:6U	
	1:1U	1:1M	1:1S	1:1S	1:1S	
Hf	0.87	1.13	1.70	1.90	2.14	M <sup>+</sup> /X <sup>4+</sup>
	**	7:6S	**	**	**	
	**	1:1S	**	**	**	
U	0.73	1.05	1.43	1.59	1.80	M <sup>+</sup> /X <sup>4+</sup>
	T7:6S	7:6S	7:6S	7:6S	7:6U	
	1:1U	1:1U	1:1U	1:1S	1:1S	
Th	0.69	0.99	1.24	1.50	1.69	M <sup>+</sup> /X <sup>4+</sup>
	T7:6S	7:6M	7:6S	7:6S	7:6U	
	1:1U	1:1S	1:1U	1:1U	1:1S	

\*Cation radius ratio M<sup>+</sup>/X<sup>4+</sup>.

\*\*Not investigated.

#### INVESTIGATION OF OTHER FUSED-SALT SYSTEMS

##### The System LiF-YF<sub>3</sub>

A phase diagram of the system LiF-YF<sub>3</sub>, derived at this Laboratory, differs substantially with that reported by Dergunov.<sup>25</sup> Results of ORNL phase studies have shown that the system contains the single binary compound LiF·YF<sub>3</sub> melting incongruently to YF<sub>3</sub> and liquid at 815°C, and two invariant points, the eutectic at 19 mole % YF<sub>3</sub> and at 695°C, and the peritectic at 49 mole % YF<sub>3</sub>. This eutectic occurs at about 50° lower temperature than that reported by Dergunov. No LiF·YF<sub>3</sub> compounds were observed by Dergunov. Crystal structure studies of the compound LiF·YF<sub>3</sub>, performed in conjunction with these phase studies, have shown that it is tetragonal,  $a_0 = 5.26 \pm 0.05 \text{ \AA}$ ,  $c_0 = 10.94 \pm 0.02 \text{ \AA}$ .<sup>26</sup> Optical Properties of LiF·YF<sub>3</sub> are given in Table 1.6. The phase diagram

of the system is shown in Fig. 1.19. A determination of the melting point of pure YF<sub>3</sub>, heretofore unreported, was made. This value is  $1412 \pm 5^\circ\text{C}$ .

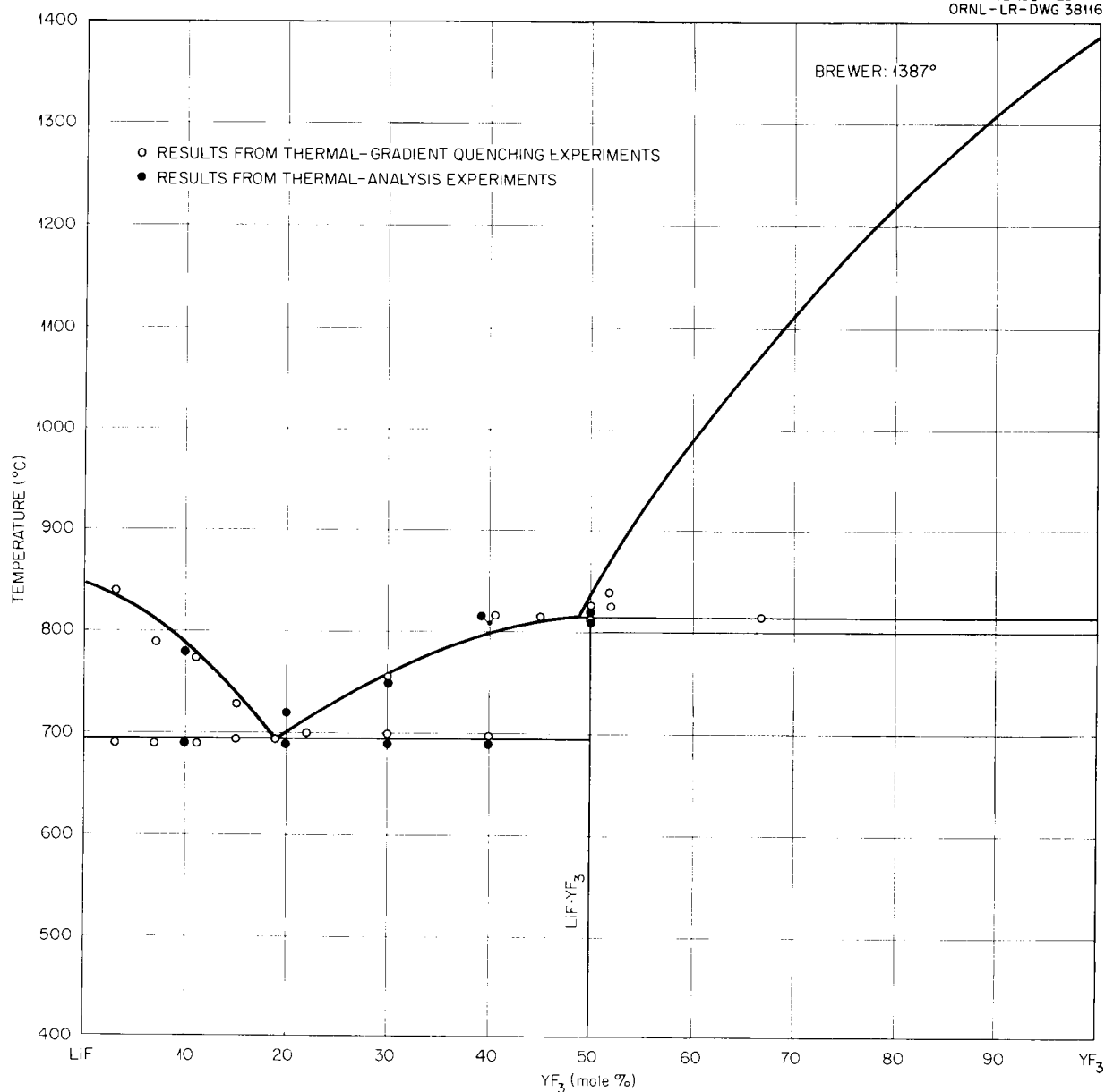
##### The System CsF-ThF<sub>4</sub>

Of the binary systems of the alkali fluorides LiF, NaF, KF, RbF, and CsF with ZrF<sub>4</sub>, ThF<sub>4</sub>, or UF<sub>4</sub>, only the system CsF-ThF<sub>4</sub> has not previously received sufficient attention to permit the construction of its phase diagram. Recent investigations at this Laboratory of CsF-ThF<sub>4</sub> phase equilibria<sup>27</sup> have shown that within the system three congruently melting compounds, 3CsF·ThF<sub>4</sub>, 2CsF·ThF<sub>4</sub>, and CsF·ThF<sub>4</sub>, and four incongruently melting compounds, 2CsF·3ThF<sub>4</sub>, CsF·2ThF<sub>4</sub>, CsF·3ThF<sub>4</sub>, and CsF·6ThF<sub>4</sub>, occur. The phase diagram of the system is shown in Fig. 1.20. Measurements of the crystal structure of the compound 3CsF·ThF<sub>4</sub> show that it has cubic symmetry (Table 1.7). Optical properties of the

<sup>25</sup>E. P. Dergunov, *Doklady Akad. Nauk S.S.S.R.* 60, 1185 (1948).

<sup>26</sup>*Met. Ann. Prog. Rep. Sept. 1, 1959*, ORNL-2839, p 288.

<sup>27</sup>This work was performed by T. S. Carlton, summer student participant, 1959.


 Fig. 1.19. The System LiF-YF<sub>3</sub>.

CsF-ThF<sub>4</sub> compounds are given in Table 1.6. As in all the other cases of alkali fluoride systems with ZrF<sub>4</sub>, ThF<sub>4</sub>, or UF<sub>4</sub>, where the cation radius ratio of the alkali ion to the quadrivalent ion is above 1.65, no 7:6 compound is formed.

#### The System LiF-UF<sub>3</sub>-UF<sub>4</sub>

Preliminary experiments in the system LiF-UF<sub>3</sub>-UF<sub>4</sub> have been made with the composition LiF-UF<sub>3</sub>-UF<sub>4</sub> (42-42-16 mole %) over the temperature

range 610 to 754°C. The liquidus temperature is 741 ± 2°C and the primary phase is UF<sub>3</sub>. At 668 ± 3°C an unidentified material appears as the secondary phase and UF<sub>3</sub> disappears. The secondary phase is uniaxial negative and brownish purple, of low birefringence with average refractive indices of 1.600. These optical properties do not correspond to the components nor to any of the compounds in the system LiF-UF<sub>4</sub>. If a solid solution of any of the LiF-UF<sub>4</sub> compounds with

$UF_3$  were involved an even boundary reaction would be expected. Consequently, it appears that

the unidentified phase is either a  $UF_3-UF_4$  or  $LiF-UF_3-UF_4$  compound.

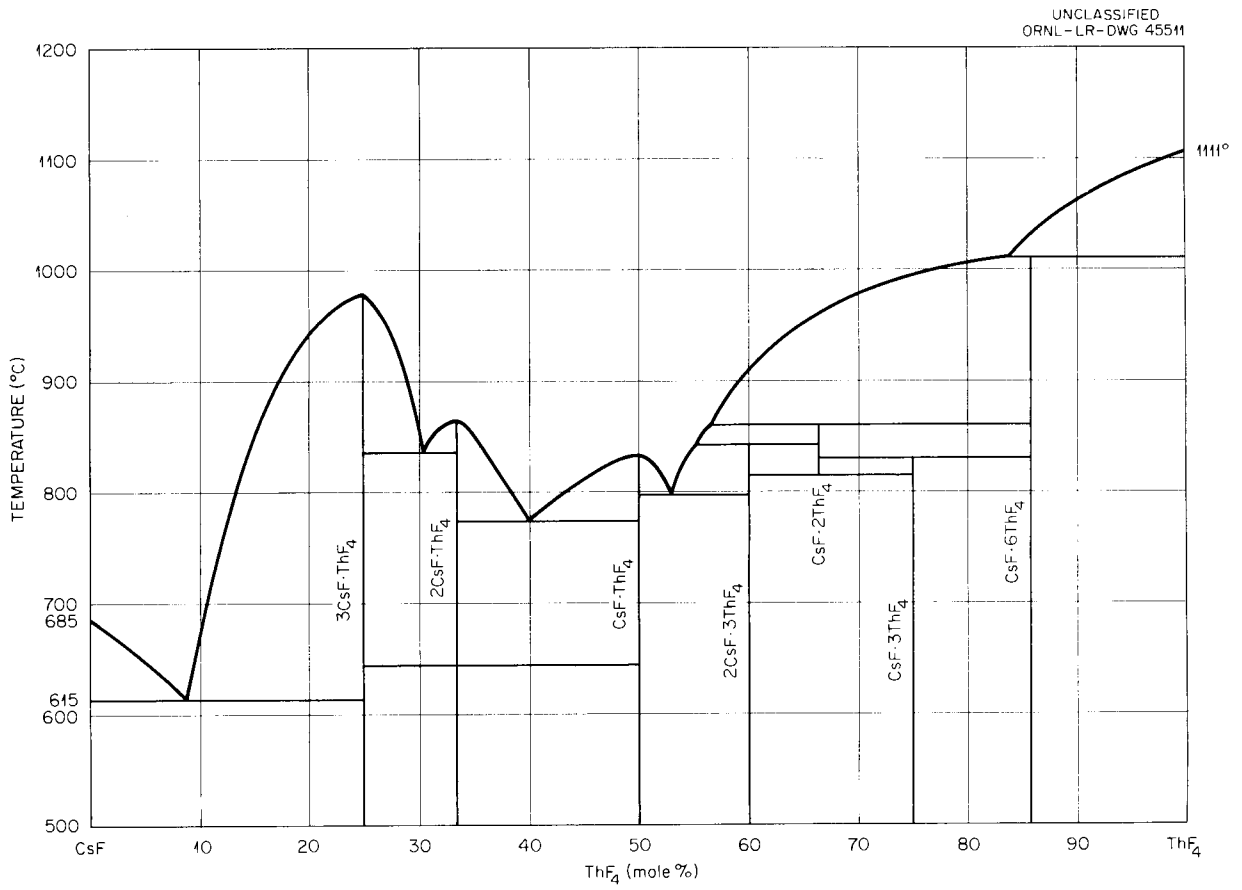


Fig. 1.20. The System CsF-ThF<sub>4</sub>.

## 2. GAS SOLUBILITIES IN MOLTEN SALTS

 SOLUBILITY OF NOBLE GASES IN  
 MOLTEN  $\text{LiF}\cdot\text{BeF}_2$ 

N. V. Smith      G. M. Watson  
 R. J. Sheil      R. B. Evans  
 W. R. Grimes

This investigation is one of a systematic series of experiments to determine the solubility of gases in molten salts. Contributions<sup>1,2</sup> resulting from the noble-gas studies include data for the  $\text{NaF}\cdot\text{ZrF}_4$  (53-47 mole %),  $\text{NaF}\cdot\text{ZrF}_4\cdot\text{UF}_4$  (50-46-4 mole %), and  $\text{LiF}\cdot\text{KF}\cdot\text{NaF}$  (ternary eutectic) mixtures. In addition, a description of the experimental techniques employed<sup>1</sup> and a relationship for predicting noble-gas solubilities in the above solvents<sup>2</sup> have been presented.

Recent extensions of this work covered solubility measurements in an  $\text{LiF}\cdot\text{BeF}_2$  (64-36 mole %) mixture. Comparisons between the measured values and those predicted by the relationship mentioned above have been made.

**Results.** – The solubility of helium, neon, argon, and xenon was isothermally determined at saturating pressures of 1.0, 1.5, and 2.0 atm. The temperature range covered was 500 to 800°C, with the exception of xenon. Experiments with xenon were performed at 600, 650, 700, and 800°C, due to the extremely low solubilities of xenon in the  $\text{LiF}\cdot\text{BeF}_2$  solvents. The solubility values presented could be duplicated within  $\pm 5\%$ .

Typical isothermal pressure dependence plots, which indicate that Henry's law is followed up to 2 atm, are presented in Fig. 2.1. The solubility is given as moles of gas per cubic centimeter of solvent. Conversions may be made to other units through the solvent density information available elsewhere.<sup>3</sup> The calculations discussed later did not require this conversion.

The Henry's law constants (obtained from pressure dependence data at various temperatures) were plotted on a semilogarithmic scale vs the reciprocal of the absolute temperature as shown

in Fig. 2.2. The enthalpy changes associated with the solution of the gas were obtained from slopes of the curves of Fig. 2.2. These plots constitute a summary of the entire series of noble-gas experiments in  $\text{LiF}\cdot\text{BeF}_2$  solvent.

**Discussion.** – The magnitudes of the solubility constants for the present solvent were essentially equal to those for the  $\text{LiF}\cdot\text{NaF}\cdot\text{KF}$  solvent and were approximately one-half to one-tenth of those for the  $\text{NaF}\cdot\text{ZrF}_4$  solvents. In general, previous findings remained unaltered. The solubilities followed Henry's law, increased with temperature, and decreased when gases with larger atomic radius (higher atomic weights) were studied. The enthalpies of solution of the heavier gases were higher than those of the lighter gases. In all cases, this function remained positive.

Predicted solubility constants, that is,

$$K_c = \frac{C_d}{C_g}$$

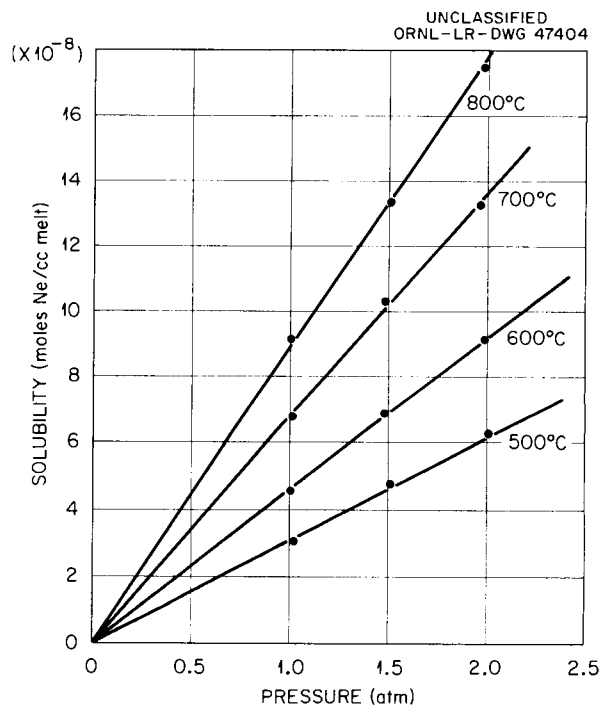


Fig. 2.1. Solubility of Neon in  $\text{LiF}\cdot\text{BeF}_2$  (64-36 mole %).

<sup>1</sup>W. R. Grimes, N. V. Smith, and G. M. Watson, *J. Phys. Chem.* **62**, 862 (1958).

<sup>2</sup>M. Blander *et al.*, *J. Phys. Chem.* **63**, 1164 (1959).

<sup>3</sup>S. I. Cohen, W. D. Powers, N. D. Greene, and H. F. Poppendiek, ORNL, personal communications.

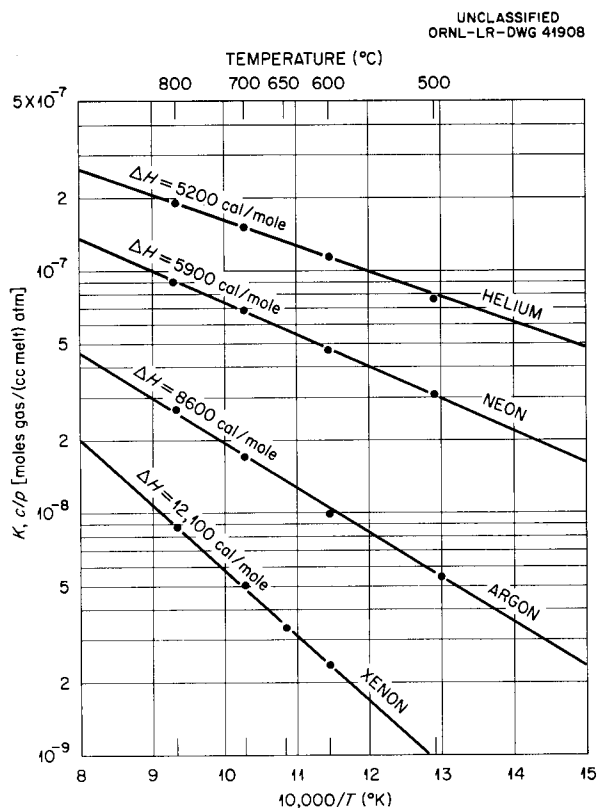


Fig. 2.2. Solubilities of Four Noble Gases as a Function of Temperature in LiF-BeF<sub>2</sub> (64-36 mole %).

were calculated by means of available surface-tension values,  $\gamma$  (dynes/cm), at applicable values of temperature,  $T$  (°K), and atomic radius,  $r$  (Å), through the relationship

$$\frac{C_d}{C_g} = e^{-18.08r^2\gamma/RT}, \quad (1)$$

the development of which is discussed<sup>2,4</sup> elsewhere. Comparisons of the predicted values and experimental values are given in Table 2.1. The magnitudes and trends indicated by the

$$\frac{K_c(\text{exp})}{K_c(\text{calc})}$$

ratios are very similar for all the solvents studied to date.

<sup>4</sup>H. H. Uhlig, *J. Phys. Chem.* **41**, 1215 (1937).

A new development, which merits some discussion, involves the magnitude of the standard entropy of solution for the various gases studied. Values of this and related functions are outlined in Table 2.2 for the solvents of interest. A review of the tabulated values will reveal that the entropy function may be of considerable importance in projected studies of BeF<sub>2</sub>-containing solvents. It should be pointed out that the effect under discussion would not be predicted by Eq. (1), since the equation was developed in terms of ideal-gas behavior. Further mention of the relatively high negative entropy value obtained will be made in the following section.

#### SOLUBILITY OF NOBLE GASES IN MOLTEN NaF-BeF<sub>2</sub>

W. T. Ward                      R. B. Evans  
G. M. Watson                  W. R. Grimes

A study of the solubilities of the noble gases in molten fluoride mixtures has been extended to include an NaF-BeF<sub>2</sub> (57-43 mole %) solvent. The method employed is the same as that described previously.<sup>5</sup> Solubilities of helium, argon, and xenon were determined at four temperatures at saturating pressures of 1.0, 1.5, and 2.0 atm. In all cases the solubility of the gas increased linearly with applied pressure of the gas and also increased with temperature. A plot of the solubility of argon as a function of saturating pressure in NaF-BeF<sub>2</sub> (57-43 mole %) is shown in Fig. 2.3 and is typical of the behavior of the noble gases in both of these solvents.

Plots of the logarithms of the Henry's law constants vs  $1/T$  are shown in Fig. 2.4.

Comparisons between predicted and experimental solubility constants cannot be made here, since surface-tension data for this solvent are not available. However, it was possible to obtain tentative values for the standard entropy change mentioned in the previous section. These values were -3.2, -3.1, and -2.3 e.u. for helium, argon, and xenon respectively. Based on the above values and similar values obtained for LiF-BeF<sub>2</sub>, an average value for the BeF<sub>2</sub>-containing solvents is -3.4 e.u., as compared with averages of -0.5 e.u. for the

<sup>5</sup>W. R. Grimes, N. V. Smith, and G. M. Watson, *J. Phys. Chem.* **62**, 862 (1958).

## REACTOR CHEMISTRY PROGRESS REPORT

 Table 2.1. Comparison of Calculated and Observed Values of Henry's Law Constants in LiF-BeF<sub>2</sub> (64-36 mole %)

Gas	Temperature (°C)	$K_c^*$		$K_c(\text{exp})$
		Experimental	Calculated	$K_c(\text{calc})$
He	500	$4.75 \times 10^{-3}$	$3.50 \times 10^{-2}$	0.136
	600	$8.27 \times 10^{-3}$	$5.92 \times 10^{-2}$	0.140
	700	$11.92 \times 10^{-3}$	$8.97 \times 10^{-2}$	0.133
	800	$17.15 \times 10^{-3}$	$12.58 \times 10^{-2}$	0.136
Ne	500	$1.96 \times 10^{-3}$	$5.54 \times 10^{-3}$	0.354
	600	$3.32 \times 10^{-3}$	$12.5 \times 10^{-3}$	0.266
	700	$5.43 \times 10^{-3}$	$23.8 \times 10^{-3}$	0.228
	800	$7.93 \times 10^{-3}$	$40.2 \times 10^{-3}$	0.197
Ar	500	$3.42 \times 10^{-4}$	$2.49 \times 10^{-4}$	1.38
	600	$7.02 \times 10^{-4}$	$9.10 \times 10^{-4}$	0.77
	700	$13.5 \times 10^{-4}$	$25.7 \times 10^{-4}$	0.53
	800	$23.4 \times 10^{-4}$	$58.8 \times 10^{-4}$	0.41
Xe	500	$0.58 \times 10^{-4}$	$0.23 \times 10^{-4}$	2.52
	600	$1.65 \times 10^{-4}$	$1.22 \times 10^{-4}$	1.35
	700	$4.07 \times 10^{-4}$	$4.62 \times 10^{-4}$	0.88
	800	$7.57 \times 10^{-4}$	$13.5 \times 10^{-4}$	0.56

$$*K_c = C_d / C_g.$$

Table 2.2. Enthalpy and Entropy Changes on Solution of Noble Gases in Molten Fluoride Mixtures at 1000°K

Solvent	Gas	$\Delta H^0$ (cal/mole)	$\Delta S^0$ (e.u.)	$T\Delta S$ , Ideal Gas Expansion (cal/mole)
LiF-BeF <sub>2</sub> (64-36 mole %)	He	5,200	-3.4	8,600
	Ne	5,900	-4.2	10,100
	Ar	8,600	-4.2	12,800
	Xe	12,100	-3.1	15,200
NaF-KF-LiF (11.5-42-46.5 mole %)	He	8,000	-0.3	8,300
	Ne	8,900	-1.0	9,900
	Ar	12,400	-0.1	12,500
NaF-ZrF <sub>4</sub> (53-47 mole %)	He	6,200	-1.0	7,200
	Ne	7,800	-0.4	8,200
	Ar	8,200	-1.5	9,700
	Xe	11,100	-0.1	11,200

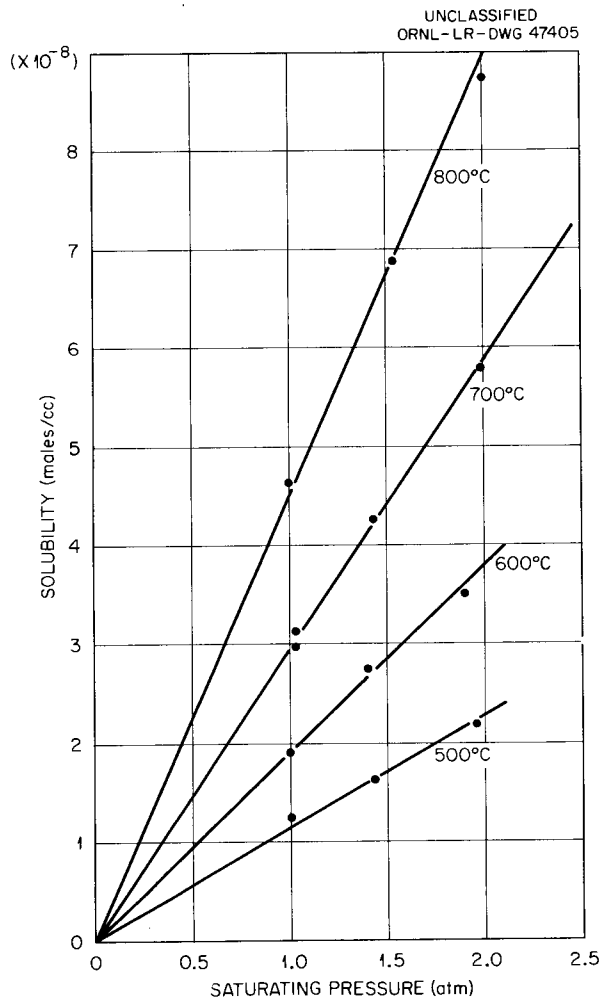


Fig. 2.3. Solubility of Argon in NaF-BeF<sub>2</sub> (57-43 mole %).

NaF-KF-LiF ternary eutectic solvent and -0.8 e.u. for the NaF-ZrF<sub>4</sub> (53-47 mole %) solvent. It is concluded that the presence of BeF<sub>2</sub> in the molten solvent has a marked effect on the environment of the dissolved gas atoms.

#### SOLUBILITY OF HF IN MOLTEN FLUORIDE MIXTURES

J. H. Shaffer      G. M. Watson

The use of HF in purifying molten fluoride mixtures for use as reactor fuels and in processing reactor fuel elements by dissolution in molten fluoride mixtures has prompted the systematic study of the solubility of HF in these mixtures. The results of determinations of the HF solubility

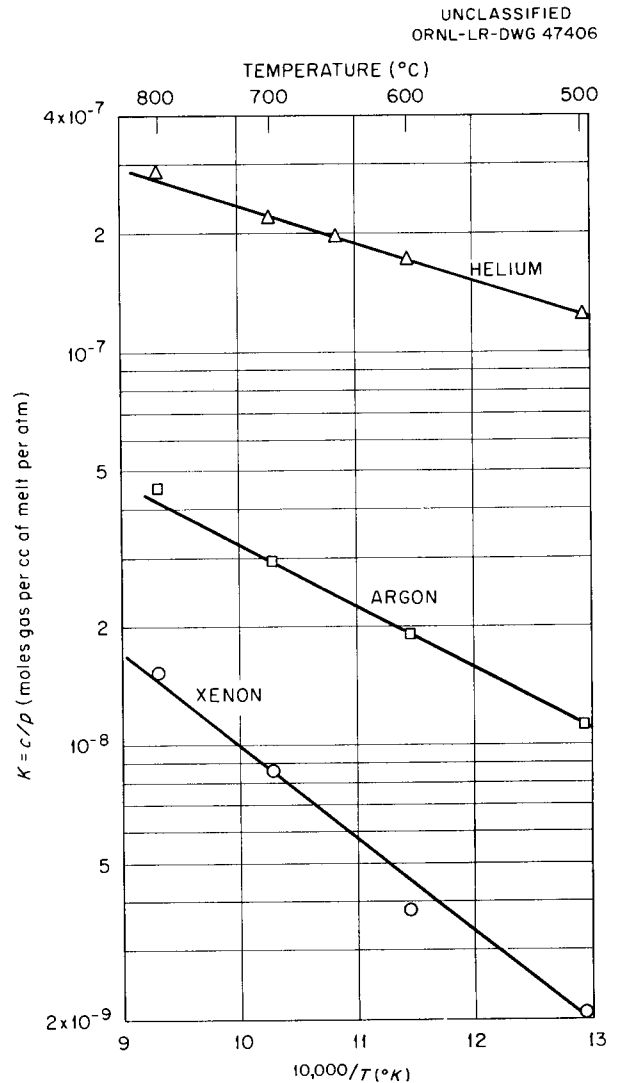


Fig. 2.4. Solubilities of Three Noble Gases as a Function of Temperature in NaF-BeF<sub>2</sub> (57-43 mole %).

in molten mixtures of NaF-ZrF<sub>4</sub> (ref 6) illustrate that this physical property might be useful to the understanding of the liquid state of molten fluoride systems. Accordingly, additional studies of the solubility of HF in mixtures of LiF-BeF<sub>2</sub> and NaF-BeF<sub>2</sub> have been made.

The experimental procedure for determining the solubility of HF in molten fluorides has been described<sup>7</sup> for measurements in the NaF-ZrF<sub>4</sub>

<sup>6</sup>J. H. Shaffer and G. M. Watson, *Chem. Ann. Prog. Rep.* June 20, 1958, ORNL-2584, p 81.

<sup>7</sup>J. H. Shaffer, W. R. Grimes, and G. M. Watson, *J. Phys. Chem.* 63, 1999 (1959).

system. This method consists in saturating the melt with HF at constant temperature and pressure, transporting a measured portion of the saturated liquid phase to an isolated section of the apparatus, and stripping the dissolved HF from the melt by helium-sparging. The evolved HF is measured by absorption in a standard solution of aqueous KOH.

Within the precision of the measurements, the solubility of HF follows Henry's law over the pressure range studied. As reported for measurements in NaF-ZrF<sub>4</sub> mixtures, the solubility of HF in the LiF-BeF<sub>2</sub> and NaF-BeF<sub>2</sub> systems increases as the saturating pressure is increased and decreases as the temperature is increased. The experimental measurements expressed as a Henry's law constant at a given temperature and melt composition were found to agree within  $\pm 5\%$ . These results are summarized in Table 2.3.

Table 2.3. Henry's Law Constants for the Solubility of HF in Mixtures of LiF-BeF<sub>2</sub> and NaF-BeF<sub>2</sub>

Melt Composition (mole % alkali fluoride)	K (moles HF per cc of melt per atm)		
	At 600°C	At 700°C	At 800°C
LiF-BeF <sub>2</sub>			
54	9.4	7.3	5.6
59	10.9	7.8	6.0
69	13.7	9.8	7.0
80	16.3*	11.7	8.8
89	17.3*	13.0*	10.3*
NaF-BeF <sub>2</sub>			
49	18.8	13.1	10.0
58	26.7	18.0	13.9
66	49.2	31.2	21.8
70	107.1	55.2	34.3
75	179.0*	93.0*	55.1

\*Extrapolated from results at higher temperatures.

A comparison of the Henry's law constants obtained for the LiF-BeF<sub>2</sub> system with those obtained for the NaF-BeF<sub>2</sub> system is shown as a function of concentration of alkali-metal fluoride at 700°C in Fig. 2.5. The weaker composition dependence

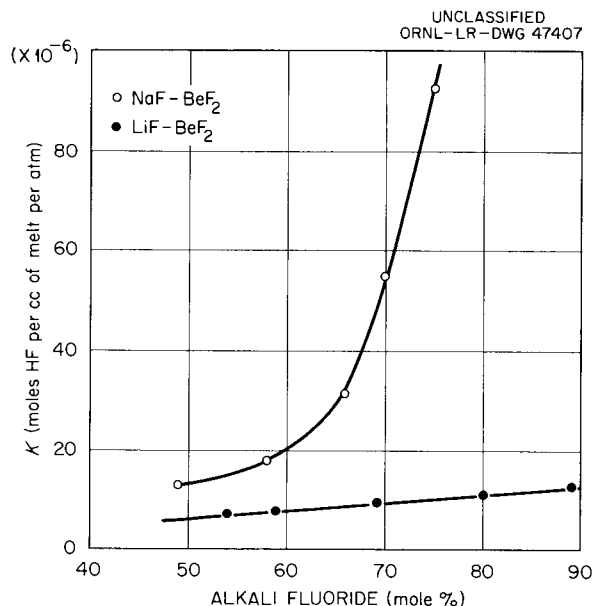


Fig. 2.5. Composition Dependence of Henry's Law Constants for the Solubility of HF in Mixtures of LiF-BeF<sub>2</sub> and NaF-BeF<sub>2</sub> at 700°C.

obtained for the LiF-BeF<sub>2</sub> system may be a result of much less stable acid fluorides being formed with LiF than with NaF (ref 8).

The temperature dependence of the Henry's law constants for the solubility of HF in the LiF-BeF<sub>2</sub> and NaF-BeF<sub>2</sub> systems indicates a constant heat of solution for each melt composition over the temperature range studied. Values for the heats of solution as well as the entropies of solution calculated at 1000°K are listed in Table 2.4. A comparison of these thermodynamic properties suggests a variation in solvent behavior in mixtures of high alkali fluoride concentrations.

Experiments are in progress to determine the solubility of HF in the system LiF-ZrF<sub>4</sub> and will be continued with other molten fluoride systems.

#### AN EMPIRICAL CORRELATION FOR THE SOLUBILITY OF HF IN MIXTURES OF NaF-BeF<sub>2</sub> AND NaF-ZrF<sub>4</sub>

J. H. Shaffer

The experimental results of measurements of the solubility of HF in various molten mixtures of the

<sup>8</sup>H. J. Emeleus, *Fluorine Chemistry*, vol 1, p 25 (ed. by J. H. Simons), Academic Press, New York, 1950.

**Table 2.4. Enthalpies and Entropies of Solution of HF in LiF-BeF<sub>2</sub> and NaF-BeF<sub>2</sub> Mixtures**

Solvent Composition (mole % alkali fluoride)	$\Delta H$ (kcal/mole)	$\Delta S_c^*$ (e.u.)	$\Delta S_p^{**}$ (e.u.)
<b>LiF-BeF<sub>2</sub></b>			
54	-5.0	-10.8	-14.9
59	-5.6	-11.2	-15.4
69	-6.4	-11.6	-15.8
80	-5.7	-10.5	-14.7
89	-4.9	-9.4	-11.3
<b>NaF-BeF<sub>2</sub></b>			
49	-5.3	-5.3	-14.1
58	-5.5	-4.8	-13.6
66	-6.8	-5.2	-13.9
70	-9.6	-6.8	-15.6
75	-10.1	-6.4	-15.1

\*Entropies of solution calculated for equal concentrations of HF in gas and dissolved phases at 1000°K.

\*\*Entropies of solution calculated for equal pressures of HF in gas and dissolved phases at 1000°K.

NaF-BeF<sub>2</sub> and the NaF-ZrF<sub>4</sub> systems have been reported.<sup>9,10</sup> By adopting a simple model for expressing the melt composition of these fluoride systems, the HF solubility can be described mathematically by an equation of the form

$$S = \exp [f(\text{temp, conc})] \quad (1)$$

If it is assumed that beryllium and zirconium are coordinated with four and seven fluoride ions respectively in the liquid states,<sup>11</sup> then the effective free-fluoride concentration in the systems NaF-BeF<sub>2</sub> and NaF-ZrF<sub>4</sub> would be based on the compounds Na<sub>2</sub>BeF<sub>4</sub> and Na<sub>3</sub>ZrF<sub>7</sub>. For mixtures of NaF with BeF<sub>2</sub> or ZrF<sub>4</sub> below these reference compounds, the free-fluoride concentration may be expressed as a deficiency in NaF and may be assigned, by convention, negative concentration

<sup>9</sup>J. H. Shaffer, W. R. Grimes, and G. M. Watson, *J. Phys. Chem.* **63**, 1999 (1959).

<sup>10</sup>"Solubility of HF in Molten Fluoride Mixtures," this report.

<sup>11</sup>Suggested by F. F. Blankenship.

terms. Similarly, the NaF concentration above the reference compounds may be expressed as excess NaF. The relation of the melt composition expressed as free fluoride to the conventional mole fraction is shown in Fig. 2.6. If the HF solubility in the NaF-BeF<sub>2</sub> and NaF-ZrF<sub>4</sub> systems is related

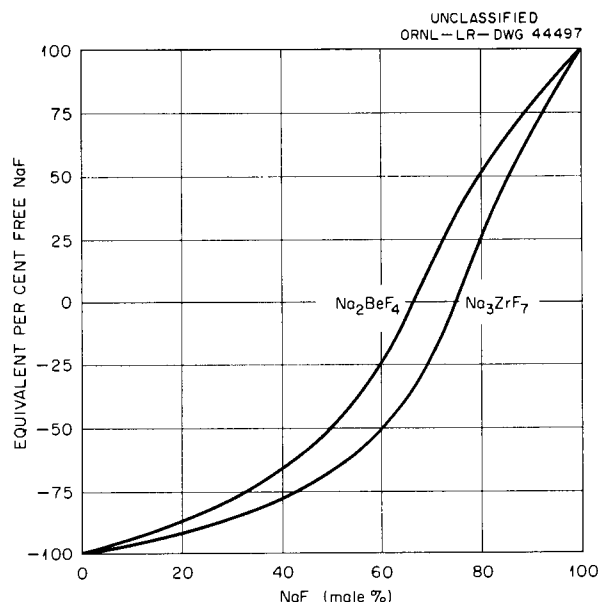


**Fig. 2.6. Correlation of Free NaF with Mole Fraction of NaF in Mixtures of NaF-BeF<sub>2</sub> and NaF-ZrF<sub>4</sub> (Based on Na<sub>2</sub>BeF<sub>4</sub> and Na<sub>3</sub>ZrF<sub>7</sub>).**

to the effective free-fluoride concentration as shown in Figs. 2.7-2.9, the same correlation of the HF solubility in both molten fluoride systems is obtained. Within the error of experimental measurements, an exponential correlation of the Henry's law constants for the HF solubility with effective free-fluoride concentration can be obtained as illustrated by Fig. 2.10. By evaluation of temperature and concentration dependencies, the Henry's law constants for the solubility of HF in the two molten fluoride systems described in this report can be obtained from the equation

$$K = \exp \left( \frac{8400 + 3263RC}{RT} - \frac{15.24 + 0.909RC}{R} \right) \quad (2)$$

where

$K$  = Henry's law constant in moles of HF per liter of melt per atm,

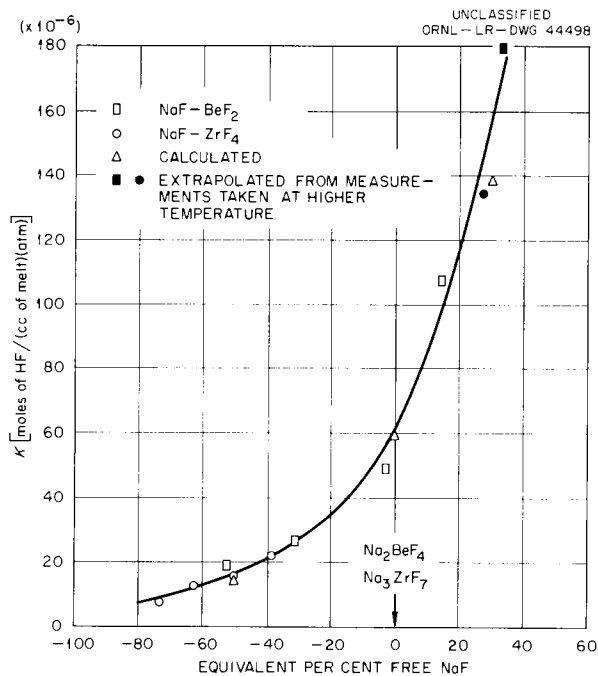


Fig. 2.7. Composition Dependence of Henry's Law Constants for the Solubility of HF in NaF-BeF<sub>2</sub> and NaF-ZrF<sub>4</sub> Mixtures at 600°C.

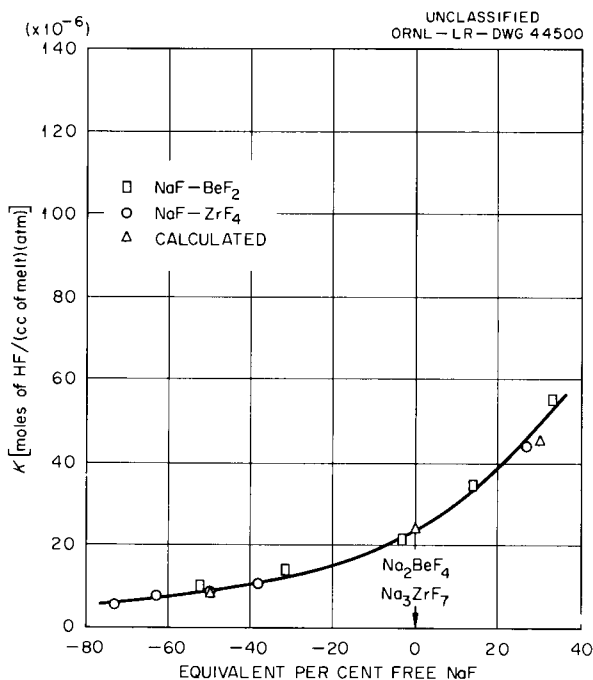


Fig. 2.9. Composition Dependence of Henry's Law Constants for the Solubility of HF in NaF-BeF<sub>2</sub> and NaF-ZrF<sub>4</sub> Mixtures at 800°C.

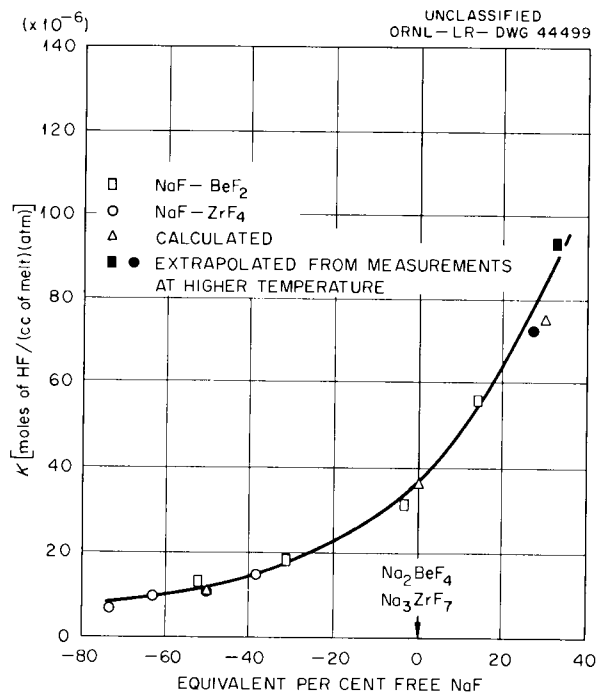


Fig. 2.8. Composition Dependence of Henry's Law Constants for the Solubility of HF in NaF-BeF<sub>2</sub> and NaF-ZrF<sub>4</sub> Mixtures at 700°C.

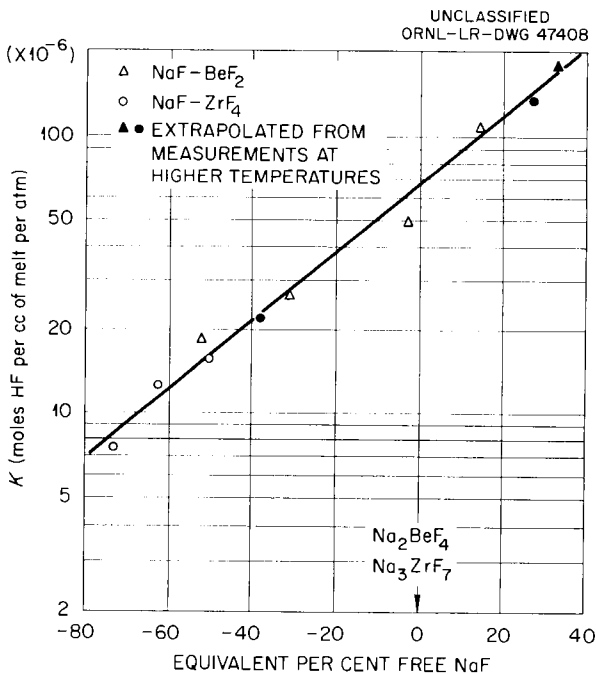


Fig. 2.10. Composition Dependence of Henry's Law Constants for the Solubility of HF in NaF-BeF<sub>2</sub> and NaF-ZrF<sub>4</sub> Mixtures at 600°C.

$C$  = concentration of effective free fluoride,

$T$  = temperature in  $^{\circ}\text{K}$ ,

$R$  = gas constant.

Calculated values from Eq. (2), denoted in Figs. 2.7–2.9, are within the experimental precision of laboratory measurements of the HF solubility.

While the melt concentration for expressing the effective free fluoride is arbitrary, it is of interest to note that a relation to a more conventional concentration concept can be obtained. If, for example, the system NaF-BeF<sub>2</sub> is considered to be composed of the systems BeF<sub>2</sub>-Na<sub>2</sub>BeF<sub>4</sub> and Na<sub>2</sub>BeF<sub>4</sub>-NaF, the postulated free-fluoride model corresponds to mole per cent BeF<sub>2</sub> in the former system and equivalent per cent NaF in the latter system. The NaF-ZrF<sub>4</sub> system also provides a corresponding correlation. The choice of the arbitrary concentration expression makes it possible to mathematically describe the HF solubility in the systems NaF-BeF<sub>2</sub> and NaF-ZrF<sub>4</sub> as a continuous concentration function. As data for the HF solubility in other fluoride systems become available, perhaps a better understanding of the liquid-fluoride state can be realized.

#### SOLUBILITY OF CO<sub>2</sub> IN MOLTEN NaF-BeF<sub>2</sub>

N. V. Smith  
R. J. Sheil

R. B. Evans  
G. M. Watson

A primary objective of the molten-salt-gas solubility program has been the elucidation of solvent properties which have an effect on gas solubilities. An indirect approach would be to investigate gases other than HF and the noble gases. Interesting speculations<sup>12</sup> have been made for dissolved non-reacting nonspherical molecules, in that these gases might increase the surface area of the "holes" in which the dissolved gases reside. Obvious candidates for study would be the permanent gases, such as hydrogen and nitrogen. These gases would be most suitable, since they are diatomic and would possess positive enthalpies of solution.

Several attempts to measure the solubility of nitrogen and hydrogen in molten salts failed. Analytical difficulties were encountered with nitrogen; dependable and consistent "blank" values

could not be obtained in the strip gas. Hydrogen could not be held in the nickel-based containers because of the high diffusion rates of hydrogen into and through the container walls. Other container materials such as quartz and aluminum lacked the structural strength required for the necessary molten-salt transfer. In lieu of hydrogen and nitrogen experiments, a decision was made to determine the solubility of CO<sub>2</sub> in an NaF-BeF<sub>2</sub> (57-43 mole %) solvent.

**Results.** – The results of CO<sub>2</sub> solubility studies are summarized in Fig. 2.11. The curve shown indicates that the Henry's law constant falls between those of helium and argon at 800°C, also that the slope of the curve becomes less negative (enthalpy of solution becomes less positive) until a minimum is reached at approximately 600°C. At this point the slope of the curve increases until the 415°C solubility constant is greater than the extrapolated value for helium. Thus CO<sub>2</sub> exhibits noble-gas behavior at temperatures greater than 600°C; at temperatures below this value, CO<sub>2</sub> solubilities simulate HF behavior. It should be mentioned that Henry's law was followed, within the experimental precision ( $\pm 5\%$ ), at 500, 600, and

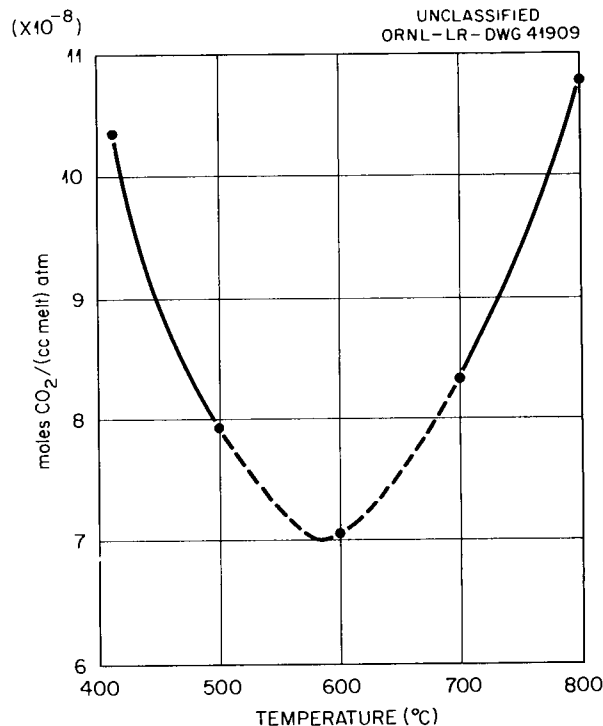


Fig. 2.11. Solubility of CO<sub>2</sub> in NaF-BeF<sub>2</sub> (57-43 mole %).

<sup>12</sup>M. Blander *et al.*, *J. Phys. Chem.* 63, 1164 (1959).

UNCLASSIFIED  
ORNL-LR-DWG 35088AR

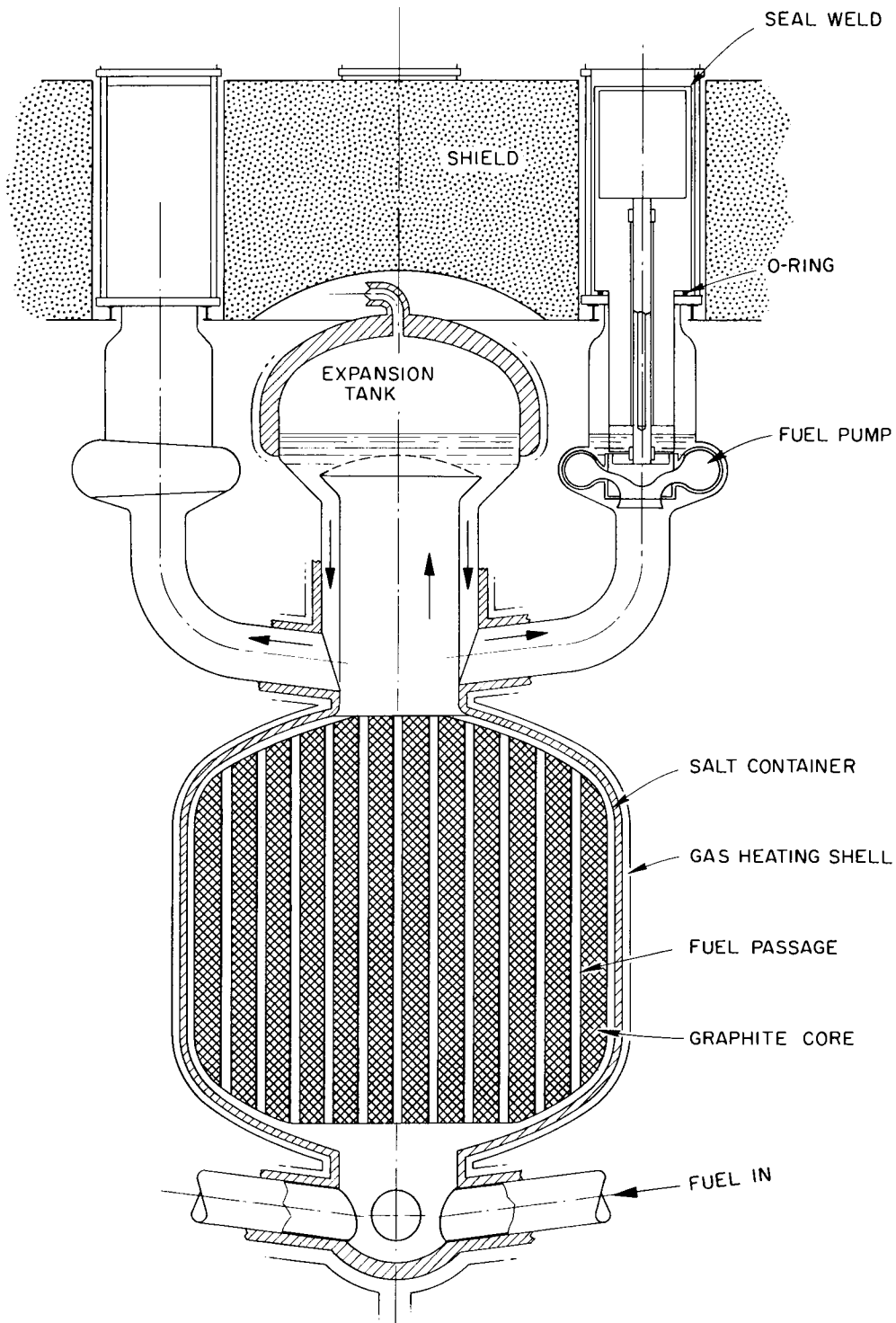


Fig. 2.12. MSR Core Conceptual Design with Expansion Tank for Xenon Decay.

700°C. At 800 and 416°C, and zero saturating pressure, an extrapolated residual of  $2 \times 10^{-8}$  mole/cc was noted. This might well be experimental error.

### XENON POISONING CONTROL IN FUSED-SALT REACTORS<sup>13</sup>

G. M. Watson

The extremely low solubility of xenon in molten fluorides led to a proposed design<sup>14</sup> in which a sufficiently large gas space is provided to permit Xe<sup>135</sup> to decay outside the core, as shown in Fig. 2.12. Xenon solubility data show that the concentration ratio for xenon in a gas phase in equilibrium with xenon in solution in molten fluorides is about 6000 at 600°C. A gas expansion tank roughly half the volume of the fuel could presumably reduce the ratio of xenon in the fuel to xenon in the tank to about 1/3000. Such a simple processing scheme, if workable, is indeed attractive.

With the present concept of breeder reactors in which the fuel is in contact with an unclad-graphite core tank, complications may arise from xenon diffusing into the graphite pores. Even "impervious-grade" graphite has a certain fraction of its volume consisting of interconnected pores which gas can penetrate. These pores could serve as receptacles for xenon gas and cause an increase in xenon poisoning. The concentration of xenon in the graphite is limited by burnup and by the diffusion rate of xenon into the graphite. The problem can be analyzed by regarding a certain volume fraction of the graphite as a gas phase adjacent to the fuel channels in equilibrium with the gas in the fuel. The xenon profile in a typical lattice cell was calculated from the diffusion coefficient and the flux, and, from this, the ratio of neutron captures where diffusion controls to the corresponding number of captures where xenon diffuses, instantaneously. This ratio is shown in Fig. 2.13. It should be noted that the mechanism of interest here is diffusion through the free

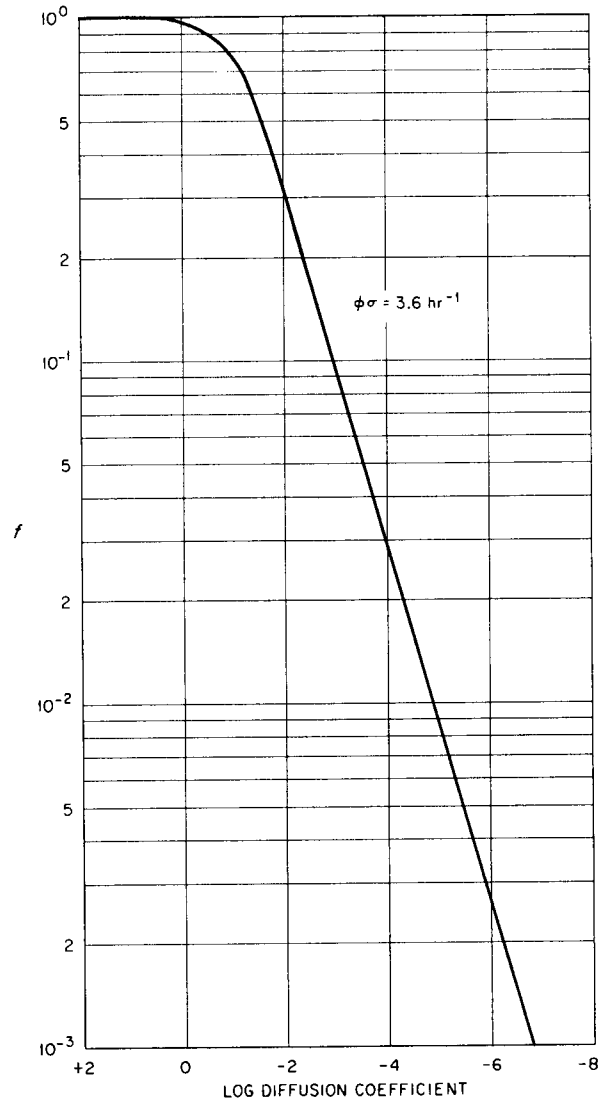


Fig. 2.13. Ratio,  $f$ , of Neutron Capture by Xenon in Graphite if Diffusion Controls to Captures if Xenon Diffusion Is Instantaneous.

graphite pores and not through the solid graphite lattice. Diffusion coefficients for the case of interest are probably in the range of  $10^{-4}$  to  $10^{-6}$  cm<sup>2</sup>/sec or possibly lower.<sup>15</sup>

By use of the data of Fig. 2.13, the xenon poison fraction was calculated as a function of diffusion

<sup>13</sup>Joint project with Chemical Technology Division; see W. D. Burch, G. M. Watson, and H. O. Weeren, *Xenon Control in Fluid Fueled Reactors*, ORNL CF-60-2-2 (to be published).

<sup>14</sup>H. G. MacPherson et al., *A Preliminary Study of a Graphite Moderated Molten Salt Power Reactor*, ORNL CF-59-1-26 (Jan. 13, 1959).

<sup>15</sup>GCR Quar. Prog. Rep. Dec. 31, 1959, ORNL-2888, p 158.

REACTOR CHEMISTRY PROGRESS REPORT

coefficient for a reactor with the following characteristics:

Power	500 Mw (thermal)
Power density	230 kw/liter
Fuel total volume	137 ft <sup>3</sup>
Average flux	$2.5 \times 10^{14}$ neutrons·cm <sup>-2</sup> ·sec <sup>-1</sup>
Total core volume	480 ft <sup>3</sup>

Fuel volume in core	77 ft <sup>3</sup>
Porosity of graphite	20%
Expansion tank volume	80 ft <sup>3</sup>

The results are plotted in Fig. 2.14.

The alternate scheme of continuous gas phase removal was also investigated. The significant feature shown is that gas phase removal is effective even if xenon diffusion rates are quite high. This is shown in Fig. 2.15, calculated for the same reactor with an expansion tank of 35 ft<sup>3</sup> rather than the 80 ft<sup>3</sup> assumed in the case of no gas removal.

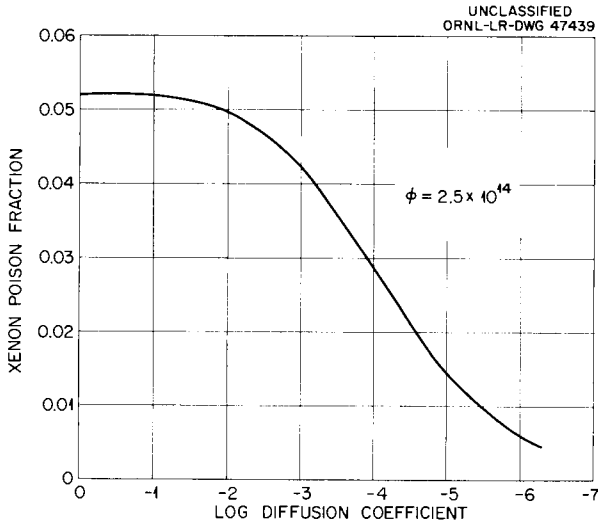


Fig. 2.14. Xenon Poison Fraction as a Function of Xenon Diffusion Coefficient in Graphite (No Gas Removal).

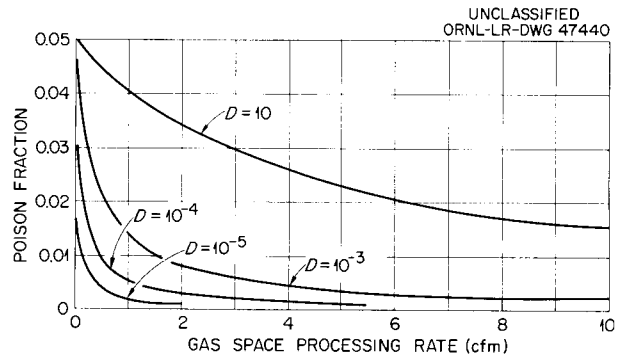


Fig. 2.15. Xenon Poisoning as a Function of Gas Processing Rate and Diffusion Coefficient of Xenon in Graphite.

## 3. THERMODYNAMIC STUDIES IN MOLTEN-SALT SYSTEMS

THERMODYNAMIC BEHAVIOR OF  
STRUCTURAL-METAL CORROSION PRODUCTS  
IN FLUORIDE MELTS

C. M. Blood                      G. M. Watson  
F. F. Blankenship              W. R. Grimes

Due to the influence of solvent composition on chemical activities, particularly on the change of activity coefficients with temperature, marked differences are found in the corrosivity of various fluoride melts toward structural metals, even when the oxidation-reduction reaction responsible for the corrosion is nominally the same. In addition, the successful exploitation of many processes to recover or regenerate reactor fuels and breeder blankets is strongly dependent on a knowledge of chemical activities of solutes in molten salts.

To supply activity coefficients pertaining to the molten fluoride corrosion of structural metals,  $M^0$ , measurements on the heterogeneous equilibrium

$$K = \frac{a_{M^0} P_{HF}^2}{a_{MF_2} P_{H_2}}$$

applying to the reduction of dissolved  $NiF_2$ ,  $FeF_2$ , or  $CrF_2$  by  $H_2$  have been carried out in a variety of fluoride fuel solvents since 1952.

Initially, it was hoped that equilibrium gas concentrations could be found by analyzing the HF content of  $H_2$  which had been bubbled through a melt containing, for example, a known concentration of  $NiF_2$ , and extrapolating to zero flow rate. Unfortunately, the lowest feasible flow rates did not provide a suitable basis for extrapolation, and it was necessary to resort to matching influent and effluent gas compositions, a very delicate and time-consuming operation. For example, with an influent gas presumed to be slightly oxidizing, gas flow was continued for three or four days, with careful adjustment and monitoring of influent and effluent gas, by which time apparent equilibrium might be reached as indicated by the effluent gas composition. Then three or four more days were required to ensure that the apparent equilibrium was not transient; meanwhile, samples of the melt for analysis are removed at least daily by means of a filter stick.

And then the process was repeated, approaching equilibrium with a slightly reducing influent gas. Thus, a minimum of two weeks of operation was required to establish a single value for the equilibrium quotient at a given concentration and temperature. Details of the apparatus and procedure have been presented previously.<sup>1</sup> The melts were contained in the metal whose reduction was under study, so that the activity of the solid phase,  $a_{M^0}$ , was always unity.

A summary of the equilibrium quotient experiments made so far, with the temperature and concentration ranges indicated, is presented in Fig. 3.1. Calculated equilibrium constants, assuming ideal behavior and based on thermodynamic data from the literature,<sup>2</sup> are included in Fig. 3.1 for comparison; the reference state for  $MF_2$  is supercooled liquid. The results for  $NiF_2$  and  $FeF_2$  in  $NaF-ZrF_4$  (53-47 mole %) have been presented previously,<sup>1</sup> and measurements on  $FeF_2$  and  $CrF_2$  in  $LiF-BeF_2$  (62-38 mole %), the fuel solvent of current interest, are in progress. The studies on  $CrF_2$  in  $NaF-ZrF_4$  (53-47 mole %) and on  $NiF_2$  in  $LiF-BeF_2$  (62-38 mole %) represent work completed during the past year.

Several points of interest are embraced by the information in Fig. 3.1. First, it was somewhat surprising that the measured equilibrium quotients for  $FeF_2$  and  $CrF_2$  agree as closely as they do with those expected for ideal behavior in accord with Raoult's law. This has been reconciled by the viewpoint, derived from related work, that the solvents employed in this experiment match the acidity, in terms of fluoride affinity or complexing, of the fluoride ion environment which prevails for  $Fe^{++}$  ions, for example, in molten  $FeF_2$ . Thus, it is not too surprising that Henry's law is obeyed, as implied by the constancy of equilibrium quotients in Fig. 3.1, to higher concentrations than

<sup>1</sup>C. M. Blood, W. R. Grimes, and G. M. Watson, "Activity Coefficients of Ferrous Fluoride and of Nickel Fluoride in Molten Sodium Fluoride-Zirconium Fluoride Solutions," presented before the Division of Physical and Inorganic Chemistry at the 132nd National Meeting of the American Chemical Society, New York, Sept. 8-12, 1957.

<sup>2</sup>L. Brewer *et al.*, *The Chemistry and Metallurgy of Miscellaneous Materials: Thermodynamics* (ed. by L. L. Quill), p 65, 110, McGraw-Hill, New York, 1950.

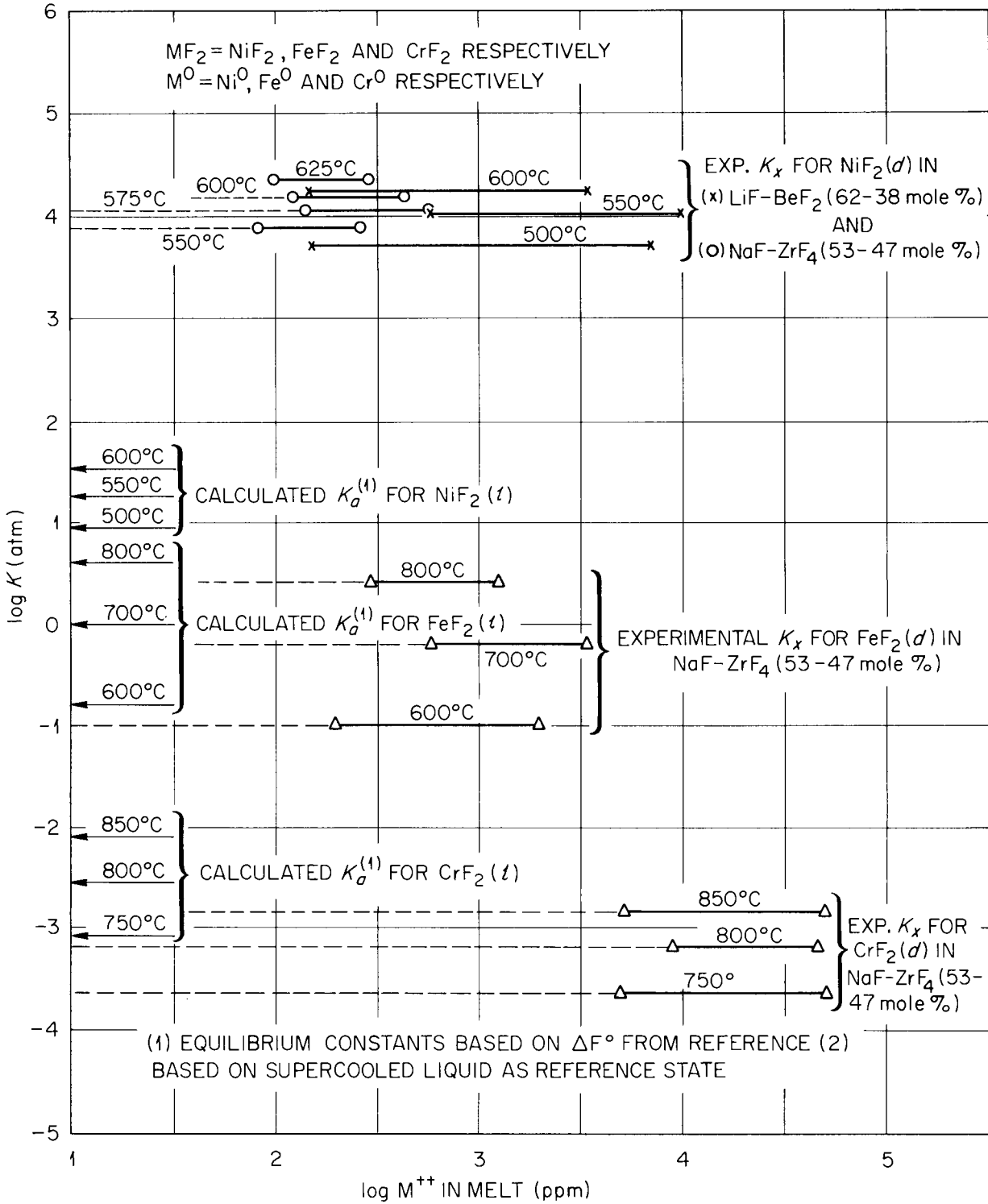


Fig. 3.1. Experimental Equilibrium Quotients for  $MF_2(d) + H_2(g) \rightleftharpoons M^0(s) + 2HF(g)$  in Fuel Solvents.

might have been expected for molten salts in general; that is, only minor negative deviations from Raoult's law are found, even at low dilutions, for cations like  $\text{Fe}^{++}$  and  $\text{Cr}^{++}$  in solvents which have proved to be useful for reactor applications.

A second point of interest is the lack of agreement in the case of  $\text{NiF}_2$  between calculated ideal behavior and the experimental results. Considerations of this point, as discussed below, have led to the conclusion that the estimates in the literature, on which the calculated equilibrium constants for  $\text{NiF}_2$  were based, are subject to considerable revision, and that values compatible with the  $\text{NiF}_2$  reduction experiment discussed below are more reliable.

The equilibrium quotients and calculated activity coefficients for  $\text{CrF}_2$  in  $\text{NaF-ZrF}_4$  (53-47 mole %) in Table 3.1 correspond to equilibrium concentrations of HF as low as  $2 \times 10^{-5}$  mole/liter in some cases. Gas concentrations of this order were very difficult to maintain and measure; consequently, melts containing less than about 1 mole %  $\text{CrF}_2$  were not amenable to study, and four to six weeks were required to obtain a single point. It was of interest, however, that Henry's law applies to concentrations of  $\text{CrF}_2$  as high as 10 mole %, as shown in Fig. 3.2. The solubility

limit of  $\text{CrF}_2$  was not reached in the ranges represented in Fig. 3.2; there was little incentive to make measurements in a saturated solution since the solid phase was known not to be the simple compound  $\text{CrF}_2$ . A temperature-dependence plot, as shown in Fig. 3.3, yields a heat of reaction of 42 kcal for the reduction by  $\text{H}_2$  of dissolved  $\text{CrF}_2$ . Calculated heats of reaction based on literature values<sup>2</sup> are included in Fig. 3.3 for comparison.

In the  $\text{NaF-ZrF}_4$  system structural-metal fluorides yield saturating phases of the type  $\text{NaF} \cdot \text{NiF}_2 \cdot 2\text{ZrF}_4$ ; however, with the  $\text{LiF-BeF}_2$  system it is, in principle, possible to make measurements on solutions that are in equilibrium with solid  $\text{NiF}_2$ ,  $\text{FeF}_2$ , or  $\text{CrF}_2$ . Solubility measurements on  $\text{NiF}_2$ , plotted in Fig. 3.4, provided activity coefficients, based on solid as reference state, which appear in Table 3.2 under the column heading  $\gamma_s$ , defined as

$$\gamma_s = \frac{1}{N_{(\text{saturation})}}$$

Direct measurements on saturated melts proved not to be as easy as with unsaturated solutions; an important feature of the usual technique of

Table 3.1. Equilibrium Constants for the Reduction of  $\text{CrF}_2$  by Hydrogen Gas; Activity Coefficients of  $\text{CrF}_2$  in  $\text{NaF-ZrF}_4$  (53-47 mole %)

Temperature (°C)	Equilibrium Constant, $K_a$			Activity Coefficients** for $\text{CrF}_2$		
	Reaction (1)	Reaction (2)	Reaction (3)	$\gamma_s$	$\gamma_l$	$\gamma_d$
	$\times 10^{-3}$	$\times 10^{-3}$	$\times 10^{-3}$			
850	4.9	7.7	$1.45 \pm 0.17$	0.296	0.188	1.00
800	1.61	2.82	$0.64 \pm 0.10$	0.394	0.225	1.00
750	0.42	0.86	$0.22 \pm 0.05$	0.526	0.257	1.00

\* $s$ ,  $g$ ,  $l$ , and  $d$  refer to crystalline solid, gaseous, supercooled liquid, and dissolved states, respectively. The  $K_a$  for reactions (1) and (2) are calculated from data in ref 2.

\*\* $\gamma_s$ ,  $\gamma_l$ , and  $\gamma_d$  are activity coefficients calculated using crystalline solid, supercooled liquid, and solution in the molten solvent, respectively, as the standard state for  $\text{CrF}_2$ .

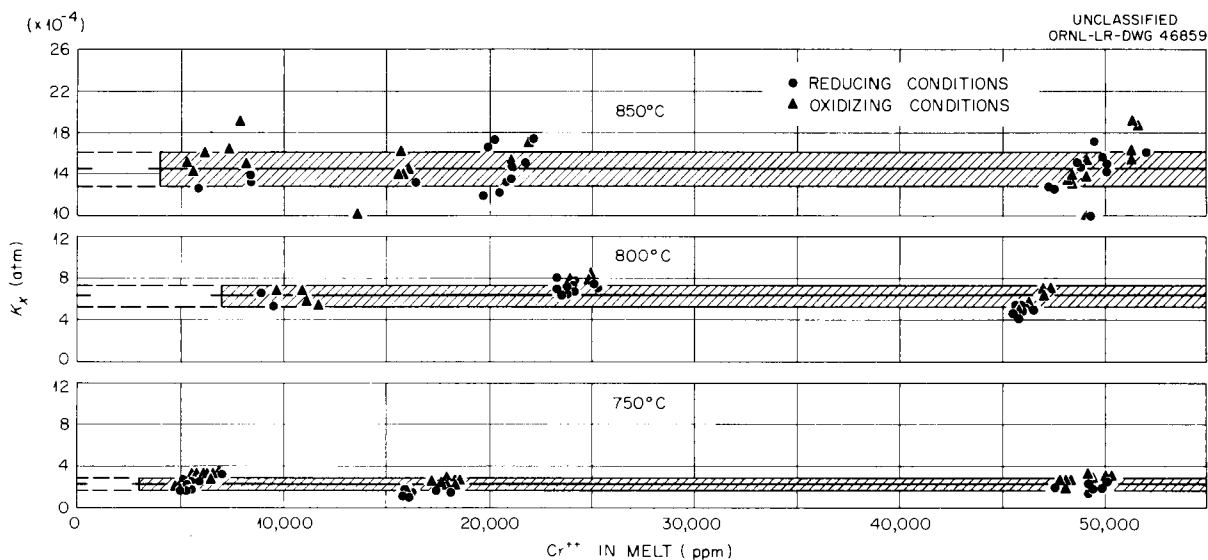


Fig. 3.2. Equilibrium Quotients for the Reduction by  $H_2$  of  $CrF_2$  in  $NaF-ZrF_4$  (53-47 mole %).

reaching equilibrium involved the slow shift of melt composition in response to the influent gas composition. With a third phase present, so that the concentrations in the melt were fixed, the effluent was much more closely coupled to changes in influent gas composition. Thus, much additional laborious adjustment was required to ensure that equilibrium had really been reached. Also, the low concentration of  $H_2$  in the gas in equilibrium with high concentrations of  $NiF_2$  was in an unfavorable range from the standpoint of gas analysis. Consequently, the most abundant and reproducible results applicable to saturated solutions could be obtained by extrapolation from solutions slightly more dilute than corresponding to saturation.

By combining the activity coefficients,  $\gamma_s$ , with experimental equilibrium quotients,  $K_x$ , values for which are shown graphically in Fig. 3.5, experimental values for the equilibrium constants,  $K_a$ , are obtained ( $K_a = K_x/\gamma_s$ ), as listed in Table 3.2. And from the equilibrium constants the standard free energy of reaction ( $\Delta F_{\text{react.}}^\circ = -RT \ln K_a$ ) is found to have the values listed under the heading  $\Delta F_{\text{react.}}^\circ$  in Table 3.3. The calculations outlined in Table 3.3 lead to revised values of  $\Delta F_{NiF_2(s)}^\circ$  which can be expressed, using  $\Delta H_{298}^\circ$  as  $-158$

kcal/mole,<sup>2</sup> as

$$\begin{aligned} \frac{\Delta F^\circ - \Delta H_{298}^\circ}{T} &= 40.9 \text{ at } 500^\circ\text{C} \\ &= 40.7 \text{ at } 550^\circ\text{C} \\ &= 40.5 \text{ at } 600^\circ\text{C} \end{aligned}$$

compared with

$$\frac{\Delta F^\circ - \Delta H_{298}^\circ}{T} = 34.9 \text{ at } 550^\circ\text{C}$$

as given in the literature.<sup>2</sup> The reproducibility of the values of  $\Delta F_{NiF_2}^\circ$  in these experiments was usually about  $\pm 2$  kcal/mole.

Even with the 5-kcal revision of  $\Delta F_{NiF_2}^\circ$  to a smaller negative value, if 1723°K is taken as the melting point of  $NiF_2$  (ref 3), and 8900 cal/mole as the heat of fusion<sup>4</sup> (corresponding to about

<sup>3</sup>L. M. Matarrese, thesis, University of Chicago, 1954; cited by J. W. Stout and E. Catalano, *J. Chem. Phys.* 23, 2015 (1955).

<sup>4</sup>A. Glasner, *The Thermochemical Properties of Oxides, Fluorides, and Chlorides to 2500°K*, ANL-5750 (1957).

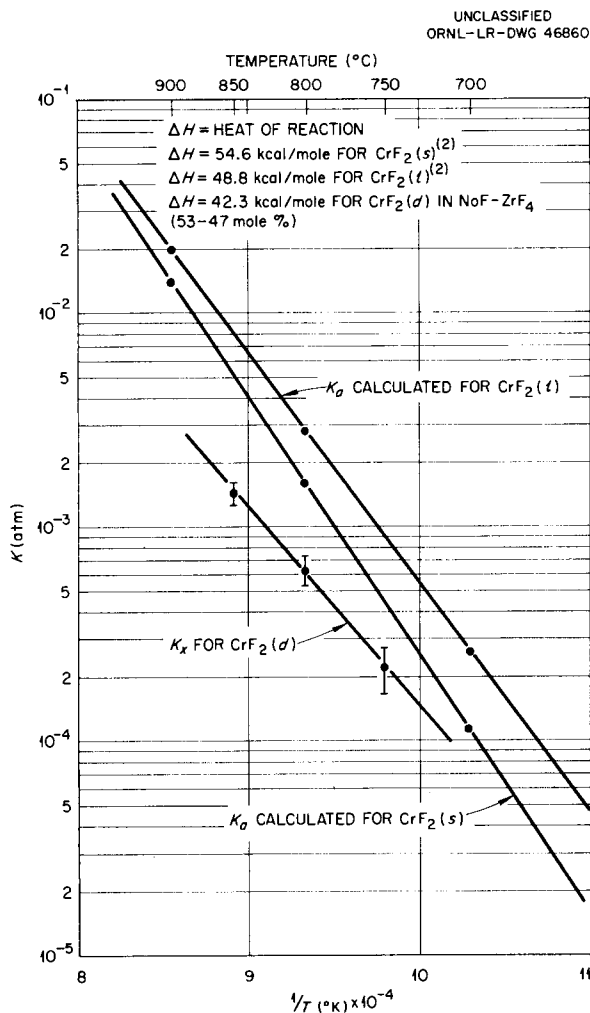


Fig. 3.3. Effect of Temperature on Equilibrium Quotient  $K_x = \frac{P_{HF}^2}{N_{CrF_2} P_{H_2}}$  in NaF-ZrF<sub>4</sub> (53-47 mole %).

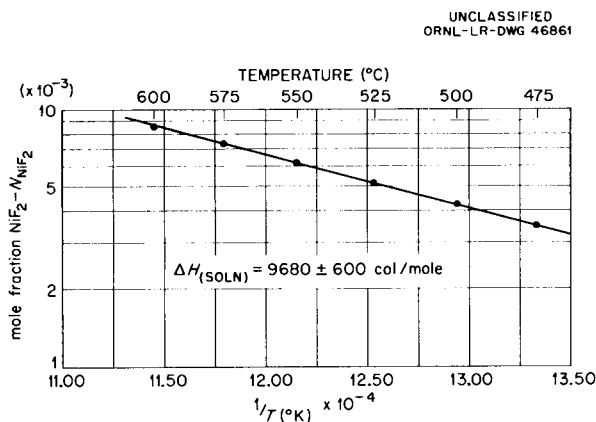


Fig. 3.4. Solubility of NiF<sub>2</sub> in LiF-BeF<sub>2</sub> (62-38 mole %).

5 e.u. for melting), the calculated activity coefficients referred to supercooled liquid as the standard state are well above unity, as shown in Table 3.2 under the column headed  $\gamma_l$ . Positive deviations of this magnitude are not expected in these fluoride melts. On the other hand, using 10 e.u. as the entropy of fusion, the calculated activity coefficients for NiF<sub>2</sub>, based on supercooled liquid as reference state, are slightly below unity, as required for consistency with FeF<sub>2</sub> and CrF<sub>2</sub>, and it may be conjectured that 10 e.u. of fusion is probably a more reliable estimate than 5 e.u.

The temperature dependence of the equilibrium quotient of the reduction of NiF<sub>2</sub> in LiF-BeF<sub>2</sub> (62-38 mole %) is shown in Fig. 3.6.

### THEORY OF MOLTEN-SALT SYSTEMS

M. Blander  
D. G. Hill<sup>5</sup>

J. Braunstein<sup>6</sup>  
R. F. Newton

A theoretical and experimental study of the thermodynamic properties of molten-salt systems containing at least two cations and two anions (reciprocal salt systems) was undertaken to provide a framework for the physical description of solution behavior in this class of systems and to attempt to understand the limitations of the conventional description of the thermodynamic properties of such systems by use of the mass action law. Some discussion of this topic has appeared.<sup>7</sup> The recent work on this class of systems has been concerned with testing the usefulness of the quasi-lattice theory in predicting solution behavior a priori, and also with generalizing the theory so as to give an insight into the meaning of conventional association constants.

### A Quasi-Lattice Model for Molten Reciprocal Salt Systems<sup>8</sup>

The activity coefficients of the component AD,  $\gamma_{AD}$ , have been calculated theoretically using two different approximations which are based on the

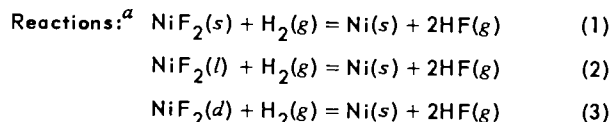
<sup>5</sup>Duke University, Durham, N.C.; consultant to Reactor Chemistry Division, summer 1959.

<sup>6</sup>University of Maine, Orono; summer research participant, Reactor Chemistry Division, 1958 and 1959.

<sup>7</sup>M. Blander, *J. Phys. Chem.* 63, 1262 (1959).

<sup>8</sup>M. Blander and J. Braunstein, *Ann. N.Y. Acad. Sci.* 79, 838 (1960).

Table 3.2. Equilibrium Constants for the Reduction of NiF<sub>2</sub> by Hydrogen Gas; Activity Coefficients of NiF<sub>2</sub> in LiF-BeF<sub>2</sub> (62-38 mole %)



Temperature (°C)	Equilibrium Constants				Activity Coefficients <sup>e</sup> (NiF <sub>2</sub> )			
	Reaction (1) <sup>b</sup>	Reaction (2) <sup>c</sup>	Reaction (2) <sup>d</sup>	Reaction (3)	γ <sub>s</sub>	γ <sub>l</sub>	γ <sub>d</sub>	γ <sub>l</sub> (revised) <sup>d</sup>
					× 10 <sup>-3</sup>			
600	149	1860	19,900	17.3 ± 1.20	120	9.3	1.00	0.87
550	61.2	1050	15,100	9.90 ± 0.57	160	9.5	1.00	0.66
500	21.3	518	10,400	5.04 ± 0.46	240	9.7	1.00	0.49

<sup>a</sup> s, g, l, and d refer to crystalline solid, gaseous, supercooled liquid, and dissolved states respectively.

<sup>b</sup> K<sub>a</sub> = K<sub>x</sub>/γ<sub>s</sub>.

<sup>c</sup> K<sub>a</sub> calculated, obtained from b, using refs 3 and 4.

<sup>d</sup> K<sub>a</sub> calculated for ΔS<sub>M</sub> ~ 10.0 e.u. using ref 3.

<sup>e</sup> γ<sub>s</sub>, γ<sub>l</sub>, and γ<sub>d</sub> are activity coefficients calculated using crystalline solid, supercooled liquid, and solution in the molten solvent, respectively, as the standard state for NiF<sub>2</sub>.

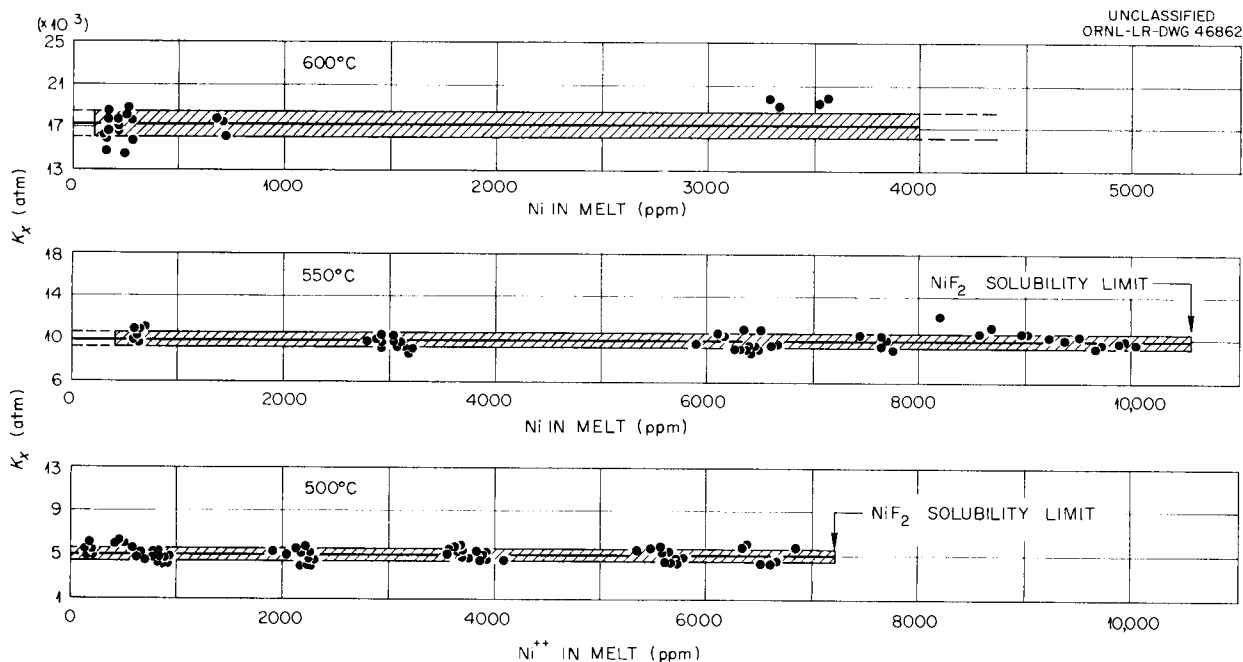
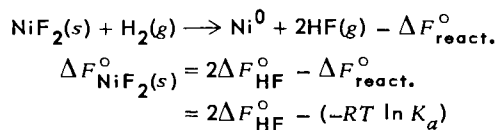


Fig. 3.5. Equilibrium Quotients for the Reduction by H<sub>2</sub> of NiF<sub>2</sub> in LiF-BeF<sub>2</sub> (62-38 mole %).

Table 3.3. Revised Standard Free Energy of Formation ( $\Delta F_{\text{NiF}_2}^\circ$ ) for  $\text{NiF}_2(s)^*$ 


Temperature (°C)	$2\Delta F_{\text{HF}}^\circ$	$\Delta F_{\text{react}}^\circ$	$\Delta F_{\text{NiF}_2(s)}^\circ$	Former $\Delta F_{\text{NiF}_2(s)}^\circ$ **
600	-131.34	-8.68	-123	-127.88
550	-131.22	-6.73	-124	-129.43
500	-131.12	-4.70	-126	-131.02

\*s and g refer to crystalline solid and gaseous states respectively;  $K_a = K_x/\gamma_s$ .

\*\*From ref 2.

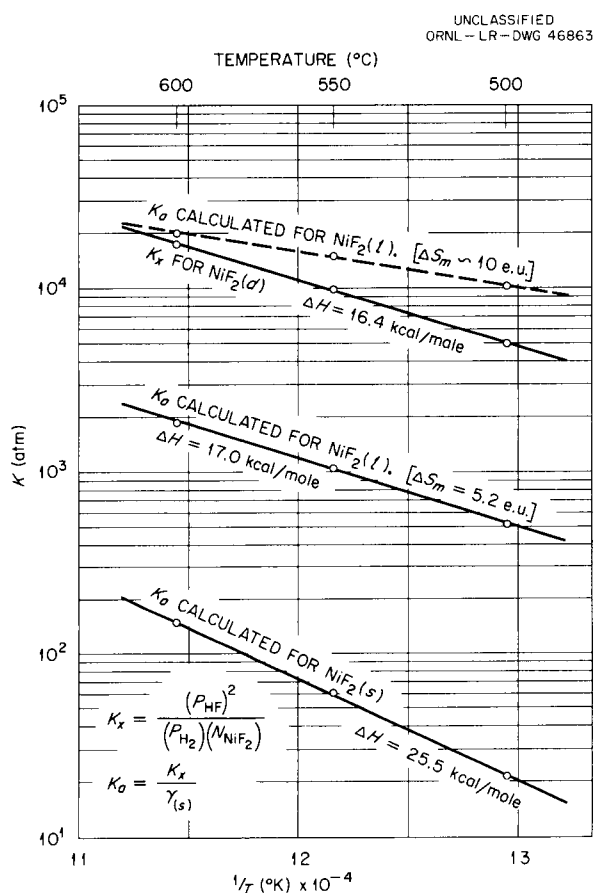


Fig. 3.6. Effect of Temperature on Equilibrium Quotient  $K_x = \frac{(P_{\text{HF}})^2}{(P_{\text{H}_2})(N_{\text{NiF}_2})}$  in  $\text{LiF-BiF}_2$  (62-38 mole %).

lattice model for the molten reciprocal salt system  $A^+$ ,  $B^+$ ,  $C^-$ ,  $D^-$ . The first is the *asymmetric* approximation in which the groupings  $AC_n^{(1-n)^+}$  are included, where  $n \leq Z$ . This leads to the relation:

$$Y_{\text{AD}} = \frac{(1-X)^Z}{N_{D^-}} \left[ 1 + \frac{X}{\beta(1-X)} \right]^{Z-1}, \quad (1)$$

where  $Z$  is the lattice coordination number,  $\beta = e^{-\Delta E/RT}$ ,  $\Delta E$  is the relative energy of interaction of a mole of  $A^+C^-$  pairs, and  $X$ , the fraction of positions adjacent to an  $A^+$  ion that are occupied by  $C^-$  ions, can be calculated from the distribution function for the *asymmetric* approximation in terms of  $Z$ ,  $\Delta E$ , and the concentrations of all the ions in solution. The second or *symmetric* approximation includes the groupings  $A_m C_n^{(m-n)^+}$ , where  $m$  and  $n$  are any integers. This method leads to the relation:

$$Y_{\text{AD}} = \left( \frac{1-Y}{1-N_{C^-}} \right)^Z, \quad (2)$$

where  $Y$  can be calculated from the distribution function for the *symmetric* approximation in terms of  $Z$ ,  $\Delta E$ , and the concentrations of the ions in solution.

The activity coefficients of  $\text{AgNO}_3$  in the two molten solvents  $\text{KNO}_3$  and  $\text{NaNO}_3$ , dilute in  $\text{Ag}^+$  and  $\text{Cl}^-$  ions, were measured in an electromotive

force cell at 402°C. The activity coefficients of  $\text{AgNO}_3$ ,  $\gamma_{\text{AgNO}_3}$ , are much lower in the  $\text{KNO}_3$  solvent than in the  $\text{NaNO}_3$  solvent at the same temperature and the same concentrations of  $\text{Ag}^+$  and  $\text{Cl}^-$  ions. The concentration dependence of  $\gamma_{\text{AgNO}_3}$  in the  $\text{KNO}_3$  solvent corresponds more closely to the concentration dependence of  $\gamma_{\text{AD}}$  as calculated from the *asymmetric* approximation (for  $Z = 6$ ,  $\Delta E = -5.6_5$ ) than to the concentration dependence calculated from the *symmetric* approximation. In the  $\text{NaNO}_3$  solvent, the concentration dependence of  $\gamma_{\text{AgNO}_3}$  corresponds more closely to the calculation based on the *symmetric* approximation (for  $Z = 6$ ,  $\Delta E = -4.5_5$ ).

The differences between the behavior in the two solvents can be correlated with the relative sizes of the  $\text{K}^+$  and  $\text{Na}^+$  ions and the relative effects of the fields of these two solvent cations on the energy of interaction of an  $\text{Ag}^+\text{-Cl}^-$  pair.

#### Electromotive Force Measurements in the System $\text{AgNO}_3\text{-NaCl-NaNO}_3$ and Their Comparison to the Quasi-Lattice Theory

Measurements of the activity coefficients of  $\text{AgNO}_3$ ,  $\gamma_{\text{AgNO}_3}$ , in dilute solutions of  $\text{Ag}^+$  and  $\text{Cl}^-$  ions in  $\text{NaNO}_3$  were made at 331, 364, 385, 402, 423, 438, and 500°C. The concentration dependence of  $\log \gamma_{\text{AgNO}_3}$  was closer to the *symmetric* approximation based on the quasi-lattice model than to the *asymmetric* approximation. Average values of the relative energies of  $\text{A}^+\text{-C}^-$  ion pair formation,  $\Delta E$ , as defined in the quasi-lattice model, were calculated by comparison of the *symmetric* approximation with the experimental results. For  $Z = 4, 5,$  and  $6$  the values of  $\Delta E$  averaged over all seven temperatures are  $-5.1_3, -4.8_3,$  and  $-4.5_9$  kcal/mole respectively. Figure 3.7 is a plot of  $-\log \gamma_{\text{AgNO}_3}$  vs the concentration of  $\text{NaCl}$  ( $R_{\text{NaCl}}$  = mole ratio of  $\text{NaCl}$ ) at a concentration of  $\text{AgNO}_3$ ,  $R_{\text{AgNO}_3} = 0.30 \times 10^{-3}$ . The dashed lines are values of  $-\log \gamma_{\text{AD}}$  as calculated from the *symmetric* theory for any one value of  $Z$  and seven values of  $\Delta E$  which differed by less than 0.05 kcal from the average. In the  $\text{AgNO}_3\text{-KCl-KNO}_3$  system, average values of  $\Delta E$  calculated from the comparison of the *asymmetric* theory and the experimental results at 370, 385, 402, 423, and 436°C were  $-6.1_8, -5.8_8,$  and  $-5.6_5$

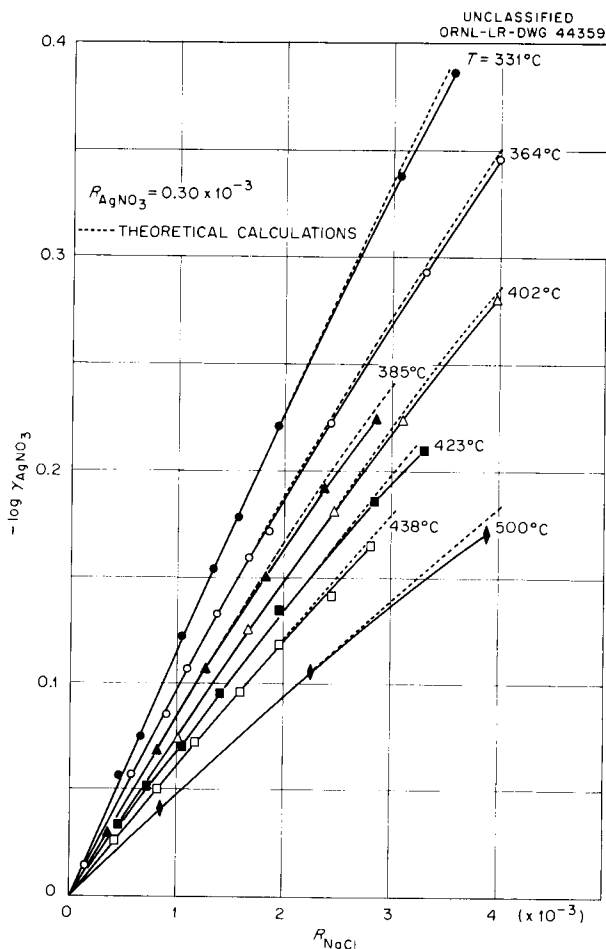


Fig. 3.7. Activity Coefficients of  $\text{AgNO}_3$  at Seven Temperatures in the  $\text{AgNO}_3\text{-NaCl-NaNO}_3$  System at  $R_{\text{AgNO}_3} = 0.30 \times 10^{-3}$  as a Function of the Concentration of  $\text{NaCl}$ .

kcal/mole for  $Z = 4, 5,$  and  $6$  respectively.<sup>9,10</sup> The values of  $\Delta E$  for any one value of  $Z$  in each of the two systems were constant, within experimental precision, at all temperatures. The conventional association constant for the formation of the ion pair  $\text{A}^+\text{-C}^-$ ,  $K_1$ , is equal to

$$Z \left[ \exp \left( -\frac{\Delta E}{RT} \right) - 1 \right].$$

The constancy of  $\Delta E$  at all temperatures studied

<sup>9</sup>M. Blander, R. F. Newton, and F. F. Blankenship, *J. Phys. Chem.* **63**, 1259 (1959).

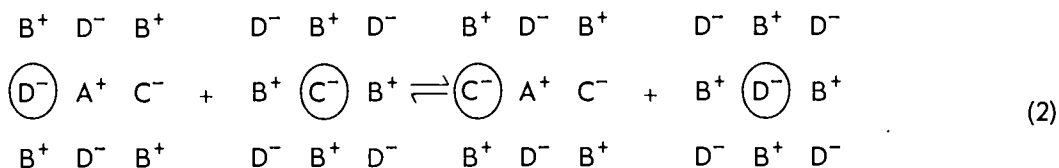
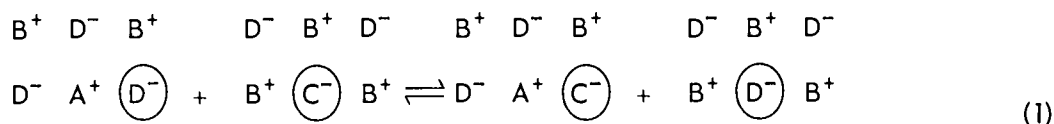
<sup>10</sup>J. Braunstein and M. Blander, *J. Phys. Chem.* **64**, 10 (1960).

and for all reasonable values of  $Z$  means that from measurements of  $K_1$  at one temperature, one may, in these two systems, correctly predict  $K_1$  at all other temperatures by use of the lattice model.

**A Generalized Calculation Based on the Quasi-Lattice Model**

A generalized statistical-mechanical calculation of the solution thermodynamics of the reciprocal molten-salt system  $A^+$ ,  $B^+$ ,  $C^-$ , and  $D^-$  dilute in  $A^+$  ions has been made. The calculation is based on the quasi-lattice model of reciprocal salt systems and treats the problem as an order-disorder problem.

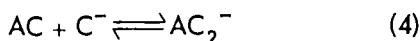
In the theory, associations of  $A^+$  and  $C^-$  ions and nearest neighbor interactions only are taken into account. A two-dimensional representation of the formation of  $A^+C^-$  ion pairs and  $C^-A^+C^-$  ion triplets is as follows:



If the symbol  $A^+$  represents an  $A^+$  ion having  $ZD^-$  ions as nearest neighbors, where  $Z$  is the coordination number of the quasi lattice,  $C^-$  represents a  $C^-$  ion having no  $A^+$  ions adjacent to it, and  $AC$  represents an  $A^+$  ion which has one  $C^-$  ion and  $(Z - 1) D^-$  ions as nearest neighbors, then Eq. (1) can be represented more conventionally as



The higher associations may be represented in a similar manner as



where  $AC_2^-$  need not be linear. Let  $\beta_i = e^{-\Delta A_i/kT}$ , where  $\Delta A_i$  is the specific Helmholtz free energy change for exchanging a particular  $D^-$  ion, which is a nearest neighbor of an  $A^+$  ion having  $(i - 1) C^-$  ions and  $(Z - i + 1) D^-$  ions as nearest neighbors, with a  $C^-$  ion which has no  $A^+$  ions as nearest neighbors. In a sense,  $-\Delta A_i$  is a "bond strength." The conventional equilibrium constants for associations as (3), (4), (5), and (6) were some of the quantities derived from a partition function for the quasi lattice.<sup>11</sup> The results are:

$$K_1 = Z(\beta_1 - 1) \tag{7}$$

$$K_1 K_2 = \frac{Z(Z - 1)}{2!} (\beta_1 \beta_2 - 2\beta_1 + 1) \tag{8}$$

$$\begin{aligned}
 K_1 K_2 K_3 = & \frac{Z(Z - 1)(Z - 2)}{3!} (\beta_1 \beta_2 \beta_3 - \\
 & - 3\beta_1 \beta_2 + 3\beta_1 - 1) \tag{9}
 \end{aligned}$$

$$\begin{aligned}
 K_1 K_2 K_3 K_4 = & \frac{Z(Z - 1)(Z - 2)(Z - 3)}{4!} (\beta_1 \beta_2 \beta_3 \beta_4 - \\
 & - 4\beta_1 \beta_2 \beta_3 + 6\beta_1 \beta_2 - 4\beta_1 + 1) \tag{10}
 \end{aligned}$$

where  $K_1$ ,  $K_2$ ,  $K_3$ , and  $K_4$  are the conventional association constants<sup>12</sup> for the equilibria (3), (4),

<sup>11</sup>The calculation was similar in some respects to that of T. L. Hill, *J. Chem. Phys.* 14, 263 (1946), for multilayer adsorption.

<sup>12</sup>In a real system the  $K_i$  must be evaluated at infinite dilution of  $A^+$  and  $C^-$  ions.

(5), and (6), respectively, where the concentration scale is either the mole fraction or the cationic or anionic fraction of the species, depending on whether a species is neutral or charged. Equations (7) through (10) constitute a separation of configurational factors from the factors containing the specific "bond strength."

A specific example for illustrative purposes is the case in which  $\beta_1 = \beta_2 = \beta_3 = \beta_4$ , or, in other words, the case in which the "bond strength" of each successive  $A^+-C^-$  interaction is the same. In this case

$$\frac{K_1}{Z} = \frac{2K_2}{Z-1} = \frac{3K_3}{Z-2} = \frac{4K_4}{Z-3},$$

a result first obtained by Bjerrum.<sup>13</sup> This demonstrates that even if the "bond strength" for the attachment of successive  $C^-$  ions is the same, the constants  $K_1$ ,  $K_2$ ,  $K_3$ , and  $K_4$  will decrease in that order.

Equation (8) is for an  $AC_2^-$  ion triplet in which the tendency for forming the second  $A^+-C^-$  bond is nondirectional. If this tendency is directional, then

$$K_1 K_2' = \frac{Z(Z-1)}{2!} \left( \frac{\beta_1 \beta_2'}{Z-1} - \frac{Z}{Z-1} \beta_1 + 1 \right),$$

where the prime (') denotes the case in which the  $AC_2^-$  triplet is linear and the second  $C^-$  ion, which is attached to an  $A^+$  ion, can have a non-zero value of  $\Delta A_2$  in only one of the  $(Z-1)$  lattice sites. If  $\beta_2' = \beta_2$ , it is easy to see that  $K_2' < K_2$ . Although "bond" strengths may not differ, the equilibrium constant for the formation of  $AC_2^-$  will be smaller if the second  $A^+-C^-$  "bond" tends to be directional than if it is nondirectional.

### FREEZING POINT DEPRESSIONS IN SODIUM FLUORIDE

S. Cantor

Depression of the freezing point of sodium fluoride by several solute fluorides of univalent and divalent cations has been examined. Sodium fluoride was chosen as the solvent for this study because (1) its heat of fusion is large, (2) its

heat capacity is well known,<sup>14</sup> and (3) crystalline NaF is the primary phase below the liquidus over the composition range from 100 to 75 mole % NaF in many binary systems.

The sodium fluoride was obtained by selecting clear crystals from slowly cooled melts of chemically pure material. Solute fluorides, other than  $BeF_2$ , were of cp quality commercial material, if available, or were prepared by treatment of cp chlorides with anhydrous HF at high temperatures. Commercial  $BeF_2$  was given a similar high-temperature hydrofluorination to minimize oxide content. Most experiments were conducted in apparatus of nickel; each experiment used about 2 moles of NaF, which was protected from the atmosphere and was stirred by a stream of argon. Temperatures and cooling rates were manually regulated. Freezing points were established within  $\pm 0.6^\circ C$  from cooling curves obtained with calibrated Pt, Pt-Rh thermocouples in a well which was bathed in the cooling liquid. (For the few materials for which nickel was unsuitable, graphite crucibles and copper thermowells and gas inlet lines were employed.)

The experimentally observed freezing points were compared with those predicted for ideal solution behavior ( $T_i$ ) calculated from:

$$-\ln N_{NaF} = \frac{\Delta H_f}{R} \left( \frac{1}{T_i} - \frac{1}{T_f} \right) + \frac{C_{P_l} - C_{P_s}}{R} \left( \ln \frac{T_f}{T_i} + 1 - \frac{T_f}{T_i} \right),$$

where  $N_{NaF}$  is the mole fraction of NaF,  $\Delta H_f$  is the molar heat of fusion (8017 cal) of pure NaF at its freezing point ( $T_f = 995.0 \pm 0.6^\circ C$ ), and  $C_{P_l} - C_{P_s}$  is the difference in molar heat capacity of pure NaF in liquid and crystalline states.

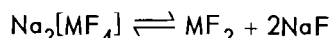
The freezing point of NaF on addition of KF and LiF in amounts to 25 mole % has been examined. Agreement between observed values and those calculated from the equation was obtained for all KF solutions studied. Ideal behavior was observed for LiF solutions containing up to 15 mole %;

<sup>13</sup>N. Bjerrum, *Z. physik. Chem.* **106**, 222 (1923).

<sup>14</sup>C. J. O'Brien and K. K. Kelly, *J. Am. Chem. Soc.* **79**, 5616 (1957).

$T_{\text{obs}} - T_i$  was  $-0.9$  and  $-1.7^\circ\text{C}$  at 20 and 25 mole % LiF. Since  $\text{Li}^+$  has a larger ratio of charge to radius than  $\text{K}^+$ , it would tend to polarize or distort the surrounding NaF lattice to a greater extent; deviation from ideal behavior should, accordingly, be expected at lower concentration of LiF. However, as expected, a simple model in which cations and anions occupy alternate sites on a hypothetical lattice and where an  $\text{M}^+$  ion substitutes for  $\text{Na}^+$  on a cation site without a new interaction in the lattice is satisfactory for these simple solutions.

Study of the freezing point of NaF on addition of up to 20 mole % of each of the alkaline earth fluorides yielded data shown in Fig. 3.8. It is apparent that lowering of the freezing point is inversely proportional to cation size in this series and that the solutions deviate markedly from simple ideal behavior. Calculation of freezing point depressions from a simple lattice model, in which substitution of  $\text{M}^{++}$  on a cation site creates an additional vacancy formerly occupied by a second  $\text{Na}^+$ , yields values which are too great for all cases except the most concentrated solutions of  $\text{BeF}_2$ . Alternatively, if one assumes the formation of complex ions of the  $\text{Na}_2\text{M}^{\text{II}}\text{F}_4$  type it is possible to calculate freezing point depressions in agreement with observations with up to 5 mole % of all solutes and up to 15 mole % of  $\text{MgF}_2$ . Although it should be possible to "fit" the experimental data by assuming reactions such as



and



in the complex ion model (or by adding "polarization" corrections to the lattice model), it is clearly futile to attempt unequivocal structural interpretations from these thermodynamic data.

The cation sizes in the divalent ions of the transition metals are quite similar; the stability constants of a variety of complex ions of these cations, however, decrease in the order  $\text{Cu}^{++}$ ,  $\text{Ni}^{++}$ ,  $\text{Co}^{++}$ ,  $\text{Zn}^{++}$ ,  $\text{Fe}^{++}$ ,  $\text{Mn}^{++}$ . Results obtained from experiments with the fluorides of these cations as solutes indicate, as shown in Fig. 3.9, that the magnitudes of freezing point depressions also follow this order. The behavior of these solutes is approximately that predicted if undissociated  $[\text{MF}_4]^{--}$  ions existed in the solutions.

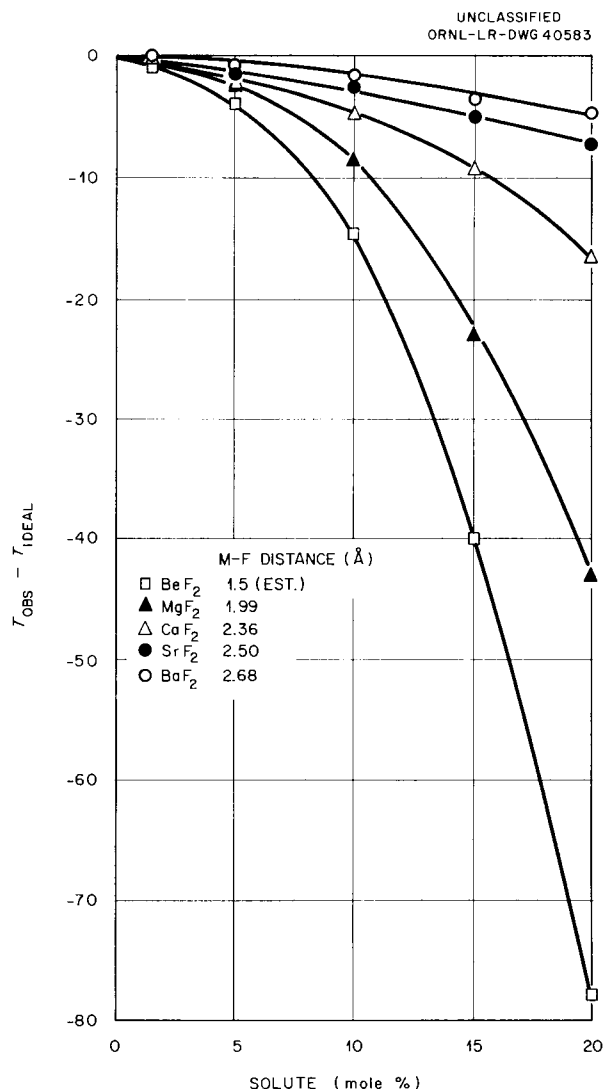


Fig. 3.8. Freezing Point Depressions in NaF Caused by the Alkaline Earth Fluorides.

Moreover, as shown in Fig. 3.10, a plot of  $T_{\text{obs}} - T_i$  vs atomic number is qualitatively similar to that of lattice energy of the fluoride vs atomic number of its cation and also to curves used to illustrate crystal field stabilization energies in complex ion formation.<sup>15</sup> It is hoped that absorption spectra of such solutions in the visible region will provide supplementary information concerning structures.

<sup>15</sup>L. E. Orgel, "Some Applications of Crystal-Field Theory to Problems in Transition-Metal Chemistry," in the proceedings of the tenth international congress of the Solvay Institute, Brussels, 1956.

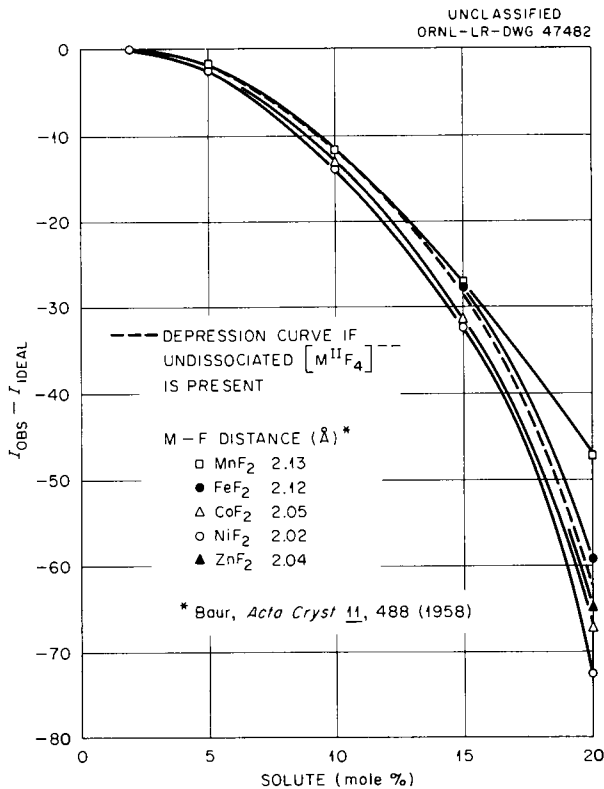


Fig. 3.9. Freezing Point Depressions in NaF Caused by Transition Metal Difluorides.

VAPOR PRESSURES OF SYSTEMS CONTAINING URANIUM HALIDES

S. Langer<sup>16</sup>

Uranium Tetrafluoride

The vapor pressure of liquid uranium tetrafluoride has been measured over the temperature interval 1018 to 1302°C by a boiling point method and by the quasi-static method of Rodebush and Dixon.<sup>17</sup> The vapor pressures obtained (4 to 180 mm Hg) are represented by

$$\log P = - \frac{16,840 \pm 44}{T} - 7.549 \log T + 37.09 \pm 0.03 ,$$

<sup>16</sup>Present address: General Atomic, P.O. Box 608, San Diego, Calif.

<sup>17</sup>W. H. Rodebush and A. L. Dixon, *Phys. Rev.* 26, 851 (1925).

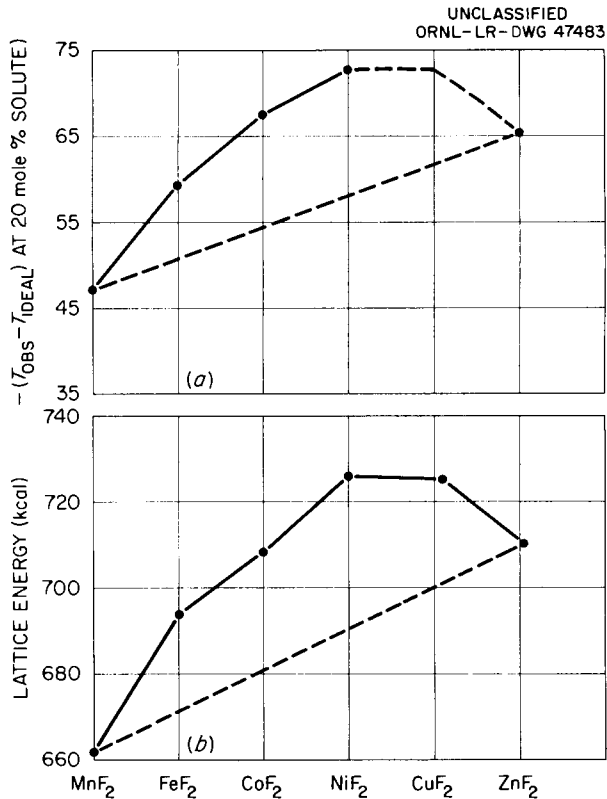


Fig. 3.10. (a) NaF Freezing Point Depressions Caused by Transition Metal Difluorides. (b) Lattice Energies of Transition Metal Difluorides.

with  $P$  in millimeters of mercury and  $T$  in degrees Kelvin.

Extrapolation of the data to the normal boiling point of 1729°K, with the assumption of a  $\Delta C_p$  of vaporization of  $-15 \text{ cal}\cdot\text{deg}^{-1}\cdot\text{mole}^{-1}$ , gives a heat of vaporization of  $51.2 \pm 0.2 \text{ kcal/mole}$  at the boiling point. The entropy of vaporization at the normal boiling temperature is 29.7 e.u., in reasonable agreement with those of other heavy metal tetrafluorides. A paper describing this work has been accepted for publication.<sup>18</sup>

If the data of Ryon and Twichell,<sup>19</sup> who used an effusion method with solid  $UF_4$  and implicitly assumed that the vapor was monomeric, are extrapolated to this temperature region, values in good

<sup>18</sup>S. Langer and F. F. Blankenship, *J. Inorg. & Nuclear Chem.* (in press).

<sup>19</sup>A. D. Ryon and L. P. Twichell, *Vapor Pressure and Related Physical Constants of Uranium Tetrafluoride*, H-5.385.2 (July 25, 1947).

agreement with those of the present study are obtained. This agreement would seem to demonstrate the virtual absence of associated molecules in the vapor above pure UF<sub>4</sub>.

### Uranium Tetrachloride

A similar study, using the Rodebush and boiling point methods, was made of the vapor pressure of UCl<sub>4</sub> as an initial step in a study of UCl<sub>4</sub>-alkali chloride binary systems. The data obtained are represented by

$$\log P = -\frac{9885 \pm 34}{T} - 7.046 \log T + 33.28 \pm 0.04, \quad (1)$$

with  $P$  in millimeters of mercury and  $T$  in degrees Kelvin. These values are in considerable disagreement with those obtained prior to 1947 by Wagner and Grady,<sup>20</sup> who also made measurements of total pressure over molten UCl<sub>4</sub>. These data, when recalculated using  $-14 \text{ cal}\cdot\text{deg}^{-1}\cdot\text{mole}^{-1}$  for  $\Delta C_p$  of vaporization, yield the equation

$$\log P = -\frac{10,200 \pm 47}{T} - 7.046 \log T + 33.79 \pm 0.05. \quad (2)$$

Unfortunately, the purity of samples used in the present investigation is not established, and it is not possible to resolve the discrepancy. The vapor pressure of molten UCl<sub>4</sub> seems to require further investigation.

### Vapor Pressures of LiF-UF<sub>4</sub> Mixtures

The vapor pressures of mixtures of UF<sub>4</sub> with 10 and with 20 mole % of LiF have been examined by use of the two methods mentioned above. The data obtained are shown, along with those for UF<sub>4</sub>, as Fig. 3.11. The total pressure of all species in the vapor is given for 90 mole % UF<sub>4</sub>-10 mole % LiF by

$$\log P = -\frac{16,550 \pm 150}{T} - 7.046 \log T + 35.22 \pm 0.10,$$

and for 80 mole % UF<sub>4</sub>-20 mole % LiF by

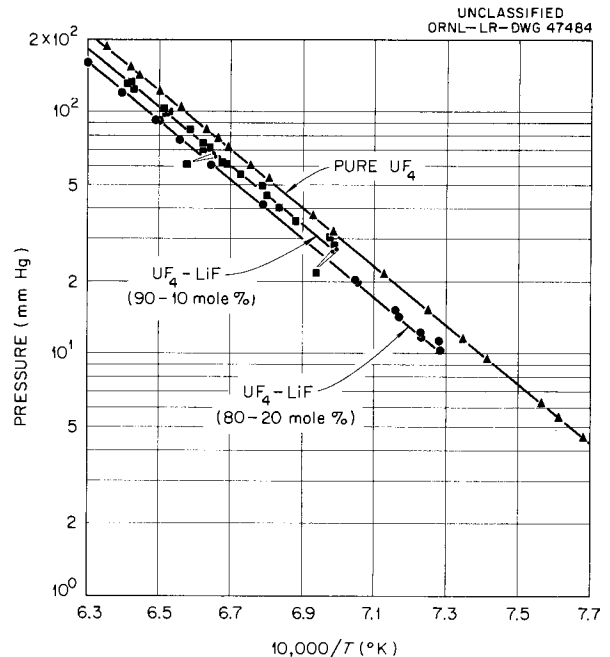


Fig. 3.11. Vapor Pressures of LiF-UF<sub>4</sub> Mixtures.

$$\log P = -\frac{16,215 \pm 36}{T} - 7.046 \log T + 34.94 \pm 0.002,$$

with  $P$  in millimeters of mercury,  $T$  in degrees Kelvin, and with  $\Delta C_p$  of vaporization assumed to be  $-14 \text{ cal}\cdot\text{deg}^{-1}\cdot\text{mole}^{-1}$ .

The partial pressure of LiF in these melts should be about 100-fold less than that of UF<sub>4</sub>. However, examination by chemical analysis and by x-ray diffraction of material condensed from the vapor phase in these experiments showed LiF-UF<sub>4</sub> mole ratios ranging from unity to 113. It seems obvious that such ratios are the result of a vapor compound; the measured pressure is, accordingly, the sum of the partial pressure of UF<sub>4</sub>, the partial pressures of LiF-UF<sub>4</sub> compounds, and the (negligible) partial pressure of LiF. Before activities of species in the melt can be obtained it will be necessary to evaluate the partial pressures of the vapor species by some direct technique.

<sup>20</sup>E. L. Wagner and H. F. Grady, *The Vapor Pressure Curves of Tuballoy Tetrachloride*, C-2.350.4 (Sept. 18, 1945).

4. SELF-DIFFUSION OF CHROMIUM IN INCONEL EXPOSED TO MOLTEN SALTS

G. M. Watson  
N. V. Smith

R. B. Evans  
W. R. Grimes

OVER-ALL DIFFUSION COEFFICIENTS

**Introduction.** – The results of recent studies<sup>1</sup> of the migration of metals (corrosion) resulting from temperature gradients in a molten-salt environment have indicated that the over-all migration rate is controlled by the diffusion rates within the metal. Chromium is of particular interest in this respect as it is present in alloys suitable for molten-salt applications.<sup>2</sup> Of all the alloy constituents, chromium has the greatest tendency to migrate. This investigation was performed to support directly and augment related corrosion studies.

Initial studies and reviews revealed that several investigations of solid-state diffusion phenomena have been reported, but only a portion of the reported work covered cases in which molten salts and chromium alloys were involved.

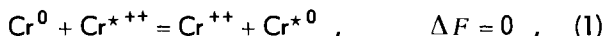
A large portion of the chromium diffusion coefficients available in the literature were applicable at temperatures above 900°C (ref 3). However, extrapolation of this information to temperatures of interest (600 to 900°C) could be misleading if the diffusion mechanism were to change<sup>4</sup> within the extrapolated region. Accordingly, an investigation was initiated of the over-all transfer rate of Cr<sup>51</sup> within isothermal systems comprised of Inconel containers and molten NaF-ZrF<sub>4</sub> mixtures. The first experiments were performed elsewhere<sup>5</sup> through a subcontract arrangement.<sup>6</sup> These initial uncorrelated data have been utilized and considerably extended. The objective of this investigation was to determine over-all self-diffusion

coefficients which include the combined effects of all diffusional processes for chromium that might occur within the Inconel at various temperatures.

The over-all coefficients were determined by following the depletion rate of Cr<sup>51</sup> (as Cr<sup>++</sup>) charged to molten salts in Inconel containers; they were also estimated by comparing the total radioactivity of salt-exposed metal specimens with the specific radioactivity of the salt at particular times.

Wall Exchange Reaction

If consideration is given to a semi-infinite isothermal system wherein an alloy containing chromium is in contact (at one face) with a molten salt containing a fixed amount of CrF<sub>2</sub>, it may be seen that the net rate of transfer of chromium between the metal and salt is zero at equilibrium, although a random dynamic exchange of chromium takes place. If a small amount of the CrF<sub>2</sub> is removed and replaced by an equal amount of labeled chromium fluoride (Cr<sup>\*</sup>F<sub>2</sub>), the random dynamic exchange can be studied by following the exchange rate of the Cr<sup>\*</sup>F<sub>2</sub>. The expression which relates the quantities of interest in terms of the surface exchange reaction or "wall reaction,"



is

$$K_{wt \text{ frac}} = \frac{[Cr^{*0}] [CrF_2]}{[Cr^0] [Cr^*F_2]} .$$

The equilibrium of Eq. (1) is established within a short time after the Cr<sup>\*</sup>F<sub>2</sub> is added. Since

$$K_a = 1 \approx K_{wt \text{ frac}} ,$$

the concentration of Cr<sup>\*0</sup> at the surface (x = 0) of the alloy at any time or temperature is given by

$$[Cr^{*0}]_{x=0} = [Cr^0] \frac{[Cr^*F_2]}{[CrF_2]} . \quad (2)$$

The Cr<sup>\*0</sup> initially distributed on the wall surface diffuses into the metal as time progresses,

<sup>1</sup>W. D. Manly *et al.*, "Metallurgical Problems in Molten Fluoride Systems," *Second U.N. International Conference on Peaceful Uses of Atomic Energy*, 1958, paper A/Conf/15/P/1990.

<sup>2</sup>J. A. Lane, H. G. MacPherson, and F. Maslan, *Fluid Fuel Reactors*, chaps. 12 and 13, Addison-Wesley, Reading, Mass., 1958.

<sup>3</sup>P. L. Gruzin and G. B. Federov, *Doklady Akad. Nauk S.S.S.R.* **105**, 264-67 (1955).

<sup>4</sup>J. S. Fisher, *J. Appl. Phys.* **22**, 74 (1951).

<sup>5</sup>R. P. Price *et al.*, Battelle Memorial Institute, private communication, March 1958.

<sup>6</sup>W. R. Grimes, private communication, 1956.

which tends to deplete both the  $\text{Cr}^{*0}$  at the surface and the  $\text{Cr}^*\text{F}_2$  in the salt unless  $\text{Cr}^*\text{F}_2$  is added to the system at a rate equal to the diffusion rate.

### Depletion Method

If  $\text{Cr}^*\text{F}_2$  is not added to the salt after time zero, and the subsequent depletion of  $\text{Cr}^*\text{F}_2$  activity in the salt (corrected for time decay) is measured as a function of time, a diffusion coefficient for chromium in the metal may be calculated by means of the following relationship:

$$\frac{b_{t=0} - b_t}{b_{t=0}} = 1 - e^{-a^2 t} \operatorname{erfc}(a\sqrt{t}), \quad (3)$$

where

$t$  = time, sec,

$b_{t=0}$  = counts  $\cdot$  g<sup>-1</sup>  $\cdot$  min<sup>-1</sup> at  $t$  of a filtered salt sample taken at  $t_0$ ,

$b_t$  = counts  $\cdot$  g<sup>-1</sup>  $\cdot$  min<sup>-1</sup> at  $t$  of a filtered salt sample taken at  $t$ ,

$$a = \frac{A}{V} \frac{[\text{Cr}^0]}{[\text{CrF}_2]} \frac{\rho_{\text{metal}}}{\rho_{\text{salt}}} \sqrt{D}, \text{ sec}^{-1},$$

where

$\frac{A}{V}$  = ratio of the salt-exposed area of Inconel to the salt volume, cm<sup>-1</sup>,

$\frac{[\text{Cr}^0]}{[\text{CrF}_2]}$  = weight-fraction ratio of chromium in Inconel to chromous fluoride (as  $\text{Cr}^{++}$ ) in the salt,

$\frac{\rho_{\text{metal}}}{\rho_{\text{salt}}}$  = density ratio of metal to salt,

$D$  = diffusion coefficient, cm<sup>2</sup>/sec.

Equation (3) was used to correlate data from two types of capsule experiments. Isothermal depletions were determined as a function of time in one experiment,<sup>5</sup> whereas depletions as a function of temperature (at identical molten-salt exposure times) were determined in the second type of experiment. The ratio  $A[\text{Cr}^0]\rho_{\text{metal}}/V[\text{CrF}_2]\rho_{\text{salt}}$  was held constant in both cases. The corrected depletions were plotted vs the independent variable measured, and this curve was compared with a

plot of the function  $1 - e^{-u^2} \operatorname{erfc}(u)$  vs  $u$ , where  $u$  was considered to be  $(a\sqrt{t})$ . Values of  $a$  and  $D$  were readily calculated by this method.

### Constant-Potential Method

Initial experimentation indicated that a depletion of the  $\text{Cr}^*\text{F}_2$  content of a melt by a test specimen could be prevented and the  $\text{Cr}^*\text{F}_2$  maintained at a constant concentration during a test if, prior to the test, the molten salt was equilibrated with the relatively large surface of an Inconel container at 900°C and then the temperature was lowered to the test temperature, about 700°C. By this procedure, the Inconel walls acquired a surface concentration of  $\text{Cr}^{*0}$  which, at 700°C, did not diffuse away into the Inconel. The small amounts of  $\text{Cr}^{*0}$  absorbed by the test-metal specimens (Inconel thermocouple wells, 1/4-in. OD) that were subsequently immersed in the salt did not alter the  $\text{Cr}^*\text{F}_2$  concentration of the melt because of the low ratio of test surface to container surface.

The corresponding  $\text{Cr}^{*0}$  transfer equation<sup>7</sup> is

$$\Delta m_{\text{Cr}^{*0}} = 2AC_{\text{Cr}^{*0}} \left(\frac{Dt}{\pi}\right)^{1/2}. \quad (4)$$

The variable  $C$  denotes concentration as g/cm<sup>3</sup>. Rearranging Eq. (4),

$$D = \frac{1}{16\pi t} \left( \frac{y}{z} \frac{[\text{CrF}_2]}{[\text{Cr}^0]} \frac{1}{r h \rho_{\text{metal}}} \right)^2, \quad (5)$$

where

$h$  = height of the immersed specimen,

$r$  = radius of the immersed specimen,

$y$  = total counts of the entire specimen (without alteration) per minute at  $t$ ,

$z$  = counts of the salt per gram-minute at  $t$ ,

$m$  = grams of  $\text{Cr}^{51}$ .

The variable  $y$  is a measure of the total amount of tracer gained by the specimen;  $z$  is an indirect measure of the tracer concentration which is maintained on the specimen surface during immersion.

<sup>7</sup>R. V. Churchill, *Modern Operational Mathematics in Engineering*, 1st ed., p 117, McGraw-Hill, New York, 1944.

Four series of experiments were performed by means of the constant-potential method. Three series involved Inconel specimens which had been subjected to three types of pretreatment conditions, and the fourth series involved INOR-8 specimens. The development and utilization of this method was partially stimulated by the need for tracer-containing alloy specimens for subsequent electropolishing experiments. Specimens from a constant-potential experiment were desirable in this respect as they were related to a convenient set of solutions of the diffusion equations.

**Results**

Over-all coefficients, as a function of temperature and grain size, were obtained from six series of experiments. The experiments could be conveniently grouped according to experimental method, alloy pretreatment, and type of alloy. An outline of the experiments is shown in Table 4.1.

Experimental points for groups I to IV and reported<sup>3</sup> high-temperature values for a similar alloy are plotted on Fig. 4.1. The experimental points for groups V and VI are not shown, since the general appearance, scatter, and slope of a

UNCLASSIFIED  
ORNL-LR-DWG 47491

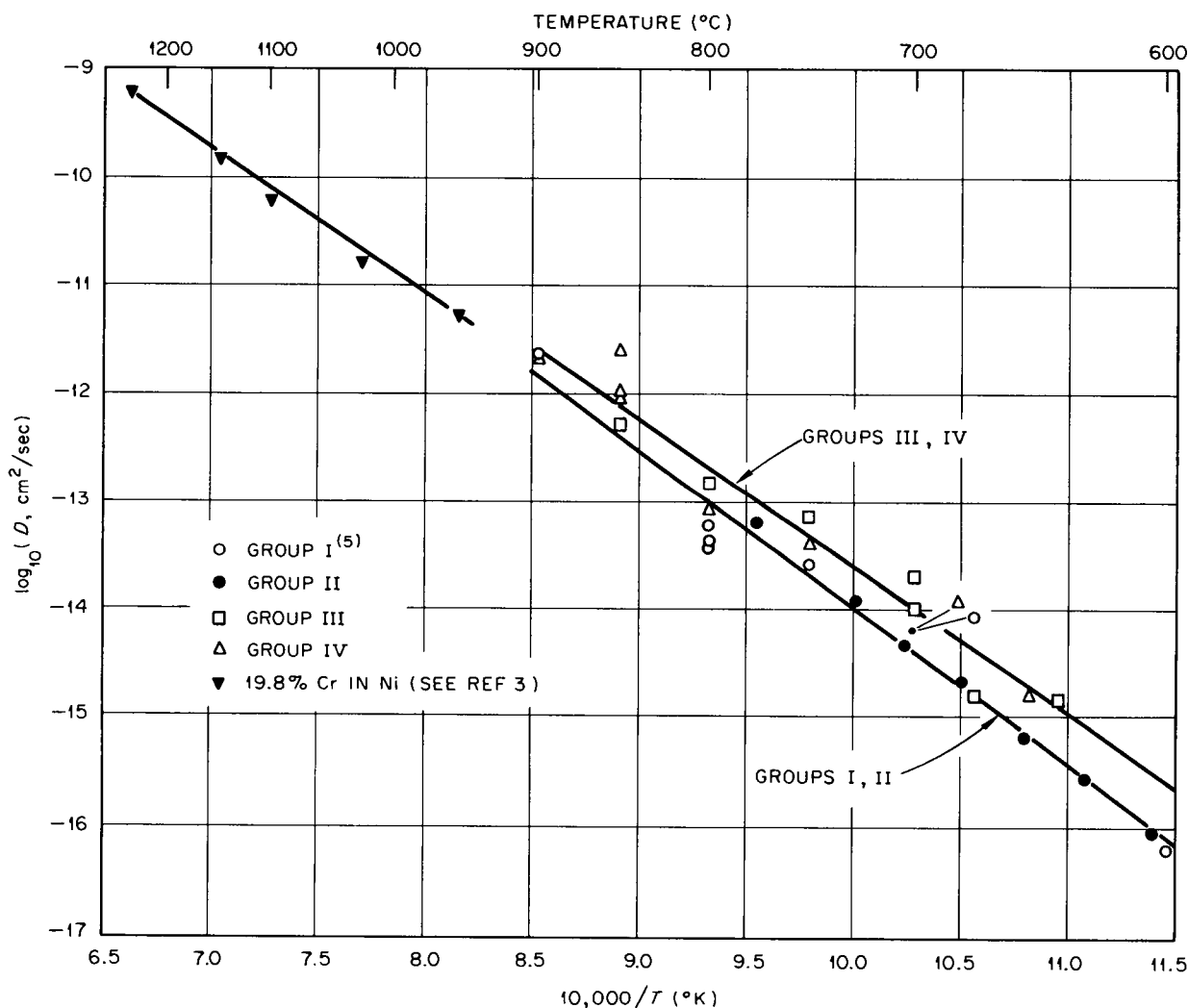


Fig. 4.1. Experimental Results for 1150°C-Annealed Inconel. Over-all coefficients.

Table 4.1. Summary of Experiments to Determine Over-All Diffusion Coefficients

Experiment Group Number	Type of Experiment	Chromium Content of Alloy (wt %)	Solvent Composition (mole %)	Alloy Material and Dimensions	Alloy Pretreatment or Annealing Conditions	Remarks
I	Isothermal capsule (depletion)	16.0	NaF-ZrF <sub>4</sub> (50-50)	Inconel: sides, 3/8-in. tubing; bottom, plate	Welding temperature, then normalized under H <sub>2</sub> for 4 hr at 900°C	Previously uncorrelated data obtained from ref 5 at 3 temperatures
II	Polythermal capsule (depletion)	14.4	NaF-ZrF <sub>4</sub> (53-47)	Inconel: capsules machined from bar stock 3/8-in. OD, 5/16-in. ID, 25/64-in. inside length	Annealed under H <sub>2</sub> for 8 hr at 1150°C	Experiment performed to verify and augment group I results
III	Constant potential	15.2	NaF-ZrF <sub>4</sub> (53-47)	Inconel: 1/4-in. tubing, 0.035-in. wall	Annealed under H <sub>2</sub> for 2 to 4 hr at 1150°C	Several groups of isothermal experiments performed to verify Eq. (4) and to evaluate the experimental method
IV	Constant potential	15.1	NaF-ZrF <sub>4</sub> (53-47)	Inconel: 1/4-in. tubing, 0.035-in. wall	Annealed under He for 2 to 4 hr at 1150°C	Single 1-day exposure time; experiments performed to show effects of H <sub>2</sub> vs He annealing
V	Constant potential	14.8	NaF-ZrF <sub>4</sub> (53-47)	Inconel: 1/4-in. tubing, 0.035-in. wall	Annealed under H <sub>2</sub> for 8 to 12 hr at 800°C	Single 2-week exposure-time experiments performed to show effects of lower annealing temperatures and to provide specimens for electropolishing experiments
VI	Constant potential	7.03	NaF-ZrF <sub>4</sub> (53-47)	INOR-8: 1/4-in. tubing, 0.028-in. wall	Annealed under H <sub>2</sub> for 8 to 12 hr at 800°C	Single 2-week exposure-time experiments performed to obtain preliminary INOR-8 over-all coefficients comparable to Inconel coefficients

plot of these points are very similar to those of Fig. 4.1.

It should be mentioned that an isothermally determined over-all coefficient depends on the measurement, control, or knowledge of ten variables. Seven of these variables are squared in the final equation; also, the coefficient changes approximately 4%/°C at 700°C. The maximum error in any single coefficient could be ±0.4 of a cycle shown on Figs. 4.1 and 4.2. This estimate excludes the effects of grain-size variations.

In view of the over-all precision involved, the most realistic summary of the results might consist of a comparison of the average curves for all

the available data. Such a comparison is presented in Fig. 4.2.

Discussion and Conclusions

A comparison of results obtained with an unannealed Inconel specimen (point A, Fig. 4.2) and those obtained with three annealed specimens (point B, Fig. 4.2) presents a pointed illustration of the effects associated with grain size. Photomicrographs showing the grain size of the actual specimens may be found in Fig. 4.3. All these specimens were exposed to the same pot-salt system at the same temperature. The same trend

UNCLASSIFIED  
ORNL-LR-DWG 47492

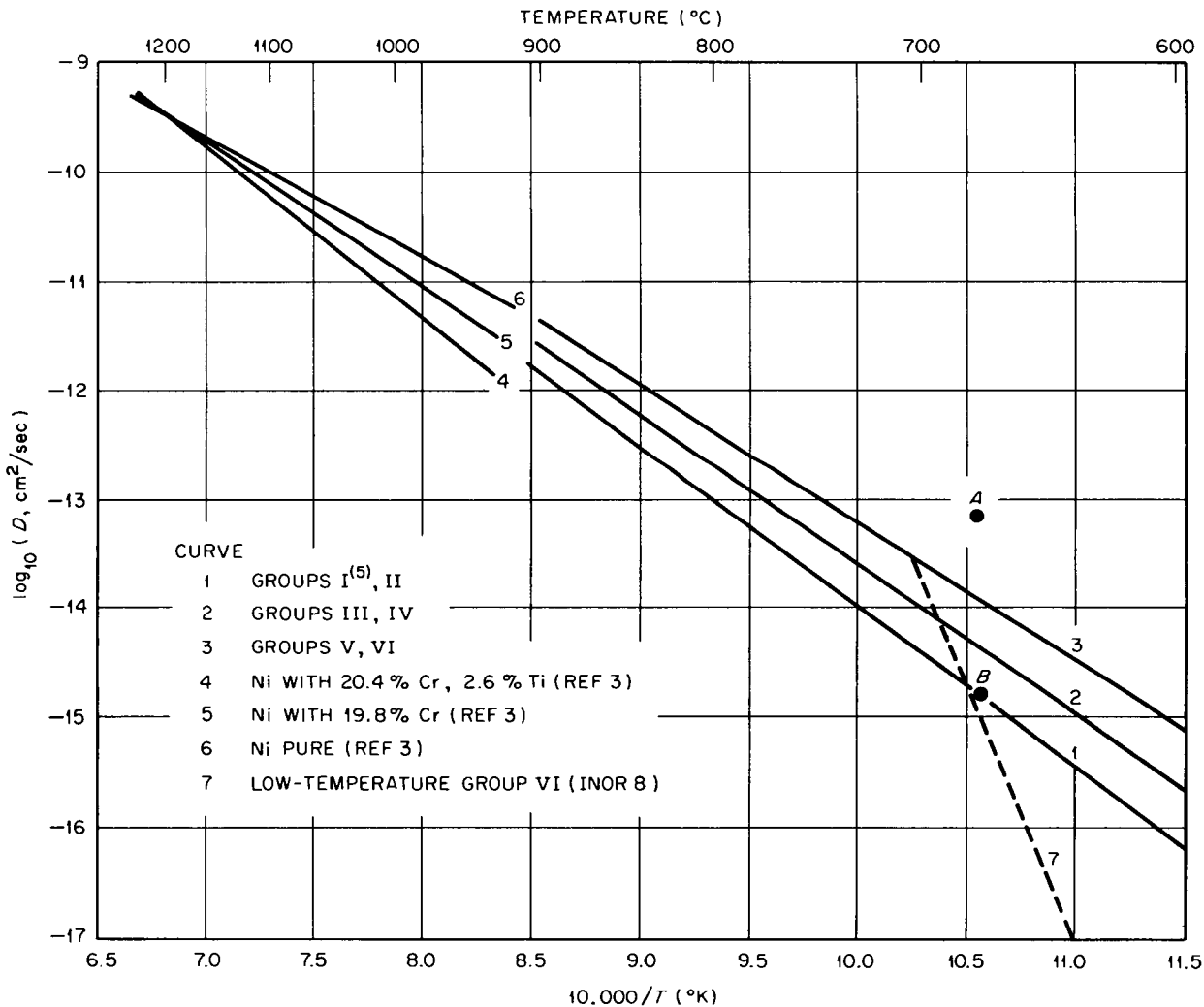
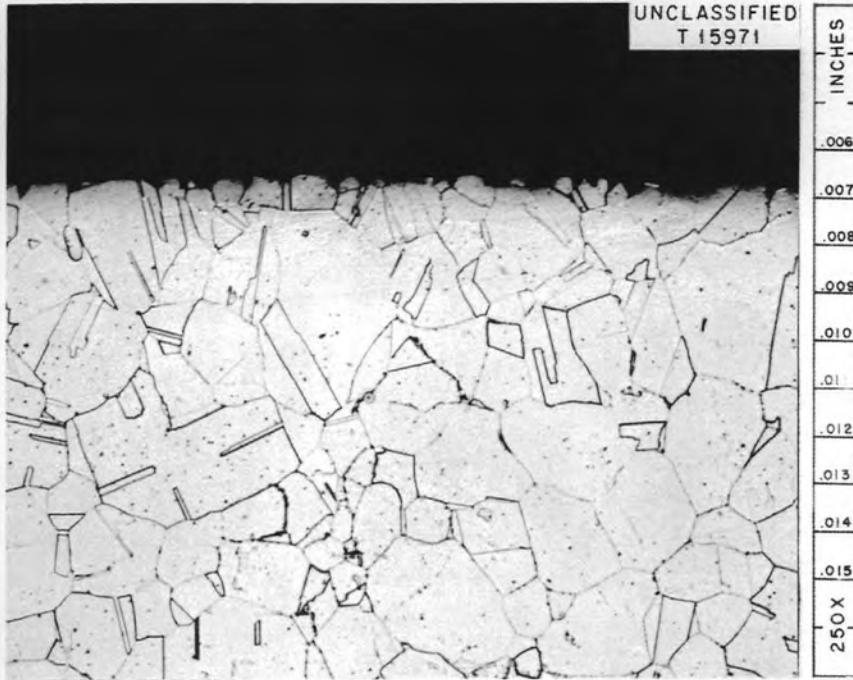


Fig. 4.2. Chromium-51 Diffusion Coefficients in Nickel-Base Alloys. Over-all values.

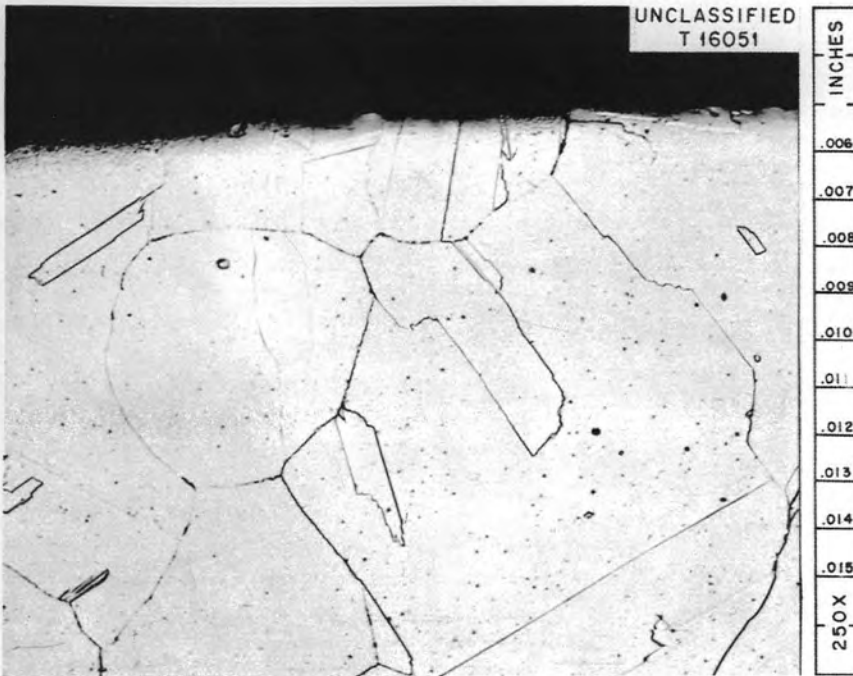
UNCLASSIFIED  
ORNL-LR-DWG 47493



SPECIMEN UNANNEALED  
(POINT A, Fig. 4.2)

$$D = 78 \times 10^{-15} \text{ cm}^2/\text{sec}$$

$T_{\text{SALT}} = 675 \text{ }^\circ\text{C}$  FOR  
BOTH EXPERIMENTS



SPECIMEN ANNEALED  
AT  $1150 \text{ }^\circ\text{C}$  FOR 4 hr

$$D = 1.7 \times 10^{-15} \text{ cm}^2/\text{sec}$$

Fig. 4.3. Photomicrographs of Group III Inconel Specimens After Diffusion Experiments.

was shown by all the results in that increases in the time and temperature of the pretreatment increased the grain size which, in turn, led to a decrease in the over-all coefficient. It was concluded that grain-size effects had a marked influence on the over-all diffusion coefficient.

The above conclusion formed the basis for another interpretation; that is, specimens with the highest number of grains also contained the highest number of "grain boundaries." Accordingly, one might suspect that a certain fraction of the diffusion took place along grain boundaries at temperatures around 700°C.

Thus one would be tempted to think in terms of two coefficients, for example, volume and grain boundary. A treatment of a similar case by Fisher<sup>4</sup> revealed that the time dependence of the penetration relationships would be altered when both mechanisms are combined. Such was not the case in this investigation. The data appeared to follow the equations presented. These equations were based on a single phenomenological coefficient which could be used to represent a homogeneous diffusion process taking place in an isotropic medium.

An encouraging feature of the results shown on Fig. 4.2 is the relatively good agreement between the high- and low-temperature data. A break in the over-all curves indicating a change in mechanism was not found for the Inconel specimens; however, a marked downward trend was noted for the INOR-8 values at temperatures below 700°C. The breaks in other systems (generally obtained from concentration profiles) result in curves with relatively low negative slopes in low-temperature regions.

Coefficients presented in Fig. 4.2 represent alloys with chromium contents ranging from 0 to 20.4 wt %. In view of the precision of the measurements and grain-size effects, it was concluded that the over-all coefficients above 700°C did not depend on the chromium concentration in the alloys. The amount of diffusion did depend on the concentration in a manner predicted by Eqs. (3) and (4).

#### CHROMIUM-51 DIFFUSION COEFFICIENTS FROM ELECTROPOLISHING EXPERIMENTS<sup>8</sup>

**Introduction.** - Practically all the solid-state diffusion data in the literature are based on the

experimental determination of tracer concentration profiles as a function of penetration distance. The experiments differ as to the boundary conditions, tracer placement techniques, and sectioning procedures employed. However, determination of the tracer profile is the basic objective common to all experiments of this type. The profile data are then converted to diffusion coefficients through a knowledge of the proper concentration equations.

It was believed that a series of experiments of this type would constitute an interesting complement to the Inconel experiments discussed in the preceding section of this report. Two estimates of the coefficient for a given specimen would be available. One would be based on the measurement of the over-all amount of tracer which diffused into the specimen under a known surface potential; the second would be based on the tracer concentration profile within the specimen.

#### Experimental Approach

Three major considerations governed the choice of a method for sectioning the tracer-containing specimens. First, very shallow tracer penetrations (very steep tracer concentration vs distance curves) would be involved; second, the operation should be fast and should not require particular skills; finally, the specimens would be cylindrical in shape, as they would originate from capsules, pots, or loops. It appeared that an electropolishing technique would satisfy all these requirements.

Based on the first two requirements mentioned, an integral method<sup>9</sup> was employed to correlate the data. This avoided the necessity of taking a large number of minute "cuts" and of then having to calculate a large number of "average" concentrations. The experiments were conducted as follows: after salt exposure, the specimens were counted, polished, recounted, polished again, etc., until less than 10% of the original count was present. The percentage of total counts remaining after each polishing was plotted as a function of the cumulative penetration distances (wall thickness minus the sum of the polishing increments). The experimental plot was compared with a generalized plot of an equation applicable to this procedure (constant potential, semi-infinite

<sup>9</sup>S. D. Gertsricken and I. Y. Dekhtyar, *Proc. Intern. Conf. Peaceful Uses Atomic Energy, Geneva, 1955* 15, 101 (1955).

<sup>8</sup>With J. H. DeVan, Metallurgy Division, ORNL.

system, initial tracer concentration zero, etc.). The equation is

$$y(x) = 100\sqrt{\pi} \operatorname{ierfc} \theta, \quad (6)$$

where

$$\operatorname{ierfc} \theta = \frac{1}{\sqrt{\pi}} e^{-\theta^2} - \theta \operatorname{erfc} \theta,$$

$y(x)$  = percentage of original activity remaining,

$$\theta = \frac{x}{2\sqrt{Dt}}.$$

Values of Eq. (6) are available in the literature.<sup>10</sup> A detailed description of the apparatus

and procedures used to perform the electropolishing operation may be found elsewhere.<sup>11</sup>

### Results

**Present Investigation.** — Electropolishing experiments were performed on duplicate specimens obtained from 13 separate experiments mentioned in the preceding section (see group V). Of all the constant-potential specimens processed, this series contained the largest amount of tracer at deepest penetrations. The final results are presented on Fig. 4.4 (open circles) immediately

<sup>10</sup>H. S. Carslaw and J. C. Jaeger, *Conduction of Heat in Solids*, 1st ed., p 373, Oxford University Press, New York, 1947.

<sup>11</sup>J. H. DeVan, *An Evaluation of Electro-Machining for the Analysis of Metal Surfaces*, ORNL CF-59-6-109 (June 25, 1959).

UNCLASSIFIED  
ORNL-LR-DWG 47494

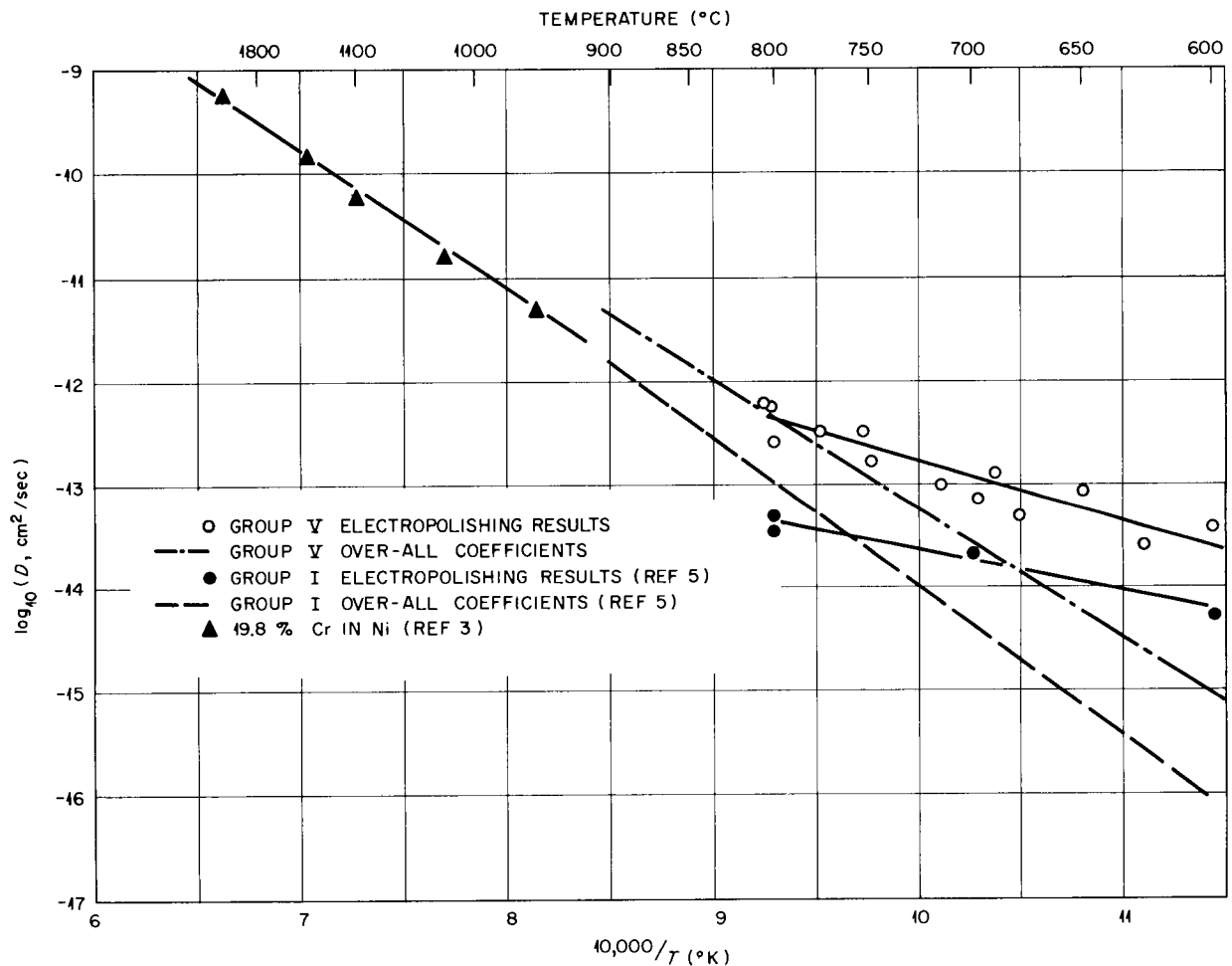


Fig. 4.4. Chromium-51 Diffusion Coefficients for Inconel, Based on Electropolishing Data.

above the average curve, which represents the over-all coefficient obtained with the same specimens. It was interesting to note that the deviations exhibited by these data were faithfully reproduced by the over-all values on the lower curve.

**Battelle Data.** - Electropolishing data submitted by Price<sup>5</sup> are shown on Fig. 4.5. In addition to the 800°C data shown, a meager amount of data was obtained for 700 and 600°C. The capsules

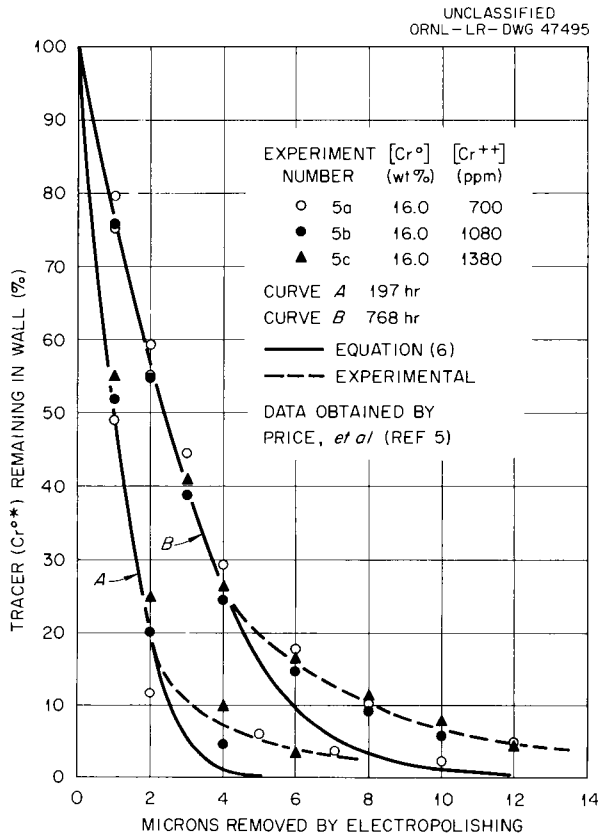


Fig. 4.5. Concentration Profiles in 800°C Depletion Capsules.

used in the over-all depletion experiments served as the electropolishing specimens which led to these results. The rigorous profile equation for a depletion experiment is

$$C(x,t) = C_0 e^{(ax/\sqrt{D}) + a^2 t} \operatorname{erfc} \left( a\sqrt{t} + \frac{x}{2\sqrt{Dt}} \right), \quad (7)$$

where  $a$  is defined in the previous section.

Since the required relationship would involve integration of Eq. (7) with respect to  $x$ , a decision was made to approximate the rigorous solution by means of Eq. (6). Past work had shown that analogous approximations with respect to the over-all transfer equations were acceptable. As it turned out, the approximate equation accurately described a major portion of the experimental profiles (see Fig. 4.5). Coefficients based on the 800°C data are shown in Table 4.2. All the available Battelle data are presented on Fig. 4.4.

**Discussion**

The 800°C data of Table 4.2 are of considerable importance, as the results of two independent series of experiments at this temperature established the equality of coefficients obtained from electropolishing experiments and over-all measurements. It is presently believed that equality of coefficients is a necessary condition for a homogeneous diffusion process.

The values given in Table 4.2 represent the results of three depletion experiments and six electropolishing experiments. The two profile coefficients shown were each obtained from the average of three similar experiments. The number of over-all coefficients available corresponded to the number of capsule experiments (involving several capsules exposed for various times) performed, that is, three. It is important to note that the initial  $[\text{Cr}^+\text{F}_2]/[\text{CrF}_2]$  ratio and the  $A/V$  ratio were identical for all experiments in the 800°C series. Thus profiles for capsules with identical salt-exposure times should be the same if the over-all diffusion equations previously presented and the assumed constant-potential boundary conditions were correct. It appears that these propositions are verified by the proximity of experimental points to the curves on Fig. 4.5.

As indicated by the curves of Fig. 4.4, the long anticipated breaks in the  $\log D$  vs  $1/T$  plots were finally acquired through the profile experiments. A discussion of the differences between the profile curves and curves for companion over-all experiments will be given separately in the next section of this report.

**INTERPRETATION OF THE CHROMIUM-51 DIFFUSION DATA**

It is observed from Fig. 4.4 of the preceding section that, at temperatures less than 800°C, the

"diffusion coefficients" obtained from tracer concentration profiles are higher than those which were based on the total amount of tracer transferred. In order to correlate both kinds of coefficients, it is useful to visualize a diffusion specimen wherein the entire diffusion process occurs in intergranular channels. If it is assumed that all the channels can be grouped together to give a certain fraction,  $f$ , of the bulk volume,  $V_b$ , then  $fV_b$  will be the "active" volume and  $(1 - f)V_b$  will be the "inactive" or dead volume. The next step concerns the selection of a reference coefficient for the active volume.

One of two suitable reference coefficients might be chosen. They are: a bulk coefficient,  $D_b$ , resulting from steady-state diffusion experiments, and a grain-boundary (or channel) coefficient,  $D_g$ , which is based on studies of single grain boundaries. To precisely illustrate the meaning of the two hypothetical coefficients, a numerical example

incorporating both coefficients was prepared. The example involved steady-state diffusion of tracer  $M^*$  through a  $1.5\text{-}\mu$  thick,  $1.025\text{-cm}^2$  cross-sectional-area, metallic membrane of  $10\text{ g/cm}^3$  density,  $10\text{ wt \% M}$ , and a  $0.1$  volume fraction,  $f$ . The membrane contained four active channels with dimensions given in Table 4.3. Both coefficients are based on the same driving force,  $\Delta C$ , as indicated by

$$\frac{\Delta M^*}{\Delta t} = D_g \left( \sum \frac{A}{L_g} \right) \Delta C_{M^*} \quad (8)$$

since

$$C_b = C_g \quad , \quad \text{at } x = 0 \text{ and } L \quad ,$$

and

$$C_b = fC_g \quad , \quad 0 < x < L \quad .$$

Subscript  $b$  refers to bulk values; subscript  $g$

Table 4.2. Comparison of Diffusion Coefficients for  $\text{Cr}^{*0}$  In Inconel at  $800^\circ\text{C}$

Data from Price *et al.* (ref 5)

According to $\text{Cr}^{*0}$ Concentration Profiles (See Fig. 4.5)		According to $[\text{Cr}^{*++}]$ Depletion	
Salt Exposure Time (hr)	$D$ ( $\text{cm}^2/\text{sec}$ )	$[\text{Cr}^{*++}]$ (ppm)	$D$ ( $\text{cm}^2/\text{sec}$ )
	$\times 10^{-14}$		$\times 10^{-14}$
197	3.47	700	4.25
768	4.75	1080	6.22
		1380	4.21

Table 4.3. Channel Parameters for Hypothetical Membrane

Channel Number	Length ( $\mu$ )	Area ( $\text{cm}^2$ )	Volume ( $\text{cm}^3$ )	$A/L$ ( $\text{cm}$ )
		$\times 10^{-2}$	$\times 10^{-6}$	
1	3.0	2.50	7.500	83.3
2	1.5	1.25	1.875	83.3
3	2.0	1.75	3.500	87.5
4	5.0	0.50	2.500	100.0
		$NA_g = 6.00$	$NV_g = 15.735$	$\Sigma(A/L) = 264.1$

refers to channel or grain-boundary values. For the example,  $D_g$  and  $\Delta C_{M^*}$  were assumed to be  $2 \times 10^{-10}$  cm<sup>2</sup>/sec and (10 g/cc) (0.1) (1.0 - 0.2) ( $10^{-8}$ ) respectively. The weight fractions were  $1.0 \times 10^{-8}$  and  $2.0 \times 10^{-9}$  at the surfaces. The corresponding rate was  $4.23 \times 10^{-16}$  g/sec. The bulk coefficient was obtained through the relationship

$$D_b = D_g \left( \frac{L_b}{A_b} \right) \sum_{i=1}^N \left( \frac{A_g}{L_g} \right)_i, \quad (9)$$

with the assumed  $D_g$  and membrane dimensions given in Table 4.3. The  $D_b$  value was  $7.73 \times 10^{-12}$  cm<sup>2</sup>/sec, which is considerably lower than the  $D_g$  value.

In many instances it will be very difficult to obtain individual  $A/L$  values which are necessary for the utilization of a true  $D_g$ . However, a model  $D_g$  or  $(D_g)_{\text{model}}$  may be estimated by visualizing a parallel series of channels with equal lengths and areas. With the example values for  $NA_g$ ,  $A_b$ ,  $f$ , and  $D_b$  and the equations

$$NA_g L_g = f A_b L_b, \quad (10a)$$

$$ND_g \frac{A_g}{L_g} = \frac{D_b A_b}{L_b}, \quad (10b)$$

which describe the model, a  $(D_g)_{\text{model}}$  value of  $2.255 \times 10^{-10}$  cm<sup>2</sup>/sec was obtained. This value is in very good agreement with the original value of  $2.0 \times 10^{-10}$  cm<sup>2</sup>/sec.

The foregoing example demonstrates that utilization of the model  $D_g$  would require information as to the average internal geometry of the diffusion media. This is not required for  $D_b$ . Nevertheless, reasonable estimates of channel behavior ( $D_g$ ) can be made through  $D_b$ , since large errors are not introduced by the model when reasonable channel-size distributions are involved. Accordingly,  $D_b$  was selected as the reference coefficient for present interpretations.

The active-volume concept implies that tracer does not accumulate in the dead volume. Thus Fick's law, from which equations describing the experiments are developed, must be modified such that

$$D_b \frac{\partial^2 C^*}{\partial x^2} = f \frac{\partial C^*}{\partial t}. \quad (11)$$

Applicable boundary conditions are

$$\lim_{x \rightarrow \infty} C^*(x,t) = 0, \quad (12a)$$

$$C^*(x,0) = 0, \quad (12b)$$

$$C^*(0,t) = C_0^*, \quad (12c)$$

which lead to a solution

$$C^*(x,t) = f C_0^* \operatorname{erfc} \frac{x}{2\sqrt{D_b t/f}}. \quad (13)$$

The corresponding equations for over-all tracer transfer,  $\Delta M^*$ , and fraction tracer remaining after electropolishing,  $y$ , are

$$\Delta M^* = 2AC_0^* \sqrt{\frac{D_b f t}{\pi}} \quad (14)$$

and

$$y = \sqrt{\pi} \operatorname{ierfc} \frac{x}{2\sqrt{D_b t/f}}. \quad (15)$$

These equations are compatible with the data, in that the basic form of the time-dependence curves corresponding to Eq. (14) and the shape of the polishing profiles of Eq. (15) are not altered by the introduction of  $f$ . Furthermore, "low" over-all coefficients are predicted by  $D_b f$  and "high" polishing coefficients by  $D_b/f$ . From the data and based on the present interpretation, values of  $D_b f$  and  $D_b/f$  were measured during the experiments. Thus

$$D_b = \sqrt{D_{\text{over-all}} D_{\text{polish}}} \quad (16)$$

and

$$f = \sqrt{\frac{D_{\text{over-all}}}{D_{\text{polish}}}}. \quad (17)$$

The term "grain-boundary diffusion," as it is generally used, refers to the portion of the electropolishing curves which we have ignored, that is, the residual 5 to 15% of the total tracer transferred which undergoes comparatively deep penetration.

This interpretation applies to 85 to 95% of the material normally classified as "volume" diffusion. We submit that this fraction of the transferred tracer follows selective diffusion paths

given by  $fV_b$ . Further, the value of  $f$  is unity at approximately 800°C for chromium in Inconel and decreases markedly with temperature reductions below 800°C.

5. PURIFICATION AND HANDLING OF MOLTEN SALTS IN QUANTITY

J. E. Eorgan      F. A. Doss      G. J. Nessle  
 J. Truitt          C. R. Croft

PURIFICATION OF  $\text{LiF}\text{-BeF}_2\text{-UF}_4$   
 MOLTEN SALTS

As the Molten Salt Reactor concept matured, it was logical to make use of the equipment and technical experience gained from the ANP Program in the processing of molten salts for reactor use. The MSR, however, required a salt composition involving  $\text{LiF}$  and  $\text{BeF}_2$  rather than  $\text{NaF}$  and  $\text{ZrF}_4$ . Because of this difference, and the greater difficulty of obtaining these new compounds in the required state of purity, changes in production processing were inevitable.

Because of the fact that beryllium was involved in these operations, extensive facility modifications had to be initiated to meet safety and industrial hygiene requirements. All facilities handling  $\text{BeF}_2$  were completely enclosed and filtered ventilation systems installed. Continuous monitoring of the atmosphere and working surfaces was carried out by the Health Physics Group to detect any abnormal release or spread of beryllium during operations. During this past year, approximately 1500 kg of  $\text{BeF}_2$ -based molten salts have been processed in these facilities and never has the beryllium concentration in the atmosphere or on the working surfaces exceeded or reached the tolerances set by the Industrial Hygiene Department.

A schematic diagram of the equipment is shown as Fig. 5.1. All portions of the equipment which contacted the molten salt were of nickel or copper, while gas lines, etc., were of copper. The reaction vessel, transfer line, and receiver assembly are shown in Fig. 5.2. For the 250-lb batches of  $\text{ZrF}_4$  13-in.-dia vessels were used. The reactors are 72 in. long, while the receivers are 24 in. long. The reaction vessels are fabricated from  $\frac{1}{4}$ -in.-thick stainless steel (300 series); they contain a loosely fitting cylindrical copper liner which holds the molten charge. The same construction is used for equipment handling 50-lb batch sizes. However, for the smaller batch sizes fabrication is accomplished through use of nickel pipe with no liners. The receiver vessels are fabricated from "A" nickel in all cases. Transfer lines are of  $\frac{3}{8}$ - or  $\frac{1}{2}$ -in.-dia tubing of "A" nickel.

Connections to and through the reaction vessel and receiver are made by means of Swagelok fittings welded to risers on these vessels or through bolted flanges gasketed with copper. The filters and samplers shown in Fig. 5.3 are 3 in. in diameter and fabricated from nickel. The filter medium was sintered nickel of 0.0015-in. pore diameter. The reactor and receiver are heated by commercial resistance furnaces of 50 and 25 kw, respectively, which could accommodate 15-in.-dia cylinders. Furnace liners of stainless steel protected the furnace elements from the melt in case of accidental spills or rupture of the equipment. All valves, gages, and electrical controls for the process are combined into a single control panel as shown in Fig. 5.4.

The raw materials, in batches of proper composition, were blended and charged into the reaction vessel. Prior to heating, the mixtures were purged of entrapped air by successive use of vacuum and helium gas. The salts were then melted under an atmosphere of anhydrous  $\text{HF}$  to remove  $\text{H}_2\text{O}$  with a minimum of hydrolysis. When the mixture melted, hydrogen was bubbled through the melt. At the same time the melt temperature was raised to  $1500^\circ\text{F}$ . This treatment served to reduce  $\text{U}^{5+}$  to  $\text{U}^{4+}$ , sulfur compounds to  $\text{S}^{--}$ , and extraneous oxidants ( $\text{Fe}^{+++}$ , for example) to lower valence

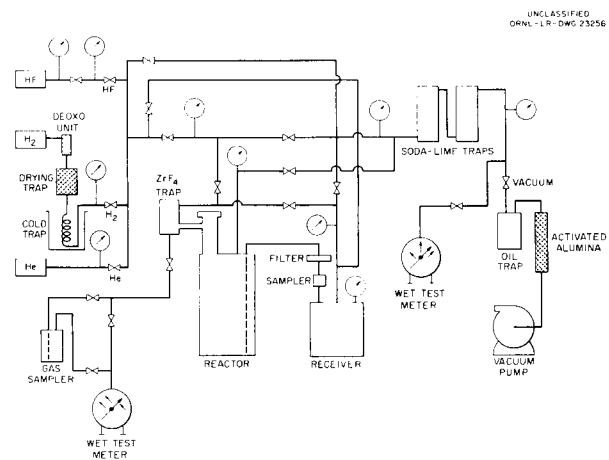


Fig. 5.1. Fluoride Preparation Apparatus Piping Diagram.

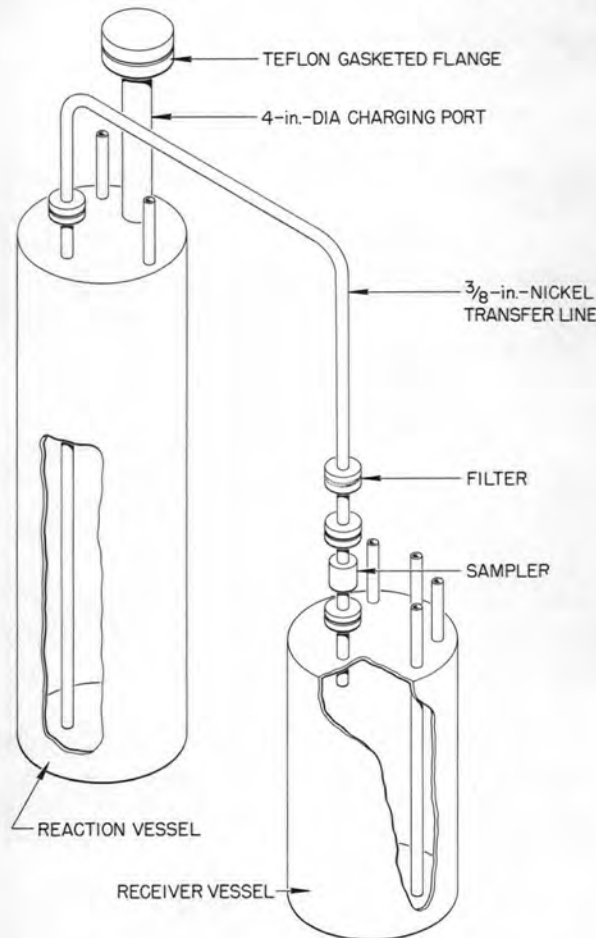
UNCLASSIFIED  
ORNL-LR-DWG 20157

Fig. 5.2. Apparatus for Purification of Fluoride Mixtures.

states. The hydrogen and all subsequent reagent gases were fed at about 4 liters/min to the reaction vessel through the molten charge. After 1 hr the hydrogen was replaced by anhydrous HF which served, during a 2 to 3 hr period at 1500°F, to volatilize  $H_2S$  and  $HCl$  and to convert oxides and oxyfluorides of uranium and beryllium into fluorides at the expense of the accumulation of considerable  $NiF_2$  or  $CuF_2$  in the melt through reaction of HF with the container. A final 24- to 36-hr treatment at 1500°F with  $H_2$  sufficed to reduce these contaminating metal fluorides and the contained  $FeF_2$  to insoluble metals.

The period of final hydrogen stripping varied with the purity of raw materials charged to the system. The process was monitored simply by

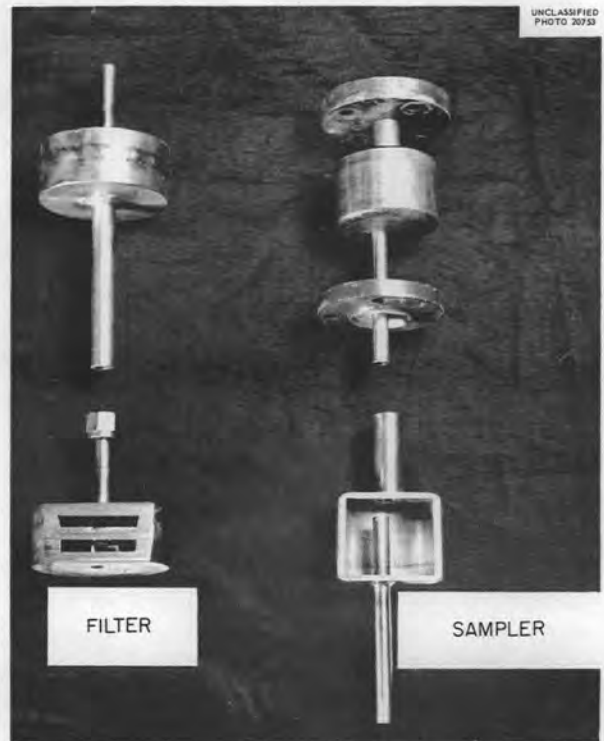


Fig. 5.3. Molten-Salt Filters and Samplers.

measuring the HF concentration of the hydrogen leaving the system. Measured quantities of the exit hydrogen were bubbled through standard aqueous solutions of boric acid. Boric and hydrofluoric acids are "weak" but fluoboric acid is "strong." Accordingly, measurement of conductivity of the resulting solution served to evaluate the quantity of HF absorbed. A batch was considered pure when the HF concentration in the exit hydrogen dropped below  $10^{-4}$  moles/liter. Subsequent chemical analyses were used to check the product purity before use.

The two most serious problems encountered were the oxide content of the  $BeF_2$  and the sulfur content of both  $BeF_2$  and  $LiF$ . The  $BeO$  impurity rapidly formed  $UO_2$  from the  $UF_4$ ; hydrofluorination of this  $UO_2$  took place at a very slow pace. Since the uranium was a minor constituent of the fuel composition ( $\sim 6\%$  by weight), losses of nearly 50% of the added uranium often occurred during the processing. This problem was ultimately resolved by hydrofluorination of the binary  $LiF-BeF_2$  prior to addition of the  $UF_4$ .

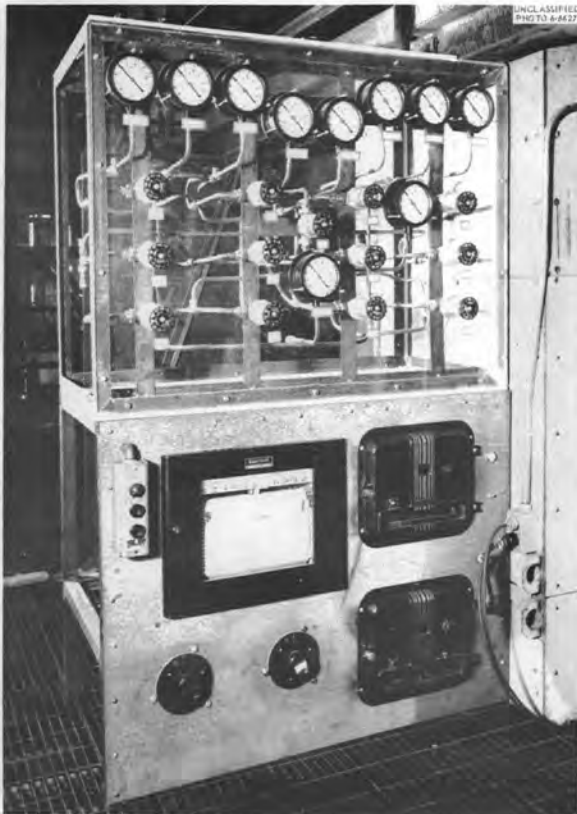


Fig. 5.4. Molten-Salt Purification Control Panel.

The large amounts of sulfur present (mostly as  $\text{SO}_4^{--}$ ) required extended hydrogen reduction and hydrofluorination for complete removal. As a result, processing time for this type of salts is nearly double that required for  $\text{ZrF}_4$ -based salts.

At the conclusion of the purification treatment a pressure of helium above the salt in the reactor vessel forced the melt through the transfer line, with its filter and sampler, into the receiver vessel. The metallic  $\text{Fe}^0$  and  $\text{Ni}^0$  were left in the reactor vessel or on the sintered nickel filter.

The purified melt was permitted to freeze under an atmosphere of helium in the receiver vessel. By appropriate manipulation of connections and valves, the cold receiver was detached and removed to storage while the helium atmosphere was maintained over the contents.

The melts were stored in the nickel receiver vessels on a manifold containing helium at 10 psig to ensure that no air or water vapor could contaminate the purified salt during storage.

The molten-salt compositions which were processed ranged from 0.5 to 120 kg in batch size; processing of salts for in-pile testing, containing  $\text{Li}^7$  and  $\text{U}^{235}$ , was included.

After the fuel has been processed and stored, the next problem is to be able to charge a nuclear reactor or some testing equipment without lowering the quality of the fuel. Of main concern in this regard is the protection of the fuel from exposure to air at all times. It has been demonstrated that molten salts, when serving as a flux for the corrosion of structural metals (such as Inconel, nickel, and stainless steel) by air at high temperatures, can cause penetration of a  $\frac{1}{4}$ -in. plate in a few hours.

Actually all manipulations necessary for transferring the molten salt into a test rig have been employed in the processing of the fuel. Molten salt at about  $300^\circ\text{F}$  above its melting point can be transferred with unheated  $\frac{3}{8}$ -in.-OD transfer lines several feet long as shown in Fig. 5.5. Where transfer lines are necessarily longer than 10 ft, heated lines are used as in Fig. 5.6.

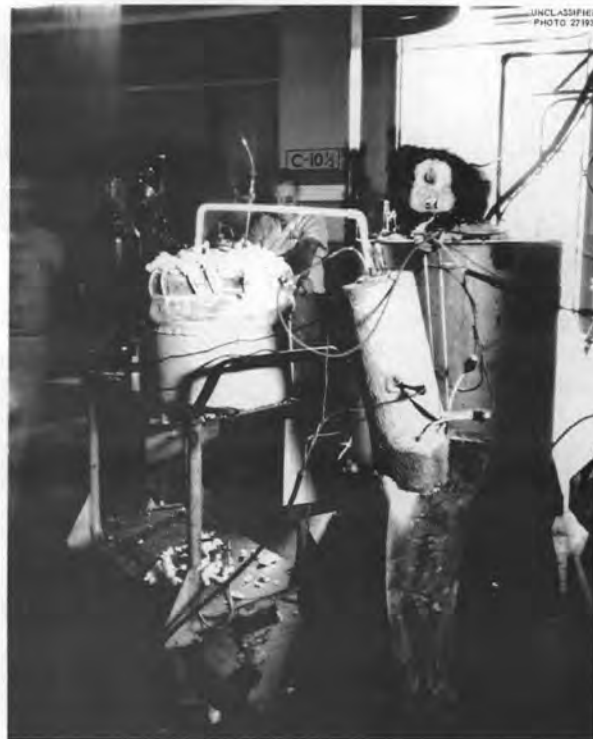


Fig. 5.5. Molten-Salt Transfer Lines.

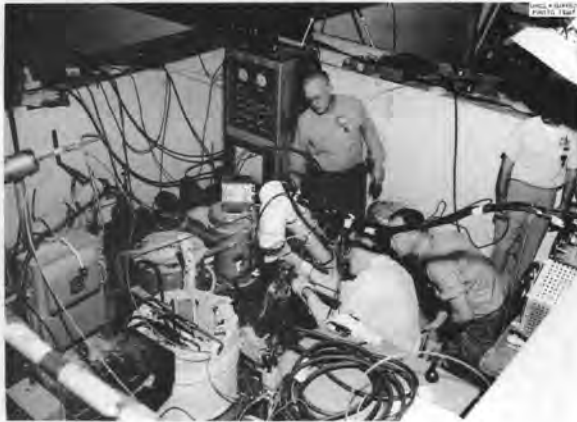


Fig. 5.6. Molten-Salt Heated Transfer Lines.

Precautions must be taken to prevent freezing of the salt in transfer lines or small diameter portions of test systems, since the thermal expansion on remelting of the salt will often result in ruptures. There seems to be some dependency on the size and shape of the apparatus as to whether remelting of the salt in a frozen section will cause a rupture. The large storage cans, for instance, have been subjected to melting and freezing cycles several times with no apparent damage, while pipes or tubing sections sometimes burst in spite of extreme care in remelting.

Due to the fact that large amounts of HF are evolved when this type fuel is exposed to moist air, good ventilation is necessary where large spills can occur.

Handling techniques are somewhat restricted because the use of valves in molten-salt flow lines is cumbersome. Simple valves for these temperatures and conditions are not yet available. Therefore, moving the molten salt from one container to another is accomplished by careful adjustment of differential pressures. Techniques have been perfected, in this regard, which permit filling the test rigs accurately to desired levels. Each time a salt batch is transferred from a storage container to a test unit, or to another container, "thief" samples of the molten salt are taken to allow continual monitoring of the salt purity. Whenever an engineering test unit is terminated, either permanently or temporarily, samples of the contained salt batch are taken for chemical analysis.

In several cases special sampling devices have been installed on test units to allow sampling

under operating conditions at specified time intervals. The graph shown in Fig. 5.7 is a plot of the chromium content of a salt batch being circulated in a forced flow corrosion test loop operating with a large temperature gradient. The loop is fabricated from INOR-8 and the salt composition is  $\text{LiF-BeF}_2\text{-ThF}_4\text{-UF}_4$  (62.0-36.5-1.0-0.5 mole %). After the steady-state equilibrium concentration of chromium is attained, any drastic change in concentration would indicate trouble. Thus, chemical control is added to the mechanical control of a loop operation.

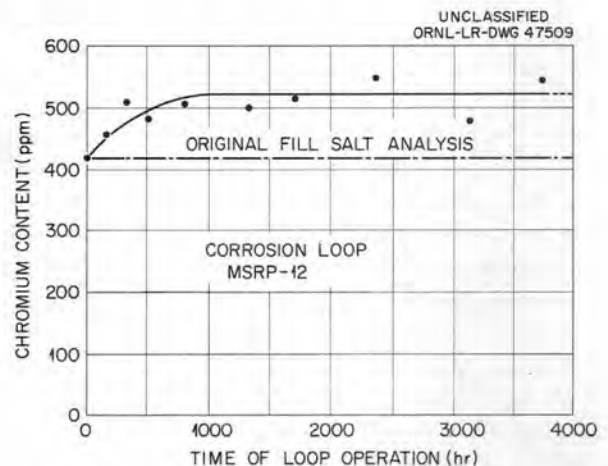


Fig. 5.7. Chromium Content of Molten Salt in Forced Flow with Large Temperature Gradient.

#### Techniques for Sampling and Enriching Molten-Salt Compositions

A device was designed to allow sampling of reactor fuel during operation and addition of  $\text{U}^{235}$  at periodic intervals to compensate for uranium burnup. A simple test unit incorporating the main features of this device was constructed and tested. An original proposal called for addition of the uranium as a binary salt of high uranium concentration. However, it later appeared probable that  $\text{UF}_4$  could be melted and cast in acceptable shapes to allow much easier handling and storage, and that the dissolution of  $\text{UF}_4$  in the molten salt would be rapid enough to satisfy operating conditions. To test this belief,  $\text{UF}_4$  was melted and cast into graphite molds in slugs weighing 20 to 40 g. These slugs were found to be very stable, easily weighed, and could be handled in the open atmosphere. The test unit was designed so that

## REACTOR CHEMISTRY PROGRESS REPORT

the uranium could be added at one end and the salt sampled at the other. Fifteen slug additions were made to a nonuranium LiF-BeF<sub>2</sub> (50-50 mole %). It was concluded that the entire slug dissolved in the molten salt in a matter of minutes, and it was found that the calculated uranium concentration of the salt agreed very well with the results of chemical analyses of the samples taken after each addition.

### SERVICE WORK FOR OTHER PROGRAMS

Considerable amounts of ZrF<sub>4</sub>-based fluoride salts are required by the Chemical Technology Division for use in their development and testing programs. Because the Reactor Chemistry Division "inherited" the capabilities for processing and handling large amounts of these salts from previous experience, it was found practical to continue this service. During the past year approximately 2000 kg of various salt compositions involving NaF, ZrF<sub>4</sub>, UF<sub>4</sub>, and LiF have been dispensed to the Chemical Technology Division for use in their experiments. At the present some 1500 kg of similar compositions are on order and are being processed as time permits.

Most of the service work performed for the GCR Program involves specialized handling of liquid metals in cooperation with the Experimental Engineering Group of the Reactor Projects Division. There have been a few instances of bulk usage of molten salts for special heat-transfer and heat-capacity studies. Because of experience in handling liquid metals, the Reactor Chemistry

Division was asked to develop a procedure for filling in-pile test capsules with NaK, where the quantities involved ranged from 30 to 100 cc and the accuracy of loading was set at  $\pm 1$  cc. The operation was unique in that the fill line to the capsule was  $\frac{1}{8}$ -in.-ID metal tubing approximately 20 ft in length which had to empty at the completion of the fill, and the operation was a "one-shot" procedure, since no provision was made for removing any excess NaK in case of an over-fill. By special adaptation of an x-ray unit with a closed-circuit television system, which allowed viewing of the filling operation, and a specially designed filling unit, a standard filling procedure was developed which has permitted some 30 successful filling operations during this past year. Other tests involving instrumentation development and physical property studies pertinent to the GCR have required larger quantities of NaK and Na. These operations are more nearly standard in requirements and are easily handled. General service work of this nature will undoubtedly be maintained for the GCR as long as such services are necessary.

Relatively small amounts of various types of molten-salt compositions are supplied to the Metallurgy Division for use in alloy development testing programs and graphite-molten-salt compatibility studies in connection with the MSR Program.

Because of experience in handling liquid metals the Reactor Chemistry Division has been called on by other divisions for advice and actual assistance on problems involving the handling and disposal of these metals.

## 6. GRAPHITE COMPATIBILITY

## PERMEATION OF GRAPHITE BY MOLTEN SALTS

R. J. Sheil	G. J. Nettle
R. B. Evans	C. R. Croft
G. M. Watson	F. F. Blankenship

The molten-salt reactor is presently designed to be graphite moderated. Although graphite is inert to fluoride fuel mixtures, the permeation of graphite is a matter of concern.

Reactor-grade AGOT graphite was known to be quite porous and susceptible to penetration by the molten salts. Experiments were initiated to determine whether this graphite could be pre-impregnated with a high-melting, inert salt [ $\text{LiF-MgF}_2$  (67.5-32.5 mole %)] to such an extent as to prevent penetration by reactor fuel salt components. The impregnation was accomplished by degassing the graphite at  $900^\circ\text{C}$  under 100  $\mu$  (or less) pressure and while holding the graphite samples at these conditions submerging them in the molten salt. With the graphite completely submerged, a helium pressure of 15 psig was applied. The pressure was then relieved and the graphite removed from the salt and cooled at 2 psig of helium. By weighing the graphite rods before and after this treatment it was determined that impregnation of the graphite was complete or nearly complete in every case. Analysis of machine cuttings of these rods showed that the  $\text{LiF-MgF}_2$  salt had penetrated uniformly to the center of the rods. However, on soaking these impregnated rods with various proposed fuel mixtures containing  $\text{LiF-BeF}_2\text{-ThF}_4\text{-UF}_4$ , it was found that the fuel components penetrated deeper and in greater quantities than in rods receiving no prior impregnation.

Consequently, the compatibility studies shifted to testing the penetration of AGOT-grade graphite in proposed molten-salt fuels at varying conditions of time, temperature, and pressures. Pressure was recognized as the most important factor and a lower limit of 50 psig was set as a possible reactor operating pressure. An extensive series of recent tests was carried out under 60 psig. At this pressure and at an upper limit temperature of  $1300^\circ\text{F}$ , AGOT-type graphite was nearly completely impregnated by the proposed molten salts.

By using AGOT graphite as a reference material, with the above pressure and temperature, an

extended testing program of various high-density, low-permeability graphite is being carried out to determine which graphites would be suitable for reactor use in a molten-salt environment. A listing of several graphites tested in this manner is given in Table 6.1. Preliminary calculations indicate that 1% (by weight) pickup of the fuel by the graphite might be tolerated. If this is so, several types of graphite are now available. The remaining problems are determination of radiation damage and fabrication of a selected graphite into the desired shapes.

Table 6.1. Permeation of Various Grades of Graphite with Typical Molten Fluoride Fuel Salts

Type Graphite	Weight Pickup (%)
AGOT	21
TSF	20
R-0013	10
ATL-82	6.2
S-4	4.6
CEY (special)	1.0
RLM-24-CEY	0.2
21-CT-158	- 0.1
18-CT-158	- 0.1
GT-123	$\pm 0.1$

In addition to the static tests, the absence of deleterious effects in flowing systems was established by an experiment which involved exposing 31 samples of GT-123-82 National Carbon Co. impervious graphite rod to molten  $\text{LiF-BeF}_2\text{-UF}_4$  (62-37-1 mole %) in a pumped corrosion test loop at  $1300^\circ\text{F}$  for a period of one year.<sup>1</sup>

The  $\frac{1}{2}$ -in. and  $\frac{3}{16}$ -in. by 11-in. graphite rods were inserted in an INOR-8 box into a pump loop<sup>2</sup> operated by the Metallurgy Division and the Experimental Engineering Section. After sealing

<sup>1</sup>R. J. Sheil, R. B. Evans III, and G. M. Watson, *Molten Salt Compatibility Test Results of Physical and Chemical Measurements*, ORNL CF-59-8-133 (Aug. 31, 1959).

<sup>2</sup>J. L. Crowley, *MSR Quar. Prog. Rep. Jan. 31, 1958*, ORNL-2474, p 27.

the box and degassing the graphite under vacuum for 24 hr at 1100°F, argon was admitted to the system before charging it with molten salt. A helium pressure of 3 psig was maintained and the salt was circulated at a rate of 1.1 gpm, resulting in a total pressure of 13 psig at the graphite. After a one-year period, the salt was drained and the samples removed for physical testing and chemical analyses. Possible changes in dimensions, weight, and chemical composition were sought.

The samples for chemical analyses were obtained by machining off successive  $\frac{1}{32}$ -in. layers from the cylinders until a core of less than  $\frac{3}{16}$  in. in diameter was left. After grinding to -100 mesh, the samples were analyzed for uranium and beryllium. As indicated in Table 6.2 the samples showed only a slight migration of the salt into the graphite. The uranium and beryllium concentrations in the graphite were between 0 and 170 ppm. The average uranium concentration in the samples was about 15 ppm. The average beryllium content of the samples was about 93 ppm. The uranium contents were fairly constant along the radius with higher values in the center and on the surface, while the beryllium concentrations exhibited more fluctuation still indicating the same trend. No macroscopic changes were detected on the graphite rods and the weight losses, averaging about 0.02%, can be attributed to the desorption of residual gases. The average cross-sectional shrinkage of about  $\frac{1}{2}$  mil was within the probable error of the measurements. The salt did not adhere to the graphite on any of the specimens.

#### INTERCALATION OF FISSION PRODUCTS WITH GRAPHITE

B. J. Sturm      F. F. Blankenship

Nuclear reactors are being considered in which the molten fuel is to be in direct contact with graphite moderator, therefore, the possible effect of fission products on the graphite is of concern. Some molten salts deprecipitate graphite by forming intercalate compounds.<sup>3</sup>

Most of the fission elements form stable fluorides which have been included in melts in graphite

crucibles in the course of other investigations in the Reactor Chemistry Division. There have been no indications of intercalation with, or other damaging effects on, the graphite. In the reactor the more noble metals would be expected to exist as free elements and, therefore, should not intercalate.

When treated with liquid  $\text{MoF}_5$  or  $\text{MoF}_6$ , the graphite swelled to form intercalate compounds; however, molybdenum fluorides are not likely to exist in the reactor.<sup>4</sup> Graphite was treated with commercial  $\text{K}_2\text{NbF}_7$  at about 800°C,  $\text{LiI}$  at about 700°C, and  $\text{LiI}$  with 10%  $\text{LiBr}$  at about 550°C without any indication of intercalation.

Intercalate compounds of salts with graphite tend to decompose at high temperatures; therefore, the high temperature of the fuel during operation of the reactor may also discourage the formation of intercalate compounds with the fission products. Consistent with this idea, a high-melting  $\text{NaCl-FeCl}_3$  (70:30) mixture did not attack graphite at 750°C, even though pure  $\text{FeCl}_3$  at 300°C readily intercalated.

#### ADSORPTION OF XENON ON GRAPHITE

M. C. Cannon<sup>5</sup>      W. T. Ward

The adsorption of xenon from xenon-helium mixtures on bulk reactor-grade graphite was determined. The volume of xenon adsorbed was measured at xenon partial pressures between 1 and 100 mm Hg at -79, 0, 20, 30, and 80°C.

The apparatus used for the xenon adsorption experiments is shown in Fig. 6.1. The method used to measure the adsorption of xenon on graphite was to circulate a xenon-helium gas mixture through a graphite cylinder enclosed in an Inconel pot. The gas mixture was circulated through the periphery of the graphite cylinder. The pressure drop on the outside of the cylinder walls was to about 2 cm above the static pressure, and inside the wall the drop was to 1 cm below. Adsorption pressure was assumed to be equal to the static pressure. The gas was circulated for 15 min and equilibrated for 45 min, repeating the cycle 4 to 5 times before sampling the gas mixture for analysis. The gas samples were analyzed by

<sup>3</sup>W. Rudorff, in *Advances in Inorganic Chemistry and Radiochemistry* (ed. by H. J. Emeleus and A. G. Sharpe), p 223-66, vol I, Academic Press, New York, 1959.

<sup>4</sup>*MSR Quar. Prog. Rep. Oct. 31, 1959, ORNL-2890, p 66.*

<sup>5</sup>Summer participant, 1959.

Table 6.2. Analyses of Machine Cuttings from Graphite Rods

Rod No.	Cutting No.	PPM		Theoretical* U/Be	Actual U/Be
		U	Be		
8	1	30	125	0.573	0.240
	2	9	175		0.051
	**	10	< 1		
11	1	22	125		0.176
	2	10	110		0.091
14	1	24	75		0.320
	2	28	105		0.267
23	1	17	125		0.136
	2	< 1	60		0.017
	**	5	< 1		
18	**	8	< 1		
	1	50	170		0.294
	2	15	130		0.115
	3	15	125		0.120
	4	12	100		0.120
	5	10	65		0.154
	6	13	105		0.124
	7	< 1	50		0.020
	8	13	140		0.093
	9	5	165		0.030
	10	< 1	< 1		1.000
	11	6	105		0.057
	12**	< 1	< 1		
Center	100	125		0.800	
31	**	5	< 1		
	1	20	165		0.121
	2	18	140		0.129
	3	24	120		0.199
	4	20	85		0.235
	5	20	75		0.267
	6	20	80		0.250
	7	17	55		0.310
	8	< 1	80		0.013
	9	< 1	95		0.011
	10	< 1	< 1		1.000
	11	< 1	90		0.011
Center	70	170		0.411	
**	< 1	< 1			

\*Based on chemical analysis of original salt batch, nominally  $\text{LiF}\cdot\text{BeF}_2\cdot\text{UF}_4$  (62-37-1 mole %).

\*\*Samples machined from "as received" material.

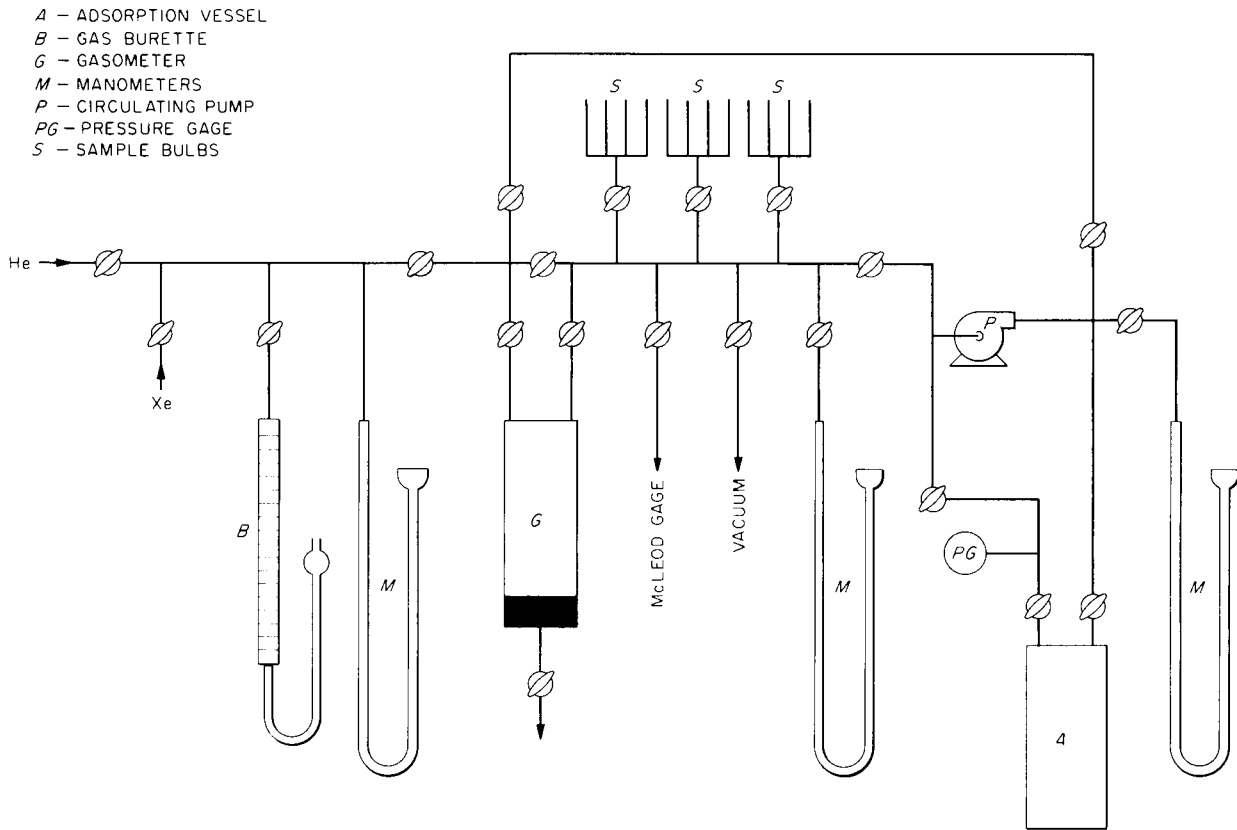


Fig. 6.1. Adsorption Apparatus.

the Mass Spectrograph Laboratory. Any residual gas on the graphite surface was eliminated by evacuating the system and heating the graphite cylinder to 800°C between runs.

As Fig. 6.2 indicates the volume of xenon adsorbed on graphite is a function of the temperature and the partial pressure of the gas. A comparison of the points obtained for the adsorption of pure xenon with those for xenon-helium mixtures shows no composition dependence for the adsorption. The amount of xenon adsorbed on graphite decreases substantially with increasing temperature; hence only a small volume of gas should be adsorbed in the graphite at the operating temperature of the molten-salt thermal breeder reactor. At 50 mm Hg xenon partial pressure the volume of xenon gas adsorbed on graphite is  $1.5 \times 10^{-3}$  cc (STP) per gram of graphite at 80°C.

This indicates that only a small poisoning effect can be attributed to the xenon adsorbed on graphite at the operating temperature of the molten-salt thermal breeder reactor. The adsorption is physical and is not a function of the mixture composition.

#### Extrapolation to Reactor Temperatures

If the experimental data obtained at 0 and 80°C is plotted in the form of isosteres ( $\log P$  vs  $1/T$ ) and extrapolated to higher temperatures, isotherms at 500 and 750°C may be constructed from the extrapolated values as shown in Fig. 6.3.

It would appear from these curves that at temperatures of 500 to 750°C the adsorption of xenon on AGOT graphite would be less than  $1 \times 10^{-5}$  cc (STP) per gram at a xenon partial pressure of 1 mm Hg and approximately  $3 \times 10^{-5}$  cc/g at 10

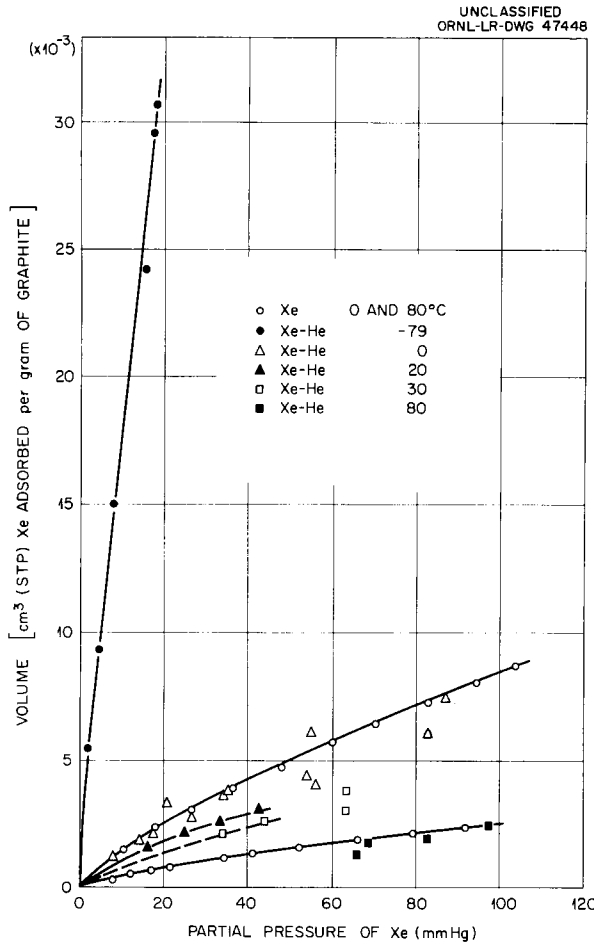


Fig. 6.2. Adsorption of Xenon on AGOT Graphite.

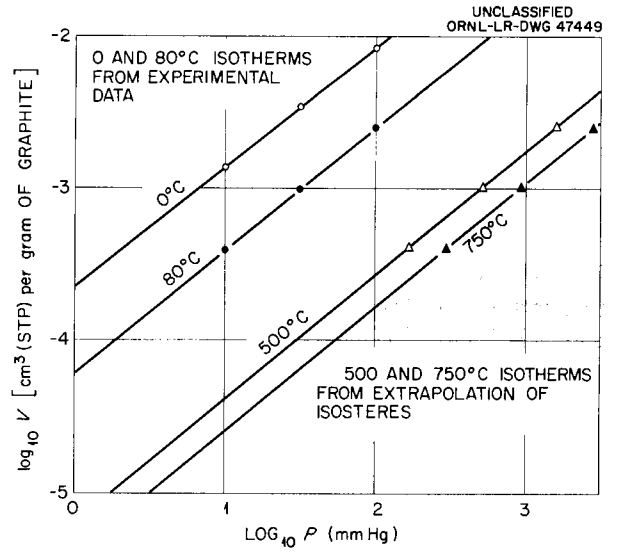


Fig. 6.3. Xenon Isotherms on AGOT Graphite.

mm Hg. The length of the extrapolation should be kept in mind when considering the validity of these values.

#### Heat of Adsorption

The heat of adsorption of xenon on graphite calculated from the isosteres ranged from 3500 to 3700 cal/mole, compared with a heat of vaporization as given by Peters and Weil<sup>6</sup> of 3270 cal/mole. This close agreement indicates that the adsorption is physical.

<sup>6</sup>K. Peters and K. Weil, *Z. physik. Chem.* A148, 1 (1930).

7. EFFECT OF RADIATION ON STATIC CORROSION OF STRUCTURAL MATERIALS BY FUSED-SALT FUELS

W. E. Browning

H. L. Hemphill

TESTS OF GRAPHITE COMPATIBILITY WITH FUSED SALTS UNDER IRRADIATION

Two fuel-filled graphite capsules were irradiated in the MTR at 1250°F for 1610 and 1492 hr, respectively, at integrated power densities of 1520 and 1375 kwhr/cm<sup>3</sup>. These graphite capsules,

illustrated in Fig. 7.1, were enclosed in Inconel containers and filled with the fuel mixture LiF-BeF<sub>2</sub>-UF<sub>4</sub> (62-37-1 mole %). Examinations have indicated that the graphite was unaffected by irradiation while exposed to the fuel mixture. The graphite was wetted by fuel in the irradiated capsules, but was not wetted in similar unirradiated

UNCLASSIFIED  
ORNL-LR-DWG 30083

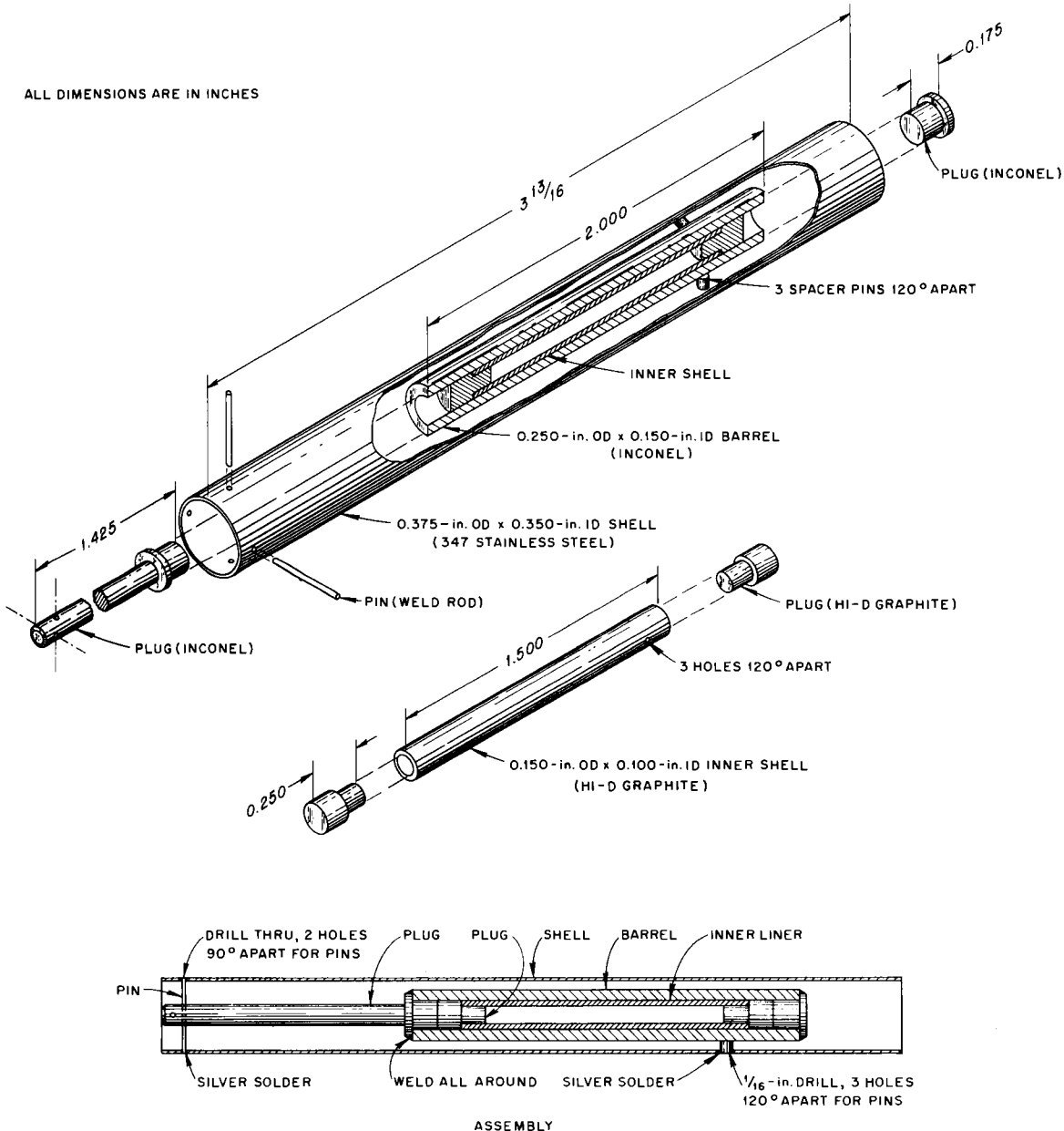


Fig. 7.1. Graphite-Fused-Salt Capsules for Irradiation in the MTR.

control capsules. A section through one of the irradiated capsules is shown in Fig. 7.2, and Fig. 7.3 shows a similar view of an unirradiated control capsule that had been held for 3389 hr at 1250°F. The irradiated fuel dissolved more rapidly in water used in cleaning than did the unirradiated fuel.

These results suggest that use of a fuel-cooled graphite moderator might not be limited by short-term damage to the graphite.

#### IN-PILE STATIC CORROSION TESTS

Two fused-salt capsules were exposed in the MTR for 5500 hr, the longest fused-salt in-pile exposure to date. The two capsules are made of INOR-8 and contain the fused salt  $\text{Li}^7\text{F}-\text{BeF}_2-\text{U}^{235}\text{F}_4$  (62-37-1 mole %). The capsules were exposed at 1250°F and at an initial power density of 1200 w/cc. It is estimated, based on flux and duration of exposure, that approximately 75% of the  $\text{U}^{235}$  was consumed by fission. The capsules were removed when one of them released

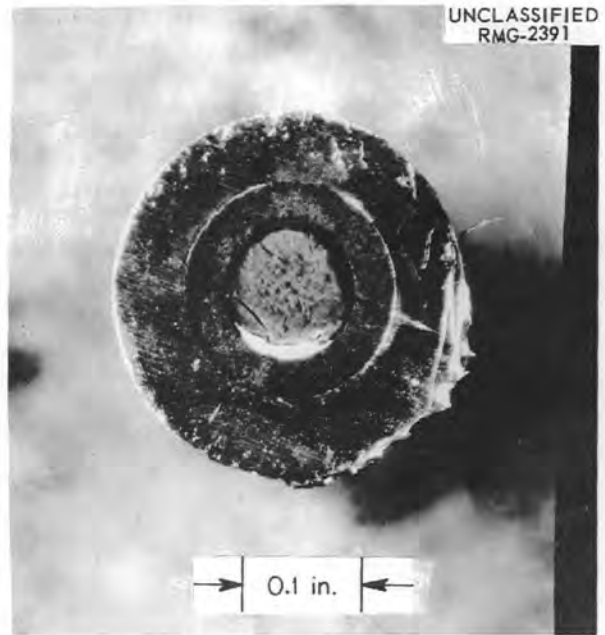


Fig. 7.2. Section of Irradiated Graphite-Fused-Salt Capsule.

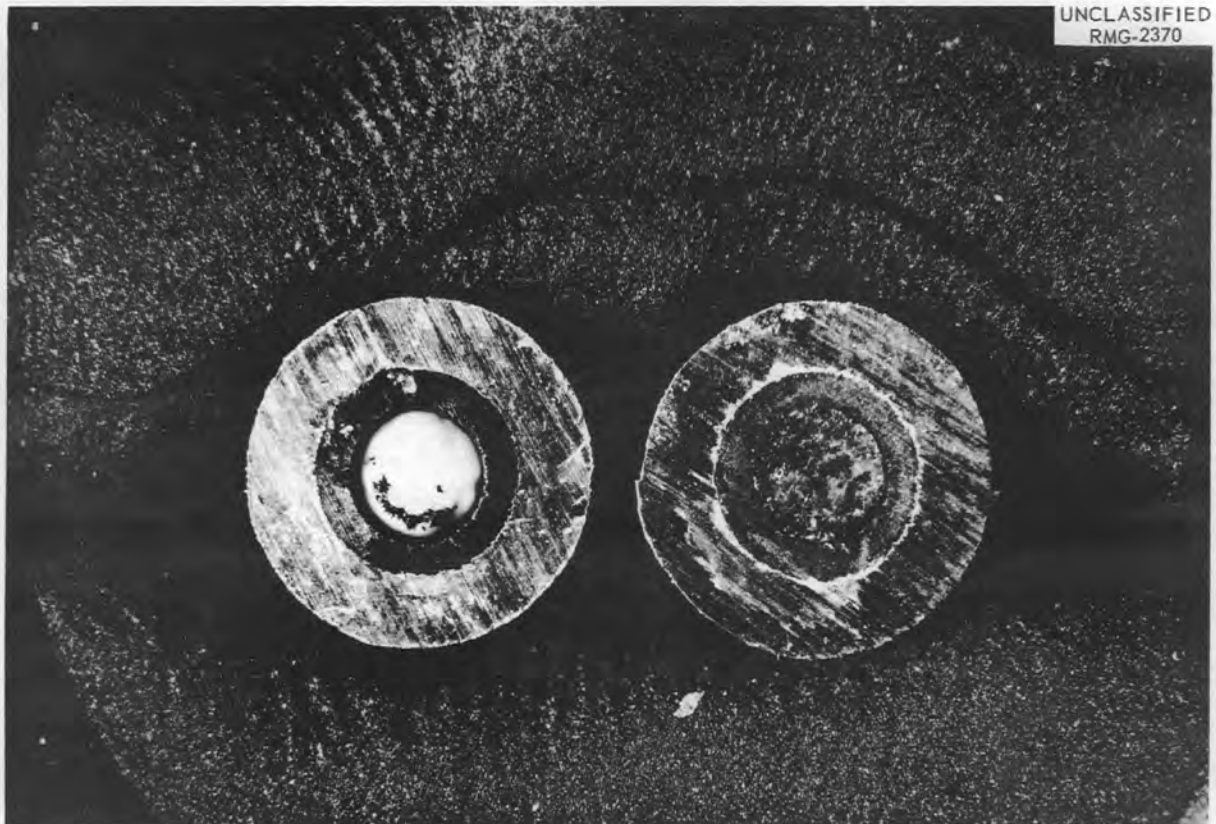


Fig. 7.3. Section of Control Graphite-Fused-Salt Capsule.

## REACTOR CHEMISTRY PROGRESS REPORT

radioactive gas. These capsules will be subjected to metallographic examination to determine the extent of corrosion.

Forty-seven fused-salt capsules have been tested in the MTR with a combined exposure time of 32,200 hr, or 3.67 years. The average irradiation time for these capsules was 685 hr. Most of them were made of Inconel, contained zirconium-based

fluoride fuel, and were exposed at 1500 or 1600°F. The amount of corrosion observed by metallographic examination was considered negligible and was the same as that observed for control experiments operated under the same conditions but in the absence of radiation. Four of these capsules contained beryllium-based fused salt and were exposed at 1250°F for an average duration of 3500 hr.

## 8. REACTIONS IN MOLTEN SALTS

RARE-EARTH FLUORIDE SOLUBILITIES  
AND EXCHANGE REACTIONS

R. A. Strehlow	G. M. Watson
W. T. Ward	W. R. Grimes

Measurements were made of some rare-earth fluoride solubilities in compositions containing  $\text{BeF}_2$  as part of a continued series of investigations on the solubility relations of selected fission product compounds in potentially useful molten-salt fuel compositions. Information derived from this work is of use in determining the potential value of precipitation techniques for processing molten fuels to decrease the concentration level of certain neutron absorbing elements such as samarium and europium as well as to provide assurance that precipitation will not occur in a fuel stream. A discussion of the methods employed and the earlier results may be obtained by referring to the published accounts of earlier work.<sup>1-4</sup>

The solubility of  $\text{CeF}_3$  was determined in a mixture composed of  $\text{NaF-LiF}$  eutectic (40-60 mole %) to which had been added varying amounts of  $\text{BeF}_2$ . The solubility at  $600^\circ\text{C}$  as a function of solvent composition is shown in Fig. 8.1, where it may be compared with those reported previously<sup>1</sup> for the  $\text{LiF-BeF}_2$  and the  $\text{NaF-BeF}_2$  systems. It is interesting to note that the minimum solubility for all these systems occurred at compositions of the solvent which contain about 63 mole % alkali fluoride. Data at several temperatures are shown in Fig. 8.2.

The solubilities of  $\text{CeF}_3$ ,  $\text{LaF}_3$ , and  $\text{SmF}_3$  were determined both singly and in pairs in a solvent composed of  $\text{LiF-BeF}_2\text{-UF}_4$  (62.8-36.4-0.8 mole %). Their behavior in this solvent was similar to that

encountered in the  $\text{NaF-ZrF}_4\text{-UF}_4$  solvent reported previously.<sup>2</sup> Plots of solubility as a function of temperature in both solvents are shown in Fig. 8.3. One of the points of similarity is the fact that when two rare-earth fluorides are present the precipitating phase is a solid solution of the rare-earth fluorides, and the total solubility lies between the solubility curves found when only one rare-earth fluoride is present. Examples of this are shown in Figs. 8.4 and 8.5. Small amounts of  $\text{UF}_4$  in the  $\text{LiF-BeF}_2$  solvents were found to have very little effect on the solubility of  $\text{CeF}_3$  (see Fig. 8.6).

The work was extended to compositions with greater thorium and uranium contents. The solubility of  $\text{CeF}_3$  was determined in two solvents relatively rich in  $\text{ThF}_4$  and/or  $\text{UF}_4$ . In the thorium-containing solvent two independent series of determinations involving different total amounts of  $\text{CeF}_3$  were made (one series of determinations was performed by J. Truitt), the results indicating

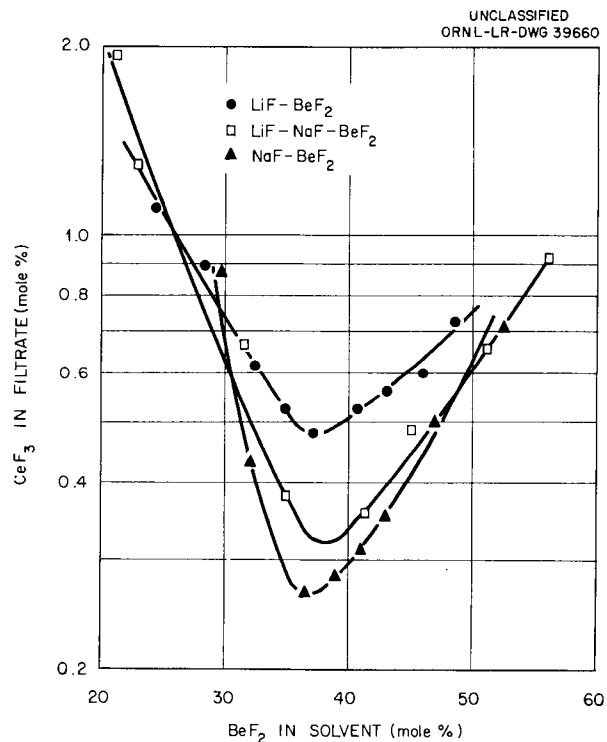


Fig. 8.1. Comparison of  $\text{CeF}_3$  Solubility (mole %) in  $\text{LiF-BeF}_2$ , in  $\text{LiF-NaF-BeF}_2$ , and in  $\text{NaF-BeF}_2$  at  $600^\circ\text{C}$ .

<sup>1</sup>W. T. Ward, R. A. Strehlow, and G. M. Watson, *Chem. Ann. Prog. Rep.* June 20, 1958, ORNL-2584, p 82.

<sup>2</sup>W. T. Ward et al., *Solubility Relations Among Some Fission-Product Fluorides in NaF-ZrF<sub>4</sub>-UF<sub>4</sub>* (50-46-4 mole %), ORNL-2421 (Jan. 15, 1958).

<sup>3</sup>W. T. Ward et al., *Solubility Relations Among Rare-Earth Fluorides in Selected Molten Fluoride Solvents*, ORNL-2749 (Oct. 13, 1959).

<sup>4</sup>W. R. Grimes et al., *Chem. Eng. Progr., Symposium Ser.* 55(27), 65 (1959).

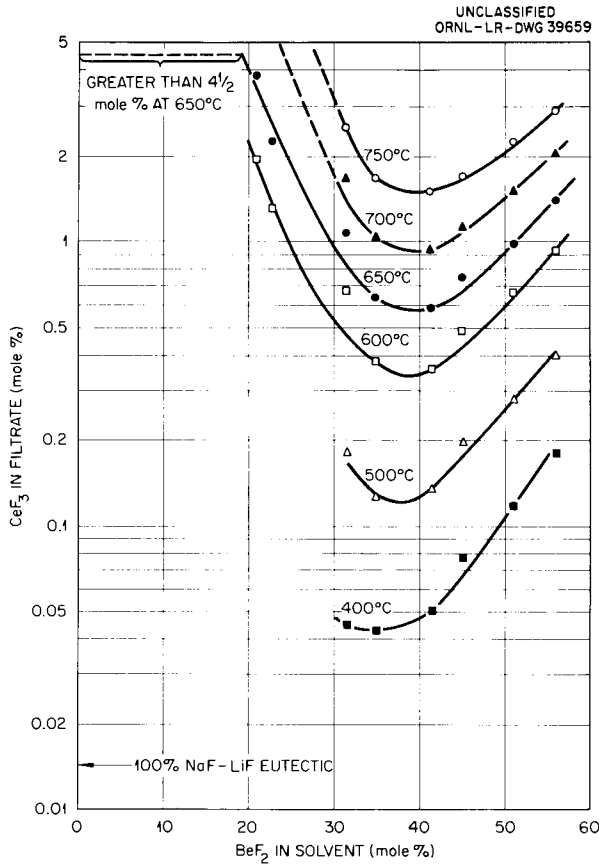
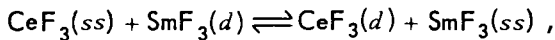


Fig. 8.2. Solubility (mole %) of  $CeF_3$  in NaF-LiF- $BeF_2$  Solvents.

that the solubility of  $CeF_3$  is independent of the amount present. Solubility data for both solvents is summarized in Table 8.1 and is shown graphically in Fig. 8.7. It may be seen that the solubility in both of these solvents is higher than in LiF- $BeF_2$  (63-37 mole %). This would be expected on the basis of the higher LiF/ $BeF_2$  ratio.

The fact that the rare-earth fluorides form solid solutions in the molten fluoride mixtures studied suggests the reprocessing scheme of precipitating out the high cross-section rare-earth fission products ( $SmF_3$ ,  $GdF_3$ , and  $EuF_3$ ) by replacing them with  $CeF_3$ . The equation representing a single equilibrium stage for the extraction of a poison (e.g.,  $SmF_3$ ) from the solvent by a solid (e.g.,  $CeF_3$ ) is



where (d) indicates that the rare-earth fluoride

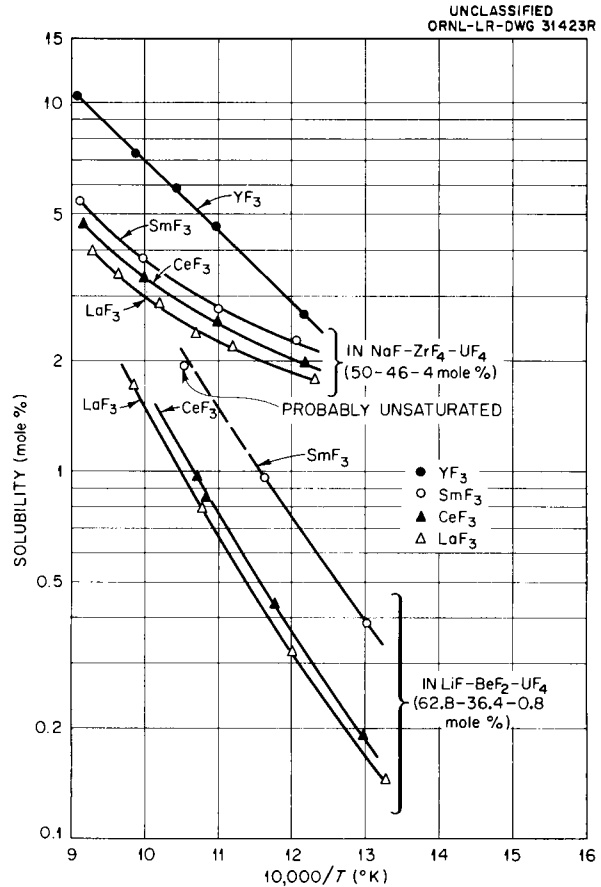


Fig. 8.3. Solubility of Some Fission Product Tri-fluorides in Molten Fluoride Fuels.

is dissolved in the solvent and (ss) that it is in solid solution. With suitable restrictive conditions the equilibrium constant for this reaction can be shown to be approximately equal to a simple solubility ratio:

$$K = \frac{N_{CeF_3(d)} N_{SmF_3(ss)}}{N_{SmF_3(d)} N_{CeF_3(ss)}} = \frac{S_{CeF_3}^0}{S_{SmF_3}^0} ,$$

where  $N$  is the mole fraction of the given species in the specified phase and  $S^0$  is the mole fraction of the given species in a saturated solution in the absence of the other rare-earth fluoride, all at the same temperature.

To demonstrate the feasibility of this exchange an experiment was performed in which a few parts per million of radioactive labeled  $SmF_3$  was dissolved in LiF- $BeF_2$ - $UF_4$  (62.8-36.4-0.8 mole %).

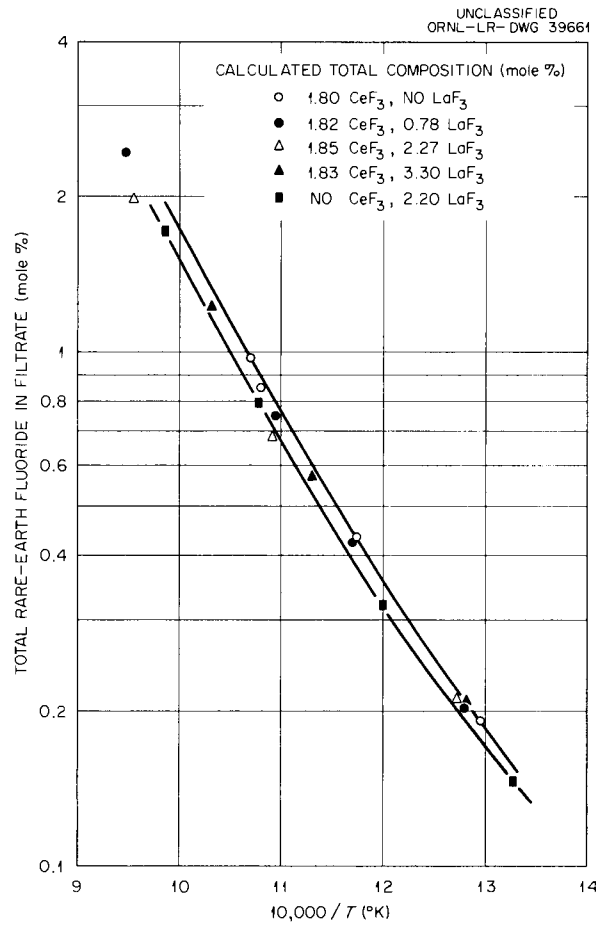


Fig. 8.4. Solubility of CeF<sub>3</sub> and of LaF<sub>3</sub> (Separately and Mixed) in LiF-BeF<sub>2</sub>-UF<sub>4</sub> (62.8-36.4-0.8 mole %).

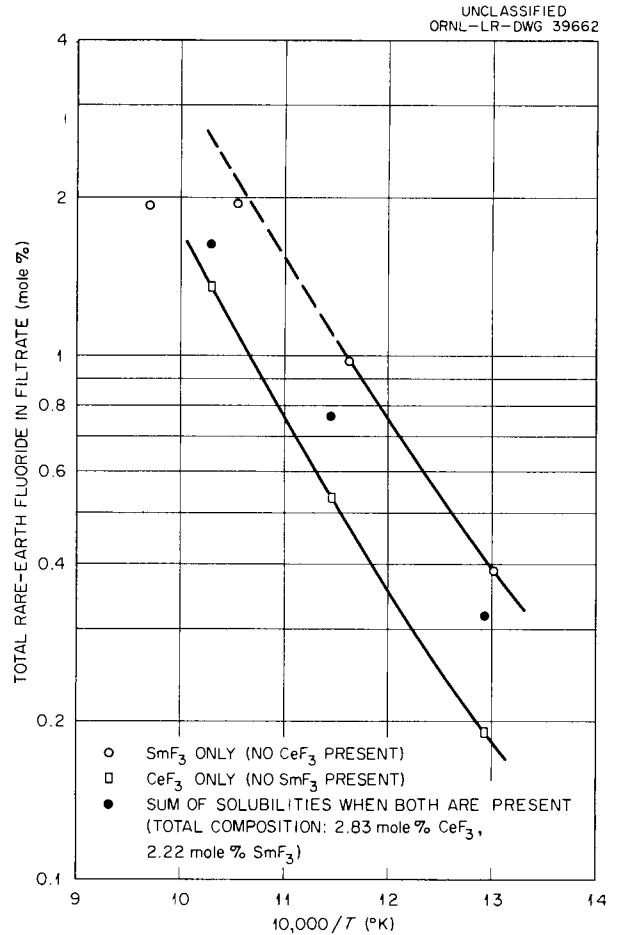


Fig. 8.5. Solubility of CeF<sub>3</sub> and of SmF<sub>3</sub> (Separately and Mixed) in LiF-BeF<sub>2</sub>-UF<sub>4</sub> (62.8-36.4-0.8 mole %).

Table 8.1. Solubility of CeF<sub>3</sub> in LiF-BeF<sub>2</sub>-UF<sub>4</sub> (73-6-21 mole %) and in LiF-BeF<sub>2</sub>-ThF<sub>4</sub>-UF<sub>4</sub> (72-15.5-11.5-1 mole %)

Temperature (°C)	CeF <sub>3</sub> Solubility in LiF-BeF <sub>2</sub> -UF <sub>4</sub>		CeF <sub>3</sub> Solubility in LiF-BeF <sub>2</sub> -ThF <sub>4</sub> -UF <sub>4</sub>	
	Weight %	Mole %	Weight %	Mole %
700	7.8	3.6	9.0	3.1
600	3.9	1.8	4.4	1.5
500	1.9]	0.86	2.05	0.68

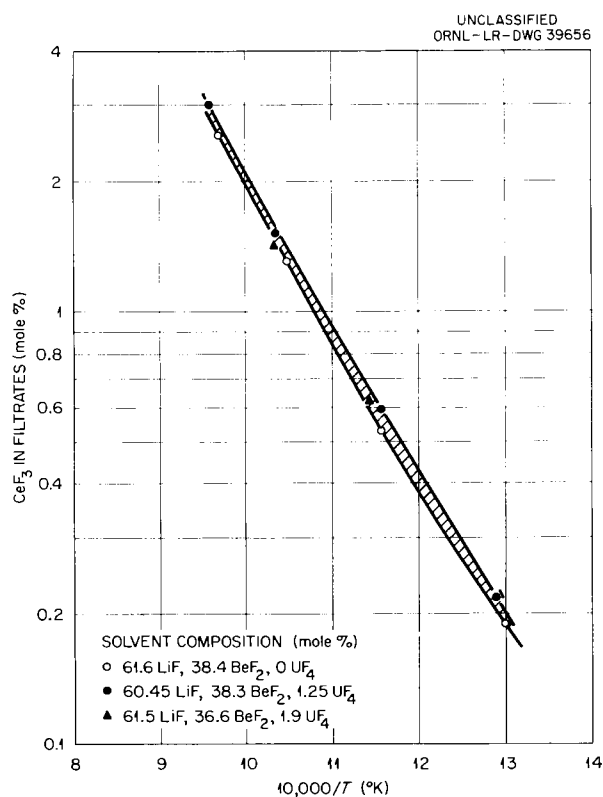


Fig. 8.6. Effect of  $UF_4$  on Solubility of  $CeF_3$  in LiF- $BeF_2$  (62-38 mole %). Solvent composition calculated from filtrate analyses (average values).

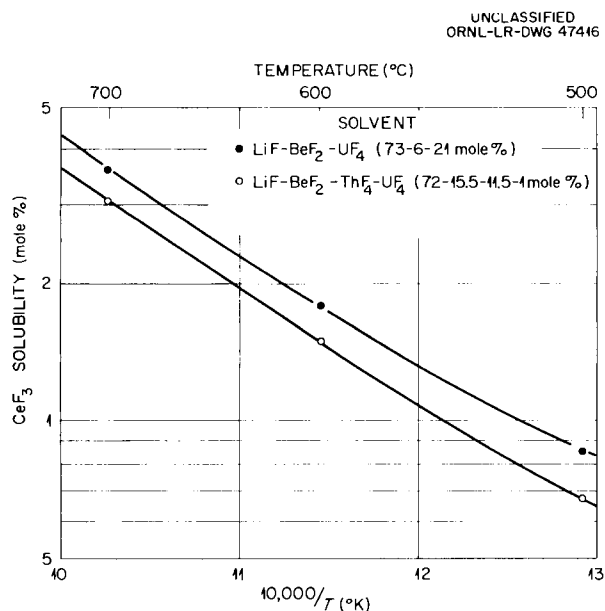


Fig. 8.7. Solubility of  $CeF_3$  in LiF- $BeF_2$ - $UF_4$  (73-6-21 mole %) and in LiF- $BeF_2$ - $ThF_4$ - $UF_4$  (72-15.5-11.5-1 mole %).

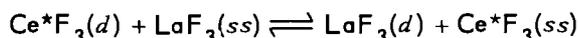
Cerous fluoride was then added and the  $SmF_3$  in solution was determined by counting the activity in filtrates obtained at several temperatures. These experimental values are shown in Table 8.2 and compared with those predicted as indicated above.

A short study was also made to determine whether  $AlF_3$  might be used in place of  $CeF_3$  as an extractant. It was found, however, that the solubilities of the rare earths in LiF- $BeF_2$ - $UF_4$  (62.8-36.4-0.8 mole %) increased with additions of  $AlF_3$  (presumably due to the change in the nature of the solvent).

#### EXCHANGE RATE STUDIES WITH RARE EARTHS

J. Truitt R. B. Evans

Previous studies<sup>5-8</sup> have shown that the total rare-earth solubilities are a function of temperature and solvent composition and are nearly independent of the type of rare earth present. The results of this study indicated that a process based on the exchange



might be feasible for fission product removal.

Radioactive tracer experiments were performed to establish the time required for the exchange to obtain equilibrium under isothermal conditions and at low  $Ce^*F_3(d)$  concentrations. A  $ThF_4$ -containing solvent, LiF- $BeF_2$ - $ThF_4$ - $UF_4$  (72.0-15.5-11.5-1.0 mole %), was utilized for these studies. Powdered  $LaF_3$  was utilized as the exchange material in the first group of experiments.

Preliminary calculations based on available data<sup>5-8</sup> were performed to ensure that the experimental conditions would be similar to those which might be encountered under reactor operating

<sup>5</sup>W. R. Grimes *et al.*, *Chem. Eng. Progr., Symposium Ser.* 55(27), 65 (1959).

<sup>6</sup>W. T. Ward *et al.*, *Solubility Relations Among Rare-Earth Fluorides in Selected Molten Fluoride Solvents*, ORNL-2749 (Oct. 13, 1959).

<sup>7</sup>W. T. Ward *et al.*, *Solubility Relations Among Some Fission-Product Fluorides in NaF-ZrF<sub>4</sub>-UF<sub>4</sub> (50-46-4 mole %)*, ORNL-2421 (Jan. 15, 1958).

<sup>8</sup>W. T. Ward *et al.*, "Solubility Relations of Rare-Earth Fluorides and Yttrium Fluoride in Various Molten NaF-ZrF<sub>4</sub> and NaF-ZrF<sub>4</sub>-UF<sub>4</sub> Solvents," *J. Chem. Eng. Data* (in press).

Table 8.2. Removal of Traces of SmF<sub>3</sub> by Addition of CeF<sub>3</sub> to LiF-BaF<sub>2</sub>-UF<sub>4</sub> (62.8-36.4-0.8 mole %)

	Total Rare-Earth Fluoride (wt %) in System (calc)		Filtrate Temperature (°C)	Rare-Earth Fluoride (wt %) in Filtrates		
	CeF <sub>3</sub>	SmF <sub>3</sub>		CeF <sub>3</sub> <sup>a</sup>	SmF <sub>3</sub>	
					Observed	Predicted <sup>b</sup>
Before CeF <sub>3</sub> Addition	0	0.0795	749		0.0795	
First CeF <sub>3</sub> Addition	2.12	0.0778	695	2.1 <sup>c</sup>	0.0750	
	2.12	0.0780	580	2.1 <sup>c</sup>	0.0757	
	2.12	0.0781	487	0.90	0.0542	0.0471
Second CeF <sub>3</sub> Addition	10.1	0.0731	736	8.34	0.0662	0.0662
	10.2	0.0735	587	2.57	0.0397	0.0300
	10.7	0.0757	492	0.96	0.0262	0.0131

<sup>a</sup>Determined in a separate experiment; disregards effect of small amount of SmF<sub>3</sub> in system.

<sup>b</sup>Calculated from relationship 
$$N_{SmF_3(d)} = \frac{S_{SmF_3}^0 N_{SmF_3(ss)}}{S_{CeF_3}^0 N_{CeF_3(ss)}} N_{CeF_3(d)}$$

<sup>c</sup>Unsaturated.

conditions. The results of the calculations are shown in Fig. 8.8. It was found that the family of curves shown in Fig. 8.8 would be valid for mixtures with initial CeF<sub>3</sub> concentrations ranging from 50 to 1000 ppm CeF<sub>3</sub>. The curves demonstrate that small additions of LaF<sub>3</sub>(s) result in efficient removal, but large additions are very inefficient.

Individual tests were then performed to determine the time required to attain equilibrium at

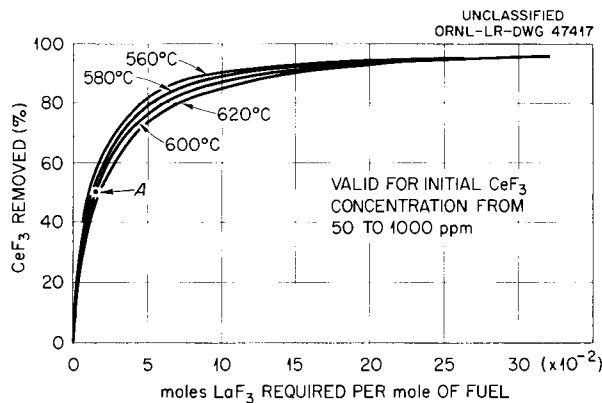


Fig. 8.8. Calculated Removal of CeF<sub>3</sub>(d) by Addition of LaF<sub>3</sub>(s).

point A in Fig. 8.8. The tests were conducted in small copper containers, which were charged with 100 g of solvent containing saturation amounts (at 580°C) of rare-earth fluorides (3.83 wt % LaF<sub>3</sub> and 0.1 wt % CeF<sub>3</sub>). These mixtures were heated to 600°C for 1 hr, sampled, and the amount of LaF<sub>3</sub>(s) required to produce an ultimate 50% CeF<sub>3</sub> concentration reduction was added to each mixture. After a preset interval the solutions were sampled to determine the amount of exchange attained. The results of eight tests utilizing powdered LaF<sub>3</sub> are shown in Fig. 8.9. Based on the

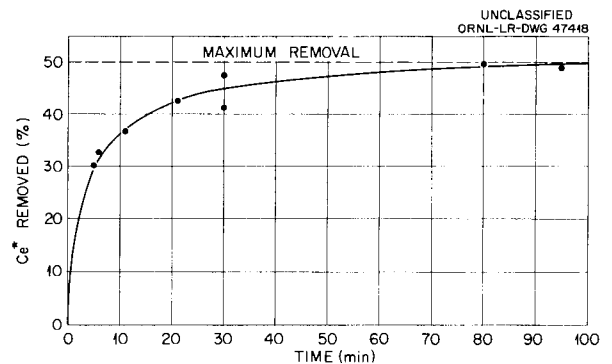


Fig. 8.9. Removal of CeF<sub>3</sub>(d) by LaF<sub>3</sub>(s) as a Function of Time.

average curve it can be concluded that 60% of ultimate removal was attained in 5 min, 85% in 20 min, and 95% in 1 hr.

Similar experiments were conducted with coarse ground (-8 +20 US sieve) 900°C sintered LaF<sub>3</sub> immersed via 30 mesh nickel screen baskets. The data summarized in Table 8.3 indicate that the sintered material is not suitable for the ThF<sub>4</sub> solvent even though the results were encouraging with the NaF-ZrF<sub>4</sub> solvent.

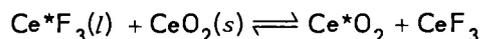
It was concluded that a fine-ground exchange reagent would be required for the proposed removal process.

### EXCHANGE REACTIONS WITH OXIDES AND CARBIDES IN MOLTEN FLUORIDES

J. H. Shaffer      G. M. Watson

The removal of radioactivity from fused-salt solutions is being investigated by exchange reactions for possible application in reprocessing molten-salt reactor fuels. Reactions of this type which would cause the radioactive cations to be held on a solid material by isotopic exchange, adsorption, or by other similar processes are of interest in this program. To be applicable for reprocessing molten-salt reactor fuels, solid exchange reactants must be relatively insoluble in molten fluorides and chemically inert toward reactor fuel constituents. Accordingly, the exchange properties of various possible materials are being studied in the presence of the proposed reactor fuel constituents (i.e., LiF, BeF<sub>2</sub>, ThF<sub>4</sub>, and UF<sub>4</sub>).

Studies of oxide reactions in molten fluorides have shown that the rare-earth oxides are sufficiently insoluble to be of interest in this investigation. The exchange of CeO<sub>2</sub> with cerium activity in the solvent LiF-NaF (60-40 mole %) and the subsequent effect of added CeF<sub>3</sub> on the equilibrium



are shown in Fig. 8.10. Similarly, the removal of lanthanum activity with La<sub>2</sub>O<sub>3</sub> in the same solvent together with the effect of added CeF<sub>3</sub> is shown in Fig. 8.11. These experiments, while not conclusive, illustrate the effectiveness of an exchange process in molten fluorides. The exchange of lanthanum with cerium is interesting in that nuclear poisons such as samarium, gadolinium, and

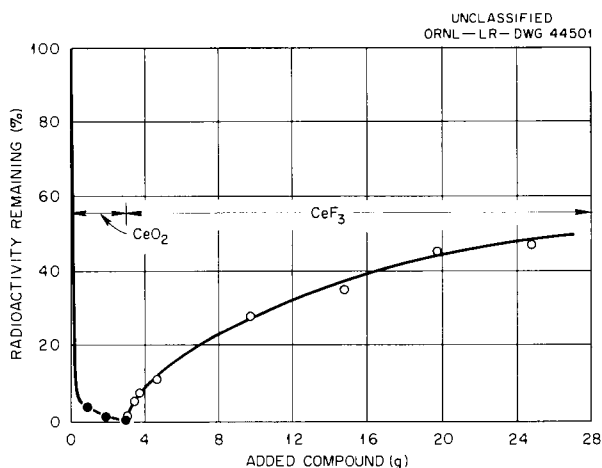


Fig. 8.10. Exchange of Cerium Activity with CeO<sub>2</sub> and CeF<sub>3</sub> in LiF-NaF (60-40 mole %) at 750°C.

Table 8.3. Test Conditions and Results of the Basket Experiment

Test No.	Solvent	Rare-Earth-Saturated Solvent Charged (Ce*F <sub>3</sub> + LaF <sub>3</sub> ) (g)	LaF <sub>3</sub> Charged (g)	Weight of LaF <sub>3</sub> and Basket Before Charging (g)	Weight of Basket After Removal (g)	Maximum Calculated CeF <sub>3</sub> Removal (%)	Experimental Removal (%)		Maximum Experimental Removal (%)	Total Contact Time (hr)
							After 8 hr	After 24 hr		
1	C-45 (53-47)	2000	150	445	590	67	23	30	41	97.5
2	C-45 (53-47)	1855	150	417	<i>a</i>	69	23	<i>a</i>	46	<i>a</i>
3	LiF-BeF <sub>2</sub> -ThF <sub>4</sub> -UF <sub>4</sub> (72.0-15.5-11.5-1.0)	2000	160	367	500	76	4.5	7.5	8.5	55

<sup>a</sup>Basket failed.

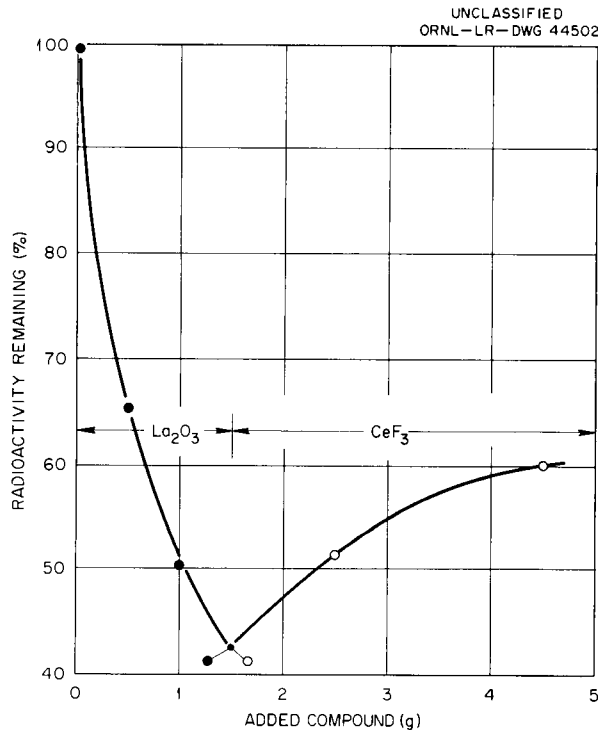


Fig. 8.11. Exchange of Lanthanum Activity with  $\text{La}_2\text{O}_3$  and  $\text{CeF}_3$  in  $\text{LiF-NaF}$  (60-40 mole %) at  $750^\circ\text{C}$ .

europium might be replaced with rare earths such as cerium and lanthanum which have lower neutron absorption cross sections. However, as shown in Fig. 8.12,  $\text{CeO}_2$  reacts readily with  $\text{UF}_4$  in the solvent  $\text{LiF-NaF}$  (60-40 mole %). These results indicate that a rare-earth oxide reprocessing scheme would be limited to reactor fuels which have had uranium removed. Figure 8.13 illustrates the effect of  $\text{ThF}_4$  and  $\text{BeF}_2$  on the removal of cerium activity from solution by exchange with  $\text{CeO}_2$ .

Experiments to investigate the exchange properties of carbides are in progress. The results of two experiments to study the removal of hafnium activity with  $\text{HfC}$  are shown in Fig. 8.14. These results illustrate the effect of  $\text{UF}_4$  on the exchange reaction in the solvent  $\text{LiF-BeF}_2$  (63-37 mole %).

Attempts to remove barium activity with  $\text{Cr}_2\text{O}_3$  and  $\text{BeO}$  in the solvent  $\text{LiF-BeF}_2\text{-ThF}_4$  (67-18-15 mole %) were not successful. Similarly an attempt to remove cerium activity from the same solvent with  $\text{BeO}$  was unsuccessful. The addition of  $\text{Al}_2\text{O}_3$  to  $\text{LiF-BeF}_2\text{-ThF}_4$  (67-18-15 mole %) containing cerium activity caused the precipitation

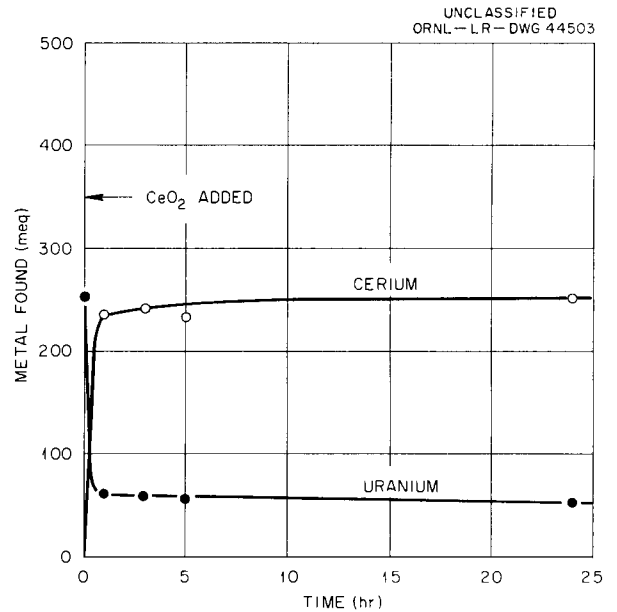


Fig. 8.12. Reaction of  $\text{UF}_4$  with  $\text{CeO}_2$  in  $\text{LiF-NaF}$  (60-40 mole %) at  $750^\circ\text{C}$ .

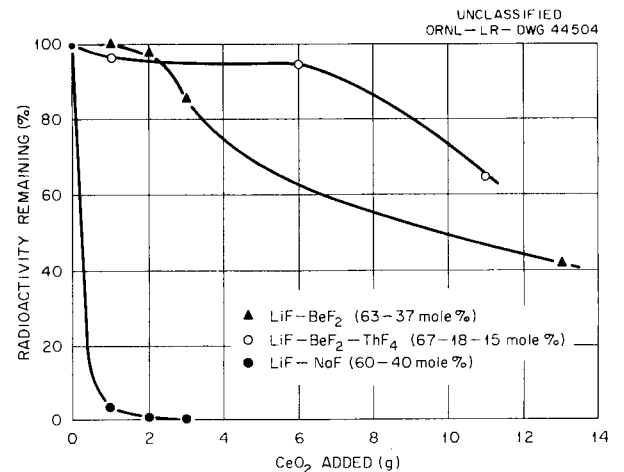


Fig. 8.13. Removal of Cerium Activity by Exchange with  $\text{CeO}_2$  in Molten-Fluoride Systems.

of  $\text{ThF}_4$  without any detectable removal of cerium activity from solution.

It may be concluded from these data that the merit of an exchange reaction concept for reprocessing molten-salt reactor fuels will depend on the compatibility of the solid exchange reactant with the reactor fuel constituents. The presence of thorium and beryllium has been shown to affect

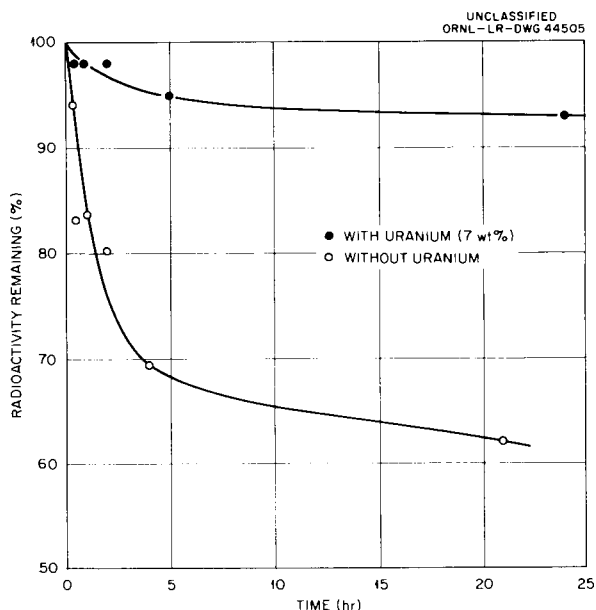


Fig. 8.14. Effect of  $UF_4$  on the Removal of  $Hf^{181}$  Activity with  $HfC$  (5 wt %) in  $LiF-BeF_2$  (63-37 mole %) at  $600^\circ C$ .

the efficiency of exchange reactions with  $CeO_2$  and  $HfC$ . Further experiments will be conducted to study the exchange properties of the rare-earth carbides as well as other materials of interest in this investigation.

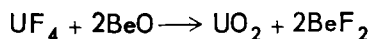
#### CHEMICAL REPROCESSING OF REACTOR FUELS BY OXIDE PRECIPITATIONS

J. H. Shaffer      G. M. Watson  
W. R. Grimes

#### Extraction of Uranium by Surface Precipitation on Beryllium Oxide

The chemical reactions of oxides with compounds associated with nuclear reactor fuels are being investigated to determine the feasibility of reactor fuel reprocessing by oxide precipitations from molten fluoride solutions. Of the various oxide reactions studied during this investigation, the extraction of uranium from solution as  $UF_4$  in  $LiF-BeF_2-ThF_4$  (67-18-15 mole %) by the surface precipitation of  $UO_2$  on  $BeO$  appears to be directly applicable to a reprocessing scheme for the breeder blanket fuel of a fused-salt nuclear reactor.

The precipitation of  $UO_2$  by the reaction



has been noted in several separate experiments.<sup>9,10</sup> The stoichiometry of this reaction by using powdered  $BeO$  is shown in Fig. 8.15 for the solvents  $LiF-BeF_2$  (63-37 mole %),  $LiF-KF$  (50-50 mole %), and  $LiF-NaF$  (60-40 mole %). The relative reaction rate of  $UF_4$  with a one-fold excess  $BeO$  as a function of the particle size (see Fig. 8.16) indicates that the surface area of the  $BeO$  should prove to be an important variable for this extraction process.

Observations of an experiment designed to investigate the reaction of  $UF_4$  with  $BeO$  in an extraction column<sup>11</sup> show two interesting characteristics. First, the  $UO_2$  precipitated by  $BeO$  appeared to be tenaciously held on the surface of the  $BeO$  packing in the extraction column. Second, in reacting 16% of the  $BeO$ , the retention of 82% of the  $BeF_2$  produced by the reaction with  $UF_4$  was sufficient to plug the extraction column. This second characteristic will probably limit the use of  $BeO$  extraction columns to dilute solutions of  $UF_4$  in molten fluorides.

With the advent of the molten-salt nuclear reactor as a thermal breeder, the process of removing trace quantities of uranium, and possibly protactinium, from the breeder blanket fuel by extraction with  $BeO$  appeared to be unique. Previous attempts to extract uranium from fused-fluoride solution were successful in reducing the apparent uranium concentration to approximately 150 ppm. However, in renewed observations of the reaction of  $BeO$  with  $UF_4$  in the solvent  $LiF-BeF_2-ThF_4$  (67-18-15 mole %) a fluorometric method for determining the uranium concentration<sup>12</sup> in the molten fluoride solution was employed. In two experiments, the addition of 30 g of  $BeO$  per kilogram of a molten mixture containing 1800 ppm uranium as  $UF_4$  in  $LiF-BeF_2-ThF_4$  (67-18-15 mole %) reduced the soluble uranium concentration to less than 1 ppm (see Fig. 8.17). This behavior may provide the basis for a processing scheme to recover uranium from the breeder blanket of a

<sup>9</sup>J. H. Shaffer, *MSR Quar. Prog. Rep. Oct. 31, 1958*, ORNL-2626, p 92.

<sup>10</sup>*MSR Quar. Prog. Rep. Jan. 31, 1959*, ORNL-2684, p 101.

<sup>11</sup>*MSR Quar. Prog. Rep. Apr. 30, 1959*, ORNL-2723, p 82.

<sup>12</sup>C. J. Rodden (ed.), *Analytical Chemistry of the Manhattan Project*, p 122, McGraw-Hill, New York, 1950.

UNCLASSIFIED  
ORNL-LR-DWG 40627

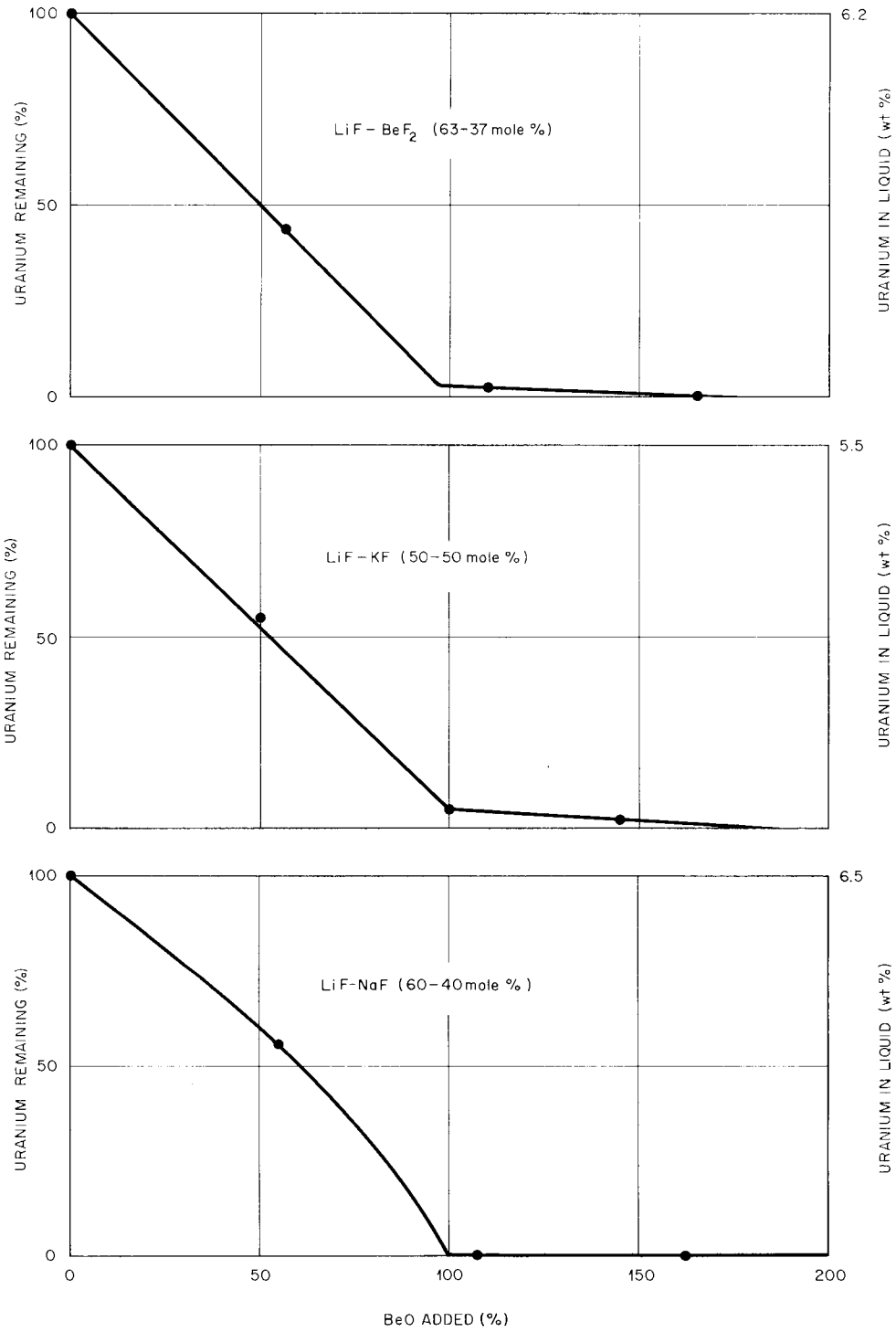


Fig. 8.15. Reaction of BeO (>325 mesh) with UF<sub>4</sub> in Molten Fluorides.

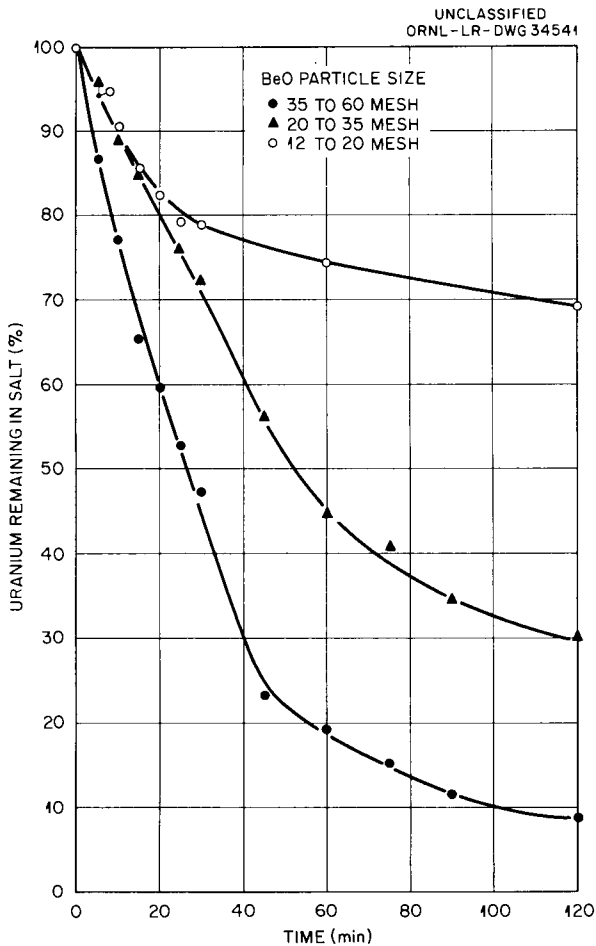


Fig. 8.16. Rate of Reaction of BeO (100% Excess) with  $UF_4$  in  $LiF-BeF_2$  (63-37 mole %) at  $600^\circ C$ .

fused-salt reactor. Further experiments are scheduled to study the extraction of trace quantities of protactinium from similar molten fluoride solutions by this process.

### The Reactions of Beryllium Oxide in Molten Fluorides

The use of BeO has been noted as a possible means for reprocessing nuclear reactor fuels by oxide precipitations from molten fluoride solutions. In addition to the reaction of BeO with  $UF_4$  to remove uranium from solution as  $UO_2$ , the behavior of BeO toward other compounds associated with nuclear reactor fuels would be important to the development of this fuel reprocessing scheme.

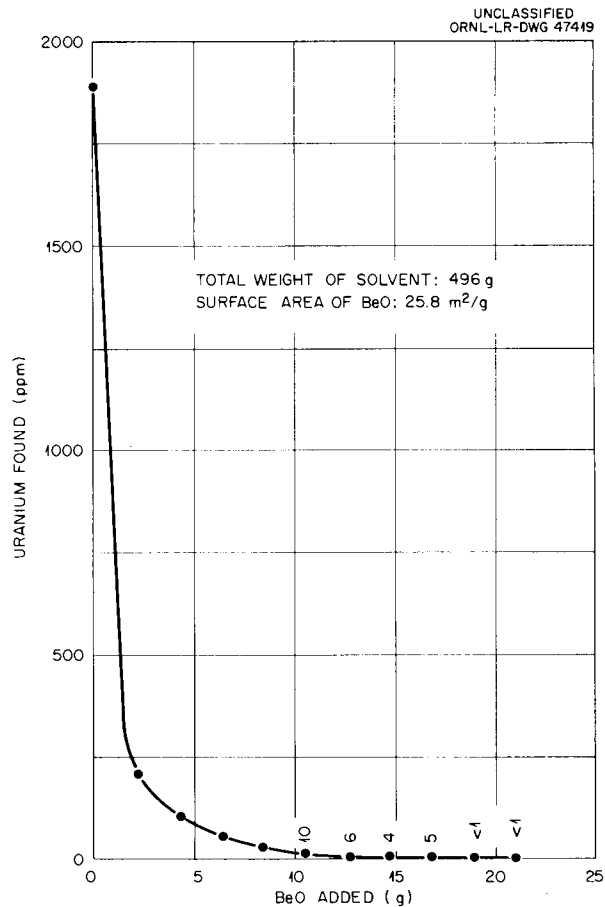


Fig. 8.17. Reaction of BeO with Trace Quantities of  $UF_4$  in  $LiF-BeF_2-ThF_4$  (67-18-15 mole %) at  $650^\circ C$ .

The behavior of BeO toward rare earth fluorides has been described previously.<sup>13</sup> In these experiments the rare earths were represented as cerium in studying the equilibrium



In one experiment CaO was added to an approximately equimolar concentration mixture of  $CeF_3$  and  $BeF_2$  in the solvent  $LiF-KF$  (50-50 mole %) at  $600^\circ C$ . The results, by illustrating the coprecipitation of cerium and beryllium, indicated that the equilibrium shown in Eq. (1) might occur. In a second experiment, BeO was added to a mixture containing  $CeF_3$  in the solvent  $LiF-KF$

<sup>13</sup>J. H. Shaffer, *MSR Quar. Prog. Rep.* June 30, 1958, ORNL-2551, p 90.

(50-50 mole %) at 600°C, further illustrating the equilibrium as shown in Fig. 8.18. An additional experiment in which BeO was added to a 5 wt % mixture of CeF<sub>3</sub> in the solvent LiF-BeF<sub>2</sub> (63-37 mole %) failed to indicate any detectable precipitation of cerium. These results illustrate that in processing a molten-salt reactor fuel containing appreciable concentrations of BeF<sub>2</sub>, the use of BeO will not cause any detectable precipitation of the trivalent rare earths.

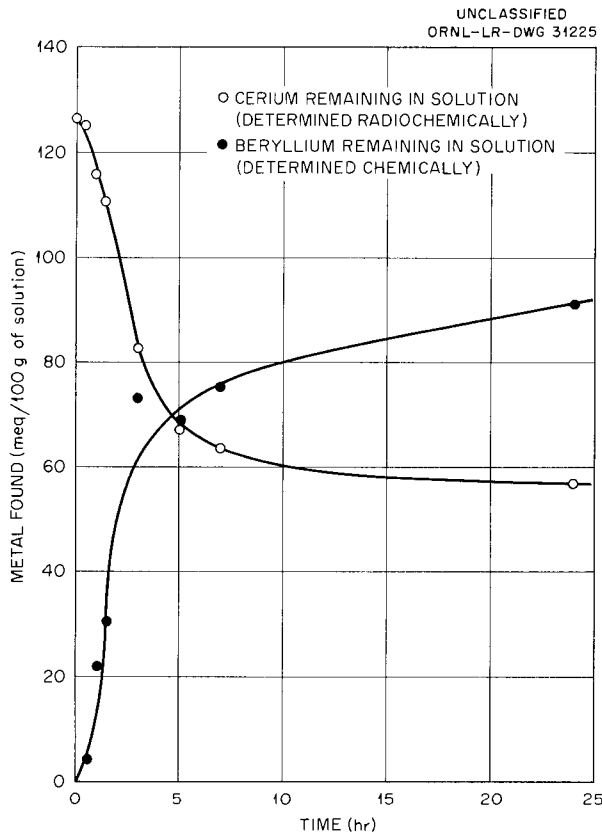


Fig. 8.18. Results of Reaction of CeF<sub>3</sub> with BeO in LiF-KF (50-50 mole %) at 600°C.

As shown in Fig. 8.19, the addition of BeO to a mixture ZrF<sub>4</sub> in the solvent LiF-KF (50-50 mole %) yielded results typical of those obtained for the precipitation of uranium. However, the addition of a large excess of BeO to a mixture of UF<sub>4</sub> and ThF<sub>4</sub> in the solvent LiF-BeF<sub>2</sub> (63-37 mole %) caused the precipitation of uranium, but failed to indicate the precipitation of thorium (see Fig. 8.20).

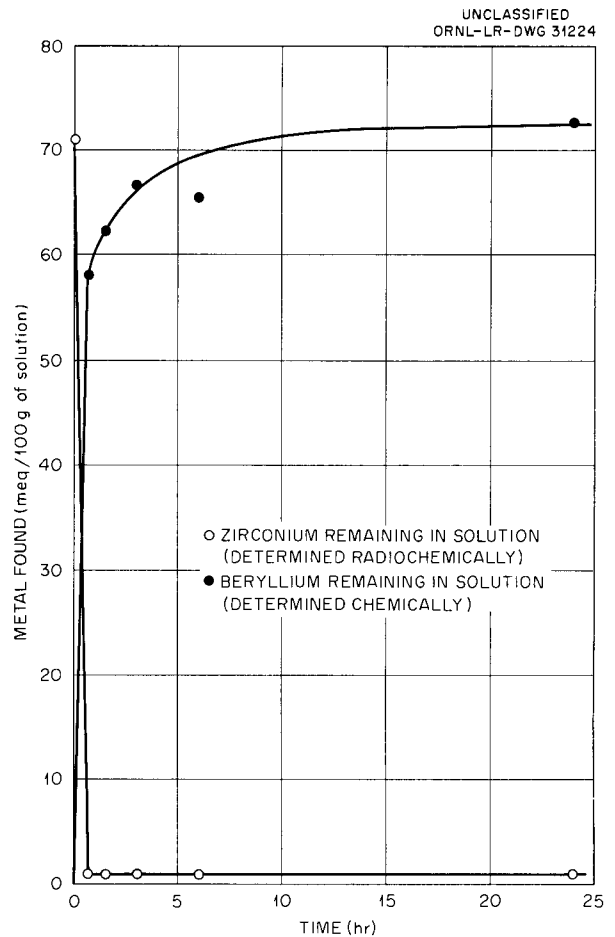


Fig. 8.19. Results of Reaction of ZrF<sub>4</sub> (Hf<sup>181</sup>F<sub>4</sub>) with BeO in LiF-KF (50-50 mole %).

#### Extraction of Uranium by Reaction with Water Vapor

In addition to the reprocessing of molten-salt reactor fuels by extracting uranium with BeO, the precipitation of UO<sub>2</sub> by reaction with water vapor is of current interest. The primary advantage of this reaction used as a steam stripping process is that relatively large quantities of uranium can be removed from solution in molten fluorides without composition alteration or contamination of the reactor fuel solvent.

The results of several experiments have indicated that this steam stripping process would provide for the selective removal of uranium from mixtures of LiF-BeF<sub>2</sub> and LiF-BeF<sub>2</sub>-ThF<sub>4</sub> mixtures without contamination by fission products.

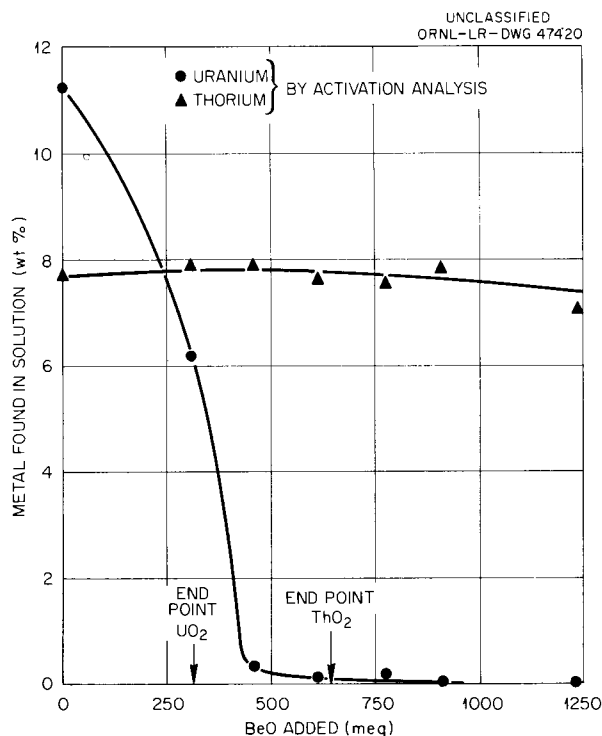


Fig. 8.20. Reaction of BeO with  $UF_4$  and  $ThF_4$  in  $LiF-BeF_2$  (63-37 mole %) at  $600^\circ C$ .

The results of previously reported experiments,<sup>14</sup> as illustrated by Fig. 8.21, show that in the presence of 1.25 wt %  $CeF_3$  in  $LiF-BeF_2$  (63-37 mole %) containing 1 mole %  $UF_4$ , the uranium was quantitatively precipitated from solution as  $UO_2$  without any detectable precipitation of cerium. In an additional experiment, the passage of water vapor through a mixture of  $ThF_4$  (7.25 wt %) in  $LiF-BeF_2$  (63-37 mole %) was found not to cause a reaction with thorium. Similarly, water vapor was found not to precipitate cerium from a mixture of 2.25 wt %  $CeF_3$  in  $LiF-BeF_2$  (63-37 mole %). However, in these two experiments the constant evolution of HF indicated the precipitation of BeO. Subsequent experiments verified these findings.

Although the study of the reaction of water vapor with  $UF_4$  as a fuel reprocessing scheme is incomplete, several interesting conclusions by analogy can be made. First, recent studies of the crystal properties and precipitation techniques

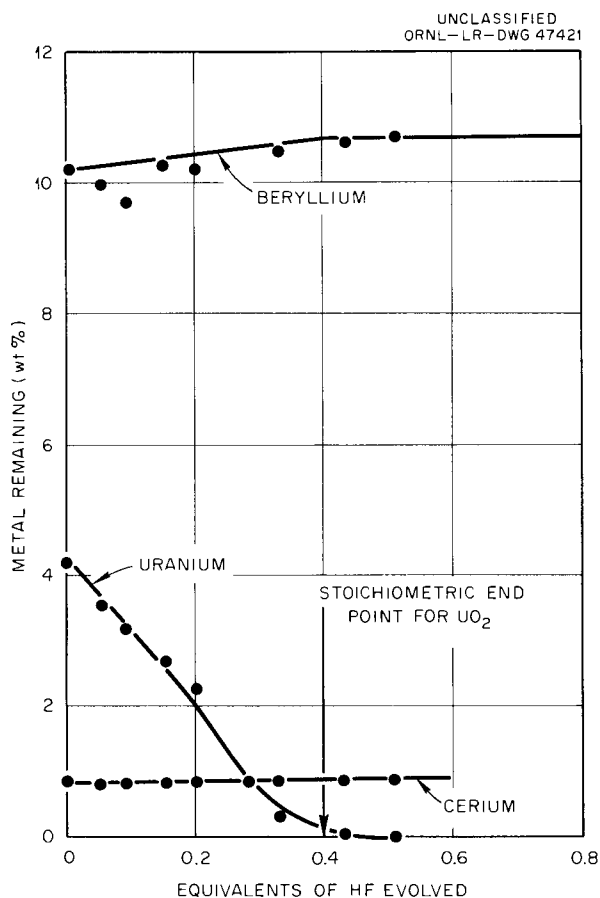


Fig. 8.21. Reaction of  $H_2O$  with  $UF_4$  in  $LiF-BeF_2$  (63-37 mole %) at  $600^\circ C$ .

of  $UO_2$  by this method suggest that the recovery of  $UO_2$  for subsequent refueling of a molten-salt reactor is feasible. Further, any oxidation products introduced by this process can be removed by  $HF-H_2$  treatment of the fuel solvent. Second, the selectivity of the reaction of water vapor with the proposed molten salt reactor fuels has been shown to be in the order



This order of reactivity indicates that by allowing the steam stripping reaction to proceed beyond the stoichiometric end point for  $UO_2$  precipitation, the complete removal of uranium from the molten fluoride system can be insured. This operation would not be detrimental to solvent recovery or to uranium reclamation. Further refinement in the experimental techniques for this steam stripping process are in progress.

<sup>14</sup>MSR Quar. Prog. Rep. Apr. 30, 1959, ORNL-2723, p 83.

**Reactions of the Alkaline Earth Oxides  
in Molten Fluorides**

The reactions of the alkaline earth oxides with the proposed reactor fuel constituents are of interest in characterizing the stability of various oxides in molten fluoride solutions. The use of these alkaline earth oxides in reprocessing schemes for molten-salt reactor fuels is of dubious importance in that their use as precipitating agents would introduce extraneous ions into the solvent. However, the reactions of the oxides with  $CeF_3$  indicate that their use may be of some merit in fission product recovery.

The reactions of  $CaO$  with  $UF_4$  and  $CeF_3$  in the solvent  $LiF-KF$  (50-50 mole %) have illustrated that uranium is preferentially precipitated prior to the precipitation of cerium. Typical results of these reactions are shown in Fig. 8.22. Similarly,  $CaO$  reacts stoichiometrically with  $ZrF_4$  to form  $ZrO_2$  prior to the precipitation of cerium. These results illustrate that  $UO_2$  and  $ZrO_2$  are more stable than  $Ce_2O_3$ .

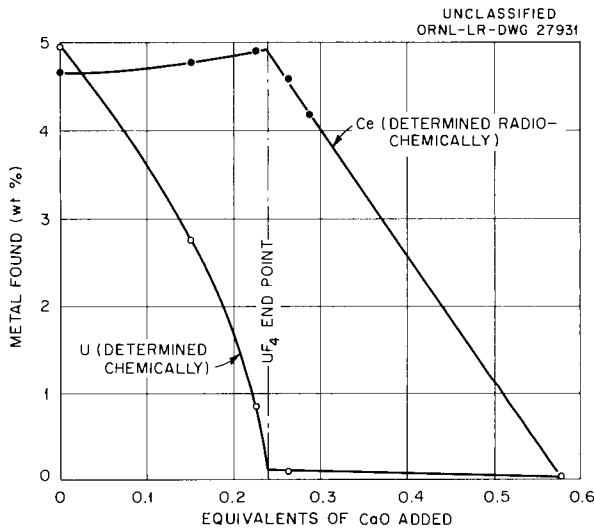
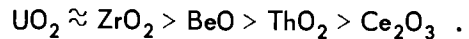


Fig. 8.22. Titration of  $CeF_3$  and  $UF_4$  with  $CaO$  in  $LiF-KF$  (50-50 mole %).

As mentioned previously in this report, the reaction of  $CaO$  with  $CeF_3$  and  $BeF_2$  in approximately equal concentrations in  $LiF-KF$  (50-50 mole %) causes the coprecipitation of  $Ce_2O_3$  and  $BeO$ . A subsequent experiment in which  $BeO$  was reacted with  $CeF_3$  illustrated that  $BeO$  was slightly more stable than  $Ce_2O_3$ .

The reactions of  $CaO$  with thorium have been studied in two experiments. First, the reaction of  $CaO$  with  $ThF_4$  (11.5 wt %) and  $CeF_3$  (3.25 wt %) in the solvent  $LiF-NaF$  (60-40 mole %) at  $750^\circ C$  illustrated (see Fig. 8.23) that thorium was selectively precipitated prior to the precipitation of cerium. In the second experiment,  $CaO$  was added to a mixture containing  $UF_4$  (9.7 wt %),  $ThF_4$  (10.3 wt %), and  $CeF_3$  (2.5 wt %) in the solvent  $LiF-NaF$  (60-40 mole %) at  $750^\circ C$ . These results, shown in Fig. 8.24, illustrate the selective precipitation of  $UO_2$ ,  $ThO_2$ , and  $Ce_2O_3$ . Correlations from experiments with the reaction of water vapor with  $ThF_4$  in  $LiF-BeF_2$  (63-37 mole %) indicate that  $BeO$  is more stable than  $ThO_2$ . By use of this analogy, it might be suggested that the order of stability of the oxides of interest in this investigation is



However, the study of the reactions of  $CaO$  with  $ThF_4$  and  $BeF_2$  and with  $ZrF_4$  and  $BeF_2$  is suggested to confirm these results.

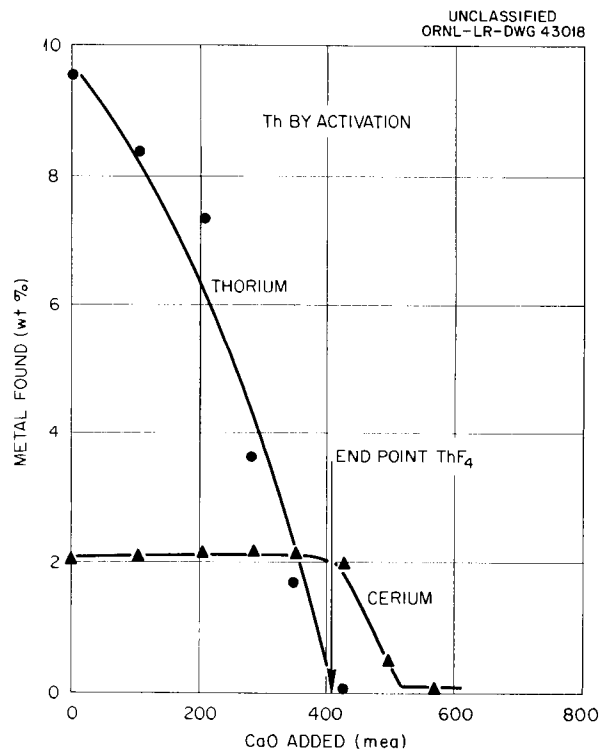


Fig. 8.23. Reaction of  $CaO$  with  $ThF_4$  and  $CeF_3$  in  $LiF-NaF$  (60-40 mole %) at  $750^\circ C$ .

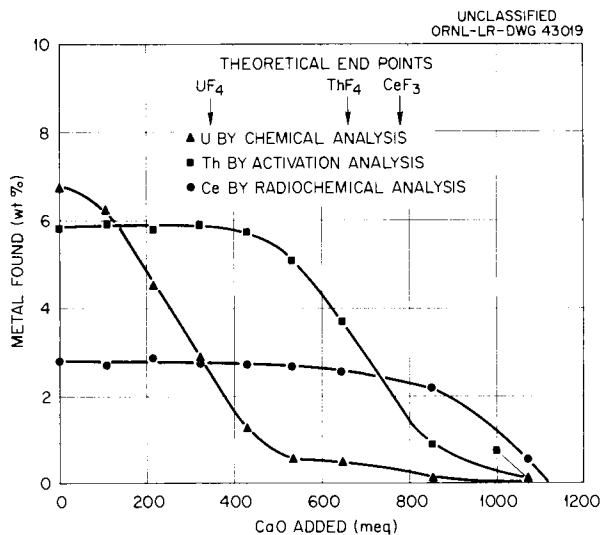


Fig. 8.24. Reaction of CaO with  $UF_4$ ,  $ThF_4$ , and  $CeF_3$  in LiF-NaF (60-40 mole %) at  $750^\circ C$ .

The reactions of BaO, SrO, and MgO with  $UF_4$  and  $CeF_3$  in the solvent LiF-NaF (60-40 mole %) were studied during this investigation.<sup>15</sup> Without exception, these reactions were typical of similar reactions with CaO. Figure 8.25 illustrates the precipitation of uranium and cerium by reaction of  $UF_4$  and  $CeF_3$  in LiF-NaF (60-40 mole %) with SrO.

The apparent stability of the oxides of elements associated with nuclear reactor fuels provides a basis for a separations scheme for these compounds. Further research efforts with these reactions will be primarily aimed at the development of a suitable method for fission product recovery from nuclear reactor fuels.

COLD-ZONE DEPOSITION OF SOLUTES

R. B. Evans	W. T. Ward
G. M. Watson	W. R. Grimes

The possibility of removing slightly soluble contaminants or constituents from fuel melts by cooling to produce a precipitate leads to an interest in the nucleation and growth of crystals on removable cold surfaces. While ideal equilibrium freezing on a cold finger is extremely

<sup>15</sup>Experimental work performed by R. St. James, DCMA, CEN Saclay, while with the Reactor Chemistry Division, ORNL, June 1959.

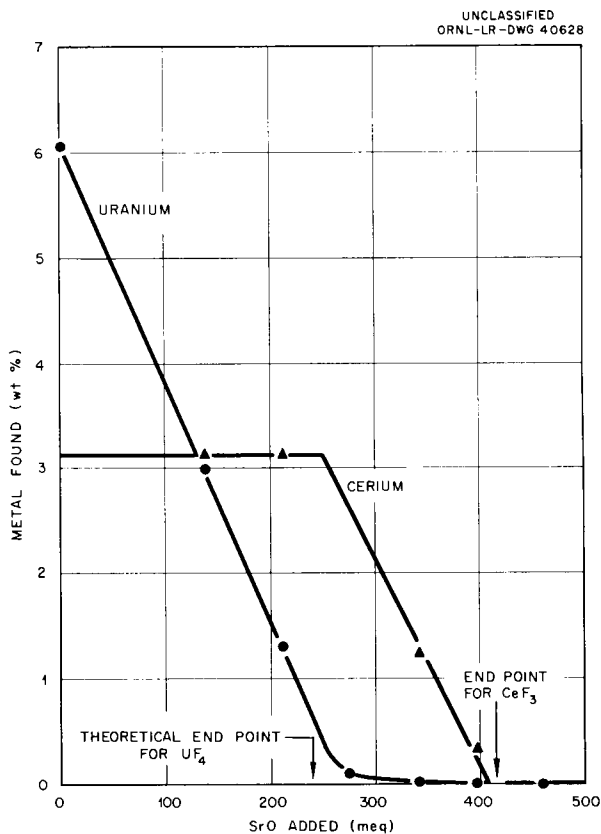


Fig. 8.25. Reaction of SrO with  $UF_4$  and  $CeF_3$  in LiF-NaF (60-40 mole %) at  $750^\circ C$ .

difficult to achieve, primarily because of the delicate heat balances involved, an inefficient version of the process might be very useful if it were simple enough to be easily executed repeatedly on a reprocessing side stream.

A cold finger was used to precipitate tracer labeled  $CeF_3$  from LiF-BeF<sub>2</sub> (63-37 mole %, melting point  $450^\circ C$ ) in a 2-in.-dia nickel pot 17 in. deep. Both hydrogen and water were used as coolants in a series of trials. Solutions containing about 5 wt %  $CeF_3$ , corresponding to saturation at about  $600^\circ C$ , furnished deposits which, on removal from the melt, were found to contain occluded and adherent solvent to the extent that the  $CeF_3$  content generally ranged from 20 to 40%. On the basis of this performance with a relatively crude control of heat flow, as obtained in these experiments, the process appeared to have a definite promise of feasibility.

Part II

AQUEOUS HOMOGENEOUS REACTOR PROGRAM

•  
•

•  
•

•  
•

## 9. PHASE EQUILIBRIA IN AQUEOUS SYSTEMS AT ELEVATED TEMPERATURE

W. L. Marshall

C. J. Barton  
J. S. Gill  
G. M. Hebert

E. V. Jones  
R. E. Moore  
R. Slusher

Dilute solutions of uranyl sulfate and sulfuric acid in water (or heavy water) at temperatures above 250°C and under relatively high pressures serve as fuels for aqueous homogeneous reactors. Copper sulfate is incorporated to catalyze the recombination of H<sub>2</sub> (or D<sub>2</sub>) and O<sub>2</sub> from radiolysis of the water, and nickel sulfate appears in solution as a consequence of corrosion of the stainless steel reactor system. A detailed knowledge of the phase behavior of the five-component system UO<sub>3</sub>-CuO-NiO-SO<sub>3</sub>-H<sub>2</sub>O (ref 1) and of its D<sub>2</sub>O counterpart at elevated temperatures is, accordingly, clearly necessary.

Investigations of this system carried out in the Reactor Chemistry Division are described in this chapter. In addition, investigations of alternate homogeneous reactor fuels, some current attempts to find a suitable thorium breeder blanket, and development of phase-study apparatus for use at elevated temperature are described. Detailed information on these various topics is given in recent Homogeneous Reactor Project Progress Reports<sup>2-4</sup> and other ORNL reports.<sup>5-12</sup>

### SOLID-LIQUID EQUILIBRIA IN THE SYSTEM UO<sub>3</sub>-CuO-NiO-SO<sub>3</sub>-H<sub>2</sub>O AND ITS D<sub>2</sub>O ANALOG AT 300°C

During the past year portions of the system UO<sub>3</sub>-CuO-NiO-SO<sub>3</sub>-H<sub>2</sub>O and its D<sub>2</sub>O counterpart at 300°C were investigated in order to have a general insight into solubility equilibria, the knowledge of which is of considerable importance

<sup>1</sup>These designations (e.g., UO<sub>3</sub>) are used throughout this chapter to indicate the system components and are not intended to define the species in solution. SO<sub>3</sub>, for example, is used to designate total sulfate in the system.

<sup>2</sup>HRP Quar. Prog. Rep. Jan. 31, 1959, ORNL-2696, p 205-14.

<sup>3</sup>*Ibid.*, Apr. 30, 1959, ORNL-2743, p 227-38.

<sup>4</sup>*Ibid.*, Oct. 31, 1959, ORNL-2879, p 99-125.

<sup>5</sup>W. L. Marshall, J. S. Gill, and R. E. Moore, *Two-Liquid-Phase Temperature Limits in the Homogeneous Reactor Fuel Solution and Its Concentrates; Comments on Solid-Liquid Equilibria*, ORNL CF-59-8-41 (1959).

and use in the selection of fuel compositions for aqueous homogeneous reactors. A temperature of 300°C was selected for the investigation, since the design of the HRE-2 specified that its fuel be held at or below this temperature, and since solubilities for the solids investigated showed or were expected to show negative temperature coefficients of solubility.

Detailed definition of phase behavior in a five-component system is a difficult experimental feat at best. Study of this system is further complicated by the high vapor pressure (ca. 83 atm) of the system at 300°C, by the occurrence of a second liquid phase over a wide range of compositions, and by the need to avoid reduction of uranyl ion and consequent oxidation of the container metal. Accordingly, the following experimental program was conducted to obtain a general description of the relevant portions of this system. Solubility relationships were determined after equilibration of solution-solid mixtures of chosen composition in the presence of saturated vapor at 300°C in pressure vessels of titanium. Compositions of

<sup>6</sup>R. E. Moore and W. L. Marshall, *Effect of Excess Acid on Two-Liquid-Phase Temperature Limits for the Homogeneous Reactor Fuel Solution and Its Concentrates*, ORNL CF-59-11-27 (1959).

<sup>7</sup>C. J. Barton et al., *Phase Stability of Homogeneous Reactor Hot Fuel Solutions*, ORNL CF-59-8-72 (1959).

<sup>8</sup>J. S. Gill and W. L. Marshall, *The Compound CuO·3UO<sub>3</sub>*, ORNL CF-59-8-95 (1959).

<sup>9</sup>W. L. Marshall and J. S. Gill, *Investigation of the System UO<sub>3</sub>-CuO-NiO-SO<sub>3</sub>-H<sub>2</sub>O at 300°C*, ORNL CF-59-12-60, rev 1<sup>3</sup> (1959).

<sup>10</sup>C. J. Barton, G. M. Hebert, and W. L. Marshall, *Liquid-Liquid Immiscibility above 300°C in the System UO<sub>3</sub>-SO<sub>3</sub>-N<sub>2</sub>O<sub>5</sub>-H<sub>2</sub>O*, ORNL CF-59-11-64 (1959).

<sup>11</sup>W. L. Marshall, *Consideration of UO<sub>2</sub>(NO<sub>3</sub>)<sub>2</sub>-HNO<sub>3</sub>-H<sub>2</sub>O(D<sub>2</sub>O) as a High Temperature Homogeneous Reactor Fuel*, ORNL CF-59-5-100 (1959).

<sup>12</sup>W. L. Marshall, *Further Consideration of UO<sub>3</sub>-HNO<sub>3</sub>-H<sub>2</sub>O as a Homogeneous Reactor Fuel; Investigation of Solution Stability of Solutions Suitable for HRT Operation*, ORNL CF-59-8-27 (1959).

the solutions were obtained by chemical analysis for  $\text{SO}_3$ ,  $\text{UO}_3$ ,  $\text{CuO}$ , and  $\text{NiO}$  of samples drawn at equilibrium; solids were examined at the conclusion of each experiment to ascertain the number and identity of the solid phases. By proper choice of materials loaded into the pressure vessels, the compositions of solutions in equilibrium at  $300^\circ\text{C}$  with one, two, or three solid phases of known identity were obtained. In separate experiments, concentrations of metallic species in solution at equilibrium with each solid phase or phases were also examined as functions of  $\text{SO}_3$  concentration from approximately 0.04 to 0.2  $m$ . From the resulting data a general description of solubility equilibria at  $300^\circ\text{C}$  was obtained for the five-component system and its included quaternary and ternary aqueous systems.

A cubic representation of solubilities, shown in Fig. 9.1, indicates the saturation concentrations of metal oxide components in solutions which are 0.06  $m$  in  $\text{SO}_3$ . Saturation concentrations are shown on the edges of the cube for the separate three-component systems, on the external planes for the four-component systems, and within the cube for the five-component system. The solid-phase compositions at the solution saturation boundaries cannot be expressed using this representation, but their identities and the saturation surfaces over which they are stable are designated on the figure. A complete diagram shows saturation surfaces defined by skeletal boundary points at constant  $\text{SO}_3$  concentration. These boundary points are determined from reference curves for the solubilities of solids of known identity as a function of  $\text{SO}_3$  concentration. As a first approximation this skeletal approach gives a description of the solubility surfaces, specifying the stable phases and their regions of stability.

Figure 9.2 shows a projection on the  $\text{UO}_3$ - $\text{CuO}$  face of the cube shown in Fig. 9.1. Saturation concentrations of the component  $\text{NiO}$  are indicated in parentheses. The outer curve, A-RA-RU-U, is described on the external  $\text{UO}_3$ - $\text{CuO}$  plane, where the  $\text{NiO}$  concentration = 0, whereas the inner curves, NA-ZAN, ZN-ZAN, ZU-ZUR, and RA-ZAR, originate on the  $\text{CuO}$ - $\text{NiO}$ ,  $\text{UO}_3$ - $\text{NiO}$ , and  $\text{UO}_3$ - $\text{CuO}$  external planes and project into the cube to ternary points. The letters refer to saturating solid phases which are stable at the various designated points and along the curves in Fig. 9.2

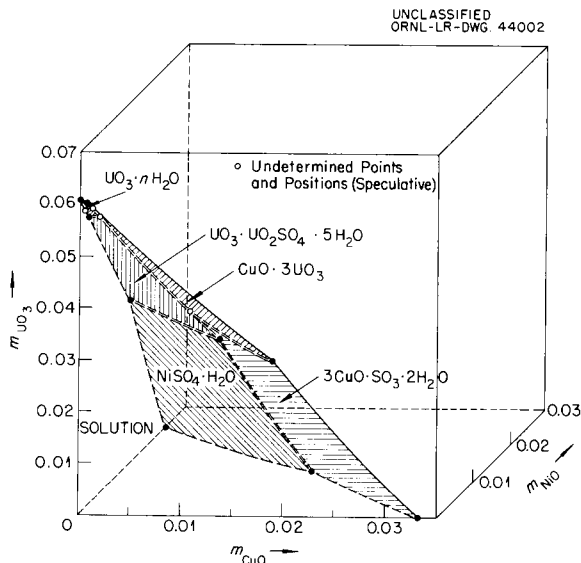


Fig. 9.1. System  $\text{UO}_3$ - $\text{CuO}$ - $\text{NiO}$ - $\text{SO}_3$ - $\text{H}_2\text{O}$  at  $300^\circ\text{C}$  ( $\text{SO}_3 = 0.06 m$ ).

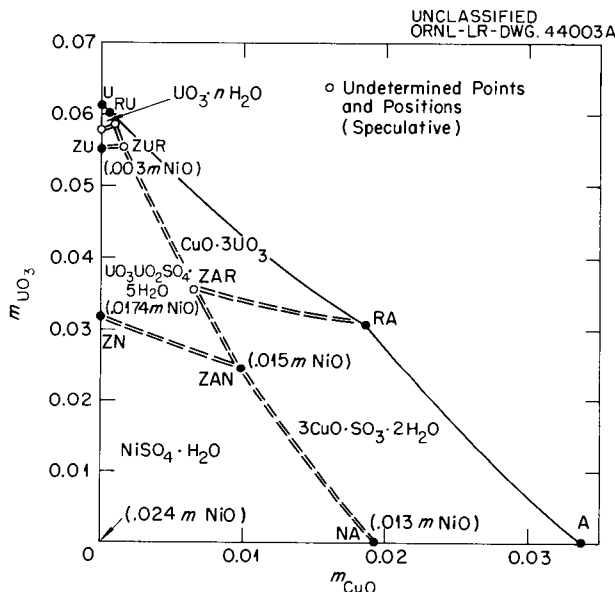


Fig. 9.2. Projection on  $\text{UO}_3$ - $\text{CuO}$  Face of Cube Representing System  $\text{UO}_3$ - $\text{CuO}$ - $\text{NiO}$ - $\text{SO}_3$ - $\text{H}_2\text{O}$  at  $300^\circ\text{C}$  ( $0.06 m \text{ SO}_3$  Is Constant).

and are defined as follows:

- U =  $\text{UO}_3 \cdot n\text{H}_2\text{O}$
- A =  $3\text{CuO} \cdot \text{SO}_3 \cdot 2\text{H}_2\text{O}$  (antlerite)
- N =  $\text{NiSO}_4 \cdot \text{H}_2\text{O}$
- Z =  $\text{UO}_3 \cdot \text{UO}_2\text{SO}_4 \cdot 5\text{H}_2\text{O}$  (zippeite)
- R =  $\text{CuO} \cdot 3\text{UO}_3$

Examples of interpretation are: (1) at point ZAN, there are three solid phases,  $\text{UO}_3 \cdot \text{UO}_2\text{SO}_4 \cdot 5\text{H}_2\text{O}$ ,  $3\text{CuO} \cdot \text{SO}_3 \cdot 2\text{H}_2\text{O}$ , and  $\text{NiSO}_4 \cdot \text{H}_2\text{O}$ , at equilibrium with saturated solution phase, (2) along the binary curve NA-ZAN, there are two solid phases,  $\text{NiSO}_4 \cdot \text{H}_2\text{O}$  and  $3\text{CuO} \cdot \text{SO}_3 \cdot 2\text{H}_2\text{O}$ , present at equilibrium, and (3) the solid which is stable at the saturation surface bounded by points A, NA, ZAN, ZAR, and RA is  $3\text{CuO} \cdot \text{SO}_3 \cdot 2\text{H}_2\text{O}$ . The ternary points, ZUR and ZAR, however, are speculative at this time with regard to both position and all equilibrium solid phases.

#### New Solids of Special Interest: Laboratory Preparation of Solids

During the course of this investigation, the compound  $\text{CuO} \cdot 3\text{UO}_3$  was discovered and characterized. A detailed discussion of this work is given in an ORNL report.<sup>8</sup> A picture of crystals of the solid is shown in Fig. 9.3; its x-ray diffraction pattern is presented in Fig. 9.4. A large amount of the compound was made in the laboratory by reaction in a high-pressure vessel at  $300^\circ\text{C}$  of a mixture of  $\text{CuO}$  and  $\text{UO}_3 \cdot n\text{H}_2\text{O}$  solids which were slurried in a  $0.05\ m\ \text{H}_2\text{SO}_4$  solution. A similar procedure was used for the synthesis of a new mixed oxide of nickel and uranium which appears to be isomorphous with  $\text{CuO} \cdot 3\text{UO}_3$  and which may be a stable solid phase at  $300^\circ\text{C}$  in the multicomponent system.

A known compound,  $3\text{CuO} \cdot \text{SO}_3 \cdot 2\text{H}_2\text{O}$ , was not available for use in these studies but was prepared by refluxing solid  $\text{CuCO}_3$  (readily available) at  $100^\circ\text{C}$  with an  $\text{H}_2\text{SO}_4 \cdot \text{H}_2\text{O}$  solution at a mole ratio,  $\text{H}_2\text{SO}_4/\text{CuCO}_3 = \frac{1}{3}$ . The solid after refluxing the mixture for 24 hr was found to be  $3\text{CuO} \cdot \text{SO}_3 \cdot 2\text{H}_2\text{O}$ . Preparational methods of this type are being used for the synthesis at  $300^\circ\text{C}$  of new uranium-containing solids of special interest to the aqueous homogeneous reactor program.

#### Solubilities in $\text{D}_2\text{O}$ Media

Solubilities in  $\text{D}_2\text{O}$  media along a ternary curve where  $\text{UO}_3 \cdot \text{UO}_2\text{SO}_4 \cdot 5\text{D}_2\text{O}$ ,  $3\text{CuO} \cdot \text{SO}_3 \cdot 2\text{D}_2\text{O}$ , and  $\text{NiSO}_4 \cdot \text{D}_2\text{O}$  are the stable solids (Fig. 9.5) indicate little difference from similar solubilities in  $\text{H}_2\text{O}$  (Fig. 9.6). In a similar manner, the solubility of  $\text{UO}_3 \cdot \text{H}_2\text{O}$  in  $\text{H}_2\text{SO}_4 \cdot \text{H}_2\text{O}$  solutions was found to be nearly the same as that of its  $\text{D}_2\text{O}$  analog in

$\text{D}_2\text{SO}_4 \cdot \text{D}_2\text{O}$  solutions (Fig. 9.7). Therefore, as a first approximation, the solubility data obtained for  $\text{H}_2\text{O}$  systems can be applied to systems containing  $\text{D}_2\text{O}$  and be used for the selection of compositions for homogeneous reactor fuels as discussed below.

#### Application of Multicomponent Solubility Data to Aqueous Homogeneous Reactors

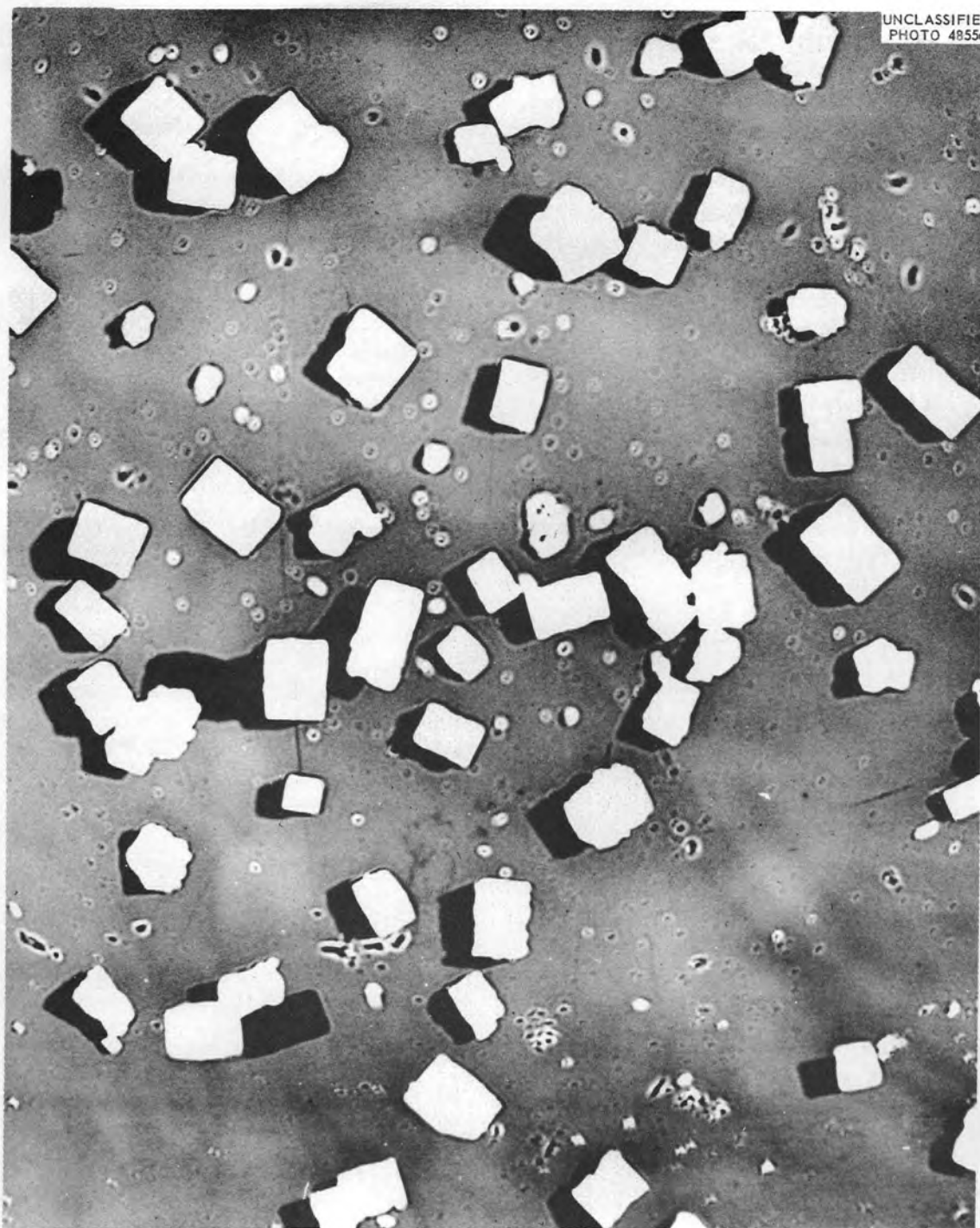
In order to apply the solubility data to the selection of homogeneous reactor fuel compositions, the appropriate  $\text{SO}_3$  concentration of the fuel is established. A volume model, like that shown in Fig. 9.1, is constructed from the basic solubility data and shows the solubility relationships of the various solids at the specified  $\text{SO}_3$  concentration.

Nickel oxide as a soluble corrosion product is not present in the initial fuel. However, corrosion of the container material occurs during reactor operation, nickel dissolves into the solution, and the over-all composition point moves away from the side representing the four-component system  $\text{UO}_3 \cdot \text{CuO} \cdot \text{SO}_3 \cdot \text{H}_2\text{O}$  and into the cube volume representing the five-component system. Depending upon the initial composition, any one of several solids may be the first one to appear at the saturation point. It might prove very desirable to select a fuel composition such that a potential saturating solid phase, however unlikely, would not contain uranium. Upon consideration of Fig. 9.2, this procedure would involve selecting a fuel containing  $\text{CuO}$  and  $\text{UO}_3$  components not exceeding concentrations delineated by lines A-RA, RA-ZAR, ZAR-ZAN, and ZAN-ZN.

After an over-all examination of solubility data at constant  $\text{SO}_3$  concentration, an empirical rule was formulated to define approximate solution saturation limits for use in the rapid estimation of phase stability of proposed reactor fuel compositions (Fig. 9.1). In addition to being based on the experimental data, this relationship involves a concept that the  $\text{HSO}_4^-$  species is the predominant anionic species in solution and that uranium behaves as a dimer at  $300^\circ\text{C}$ . The empirical rule follows: If

$$R = \frac{m_{(1/2)\text{UO}_3} + m_{\text{CuO}} + m_{\text{NiO}}}{m_{\text{SO}_3}}$$

is less than approximately 0.5 for a specific composition, this composition will represent a



40  $\mu$

Fig. 9.3. The Compound  $\text{CuO} \cdot 3\text{UO}_3$ . 500X. Reduced 15%.

UNCLASSIFIED  
ORNL-LR-DWG. 38749B

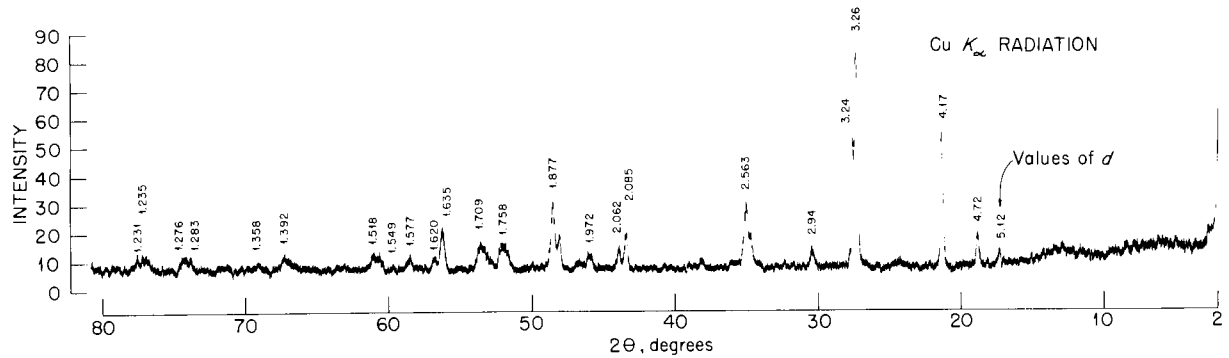


Fig. 9.4. The X-Ray Diffraction Pattern for  $\text{CuO}\cdot 3\text{UO}_3$ .

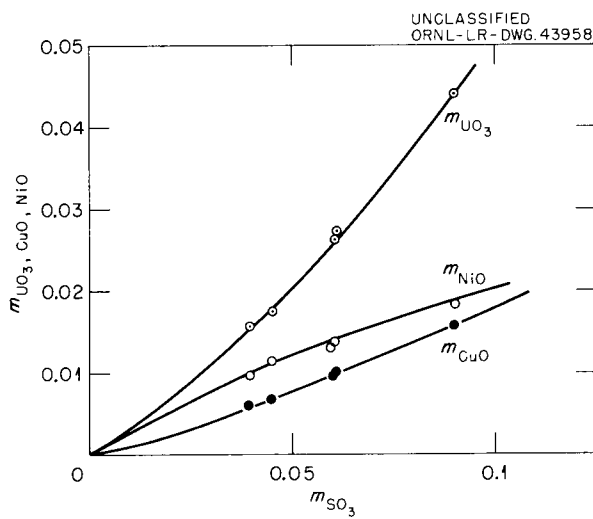


Fig. 9.5. Mutual Solubilities at  $300^\circ\text{C}$  of  $\text{UO}_3$ ,  $\text{UO}_2\text{SO}_4\cdot 5\text{D}_2\text{O}$ ,  $3\text{CuO}\cdot \text{SO}_3\cdot 2\text{D}_2\text{O}$ , and  $\text{NiSO}_4\cdot \text{D}_2\text{O}$  in  $\text{D}_2\text{SO}_4\text{-D}_2\text{O}$  Solutions.

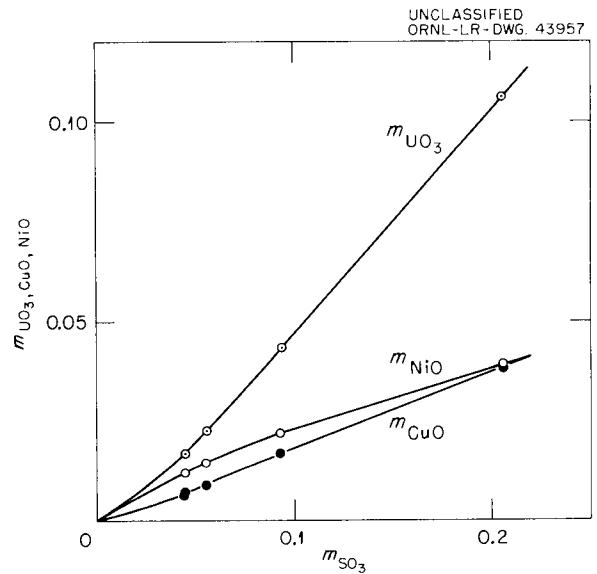


Fig. 9.6. Mutual Solubilities at  $300^\circ\text{C}$  of  $\text{UO}_3$ ,  $\text{UO}_2\text{SO}_4\cdot 5\text{H}_2\text{O}$ ,  $3\text{CuO}\cdot \text{SO}_3\cdot 2\text{H}_2\text{O}$ , and  $\text{NiSO}_4\cdot \text{H}_2\text{O}$  in  $\text{H}_2\text{SO}_4\text{-H}_2\text{O}$  Solutions.

phase-stable solution at least to  $300^\circ\text{C}$  for sulfate-based aqueous homogeneous reactor fuels in the 0.04 to 0.2  $m \text{SO}_3$  range. The experimental data show that this rule is violated at excessively high values of

$$\frac{m_{\text{NiO}}}{m_{(1/2)\text{UO}_3} + m_{\text{CuO}} + m_{\text{NiO}}} = R_{\text{NiO}}$$

In all conditions which have been applied so far to ORNL aqueous reactor fuels,  $R_{\text{NiO}}$  has not been excessively high; it has been  $< 0.5$ .

#### Boundary Curves Between Liquid-Solids and Liquid-Liquid-Solids Equilibria

A major objective of this investigation is the ultimate determination of the boundary curves

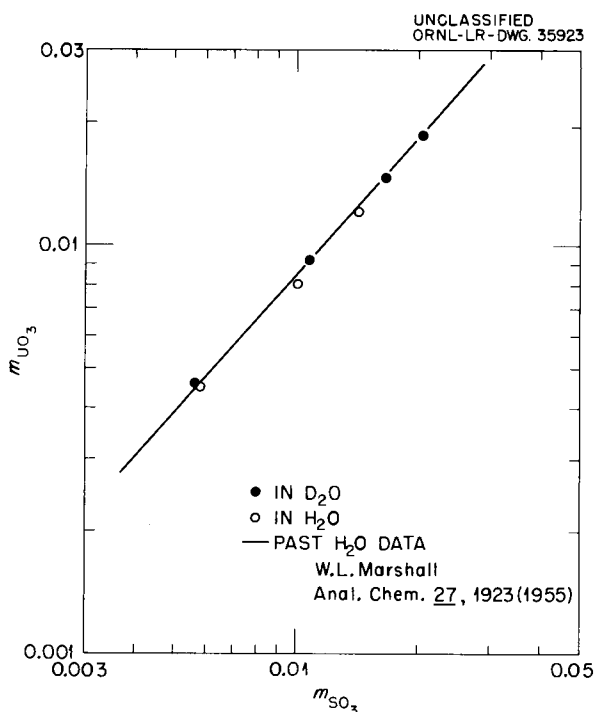


Fig. 9.7. Comparative Solubilities at 300°C of  $\text{UO}_3 \cdot \text{H}_2\text{O}$  in  $\text{H}_2\text{SO}_4\text{-H}_2\text{O}$  Solutions and of  $\text{UO}_3 \cdot \text{D}_2\text{O}$  in  $\text{D}_2\text{SO}_4\text{-D}_2\text{O}$  Solutions.

between liquid-solids and liquid-liquid-solids equilibria. Considerable experimental data above 300°C in the two-liquid-phase regions of the systems  $\text{UO}_3\text{-SO}_3\text{-H}_2\text{O}(\text{D}_2\text{O})$ ,  $\text{UO}_3\text{-CuO-SO}_3\text{-H}_2\text{O}$ , and  $\text{UO}_3\text{-NiO-SO}_3\text{-H}_2\text{O}$  have been<sup>13,14</sup> and are being obtained as described in this chapter, but as yet the over-all connection with solid-liquid boundaries is incomplete. On the basis of the observed behavior of two-liquid-phase regions above 300°C in the systems  $\text{UO}_3\text{-SO}_3\text{-H}_2\text{O}(\text{D}_2\text{O})$  and  $\text{UO}_3\text{-CuO-SO}_3\text{-H}_2\text{O}$  as a function of concentration and temperature, it is anticipated that liquid-liquid immiscibility regions for the five-component system  $\text{UO}_3\text{-CuO-NiO-SO}_3\text{-H}_2\text{O}$  and its  $\text{D}_2\text{O}$  analog may ultimately engulf the liquid-solid regions in the 0.04 to 0.2  $m \text{SO}_3$  range as temperatures extend higher than 300°C.

<sup>13</sup>H. F. McDuffie (compiler), section entitled "Properties of Aqueous Fuels," p 85-129 in *Fluid Fuel Reactors*, Addison-Wesley, Reading, Mass., 1959.

<sup>14</sup>F. E. Clark *et al.*, *J. Chem. Eng. Data* **4**, 12 (1959).

### LIQUID-LIQUID EQUILIBRIA IN THE SYSTEM $\text{UO}_3\text{-SO}_3\text{-H}_2\text{O}$ , ITS $\text{D}_2\text{O}$ ANALOG, AND SIMILAR SYSTEMS CONTAINING $\text{CuO}$ AND $\text{NiO}$ COMPONENTS

The system  $\text{UO}_3\text{-SO}_3\text{-H}_2\text{O}$  at high temperature is characterized by a range of compositions in which liquid-liquid immiscibility occurs. This observation was first made by Secoy in his study of the system  $\text{UO}_2\text{SO}_4\text{-H}_2\text{O}$  above 175°C.<sup>15</sup> Temperatures at which a second liquid phase appears constitute an upper limit for the use of  $\text{UO}_2\text{SO}_4\text{-H}_2\text{O}$  or  $\text{UO}_2\text{SO}_4\text{-D}_2\text{O}$  solutions as aqueous homogeneous reactor fuels. The comprehensive investigation of regions of liquid-liquid immiscibility in the three-component system  $\text{UO}_3\text{-SO}_3\text{-H}_2\text{O}$  as well as in the related four- and five-component systems  $\text{UO}_3\text{-CuO-SO}_3\text{-H}_2\text{O}$  and  $\text{UO}_3\text{-CuO-NiO-SO}_3\text{-H}_2\text{O}$  is therefore of considerable interest.

Phase equilibrium information on the liquid-liquid immiscibility temperature-composition boundaries is being obtained. In addition, it is necessary to know the compositions of the two phases at equilibrium with each other as described by "tie lines." Details of the investigations of (1) the compositions of two coexisting liquid phases in these systems and (2) the liquid-liquid boundary limits follow.

#### The Compositions of the Two Liquid Phases of the Systems

Briefly, the experimental method for the determination of compositions of two immiscible liquid phases consists of the following steps: Aqueous solutions of stoichiometric  $\text{UO}_2\text{SO}_4$  or of  $\text{UO}_2\text{SO}_4$  containing a dissolved excess of  $\text{H}_2\text{SO}_4$  or  $\text{UO}_3$  are sealed in Pyrex tubes. A set of sealed tubes containing solutions of varying composition is placed in a stainless steel autoclave to which some water is added to counterbalance the vapor pressure generated within the various tubes at temperature. The autoclave is then rocked at 300, 325, or 350°C until equilibrium is established between the two liquid phases which coexist at these temperatures. The autoclave is set in an upright position, thus allowing the liquid phases of higher density to flow to the bottom of the tubes. The autoclave containing the tubes is

<sup>15</sup>C. H. Secoy, *J. Am. Chem. Soc.* **72**, 3343 (1950).

cooled rapidly by immersion in an ice-water mixture, the tubes are removed, and the heavy and light phases are separated by cutting the tubes at appropriate positions, in order to recover for analysis only the central portion of each liquid phase. At ice-water temperature the heavy-liquid phase behaves as a gel for most concentrations, thereby reducing the probability of mutual contamination of the phases during the cooling and separation procedure. Both phases are analyzed for uranium by controlled-potential coulometric titration and for sulfate by removal of  $\text{UO}_2^{++}$  by a cation exchange resin and subsequent titration of  $\text{H}_2\text{SO}_4$ .

Experimental data are presented graphically in Fig. 9.8. This method of representation is convenient for displaying data covering a wide range

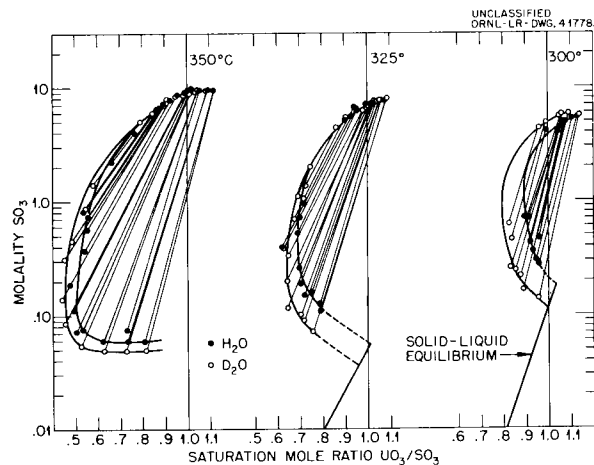


Fig. 9.8. Two-Liquid-Phase Regions in the System  $\text{UO}_3\text{-SO}_3\text{-H}_2\text{O}(\text{D}_2\text{O})$ .

of concentration. It is evident that, as the temperature rises from 300 to 350°C, the heavy-liquid phase becomes very concentrated and the light-liquid phase becomes very dilute. Under these conditions, the heavy phase at the highest concentration approaches a mole ratio,  $\text{UO}_3/\text{SO}_3$ , of 1.0, contains very little  $\text{H}_2\text{O}$ , and perhaps may approach a "liquid-salt hydrate" composition, such as  $\text{UO}_2\text{SO}_4 \cdot 3\text{H}_2\text{O}$  or  $\text{UO}_2\text{SO}_4 \cdot 4\text{H}_2\text{O}$ . The composition of the light phase in equilibrium with the heavy phase, as indicated by the connecting lines, is in the range of 0.01 to 0.1  $m \text{SO}_3$ . Since the HRE-2 fuel solution is in this same concentration range, the heavy-liquid phase formed initially upon reaching the immiscibility boundary

must probably be stoichiometric  $\text{UO}_2\text{SO}_4 \cdot \text{XH}_2\text{O}$  which also contains  $\text{CuSO}_4$  and  $\text{NiSO}_4$  (*vide infra*).

Comparison of the  $\text{UO}_3\text{-SO}_3\text{-H}_2\text{O}$  and  $\text{UO}_3\text{-SO}_3\text{-D}_2\text{O}$  systems (Fig. 9.8) shows relatively little difference in solubility behavior at high concentrations of  $\text{SO}_3$ . However, at low concentrations of  $\text{SO}_3$ , the saturation mole ratios,  $\text{UO}_3/\text{SO}_3$ , are somewhat lower for the  $\text{D}_2\text{O}$  than for the  $\text{H}_2\text{O}$  system.

Since the homogeneous reactor fuel contains copper and nickel, preliminary investigations were made of the relative distribution of these two components between the light- and heavy-liquid phases of the system  $\text{UO}_3\text{-SO}_3\text{-H}_2\text{O}$ . Some of the experimental data for the multicomponent system  $\text{UO}_3\text{-CuO-NiO-SO}_3\text{-H}_2\text{O}$  are shown in Fig. 9.9. The initial solutions contained 1.25  $m \text{UO}_2\text{SO}_4$ , 0.23  $m \text{CuSO}_4$ , and 0.24  $m \text{NiSO}_4$ , plus 10 to 40 mole % excess  $\text{H}_2\text{SO}_4$ . The concentrations of  $\text{UO}_2\text{SO}_4$ ,  $\text{CuSO}_4$ , and  $\text{NiSO}_4$  were kept constant in order to attempt to approximately represent the data on three correlating curves, one for each cationic component. Experimental data for the quaternary systems  $\text{UO}_3\text{-CuO-SO}_3\text{-H}_2\text{O}$  at 350°C and  $\text{UO}_3\text{-NiO-SO}_3\text{-H}_2\text{O}$  at 325 and 350°C are shown in Figs. 9.10 and 9.11. The initial concentrations of components are designated on the figures.

If the saturation mole ratios,  $\text{CuO}/\text{SO}_3$ ,  $\text{NiO}/\text{SO}_3$ , and  $\text{UO}_3/\text{SO}_3$ , either for the light or heavy phase at constant  $m \text{SO}_3$  are added together, the resulting summation ratio appears to fall on an immiscibility curve for the system  $\text{UO}_3\text{-SO}_3\text{-H}_2\text{O}$  (Fig. 9.8). This observation leads to the belief that violation of the immiscibility boundary curve by solution compositions near that of the HRE-2 fuel will result in the separation of a heavy-liquid phase which corresponds approximately to stoichiometric  $\text{UO}_2\text{SO}_4$ ,  $\text{CuSO}_4$ , and  $\text{NiSO}_4$  plus  $\text{H}_2\text{O}$ ; that is, there will be little or no excess  $\text{H}_2\text{SO}_4$  or metal oxides in the heavy-liquid phase. In actual reactor operation, this condition does not preclude the reasonable probability that the temperatures of any heavy-liquid phase formed initially will rise rapidly, due to the higher internal fission density, and dehydrate to produce solids. These solids may be sulfates or oxy-sulfates which, upon attainment of temperatures in excess of approximately 800°C, should convert to oxides.

Further investigations of the distribution of cationic species between light- and heavy-liquid layers in the system  $\text{UO}_3\text{-SO}_3\text{-H}_2\text{O}$  and its  $\text{D}_2\text{O}$

UNCLASSIFIED  
ORNL-LR-DWG. 45323

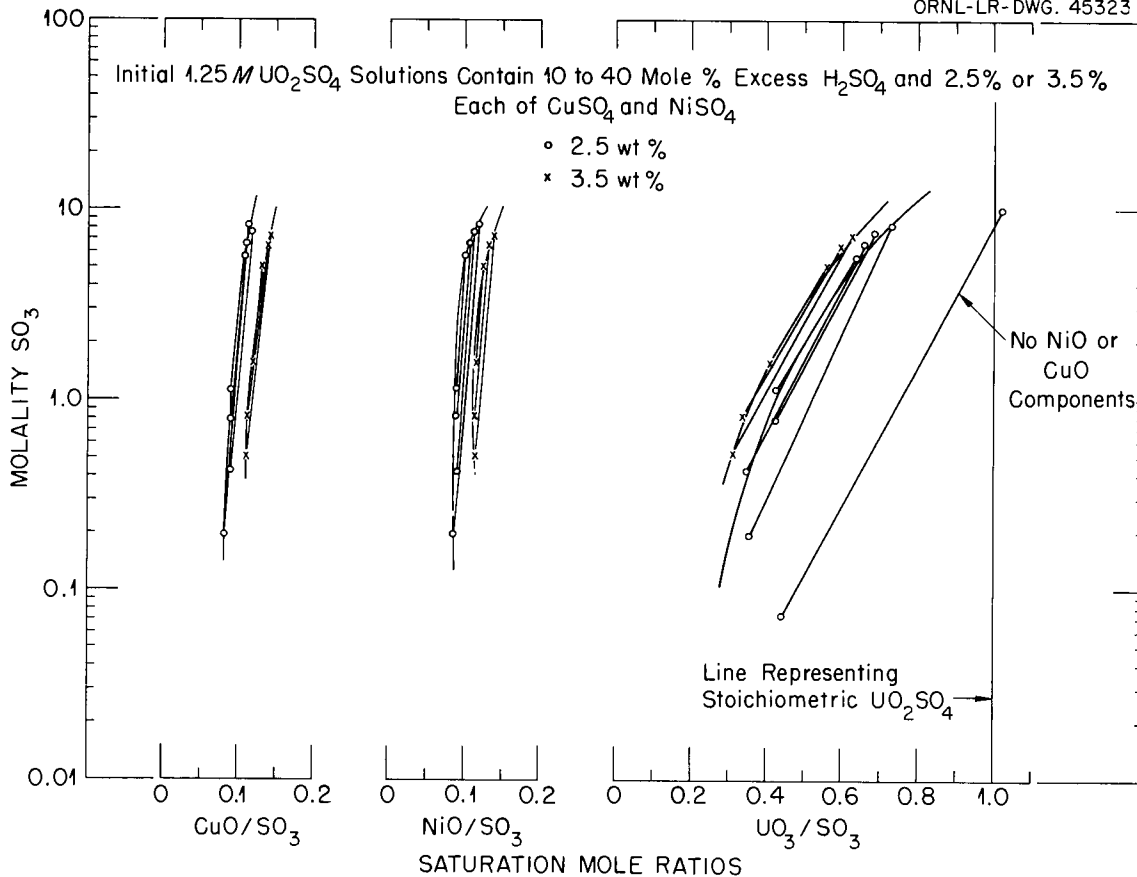


Fig. 9.9. Distribution of  $UO_3$ ,  $CuO$ , and  $NiO$  Components in the Two Liquid Phases, System  $UO_3-CuO-NiO-SO_3-H_2O$  at  $350^\circ C$ .

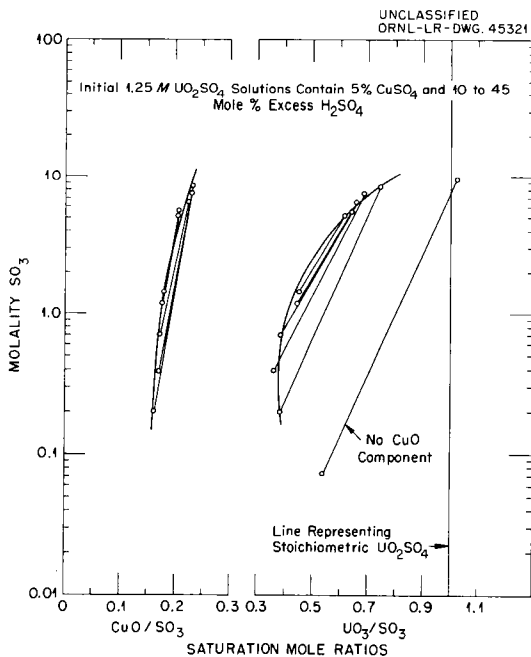


Fig. 9.10. Distribution of  $UO_3$  and  $CuO$  Components in the Two Liquid Phases, System  $UO_3-CuO-SO_3-H_2O$  at  $350^\circ C$ .

counterpart may lead to methods for using the phase-separation phenomenon in chemical processing, purification, or separations involving  $UO_2SO_4$  or other uranium compounds.

**Effect of the Mole Ratio,  $UO_3/SO_3$ , on Immiscibility Temperatures of 0.02, 0.05, 0.10, and 0.20 m Sulfate Solutions**

During the past year increasing use, for the prediction of immiscibility boundaries, was made of a previously unpublished, although frequently discussed, relationship between solution composition and liquid-liquid-immiscibility temperature. It appears that this temperature is an approximately linear function of the mole ratio,  $UO_3/SO_3$ , for a constant  $SO_3$  concentration as shown by Figs. 9.12 and 9.13. These are revised plots of information previously presented<sup>16</sup> for the

<sup>16</sup>H. W. Wright and W. L. Marshall, *HRP Quar. Prog. Rep. Oct. 1, 1952*, ORNL-1424, p 108.

UNCLASSIFIED  
ORNL-LR-DWG. 45322

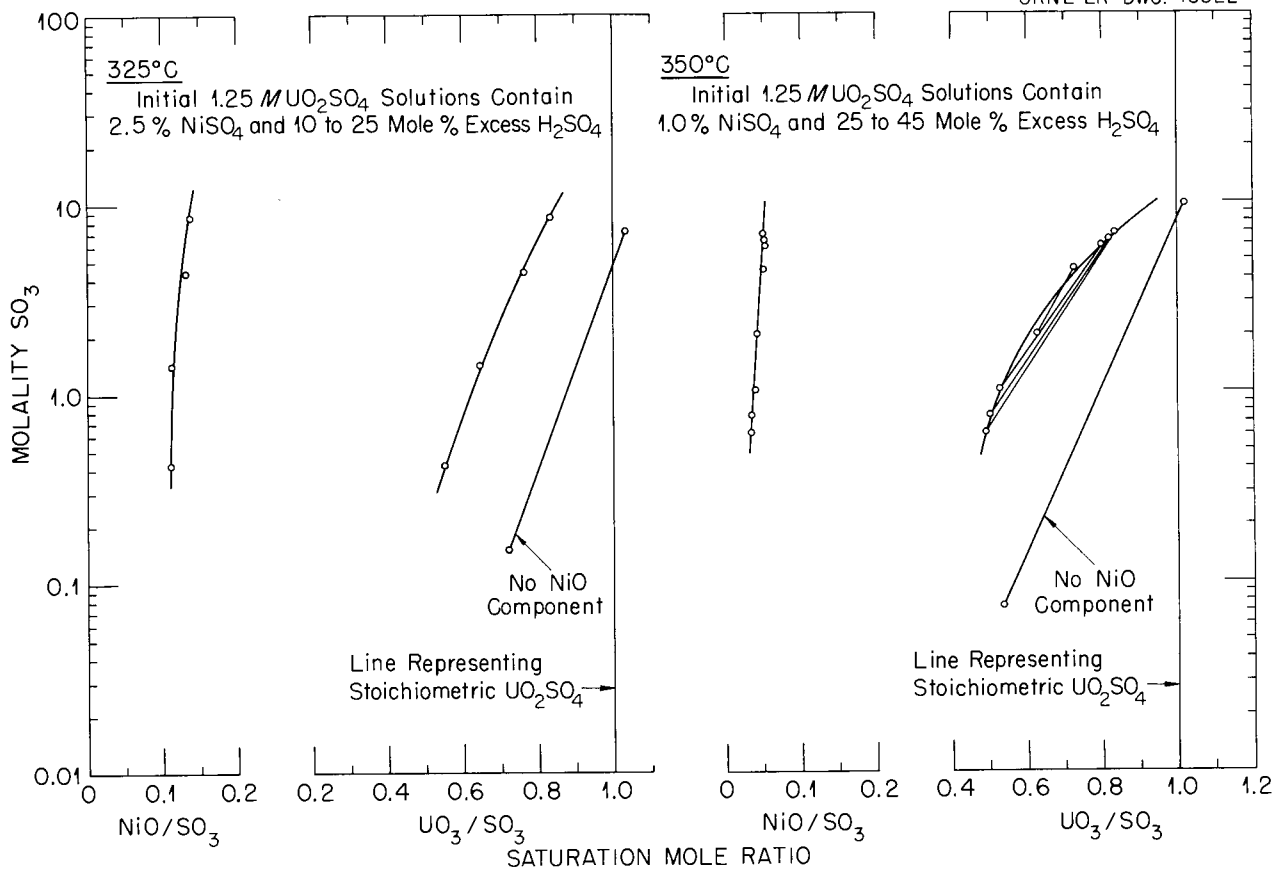


Fig. 9.11. Distribution of  $UO_3$  and  $NiO$  Components in the Two Liquid Phases, System  $UO_3-NiO-SO_3-H_2O$  at 325 and 350°C.

system  $UO_3-SO_3-H_2O$ . Extrapolation of the data to low mole ratios,  $UO_3/SO_3$ , suggests that the lines intersect the critical curve for the  $SO_3-H_2O$  system and that, accordingly, there must be solubility of  $UO_3$  in the supercritical fluid of this system, confirming an observation which was experimentally established by Secoy in 1949.<sup>17</sup>

By analogy, it appears that the mole ratio,  $(UO_3 + CuO + NiO)/SO_3$ , or mole ratio function,

$$f \left[ \frac{(UO_3 + CuO + NiO)}{SO_3} \right],$$

might also show a relationship with temperature which would be sufficiently close to linearity to be useful; preliminary evaluation of available data indicates that this may be the case. The

ultimate goal of this investigation is to attempt to define this relationship.

Immiscibility temperatures obtained during the past year for systems containing 0.02, 0.05, 0.10, and 0.20  $m$   $SO_3$  having a varying mole ratio,  $UO_3/SO_3$ , are shown in Fig. 9.14. Upon considering the 0.10  $m$   $SO_3$  solutions it is apparent that the immiscibility temperature increased from 309°C for the 0.10  $m$   $UO_2SO_4$  solution, for which  $m_{UO_3}/m_{SO_3} = 1$ , to 377.5°C for the 0.02  $m$   $UO_2SO_4$  solution, 0.08  $m$  in  $H_2SO_4$ , for which  $m_{UO_3}/m_{SO_3} = 0.2$ . The critical temperature of the light-liquid phase portion of the latter solution was approximately 2°C above the immiscibility temperature. No phase separation was observed in the 0.01  $m$   $UO_2SO_4$  solution, 0.09  $m$  in  $H_2SO_4$ , for which  $m_{UO_3}/m_{SO_3} = 0.1$ , up to the critical temperature (386°C). Similar observations were made for the

<sup>17</sup>C. H. Secoy, *Chem. Quar. Prog. Rep.*, Dec. 31, 1949, ORNL-607, p 33-38.

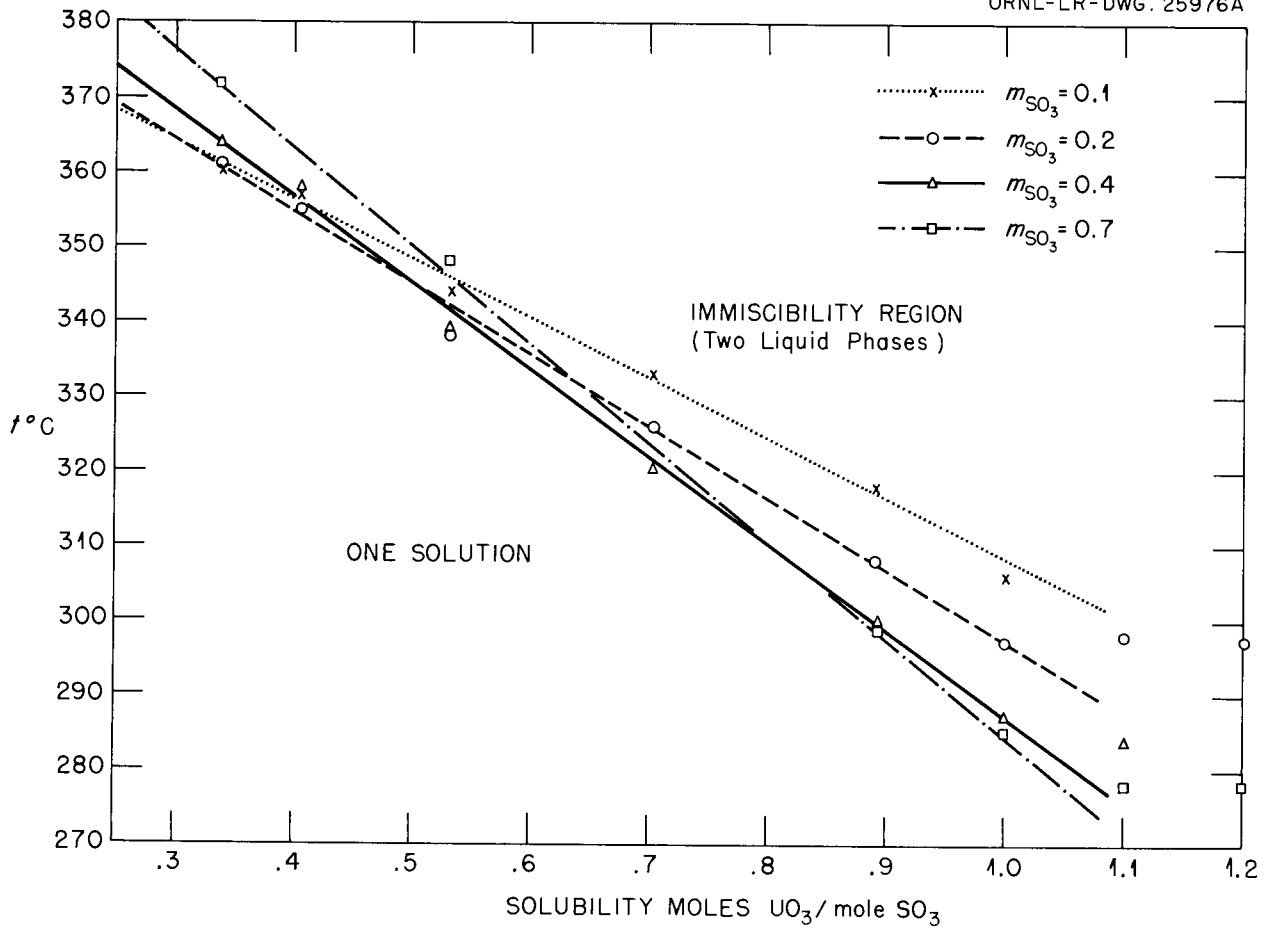


Fig. 9.12. Two Liquid Phases, System  $UO_3-SO_3-H_2O$ .

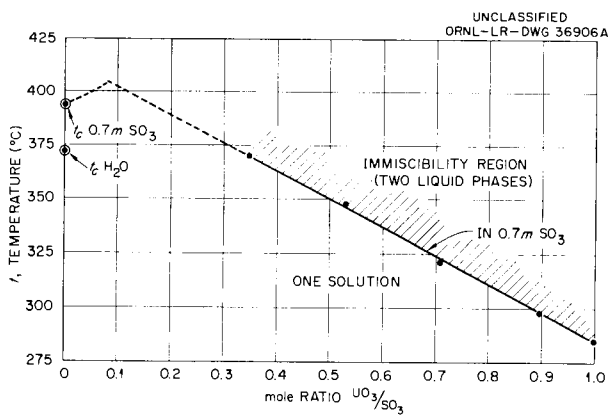


Fig. 9.13. Liquid-Liquid Immiscibility, System  $UO_3-SO_3-H_2O$  ( $0.7 m SO_3$ ).

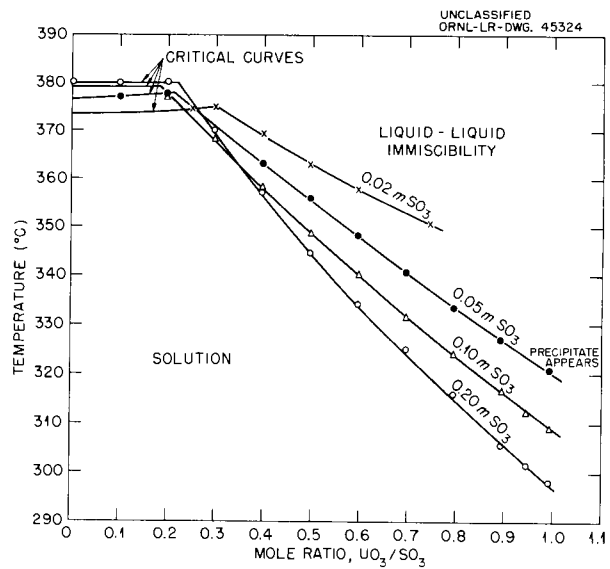


Fig. 9.14. Temperature of Two-Liquid-Phase Formation for the System  $UO_3-SO_3-H_2O$ .

0.02, 0.05, and 0.20 *m* SO<sub>3</sub> solutions. These observations, in addition to showing the approximate linearity of relationships when plotted as shown in Fig. 9.14, indicate that when the mole ratio, UO<sub>3</sub>/SO<sub>3</sub>, is relatively low, UO<sub>3</sub> is soluble in supercritical sulfuric acid fluid.

#### AQUEOUS HOMOGENEOUS REACTOR FUEL STUDIES

##### Phase Stability of Synthetic HRE-2 Fuel Solutions and their Concentrates

One of the primary requirements of an aqueous homogeneous reactor fuel solution is that it be stable toward both separation into two liquid phases and precipitation of hydrolytic solid phases at the operating temperature of the reactor. A knowledge of how the tendency toward the formation of a second liquid phase, or of a hydrolytic solid, changes as the fuel solution is concentrated by evaporation of D<sub>2</sub>O or diluted by D<sub>2</sub>O is important, since both of these processes may occur during reactor operation. It has been suggested that localized boiling is a mechanism for concentration either within the core solution or at certain limited locations on surfaces in the reactor core. Dilution of the fuel solution by D<sub>2</sub>O occurs at the connection to the pressurizer which contains both D<sub>2</sub>O and fuel solution under operating conditions of the HRE-2. During the past year studies of the phase-stability boundaries, particularly the liquid-liquid-immiscibility boundaries, of homogeneous-reactor fuel solutions have provided considerable insight concerning the peculiarities of HRE-2 operation.

In recent months several additions of deuterated sulfuric acid have been made to the HRE-2 fuel solution. Before these additions the HRE-2 fuel solution was of approximately the following composition:

Compound	Molarity at 25°C
UO <sub>2</sub> SO <sub>4</sub>	0.0258
CuSO <sub>4</sub>	0.0126
NiSO <sub>4</sub>	0.0058
MnSO <sub>4</sub>	0.0004
D <sub>2</sub> SO <sub>4</sub>	0.0166

The temperature for the formation of a second liquid phase for a synthetic solution of this composition was determined to be 332°C.<sup>5</sup> This

temperature is well above the average core temperatures (240–280°C) during power operation of the HRE-2. The results of several different experiments carried out in silica tubes have shown that solid phases will not precipitate from the homogeneous solution, from the two liquid phases, or from the subsequent supercritical fluid and heavy-liquid phase as the temperature is raised to 500°C. In one experiment 3 ml of the synthetic fuel solution, sealed in a large-diameter tube (8-mm ID, 2-mm wall), was held for 17 hr at 329°C with no indication of solid precipitation.<sup>2</sup> Other experiments have been carried out in which solutions of approximately the composition of the HRE-2 fuel were observed while being heated from 200 to 500°C under an oxygen overpressure of about 200 psi.<sup>2</sup> Oxygen overpressure is a design condition of the HRE-2. The heavy phase remained a clear yellow liquid. No solid phases were seen even after holding the temperature at 500°C for 16 hr.

Laboratory experiments have shown that when the synthetic HRE-2 fuel solution is concentrated by evaporation of D<sub>2</sub>O, the temperature for the appearance of a second liquid phase falls to a minimum value of about 305°C at an eightfold concentration and rises slowly as the concentration is further increased. Dilution of the fuel by a factor of two with D<sub>2</sub>O causes a rise in the second-liquid-phase temperature from 332 to 342°C. The higher acidity of solutions more concentrated than the HRE-2 fuel should place these solutions even further from a hydrolytic solid-liquid solubility boundary than the HRE-2 fuel. Therefore, the precipitation of a hydrolytic solid while the fuel solution is undergoing concentration would be less likely. On the other hand, if the fuel solution is diluted, it will become less acidic, and the precipitation of hydrolytic solid products would be more likely. Indeed, D. M. Richardson<sup>18,19</sup> has reported finding crystals of a material, with an analysis and x-ray diffraction pattern which correspond to the newly discovered compound CuO·3UO<sub>3</sub> (ref 8), in the pressurizer lines of both the HRE-2 mockup and the HRE-2 after a run with

<sup>18</sup>D. M. Richardson, *Composition of Solids from the HRT Mockup Pressurizer*, ORNL CF-56-6-56 (1956).

<sup>19</sup>D. M. Richardson, *Composition of Solids from the HRT Pressurizer Line*, ORNL CF-57-5-36 (1957).

depleted fuel solution. Both the increased temperature and the dilution of the fuel at the pressurizer would favor hydrolytic-solid precipitation.

During the past year the operation of the HRE-2 revealed that the power-dependent loss of circulating-uranium inventory was aggravated by raising the reactor pressure (by raising the pressurizer temperature) but substantially eliminated by reducing the reactor pressure.<sup>4</sup> It was suggested that the minimum two-liquid-phase temperature (305°C) obtained on concentrating the fuel solution was of significance for reactor operation in that, when the reactor pressurizer temperature was higher than this, the temperature of local boiling would also be higher and the resulting concentrated solution could reach the two-liquid-phase boundary. At this point, the hundredfold increase in uranium concentration in the heavy-liquid phase and the concomitant hundredfold increase in fission power density would tend to aggravate the situation further until the second liquid phase was heated to the decomposition point and perhaps converted into metal oxides. If, on the other hand, the pressurizer temperature were maintained below 305°C, then local boiling would maintain the temperature of the fuel solution near this value and boiling concentration could not cause the appearance of the concentrated second liquid phase. Of course, HRE-2 fuel solutions which continued to concentrate at temperatures below 305°C would ultimately form a solid phase or phases instead of a second liquid phase. This would, however, require concentration by a factor of 150 or greater in molar units and the solid phases would be stoichiometric salts or acid salts rather than hydrolytic solids.

The second-liquid-phase temperatures were known to be elevated by addition of acid to uranyl sulfate solutions. The minimum second-liquid-phase temperature, which might be obtained on concentrating such solutions, should likewise be raised upon addition of acid. Consequently, the possibility of adding more acid to the fuel solution to achieve greater reactor operational stability was considered. The liquid-liquid-immiscibility boundary limits for synthetic HRE-2 fuel solutions containing several different amounts of excess acid and for a number of concentrates of these solutions were determined<sup>6</sup> and are shown in Fig. 9.15. The minimum values are 305, 322, 330, and 342°C for excess acid concentrations of 0.0166, 0.0234,

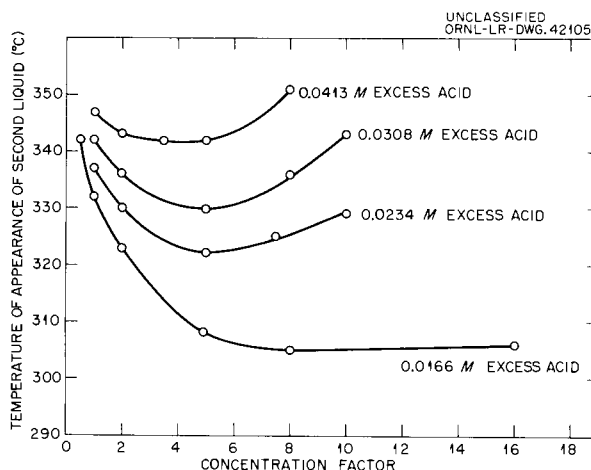


Fig. 9.15. Temperature of the Appearance of the Second Liquid Phase as a Function of Dilution and Concentration of HRE-2 Fuel Containing Various Amounts of Excess Acid.

0.0308, and 0.0413 M. From a series of plots of two-liquid-phase temperature vs excess acid at various concentration factors chosen from Fig. 9.15 a curve of two-liquid-phase temperature vs concentration factor may be constructed for any chosen quantity of excess acid between 0.0166 and 0.0413 M.

From the information obtained in these laboratory tests it was expected that:

1. The HRE-2 fuel containing 0.0166 M excess acid would become unstable in the presence of local hot spots if the pressurizer temperature were maintained at or above 305°C (1353.4 psia reactor total pressure).
2. A fuel containing 0.0234 M excess acid would become unstable with a pressurizer temperature maintained at or above 322°C (1706 psia total pressure).
3. A fuel containing 0.0308 M excess acid would become unstable with a pressurizer temperature maintained at or above 330°C (1895 psia total pressure).

Several quantities of deuterated sulfuric acid have been added to the HRE-2 solution in recent months in an attempt to achieve operational stability at higher pressurizer temperatures. Reactor experiments in which the pressure was held constant at various values while the reactor power was increased until instability was noted by a drop in the nuclear average temperature indicated

semiquantitative agreement with the theory discussed above. In another series of reactor experiments the reactor power was held constant and the pressure was increased until instability was noted. The results were also in approximate agreement with the theory.

### Phase Stability of Radioactive HRE-2 Fuel Solutions

Liquid-liquid-immiscibility temperatures of two samples of HRE-2 fuel solution were determined by visual observation of phase separation in sealed silica tubes approximately three weeks after the samples were removed from the reactor during power operation. These tests were performed to check the validity of the assumption that the phase behavior of a radioactive fuel solution is the same as that of a non-radioactive solution having the same composition. Details of this investigation were presented.<sup>7</sup> The immiscibility temperatures were determined to be  $325 \pm 1^\circ\text{C}$  for one sample and  $326 \pm 0.5^\circ\text{C}$  for the other. These values were slightly lower than the values predicted by experiments with similar synthetic fuel solutions ( $329 \pm 0.5^\circ\text{C}$ ), but the discrepancies were small enough so that they could be accounted for by minor differences in composition between the synthetic and the reactor fuel solutions. There appeared to be little reason to believe that the high radiation level to which the fuel solution was exposed in the reactor had a significant effect on its phase behavior, at least after it had cooled to 2 r/ml. Neither dilution of fuel solution with 8 vol % of 30%  $\text{H}_2\text{O}_2$  (which decomposed to produce a small, desired oxygen overpressure) nor with the amount of  $\text{H}_2\text{O}$  equivalent to that produced by the decomposed  $\text{H}_2\text{O}_2$  increased the immiscibility temperature more than  $2^\circ\text{C}$ . However, increasing the free  $\text{D}_2\text{SO}_4$  concentration from about 0.017 to 0.04 *m* raised the immiscibility temperature from  $326$  to  $345^\circ\text{C}$ .

### Effect of Increased Temperature on the Heavy-Liquid Phase

If the heavy-liquid phase is produced in the reactor core as a result of localized boiling or a temporary overheating at some limited location on the surface of the core vessel, its temperature would be expected to increase due to the higher

fission density within its volume. The resulting higher vapor pressure should produce a vapor space around the heavy-phase droplet when its temperature approximates that of the reactor pressurizer. If the temperature of the droplet increases further, a transfer of vapor from the heavy phase through the vapor space and into the bulk solution should occur.

Laboratory experiments attempting to simulate this situation were carried out with a  $\Delta t$  between two legs of an inverted U tube.<sup>2</sup> One leg contained  $\text{H}_2\text{O}$  at  $270^\circ\text{C}$  in order to approximate the vapor pressure of a bulk solution; the other leg contained a concentrated  $\text{UO}_2\text{SO}_4$  solution at a higher temperature. It was found that a solid phase was produced in the  $\text{UO}_2\text{SO}_4$  solution when its temperature was held at  $290$  to  $300^\circ\text{C}$ . Although the investigation was carried out at temperatures below those expected in the HRE-2 pressurizer, as a first approximation, it may be that if the temperature of the heavy-liquid phase becomes greater than  $20$  to  $30^\circ\text{C}$  above that of the pressurizer, the heavy-liquid phase in the reactor will lose water, and a solid phase or phases will be formed. Other experiments showed that if the temperature of solid  $\text{UO}_2\text{SO}_4$  produced in this process went above approximately  $800$  to  $900^\circ\text{C}$ , the solid  $\text{UO}_2\text{SO}_4$  would decompose to oxides, liberating  $\text{SO}_3$  to the bulk solution.

### Observations on Rate of Solution of Heavy Phase

When the temperature of a synthetic HRE-2 fuel solution contained in a silica tube becomes just greater than the two-liquid-phase boundary temperature, the heavy phase is immediately produced throughout the bulk of the solution in the form of very small droplets. No delay in the formation process has ever been observed once the immiscibility temperature has been reached. After formation, the small droplets of heavy phase coalesce to produce larger drops which settle to the bottom. On cooling of the system, the heavy phase does not redissolve quickly at temperatures just below the immiscibility temperature unless good mixing is provided. Qualitative laboratory experiments have shown that as the temperature is decreased the heavy phase dissolves faster into the light phase. This effect was noted both when the solution was agitated and when it was not; the rate at which the heavy phase dissolved was, of course, much greater under agitation.

By cooling the synthetic fuel solution without agitation, it was possible to maintain a considerable quantity of the heavy phase in contact with the light phase down to a temperature of about 270°C. However, at this temperature a qualitative change took place; the interface between the phases disappeared, leaving only a concentration gradient where the interface had been. Experiments with  $\text{UO}_2\text{SO}_4\text{-H}_2\text{O}$  solutions of various concentrations of  $\text{UO}_2\text{SO}_4$  showed the same effect, but the temperature of disappearance of the interface was not so easily observed as in the case of the synthetic homogeneous reactor fuel solution. This phenomenon has aspects which may be relevant to reactor operation and instability. If droplets of heavy phase have been formed and are suspended in the fuel solution but have moved to a position of low fission power density (so that they are not undergoing thermal decomposition or surface boiling) they will be re-dissolved by the continuous phase only as rapidly as material can be transferred across a definite liquid-liquid interface. There will, of course, be a concentration gradient on each side of the boundary but the boundary is still there. However, if their temperature becomes lowered to a point below the *minimum* temperature at which the heavy phase can maintain its identity as a separate phase, then the interfacial barrier to mass transfer *disappears* and there remain only local regions of higher concentration which have become part of the continuous phase; their dispersal is, obviously, much easier than the attack on discrete droplets.

The minimum immiscibility temperature for the system  $\text{UO}_2\text{SO}_4\text{-D}_2\text{O}$  is 274°C at 1 *m*  $\text{UO}_2\text{SO}_4$ . The minimum temperature for two-liquid-phase formation in the system formed from  $\text{CuSO}_4$ ,  $\text{UO}_2\text{SO}_4$ , and  $\text{H}_2\text{O}$  is slightly below 285°C at 18 wt %  $\text{UO}_2\text{SO}_4$  and 3 wt %  $\text{CuSO}_4$ . Lower temperatures should occur in acid-deficient portions of the five-component system  $\text{UO}_3\text{-CuO-NiO-SO}_3\text{-D}_2\text{O}$ .

#### LIQUID-LIQUID EQUILIBRIA IN THE SYSTEM $\text{UO}_3\text{-SO}_3\text{-N}_2\text{O}_5\text{-H}_2\text{O}$

During the past year a fairly comprehensive study of liquid-liquid-immiscibility boundary temperatures in the system  $\text{UO}_3\text{-SO}_3\text{-N}_2\text{O}_5\text{-H}_2\text{O}$  was completed with 0.04-, 0.08-, and 0.16-*m* uranyl solutions. This work is discussed in detail in a

recent report.<sup>10</sup> The twofold purpose of this investigation was to determine whether  $\text{UO}_2\text{SO}_4\text{-HNO}_3\text{-H}_2\text{O}$  solutions have significantly higher immiscibility temperatures than  $\text{UO}_2\text{SO}_4\text{-H}_2\text{SO}_4\text{-H}_2\text{O}$  solutions and to furnish data which may help to provide a better understanding of the nature of the immiscibility phenomenon in uranyl sulfate solutions. The appearance and disappearance of a second liquid phase was observed in small samples of solutions sealed in silica tubes suspended in a liquid nitrate bath. The metal container, equipped with glass windows, used to contain the nitrate bath is described in "Liquid-Salt Bath for High-Temperature Aqueous Studies," this chapter.

Comparison of the effects of nitric and sulfuric acids can be made either on the basis of the total  $\text{H}^+$ , which in sulfuric acid is twice the  $\text{H}^+$  in equimolar nitric acid, or on the basis of the probable free  $\text{H}^+$  in the system. Since the second ionization constant of sulfuric acid is very low at the elevated temperatures of interest, it may be assumed that the  $\text{HSO}_4^-$  ions do not dissociate appreciably. Thus, one mole of  $\text{H}_2\text{SO}_4$  may be compared with one mole of  $\text{HNO}_3$ .

The data plotted in Fig. 9.16 reveal that sulfuric acid is initially more effective than nitric acid in raising the two-liquid-phase temperature if it is considered a monobasic acid, but less if it is considered a dibasic acid. The nitric acid and sulfuric acid curves for all three  $\text{UO}_2^{++}$  concentrations show "crossover" points at temperatures

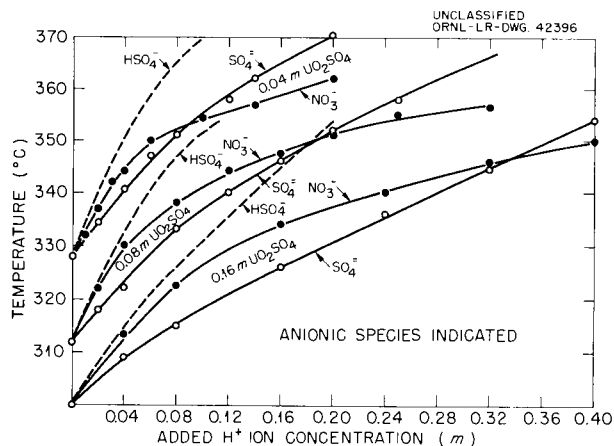


Fig. 9.16. Effect of  $\text{HNO}_3$  and  $\text{H}_2\text{SO}_4$  on Liquid-Liquid Immiscibility Temperatures of  $\text{UO}_2\text{SO}_4$  Solutions.

ranging from 353°C for 0.04  $m$   $UO_2^{++}$  solutions to 347°C for 0.16  $m$   $UO_2^{++}$  solutions. The mole ratios,  $UO_2^{++}/(\text{added } H^+)$ , at the "crossover" points were found to be relatively constant (0.455, 0.426, and 0.470 for 0.04-, 0.08-, and 0.16- $m$   $UO_2^{++}$  solutions, respectively). The significance of this constancy has not been established.

Data from Fig. 9.16, with additional data obtained by using mixtures of uranyl sulfate and uranyl nitrate as well as uranyl sulfate-sulfuric acid-nitric acid solutions, are plotted in Figs. 9.17-9.19 vs

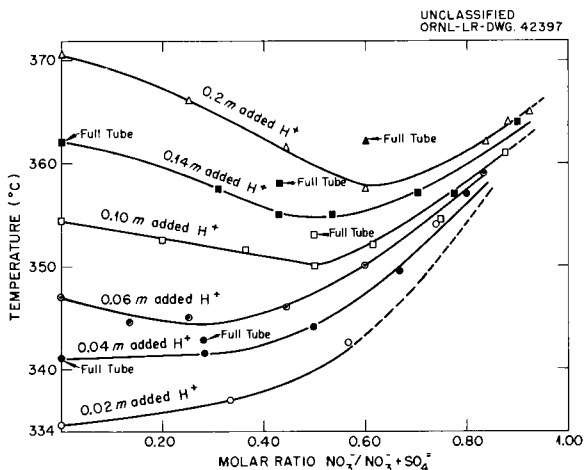


Fig. 9.17. Temperature of Separation of Heavy-Liquid Phase from 0.04  $m$   $UO_2^{++}$  Solutions as a Function of Acidity and Mole Ratio  $NO_3^- / (NO_3^- + SO_4^{--})$ .

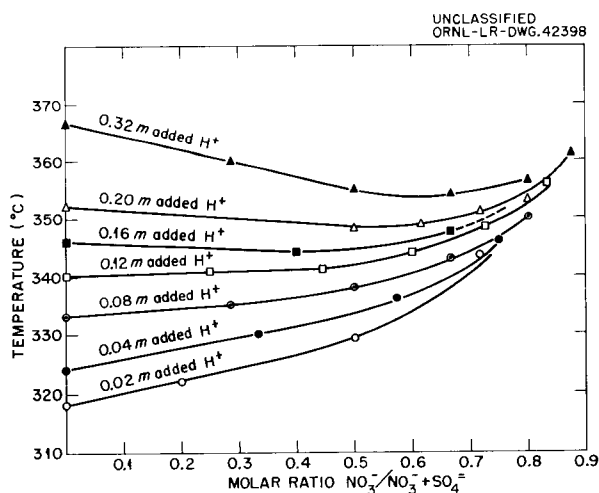


Fig. 9.18. Temperature of Separation of Heavy-Liquid Phase from 0.08  $m$   $UO_2^{++}$  Solutions as a Function of Acidity and Mole Ratio  $NO_3^- / (NO_3^- + SO_4^{--})$ .

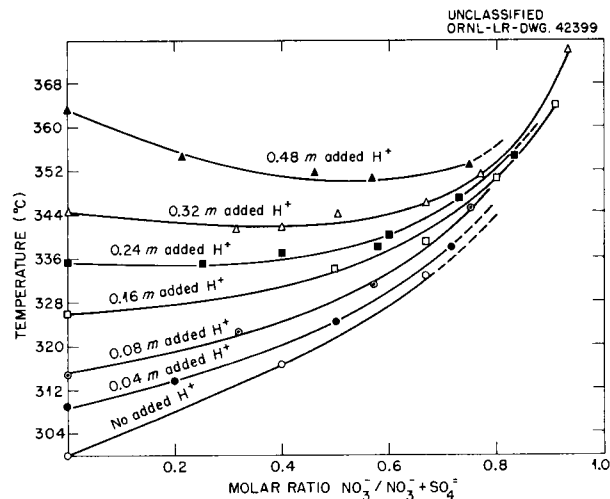


Fig. 9.19. Temperature of Separation of Heavy-Liquid Phase from 0.16  $m$   $UO_2^{++}$  Solutions as a Function of Acidity and Mole Ratio  $NO_3^- / (NO_3^- + SO_4^{--})$ .

the mole ratio,  $NO_3^- / (NO_3^- + SO_4^{--})$ , in order to show the effect of substituting  $NO_3^-$  for  $SO_4^{--}$  ions at different levels of added acid. It is apparent that, for solutions containing a low concentration of added acid, substitution of nitrate for sulfate raises the two-liquid-phase temperature but, for solutions of higher acid concentrations, the substitution of nitrate for sulfate lowers the immiscibility temperature through a minimum as the mole ratio,  $NO_3^- / (NO_3^- + SO_4^{--})$ , is increased. Since the immiscibility temperature increases with increasing acid concentration, it was first thought that this decrease might be due to increased transfer of nitrate from liquid to vapor phase with increasing temperatures. In order to determine the magnitude of this effect, immiscibility temperatures were determined for several 0.04  $m$  uranyl solutions as a function of the fractional filling of the sample container at the separation temperature. The data plotted in Fig. 9.20 show that there is an approximately linear relationship between immiscibility temperature and volume fraction of liquid in the tube. Extrapolation of the lines to zero vapor volume gave the immiscibility-temperature values marked "full tube" in Fig. 9.17. The data show that the dip in the curves at higher acidities is reduced but not completely removed by eliminating the vapor phase.

An interesting observation, made during the course of the volume-filling experiments, was that a solution containing 0.04  $m$   $UO_2SO_4$ , 0.02  $m$

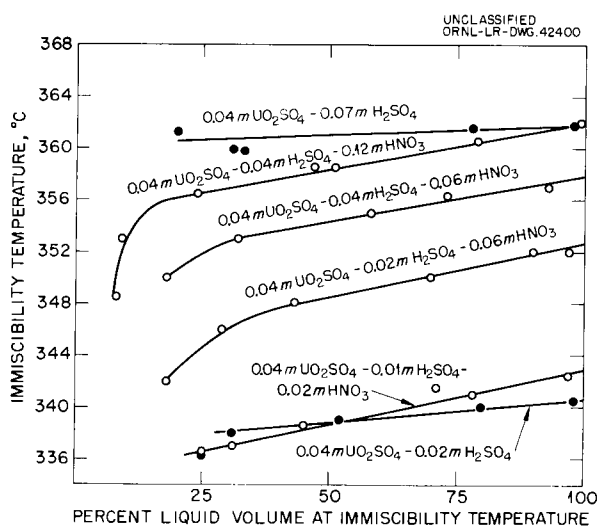


Fig. 9.20. Variation of Immiscibility Temperature with Volume Per Cent of Liquid in Sample Container.

H<sub>2</sub>SO<sub>4</sub>, and 0.06 *m* HNO<sub>3</sub> ("full tube" immiscibility temperature = 352.6°C) did *not* show a phase separation at temperatures up to 360°C, the maximum temperature to which it was heated, in a tube that was completely full at 351.5°C. This indicates that the immiscibility temperature may be raised significantly by the application of high pressures.

From the standpoint of possible application to homogeneous reactors, the data obtained indicate that there is some advantage in using mixed nitrate-sulfate anions in uranyl solutions, as compared to UO<sub>2</sub>SO<sub>4</sub>-H<sub>2</sub>SO<sub>4</sub>-H<sub>2</sub>O solutions, for the purpose of raising liquid-liquid-immiscibility temperatures of aqueous homogeneous reactor fuels. The theoretical significance of the data is not clear at this time, but in this system an interdependent relationship between acidity and complexing of the uranyl ion seems to be indicated.

#### SOLID-LIQUID EQUILIBRIA IN THE SYSTEMS UO<sub>3</sub>-N<sub>2</sub>O<sub>5</sub>-H<sub>2</sub>O, 25 TO 350°C, AND UO<sub>3</sub>-CuO-NiO-N<sub>2</sub>O<sub>5</sub>-H<sub>2</sub>O, 300°C

##### The System UO<sub>3</sub>-N<sub>2</sub>O<sub>5</sub>-H<sub>2</sub>O

During the past year two memoranda were written to emphasize potential advantages of nitrate-compared to sulfate-based aqueous fuel systems.<sup>11,12</sup> Briefly, these pointed to absence of a liquid-liquid-immiscibility region, oxides instead of salts as the stable solid phases, possible low

or no radiolytic production of free N<sub>2</sub> gas, possible corrosion benefits, and potential economies in fuel processing. It was recalled that earlier experimental investigations at high temperatures had been undertaken on concentrated nitrate solutions and that these current phase studies were the first to be undertaken in the low-concentration range. With these facts in mind, the system UO<sub>3</sub>-N<sub>2</sub>O<sub>5</sub>-H<sub>2</sub>O was investigated from 25 to 350°C. Details concerning past data and experimental procedure were presented in past HRP quarterly reports.<sup>2-4</sup> In addition to an insight into the over-all phase behavior of uranyl nitrate solutions for use as homogeneous reactor fuels, precise and accurate measurements were obtained to glean further information on the general behavior of hexavalent uranium salts at elevated temperature in aqueous media. Information of this general type can be applied to the further understanding of the behavior of sulfate systems.

The best experimental data to date are shown in Fig. 9.21. The solubility curves are extended down to  $5 \times 10^{-4}$  *m* total NO<sub>3</sub><sup>-</sup> and up to 5 *m* total NO<sub>3</sub><sup>-</sup>. The apparent reversal of curvature in the 10<sup>-2</sup> to 10<sup>-4</sup> *m* NO<sub>3</sub><sup>-</sup> range at high temperature may be real, as evidenced by repeated agreement of data and by the reverse slope at 25°C. In fact, as the NO<sub>3</sub><sup>-</sup> concentration approaches zero, the saturation mole ratio, UO<sub>3</sub>/NO<sub>3</sub><sup>-</sup>, must approach infinity, since there is a finite solubility of UO<sub>3</sub> in pure H<sub>2</sub>O.

The data from 10<sup>-2</sup> and 10<sup>-4</sup> *m* NO<sub>3</sub><sup>-</sup> were obtained by a new method. When the pH values at 25°C for pure HNO<sub>3</sub>-H<sub>2</sub>O solutions and for several HNO<sub>3</sub>-H<sub>2</sub>O solutions containing dissolved UO<sub>3</sub> were plotted against the logarithm of the calculated "free" acid concentration,  $[\text{total } m_{\text{NO}_3^-}] - 2[m_{\text{UO}_2(\text{NO}_3)_2}]$ , for each solution, then all values fell approximately on the same curve (Fig. 9.22). Therefore, the pH at 25°C of an experimental sample, saturated at high temperature with UO<sub>3</sub>, was measured; reference to the curve of Fig. 9.22 gave the "free acid" concentration required for this pH. Uranium was analyzed by the controlled-potential coulometric-titration method.<sup>20</sup> From these two values the mole ratio, UO<sub>3</sub>/NO<sub>3</sub><sup>-</sup>, was obtained at very low concentration, where the

<sup>20</sup>W. D. Shults and P. F. Thomason, *Anal. Chem.* 31, 492 (1959).

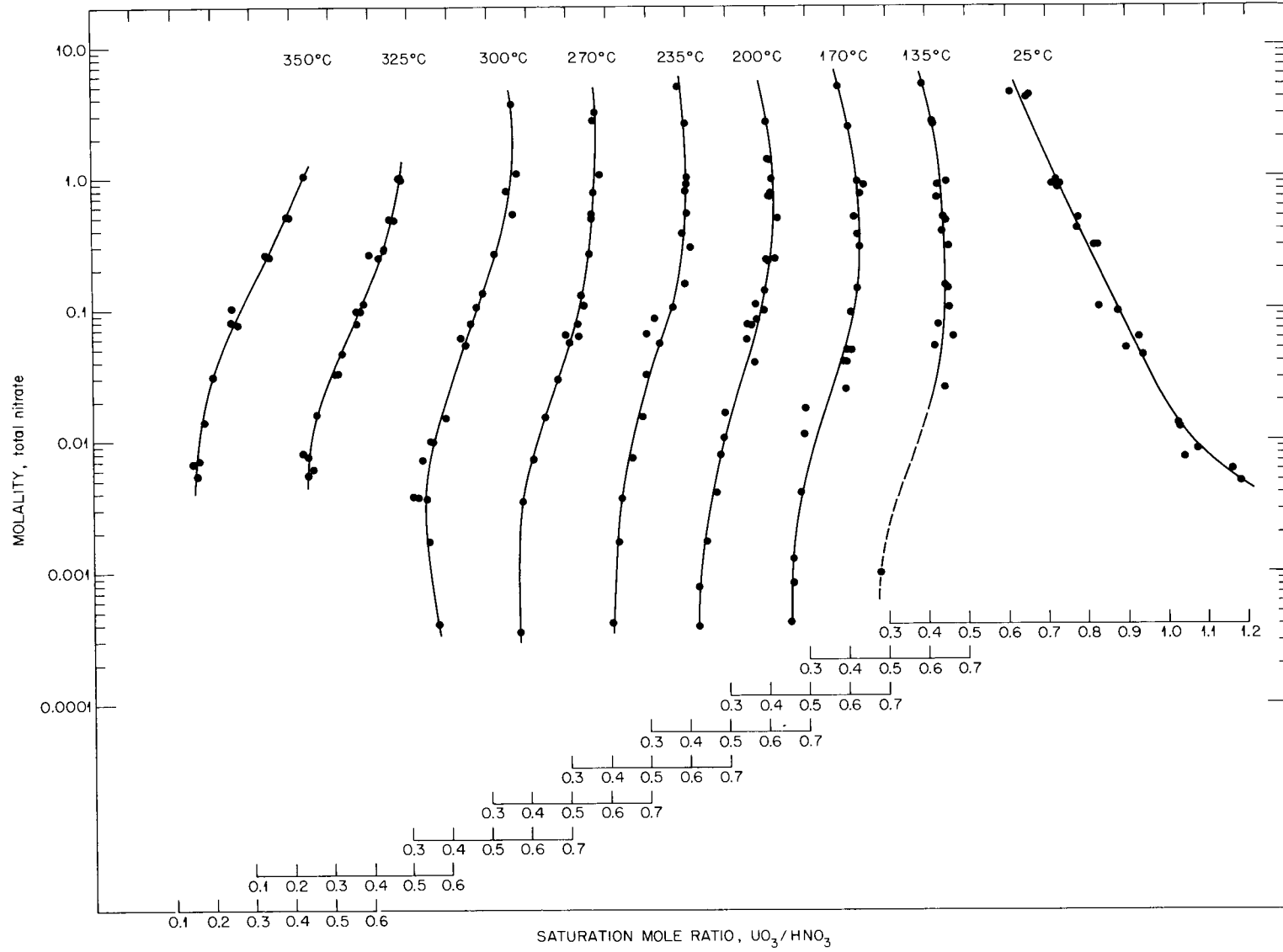


Fig. 9.21. The Solubility of  $UO_3 \cdot 7H_2O$  in  $HNO_3-H_2O$  Solutions, 25 to 350°C.

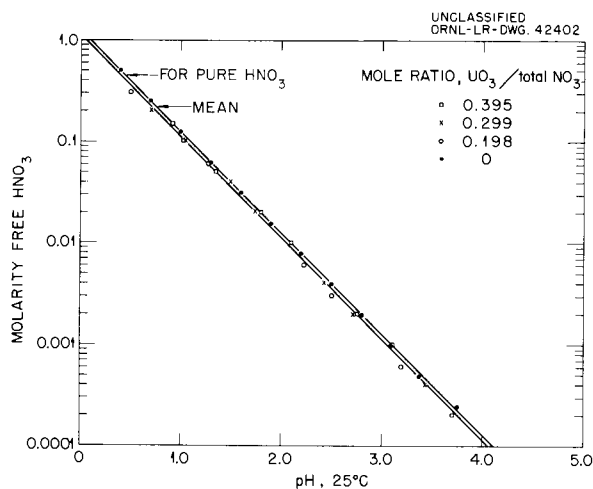


Fig. 9.22. The pH at 25°C of  $\text{HNO}_3\text{-H}_2\text{O}$  and  $\text{UO}_3\text{-H}_2\text{O}$  Solutions.

direct titration of  $\text{HNO}_3$  is very difficult due to the low concentration of  $\text{HNO}_3$  and the small volume of the sample (5 ml).

The solubility data obtained to date give further evidence of the thermal phase stability of the nitrate system. There is, however, some uncertainty concerning  $\text{NO}_2\text{-HNO}_3\text{-N}_2\text{O}_5$  equilibria in the vapor and liquid phases and the effect of oxygen overpressure on this system.

#### The System $\text{UO}_3\text{-CuO-NiO-N}_2\text{O}_5\text{-H}_2\text{O}$ and Its Relation to Homogeneous Reactors

The encouraging results of the preliminary investigation of the system  $\text{UO}_3\text{-N}_2\text{O}_5\text{-H}_2\text{O}$  supported further consideration of nitrate-based homogeneous reactor fuels<sup>11,12</sup> in order to learn whether stability difficulties might arise with fuels containing copper and nickel in addition to uranium. In particular, it was considered important to establish the general nature of the solid phases and to ascertain whether there would be any regions of composition showing very low solubility of the metallic-oxide components.

The preliminary experimental approach was the same as that used for the over-all study of solid-liquid equilibrium in the multicomponent sulfate system. Briefly, excess amounts of particular solids were added to  $\text{HNO}_3\text{-H}_2\text{O}$  solutions of 0.02, 0.06, 0.2, and 0.6 *m*  $\text{HNO}_3$  in pressure vessels. The solution-solid mixtures were equilibrated successively at 200 and 300°C; at each temperature liquid samples were withdrawn for analysis.

After a run the vessels were cooled rapidly to low temperature, and the solids were removed and submitted for x-ray diffraction analysis. The starting compositions were so chosen as to give the maximum permissible number of solid phases at constant temperature, saturation pressure, and variable  $\text{N}_2\text{O}_5$  concentration, thus producing ternary, binary, and monary curves for the five-component system and its included four- and three-component systems as a function of  $\text{N}_2\text{O}_5$  concentration.

The results showed no apparent significant decreases in solubility in the region from 0.02 to 0.6 *m* total  $\text{NO}_3^-$ . From these preliminary data, compositions having mole ratios,  $(\text{UO}_3 + \text{CuO} + \text{NiO})/\text{NO}_3^-$ , of less than 0.3 to 0.4 appear to be phase-stable at 300°C for this system. The solid phases identified were all oxides, such as  $\text{CuO}$ ,  $\text{NiO}$ , and  $\text{UO}_3 \cdot n\text{H}_2\text{O}$ , as had been expected for the nitrate system. One unidentified oxide, presumably a double oxide of nickel and uranium, was found. The oxide,  $\text{CuO} \cdot 3\text{UO}_2$ , found in the analogous sulfate system,<sup>8</sup> was also identified. Based on this preliminary evaluation, the system  $\text{UO}_3\text{-CuO-NiO-N}_2\text{O}_5\text{-H}_2\text{O}$  appears to present no thermal-phase-stability problem in the concentration ranges of specific homogeneous reactor interest at least to 300°C. It is anticipated that the analogous  $\text{D}_2\text{O}$  system will show no marked deviation in behavior from the  $\text{H}_2\text{O}$  system.

#### INVESTIGATION OF THORIUM-CONTAINING NITRATE AND FLUORIDE SOLUTIONS FOR BREEDER-BLANKET USE

Efforts to find a thorium-containing solution suitable for a breeder-blanket operation at 300°C were unsuccessful.<sup>3</sup> Solutions containing  $\text{Th}(\text{NO}_3)_4$ ,  $\text{LiNO}_3$ , and  $\text{H}_2\text{O}$  in the mole ratios 6:71:23 and 7:62:31 were observed to precipitate a solid phase at 290°C which did not redissolve until the mixtures had cooled to 240°C. Solutions containing  $\text{Th}(\text{NO}_3)_4$ ,  $\text{Be}(\text{NO}_3)_2$ , and  $\text{H}_2\text{O}$  in the mole ratios 15:6:79, 8:15:77, 11:11:78 were observed to precipitate a solid phase at 290, 280, and 280°C, respectively. The precipitated solids either did not redissolve on cooling or redissolved only when the temperature had dropped below 250°C. The addition of just enough water to dissolve the latter two mixtures at room temperature raised the precipitation temperature to 300 and 290°C, respectively, but the solids formed did

not redissolve above 250°C on cooling. Several attempts to dissolve  $\text{ThF}_4$  in moderately concentrated aqueous solutions of  $\text{BeF}_2$  at 300°C were unsuccessful. All the work described above was done by sealing mixtures into small-diameter quartz tubes, agitating the tubes in an aluminum block furnace, and observing visually while the tubes were being heated and cooled.

#### LIQUID-SALT BATH FOR HIGH-TEMPERATURE AQUEOUS STUDIES

In the synthetic method for the determination of phase equilibria, known mixtures of components are placed in containers and are heated or cooled. The temperature at which a phase transition occurs is noted by some means; this defines a saturation limit for the particular synthetic mixture. The usual procedure for aqueous systems at high temperature involves sealing a known mixture in a glass tube and visually observing the phase-transition temperature.<sup>21</sup> The semi-micro equipment used for this purpose at ORNL consisted of cylindrical aluminum blocks heated with spiral-wound resistance wire and containing slits for observation. A Vibro-Tool was used for vibrating the glass tube, thus mixing the solution, and a short-range telescope was used for

observing phase transitions.<sup>22</sup> Later, stirred liquid salt baths in glass containers were used in order to minimize the effects of temperature gradients.<sup>14</sup> These baths, however, constituted a potential hazard since, upon the explosion of a tube, liquid salt was sprayed up and out of the bath and, usually, the all-glass container would break.

In order to remedy these difficulties metal units were developed to contain the liquid salt, and these are now in use. Figure 9.23 shows such a unit. The container units have heavy-duty glass windows on the back and front faces. The top is covered with a metal plate and the whole unit is placed in a wooden box with front and back windows. A light is placed behind the back window and a small telescope is used for observation of phase transitions. A constant amount of heat is supplied by a hot plate beneath the unit and a variable amount is furnished by an Inconel-covered Calrod loop heater immersed in the bath and controlled by a variable transformer. The capillary tubes containing the compositions being tested are agitated periodically, while they are heated or cooled in the bath, by means of a Vibro-Tool controlled by an interval timer.<sup>22</sup> This equipment was used for the determination of liquid-liquid-immiscibility boundaries by the synthetic method for the systems  $\text{UO}_3\text{-SO}_3\text{-N}_2\text{O}_5\text{-H}_2\text{O}$ ,  $\text{UO}_3\text{-CuO-NiO-SO}_3\text{-D}_2\text{O}$ , and  $\text{UO}_3\text{-SO}_3\text{-H}_2\text{O}$  discussed in this chapter.

<sup>21</sup>See papers of A. W. C. Menzies, A. Benrath, and others.

<sup>22</sup>W. L. Marshall, H. W. Wright, and C. H. Secoy, *J. Chem. Educ.* 31, 34 (1954).

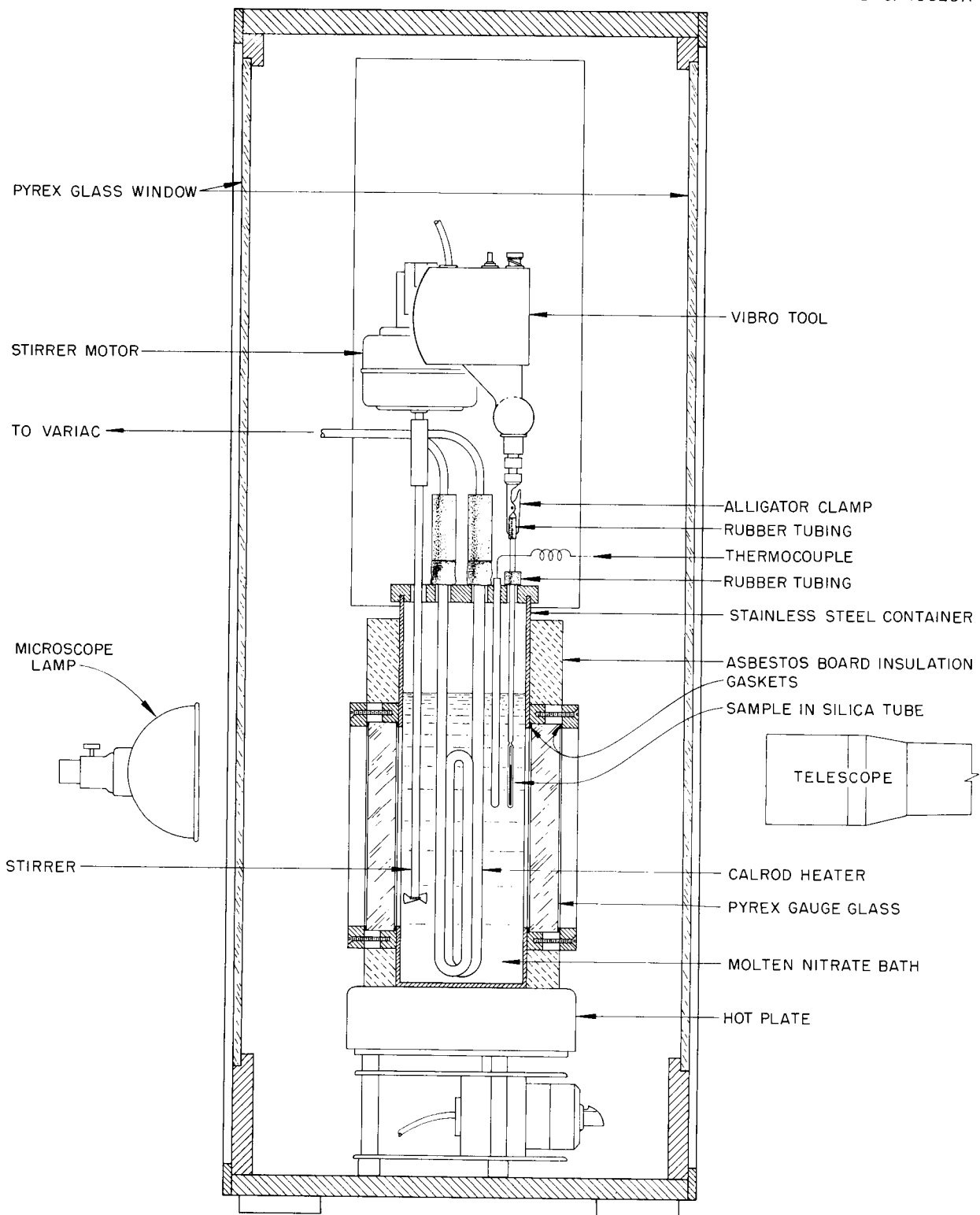


Fig. 9.23. Equipment for Solubility Studies at Elevated Temperatures.

## 10. REACTIONS IN AQUEOUS SOLUTIONS

## RECOMBINATION OF HYDROGEN AND OXYGEN

Disposal of the 2:1 mixture of hydrogen (or deuterium) and oxygen created by the radiolytic decomposition of water in fissioning aqueous solutions presents a substantial technical and engineering problem in connection with the development of aqueous homogeneous reactors.

The fact that dissolved hydrogen (or deuterium) and oxygen will react smoothly at elevated temperatures to form water if a suitable catalyst is present in solution makes recombination of the radiolytic gases *in situ* possible.

Elucidation of the kinetics and mechanisms of recombination catalysis is therefore of both practical and fundamental significance.

## Cupric Ion as a Homogeneous Catalyst in Nitrate Solutions

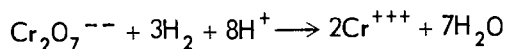
M. J. Kelly            H. H. Stone  
M. D. Silverman

The system  $\text{UO}_3\text{-HNO}_3\text{-H}_2\text{O(D}_2\text{O)}$  has been suggested as an alternate fuel for homogeneous reactor operations.<sup>1</sup>

Since dissolved cupric sulfate has proved extremely successful in suppressing gas evolution in the sulfate system used in HRE-2 under actual reactor operations, a series of experiments was carried out to determine the effectiveness of cupric nitrate as a recombination catalyst in the proposed nitrate system.

**Light-Water-Hydrogen System.** — For this system  $k_{\text{Cu}}$  was determined by the technique described by Peters and Halpern<sup>2</sup> using  $\text{Cr}_2\text{O}_7^{--}$  as the oxidant instead of oxygen gas,<sup>3</sup> since the two methods had been shown to give the same value for the rate constant and since the results, at constant hydrogen pressure, would be useful for other studies.

The stoichiometry of the reaction is considered to be



<sup>1</sup>W. L. Marshall, *Consideration of  $\text{UO}_2(\text{NO}_3)_2\text{-HNO}_3\text{-H}_2\text{O(D}_2\text{O)}$  as a High Temperature Homogeneous Reactor Fuel*, ORNL CF-59-6-100 (May 26, 1959).

<sup>2</sup>E. Peters and J. Halpern, *J. Phys. Chem.* **59**, 793 (1955).

<sup>3</sup>H. F. McDuffie *et al.*, *J. Phys. Chem.* **62**, 1030 (1958).

and the rate expression for the consumption of hydrogen is

$$\text{rate} = k_{\text{Cu}} [\text{Cu}^{++}] [\text{H}_2] [\text{O}_x]^0 .$$

The disappearance of the  $\text{Cr}_2\text{O}_7^{--}$  with time was followed with a spectrophotometer using samples drawn from the reaction vessel. The hydrogen pressure within the reaction vessel was maintained constant and, therefore, the hydrogen concentration in the liquid phase remained constant as did the  $\text{Cu}^{++}$  concentration. Therefore, at any two times  $t_1$  and  $t_2$  will be

$$k_{\text{Cu}} = \frac{3\{[\text{Cr}_2\text{O}_7^{--}]_1 - [\text{Cr}_2\text{O}_7^{--}]_2\}}{[\text{Cu}^{++}][\text{H}_2](t_2 - t_1)} .$$

The 3 appears in the numerator because of the stoichiometry of the reaction. The values for the concentration of  $\text{H}_2$  in solution were calculated from values of its solubility in water at temperatures as had been done previously<sup>3</sup> (and are subject to substantial recognized uncertainties). The results obtained for this system are shown on Fig. 10.1 and can be represented by the expression

$$k_{\text{Cu}^{++}} = (6.56 \times 10^{14}) e^{-27,000/RT} \text{ liters}\cdot\text{mole}^{-1}\cdot\text{hr}^{-1} .$$

Since some question might arise concerning the use of an oxidant other than oxygen, several  $k_{\text{Cu}}$  values at various temperatures were determined for simulated *sulfate-based* reactor fuel solutions using dichromate as the oxidant. These values were found to agree very well with values previously determined by the hydrogen-oxygen recombination method. These data are also plotted on Fig. 10.1.

Figure 10.1 shows the activation energy to be approximately the same for both sulfate and nitrate systems. The catalytic effect of the cupric ion in the nitrate system is not so great as it is in the sulfate system. The value of  $k_{\text{Cu}^{++}}$  in the sulfate system is some 2.2 to 2.5 times greater than the value at the same temperature in the nitrate system.

**Heavy-Water-Deuterium System.** — Since the moderating properties of heavy water are required in the present breeder concept of homogeneous

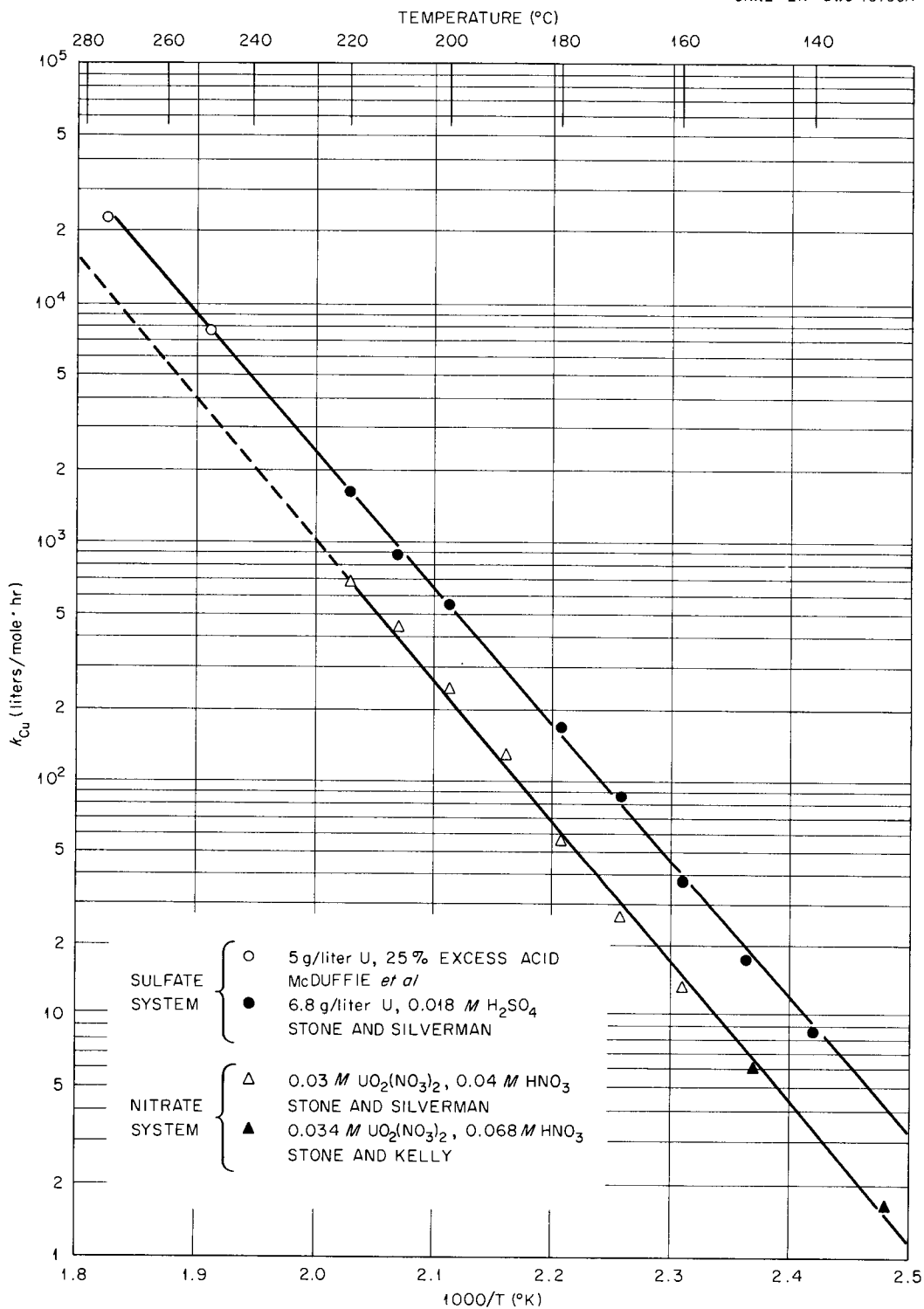


Fig. 10.1. Comparison of Sulfate and Nitrate Systems: Effect of Temperature on Recombination Rate.

reactors, data on the deuterium-oxygen recombination in heavy water with cupric ion as the catalyst became desirable. A series of experiments using D<sub>2</sub>O as the solvent and D<sub>2</sub> as the reductant was instituted. Initial experiments carried out, using Cr<sub>2</sub>O<sub>7</sub><sup>2-</sup> as the oxidant as previously described, resulted in anomalous results at high temperatures, with the observed rate being both slower than expected from data obtained in the sulfate solutions in heavy water by McDuffie and Stone<sup>4</sup> and definitely not appearing as zero order with respect to the concentration of oxidant. cursory investigation of these difficulties showed that decomposition of the nitric acid in the D<sub>2</sub>O solutions formed soluble nitrogen oxides which interfered with the spectrophotometric determination of the Cr<sub>2</sub>O<sub>7</sub><sup>2-</sup> present in the solutions. This decomposition, while of interest, was not studied further, but the techniques described by McDuffie *et al.*<sup>3</sup> were used for the balance of the experimental work.

The catalyst was cupric ion and the system 0.03 *m* UO<sub>2</sub>(NO<sub>3</sub>)<sub>2</sub>, 0.08 *m* DNO<sub>3</sub> with D<sub>2</sub>O as the solvent. Experiments were performed over a temperature range of 200 to 300°C. The results are shown in Fig. 10.2 compared with results ob-

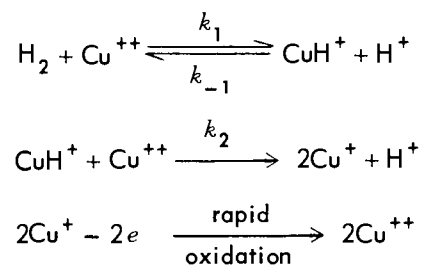
tained by McDuffie and Stone in the sulfate system by similar methods. It can be seen that the activity of the copper was considerably lower in the nitrate system, as had been observed in the light-water system. The activation energy calculated from this data is 26.0 kcal/mole. This compares with 27.0 kcal/mole for the light-water system. The apparent difference in temperature coefficients between the nitrate and sulfate systems, as shown in Fig. 10.2, may be due to insufficient experimental data for the sulfate system. It is not inconceivable that the decomposition of the nitrates at the higher temperatures results in enough lowering of the acidity to cause the apparent increase in temperature coefficient in the nitrate system.

In a homogeneous reactor with a total pressure of 2000 psia, including 100 psi of excess oxygen, the maximum power densities which could be achieved without radiolytic gas evolution with 0.02 *M* Cu(NO<sub>3</sub>)<sub>2</sub> as the catalyst were calculated to be 36 and 18 w/cc at 300 and 275°C respectively.

### Rate of Oxidation of Dissolved Hydrogen or Deuterium Catalyzed by Cu(ClO<sub>4</sub>)<sub>2</sub> in Light and Heavy Water

H. H. Stone      M. J. Kelly      G. M. Watson  
H. F. McDuffie

A mechanism for the homogeneous catalysis of the oxidation of dissolved hydrogen by dissolved cupric salts was proposed by Halpern<sup>5</sup> as follows:



This mechanism was based on the interpretation of the effects of changes in acidity and copper concentration in the cupric perchlorate-perchloric acid system at 110°C.

The interest of this Laboratory in the mechanism of recombination reactions initiated a thorough

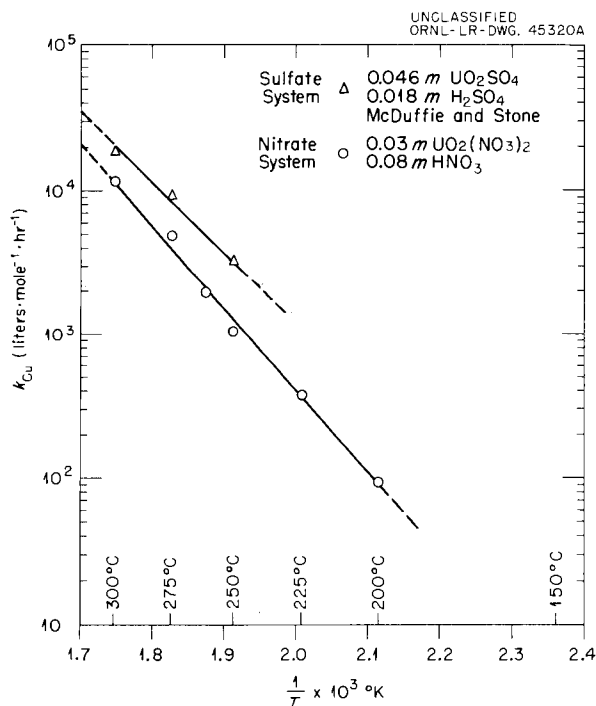


Fig. 10.2. Effect of Temperature on Recombination Rate. Heavy water solvent, deuterium gas.

<sup>4</sup>H. F. McDuffie and H. H. Stone, *HRP Quar. Prog. Rep. Jan. 31, 1958*, ORNL-2493, p 181-83.

<sup>5</sup>J. Halpern, E. R. Macgregor, and E. Peters, *J. Phys. Chem.* 60, 1455 (1956).

survey of this reaction to determine the mechanism unequivocally if possible.

It was suggested by P. H. Emmett<sup>6</sup> that this mechanism would give rise to isotope exchange if deuterium gas were used in connection with a light-water solution of the catalyst; any  $D^+$  formed in the first step would immediately exchange with the  $H_2O$  to form  $H^+$  which in the  $k_{-1}$  reaction would regenerate HD instead of DD. If no isotope exchange were observed, or if it were substantially less than calculated, the adequacy of this mechanism would be challenged. For accurate calculations of the expected amount of exchange, it is necessary to have estimates of the rates of the various component reactions. To entirely delineate the conditions imposed by the postulated mechanism, the rates of reaction of hydrogen and deuterium in light-water solutions with varying acidity, and the rates of reaction of hydrogen and deuterium in heavy-water solutions with varying acidities and copper concentrations, as well as the solubility of hydrogen and deuterium in these various solutions at several temperatures must be known.

A program to obtain these data has been in progress during the past year.

The reaction rate constants for the homogeneously catalyzed activation of molecular hydrogen and deuterium by cupric ion were determined at 100, 110, 120, 130, and 140°C for the following systems:

- 20 atm  $H_2$ ,  $H_2O$ , 0.1 M  $Cu(ClO_4)_2$ , 0.01 and 1.0 M  $HClO_4$
- 20 atm  $D_2$ ,  $H_2O$ , 0.1 M  $Cu(ClO_4)_2$ , 0.01 and 1.0 M  $HClO_4$
- 20 atm  $H_2$ ,  $D_2O$ , 0.1 M  $Cu(ClO_4)_2$ , 0.01 and 1.0 M  $DClO_4$
- 20 atm  $D_2$ ,  $D_2O$ , 0.1 M  $Cu(ClO_4)_2$ , 0.01 and 1.0 M  $DClO_4$

These experimental data are presented in Figs. 10.3 and 10.4.

The rate constants are calculated on the basis of

$$r = k_{Cu} [Cu][H_2]$$

in order that the data may be internally consistent. No interpretation of mechanism can be attempted until the solubilities of hydrogen and deuterium become available. The activation energy for each system was calculated and found to be independent

of the choice of solute gas (hydrogen or deuterium) or solvent ( $D_2O$  or  $H_2O$ ). However, as the hydrogen (or deuterium) ion concentration, that is, the acidity, was increased from 0.01 to 1.0 M the energy of activation decreased from  $27.0 \pm 0.5$  to  $24.0 \pm 0.5$  kcal/mole. The observed reaction rate constants were lower at higher acidities for each system. The reaction rate constants were lower for  $D_2$  than for  $H_2$  in similar systems.

The rate constants for the systems previously mentioned, but with cupric perchlorate concentrations of 0.190, 0.325, and 1.0 M, were determined to check the effect of variations of copper concentration. These data are plotted in Figs. 10.5 and 10.6. At the low acid concentration (0.01 M) the effect of copper is consistent with the rate equation used for calculations. At high acid concentrations variations appear as the copper concentration changes. At high copper concentrations the rate constant again becomes consistent with first-order copper behavior. This same system was also investigated at constant 0.1 M copper perchlorate with variations in acid concentration of 0.2575, 0.505, and 0.7525 M. These data combined with data from previous experiments at 0.01 and 1.0 M acid are plotted in Fig. 10.7. An increase in acid concentration effectively lowers the observed rate of reaction.

All the results reported here are based on the assumption that the solubilities of  $H_2$  and  $D_2$  are equal and do not change over the temperature range studied. They are subject to correction when solubility information for these solutions becomes available. Experimental work is in progress to determine these solubilities.

#### PEROXIDE STUDIES

##### The Concentration of Peroxide in Uranyl Sulfate Solutions at Incipient Precipitation

L. O. Gilpatrick                      M. J. Kelly  
 H. R. Jolley<sup>7</sup>                          M. D. Silverman  
 G. M. Watson

The allowable power level of an aqueous homogeneous reactor could be limited by the concentration of peroxide produced by fission fragments acting on the solution; uranium peroxide, formed by the reaction of peroxide with uranyl ion, has a

<sup>6</sup>H. F. McDuffie and H. H. Stone, *HRP Quar. Prog. Rep.* Jan. 31, 1957, ORNL-2272, p 170-71.

<sup>7</sup>Summer participant from Loyola University of the South.

UNCLASSIFIED  
ORNL-LR-DWG 42537A

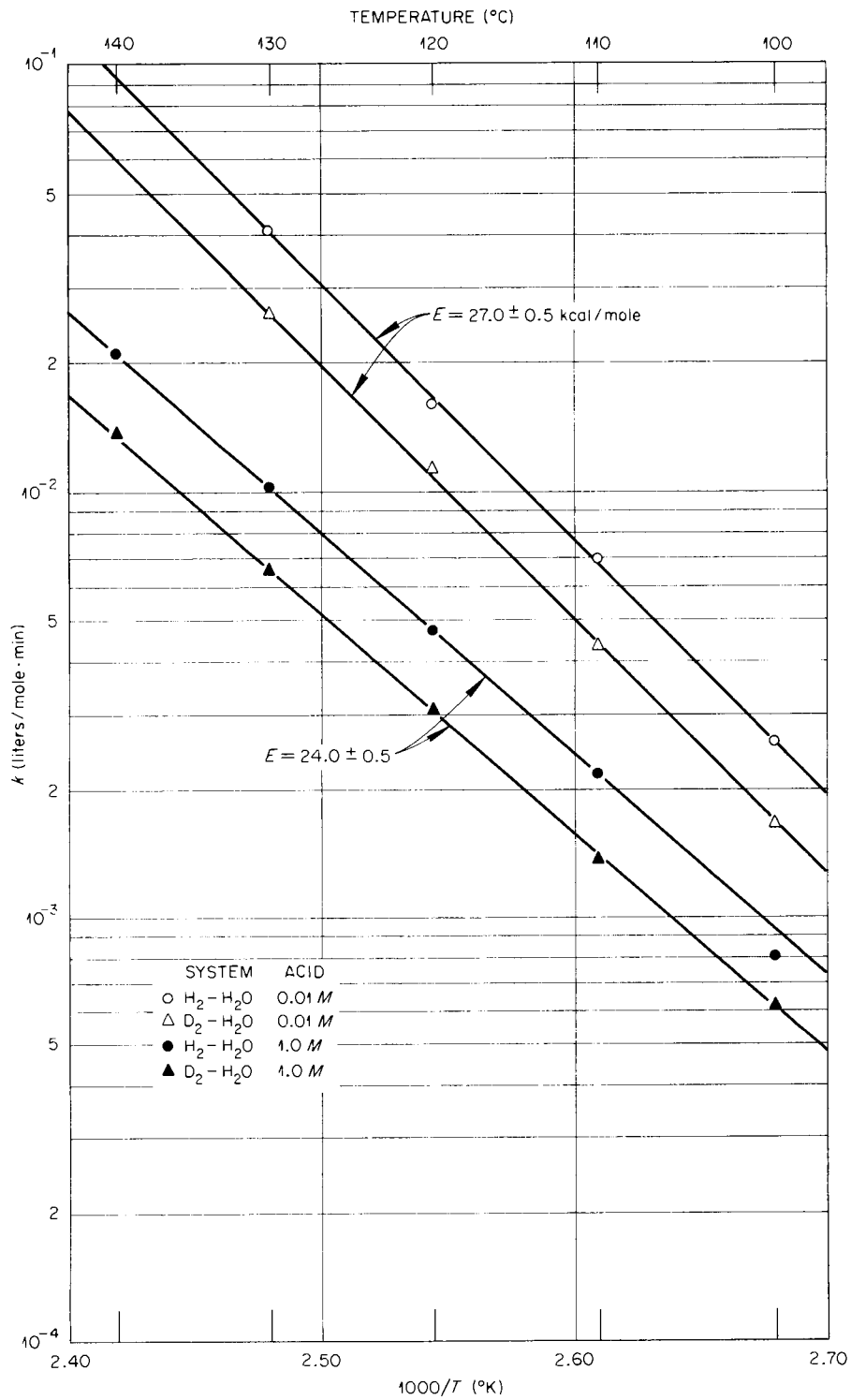


Fig. 10.3. Effect of Temperature on Recombination Rates (Perchlorate-H<sub>2</sub>O System).

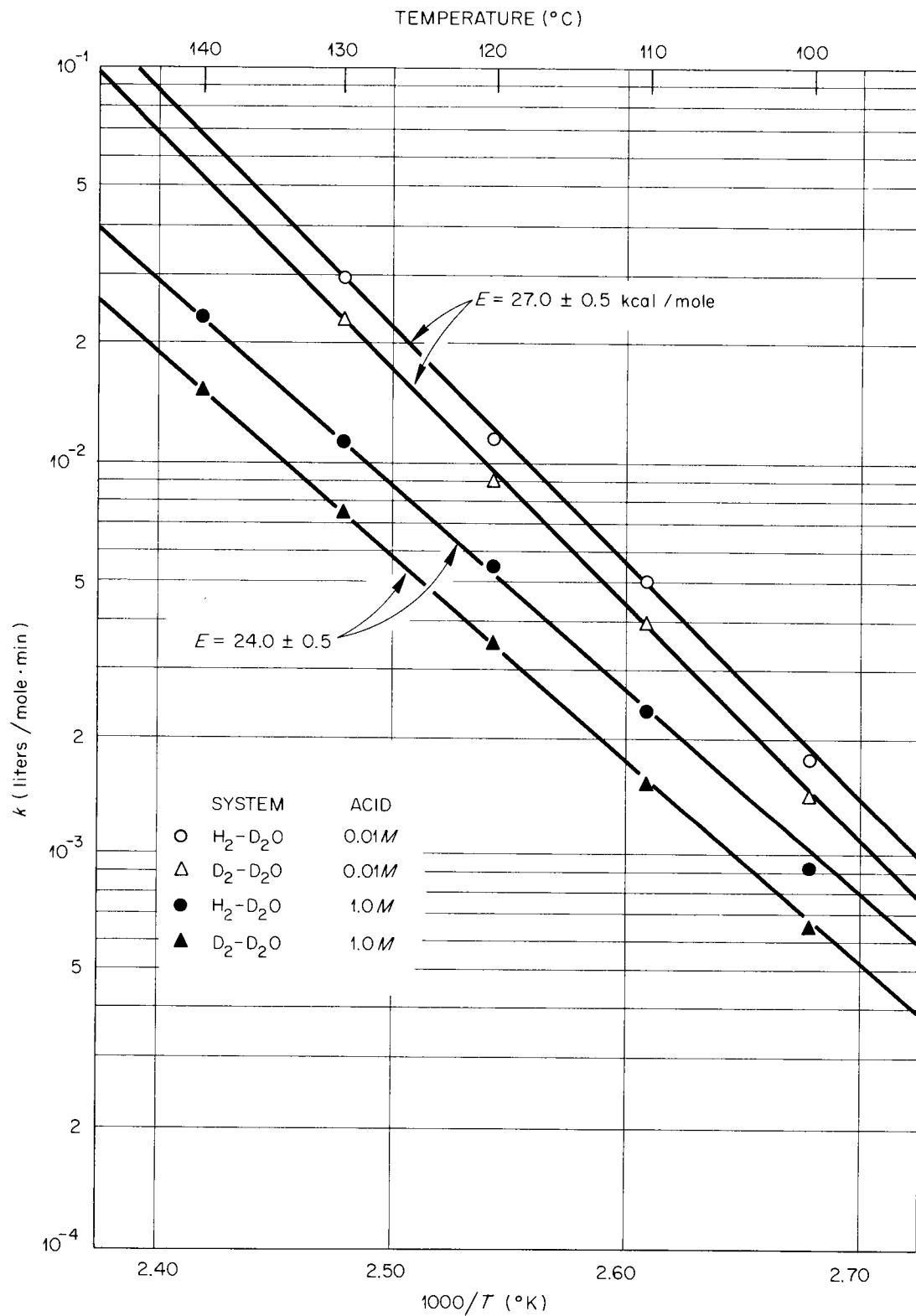


Fig. 10.4. Effect of Temperature on Recombination Rates (Perchlorate- $D_2O$  System).

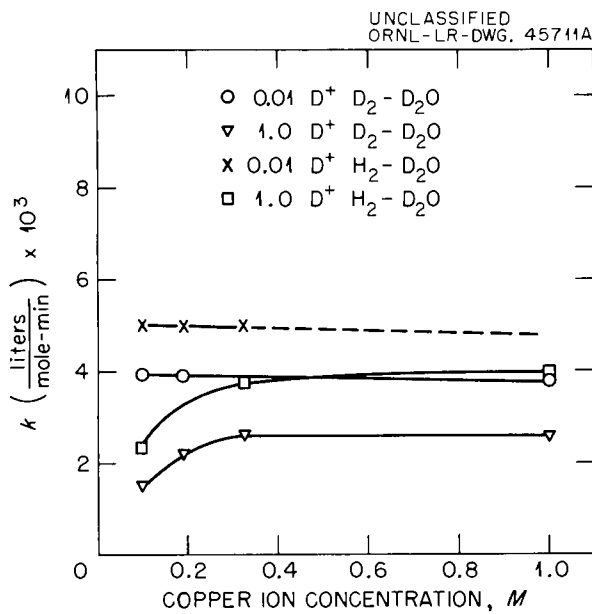


Fig. 10.5. Effect of Copper Ion Concentration on Calculated Rate Constants at 0.01 M and 1.0 M Acid. 110°C, 20 atm.

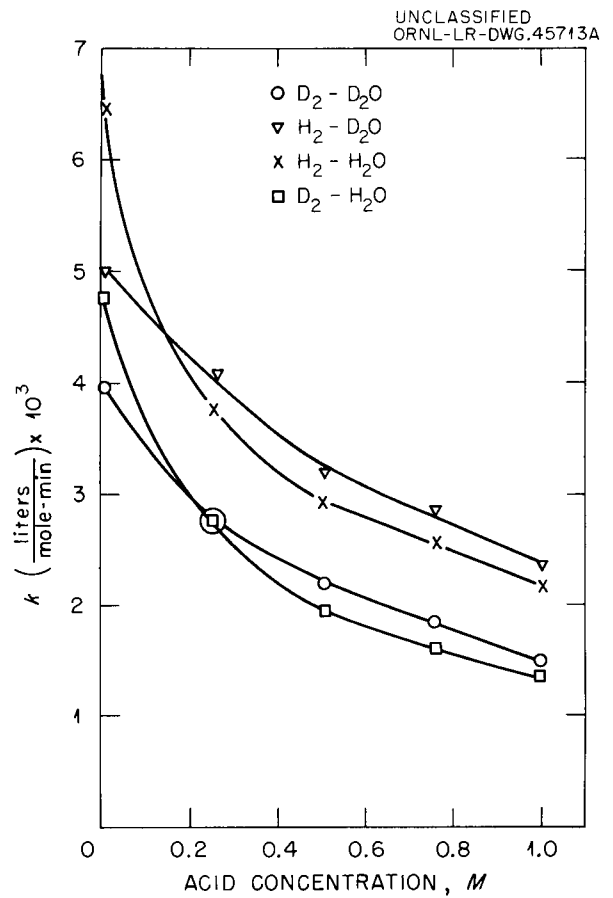


Fig. 10.7. The Effect of Acid on the Calculated Reaction Rate Constant. 110°C, 20 atm, 0.1 M Cu(ClO<sub>4</sub>)<sub>2</sub>.

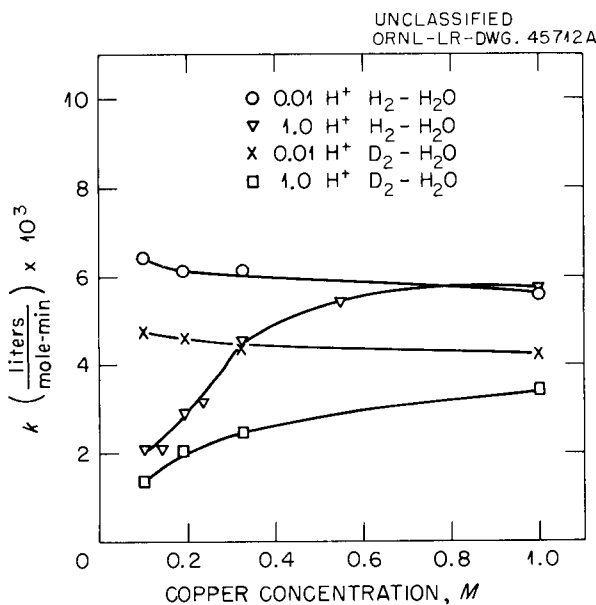


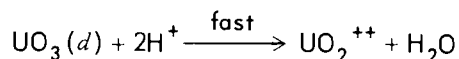
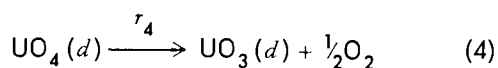
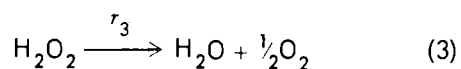
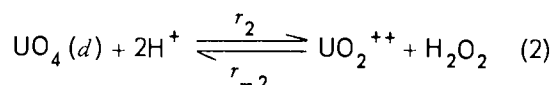
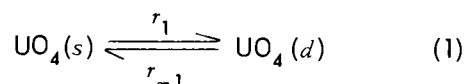
Fig. 10.6. Effect of Copper Ion Concentration on Calculated Rate Constants at 0.01 M and 1.0 M Acid. 110°C, 20 atm.

quite low solubility, and its precipitation in a circulating homogeneous reactor system would pose serious problems.

Precipitation of uranium peroxide from uranyl sulfate solutions occurs when the concentration of total peroxide exceeds an allowable equilibrium peroxide concentration for saturation. This equilibrium concentration is a function of the environmental conditions. This investigation examined the effects on the magnitude of the total peroxide concentration at saturation resulting from changing the concentrations of acid or uranium and altering the temperature. The results of the experimental observations were used in an attempt to arrive at a self-consistent set of numerical parameters related

to the equilibrium involving hydrogen peroxide, uranium peroxide, uranyl ion, and hydrogen ion.

The chemical reactions in this system involve some reversible processes, and some unidirectional decomposition reactions, which are all intimately related. While the mechanisms of the reactions in this system are not completely understood, the following set of equations is presented for purposes of the discussion:<sup>8,9</sup>



The notations (s) and (d) signify solid or dissolved species, and the symbols  $r_1$  and  $r_{-1}$  represent the forward and reverse rates of the indicated process. In the present discussion, solid uranium peroxide existing under the experimental conditions is denoted as  $\text{UO}_4(s)$  without attempting to express explicitly the number of molecules of water of hydration involved and ignoring the question as to whether the solid phase is  $\text{UO}_4 \cdot (\text{H}_2\text{O})_x$  or  $\text{UO}_3 \cdot \text{H}_2\text{O}_2 \cdot (\text{H}_2\text{O})_{x-1}$  (ref 10).

Equations (1) and (2) represent reversible processes, while (3) and (4) show possible modes of decomposition which are not necessarily unique; they probably occur simultaneously and to a varying degree, depending on the experimental conditions of concentrations, catalysis, and temperature. The modes of decomposition of peroxide, and the interactions caused by (2), have a common factor – the net production of uranyl ions and consumption of acid. The changes in concentrations brought

about by the decomposition reactions affect the equilibrium processes, which, in turn, are sources of reactants for the decomposition steps, etc. Unfortunately, in this system, it is not possible to isolate for purposes of study any one of the reactions listed above, but the entire set of reactions must be studied simultaneously. It is obvious that this condition adds very substantially to the complexity of the system, and, at least at the beginning, the investigation must be carried out on a phenomenological basis.

Simplification can be attained in the numerical treatment of the system involving *solid* uranium peroxide in contact with a *solution* of uranyl ions if the reversible processes (1) and (2) can be made to approach equilibrium through the proper choice of experimental conditions; this can be achieved if the rates  $r_1$ ,  $r_{-1}$ ,  $r_2$ , and  $r_{-2}$  are considerably greater than  $r_3$  and  $r_4$  combined. Explicitly this is equivalent to stating that steps (3) and (4) are rate determining, or much slower than the initial rate of solution  $r_1$  of the solid phase, and that both equilibria are mobile. If these conditions are attained, a nearly saturated solution of uranium peroxide will prevail in the system in spite of the decomposition reactions. This, to a first approximation, will fix the concentration of dissolved uranium peroxide and effect considerable simplification in the numerical treatment. The total concentration of  $\text{H}_2\text{O}_2$  in solution can then be stated in terms of the concentration of  $\text{H}^+$  and  $\text{UO}_2^{++}$ , the solubility of  $\text{UO}_4$ , and an equilibrium quotient  $K_c$  (if it is assumed that for the prevailing conditions  $K_c$  remains sensibly constant during the measurements). If equilibrium conditions prevail, the experimental measurements provide the basis for arriving at an order of magnitude for the ratio  $\text{UO}_4(d)/K_c$  where  $\text{UO}_4(d)$  is the solubility in moles per liter of uranium peroxide.

Experimentally, two methods are suited for the study of the system. The first method consists in adding excess  $\text{H}_2\text{O}_2$  to a solution of uranyl ion of known acidity held in a stirred autoclave at constant temperature and obtaining, through a filter, serial samples of solution at definite times. The filtrates are then analyzed for total uranium, total peroxide, and changes in hydrogen ion concentration. The uranium concentration is observed to go through a minimum after the addition of  $\text{H}_2\text{O}_2$  and then to increase with time until it returns approximately to its original value. The total peroxide

<sup>8</sup>M. D. Silverman, G. M. Watson, and H. F. McDuffie, *Ind. Eng. Chem.* 48, 1238 (1956).

<sup>9</sup>G. M. Watson, M. D. Silverman, and H. F. McDuffie, *Anal. Chem.* 28, 1107 (1956).

<sup>10</sup>C. Duval, *Anal. Chim. Acta* 3, 337 (1949).

gradually decreases with time, while the acidity goes through a maximum and then returns gradually to the neighborhood of its initial value. The experimental data are values of concentrations in the filtrates of total uranium, total peroxide, and total acid, all of which are determined as functions of time.

A plot of the logarithm of the total peroxide concentration vs time reveals that a rather abrupt change in the observed rate of the process takes place at the same time that the total uranium attains its final concentration in the experiment. Since the rate of decomposition of peroxide in unsaturated uranyl sulfate solutions is first order with respect to total peroxide,<sup>8,9,11</sup> it appears logical to assume that the total peroxide concentration at the time when the discontinuity occurs in both curves is the amount of peroxide remaining when the last traces of solid phase dissolve. Conversely, if equilibrium has prevailed throughout the experiment for processes (1) and (2), the peroxide concentration thus determined should approximate the peroxide concentration at the point of incipient precipitation from conditions corresponding to those of the liquid phase present at the observed point of discontinuity. As the concentration of uranium increases and the peroxide decreases with time, a value is reached where the two concentrations are equal. This point will be later denoted as the "crossover" point.

The second experimental approach to the study of this system is to release suddenly solid uranium peroxide into a stirred solution held at a constant temperature and to analyze serial filtrates in the same manner as in the precipitation studies. The concentration of total uranium increases rapidly at first until it reaches the value of the "crossover" point of a similar precipitation study. After the "crossover" point the experiments are identical. The peroxide concentration is subject to the same treatment previously described at the point where the uranium attains its final concentration. This type of experimental approach gives evidence that the rate of dissolution of solid uranium peroxide is *much faster* than the rate of decomposition for the experimental conditions used and that the dissolution step is not rate determining. Accordingly, the approach to equilibrium

is probably effective throughout the experiment. The sudden decrease in rate of appearance of uranium in solution can be interpreted as attainment of equilibrium in steps (1) and (2).

In order to show that the equilibrium of Eq. (2) is approached under experimental conditions, it is necessary that the rate of solution of solid  $\text{UO}_4$  be fast compared with any decomposition process. Figure 10.8 shows the rate of solution when solid  $\text{UO}_4$  is added to an acid solution in a rapidly

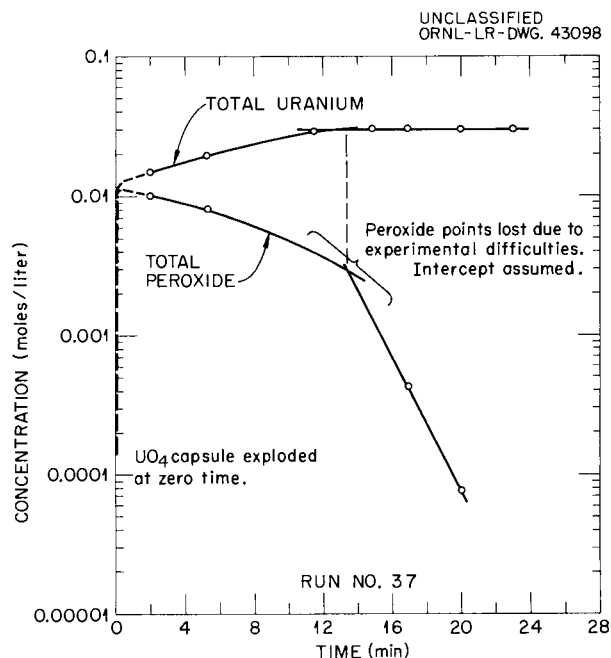


Fig. 10.8. Rate of Solution of Solid  $\text{UO}_4$  in Acid Solution.

stirred autoclave; the rate of increase in the uranium concentration in solution is extremely rapid initially. This rate then decreases, probably controlled by one or more of the possible decomposition processes previously discussed. Since the rate of solution is much greater than the decomposition rate, it is probable that equilibrium is attained if  $r_2$  and  $r_{-2}$  are fast compared with the decomposition rate. To investigate the reverse rate of the equilibrium,  $\text{H}^+$  is added to solution saturated with  $\text{UO}_4(d)$ . If  $\text{UO}_4(d)$  remains constant the addition of  $\text{H}^+$  to the solution will cause an equilibrium shift to the right in (2) with an equivalent gain in both  $\text{UO}_2^{++}$  and  $\text{H}_2\text{O}_2$ . Figure 10.9 shows the results of such an experiment; it is seen that the equilibrium shift was quite rapid and

<sup>11</sup>L. O. Gilpatrick and H. F. McDuffie, *HRP Quar. Prog. Rep.* April 30, 1958, ORNL-2561, p 313-16.

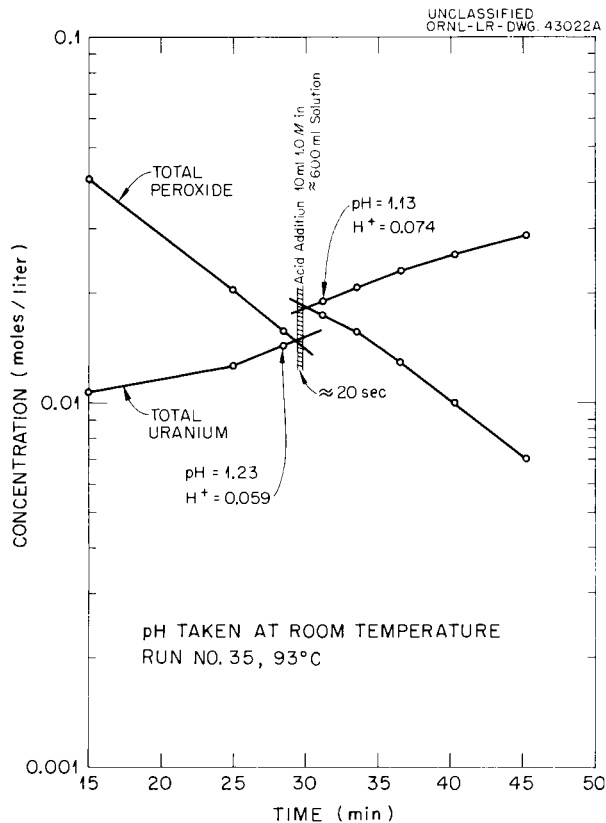
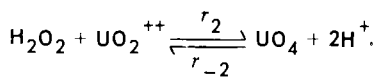


Fig. 10.9. Equilibration Shift upon Acid Addition,



indicates a large value for  $r_2$ . Figure 10.10 shows the experimental results when  $UO_2^{++}$  is added to shift the equilibrium to the left. Equilibrium is again established quickly, indicating that it is extremely mobile.

From this experimental evidence it seems likely that the system is indeed near equilibrium and that for our calculations we may assume

$$K_c = \frac{UO_4 [H^+]^2}{[UO_2^{++}] [H_2O_2]} \text{ at constant } T \quad (5)$$

The general pattern of a typical experiment is shown in Fig. 10.11. Excess  $H_2O_2$  was added to the solution and samples were withdrawn at times indicated on the graph. Total peroxide and total uranium concentrations were determined until all the uranium again appeared in solution as uranyl ion. The rate of peroxide disappearance in the

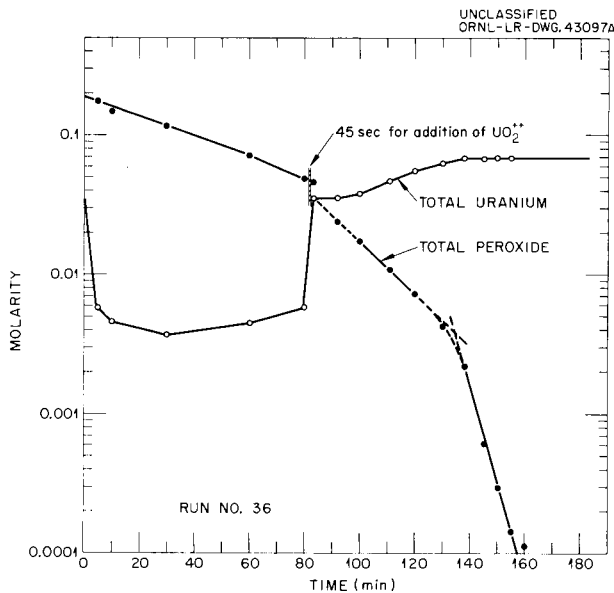


Fig. 10.10. The Effect of Addition of  $UO_2^{++}$  and  $H^+$  on Equilibrium. Initial concentrations doubled by addition.

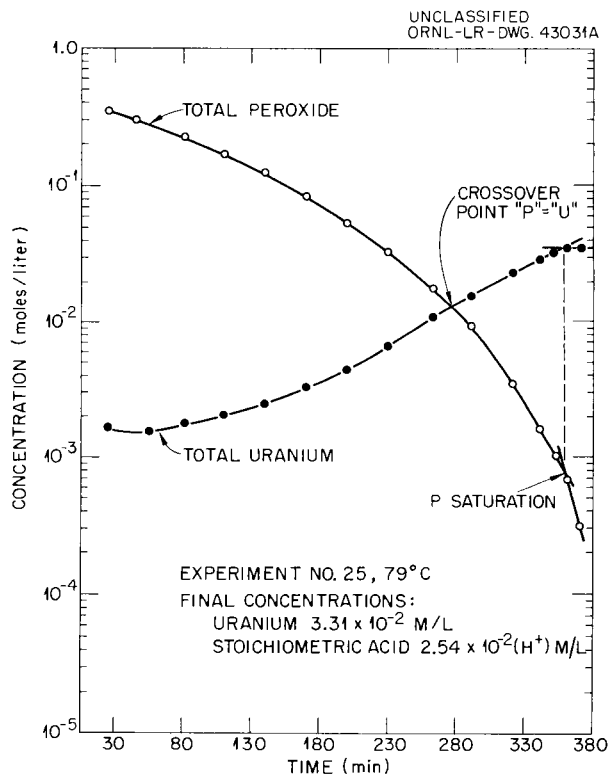


Fig. 10.11. Concentrations of Total Peroxide and Total Uranium vs Time in a Typical Experiment.

presence of  $\text{UO}_4(s)$  is slower than its rate of disappearance in the unsaturated solution. This discontinuity may be located graphically and taken as the point of peroxide saturation. Experimentally, however, it is somewhat easier to determine the time at which the uranium concentration ceases to increase in solution; the concentration of peroxide at this time is the total peroxide at saturation. Experiments similar to that shown in Fig. 10.11 were carried out at several temperatures. The experimental data have been reported elsewhere.<sup>12</sup>

In order to treat the data numerically, it was assumed that equilibrium existed. As the activities of the ionic species were unknown under experimental conditions, stoichiometric concentrations were used for calculation.

Since

$$P_{(\text{saturation})} = \text{UO}_4(d) + [\text{H}_2\text{O}_2],$$

and

$$[\text{H}_2\text{O}_2] = \frac{\text{UO}_4(d)}{K_c} \cdot \frac{[\text{H}^+]^2}{[\text{UO}_2^{++}]},$$

then

$$P_{(\text{saturation})} = \text{UO}_4(d) + \frac{\text{UO}_4(d)}{K_c} \cdot \frac{[\text{H}^+]^2}{[\text{UO}_2^{++}]}, \quad (6)$$

where  $[\text{H}^+]$  and  $[\text{UO}_2^{++}]$  concentrations are measured parameters for a given solution. The solubility of uranium peroxide was unknown in the experimental solutions. Experiments showed it was about  $1 \times 10^{-4} M$  in a solution of uranyl sulfate with no excess acid at  $78^\circ\text{C}$ . The same magnitude was assumed in the calculations.

The value of the ratio  $\text{UO}_4(d)/K_c$  was calculated from the experimental data and the equilibrium expression.<sup>12</sup> An average value of  $3.6 \times 10^{-2}$  was obtained for the ratio  $\text{UO}_3(d)/K_c$  over the range investigated, including changes in uranium concentration from 0.03 to 0.07 M, in stoichiometric  $\text{H}^+$  from 0.025 to 0.10 M, and in temperature from  $79$  to  $114^\circ\text{C}$ . The calculated values of  $P_{(\text{saturation})}$  agreed satisfactorily with those observed.

The results of the present investigation can be represented by the following relation:

$$P_{(\text{saturation})} = \left( 1.0 + 360 \frac{[\text{H}^+]^2}{[\text{UO}_2^{++}]} \right) \times 10^{-4} M \quad (7)$$

as a function of the stoichiometric acid concentration.

An equation to calculate the maximum power density ( $W_{\text{max}}$ ) of a homogeneous reactor allowable before precipitation of uranium peroxide occurs is given elsewhere.<sup>13</sup> If Eq. (7) is introduced into this expression and a value of  $G_{\text{H}_2}$  of 1.6 is used, the maximum power density is given by

$$W_{\text{max}} = \left( 1.05 + 378 \frac{[\text{H}^+]^2}{[\text{UO}_2^{++}]} \right) k_{\text{obs}}, \quad (8)$$

where  $W$  is given in watts per  $\text{cm}^3$  and  $k_{\text{obs}}$  is the observed first-order rate constant<sup>8,9,11</sup> of the decomposition of peroxide expressed in  $\text{min}^{-1}$ .

The most obvious limitation of Eq. (7) is the assumption that the ratio  $(\text{UO}_4)/K_c$  is independent of temperature. Within the narrow temperature range investigated this ratio appears to be independent of temperature within experimental variations.

#### Peroxide Decomposition in Homogeneous Reactor Fuels - Nitrate System

M. D. Silverman G. M. Watson M. J. Kelly

Reconsideration of an aqueous reactor fuel based on the nitrate ion as the anion has been suggested by Marshall.<sup>14</sup>

The power level at which this fuel can be used will be limited at low temperatures by the concentration of peroxide produced by fission fragments acting on the solution and the rate of decomposition of the peroxide in the aqueous solution. The rate of formation of peroxide in the reactor is dependent on the power density. However, the rate of decomposition is known to depend on several factors - for example, temperature, acid concentration, and the concentration of metal ions which

<sup>13</sup>J. A. Lane, H. G. MacPherson, and F. Maslan, *Fluid Fuel Reactors*, Addison-Wesley, Reading, Mass., 1958.

<sup>14</sup>W. L. Marshall, *Consideration of  $\text{UO}_2(\text{NO}_3)_2 \cdot \text{HNO}_3 \cdot \text{H}_2\text{O}(\text{D}_2\text{O})$  as a High Temperature Homogeneous Reactor Fuel*, ORNL CF-59-6-100 (May 26, 1959).

<sup>12</sup>L. O. Gilpatrick et al., *The Concentration of Peroxide in Uranyl Sulfate Solutions at Incipient Precipitation*, ORNL CF-59-10-12 (Oct. 22, 1959).

act as catalysts. Kinetic studies of the effects of these factors on the decomposition process have been made in uranyl sulfate solutions by Silverman *et al.*<sup>8</sup> and Gilpatrick.<sup>11</sup> The present work represents a similar study of those factors found to affect the rate of peroxide decomposition in reactor fuel solutions based on the nitrate anion.

The rate of disappearance of the peroxide was observed to be first order with respect to peroxide in all the experiments. This rate was followed by withdrawing samples from the reaction volume and determining the remaining peroxide by the method described by Silverman.<sup>8</sup>

Figure 10.12 shows the effect of temperature on the rate of decomposition of the peroxide. The most significant observations are that the addition of acid decreases the rate at constant temperature

but does not change the temperature dependence, and the addition of a small amount of iron to the solution increases the rate markedly but this addition also does not appear to influence the temperature dependence as indicated by the slope of the curve. The calculated energy of activation is 25 kcal/mole, which is in agreement with results in the sulfate system.<sup>8,11</sup> The energy of activation appears independent of solvent as shown by the parallel curves in Fig. 10.12.

The effect of acid on the rate of decomposition is plotted in Fig. 10.13. The acid variation has an inverse effect on the rate over the range studied.

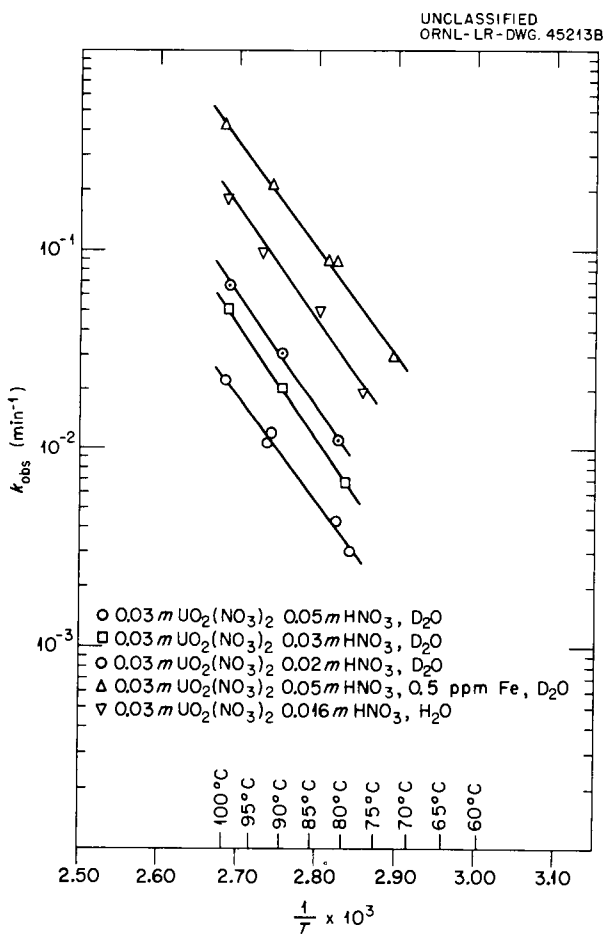


Fig. 10.12. Effect of Temperature on the Rate of Decomposition of Peroxide (Nitrate System).

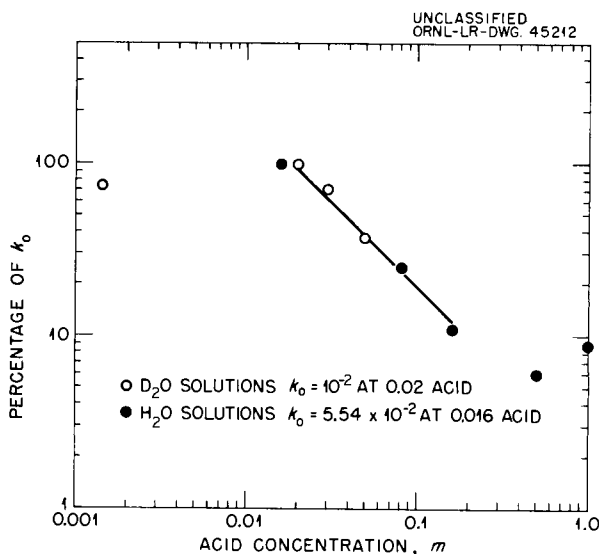


Fig. 10.13. The Effect of Acid Concentration on the Rate of Peroxide Decomposition (Nitrate System).

An increase of 0.02 to 0.2 *m* in acid resulted in a tenfold decrease in the rate of decomposition. The data at both high and low acid concentrations must be checked and extended before valid conclusions may be drawn.

Preliminary data are available on the effect of adding iron, copper, chromium, and nickel to the solution in the form of dissolved salts. The iron acts as a very effective homogeneous catalyst as shown in Fig. 10.14. The rate of decomposition is found to increase a factor of 20 for each ppm of iron in solution.

The presentation of data in this form, eliminating temperature as a variable, is possible since the temperature dependence is the same for all the

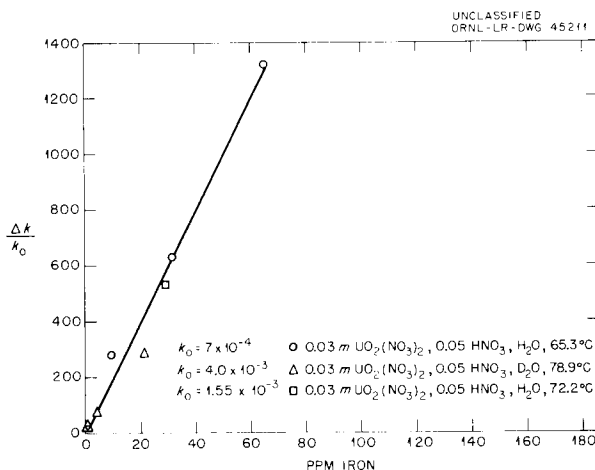


Fig. 10.14. The Effect of Iron on the Decomposition of Peroxide.

processes; that is, for a given catalyst concentration, the observed  $k$  is given as a function of temperature by the Arrhenius equation

$$k_0 = A_0 e^{-E/RT}$$

At any catalyst concentration, the rate constant is similarly expressed by

$$k_{\text{cat}} = A_{\text{cat}} e^{-E/RT}$$

where the constant  $E$  is the same in both equations.

At any fixed temperature, therefore,

$$\frac{k_{\text{cat}} - k_0}{k_0} = \frac{A_{\text{cat}} - A_0}{A_0}$$

and the catalyst concentration effect may be expressed as being independent of temperature if  $k_0$  is known.

The effects of copper, nickel, and chromium have been determined in a preliminary survey and found to be very small in comparison with iron. All three ions catalyze the system some one-thousandth as effectively as iron. Further experiments will be made to determine how nearly alike these ions are in total effect.

As has been shown in the sulfate system,<sup>8</sup> the addition of copper to an iron-containing solution enhances the observed catalysis. The addition of a large excess of copper to a fixed iron concentration does not cause this enhancement to increase without limit, but rather a saturation effect is observed at some iron-copper ratio. Further studies

of this phenomenon may result in a better understanding of the basic mechanism involved.

### Uranium Peroxide Precipitation and Structure

L. O. Gilpatrick      H. F. McDuffie

Questions concerning the composition and structure of uranium peroxide were raised when approximately 6 g of lemon-yellow solid was recovered from the fuel system of the North Carolina State Reactor following a gradual loss of reactivity.<sup>15</sup> A disagreement was brought to light when the x-ray diffraction pattern of this material was independently compared with reference patterns<sup>16</sup> for  $\text{UO}_4 \cdot 2\text{H}_2\text{O}$  in the files of two Laboratory Divisions; the two reference patterns were found to be different. This situation was resolved by the discovery that two different crystalline forms of uranium peroxide can be prepared by precipitation from the same aqueous solutions, with the occurrence of either form dependent primarily on the temperature of the precipitation.

Repeated laboratory precipitations in which 1 M hydrogen peroxide was added to 0.04 M uranyl sulfate solutions with stirring established that a low-temperature form was consistently produced below 63.5°C, while a high-temperature form was invariably produced above 64.5°C, with a mixture of both being obtained in the 63.5 to 64.5°C interval. Figure 10.15 illustrates the effect of precipitation temperature on the x-ray diffraction pattern and shows the actual x-ray data obtained.<sup>17</sup>

The low-temperature form appears to be non-hygroscopic and relatively stable in air at room temperature. Ignition to  $\text{U}_3\text{O}_8$  established the composition of the air-dried low-temperature form

<sup>15</sup>Letter from M. T. Kelley to H. A. Lamonds, April 3, 1959, reporting analytical results on samples received Feb. 18, 1959.

<sup>16</sup>Reference pattern in Analytical Chemistry Division taken from H. W. Dunn, *X-Ray Diffraction Data for Some Uranium Compounds*, ORNL-2092 (Aug. 2, 1956). This report incorrectly attributes the formula  $\text{UO}_4 \cdot 2\text{H}_2\text{O}$  to a pattern corresponding to the tetrahydrate. Reference pattern in Chemistry Division courtesy of R. D. Ellison based on material prepared in 1952 by H. W. Wright and identified as  $\text{UO}_4 \cdot 2\text{H}_2\text{O}$ .

<sup>17</sup>The x-ray diffraction patterns were obtained through the cooperation of R. E. Thoma and his group.

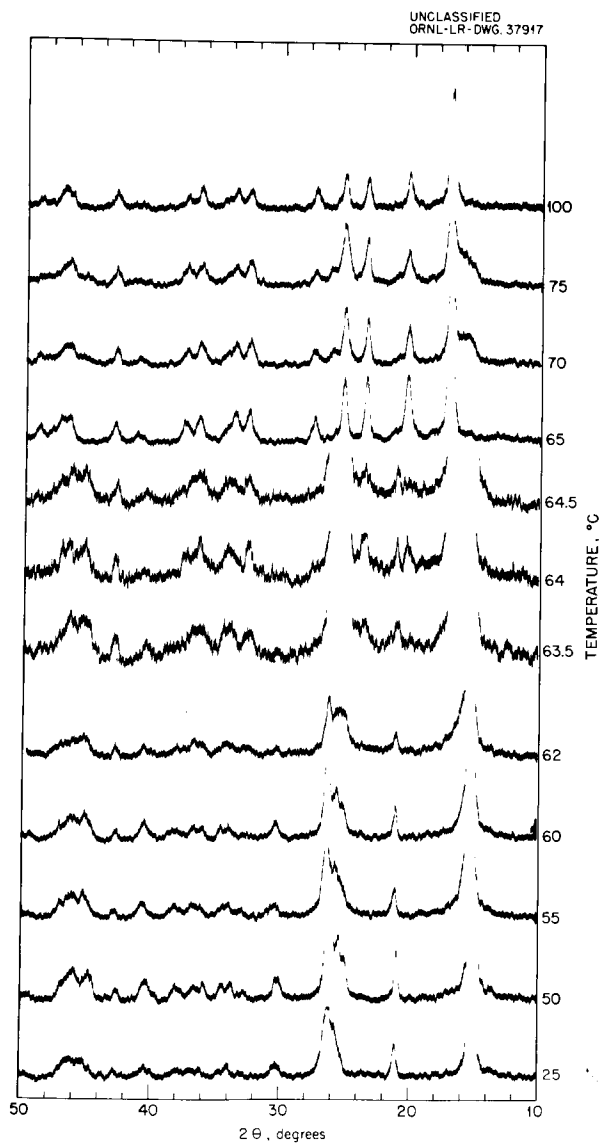


Fig. 10.15. Effect of Preparation Temperature upon Crystal Structure of Uranium Peroxide.

as corresponding very closely to  $\text{UO}_4 \cdot 4\text{H}_2\text{O}$ ; when the sample was exposed to a mild desiccant, sulfuric acid of density 1.50 at  $24.5^\circ\text{C}$  for 36 hr in a vacuum desiccator, exhausted initially to the onset of boiling in the acid, the loss of weight was 0.5% (from 0.4% over that calculated for the tetrahydrate to 0.1% under the calculated weight). However, when exposed to magnesium perchlorate overnight in an initially evacuated ( $25 \mu$ ) desiccator, the material was converted into the high-temperature form and lost weight equivalent to two

molecules of water. When heated at  $50^\circ\text{C}$  in the air for 1 hr the low-temperature form lost 80% of the two molecules of water which are easily removed; the loss of weight to the dihydrate was complete after 18 hr at 50 to  $45^\circ\text{C}$ . An unexpected stability of the tetrahydrate was noted when an attempt was made to convert it to the dihydrate by stirring in an aqueous solution of hydrogen peroxide at  $70^\circ\text{C}$  (above the temperature at which tetrahydrate is formed on precipitation). Stirring for 5 hr failed to convert the x-ray pattern from that of the tetrahydrate to that of the dihydrate.

The high-temperature form appears to be quite stable in the air even to temperatures as high as  $90^\circ\text{C}$ , at which it may be held overnight without weight change. Upon ignition to  $\text{U}_3\text{O}_8$  the loss in weight corresponds to an original formula of  $\text{UO}_4 \cdot 2\text{H}_2\text{O}$ .

Attempts have been made to convert the dihydrate into the tetrahydrate by stirring an aqueous slurry of the dihydrate for extended periods of time at various temperatures. Dihydrate, which has been prepared by dehydration of the tetrahydrate over magnesium perchlorate in a vacuum desiccator, was stirred for 20 hr in distilled water at room temperature; x-ray diffraction did not reveal any reversion of the dihydrate to the tetrahydrate.

In agreement with the literature discussed below, the dihydrate was decomposed partially by heating at  $150^\circ\text{C}$  for 20 hr in air; the loss of weight corresponded to that required for a final formula of  $\text{U}_2\text{O}_7$ , and subsequent heating at  $150^\circ\text{C}$  for an additional 50 hr failed to produce further decomposition. The material was orange and liberated gas (oxygen) on contact with water as expected. Its x-ray diffraction pattern was so indistinct as to make it impossible to assert that the material is crystalline.

The literature concerning the chemistry of the oxides and hydrated oxides of uranium has been summarized and reviewed by Katz and Rabinowitch.<sup>18</sup> Apparently  $\text{UO}_4$  has never been produced in an anhydrous form. Hydrates containing from "about four and one-half molecules of water" down to 1.5 molecules of water, with many intermediate values, have been reported by various investigators, but our information is quite consistent with that of the earliest investigator,

<sup>18</sup>J. J. Katz and E. I. Rabinowitch, *Natl. Nuclear Energy Ser. Div. VII 5*, 244-330 (1951).

Fairley,<sup>19</sup> who in 1877 reported that the air-dried form of uranium peroxide corresponded to the tetrahydrate but the material dried at 100°C corresponded to the dihydrate formula. No hydrates other than these appear to have been characterized sufficiently to merit serious consideration. Various project reports cited by Katz and Rabinowitch, and a recent paper by Boggs and El-Chehabi,<sup>20</sup> have established the thermal decomposition of the dihydrate to a material of the formula  $U_2O_7$ . This was also confirmed by our work.

Thus the tetrahydrate and the dihydrate of uranium peroxide have now been differentiated and characterized in the same laboratory on the basis of temperature of preparation, x-ray diffraction pattern, gravimetric analysis upon heating at various temperatures, and conversion of the tetrahydrate into the dihydrate by a number of procedures. The material originally recovered from the North Carolina State Reactor was the tetrahydrate; subsequent storage in a desiccator for "safety" while the various tests were performed had converted it into dihydrate. The preparation and reactions of uranium peroxide compounds are being studied further in connection with its occurrence and decomposition in homogeneous reactor fuel solutions at elevated temperatures.

#### THE USE OF CATION EXCHANGE RESINS IN THE DETERMINATION OF FREE ACID

L. O. Gilpatrick      H. F. McDuffie

A simple ion exchange method was developed for the determination of free acid in aqueous homogeneous reactor fuel solutions which contain easily hydrolyzable cations such as  $Cu^{++}$  and  $UO_2^{++}$ . These ions, which interfere with the titration of the free acid to a neutral end point, are, in the new method, adsorbed on a cation exchange resin and replaced with  $Li^+$  from the resin. The eluate solution, containing free acid ( $H_2SO_4$ ) and neutral salt ( $Li_2SO_4$ ), may be titrated to a neutral end point by conventional methods without complications due to hydrolysis.

The objective of accurate and precise determination of the free acid content of reactor fuel solutions had previously been only approached. Two general procedures had been used: in one, a complexing agent, such as potassium oxalate, was added to prevent hydrolysis of the interfering

ions,<sup>21</sup> while in the other, the interfering ions were physically separated from the solution by precipitation, as illustrated by the use of potassium ferrocyanide with uranyl solutions.<sup>22</sup> The present approach is similar to the second of these methods in that a physical separation of the interfering ions from the bulk of the solution is achieved - by deposition of them on the ion exchange resin. The method possesses additional advantages in that the analytical technique is simple and adaptable for remote operation, much of the radioactivity of the original solution is retained on the column, and a wide variety of interfering ions can be removed in one step.

An outline of the technique as applied to solutions containing  $UO_2SO_4$ ,  $CuSO_4$ , and  $H_2SO_4$  is as follows:

The ion exchange column is loaded with a cation exchange resin initially in the *lithium* form or converted to that form after loading. The test solution is then passed through the column;  $Cu^{++}$ ,  $UO_2^{++}$ , and  $H^+$  are deposited at the top of the column and replaced with  $Li^+$  ions. Elution of the column with dilute  $Li_2SO_4$  solution displaces the  $H^+$  ions but not the divalent ions. The combined eluates, containing  $H_2SO_4$  and  $Li_2SO_4$ , are titrated by any convenient method to a neutral end point.

The results of several experiments are shown in Table 10.1 and a typical elution curve is seen in Fig. 10.16, illustrating the sharp separation which it is possible to obtain. When attempts were made to utilize resin columns in the potassium form with  $K_2SO_4$  as the eluting solute the separation was not nearly so sharp between the  $H^+$  and the hydrolyzable cations as when lithium was used; uranyl ions did appear in the eluate before all the  $H^+$  had been displaced from the column. This behavior is, of course, consistent with the qualitative sequence of affinities of these ions for the resin.

This method of analysis has been successfully applied to the determination of free acid in HRE-2 fuel solutions.<sup>23</sup> It appears to merit wider usefulness as a general method for the determination of free acid in solutions containing ions which interfere with conventional methods.

<sup>21</sup>ORNL Master Analytical Manual, Procedure No. 9-012205 (Feb. 17, 1953).

<sup>22</sup>*Ibid.*, No. 9-05500 (July 1, 1953).

<sup>23</sup>F. J. Miller, *Evaluation of the Free Acid Determination in Uranyl Sulfate Solutions by the Dowex-50 Resin Separation Procedure*, ORNL CF-59-10-112 (Oct. 27, 1959).

<sup>19</sup>T. Fairley, *J. Chem. Soc.* 31, 127-33 (1877).

<sup>20</sup>J. E. Boggs and M. El-Chehabi, *J. Am. Chem. Soc.* 79, 4258-60 (1957).

REACTOR CHEMISTRY PROGRESS REPORT

Table 10.1. Free-Acid Determination in Reactor Fuel Solutions by Ion Exchange

Experiment No.	Solution*	Eluant (M Li <sub>2</sub> SO <sub>4</sub> )	Rate (ml·cm <sup>-2</sup> ·min <sup>-1</sup> )	Volume of 0.02 M NaOH (ml)		σ
				Calculated	Observed	
8	a	0.035	5.3	24.5	24.8	0.3
9	a	0.035	7.5	24.5	24.4	
10	a	0.050	6.3	24.5	24.7	
11	a	0.035	6.7	24.5	24.2	
13	a	0.050	6.7	24.5	24.0	
16	b	0.050	4.3	40.0	40.1	0.2
17	b	0.050	4.2	40.0	39.8	
24**	a	0.050	1.0	24.5	24.2	0.5
25	a	0.050	3.2	24.5	24.9	

\*Test solution composition:

Solution	UO <sub>2</sub> SO <sub>4</sub>	CuSO <sub>4</sub>	NiSO <sub>4</sub>	Li <sub>2</sub> SO <sub>4</sub>	H <sub>2</sub> SO <sub>4</sub>
a (38)	0.025 M	0.0125 M	0.003 M	2	0.0245 M
b (42)	0.025 M	0.0125 M	0.003 M	0.100 M	0.100 M

Column: Glass, 1-cm dia, 7-cm length of bed.

Resin: 5 ml Dowex 50, X8 cross linkage, 50-100 mesh.

Sample: Diluted to  $\leq 0.1 N$  acid and  $\leq 0.5$  meq total cations. Flow rate  $\leq 1$  ml/min.

Eluant: 200 ml  $\times$  0.035-0.05 M Li<sub>2</sub>SO<sub>4</sub> (pH 7.1). Flow rate,  $\leq 5$  ml·cm<sup>-2</sup>·min<sup>-1</sup>.

\*\*Later work shows Dowex 50W, 100-200 mesh, to be more convenient since colored ions can be seen visually on the lighter resin.

UNCLASSIFIED  
ORNL-LR-DWG. 45714A

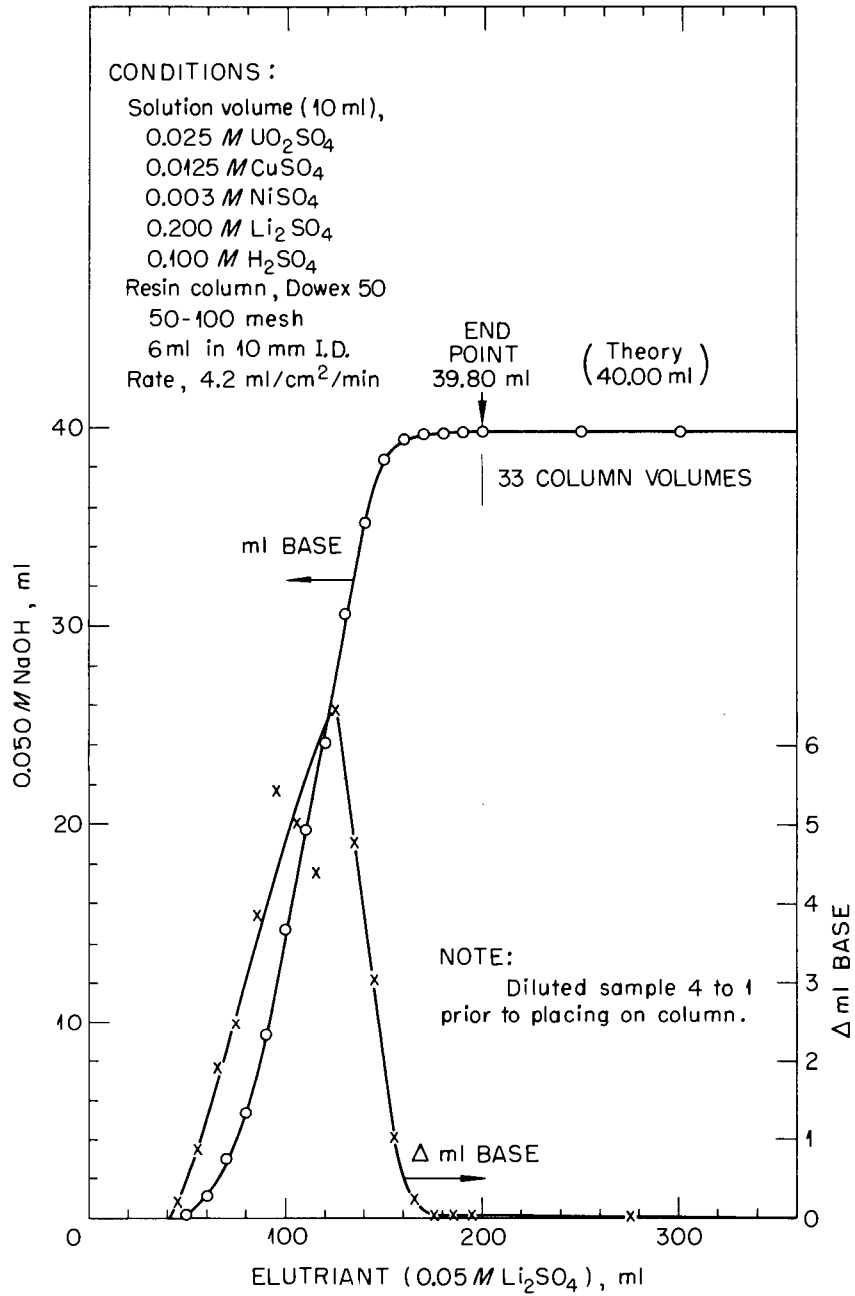


Fig. 10.16. Resin Separation for Free Acid.

## 11. THERMODYNAMIC STUDIES IN AQUEOUS SYSTEMS

A HIGH-TEMPERATURE EMF CELL FOR  
ACIDITY MEASUREMENTS;  
THE HYDROLYSIS OF URANIUM(VI) AT 94°C

C. F. Baes, Jr.

During the past year an experimental program was initiated to measure acidity in aqueous solutions at elevated temperatures. The primary objectives are to investigate the hydrolysis of uranium(VI) and sulfate ion. Subsequently, investigation of the hydrolysis and complexing of other metal ions of interest may be included.

The general procedure adopted has already been applied widely in such studies at ordinary temperatures.<sup>1</sup> It consists of potentiometric titrations using hydrogen-ion-responding electrodes in concentration cells with transference. A relatively high and nearly constant ionic strength is maintained in both half cells, primarily to reduce the variation of activity coefficients. In the absence of a salt bridge, this also serves to minimize the liquid junction potential. The cell presently being used is



in which silver-silver chloride internal electrodes are used in each glass electrode. The acidity of the solution being measured (A) is compared to that of a solution (B) containing a known concentration of a strong acid. With proper control of ionic strength and composition, and with control titrations in which the acidities of both solutions A and B are known, it is possible to relate fairly reliably the measured emf of such a cell to the acid concentration ratio of its two half cells.

To the author's knowledge, this is the first use of a cell containing only glass electrodes. Such an arrangement has the obvious advantage that the solutions measured are in contact only with the relatively inert glass electrodes and the containing vessel. It is thus relatively free of chemical interferences often encountered in high-temperature emf studies due to the increased

solubility of electrode materials and/or the increased importance of unwanted electrode reactions.

As with all cells involving glass electrodes, the resulting high electrical resistance requires the use of a sensitive potentiometer circuit, careful insulation, and shielding for precise emf measurements. It has been found that precision emf measurements are possible in the present case using a vibrating-reed electrometer arrangement described by Kraus, Holmberg, and Borkowski<sup>2</sup> for use with a glass electrode-low-resistance reference electrode combination. The presence of two high-resistance electrodes requires merely that the cell be well insulated from ground.

A cell designed for potentiometric titrations has been constructed, and measurements of the hydrolysis of uranium(VI) at 94°C have been made. The precision of emf measurement is of the order of 0.1 mv. The upper temperature limit of the cell has not yet been determined, but promising preliminary measurements have been made at 150°C.

**The Cell.** - Figure 11.1 shows the cell arrangement. The titration vessel *C* is of Teflon, containing a Teflon-encased stirring magnet *M*. It fits snugly into a pressure bomb, directly beneath which is an air-cooled magnetic stirrer unit. The reference solution *B* is contained in a quartz tube *T* with a sealed-in, fine-porosity quartz frit *F* to provide the liquid junction. The glass electrodes *G* (Beckman general purpose glass electrode bodies) contain excess silver chloride to assure saturation of the dilute HCl internal solutions at elevated temperatures. The quartz tube, the electrodes, and the main body of the cell are all fitted with Teflon covers, vented so that gas pressure equilization is obtained throughout. An overpressure of inert gas is maintained to minimize diffusion of water vapor from the cell. A Teflon thermocouple well (not shown) is also provided. It receives a thermocouple encased in a steel pressure tube carried by the bomb head. The platinum supporting wires of the silver-silver chloride electrodes are connected to platinum lead wires in the bomb head by platinum sleeves. These

<sup>1</sup>For example: S. Ahrland, *Acta Chem. Scand.*, **3**, 374 (1949) and **5**, 1151 (1951); E. Eichler and S. Rabideau, *J. Am. Chem. Soc.*, **77**, 5501 (1955).

<sup>2</sup>K. A. Kraus, R. W. Holmberg, and C. J. Borkowski, *Anal. Chem.*, **22**, 341 (1959).

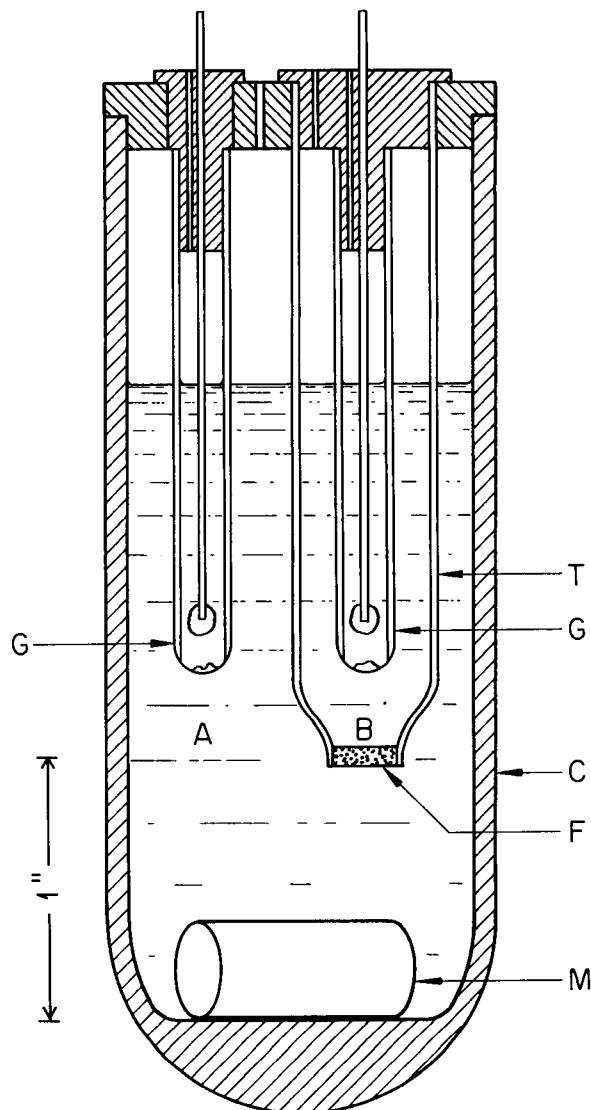
UNCLASSIFIED  
ORNL-LR-DWG. 45396

Fig. 11.1. High-Temperature Glass Electrode Cell.

lead wires are insulated from the bomb head by Teflon sealing cones and Teflon spaghetti. They terminate in external coaxial connectors. The titrating solution is delivered from a High Pressure Equipment Company "pressure generator," a screw-driven piston-cylinder combination of stainless steel with Teflon packing. The solution is carried to the cell by a connecting titanium capillary tube which passes through the bomb head. The bomb fits snugly into an aluminum furnace liner

which carries the temperature control thermocouple and also is provided with grooves through which the titanium capillary is passed in order to preheat the titrating solution. The liner fits into the tube of a vertically mounted Marshall furnace. Temperature control of the furnace ( $\pm 0.1^\circ\text{C}$ ) is obtained with a Leeds and Northrup series 60 DAT controller.

**Uranium(VI) Hydrolysis.** - In these initial measurements, all solutions were made half molar in nitrate by the addition of  $\text{KNO}_3$ . The nitrate system was chosen rather than perchlorate, primarily because of the information available for that system due to the work of Marshall *et al.*<sup>3</sup> on the solubility of  $\text{UO}_3$  at elevated temperatures.

A control titration was carried out at  $93.6^\circ\text{C}$  in which solution B was  $0.02\text{ m}$  in  $\text{HNO}_3$  and solution A was varied from 0 to  $0.02\text{ m}$  in  $\text{HNO}_3$ . The emf values obtained, when corrected for a uniform slow potential drift (*ca.*  $1\text{ mv/hr}$ ) which was observed, were related to the known acidities,  $[\text{H}^+]_A$  and  $[\text{H}^+]_B$ , of the two half cells by the expected Nernst equation

$$E = E_g - 72.8 \log \frac{[\text{H}^+]_A}{[\text{H}^+]_B} \quad (1)$$

within  $\pm 1\text{ mv}$  in the range  $0.004$  to  $0.01\text{ m}$   $\text{HNO}_3$ .

In the above equation,  $E_g$  contains (1) the difference in the asymmetry potentials of the glass electrodes, (2) any difference in the potentials of the silver-silver chloride internal electrodes, (3) the liquid junction potential, and (4) the effect of any deviation from unity of the activity coefficient ratio  $(\gamma_{\text{H}^+})_A / (\gamma_{\text{H}^+})_B$ . From its behavior, the observed slow potential drift is thought to result mainly from variation in the first two of these quantities.

A titration was then carried out in which solution A was  $0.01\text{ m}$  in  $\text{UO}_2(\text{NO}_3)_2$  and, initially,  $0.004\text{ m}$  in  $\text{KOH}$  (approximately the maximum amount of base which could be added without precipitation of uranium at the temperature of the run). During the titration, a nitric acid solution - also  $0.01\text{ m}$  in  $\text{UO}_2(\text{NO}_3)_2$  - was added. A portion of the results is shown in Table 11.1. The measured acidities  $[\text{H}^+]_A$  were obtained from Eq. (1) ( $[\text{H}^+]_B$

<sup>3</sup>This report, chap. 9.

Table 11.1. Uranium(VI) Hydrolysis at 93.6°C  
 0.5 m KNO<sub>3</sub>, 0.0099 m U(VI), initially 0.00378 m in KOH

	Excess Acid over Stoichiometric, $C_H - C_{OH}$ (m)	Measured Acidity, $[H^+]_A$ (m)	Fraction of U(VI) Hydrolyzed, $\bar{n}$
Basic side	$\left\{ \begin{array}{l} -0.00378 \\ -0.00215 \\ -0.00114 \end{array} \right.$	0.00078	0.46
		0.00106	0.32
		0.00132	0.248
Stoichiometric point	0	0.00168	0.169
Acid side	$\left\{ \begin{array}{l} +0.00170 \\ +0.00345 \\ +0.00589 \end{array} \right.$	0.00261	0.092
		0.00390	0.045
		0.00607	0.018

being known). In the last column,  $\bar{n}$  is the ratio of the acid liberated by uranium hydrolysis to the total uranium concentration  $C_U$ ; by the hydrolysis reaction given below [Eq. (3)] it is then the fraction of uranium which is hydrolyzed. It is given by

$$\bar{n} = \frac{[H^+]_A - (C_H - C_{OH})}{C_U} \quad (2)$$

wherein  $C_H$  and  $C_{OH}$  are the calculated concentrations of acid added and of base initially present, respectively, in the absence of hydrolysis. From the generally accepted initial hydrolysis reaction of uranyl ion at ordinary temperatures



it is expected that  $\bar{n}/(1 - \bar{n})^2$  should vary inversely as  $[H^+]_A^2$ . This was found to be the case within the experimental error for the present results, the resulting hydrolysis constant being

$$Q = \frac{[U_2O_5^{++}][H^+]^2}{[UO_2^{++}]^2} = 4 \times 10^{-5} \quad .$$

However, until results at other uranium concentrations are obtained, this should be considered only a tentative interpretation. Yet it may be noted that this value of  $Q$  is in reasonable agreement with an estimated value of *ca.*  $2 \times 10^{-5}$  ( $\mu = 0.5$ , 94°C) which Lietzke and Stoughton derived from

their results on the solubility of Ag<sub>2</sub>SO<sub>4</sub> in UO<sub>2</sub>SO<sub>4</sub> solution at elevated temperatures.<sup>4</sup>

In any case, the tendency of uranyl ion to hydrolyze is clearly greater at 93.6°C than at lower temperatures. Thus various estimates of the above quotient  $Q$  at 20, 25, and 40°C which may be found in the literature<sup>5</sup> are mainly in the range  $0.7$  to  $1.5 \times 10^{-6}$ . Stoichiometric 0.01 m solutions of uranyl nitrate and perchlorate at various ionic strengths at these temperatures yield  $\bar{n}$  values (based on pH) in the range 0.05 to 0.08 (5 to 8% hydrolyzed), whereas the corresponding value from the present results at 94°C is 0.17 (17% hydrolyzed).

**Future Work.** - Plans for future work include (1) determination of the practical upper temperature limit of the present emf cell, (2) study of uranium(VI) hydrolysis at several concentrations in nitrate and perchlorate solutions at several temperatures, and (3) study of bisulfate ionization in acidic sulfate-nitrate solutions in the absence and in the presence of uranium.

The maximum temperature at which the glass electrode can be used is probably in the vicinity of 200°C.<sup>6</sup> For measurements at higher temperatures the hydrogen electrode probably can be used in the

<sup>4</sup>M. H. Lietzke and R. W. Stoughton, ORNL CF-59-11-41 (1959).

<sup>5</sup>J. Bjerrum, G. Schwarzenbach, and L. Sillen, *Stability Constants; Part II, Inorganic Liquids*, p 9, The Chemical Society, London, 1958.

<sup>6</sup>M. H. Lietzke and J. R. Tarrant, ORNL CF-57-11-87 (1957).

present cell in the absence of reducible solutes,<sup>7</sup> but for uranium solutions some other hydrogen-ion-responding electrode must be formed since uranium(VI) is reduced by hydrogen. One possibility which is to be investigated is the oxygen-on-platinum electrode.

THE OSMOTIC BEHAVIOR OF  
REPRESENTATIVE AQUEOUS SALT  
SOLUTIONS AT 100°C<sup>8</sup>

C. S. Patterson<sup>9</sup>      L. O. Gilpatrick  
B. A. Soldano

The recent emergence of aqueous homogeneous reactors has focused attention on the limited amount of experimental information available concerning the thermodynamic behavior of aqueous solutions at elevated temperatures. Under the most ideal conditions, however, the interpretation of concentrated solution behavior constitutes a formidable task. Therefore, a comprehensive experimental program at elevated temperatures provides a reasonable method of obtaining the performance characteristics of those salt solutions whose properties might be of potential reactor use.

Since the isopiestic technique provides a direct experimental probe, depending solely upon the precision of weighing, it has been adapted for study of solution behavior at elevated temperatures. It becomes a relatively simpler task then to translate the osmotic coefficients so obtained into the various terms employed to describe solution behavior, that is, free energies, activity coefficients, etc.

The osmotic coefficient is directly derivable from experimental data and does not require numerical integration nor a theoretical description of the behavior of the system. It is defined in terms of the activity of water<sup>10</sup> by Eq. (1),

$$\ln a_A \equiv - \frac{\nu m W_a}{1000} \phi, \quad (1)$$

where  $a_A$  is the activity of water,  $\nu$  is the idealized number of ions formed per mole of salt in the assumed standard state (i.e.,  $\nu = 3$  for  $\text{Na}_2\text{SO}_4$ ),  $m$  is the molality of the solute,  $W_a$  is the molecular weight of water, and  $\phi$  is the molal osmotic coefficient.

The present investigation was primarily concerned with an examination of the osmotic behavior of a variety of salt solutions over a limited concentration range above 1 *m* at 99.6°C. The systems studied were LiCl, KCl, CsCl,  $\text{Na}_2\text{SO}_4$ ,  $\text{BaCl}_2$ ,  $\text{MgSO}_4$ , and  $\text{UO}_2\text{SO}_4$ , which were selected to represent the behavior of typical 1-1, 1-2, 2-1, and 2-2 electrolytes. Their behavior at 25°C was compared with that at 100°C. The method used in this study was the isopiestic (equal water vapor pressure) method pioneered by Stokes and Robinson<sup>11</sup> but extended to a higher temperature range.

The measurements of the osmotic coefficients of NaCl at 100°C by Smith and Hirtle<sup>12</sup> were used as a standard for comparison to avoid the complications of an independent or simultaneous determination of the activity of water. The experimentally determined quantity therefore is the osmotic ratio  $R$ , obtained by dividing the defining equation for  $\phi$  by the same relation for the standard salt and rearranging. The primed values refer to the standard:

$$R = \frac{\phi}{\phi'} = \frac{\nu' M'}{\nu M}. \quad (2)$$

Apparatus suitable for the studies of aqueous electrolytes by the isopiestic technique was designed and built to be capable of withstanding pressures well above atmospheric and to be operated at controlled temperatures from room temperature to well above 100°C. Construction and design details of the apparatus have been presented elsewhere.<sup>13</sup> In essence it consists of a magnetic balance operated in a sealed water vapor chamber

<sup>7</sup>R. S. Greeley, *Thermodynamic Properties of Dilute Aqueous Hydrochloric Acid Solutions at Elevated Temperatures from Electromotive-Force Measurements*, thesis, University of Tennessee, 1959.

<sup>8</sup>This work is a continuation of that reported in ORNL-2782 (1959) and ORNL-2386, p 74 (1957).

<sup>9</sup>Research participant, Oak Ridge Institute of Nuclear Studies, summer 1958. Present address: Department of Chemistry, Furman University, Greenville, S.C.

<sup>10</sup>R. A. Robinson and R. H. Stokes, *Electrolyte Solutions*, p 28, Butterworth Scientific Publications, London, England, 1955.

<sup>11</sup>R. H. Stokes and R. A. Robinson, *Trans. Faraday Soc.* **37**, 419 (1941).

<sup>12</sup>R. P. Smith, *J. Am. Chem. Soc.* **61**, 500 (1939); R. P. Smith and D. S. Hirtle, *ibid.* **61**, 1123 (1939).

<sup>13</sup>B. A. Soldano *et al.*, *The Structure of Electrolytic Solutions*, p 224-35, Wiley, New York, 1958.

contained in a constant temperature air bath. This arrangement permits an *in situ* weighing of equilibrated solutions contained in 20 titanium dishes. The design permits all transfer operations of dishes to and from the balance to be made without opening the chamber. The balance is of the platform type with torsion ribbon suspensions. The null point is determined by measuring the position of a nickel core moving in a small differential transformer, whose signal is continuously recorded. An independent direct current circuit driving a small coil of silver wire beneath the load pan and opposing a small permanent magnet fixed to the balance beam provides the restoring force necessary to provide balance. An accurate relative measurement of the current flowing in this circuit is the measured quantity from which weights are determined.

The balance is calibrated frequently during the sequence of weighings by placing four graded platinum weights in the four empty dishes of the set of 20. These standards were chosen of such weights as to bracket all the weights to be determined. A given unknown weight was always evaluated by interpolation (using the analytical equation for a straight line in the two-point form) between a standard weight just heavier and one just lighter. The sequence of weighings was repeated until the results for several consecutive sets showed satisfactory reproducibility.

Where practical the solutes were weighed directly into the titanium dishes. A concentration range from about 1 to 4.2 *m* (reference salt) was covered by a series of equilibrations using the same salt samples. Solution concentrations were changed by opening the unit and replacing a 100-ml reservoir solution of NaCl with one of the desired strength, or by simply adding to it a calculated volume of water. This large reservoir acted as a ballast to adjust the approximate concentration of water in the test solutions. As a check on technique, the concentrations were initially selected in a few cases so that about half the dishes approached equilibrium from the lower side and half from the upper side with respect to concentration. This would have exposed any inconsistencies caused by differences in rate of evaporation or condensation among the various solutions or by failure to allow enough time for equilibration. At equilibrium for a constant temperature in the closed system each solution will have lost or gained water until its

vapor pressure equals all the others. When this condition has been established, each dish is weighed, the water content determined by difference, and the molality of each solution calculated. The average osmotic ratios *R* calculated for pairs of dishes are shown in Table 11.2. The osmotic coefficients listed in Table 11.3 were taken at round molalities from smoothed graphs of the osmotic coefficients plotted vs the molality of each solute.

The performance of the apparatus can be evaluated from data contained in Table 11.2. The last line records the mean standard deviation for the sets of pairs for each experiment averaged over all experiments and demonstrates that the precision of the data is closely allied to the magnitude of the change in molality over the concentration range. For example, MgSO<sub>4</sub> exhibits the best precision ( $\sigma = 0.0010$ ) and the smallest change in molality (97%). Uranium sulfate shows the next best precision ( $\sigma = 0.0022$ ) and the next smallest change in molality (142%). A similar treatment for the other solutes demonstrates a good inverse relation between water transport from the dish and precision. Therefore the rate of attainment of equilibrium must have affected the over-all precision. It is to be expected that longer equilibration periods will contribute to an improvement in precision. In addition mean standard deviations calculated for each experiment (not shown) demonstrate that the over-all precision is reduced as smaller absolute amounts of water are determined at the higher molalities. This latter result is to be expected whenever progressively smaller quantities are weighed with a balance having a fixed minimum source of error.

The osmotic coefficients (Table 11.3) are compared with those of the same molality at 25°C tabulated by Stokes and Robinson.<sup>10</sup> The results of these comparisons are shown in Figs. 11.2 and 11.3.

**Discussion.** — The osmotic coefficient is so defined that for the standard state at infinite dilution the molal osmotic coefficient  $\phi$  is equal to 1 for all solutes. For real electrolytes in this study the value of  $\phi$  decreases at small molalities, passes through a minimum value, and then increases regularly to values in excess of 1 for some cases such as LiCl and BaCl<sub>2</sub> at molarities in excess of 2. This pattern of behavior is obscured in many cases by the limited range of the data. The

Table 11.2. Experimental Isopiestic Ratios Measured at 99.6°C<sup>a</sup>

Experiment No.	Average Molality of NaCl	Average Isopiestic Ratios Relative to NaCl						
		LiCl	KCl	CsCl	Na <sub>2</sub> SO <sub>4</sub>	BaCl <sub>2</sub>	MgSO <sub>4</sub>	UO <sub>2</sub> SO <sub>4</sub>
1	0.958	1.008	0.964	0.911	0.717	0.895	0.504	0.460
2	1.096	1.012	0.961	0.900	0.697	0.897	0.521	0.465
3 <sup>b</sup>	1.272	1.013	0.952	0.890		0.904	0.541	0.496
4 <sup>b</sup>	1.850	1.035	0.938	0.873		0.930	0.624	0.549
5	1.955	1.040	0.938	0.872	0.635	0.933	0.636	0.553
6	2.360	1.049	0.928	0.862	0.626	0.942	0.693	0.587
7 <sup>b</sup>	2.726	1.065	0.922	0.850		0.950	0.734	0.607
8	2.889	1.068	0.916	0.840	0.606	0.949	0.753	0.620
9	3.176	1.073	0.918			0.963	0.785	0.630
10	4.230	1.100	0.892				0.891	
	$\sigma^c$	0.0032	0.0047	0.0080	0.0032	0.0039	0.0010	0.0022

<sup>a</sup>Data included in this table represent values which had remained constant within experimental error for sets of weighings taken on at least two successive days after an initial equilibration period.

<sup>b</sup>Data for Na<sub>2</sub>SO<sub>4</sub> are missing in experiments 3, 4, and 7 because Na<sub>2</sub>SO<sub>4</sub> was substituted for K<sub>2</sub>SO<sub>4</sub>, the original solute, which saturated at an early stage. The values for the highest molalities of Na<sub>2</sub>SO<sub>4</sub> and BaCl<sub>2</sub> are missing also because of saturation.

<sup>c</sup>Standard deviation calculation for  $\sigma = \sqrt{\sum (\Delta x)^2 / 2n}$ , where  $\Delta x$  = difference between pairs and  $n$  = total experiments per salt.

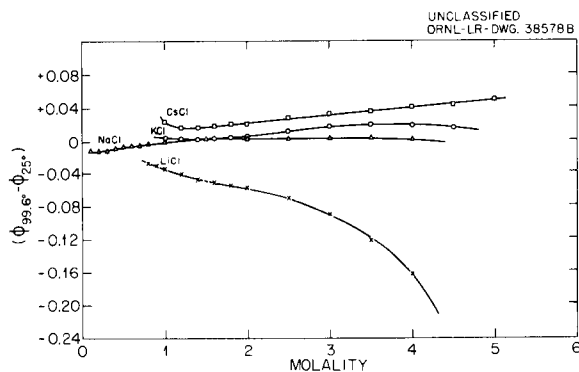


Fig. 11.2. Comparative Osmotic Behavior of Monovalent Electrolytes at 99.6 and 25.0°C.

alkali halides KCl, NaCl, and CsCl show modest changes from ideal behavior and are ranked in the order of their molecular weights and ionic radii with NaCl exhibiting the least and CsCl the greatest deviations. The changes in  $\phi$  when increasing the temperature from 25 to 100°C reveal

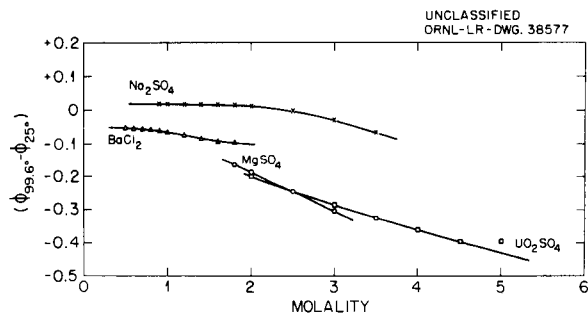


Fig. 11.3. Comparative Osmotic Behavior of Multivalent Electrolytes at 99.6 and 25.0°C.

very small shifts as shown in Fig. 11.2, but the solutes still maintain their relative order. Lithium chloride occupies a unique position whether one is considering the effective pressures of salt solutions, osmotic coefficients, entropies, etc. It has a negative and larger change in  $\phi$  when compared at the two temperatures than the other 1-1 alkali halides. In other words, the pronounced

Table 11.3. Osmotic Coefficients for Round Molalities at 99.6°C

Molality	LiCl	NaCl*	KCl	CsCl	Na <sub>2</sub> SO <sub>4</sub>	MgSO <sub>4</sub>	BaCl <sub>2</sub>	UO <sub>2</sub> SO <sub>4</sub>
0.8	(0.967)**	0.926					0.846	
0.9	(0.974)	0.930			0.667		0.858	
1.0	0.982	0.935	0.901	(0.880)	0.658		0.869	
1.2	0.999	0.945	0.902	0.872	0.648		0.893	
1.4	1.018	0.955	0.903	0.872	0.642		0.917	
1.6	1.039	0.965	0.907	0.875	0.638		0.942	
1.8	1.061	0.976	0.912	0.879	0.635	(0.463)	0.966	
2.0	1.084	0.986	0.918	0.884	0.633	0.477	0.991	(0.424)
2.5	1.141	1.016	0.935	0.898	0.631	0.534	1.053	0.463
3.0	1.194	1.048	0.953	0.912	0.630	0.616		0.505
3.5	1.243	1.077	0.969	0.926	(0.629)	0.712		0.548
4.0	(1.281)	1.105	0.983	0.941		0.822		0.591
4.5			0.995	0.956		0.936		0.630
5.0				0.972		(1.052)		0.666

\*Standard values with interpolations taken from R. P. Smith, *J. Am. Chem. Soc.* **61**, 500 (1939) and R. P. Smith and D. S. Hirtle, *ibid.* **61**, 1123 (1939).

\*\*Values in parentheses determined by a short extrapolation.

effect of the lithium ion on the structure of water at 25°C is decreased at higher temperatures as the system moves in the direction of more ideal behavior at 100°C. The remaining electrolytes, BaCl<sub>2</sub>, MgSO<sub>4</sub>, Na<sub>2</sub>SO<sub>4</sub>, and UO<sub>2</sub>SO<sub>4</sub>, all show considerably larger deviations from ideal behavior than the 1-1 alkali halides as the temperature is elevated. These solutes show much larger negative changes in  $\phi$  with temperature (Fig. 11.3) and increasingly larger temperature effects at higher molalities. The multicharged cations with their generally larger ionic charge to ionic radius ratio exhibit stronger interactions with the polar solvent water than the singly charged ions. Their behavior is therefore less ideal than the simpler solutes, and the reduction in the dielectric constant of the solvent due to elevations of the temperature results in marked changes in their ability to affect water.

This study demonstrates the usefulness and practicability of the isopiestic method for the study of electrolyte solutions at elevated temperatures. The data available thus far are adequate only to point the way ahead and to reveal comparative behavior over a limited concentration

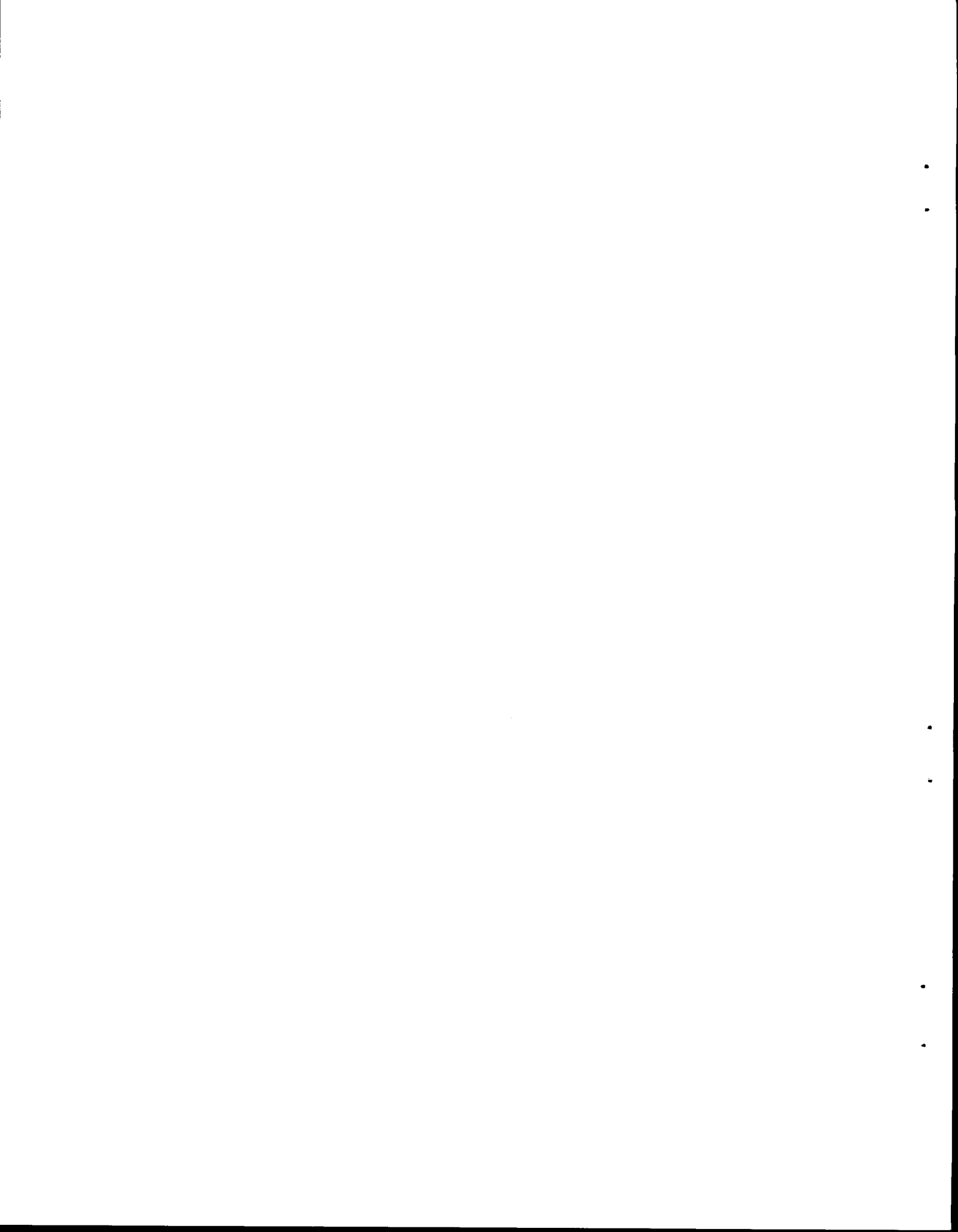
range for a limited selection of solutes. An extension of the concentration range downward to 0.1 *m* or less is urgently needed and will be given early consideration in future planning. The standard state for electrolyte solutions is one of infinite dilution, and an integration of  $\phi$  for the range of molalities is necessary from higher concentrations to zero in order adequately to describe the system in such usual terms as activity coefficients. The region from 0.1 to 1 *m* is one of rapid change in solution behavior and inadequate theoretical development for most systems, so that measurements are most necessary in this range in order to perform useful integrations. The situation is better in the concentration range from zero to 0.1 *m*, where useful extrapolations can be attempted to complete the concentration range. The investigation of a wide variety of salts and especially of higher temperatures is of great interest. The isopiestic equipment used in collecting these data is presently undergoing modifications involving the introduction of a direct optical system for balance monitoring. This should improve the speed with which data can be collected and the reliability of performance.

•  
•

**Part III**  
**GAS-COOLED REACTOR PROGRAM**

•  
•

•  
•



## 12. GAS EVOLUTION FROM GRAPHITE

L. G. Overholser

J. P. Blakely

Graphite has extensive use as a moderator in various reactors because of its physical, mechanical, and nuclear properties. Most of these applications are for systems in which the graphite is not in direct contact with the coolant or in those instances where the coolant contacts the graphite, the coolant and graphite temperatures are sufficiently low to preclude any significant reaction of the coolant with the graphite. The successful use of CO<sub>2</sub> as a coolant by the British in the unclad-graphite-moderated Calder Hall reactors stimulated interest in the gas-cooled reactor field and resulted in studies pointed toward the use of less reactive coolants than CO<sub>2</sub> in order to achieve higher outlet gas temperatures and thereby increase the thermal efficiency of graphite-moderated reactors.

In view of the ample helium supplies available in this country it is only natural that such an inert gas should find favor for projected gas-cooled reactors. Although sufficiently pure helium is available for such applications it is anticipated that contamination of the helium by water vapor, carbon dioxide, carbon monoxide, oxygen, nitrogen, and hydrocarbons may occur from such sources as leaks in the valves, seals, heat exchanger tubes, and outgassing of the graphite. The contaminants resulting from this outgassing will probably be of most concern during startup and early stages of reactor operation. The reaction  $C + CO_2 \rightleftharpoons 2CO$  which can produce burnout of graphite in the hot regions and deposition of carbon in the cooler areas of the reactor is of particular importance since most of the oxygen present in the gas, either as oxygen or in the water vapor, will react with the graphite to yield CO<sub>2</sub> and/or CO at the temperatures of interest. The possible interaction of the contaminants with metal surfaces resulting in oxidation, carburization, or decarburization, especially of the fuel element cladding, must also be considered.

Experimental studies are being made that are designed to yield information on the quantity and composition of the gas evolved by different types of graphite at various temperatures. Other factors such as the geometry of the graphite specimen, the effect of exposure of graphite to various atmospheres,

and the rates of gas evolution which have been studied to a limited extent are to be investigated more thoroughly. The results of these studies should be of assistance in the evaluation of the level of contaminants likely to occur in the helium, helpful in an appraisal of the interaction of these contaminants with the graphite and the metal surfaces, and of aid in the design of the purification system for the helium.

Six reactor grades<sup>1</sup> of graphite manufactured by three companies have been or are being studied. These include: TSF and AGOT grades from the National Carbon Co., Speer Moderator Nos. 1 and 2 from the Speer Carbon Co., and R-1HLM and R-6HLM from the Great Lakes Carbon Co. These graphites have nominal densities in the range 1.6–1.7 g/cm<sup>3</sup> and in most instances test specimens were cut from bars or pieces of bars extruded to 4 × 4 × 50 in. in size. In addition to the reactor grades of graphite three graphites of interest to the Los Alamos reactor program were studied. They are National Carbon Porous No. 60, Great Lakes H4LM, and Great Lakes 4HLM reimpregnated. The first has a density of ~1.0 g/cm<sup>3</sup> and the last a density of ~1.8 g/cm<sup>3</sup>. Two graphites, National Carbon ATJ and C-18, were studied on request for the ORNL thermonuclear project. These two graphites are commonly used for fabrication of various graphite forms because of their machining qualities.

A general view of the apparatus used in the gas evolution studies is presented in Fig. 12.1. External resistance heating of the graphite specimen (usually 1½ in. in diameter and 2 in. long; a few studies have been made with specimens ¾ in. in diameter and 2 in. long) is used for temperatures up to 1000°C; induction heating (specimens 1¼ in. in diameter × 1 in. long) is used for temperatures from 1000 to 2000°C. For either method of heating, the graphite specimen is loaded into a quartz tube,

---

<sup>1</sup>A more complete description of the graphites, a detailed description of the equipment and experimental methods, and an exhaustive presentation of the experimental data have been presented in the GCR Project progress reports: Dec. 31, 1958, ORNL-2676; June 30, 1959, ORNL-2767; Sept. 30, 1959, ORNL-2835; and Dec. 31, 1959, ORNL-2888.

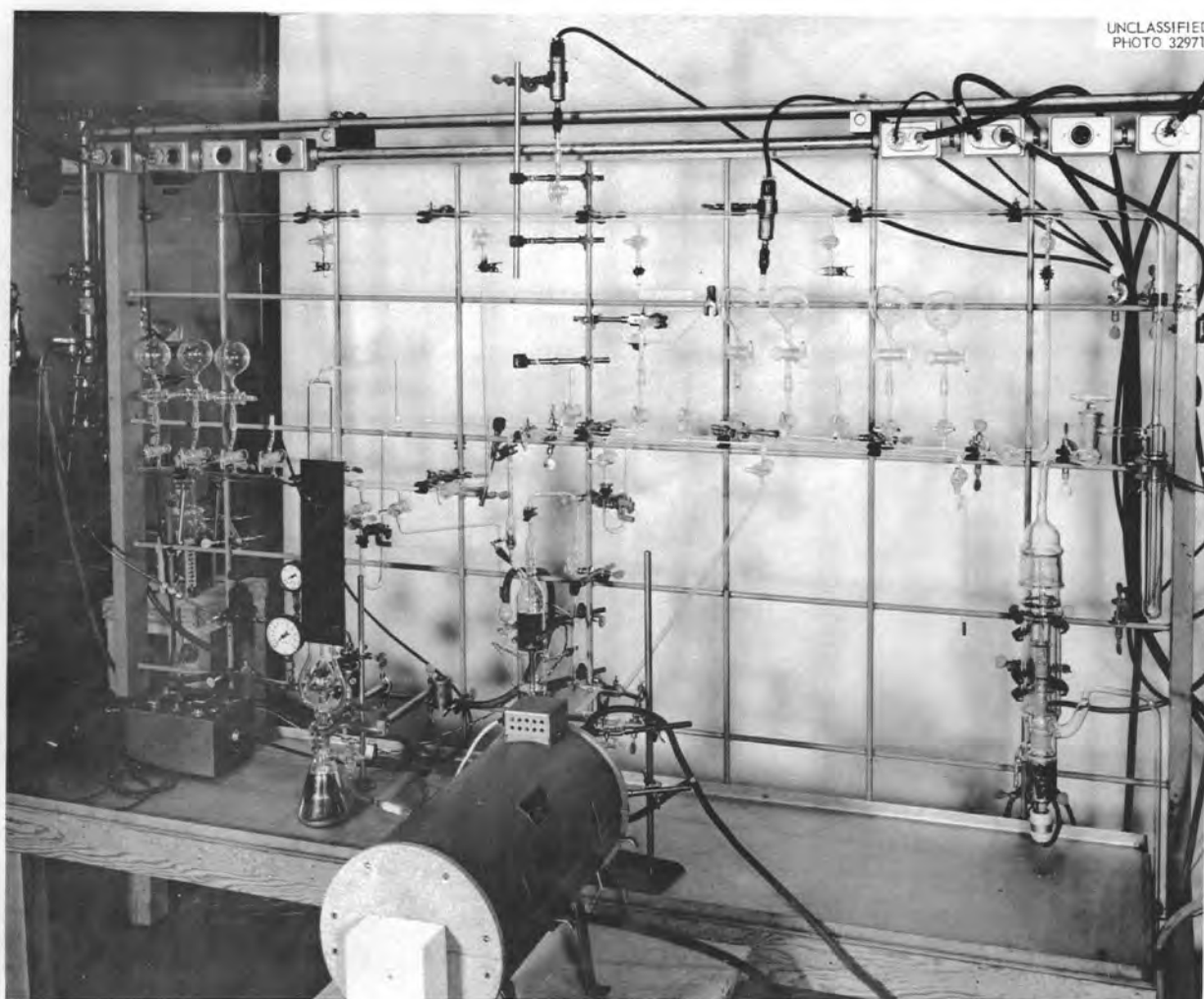


Fig. 12.1. Apparatus for Studying the Gas Evolution of Graphite at Various Temperatures.

and the entire system including the sample bulbs is pumped down to 1 to 2  $\mu$  pressure at room temperature. The gas evolved upon heating is removed by a Toepler pump and collected in a calibrated manifold where the pressure is measured by a McLeod gage before the gas is sampled. The composition of the gas sample is determined by a mass spectrometer and a gas chromatograph, the latter being used primarily to distinguish between  $N_2$  and  $CO$ . Volumes are arbitrarily expressed as  $cm^3$  per 100  $cm^3$  of graphite. The manifold is routinely pumped out after the collection of gas is complete for any given temperature. Therefore, the volume

of gas given for a particular temperature represents that evolved between this temperature and the next lower temperature (where no lower temperature appears it is room temperature), with most of the gas being evolved at the designated temperature. Since the gas is being pumped off during the rise in temperature, the composition of the gas is somewhat different from that which would be obtained if all the gas came off at the designated temperature. The time of heating at any given temperature varies considerably. In general, 3 to 6 hr suffices to remove the bulk of the gas. However, as will be seen from the rate data, graphites

continue to release small amounts of gas for prolonged periods of time. In many instances the heating is continued until the rate of evolution is approximately 2% per hour of the total amount evolved at that temperature. At temperatures up to  $\sim 1200^{\circ}\text{C}$ , a burst of gas is always observed when the temperature is raised even though the rate of evolution may be very low prior to the increase in temperature.

A breakdown of mass No. 28 into  $\text{N}_2$  and  $\text{CO}$  is not given although it is available for most of the data presented. Nitrogen accounts for only a few per cent of the total gas evolved through either  $1000$  or  $2000^{\circ}\text{C}$ . At the lower temperatures ( $200$ – $400^{\circ}\text{C}$ ) most of mass No. 28 consists of  $\text{N}_2$ , but at higher temperatures it is 80 to 95%  $\text{CO}$ . There does appear to be an increase in the  $\text{N}_2$  to  $\text{CO}$  ratio above  $1400^{\circ}\text{C}$ , but  $\text{N}_2$  remains the minor constituent.

Data are presented in Tables 12.1 and 12.2 which show the differences in quantity and composition of gas evolved by AGOT and TSF graphites as a function of temperature. AGOT graphite is a thermally purified graphite whose purity is effected in part by careful selection of raw materials, but mainly by volatilization of impurities at the graphitization temperature of  $\sim 2800^{\circ}\text{C}$ . TSF, a gas-purified graphite, may or may not see as high a

graphitization temperature as AGOT, but in addition receives a high-temperature halogen treatment (probably Freon) which produces a graphite with lower neutron absorption cross section and lower ash content, and, as seen from the data in Tables 12.1 and 12.2, a graphite that also evolves less gas than AGOT. The gas from TSF also contains a higher ratio of  $\text{H}_2$  to  $\text{CO} + \text{CO}_2$  than does that evolved by AGOT. The change in composition of the evolved gas for the two graphites with temperature is shown clearly in Figs. 12.2 and 12.3, and the differences in volumes as well as composition are depicted in Fig. 12.4. The data presented in Figs. 12.2–12.4 were not obtained from the same specimens of AGOT and TSF graphite which were used for obtaining the results given in Tables 12.1 and 12.2. Bars from several furnace loads of each of the two graphites have been studied and some differences observed. However, it should be pointed out that graphite is an extremely variable material and that it is not uncommon for specimens machined from the same bar to yield values which differ by 50% for the gas evolved.

Data obtained at  $300$ ,  $600$ , and  $1000^{\circ}\text{C}$  for the various graphites studied, are presented in Table 12.3. In all but one case (ATJ), the run given was selected as representative for the particular graphite. It may be noted that Speer moderators Nos. 1 and 2 evolve gas with a  $\text{H}_2$  to  $\text{CO} + \text{CO}_2$

Table 12.1. Interval Profile of the Volume and Composition of Gas Evolved by a Typical Thermally-Purified Graphite (National Carbon AGOT)

Temperature ( $^{\circ}\text{C}$ )	Volume ( $\text{cm}^3/100 \text{ cm}^3$ graphite)	Volume Per Cent of Constituents in Evolved Gas				
		$\text{H}_2$	Hydrocarbons	$\text{H}_2\text{O}$	$\text{CO}_2$	Mass 28
200	1.2	1	6	70	3	11
400	1.8	3	10	50	20	14
500	2.2	7	8	12	39	29
600	2.6	11	3	3	50	32
700	2.5	15	0.4	6	37	41
800	5.7	28	0.6	2	25	48
900	6.3	44		5	1	50
1000	10.1	55		0.2	0.3	43
Total	32.4	11.0*	0.6*	2.7*	4.8*	13.1*

\*Total volume,  $\text{cm}^3$  per  $100 \text{ cm}^3$  of graphite.

REACTOR CHEMISTRY PROGRESS REPORT

Table 12.2. Interval Profile of the Volume and Composition of Gas Evolved by a Typical Gas-Purified Graphite (National Carbon TSF)

Temperature (°C)	Volume (cm <sup>3</sup> /100 cm <sup>3</sup> graphite)	Volume Per Cent of Constituent in Evolved Gas				
		H <sub>2</sub>	Hydrocarbons	H <sub>2</sub> O	CO <sub>2</sub>	Mass 28
300	0.9	2	34	26	4	30
400	1.1	9	16	26	6	40
500	2.2	14	23	12	13	25
600	3.1	29	39	6	6	22
700	2.7	42	34	2	1	21
800	2.0	83	5	1	0.4	10
900	2.4	75	1	2	0.3	21
1000	2.7	79	0.5	4	0.2	17
Total	17.1	8.0*	3.2*	1.3*	0.6*	3.7*

\*Total volume, cm<sup>3</sup> per 100 cm<sup>3</sup> of graphite.

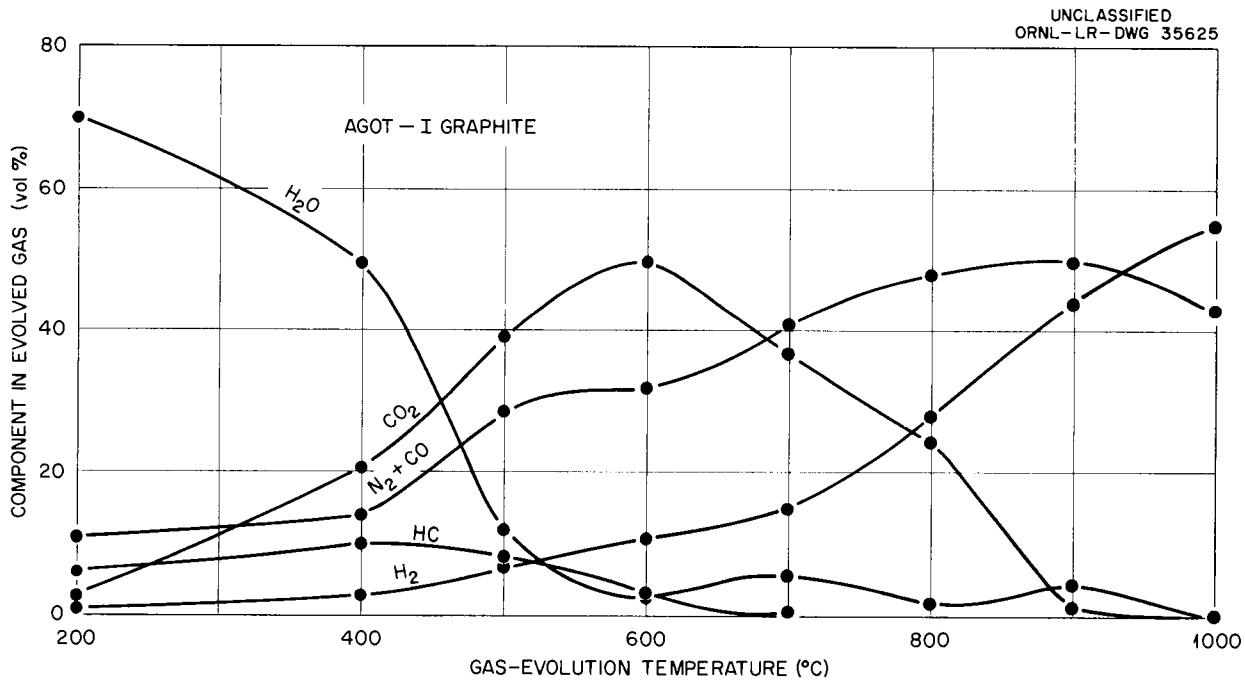


Fig. 12.2. Volume and Composition of Gases Evolved by AGOT-1 Graphite at Various Temperatures.

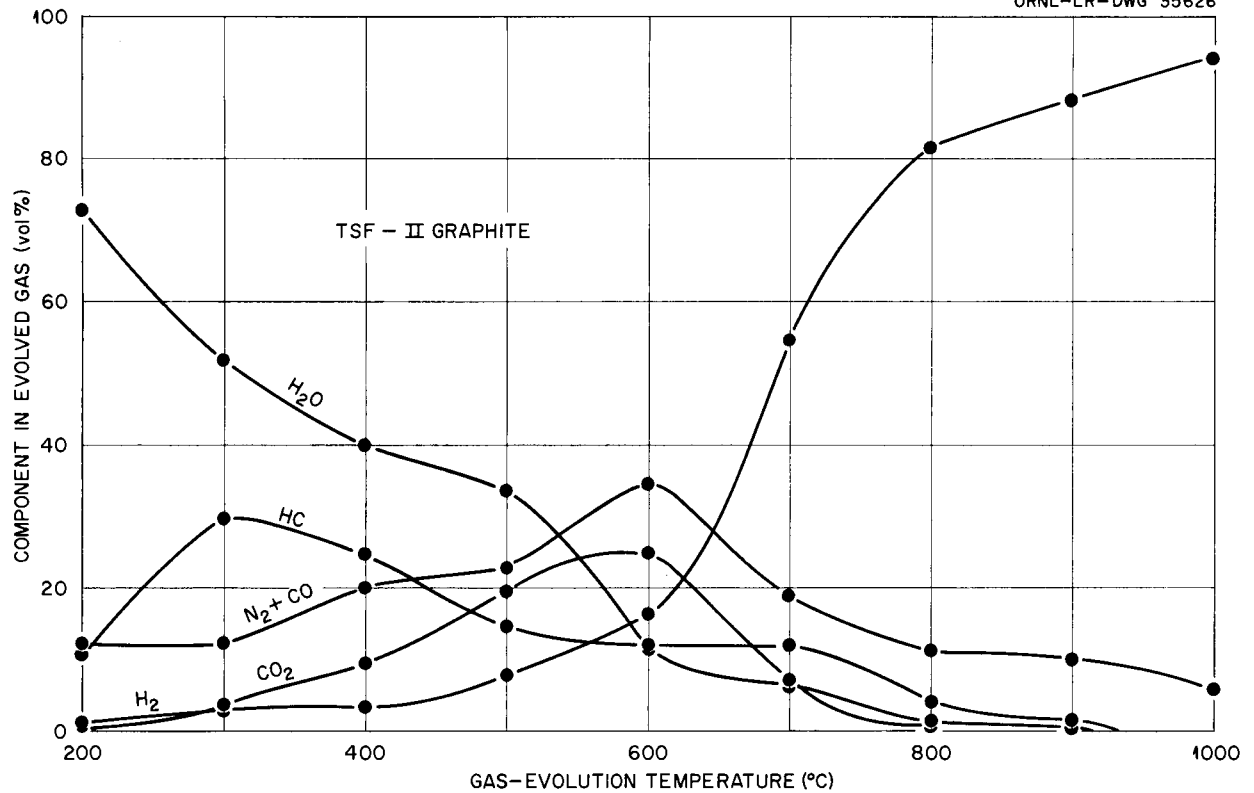
UNCLASSIFIED  
ORNL-LR-DWG 35626

Fig. 12.3. Volume and Composition of Gases Evolved by TSF-II Graphite at Various Temperatures.

ratio greater than one. Since these are gas-purified graphites it would be expected that the composition of the evolved gas be similar to that found for TSF. The total quantity of gas also falls in the same region for all three of these gas-purified graphites. It is not known for certain whether or not R-1HLM is a gas-purified graphite. Judging from the similarity of both the composition and total volume of the evolved gas to those for AGOT, it is not a gas-purified graphite. The non-reactor grades of graphite are listed for general interest. H4LM, whose degassing behavior suggests that it has been gas-purified, behaves quite differently after being reimpregnated (similar to that for AGOT).

Data obtained at 1000, 1400, and either 1800 or 2000°C for the different graphites studied are presented in Table 12.4. The volume of gas evolved through the maximum temperature is in all cases at least double that observed for external resistance heating through 1000°C. It will be noted that

the volume evolved at 1000°C by using induction heating also is greater than that observed for external resistance heating through 1000°C. The reason for this difference in behavior is not yet understood. The gas-purified graphites under induction heating also evolve a larger volume of H<sub>2</sub> than the combined volume of CO + CO<sub>2</sub>. Surprisingly small volumes of gas are reported for porous No. 60 and ATJ graphites and, as expected, C-18 evolved a relatively large volume.

Preliminary rate data for the evolution of gas from TSF graphite are shown in Table 12.5 and Fig. 12.5. The data are incomplete in many instances but do provide some insight into the degassing behavior. Temperature has a marked effect on the rate of gas evolution and, as indicated earlier, the rate of release is high during the early stages of heating. Accurate measurements of the rate changes after prolonged heating also are difficult to obtain since the rates change

## REACTOR CHEMISTRY PROGRESS REPORT

Table 12.3. Volume and Composition of Gas Evolved by Various Graphites at 300, 600, and 1000°C

Graphite	Temperature (°C)	Volume (cm <sup>3</sup> /100 cm <sup>3</sup> graphite)	Volume Per Cent of Constituents in Evolved Gas				
			H <sub>2</sub>	Hydrocarbons	H <sub>2</sub> O	CO <sub>2</sub>	Mass 28
National Carbon AGOT	300	1.9	0.8	0.5	85	2.0	11
	600	8.3	5.7	4	38	44	10
	1000	17.2	18	0.7	2	22	53
Total		27.4	3.6*	0.4*	5.0*	7.4*	10.2*
National Carbon TSF	300	0.9	1.8	36	27	4	30
	600	4.8	19	51	5	5	20
	1000	8.5	84	1	1	0.5	14
Total		14.2	8.1*	2.8*	0.5*	0.2*	2.5*
Speer moderator No. 1	300	0.7	1.9	9	61	6.5	18
	600	3.7	6.7	16	19	14	46
	1000	11.1	64	2	1	1	29
Total		15.5	7.4*	0.8*	1.2*	0.7*	5.4*
Speer moderator No. 2	300	0.5	1.2	5	77	4	13
	600	3.1	14	24	18	14	30
	1000	6.6	75	2	1	0.2	18
Total		10.2	5.3*	0.8*	0.9*	0.4*	2.4*
Great Lakes R-1HLM	300	0.6	3.1	3	73	4.6	16
	600	5.1	6	29	32	12	20
	1000	28.8	31	4	3	5	56
Total		34.5	9.2*	2.7*	2.8*	2.1*	17.1*
Great Lakes H4LM	300	0.6	40	5	73	5	13
	600	3.3	16	30	23	9	22
	1000	10.3	81	4		1	14
Total		14.2	8.8*	1.4*	1.2*	0.4*	2.2*
Great Lakes H4LM reimpregnated	300	0.9	1.5	2	70	14	13
	600	12.2	11	8	13	50	18
	1000	16.3	41	3		2	51
Total		29.4	8.1*	1.5*	2.3*	6.5*	10.7*
National Carbon porous No. 60	300	0.9	2.3	1	74	6	16
	600	14.8	12	16	8	48	17
	1000	17.8	49	3	1	1	46
Total		33.5	10.5*	2.8*	1.9*	7.3*	10.9*
National Carbon ATJ	300	0.5	1.4	3	68	10	16
	600	11.5	1.6	4	21	65	7
	1000	9.5	40	1	2	12	45
Total		21.5	4.0*	0.5*	2.9*	8.7*	5.0*
National Carbon C-18	300	0.9	1.9	1	72	8	16
	600	23.4	4.7	17	3	68	9
	1000	18.4	30	3	1	18	48
Total		42.7	6.6*	4.3*	1.0*	19.2*	11.1*

 \*Total volume, cm<sup>3</sup> per 100 cm<sup>3</sup> of graphite.

Table 12.4. Volume and Composition of Gas Evolved by Various Graphites in the Temperature Range 1000–2000°C

Graphite	Temperature (°C)	Volume (cm <sup>3</sup> /100 cm <sup>3</sup> graphite)	Volume Per Cent of Constituents in Evolved Gas				
			H <sub>2</sub>	Hydrocarbons	H <sub>2</sub> O	CO <sub>2</sub>	Mass 28
National Carbon AGOT	1000	59.9	42	0.2	6	14	37
	1400	13.8	20	0.5		1.0	78
	2000	1.4	9	0.6		0.2	91
Total		75.1	28.2*	0.2*	3.6*	8.4*	34.5*
National Carbon TSF	1000	39.6	48	5	10	2	35
	1400	10.7	53	2		2	39
	1800	2.4	1				98
Total		52.7	24.8*	0.4*	4.1*	1.1*	20.3*
Speer moderator No. 1	1000	21.1	51	3	2	2.4	42
	1400	16.7	68	1		0.3	19
	1800	5.1	4	1		0.2	94
Total		42.9	22.9*	0.2*	0.1*	0.1*	17.0*
Speer moderator No. 2	1000	29.0	77	1	2	0.9	22
	1400	4.0	44	2		0.3	53
	1800	2.0	6			0.4	93
Total		35.0	23.3*	0.4*	0.6*	0.3*	10.4*
Great Lakes R-1HLM	1000	41.2	32		1	1.4	66
	1400	10.6	6		0.3	1.2	93
	1800	0.2	10	0.5		0.2	88
Total		52.0	13.8*	<0.1*	0.4*	0.7*	37.3*
Great Lakes H4LM	1000	22.8	48	0.5	4	0.3	47
	1400	9.5	61	0.7		0.4	36
	1800	4.3	27				73
Total		36.6	17.9*	0.2*	0.9*	0.1*	17.2*
Great Lakes H4LM reimpregnated	1000	61.7	22	0.4	4	2.7	71
	1400	10.0	44	0.7		0.3	54
	1800	6.6	81	0.3			17
Total		78.3	23.4*	0.3*	2.5*	1.7*	50.3*
National Carbon porous No. 60	1000	51.5	38	2	5	2.6	52
	1400	3.0	15				85
	1800	1.5	67	0.5			33
Total		56.0	21.0*	1.0*	2.6*	1.3*	29.7*
National Carbon ATJ	1000	46.3	16	2	4	37	41
	1400	3.6	2.5	3		3	92
	2000	0.2	**	**	**	**	**
Total		50.1	7.6*	1.0*	1.9*	17.1*	22.2*
National Carbon C-18	1000	88.2	35	1	1	10	52
	1400	31.0	11			3	85
	1800	4.3	83	2		0.7	10
Total		123.5	37.8*	1.3*	0.9*	9.7*	72.7*

\*Total volume, cm<sup>3</sup> per 100 cm<sup>3</sup> of graphite.

\*\*Not analyzed.

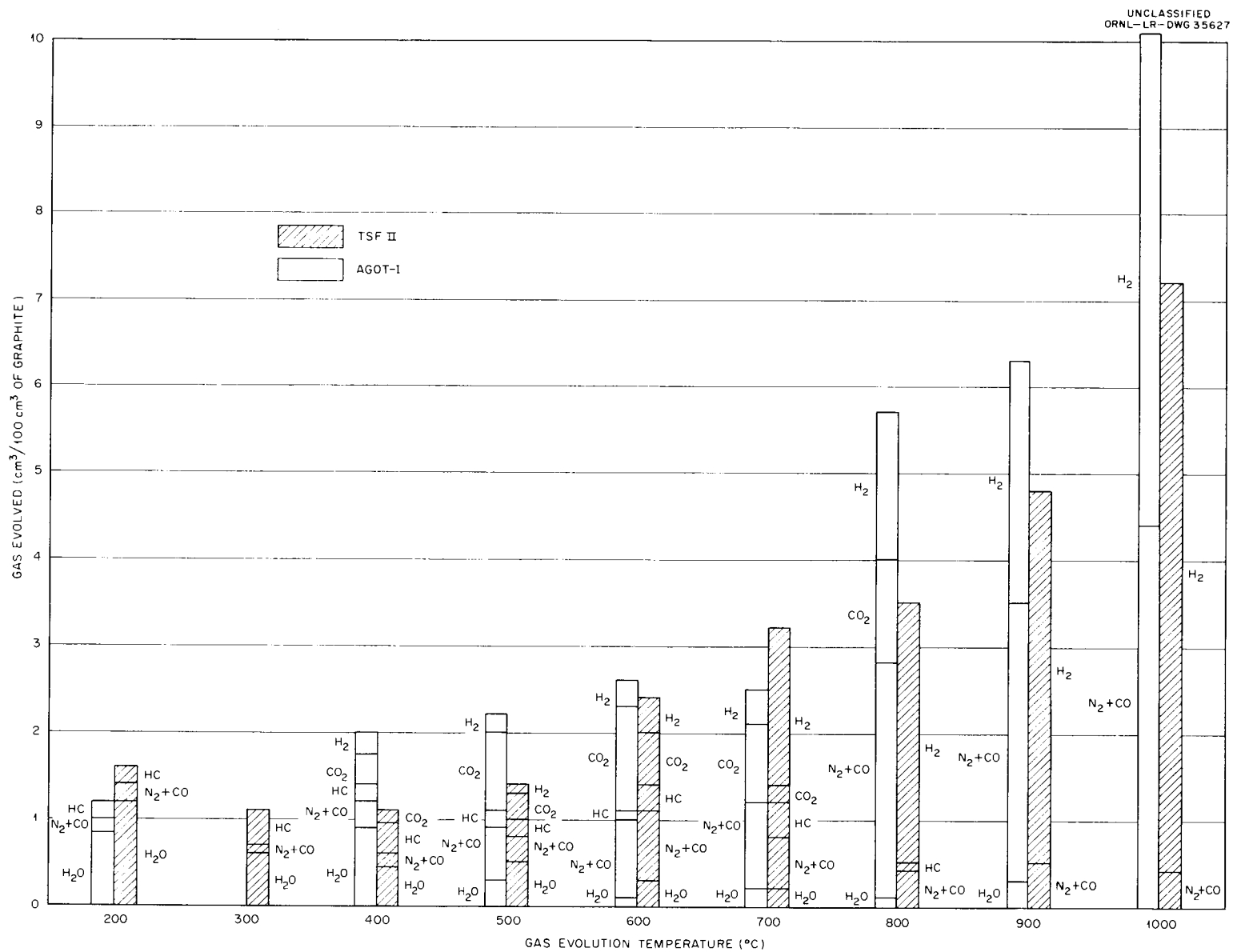


Fig. 12.4. Volumes of the Various Gases Evolved by AGOT-1 and TSF-II Graphite in the Temperature Range 200–1000°C.

Table 12.5. Rate of Gas Evolution by TSF-II Graphite  
 $1\frac{1}{2} \times 2$  in. specimen

Elapsed Time (hr)	Temperature (°C)	Run 1		Run 2	
		Rate*	Volume (cm <sup>3</sup> )	Rate*	Volume (cm <sup>3</sup> )
1	300		1.0		0.9
3	300	0.09		0.1	
8	300	0.04			
18	300	0.02			
23	300		1.5		
27	300			0.01	1.8
1	600	0.6	3.1		2.1
2	600	0.31			
3	600	0.22			
4	600	0.19			
6	600			0.11	
10	600	0.08			
16	600			0.05	4.1
22	600	0.06			
38	600	0.03			
48	600	0.03	6.2		
2	1000	2.0	9.3	1.1	6.5
6	1000	0.50			
22	1000	0.25		0.16	12.1
25	1000	0.25			
40	1000	0.15	19.5		

\*Rate given as cm<sup>3</sup> per 100 cm<sup>3</sup> of graphite per hour.

extremely slowly. The values reported were obtained by using a certain defined set of experimental conditions. Aside from the temperature, the pressure of the gas in contact with the graphite specimen is probably the single factor having the greatest effect on the rate of evolution. The gas was pumped off continuously with a Toepler pump and, except during the early stages of heating at a given temperature, the pressure of the gas over the specimen was relatively low and decreased as the rate of evolution decreased. These dynamic conditions yield rates quite different from those seen when the evolved gas is not removed but, rather, equilibrium conditions are attained, characterized by a constant pressure. For run No. 1 the pressure in the quartz tube was 180  $\mu$  15 min after reaching 300°C, 20  $\mu$  after 2 hr, 10  $\mu$  after 6 hr, and 3 to 5  $\mu$  after 18 hr. At 600°C a maximum pressure of 320  $\mu$  was measured, 35  $\mu$  at 2 hr, 12  $\mu$

at 10 hr, 5  $\mu$  at 22 hr, and 3  $\mu$  at 48 hr. At 1000°C the pressure was 25  $\mu$  at 6 hr, 15  $\mu$  at 20 hr, and 10  $\mu$  at 40 hr. Further measurements will be made by using a mercury diffusion pump to remove the gas in an attempt to maintain the pressure over the specimen at some lower and more constant value.

Attempts have been made to correlate the outgassing behavior of the graphites with such properties as ash content, surface area, loss in weight upon degassing, and porosity. Aside from possibly the ash content and the loss in weight it does not appear that any correlation between these properties and the volume of gas released exists. Control of manufacturing processes including the selection of raw materials and the graphitization conditions is most likely to result in a better correlation with the outgassing behavior of the various graphites.

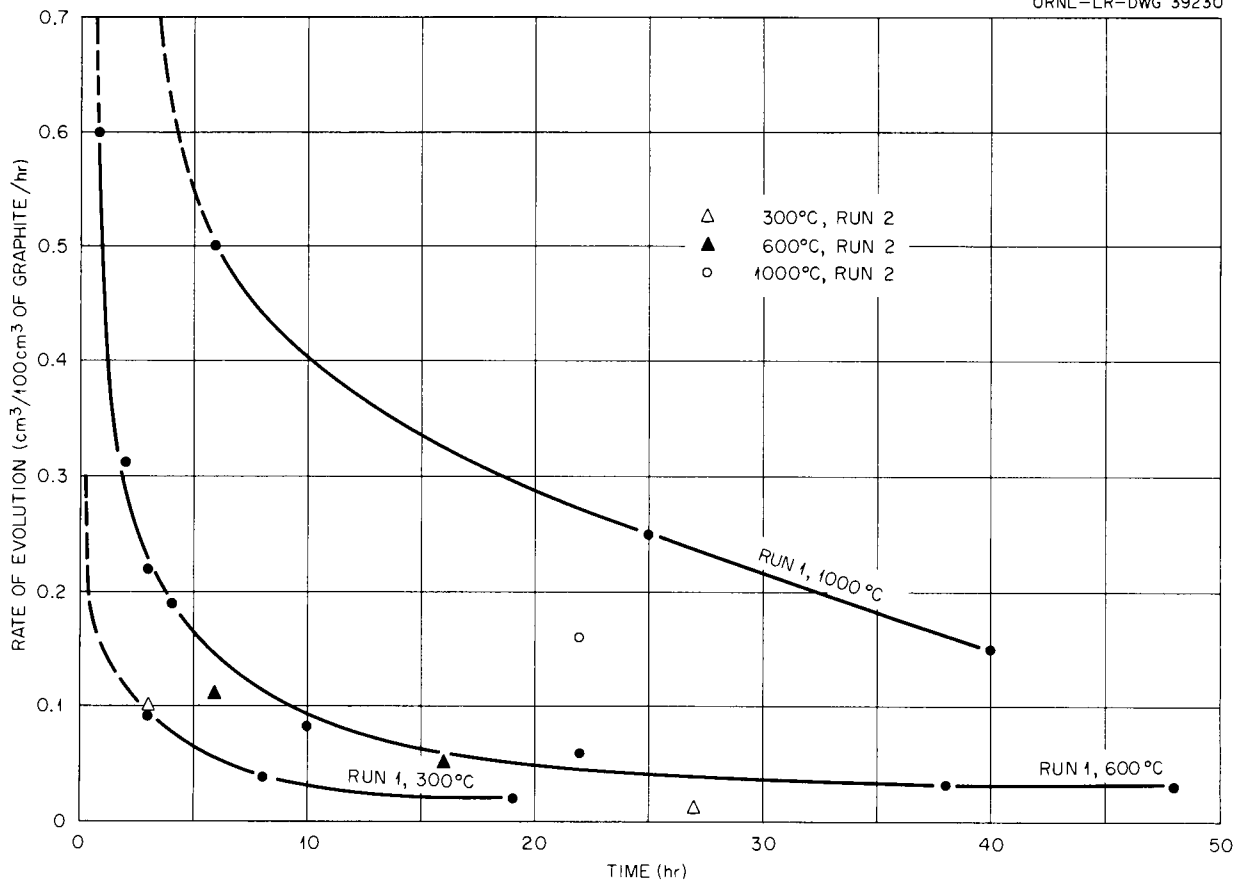


Fig. 12.5. Rate of Evolution of Gas by TFS-II Graphite Specimens 1½ in. in Diameter and 2 in. Long, at 300, 600, and 1000°C.

## 13. TRANSPORT OF GASES THROUGH CERAMIC MATERIALS

J. Truitt

R. B. Evans

N. V. Smith

G. M. Watson

During the course of design studies of an enriched-uranium-fueled, helium-cooled reactor (GCR-2), it became clear that increasing the allowable operating temperature of projected fuel elements would advance calculated efficiencies to levels which could not be ignored.<sup>1</sup> This development created a marked impact on design concepts and fuel-element technology. The pivotal consideration involved release rates of volatile fission products from high-temperature fuel elements and resultant coolant contamination.<sup>2</sup> Metal claddings are not feasible at these temperatures<sup>2</sup> ( $t_{\text{surface}} > 2000^{\circ}\text{F}$ ), and the reliabilities of ceramic coatings (low-permeability graphites and carbides) are undetermined.<sup>3</sup> In some designs, contamination of the coolants has been assumed to be inevitable.<sup>2</sup>

The controlling release rates of fission products from  $\text{UO}_2$ -impregnated graphite are those in the  $\text{UO}_2$  particle. In this case, the rates are so low that intentional extraction of  $\text{Xe}^{135}$  to enhance neutron efficiencies appears to be impractical.<sup>4</sup> Experiments related to mechanisms of fission product release from fuel materials have been performed elsewhere<sup>5-7</sup> and are being continued locally.<sup>8</sup>

<sup>1</sup>The ORNL Gas-Cooled Reactor. *Advanced Concepts*, ORNL-2510 (Oct. 2, 1958).

<sup>2</sup>The HGCR-1, a Design Study of a Nuclear Power Station Employing a High-Temperature Gas-Cooled Reactor with Graphite- $\text{UO}_2$  Fuel Elements, ORNL-2653 (July 14, 1959).

<sup>3</sup>A Study of Problems Associated with Release of Fission Products from Ceramic Fuels in Gas Cooled Reactors, ORNL-2851 (Oct. 27, 1959).

<sup>4</sup>A. M. Perry, "Advanced Design Studies," p 338 in *ORNL Information Meeting on Gas Cooled Reactors*, USAEC TID-7564 (December 1958).

<sup>5</sup>D. Cubicciotti, *The Diffusion of Xenon from Uranium-Carbide Impregnated Graphite at High Temperatures*, NAA-SR-194 (Oct. 13, 1952).

<sup>6</sup>C. T. Young and C. A. Smith, *Preliminary Experiments on Fission Product Diffusion from Uranium-Impregnated Graphite in the Range 1800-2000°C*, NAA-SR-232 (June 17, 1953).

<sup>7</sup>A. H. Booth and G. T. Rymer, *Determination of the Diffusion Constant of Fission Xenon in  $\text{UO}_2$  Crystals and Sintered Compacts*, CRDC-720 (August 1958).

<sup>8</sup>J. L. Scott and D. F. Toner, *The Study of Fission Product Release from Ceramic Fuels*, ORNL CF-59-12-82 (Dec. 23, 1959).

The subject research program covers theoretical and experimental studies on forced gas flow,<sup>9</sup> diffusion phenomena,<sup>10</sup> and porosity as they affect or occur in ceramic fuel-element and moderator materials. Recent work has involved reactor-grade graphites of relatively high porosity and permeability. Although these studies have been of fundamental nature, an excellent illustration of the immediate applicability of this work has been proposed<sup>11,12</sup> and completed<sup>13</sup> elsewhere.

This chapter illustrates the type and scope of the gas-transport studies currently being conducted at low temperatures. Plans for extending the investigation to high-temperature and pressure regions are being formulated.

## PERMEABILITY

Examination of parameters associated with forced-flow behavior affords a rapid method of characterizing fluid-transport mechanisms as they occur in the interstices of a ceramic material. Since many problems arise from the geometrical complexity of the pore structures, previous investigators have often employed an analog or model which consists of a group of parallel circular capillaries with equal "average" diameters and lengths. This is an oversimplification of the problem; however, use of this analog leads to concise presentations of definitions, data, and results in terms of established concepts.

The definitive steady-state isothermal relationship for fluid flow in circular conduits is given

<sup>9</sup>J. M. Hutcheon, B. Longstaff, and R. K. Warner, "The Flow of Gases Through a Fine Pore Graphite," p 259 in *Industrial Carbon and Graphite*, Society of Chemical Industry, London, 1957.

<sup>10</sup>A. Wheeler, "Reaction Rates and Selectivity in Catalyst Pores," p 260-75 in *Advances in Catalysis-III*, Academic Press, New York, 1951.

<sup>11</sup>*High Temperature Gas-Cooled Graphite-Moderated Power Station*, GA-593, GACP-595, GA-598, General Atomics, San Diego (November 1958).

<sup>12</sup>Personal communication from W. B. Cottrell, ORNL, to A. S. Berman, ORGDP (January 1959).

<sup>13</sup>H. L. Weissberg and A. S. Berman, *Diffusion of Radioactive Gases Through Power Reactor Graphite*, ORGDP-KL-413 (Apr. 6, 1959).

by Poiseuille's law, that is,

$$Q = \frac{d^2}{32\mu} A \frac{\Delta P}{L} = \frac{k_c}{\mu} A \frac{\Delta P}{L} \quad (1a)$$

The identities (see "Nomenclature," this section) clearly define a commonly used permeability constant  $k_c$  ( $\text{cm}^2$ ).

Equation (1a) is restricted to the viscous-flow region, as the relationship in the turbulent region involves  $(\Delta P)^2$ . Viscous flow is characterized by a parabolic velocity profile along the diameter normal to  $Q$ ; for liquids,  $Q/A$  is a maximum at the center and zero at the walls. The change from viscous to turbulent flow (in carefully conducted experiments) occurs at a Reynolds number ( $N_{Re} = 4Q \cdot \rho / \pi \cdot \mu \cdot d$ ) greater than 2000. Precisely, Eq. (1a) applies to liquids, and is approximated by gases flowing at high pressures, under low  $\Delta P/L$ , where  $Q$  is measured at the flowing pressure. A modified equation for gases undergoing considerable isothermal expansion is:

$$Q_a P_a = \frac{d^2}{32\mu} A \frac{\Delta P}{L} P_m = \frac{k_c}{\mu} A \frac{\Delta P}{L} P_m = K_c A \frac{\Delta P}{L} \quad (1b)$$

The identities define another popular permeability constant (applicable to gases only),  $K_c$  ( $\text{cm}^2/\text{sec}$ ). A striking and often overlooked feature of these equations is the absence of a fluid-mass-density term,  $\rho$ ; viscosity is the only contributing fluid property.

Up to this point, the discussion has been restricted to circular conduits; however, conversion to a porous medium may be readily accomplished through the model by equating simple volume and rate parameters which contain  $N$ , the number of capillaries and  $\epsilon$ , the open porosity, that is,  $N(Q_a P_a)_c = (Q_a P_a)_{\text{gross}}$  or  $N(k_c A_c/L_c) = kA/L$ , and  $NA_c L_c = \epsilon AL$ . Combining these equations, one obtains

$$k = \frac{\epsilon}{(L_c/L)^2} k_c \quad (2)$$

which indicates that an over-all  $k$  for a porous material differs from  $k_c$ , that of a capillary, through geometrical factors only. These factors, in turn, depend on the assumed model. One may use the

previous flow equations for porous materials with the understanding that  $A$ ,  $L$ ,  $k$ , and  $K$  are "gross" values which refer to the material under study. Under these conditions Eq. (1b) is referred to as "Darcy's law."<sup>14</sup>

The first experimental point of interest involved the determination of the viscous region of these materials. Previous work has indicated that the Reynolds number (using an average  $d$ ) at which turbulent flow begins to appear in porous media is essentially unity.<sup>14</sup> Since use of an average  $d$  is uncertain, and velocity profiles cannot be obtained, the only criterion remaining required experimental determinations of the linear portions of curves of pressure drop vs flow rate. Typical results are shown on Fig. 13.1 for AGOT graphite.

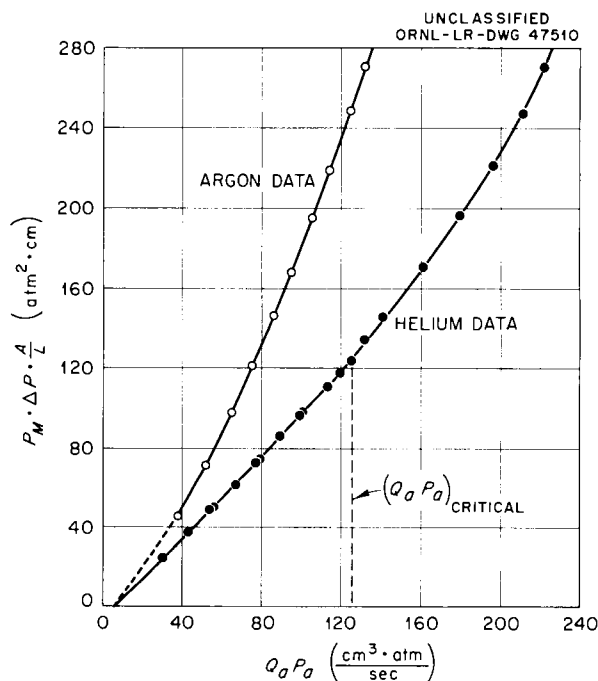


Fig. 13.1. Pressure Drop vs Flow Rate Characteristics for AGOT Graphite at 20°C.

The only linear curves are those for helium at  $Q_a P_a$  values less than 125  $\text{cm}^3/\text{sec}$  at 1 atm and 20°C. Since the Reynolds numbers for the two gases should be equal at the transition point,

$$(Q_a P_a)_{Ar} = (Q_a P_a)_{He} \left( \frac{M_{He}}{M_{Ar}} \cdot \frac{\mu_{Ar}}{\mu_{He}} \right) \quad (3)$$

<sup>14</sup>M. Muskat, chap. 3 in *Physical Principles of Oil Production*, McGraw-Hill, New York, 1949.

Based on this relationship and the helium value, an argon transition value of 14.3 cm<sup>3</sup>/sec was obtained. Thus, it appears that all of the argon experiments (corresponding to the points on Fig. 13.1) were conducted in the transition region or the turbulent-flow region. It is reasonable to expect, as indicated by the Reynolds number, that turbulent flow could occur in the smaller channels while viscous flow prevailed in the larger channels; an increasing number of channels would undergo transition as the velocity was increased. Thus, transition regions in porous media cover a wide range of velocities and depend on the pore-size distribution.

Another forced-flow phenomenon of importance concerns "slip" flow which is peculiar to gases and very viscous non-Newtonian liquids. In the case of gases, a naive explanation may be offered in terms of the velocity profile along the diameter - particularly at the walls. The velocity at the walls is zero for liquids and a constant positive value for a gas. The latter is a result of the thermal agitation of gas molecules (expressed as  $\bar{v}$ , the average thermal velocity) which causes the first layer to "slip" due to the collisions of un-directed molecules with the walls. As one might suspect, and as shown on Fig. 13.2, this effect

is important at low pressures but diminishes at high pressures, where the gases tend to take on liquid properties. The net effect is less resistance to flow than predicted by Darcy's law, or

$$Q_a P_a = \frac{k}{\mu} A \frac{\Delta P}{L} P_M \quad (1c)$$

where, as suggested by the data of Fig. 13.2,

$$k = k_a \left( 1 + \frac{a}{P_M} \right) \quad (4)$$

This form is utilized by many investigators<sup>14</sup> who also proposed that<sup>15</sup>

$$a_c = \frac{4}{3} b_c \cdot \frac{d_c}{L} \cdot \frac{\bar{v}}{P_M} \cdot \frac{32}{\mu} \quad (5)$$

which is written for capillaries. The original definition of  $k$  (cm<sup>2</sup>) was based on the thought that this parameter should be a function of the conduit and not of the fluid. Unfortunately, as shown by the three preceding equations, one must take several gas-permeability values and extrapolate to  $1/P_M = 0$  to obtain a parameter which is a characteristic of the material. The intercept  $k_a$  should be the same value one acquires from liquid flow experiments with the same medium.

Equations (1c) and (4) are excellent forms for relatively high-permeability materials and/or high-pressure applications. However, other forms are more suited to considerations involving very low-permeability materials at high pressures or intermediate materials at low pressures. Rearrangement of preceding equations, in terms of  $K$  (cm<sup>2</sup>/sec), yields

$$K_c = \frac{d_c}{32\mu} \cdot P_M + \frac{4}{3} b_c d_c \bar{v} \quad (6a)$$

for capillaries, and

$$K = B_o \frac{P_M}{\mu} + \frac{4}{3} K_o \bar{v} \quad (6b)$$

for porous media.<sup>15</sup> A plot of permeability data for

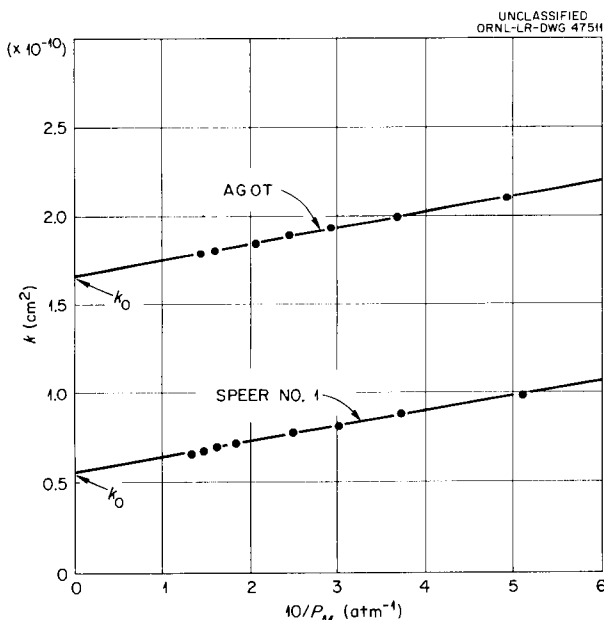


Fig. 13.2. Interpretation of High-Pressure Graphite Permeability Data at 20°C.

<sup>15</sup>P. C. Carman, *Flow of Gases Through Porous Media*, Academic Press, New York, 1956.

Speer No. 1 graphite in terms of the definitions given by Eq. (6b) is presented on Fig. 13.3. As the pressure and/or average pore diameter is decreased, the viscous-flow term (involving  $B_o$ ) loses significance. Under these conditions, the flow is given by

$$Q_a P_a = \frac{4}{3} K_o \frac{A}{L} \bar{v} \Delta P, \quad (7)$$

which is an expression for Knudsen flow. This is an important point, as it has been implied<sup>15</sup> that one can obtain Knudsen diffusion coefficients from the results of forced-flow experiments if the pores involved are very small.

Although attempts to correlate the  $B_o$  from Fig. 13.3 with the diffusion coefficients obtained experimentally on the same graphite have been unsuccessful, we anticipate much better correlations along these lines as the experiments are extended to include very low-permeability materials.

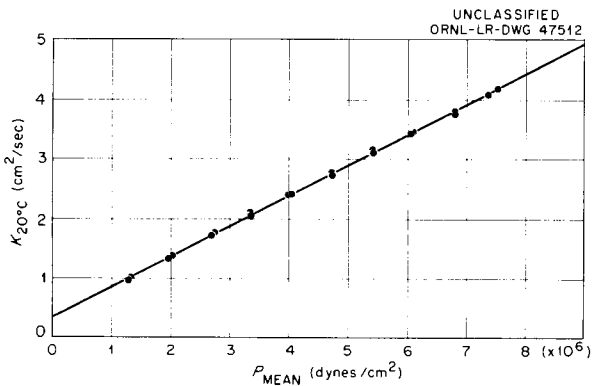


Fig. 13.3. Permeability of Speer No. 1 Graphite to Helium.

#### DIFFUSION OF GASES

A series of constant-pressure-diffusion experiments have been conducted at low pressures and temperatures using Speer No. 1 and AGOT graphites with helium and argon as the diffusing gases. With the knowledge and experience gained from these experiments, it should be possible to design a series of experiments with very low-permeability ceramics at or near reactor operating conditions of pressure and temperature. The experimental results for the diffusion experiments performed to date are summarized in Fig. 13.4. The results are expressed in terms of a diffusion coefficient for

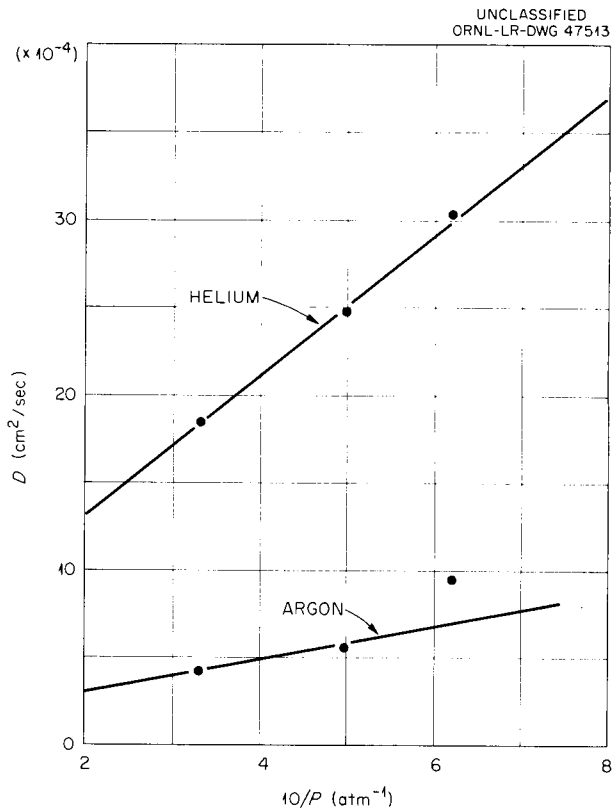


Fig. 13.4. Apparent Diffusion Coefficients for Argon and Helium in Speer No. 1 Graphite at 25°C.

each gas. A definition of the coefficient,  $D_{Ar}$  or  $D_{He}$ , may be obtained from the expression applicable to the isothermal-isobaric steady-state experimental conditions. This expression is

$$(Q_a P_a)_{Ar, He} = D_{Ar, He} A \frac{\Delta y}{L} P, \quad (8)$$

where  $y$  represents mole fraction of argon or helium.

The experiments were carried out by simultaneously sweeping initially pure argon past one face of a cylindrical graphite septum and helium past the other face. The diffusion rates for each component were obtained through determination of the composition and rate of the effluent sweep streams. The variable  $\Delta y$  was also based on the effluent composition; for argon, for example,

$$\Delta N_{Ar} = 50 + 0.5(Ar \text{ in } Ar_{stream} - Ar \text{ in } He_{stream}).$$

A great deal of care was taken to maintain equal pressures on each side of the septum so that  $\Delta P$

would be zero. These experiments were conducted with relatively low sweep velocities ( $N_{Re} < 10$ ) in order to avoid large pressure drops in the entrance lines and to keep diffused-gas concentrations at measurable levels in the effluent.

Information pertinent to the experimental results shown on Fig. 13.4 is outlined in Table 13.1; the permeability constants, determined graphically through Eq. (6b) and Fig. 13.3, were included, as these factors were used to calculate<sup>9</sup> the tortuosity ratio  $L_c/L$  shown. It should be noted that the determination of "open" porosity is included as part of the experimental program.

One of the primary objectives of the initial diffusion experiments was to establish the mechanism or mode of noble-gas diffusion through a graphite environment. If diffusion occurs in relatively-large diameter pores, the over-all mechanism should be classical in nature and would be characterized by equal coefficients (for each gas). If Knudsen and/or surface diffusion effects are involved (flow through small pores), the coefficients will differ and be independent of  $P$  or  $1/P$ . The curves shown

on Fig. 13.4 suggest that both types of mechanism contribute to the over-all diffusion encountered in the present experiments. The curves shown on Fig. 13.4 tend to follow those proposed by Wheeler.<sup>10</sup> The experimental results for Speer No. 1 graphite show a definite correspondence with initial results for AGOT graphite. Inspection of the values in Table 13.2 will reveal that the ratios of diffusion coefficients and permeability constants for AGOT graphite to comparable values for Speer No. 1 graphite range from 2.1 to 3.3.

The magnitudes of the experimental diffusion rates were much lower than those anticipated through preliminary calculations based on a model suggested by Carman,<sup>16</sup> the characterization parameters of Table 13.1 and classical He-Ar diffusion coefficients. For example, at 1 atm and 25°C, the classical He-Ar coefficient is  $8.1 \times 10^{-1}$  cm<sup>2</sup>/sec, the model value for Ar in a helium-saturated Speer No. 1 graphite is  $4.8 \times 10^{-2}$  cm<sup>2</sup>/sec, and the extrapolated experimental values for Speer No. 1 graphite are  $8.8 \times 10^{-4}$  cm<sup>2</sup>/sec for Ar and  $4.4 \times 10^{-3}$  for He. Coefficients obtained to date are of the same magnitude as those for CO<sub>2</sub> in a nitrogen-charcoal system as reported by Wicke and Kallenbach,<sup>17</sup> who performed the first experiments of this type.

Table 13.1. Speer No. 1 Graphite Characterization Factors and Dimensions for Diffusion Septum

Open porosity (with helium)	17.8 vol %
$K_o$ (with helium)	$2.23 \times 10^{-6}$ cm
$B_o$ (with helium)	$9.64 \times 10^{-11}$ cm <sup>2</sup>
Tortuosity factor, $L_c/L$	1.73
Septum shape	cylindrical
Inside diameter	0.5 in.
Outside diameter	0.8 in.
Exposed surface length	4 in.
Effective area-to-length ratio	135.8 cm

### POROSITY

The open-pore porosities, that is, the number of interconnected voids, of several different graphites were determined by the helium-gas penetration

<sup>16</sup>P. C. Carman, *Ibid.*, p 110.

<sup>17</sup>E. Wicke and R. Kallenbach, *Kolloid-Z.* **97**, 135 (1941).

Table 13.2. Summary Results of Diffusion Experiments with Two Reactor-Grade Graphites

Type of Graphite	Porosity to Helium (vol %)	Absolute Permeability (cm <sup>2</sup> )	Diffusion Coefficient (cm <sup>2</sup> /sec) at 25°C and 3.0 atm	
			Helium	Argon
		$\times 10^{-10}$	$\times 10^{-3}$	$\times 10^{-3}$
AGOT	22.0	1.65	3.7	1.4
Speer No. 1	17.8	0.56	1.8	0.42

REACTOR CHEMISTRY PROGRESS REPORT

technique<sup>18</sup> in combination with bulk-density determinations by the mercury-displacement method.<sup>18</sup> The method is based on determinations of the fluid displacements by the samples under pressure. A helium pressure of 6 atm was used in these tests.

<sup>18</sup>C. G. Rall, H. C. Hamontre, and D. B. Taliaferro, "Determination of Porosity by a Bureau of Mines Method: A List of Porosities of Oil Sands," *U.S. Bur. Mines Rep. Invest. No. 5025* (July 1953).

As Table 13.3 indicates, the porosities varied from 17.6 to 28.4% and the averages varied from 17.8 to 25.9%. Reproducibility of the method appears to be within about ±3% for samples run at different times. The variations in porosities appear to be smaller for the AGOT specimens than for the other types tested. After outgassing the samples at 1100°C an increase of about 1–3% was found in the open-pore porosities.

Table 13.3. Porosity of Reactor-Grade Graphites

Graphite Type	Open-Pore Porosity (%)		Total Porosity (%)	Graphite Type	Open-Pore Porosity (%)		Total Porosity (%)
	Experimental*	Mean			Experimental*	Mean	
AGOT-I <sup>1</sup>	20.2	20.0	24.1	Great Lakes H4LM	20.6	21.0	24.6
	19.8				20.9		
	19.9				21.4		
AGOT-III	22.0	22.1	25.7	TSF-II	26.8	25.9	28.4
	22.1				25.7		
	22.2				25.7		
Speer moderator No. 1	17.6	17.8	23.2		26.3		
	17.8				24.2		
	17.8				26.7		
	18.1				28.4		
Speer moderator No. 2	20.4	20.6	29.4	TSF-III	19.0	19.1	25.1
	20.2				18.1		
	18.9				20.1		
	21.0						
	20.9						

\*Each value represents average of three determinations.

NOMENCLATURE

- $a_c$  slip factor,  $\text{cm}^2/\text{dyne}$  or  $\text{atm}^{-1}$
- $A$  cross sectional area normal to flow,  $\text{cm}^2$
- $b_c$  geometrical correction factor for Knudsen flow
- $B_o$  viscous flow permeability constant,  $\text{cm}^2/\text{sec}$
- $d$  diameter of a circular conduit,  $\text{cm}$
- $d_c$  diameter of a capillary
- $D$  diffusion coefficient,  $\text{cm}^2/\text{sec}$
- $k$  permeability coefficient for porous media,  $\text{cm}^2$

$k_c$	permeability coefficient for a circular conduit, $\text{cm}^2$
$K$	permeability coefficient for porous media, $\text{cm}^2/\text{sec}$
$K_c$	permeability coefficient for a circular conduit, $\text{cm}^2/\text{sec}$
$K_o$	Knudsen flow permeability constant, cm
$L$	length along path of flow, cm
$M$	molecular or atomic weight, g/mole
$N$	number of capillaries involved in flow
$P$	pressure, atm or dynes/ $\text{cm}^2$
$P_a$	pressure at which effluent $Q_a$ is measured, atm or dynes/ $\text{cm}^2$
$Q$	volumetric flow rate, $\text{cm}^3/\text{sec}$
$Q_a$	volumetric flow rate of effluent gas (generally at $P_a =$ barometric pressure), $\text{cm}^3/\text{sec}$
$R$	gas constant
$T$	temperature, $^\circ\text{K}$
$\bar{v}$	average thermal velocity $(8RT/\pi M)^{1/2}$ , cm/sec
$y$	mole fraction in gas phase
$\Delta P$	pressure drop along $L$ , atm or dyne/ $\text{cm}^2$
$\epsilon$	open or connected porosity
$\mu$	fluid viscosity, dyne-cm/sec
$\rho$	fluid mass density, $\text{g}/\text{cm}^3$

## 14. IMPORTANCE OF ALKALI-METAL FISSION PRODUCTS IN EGCR FUEL CAPSULES

S. Cantor

Since the yield of cesium and rubidium nuclides of long half life is high (18.4 atoms per 100 fissions), the behavior of these fission products in long-lived reactor fuels may be of especial importance. In the EGCR, for example, whose fuel is pellets of  $\text{UO}_2$  in relatively thin-walled elements of stainless steel, these materials may contribute to excessive pressures within the fuel element or may interact with the container.

Tables giving the free energy of oxide formation<sup>1</sup> indicate that other fission products occurring in high yield (Zr, La, rare earths, Y, Sr, Ba, and Mo) form more stable oxides than  $\text{Cs}_2\text{O}$  or  $\text{Rb}_2\text{O}$ . These other fission products would react preferentially with all the oxygen made available as a by-product of fission. At the high temperature of the  $\text{UO}_2$  pellets (1200–1900°K) the equilibrium with respect to  $\text{O}^{--}$  ions should be attained fairly rapidly as surmised from self-diffusion measurements of oxygen in  $\text{UO}_2$  (ref 2). Therefore it is concluded that cesium and rubidium will be present mainly as metal. A small fraction of the alkali metals will be bound by the nonmetals (Br, I, Se, Te), whose effective fission yield is 4.4 atoms per 100 fissions. In addition, it is known that the CsI and CsBr so formed would be soluble in liquid cesium at reactor temperature.<sup>3</sup>

As burnup of the fuel progresses, cesium and rubidium will vaporize from the fuel into the cooler

vapor space that is present in each fuel capsule. When enough of the alkali metal gets into the vapor to exert a partial pressure equal to that exerted by liquid cesium at the same temperature, condensation will occur. Of course, the expected vapor pressure will be a function of the lowest temperature in each fuel rod. These vapor pressures are expected to be between 1 and 7 atm.

A stainless steel rod was soaked in cesium at 850°C for 22 hr. After the adhering cesium was wiped off, the rod was washed in successive portions of fresh acid. Analysis for cesium in the acid indicated that some diffusion of cesium into the rod had occurred. A more sophisticated experiment to determine diffusion rates is in progress.

While pressure buildup due to the alkali metals is of only moderate significance in the life of each fuel capsule, diffusion into stainless steel might be serious. A method of trapping the alkali-metal fission products would solve the pressure and diffusion problems simultaneously. Some trapping substances with acceptable physical and nuclear properties have been listed by Brewer.<sup>4</sup> Among them is tin. To the list may be added bismuth, which is known to alloy quite easily with cesium.<sup>5</sup> If either tin or bismuth were used it could be contained in recesses cut in the magnesia spacers that are now present in each fuel capsule.

<sup>1</sup>J. P. Coughlin, "Heats and Free Energies of Formation of Inorganic Oxides," *U.S. Bur. Mines, Bull. No. 542* (1954).

<sup>2</sup>J. Belle, *Second U.N. International Conference on Peaceful Uses of Atomic Energy, 1958, paper A/Conf. 15/P/2404*.

<sup>3</sup>M. A. Bredig, H. R. Bronstein, and W. T. Smith, Jr., *J. Am. Chem. Soc.* **77**, 1454 (1955).

<sup>4</sup>L. Brewer, *Trap for Alkali and Alkaline Earth Metal Fission Products*, GAMD-902 (Aug. 4, 1959).

<sup>5</sup>P. Gorlich, *Z. Physik* **101**, 337 (1936).

## 15. EFFECT OF REACTOR IRRADIATION ON BERYLLIUM OXIDE

R. P. Shields

J. E. Lee

Beryllium oxide has for many years been considered as a moderator material for high-temperature reactor systems. The low ductility of this ceramic material, however, has led to some doubts of its resistance to thermal stress under reactor conditions. An experimental program to determine the resistance of BeO to reactor irradiations at a variety of temperatures is in progress.

In this program, cylindrical specimens 1 in. in length and 0.43 to 0.80 in. in diameter have been irradiated in position C33H10 of the Engineering Test Reactor. In this position, gamma fluxes corresponding to 25 w/g and neutron fluxes<sup>1</sup> of  $6.2 \times 10^{14}$  and  $4.3 \times 10^{14}$   $\text{sec}^{-1}\cdot\text{cm}^{-2}$  for thermal and fast neutrons, respectively, are available. Exposure of the BeO cylinders in capsules of stainless steel cooled by inert gas can effect

temperature differences of *ca.* 100°C from the center to the edge of the specimen; by control of position and amount of coolant gas, temperatures from 400 to 1000°C can be obtained.

In the first experiment, irradiated at relatively low temperature to a thermal-neutron dose of  $2.2 \times 10^{20}$  *nvt*, three specimens of 0.636-in. diameter were exposed. Hot-cell examination of these specimens, which is nearly complete, reveals no cracking or damage as a consequence of the thermal stress or shocks.

A second experiment containing nine specimens and irradiated to nearly twice this neutron dosage is under examination at present. No damage has been detected on the three specimens so far examined.

A third experiment which contains nine specimens of three different diameters has been irradiated and removed from the reactor.

---

<sup>1</sup>Values obtained by Phillips Petroleum Co. in ETR cycle 18, using cobalt and nickel wire monitors.

## 16. GASEOUS ALUMINUM CHLORIDE AS A THERMODYNAMIC WORKING FLUID AND HEAT TRANSFER MEDIUM<sup>1</sup>

M. Blander

R. F. Newton

Dissociating gases, such as aluminum chloride, are attractive as heat transfer media and as thermodynamic-cycle working fluids because they are associated at low temperatures and dissociated at high temperatures. Lowering the temperature of monomeric  $\text{AlCl}_3$  will yield not only the heat given off if the composition of the gas were "frozen" but also, since the gas is more highly associated at lower temperatures, the chemical heat due to the association of some of the monomer to  $\text{Al}_2\text{Cl}_6$ . The same phenomenon increases the thermal conductivity. A temperature gradient in a system at constant total pressure leads to a gradient of the partial pressures of monomer and of dimer in a direction such that more monomer tends to diffuse to lower temperatures and more dimer to higher temperatures than if the composition were "frozen." The monomer composition tends to equilibrium at the lower temperature by associating and giving off heat. This extra heat is part of the total heat flux and considerably enhances the effective thermal conductivity at temperatures where there is an appreciable fraction of both monomer and dimer. The effective heat capacity and thermal conductivity of gaseous aluminum chloride were estimated by use of the quantitative expressions of Butler and Brokaw<sup>2</sup> and what are believed to be conservative estimates of the necessary physical parameters;<sup>3-6</sup> the values so obtained are plotted in Figs. 16.1 and 16.2. Calculations of two possible corrosion reactions each with chromium and nickel indicate that chromium would corrode badly but may be usable if it is a minor constituent of an alloy, and that unprotected nickel may be suitable for an intermediate-term reactor. (It may be feasible

to develop an alloy with a protective oxide coating and thus eliminate corrosion as a difficulty.)

These calculations are uncertain, since none of the properties calculated and very few of the parameters used in the calculations have been measured directly. A conscious attempt was made to be conservative in these estimates, however. The calculations do indicate that gaseous heat transfer media with properties superior to those of helium (e.g., aluminum chloride) may exist and that a concerted theoretical and experimental investigation of  $\text{Al}_2\text{Cl}_6$  and other dissociating gases (as, for example,  $\text{Be}_2\text{Cl}_4$ ,  $\text{Be}_2\text{Br}_4$ ,  $\text{Al}_2\text{Br}_6$ ) and mixtures of these gases (with helium, for example) may be warranted.

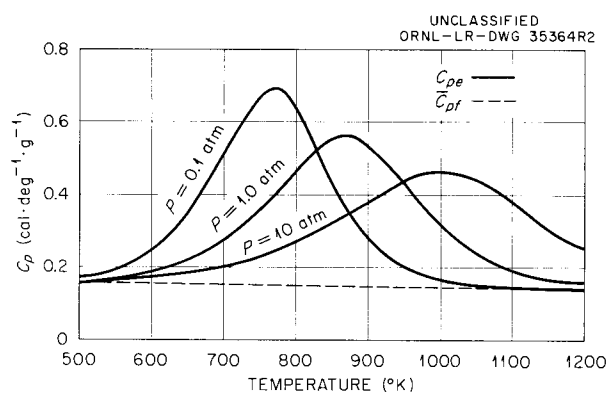


Fig. 16.1. The Calculated Effective Specific Heats of  $\text{AlCl}_3$  as a Function of Temperature at Three Pressures.

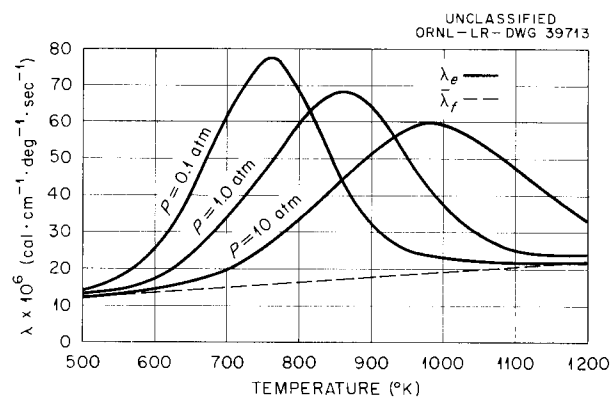


Fig. 16.2. The Calculated Effective Thermal Conductivities of  $\text{AlCl}_3$  as a Function of Temperature at Three Pressures.

<sup>1</sup>This material is contained in a report written jointly with members of the Reactor Projects Division; see M. Blander *et al.*, *Aluminum Chloride as a Thermodynamic Working Fluid and Heat Transfer Medium*, ORNL-2677 (Sept. 21, 1959).

<sup>2</sup>J. N. Butler and R. S. Brokaw, *J. Chem. Phys.* 26, 1636 (1957).

<sup>3</sup>W. Klemperer, *J. Chem. Phys.* 24, 353 (1956).

<sup>4</sup>A. Shepp and S. H. Bauer, *J. Am. Chem. Soc.* 76, 265 (1954).

<sup>5</sup>J. O. Hirschfelder, C. F. Curtiss, and R. B. Byrd, *Molecular Theory of Gases and Liquids*, Wiley, New York, 1954.

<sup>6</sup>L. R. Maxwell, *J. Opt. Soc. Am.* 30, 374 (1940).

## 17. MEASUREMENT OF TEMPERATURE IN REACTOR ENVIRONMENTS

G. W. Keilholtz

W. E. Browning

H. L. Hemphill

W. H. Montgomery

R. P. Shields

J. E. Lee

R. L. Bennett

W. T. Rainey

## THERMOCOUPLES FOR MEASUREMENT OF TEMPERATURE OF GAS-COOLED SURFACES

W. E. Browning

H. L. Hemphill

When thermocouples are used to measure the temperature of gas-cooled surfaces, corrections must be made for the cooling action of the gas upon the thermocouple. The cooling gas removes heat from the surface of the thermocouple leads, inducing a flow of heat outward through the thermocouple with a consequent thermal gradient in the region between the original surface and the junction of the thermocouple inside the thermocouple bead. The magnitude of the correction is proportional to the distance separating the thermocouple junction from the original metal surface and is also proportional to the thermal gradient in this region. The distance separating the thermocouple junction from the original metal surface, which we shall call the height of the junction, is fixed at the time the thermocouple is fabricated. The thermal gradient through the thermocouple depends upon the various geometrical factors and gas flow conditions which affect the heat transfer through the thermocouple and the lead wires. These factors include the diameter and exposed length of the thermocouple lead wires, the composition and pressure of the cooling gas, the dimensions of the cooling channel, the velocity of the cooling gas, and the thermal conductivity of the thermocouple metals.

Methods of fabricating bare wire thermocouples which have reproducible cooling corrections have been developed and previously reported.<sup>1</sup> Thermocouples of this type are fabricated by electrical resistance welding using the technique illustrated in Fig. 17.1. One thermocouple wire is placed over the other and pressed by a copper electrode against the metal surface whose temperature is to be measured, and the assembly is welded in place by passing controlled electrical current through the wires under controlled pressure. The result

of this operation is shown in Fig. 17.2. It can be seen that the two wires are fused together at the point where they cross and are fused to a metal surface below. The ceramic insulator is pushed close to the bead to provide protection from the cooling gas stream, as shown in Fig. 17.3. Figure 17.4 shows a photomicrograph of a section through the thermocouple bead at a point displaced toward the end of the thermocouple wires about 0.005 in. from the center of the bead. Sections taken near the center of the bead show the Alumel region resting above the Chromel region. The location of the thermocouple junction in a thermocouple of this type cannot be determined by examination. Various points of contact between the Chromel and Alumel contribute in differing degrees to the electrical junction. The effective location may be at any point along the boundary of the Chromel-Alumel.

Methods for determining the cooling correction were developed, and corrections were evaluated for attached thermocouples under one set of operating conditions at various gas flow rates. This work was also previously reported,<sup>1</sup> and the apparatus is illustrated in Fig. 17.5. The metal specimen is heated electrically while being cooled

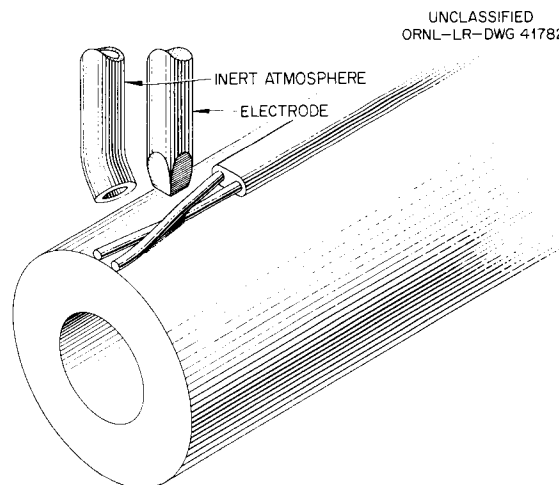


Fig. 17.1. Thermocouple Assembly Prior to Resistance Welding.

<sup>1</sup>W. E. Browning and H. L. Hemphill, *Solid State Semiann. Prog. Rep.* Feb. 28, 1955, ORNL-1851, p 19.

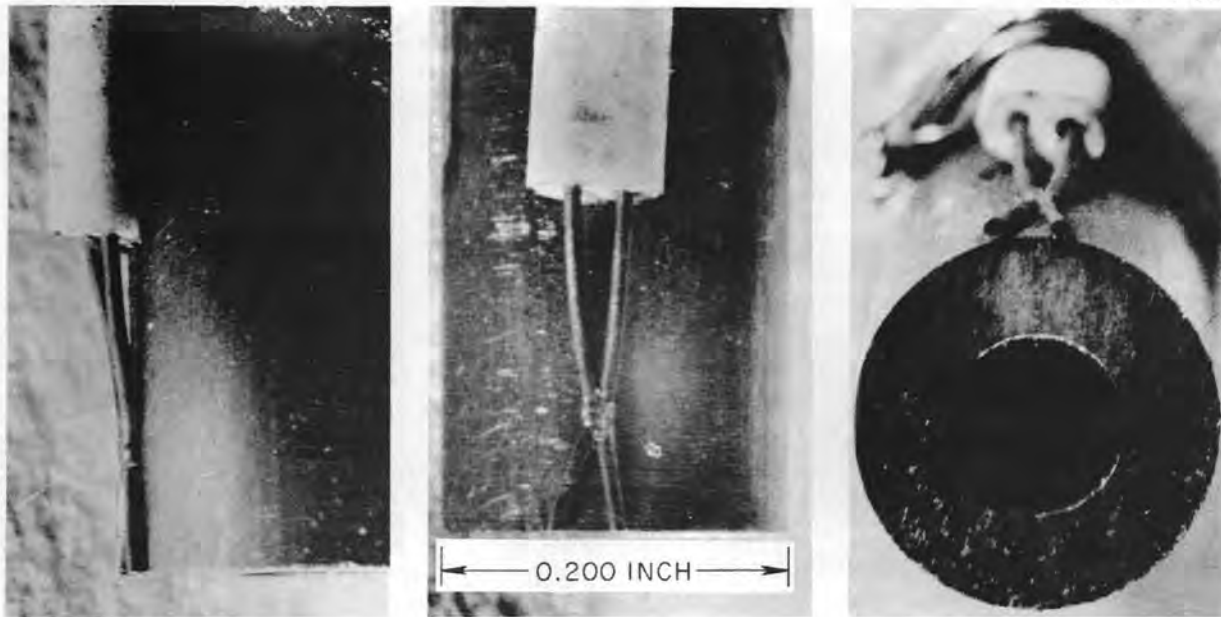
UNCLASSIFIED  
PHOTO 47418A

Fig. 17.2. Thermocouple Assembly After Resistance Welding.

by gas passing through a cooling annulus defined by a quartz tube. The metal surface temperature is determined by viewing through the quartz with an optical pyrometer and compared with the temperature indicated by the attached thermocouples.

It would be desirable to be able to predict the cooling corrections necessary for thermocouples under a variety of cooling conditions based on tests conducted under a limited number of cooling conditions. A calculation procedure has been developed using the Oracle electronic computer to predict the variation of cooling corrections with the cooling conditions surrounding the thermocouples. The results of these theoretical calculations are being used to correlate cooling correction data obtained under a variety of cooling conditions. The ideal model shown in Fig. 17.6 was used to perform the calculation of heat transfer within an attached thermocouple exposed to a coolant stream. The thermocouple was represented as two isolated wires whose ends are attached to the surface whose temperature is to be measured. It is desired to calculate the temperature at a point within the thermocouple at the location of

the thermocouple junction. To perform this calculation, it is necessary to evaluate the heat flux profile and temperature distribution throughout the thermocouple. The exposed thermocouple lead wire was divided into 100 elements of length for this calculation, and a heat flow balance was established for each element. An initial estimate was made of the heat flux into the base of the thermocouple from the hot surface. The temperature of the first length element was calculated using the heat flux and the thermal conductivity of the thermocouple metal. The convective heat losses from this heat element to the coolant were calculated using the temperature of the element and the heat transfer film coefficient determined from the cooling conditions for the case being calculated. The convective heat losses were subtracted from the heat flux entering the element to yield the heat flowing from the first element to the second length element. The temperature of the second element was then calculated, and the process was repeated for each of the 100 heat transfer elements. If the initial estimate of the heat flux into the base of the thermocouples were

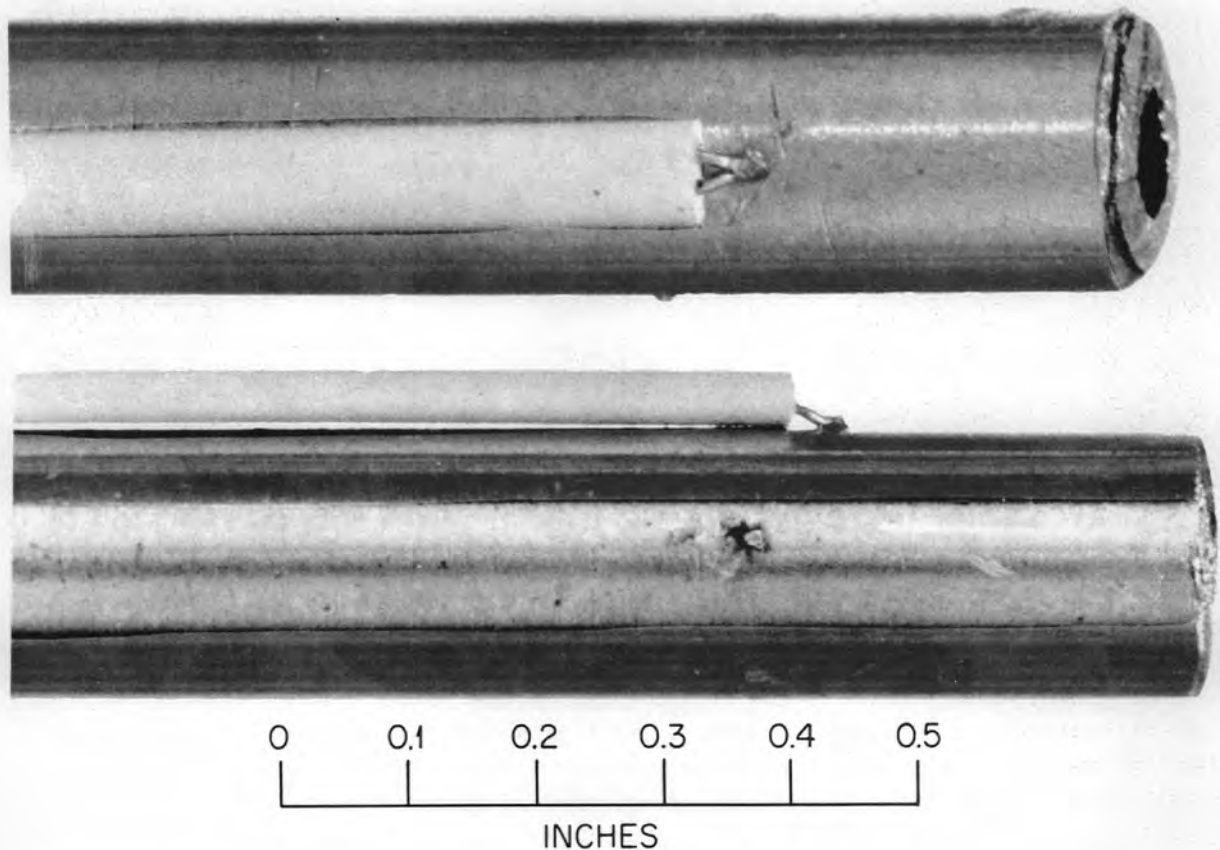
UNCLASSIFIED  
ORNL-LR-DWG 20172

Fig. 17.3. Completed Thermocouple for Measurement of Temperature of Gas-Cooled Surfaces.

correct, the residual heat flux remaining at the end of the thermocouple lead wire would be zero. The magnitude of this residual heat flux was used to construct a revised estimate of the heat flux at the base of the thermocouple, and the calculations were repeated until the residual heat flux was sufficiently close to zero. The calculation procedure used converged usually after only two or three iterations. This calculation yielded a temperature profile in the thermocouple and therefore could be used to predict the temperature cooling correction provided the height of the thermocouple junction inside the thermocouple is known. Since the height of the thermocouple junction cannot be observed directly, but is

presumably fixed for each thermocouple, it is of interest to express the results of these calculations in terms of the thermal gradient near the base of the thermocouple. This thermal gradient should be proportional to the cooling correction for each thermocouple and should vary with cooling conditions in the same way as far as thermocouple cooling correction is concerned. Some of the results of the calculations are given in Figs. 17.7 and 17.8. Figure 17.7 shows the thermal gradient at the base of the thermocouple vs the Reynolds number of the coolant for various lengths of exposed thermocouple leads. The calculations were made for 0.010-in. Chromel-Alumel wires with air at atmospheric pressure passing through a

UNCLASSIFIED  
RMG 2735

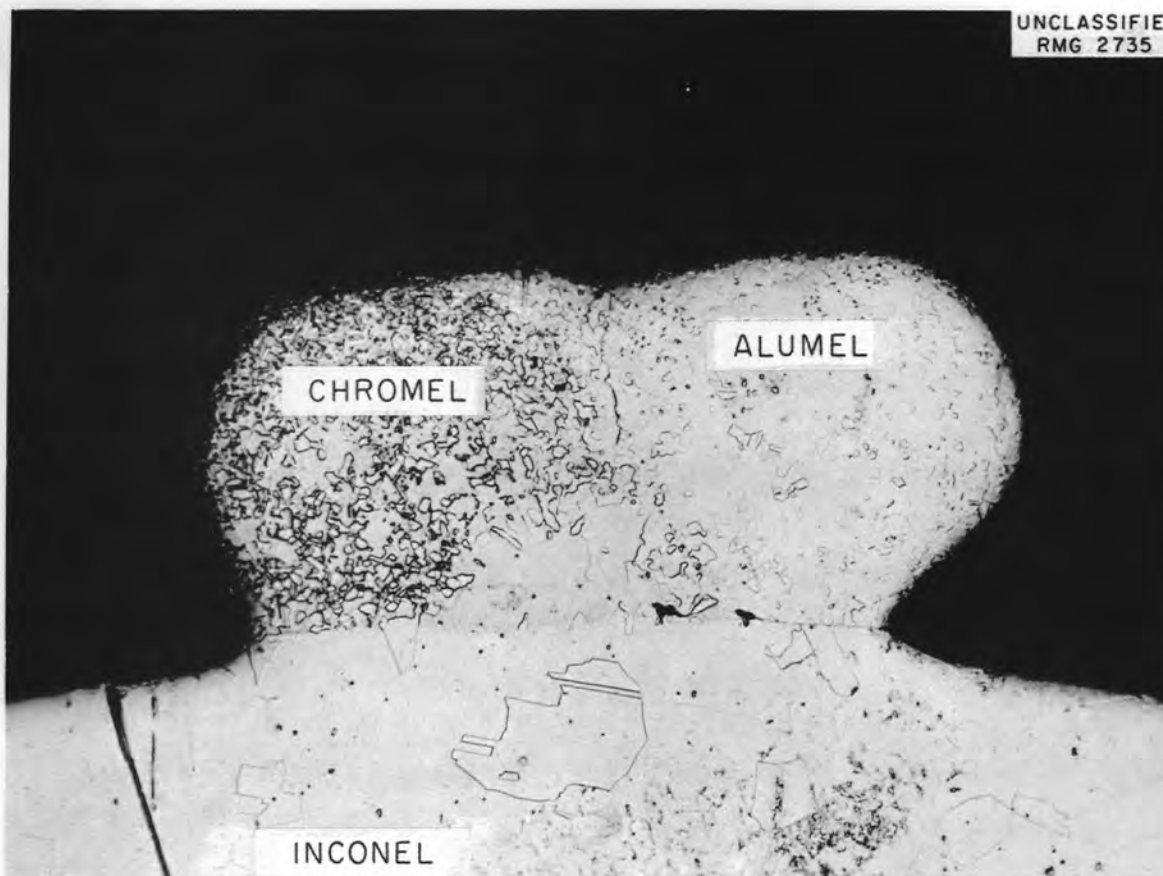


Fig. 17.4. Photomicrograph of Attached Thermocouple.

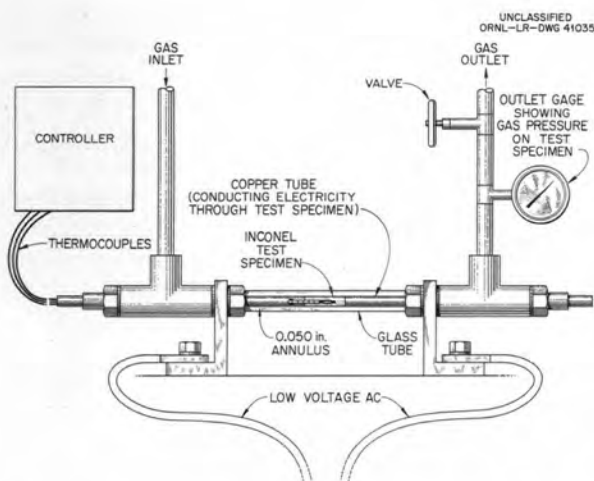


Fig. 17.5. Apparatus for Measurement of Thermocouple Cooling Corrections.

0.050-in.-thick annular channel. The thermal gradient increases with Reynolds number and is quite sensitive to length of exposed lead wire for values less than 0.100 in. In Fig. 17.8 the calculated thermal gradient is plotted vs the length of exposed lead wire for two values of the Reynolds number.

Thermocouple cooling corrections were determined experimentally for a series of thermocouples under the conditions used in the calculations. The results of these tests together with the information in Fig. 17.7 were used to evaluate an effective height of the thermocouple junction for each individual thermocouple. The effective heights so obtained were used, together with information in Fig. 17.7, to calculate the theoretical thermocouple cooling corrections as functions of Reynolds numbers shown in Fig. 17.9. The experimentally determined cooling corrections are shown also in Fig. 17.9 for comparison.

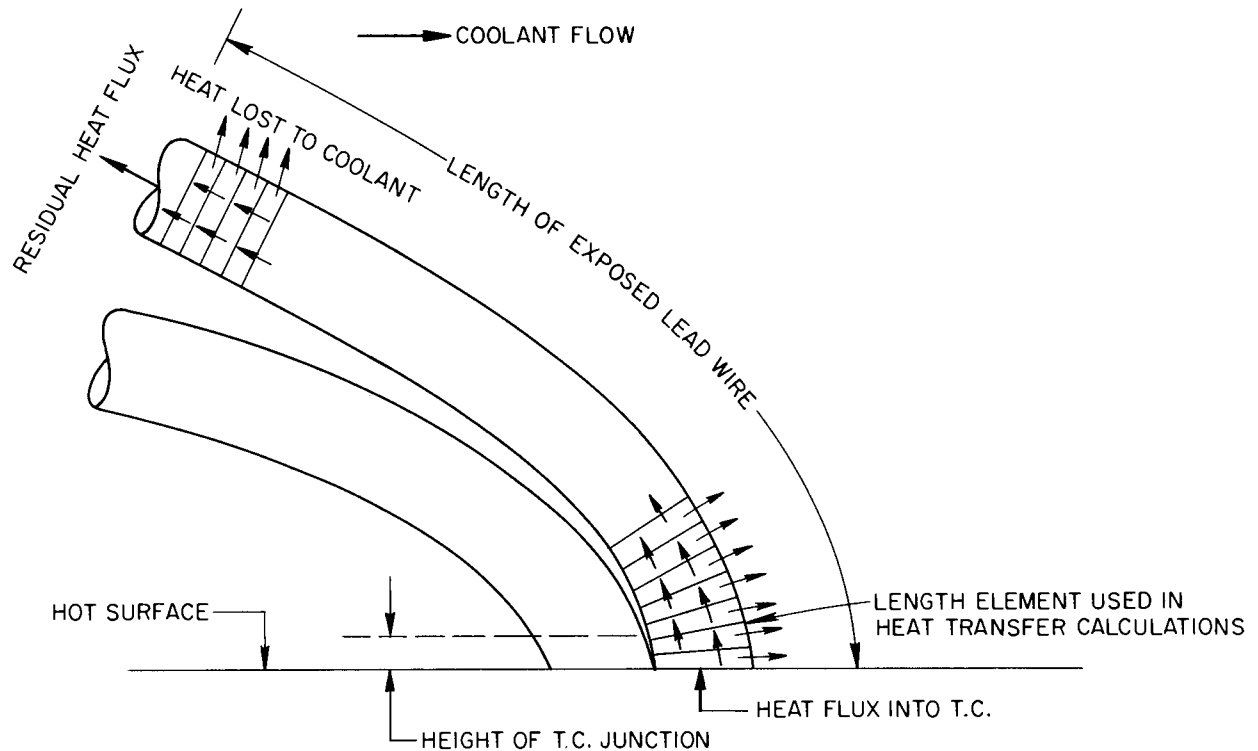


Fig. 17.6. Model for Thermocouple Heat Transfer Calculations.

It can be seen that the theoretical heat transfer calculations were successful in predicting the variation of thermocouple cooling correction with Reynolds number. Additional experimental tests and calculations are being conducted to determine whether this method of calculation can be used to predict the variation of cooling correction with other factors such as length of exposed thermocouple lead, composition of coolant, coolant pressure, coolant channel dimensions, and other factors. If this procedure is successful, it will be possible to predict the accuracy of thermocouples under any cooling conditions based on tests conducted under a small number of cooling conditions. While these calculations were applied to bare thermocouples, the results can be applied to any thermocouple assembly in which a cooling fin action occurs. For each thermocouple type it will be necessary to experimentally determine the effective height of the thermocouple junction within the thermocouple assembly. For a particular

method of fabrication, it may be possible to evaluate the effective height of the junction for individual thermocouples before they are put into service. This empirically determined effective height could be used with the calculation procedure developed here to predict thermocouple accuracy under various conditions such as might be encountered in measuring the temperatures of components of nuclear reactors.

#### DEVELOPMENT OF THERMOCOUPLES FOR USE IN A THIN ANNULUS

R. P. Shields      J. E. Lee

Beryllium oxide specimens, in the in-pile tests described in Chap. 15, were exposed in cylindrical capsules mounted within a metal tube which provided an annular passage of 0.010 to 0.15 in. Inert gas was passed through this annulus to provide temperature control of the specimens.

Inconel-sheathed Chromel-Alumel wires inserted through  $\frac{1}{4}$ -in. radial ports on the outer wall of the

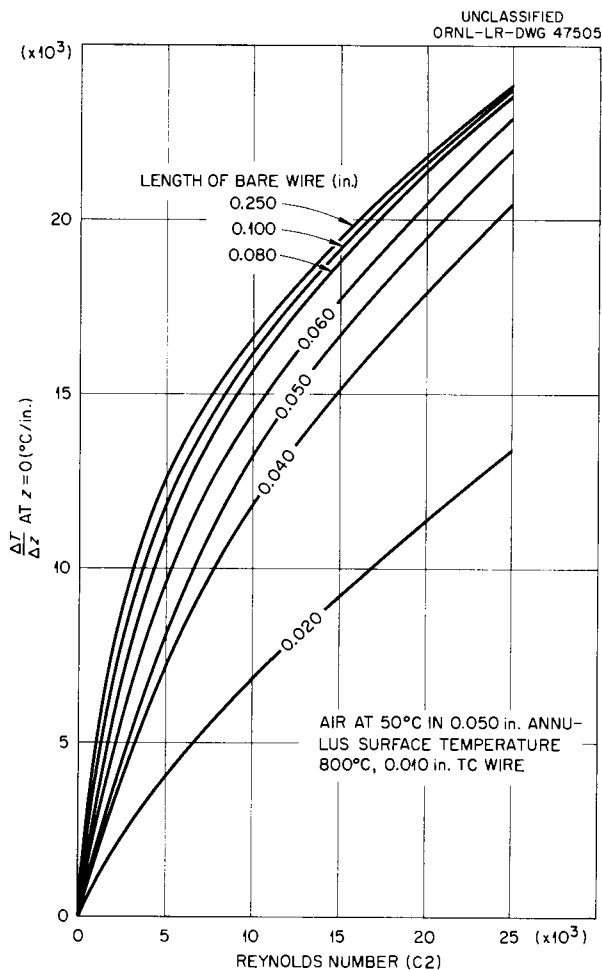


Fig. 17.7. Calculated Thermal Gradient in Thermocouples vs Reynolds Number of Coolant.

gas annulus were used to provide adequate measurements of the capsule wall. Linear thermal expansion of the capsule was carried by the end mounts so that surface movement at the access port was reduced to approximately 0.005 in. Each wire of the thermocouple pair was spot-welded separately to the capsule wall; a single-turn spiral wound in each wire gave the necessary mechanical flexibility. The sheathed wires emerged from the annulus through a small cap, which was silver-soldered in place by induction heating to seal the access hole and the sheathed wires. Although this type of installation requires stripping of the sheath and wire insulation within the annulus, the advantages of a sealed mount are obtained, and the wires are easily conducted through the water and auxiliary hardware to a convenient junction

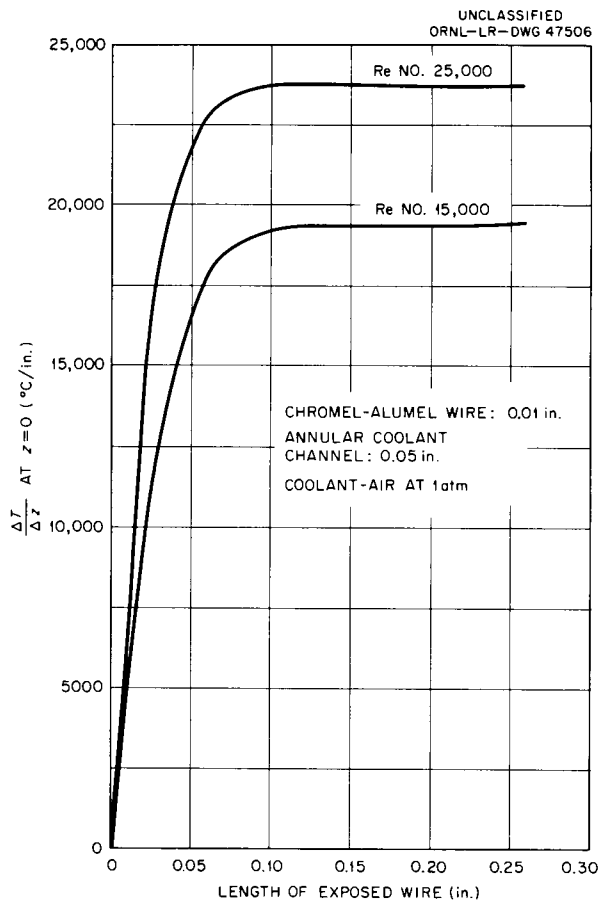


Fig. 17.8. Calculated Thermal Gradient in Thermocouples vs Length of Exposed Lead Wire.

terminal. A photograph of the cap and access port is shown in Fig. 17.10 in a preassembly view.

The performance of a side-wall thermocouple mount was tested during several series of bench-test mockups. The capsule wall temperature was simulated by an electrical resistance heated tube. Thermal expansion phenomena were simulated, and temperature control was provided by gas mixture variation (helium vs argon or nitrogen) and power input regulation. Annealing of the exposed wire tips proved to be necessary before forming the spirals in order to give a temperature cycling life of 40 to 60 cycles. In each instance of normal assembly, the braze distribution was found to be completely acceptable and no detectable distortion of the gas annulus had occurred. The accuracy of the temperatures measured by the installed thermocouple was verified by other thermocouples that were attached to the inside surface of the heated

UNCLASSIFIED  
ORNL-LR-DWG 47507

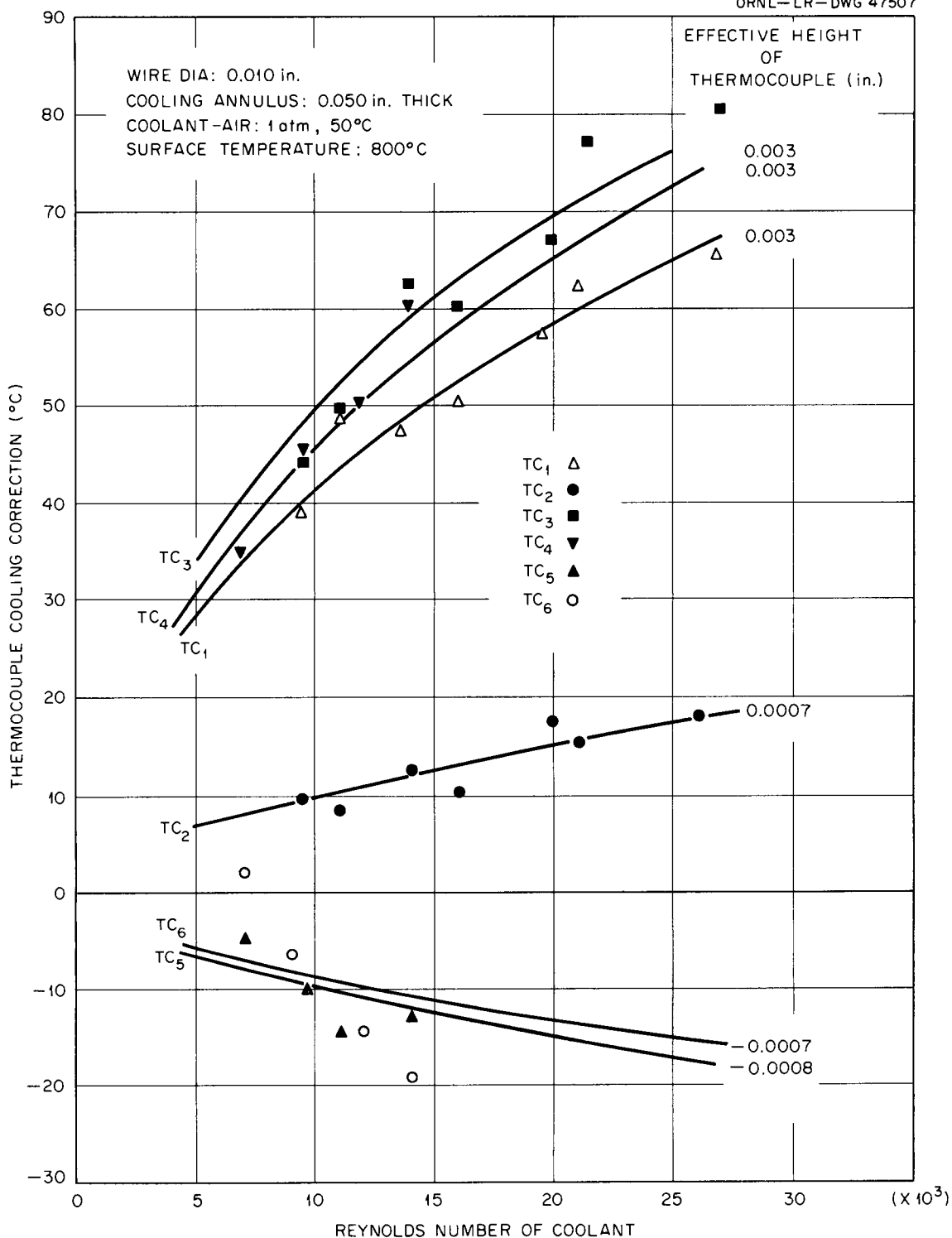


Fig. 17.9. Comparison of Experimental and Theoretical Cooling Corrections for Thermocouples in Cooling Gas Streams. Lines represent theoretical curves fitted to data from individual thermocouples.

UNCLASSIFIED  
PHOTO 44558

Fig. 17.10. Annulus Thermocouple Location Showing Access Ports and Seal Caps.

tube and found to be within 5 to 10°C. The temperature profile of the entire heated unit could be checked in this manner without interference with the gas annulus geometry.

Temperatures at the centers of BeO specimens were measured by thermocouples in wells within the capsules. Sheathed wire was used from the lead wire junction to a bushing sleeve where the wire passed through the wall of the end supports. This sleeve was induction-brazed to seal both the bushing and wire sheath. Within the assembly, the wires were exposed, mounted on insulated spacers, and welded to the bottom of the thermowell. Both Chromel-Alumel and platinum vs platinum-rhodium couples were used in such installations.

Nearly 50 of these thermocouple installations have been used in the three experiments to date. The rigors of shipping and installation in the reactor have been survived in every case. The over-all temperatures reported for each experiment assembly have been consistent with predictions based on specimen mass and position in the flux. The operational life of individual couples has been comparable in most cases to that achieved during mockup tests.

#### DRIFT STUDIES ON CHROMEL-ALUMEL THERMOCOUPLES IN UNUSUAL ATMOSPHERES

R. L. Bennett      W. T. Rainey

In many reactor installations it is necessary to measure temperatures with thermocouples which are maintained at conditions considerably less than ideal. In such installations it is often necessary to use long protection tubes (thermowells) with stagnant and possibly contaminated atmospheres. Chromel-Alumel thermocouples, which are commonly used in the 400 to 2000°F range, have been reported to behave erratically under such

conditions.<sup>2</sup> In this investigation the behavior of Chromel-Alumel thermocouples insulated with alumina and contained in 12-in. protection tubes of quartz has been examined as a function of atmosphere and the presence of various contaminants previously shown to yield occasional erratic behavior.

In stagnant air at 1000°C the drift data on 18 thermocouples during 100 hr showed a maximum deviation of  $\pm 2^\circ\text{C}$ . The data showed no significant differences between broken or solid insulators, and all drifts were positive. The Chromel leg drifted  $3 \pm 1^\circ\text{C}$  and tended to level off. The Alumel leg drifted  $6 \pm 1^\circ\text{C}$  and continued to increase in error. In flowing helium the results were approximately the same. Specially purified helium gave the same results as cylinder helium. After 140 hr of helium flow, the helium lines were replaced by air lines, and air was passed through the tubes for 60 hr. There was no change in rate of drift in any of the thermocouples.

Thermocouples in broken insulators in the presence of chromium and Inconel powder and with flowing helium atmosphere showed no greater drift than control thermocouples without metallic contaminants. It should be pointed out that the insulators in these tests were broken by cracking the ceramic into *ca.* 0.75-in. lengths with no gaps larger than 0.10 in. This resulted in only very narrow sections of the wires in the thermal gradient region being exposed to contamination. The one case of abnormal drift noted resulted from the use of chromium powder and a stagnant helium atmosphere with the thermocouple insulating tube broken at 0.75-in. intervals with 0.25 in. of metal exposed between breaks throughout its length. The protection tube was not purged of air before applying 3 psi helium pressure with no flow. The drift rate was almost linear during 24 hr at a rate of  $-2.0$  mv in 24 hr. Then the rate of drift decreased.

As a further check on oxidation changes taking place in the wires, accurate resistance measurements were made on the individual thermocouple legs during the tests in helium. The presence of metallic contaminants had no significant effect on resistance changes. In general, the sections of Alumel wire in the high-temperature zone in helium

<sup>2</sup>J. F. Potts, ORNL Instrumentation and Controls Division, and D. L. McElroy, ORNL Metallurgy Division, personal communication.

increased in resistance by approximately 50% during 200 hr. The Chromel wires increased only 5% during 200 hr. When the helium flow was replaced by air flow, the rate of change in resistance of Alumel wire increased by a factor of 4. The Chromel wires showed no appreciable changes. These resistance changes agreed with predicted results. As the cross-sectional areas of the wires were reduced by oxidation, the resistance increased. There was not necessarily any correlation between emf drift and resistance change. This was expected since any oxidation could cause resistance changes, but only oxidation resulting in a changing metal composition could cause emf changes.

It is interesting to note that no appreciable changes were noted in the resistances of either the Chromel or Alumel legs in the one instance of abnormal emf drift. The slight increases in resistance measured were much less than the usual results in helium.

The results to date indicate that Chromel-Alumel thermocouples in the presence of chromium, Inconel, and quartz insulating tape in a flowing helium atmosphere show no abnormally fast drifts when there is limited access to the wires in the thermal gradient region. However, abnormal drifts may be experienced under similar conditions in stagnant atmospheres.

#### DEVELOPMENT OF HIGH-TEMPERATURE FURNACE FOR THERMOCOUPLE STUDIES

W. E. Browning      W. T. Rainey  
W. H. Montgomery

High-temperature furnaces are required for use in investigation of thermocouples in the temperature range 1000 to 3000°C (1800 to 5400°F). For this purpose furnaces are required having a relatively small high-temperature zone of the order of  $\frac{3}{8}$  in. in diameter  $\times$  1 in. long with provision for inserting thermocouples to be tested and for viewing them with an optical pyrometer under black-body conditions. Several furnace designs have been developed; all have tantalum or tungsten heating elements supported by copper blocks, usually water-cooled, and are in an inert atmosphere contained in a quartz bell jar. Specially designed high-current, low-voltage transformers are used for power supply.

One design uses a heating element made of tantalum sheet 0.010 in. thick bent into the form of a cylinder  $\frac{3}{8}$  in. in diameter  $\times$   $2\frac{1}{2}$  in. long with

a slit left open approximately  $\frac{1}{8}$  in. for pyrometer viewing. This tantalum tube was resistance-welded to stainless steel rings which had been previously silver-soldered into copper blocks which had water cooling channels. Brass and copper tubing served the threefold purpose of supporting the water-cooled blocks, supplying coolant to the blocks, and conducting electric current to the heating element. Thermocouples to be tested are inserted through holes in the copper blocks and are suspended near the axis of the tantalum heater. Tantalum foil crimped to a V-shape is attached to the thermocouple junction for black-body viewing conditions. A furnace of this design has the advantage of uniformity of temperature and uniformity of radiation environment surrounding the thermocouple. The interior surface of the tantalum heating element itself provides a black-body surface for temperature measurement. The maximum operating temperature of a furnace of this design is limited by the mechanical strength of the tantalum heating element. Such furnaces have been operated for brief periods at up to 2600°C (4700°F) and for periods of several days at 2000°C (3600°F). For longer periods of operation serious deformation of the tantalum furnace occurs leading to nonuniformity of temperature and ultimate failure of the furnace.

Small furnaces consisting of simple tungsten ribbons have been operated up to the melting point of tungsten. Application of furnaces of this type has been limited because of the small high-temperature zone and because of the difficulty in obtaining black-body conditions for measurement of temperature at the test region.

The most successful high-temperature furnaces have used self-supporting helical heating elements made of tungsten rod 0.040 to 0.125 in. in diameter. Techniques were developed for winding tungsten helices  $\frac{3}{8}$  to  $\frac{1}{2}$  in. in diameter  $\times$   $\frac{1}{2}$  in. long. Heating elements of this type are mechanically attached to water-cooled copper blocks of the same type used in the tantalum furnace described above. Furnaces of this type have operated for periods of several days at over 2800°C (5100°F) without failure.

Quartz bell-jar-shaped enclosures approximately 4 in. in diameter have been used to contain the inert atmosphere, helium, required by these furnaces. The quartz tube is sealed to a brass base by an

O-ring. The system is evacuated to  $10 \mu$  Hg pressure and purged several times with helium before final filling. When atmospheric impurities are present, deposits of yellow or blue tungsten oxide are found on the interior surfaces of the envelope. Under good atmosphere conditions, only a slight black deposit appears on the upper portion of the envelope. The black deposit is metallic tungsten as evidenced by x-ray diffraction analysis.

The power for these furnaces has been supplied by specially built transformers designed to match the load resistance of the furnaces. The core and winding of a Variac or Powerstat autotransformer are used with the housing and brush assembly removed. The original winding of the autotransformer serves as the primary winding in the high-current transformer. The secondary winding consists of 10 or 20 turns of water-cooled copper tubing wrapped around the toroid core. The ends of this copper tube are attached to the terminals of the furnace, and the transformer and furnace are a part of the same cooling water circuit. The transformers of this type have been built using two 50-amp, 115-v Variacs in series. Secondary currents of up to 1000 amp have been obtained, at total secondary powers of over 3 kva.

These furnaces are now used routinely in the study of high-temperature thermocouples, such as rhenium-tungsten thermocouples with BeO insulation.

#### STABILITY OF RHENIUM-TUNGSTEN THERMOCOUPLES

W. E. Browning      W. H. Montgomery

It is desirable to be able to measure the center temperature of  $UO_2$  fuel elements used in high-temperature reactors, such as gas-cooled reactors. The temperatures are well above the range of conventional thermocouple materials. Thermocouples are being tested and developed for this application. Initial tests are being made on rhenium-tungsten thermocouples at temperatures from 1000 to 2000°C (1800 to 3600°F). The output of thermocouples was measured for various thermocouple temperatures determined by an optical pyrometer. The calibration curves of the thermocouples appeared to be constant with duration of exposure of the thermocouple at 1800°C up to 64 hr within experimental error. The reproducibility of results between 1000 and 1600°C was better than

between 1600 and 2000°C. The thermocouples being tested consisted of a rhenium and a tungsten wire 0.010 in. in diameter in a BeO insulator. Additional tests are being run to improve the reproducibility of results. Furnace design improvements, described elsewhere in this report, have been made using a tungsten heater instead of tantalum and using a larger power density so that these tests can be extended to higher temperatures and longer times.

A computing program for use on the IBM-704 machine was prepared by a group of students in the MIT Practice School. The computing program will statistically process experimental data obtained in thermocouple calibration experiments. The program selects the curve which fits the experimental points and determines the statistical variance of the curve. The program evaluates a series of such curves and tests the data for significance of correlation with a parameter such as duration of exposure at high temperatures, duration of exposure to neutron flux, or any other appropriate parameter. This computing program has been completed and will be used to analyze thermocouple calibration data obtained in this work.

#### EFFECTS OF RADIATION UPON THERMOCOUPLES

W. E. Browning      H. L. Hemphill

Calculations of the amounts of impurities produced in thermocouple materials by transmutation reactions are being made. A computer program using the IBM-704 was prepared by a group of MIT Practice School students to calculate the amounts of impurities as a function of neutron exposure time and flux for any material. This computer program will be used to determine the composition of thermocouple alloys after exposure to neutron flux.

Six Chromel-Alumel thermocouples which were irradiated in the MTR for 5500 hr in connection with a fused-salt capsule experiment are available for postirradiation examination. A special shearing tool was prepared and shipped to the MTR to permit removal of the experiment at its conclusion without the damage to the thermocouples which normally occurs. Five platinum-rhodium thermocouples and one rhenium-tungsten thermocouple, irradiated for 65 to 174 days in the LITR, are on

hand for postirradiation calibration. These thermocouples were used on capsules in the LITR operated for the GCR Program. The calibration curves of these thermocouples will be determined in the hot cells.

Postirradiation examination of irradiated thermocouples will indicate any permanent change in thermocouple calibration. It is possible that transient changes will occur which persist only while the thermocouple is exposed to radiation. To provide information on this point, it is desirable to calibrate thermocouples during irradiation. To do this, one must have a standard which itself is not affected by radiation. Various standards have been considered for this purpose, including boiling sodium metal at a controlled vapor pressure and

radiation pyrometers of various types. Both of these methods are quite complex. Melting point standards could be used in-pile with very little complexity. Of particular interest as a melting point standard are the fused-salt mixtures developed in connection with the MSR Program. The experience obtained operating in-pile fused-salt capsules makes the design of an in-pile thermocouple melting point calibration experiment straightforward. The results of these in-pile experiments have indicated that fused salts are not affected appreciably by radiation. A fused-salt capsule with a thermocouple well in it is being prepared for irradiation. The thermocouple output at the melting point of the fused salt before, during, and after irradiation will be measured to determine whether there is any transient effect of radiation.

## 18. REMOVAL OF RADIOACTIVE GASEOUS FISSION PRODUCTS FROM OTHER GASES

W. E. Browning

R. D. Ackley

R. E. Adams

Radioactive gaseous fission products may by accident or design be present in a flowing sweep or carrier gas in a variety of nuclear operations. Examples include reactor off-gas streams, effluent from nuclear fuel reprocessing, and off-gas from in-pile experiments. Very often the concentration of gaseous fission products in the carrier gas is such that the latter cannot be vented directly to the atmosphere because of the biological hazard; consequently, it is necessary first to reduce the concentration of radioactive gases to acceptable values. These radioactive gases consist principally of isotopes of krypton, xenon, and iodine. A two-part review article was prepared for the journal *Nuclear Safety* on the subject of removal of fission product activity from gases.<sup>1</sup>

## REMOVAL OF NOBLE GASES

## Introduction

When fission gases, particularly xenon and krypton, in a more volatile carrier gas such as helium or oxygen, pass through a column containing an adsorbent such as activated carbon, these noble-gas fission products, while not permanently adsorbed, do undergo many adsorption-desorption cycles and thereby are delayed relative to the carrier gas. This delay may provide sufficient time for radioactive decay of short-lived isotopes so that their concentration in the exit gas becomes negligible. In a variation of this method, the adsorber may be employed as a concentrator and collector of the noble gases.

A longer-range phase of this program is to develop information relating to the general problem of disposal of radioactive noble fission gases. A shorter-range phase is to provide technical information useful to ORNL reactor projects, for example, studies pertaining to the Homogeneous Reactor Test (HRT) off-gas system and to coolant purification systems for the Gas-Cooled Reactor Project.

Work previous to that covered herein has been summarized.<sup>2</sup> There, as here, a gas-solid chromatographic technique was used, with Kr<sup>85</sup> or Xe<sup>133</sup>

<sup>1</sup>W. E. Browning, "Removal of Fission Product Activity from Gases, Part I," *Nuclear Safety* 1(3) (1960); Part II to be published in June 1960.

as tracers. The data, obtained in the form of elution curves, are interpreted in terms of a theoretical plate treatment corresponding to fission gas adsorption varying linearly with fission gas pressure.<sup>3</sup> The shape of the elution curve is given by

$$P_N = \frac{P_{std} N^N A F^{(N-1)} t^{(N-1)}}{(N-1)! (km)^N} e^{-NFt/km}, \quad (1)$$

where

$P_N$  = partial pressure of fission gas, atm,

$P_{std}$  = standard pressure (1 atm),

$N$  = number of theoretical plates,

$A$  = amount of fission gas injected, cc (STP),

$F$  = flow rate of carrier gas, cc/min,

$t$  = time after fission gas injection, min,

$k$  = dynamic adsorption coefficient, cc/g,

$m$  = weight of adsorbent, g.

On setting  $dP_N/dt = 0$ , the time  $t_{max}$  for maximum fission gas partial pressure in the effluent ( $P_{N_{max}}$ ) is obtained:

$$t_{max} = \frac{(N-1) km}{NF}. \quad (2)$$

In using Eq. (2) the simplifying assumption is usually made that  $(N-1)/N = 1$  for large values of  $N$ . Theoretically,  $k$ , cc/g, is numerically equal to the slope of the static equilibrium adsorption isotherm when the units of the slope are cc(STP)/g-atm. A typical elution curve illustrating application of Eq. (1) is shown in Fig. 18.1. The earlier work included development and experimental application of the above equations involving a wide variety of adsorbents and conditions. Additional details

<sup>2</sup>W. E. Browning, R. E. Adams, and R. D. Ackley, *Solid State Ann. Prog. Rep. Aug. 31, 1958*, ORNL-2614, p 162.

<sup>3</sup>W. E. Browning and C. C. Bolta, *Measurement and Analysis of the Holdup of Gas Mixtures by Charcoal Adsorption Traps*, ORNL-2116 (July 27, 1956).

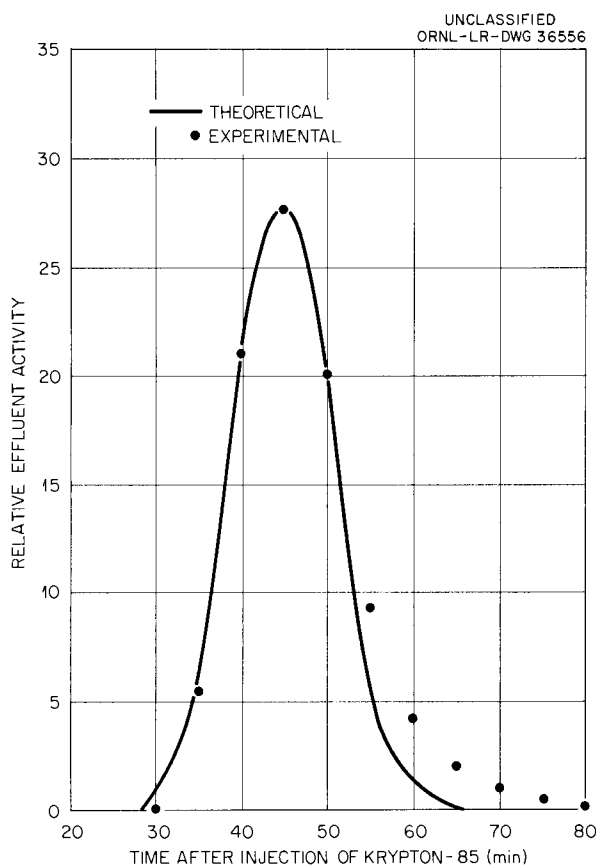


Fig. 18.1. Typical Distribution of Fission Gas Activity in Experimental Effluent Gas Stream.

pertaining to these and other studies have been reported.<sup>4,5</sup>

#### Improved Methods for Evaluating the Number of Theoretical Plates

While  $N$  (the number of theoretical plates in an adsorber bed) can be evaluated rather easily using the method similar to that employed in gas-liquid chromatography, it is occasionally preferable to base its determination on Eq. (1) in a manner which considers the shape of the elution curve in detail. Previously, determination of  $N$  by Eq. (1) involved using too few data points or using a time-consuming method. Therefore an IBM-704 computer program

<sup>4</sup>W. E. Browning, R. E. Adams, and R. D. Ackley, *Removal of Fission Product Gases from Reactor Off-Gas Streams by Adsorption*, ORNL CF-59-6-47 (June 11, 1959).

<sup>5</sup>R. E. Adams, W. E. Browning, and R. D. Ackley, *Ind. Eng. Chem.* 51, 1467 (1959).

was established for this purpose with the aid of members of the MIT Practice School.<sup>6</sup> Subsequently, it was found that Eq. (1) could be expressed in a reduced form as

$$\frac{P_N}{P_{N_{max}}} = \left[ \frac{t}{t_{max}} e^{(1-t/t_{max})} \right]^{N-1} \quad (3)$$

Use of Eq. (3) in a logarithmic form greatly facilitates the calculation of  $N$ , as the required quantities are readily obtainable directly from recorder chart paper. While application of these methods has thus far been somewhat limited, it is anticipated that they will be of considerable value in the interpretation of elution data.

#### Effect of Carrier Gas Velocity on $N$

Krypton-85 elution curves were obtained for Columbia G activated carbon, 8/14 mesh, corresponding to various flow rates of the carrier gas, oxygen, and approximate values of  $N$  were calculated by the method similar to that customarily employed in gas-liquid chromatography. Results are shown in Fig. 18.2, where  $N$  per foot of trap length is plotted vs the mean value of superficial oxygen linear velocity in ft/min. These data show that  $N$  is a function of trap length, as is obvious, and of linear velocity but not of trap diameter.

<sup>6</sup>T. J. Delaney, L. M. Davis, and M. J. Friedman, *Analysis of Experimental Data on the Holdup of Radioactive Gases on Charcoal Adsorption Traps*, EPS-X-406, KT-389 (Mar. 3, 1959).

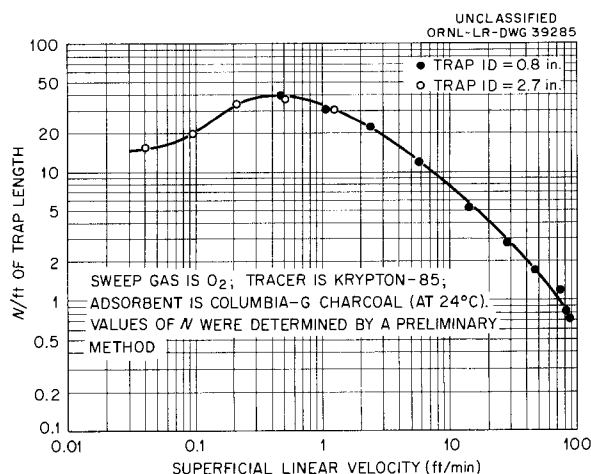


Fig. 18.2. Effect of Linear Velocity of Oxygen Carrier Gas on  $N$ , the Number of Theoretical Plates.

Also, the optimum superficial linear velocity, with respect to  $N$ , for the oxygen-Columbia G charcoal system, is indicated to be about 0.5 fpm.

**Effect of Carrier Gas Composition and Pressure on Dynamic Adsorption**

Figure 18.3 represents a revision of data previously presented.<sup>2</sup> Variation of krypton  $k$  values with different carrier gases is not as large as it appeared to be earlier.

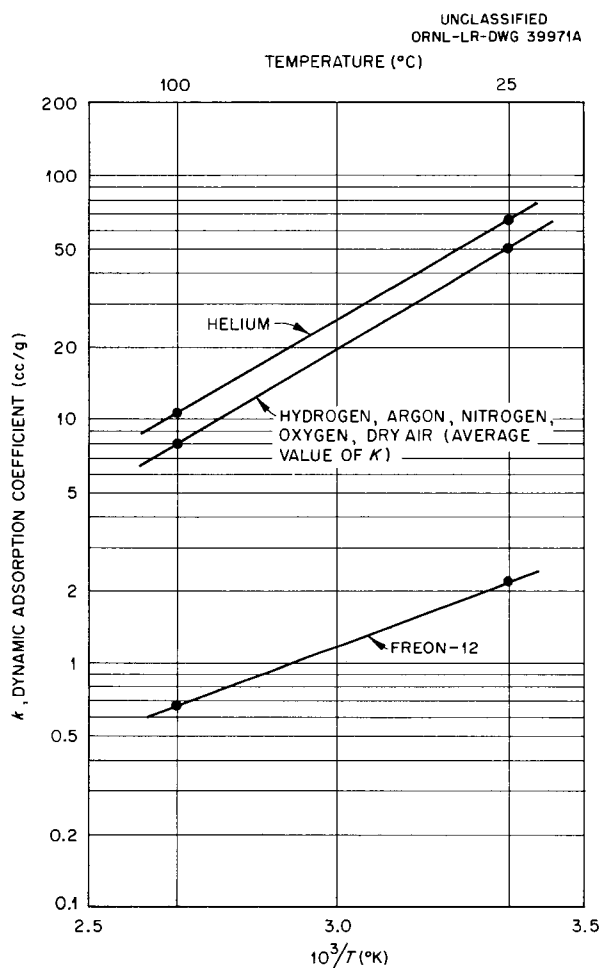


Fig. 18.3. Effect of Carrier Gas on Krypton Holdup.

The effect of adsorbed  $CO_2$  on the retention of krypton by Columbia G charcoal, with oxygen as the carrier gas, was measured and is shown in Fig. 18.4. The carrier gas was varied in  $CO_2$  concentration from 0 to 100%. As may be seen, krypton retention is considerably reduced by appreciable concentrations of  $CO_2$ .

The decrease in krypton holdup time, for a particular charcoal trap at a particular linear velocity, with increasing oxygen carrier gas pressure is shown in Fig. 18.5. The holdup time

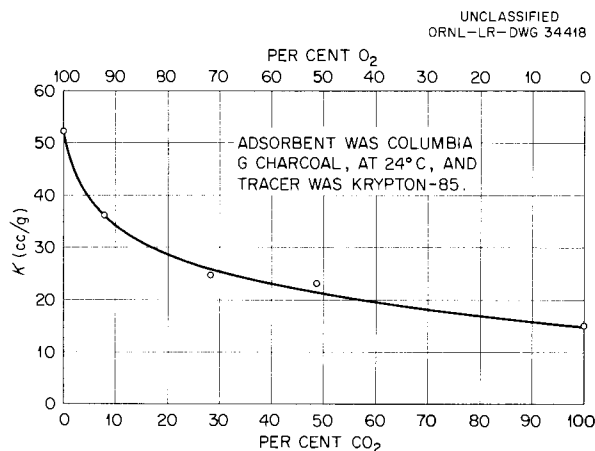


Fig. 18.4. Effect of Carbon Dioxide in Oxygen Carrier Gas on the Dynamic Adsorption Coefficient  $K$ .

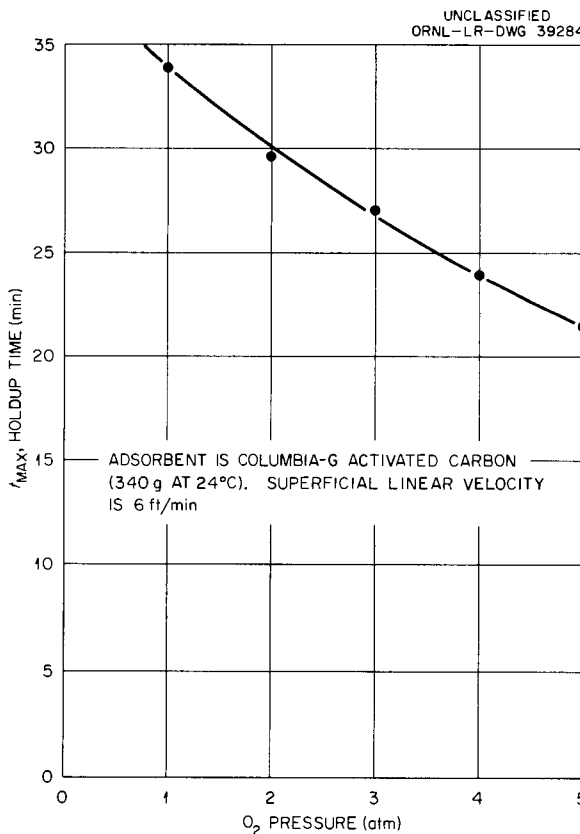


Fig. 18.5. Krypton Holdup Time vs Oxygen Carrier-Gas Pressure.

was observed to decrease by 37% as oxygen pressure increased from 1 atm to 5 atm. These results would be of interest in applications where the carrier gas is at higher than atmospheric pressure.

Data pertaining to the effect of fairly high carrier gas pressures on fission gas retention and on  $N$  are of increasing interest in connection with purification systems for gas-cooled reactors. Accordingly, appropriate equipment is being assembled preparatory to obtaining such data; initial measurements are to be made with helium at pressures up to about 400 psi, with charcoal as the adsorbent.

#### Krypton and Xenon Holdup Measurements on Various Adsorbents

Holdup data on Linde molecular sieves are of interest when a noncombustible adsorbent is required, because these materials, in particular type 5A, appear to be superior to all those tested with the exception of certain grades of charcoal. Accordingly, krypton and xenon  $k$  values with helium carrier gas were measured for types 5A, 10X, and 13X. In addition, krypton  $k$  values with oxygen carrier gas, while previously measured,<sup>2</sup> were re-evaluated, as it was convenient to do so at this time. In these more recent measurements, type 4A was not tested, as the previous work showed that its pores were too small to admit appreciable amounts of krypton or, therefore, xenon. The  $k$  values obtained, all at 25°C and in cc/g, in the order krypton with oxygen carrier gas, krypton with helium, and xenon with helium were for 5A, 12, 12, and 73; for 10X, 6, 6, and 25; and for 13X, 7, 7, and 36. As these data indicate, no appreciable difference was found for krypton holdup with the two different carrier gases oxygen and helium, and, also, xenon  $k$  values are about 4 to 6 times the krypton  $k$  values.

A total of 22 samples of charcoal, including a variety of mesh sizes from five different manufacturers, were tested for krypton holdup at room temperature, with helium or oxygen as the carrier gas. The results of these preliminary tests indicated that several of these materials would be suitable for certain applications.

Two forms of porous glass were similarly tested; however, neither of these exhibited krypton holdup to a useful degree.

#### Thermal Conductivity of Columbia G Activated Carbon in the Presence of Various Carrier Gases

In the case of removal of short-lived fission gases by adsorbents, such as charcoal, the thermal conductivity of the adsorbent and carrier-gas combination is of considerable importance in adsorber design. This is because the design must provide for dissipation of heat produced in the adsorbent by radioactive decay of fission gases. Consequently, measurements of thermal conductivity were made for 8/14-mesh Columbia G activated carbon by a direct and an indirect method. In the latter, heat generation in the charcoal resulting from radioactive decay was simulated by resistance heating of the charcoal. Also, in effect, krypton retention times were used to evaluate temperature profiles in the charcoal. Then, by assuming uniform heat generation, values of thermal conductivity could be calculated. This method probably yields low values for traps of small diameter, since the effect of the wall on packing probably results in a disproportionately high amount of heat being generated in the central zone of the charcoal. With oxygen as the carrier gas and with traps having inside diameters of 0.64, 1.03, and 2.29 in., thermal conductivities of 0.06, 0.07, and 0.08 Btu·hr<sup>-1</sup>·ft<sup>-2</sup>·(°F/ft)<sup>-1</sup>, respectively, were obtained. The corresponding values with helium carrier gas were 0.12, 0.13, and 0.15.

In the case of the direct method, the Columbia G charcoal was contained in the annular space between copper or aluminum pipes, 4 ft in length, with the ends well insulated. Known quantities of heat were applied to the inside pipe, and temperatures of both pipes were measured, thus providing, together with the pipe dimensions, the necessary information for calculating the thermal conductivities. The results for a variety of gases flowing through the charcoal are shown as a function of the thermal conductivities of the pure gases in Fig. 18.6. A comparison of curve 1 with curve 2 indicates that the wall effect is probably applicable with regard to thermal conductivity as well as to electrical conductivity, as would be expected. Furthermore, all the results obtained by the two different methods appear reasonably compatible when wall effects are considered.

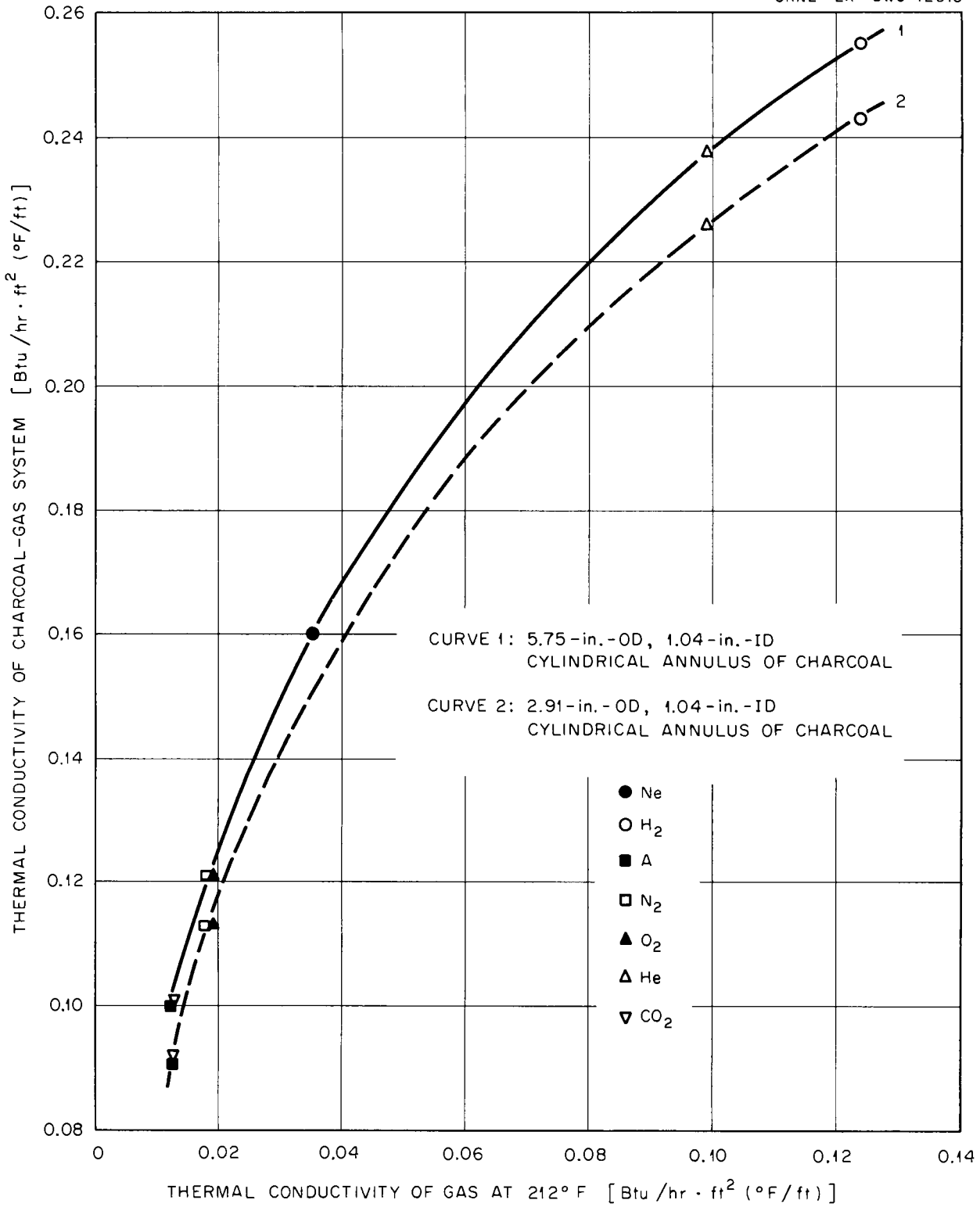


Fig. 18.6. Thermal Conductivity of Columbia G Activated Carbon-Gas Systems.

### Experiments Related to Ignition and Combustion of Charcoal in HRT Adsorber System

The HRT off-gas is normally principally oxygen, which flows at a total rate of approximately 2.5 liters/min through two charcoal adsorbers in parallel, each containing approximately 500 lb of charcoal. During the early part of run 17 of the HRT (1958), abnormal behavior of the adsorber system was observed. Thermocouples in the charcoal briefly showed unusually high temperatures, effluent off-gas flows were erratic, adsorber A was not performing in its usual satisfactory manner with respect to fission gas retention, and the effluent from A contained rather high concentrations of carbon dioxide. These observations indicated ignition and combustion of an appreciable quantity of charcoal, at least in adsorber A. Oxygen flow through A was subsequently halted; later, it was put back on stream and, after the adsorbed carbon dioxide was eluted with oxygen, it performed satisfactorily. At about this time, the D<sub>2</sub>-O<sub>2</sub> recombiner was functioning in an intermittent fashion, allowing D<sub>2</sub>-O<sub>2</sub> mixture to enter the adsorber system. Experiments were accordingly undertaken in an effort to explain the abnormal behavior of the adsorber system.

In one study, H<sub>2</sub>-O<sub>2</sub> mixtures were passed through a heated tube containing Columbia G charcoal, and the exit gas was analyzed for H<sub>2</sub>O by a dew-point meter to determine if the recombination reaction was significantly catalyzed by activated carbon. Temperatures employed were 120 and 200°C, the space velocity at the latter temperature having been 0.3 min<sup>-1</sup>. No appreciable recombination was indicated.

In later experiments, propagation of H<sub>2</sub>-O<sub>2</sub> explosions through charcoal was investigated and it was found that mixtures containing 20–74% H<sub>2</sub> would propagate flame through Columbia G activated carbon. Indication of propagation was by means of a thermocouple supplemented by visual and photographic observation, the charcoal having been in an 8-ft glass pipe, 1 in. in inside diameter. The concentration ranges for flammability were approximately the same for the three cases: upward, downward, and horizontal propagation. These range limits and the estimated average distance between the charcoal granules in the pipe appear consistent with quenching distance data for H<sub>2</sub>-O<sub>2</sub>

mixtures.<sup>7</sup> It was also observed in a number of instances that combustion of the charcoal occurred when oxygen was allowed to flow through the charcoal immediately following an H<sub>2</sub>-O<sub>2</sub> explosion. These results strongly suggest that the combustion of the charcoal in adsorber A was initiated by D<sub>2</sub>-O<sub>2</sub> flame propagation from the recombiner through the charcoal, and, as oxygen was continuously flowing, the combustion persisted until the oxygen flow was halted.

It appeared, on the basis of a comparison of the respective limits of flammability of H<sub>2</sub>-O<sub>2</sub> and D<sub>2</sub>-O<sub>2</sub> (ref 8) in the absence of charcoal, that the above range would also be applicable to D<sub>2</sub>-O<sub>2</sub>, the mixture of actual interest; nevertheless, a few propagation experiments with D<sub>2</sub>-O<sub>2</sub> mixtures were performed. No appreciable difference in limits of flammability for H<sub>2</sub>-O<sub>2</sub> and D<sub>2</sub>-O<sub>2</sub> in charcoal was observed.

The products of combustion of charcoal in oxygen were studied as a function of oxygen gas velocity (superficial). As velocity varied downward from 21.6 to 1.5 fpm, the CO<sub>2</sub> concentration in the exit gas varied from 26 to 94%, and CO from 66 to 0%, or, in effect, the ratio of CO<sub>2</sub> to CO increased as reaction temperature decreased, in accordance with expectation.

These various results, together with those shown in Fig. 18.4, appeared to explain satisfactorily and to be in accordance with the observed behavior of the HRT adsorber system.

### Potential Hazard Resulting from Oxygen Adsorption on Charcoal

Some preliminary calculations have been made pertaining to the potential hazard which exists when oxygen is adsorbed on charcoal at low temperatures. This hazard will vary considerably, corresponding to such factors as quantity of charcoal and its temperature, nature of carrier gas, its flow rate and oxygen content, etc. The calculations were based on the adiabatic heat of reaction of

<sup>7</sup>B. Lewis and G. von Elbe, *Combustion, Flames and Explosions of Gases*, Academic Press, New York, 1951.

<sup>8</sup>H. F. Coward and G. W. Jones, "Limits of Flammability of Gases and Vapors," *U.S. Bur. Mines, Bull. No. 503* (1952).

oxygen with the charcoal or with a combustible component of the carrier gas and on enthalpies as a function of temperature for charcoal and the associated gases. The mechanism by which the reaction might be initiated is not apparent; however, because of radiation and, thus, possible ozone formation, consideration of this possible reaction does appear warranted. The resulting increase in charcoal temperature would cause a desorption of adsorbed gases, with a consequent increase in pressure. In estimating the pressure developed, no allowance was made for any escape of gases from the adsorber.

The results of such calculations for a particular adsorber, namely, one of three similar charcoal traps for the NS "Savannah," appear in Fig. 18.7.

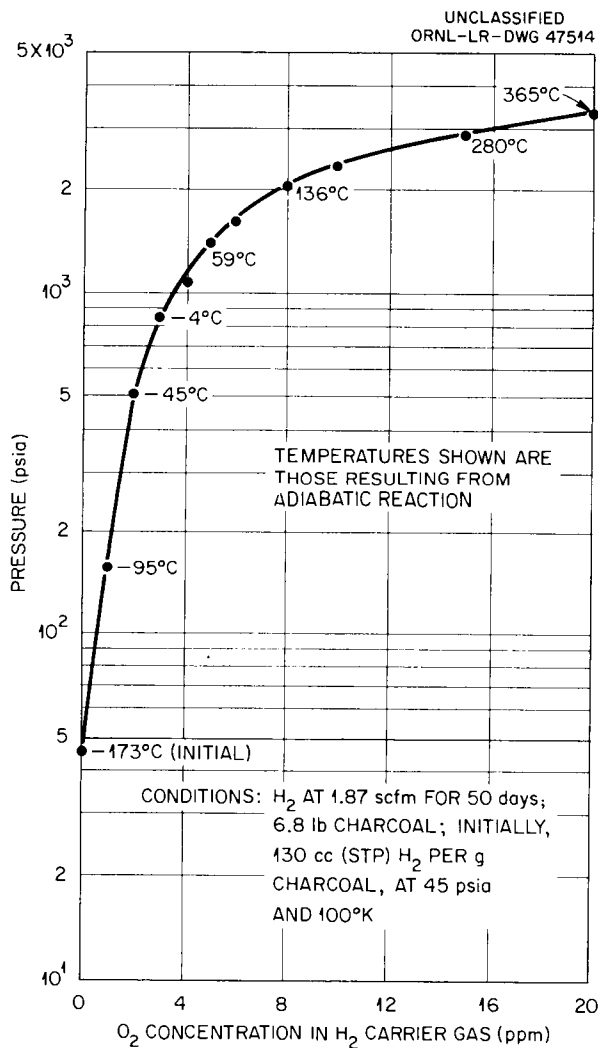


Fig. 18.7. Calculated Potential Pressure Buildup in Charcoal due to H<sub>2</sub>-O<sub>2</sub> Reaction (Adiabatic).

(This fission gas system is briefly described below, under "Applications to Reactor Systems," where the method for removing oxygen from the carrier gas, upstream of the charcoal, is mentioned.) The figure shows that, under certain conditions, oxygen concentrations as low as a few parts per million in the inlet gas to a low-temperature adsorber, over an extended period of time, may give rise to a potentially hazardous situation.

#### REMOVAL OF RADIOIODINE VAPOR

Several materials were studied for application in removing radioiodine vapor from air streams. Preliminary studies<sup>9</sup> indicated that iodine vapor is strongly held after adsorption occurs and that the tracer method used in the noble-gas studies could not be utilized for iodine adsorption studies. A method which gave positive results is described as follows, with reference to the apparatus shown in Fig. 18.8. Elemental iodine crystals (I<sup>127</sup> containing radioactive I<sup>131</sup>) were contained in the U-tube, and a portion of the air supply was routed through the U-tube to transport iodine vapor into the main air stream. The time required for introduction of all the iodine vapor into the adsorber column was approximately 15 min, and the average iodine concentration during this time was 0.18 mg of I<sup>127</sup> and 54 μC of I<sup>131</sup> per cubic foot of air. Air flow was continued through the system for 24 hr. Iodine vapor escaping through the column was collected downstream by the combination of a plug of carbon wool fibers (available from Bameby-Cheney Co., Columbus, Ohio), a CWS-6 absolute filter, and an electrostatic precipitator. After completion of the run, the system was disassembled and the distribution of iodine radioactivity in the column determined by scanning with a sodium iodide scintillation crystal, viewing through a small slit in a lead shield. The over-all efficiency was then determined by radiochemical iodine assay of the system from point A to point B, as shown in Fig. 18.8. An adsorption efficiency was determined by comparing the amount of iodine residing in the adsorber column with the amount found in the total system. The accuracy of this method for determining adsorption efficiency depends upon the premises that all the iodine passing through the experimental column was

<sup>9</sup>W. E. Browning, R. E. Adams, and R. D. Ackley, *Solid State Ann. Prog. Rep. Aug. 31, 1958*, ORNL-2614, p 162.

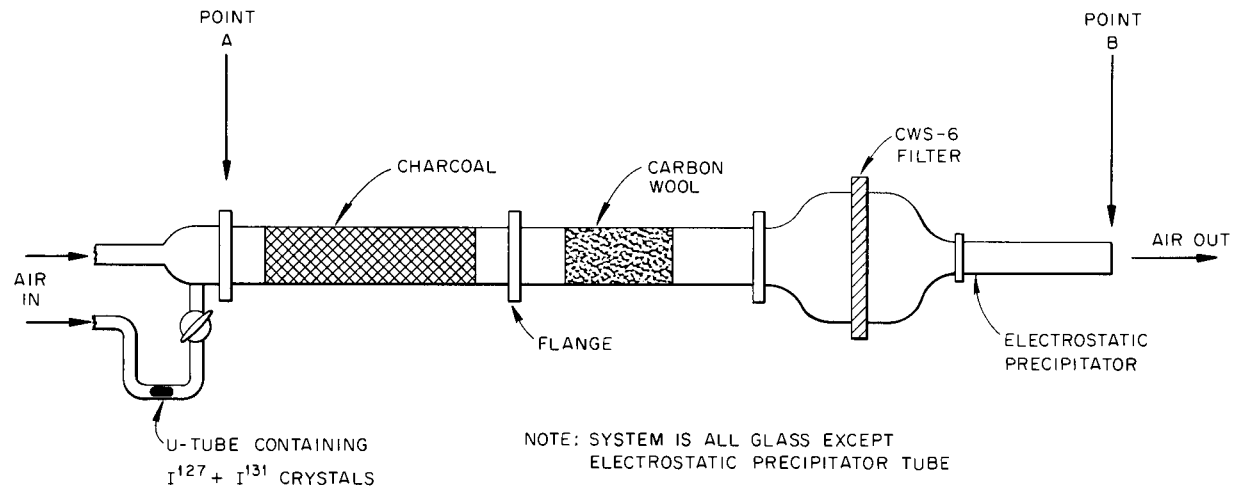


Fig. 18.8. Experimental System Used in Iodine Adsorption Studies.

collected downstream and that none was allowed to escape. Efforts to detect iodine activity in the effluent air stream were unsuccessful.

#### Activated Charcoal

Various parameters which could influence the adsorption of iodine vapor by charcoal at room temperature were studied. Early in the study it appeared that dust particles in the air sweep might be responsible for the transport of iodine through an adsorber. Iodine adsorbed on a particle of dust would not be available for reaction at the charcoal surface. In addition, fine particles of charcoal containing iodine might be carried from the adsorber by the air sweep. For these reasons the absolute filter (CWS-6) and the electrostatic precipitator were included in the experimental system in addition to the carbon wool. In one run, the CWS-6 filter was placed immediately downstream from the charcoal mass, and particularly dusty charcoal was used. A significant amount of dust and iodine activity was found on the filter and a detectable trace on the inner surface of the electrostatic precipitator. In all later runs the charcoal was "dedusted" before iodine injection by introducing air at a flow rate greater than that to be used in the experiment; the dust problem was greatly reduced by this method.

The effect of superficial air velocity (volumetric air flow rate divided by cross-sectional area of

adsorbent container) was examined at velocities of 82, 170, and 275 fpm, and very little effect was noted. The depth of penetration into the charcoal mass and the over-all efficiency were very similar for the three air velocities. The size of the charcoal particles does affect the adsorption efficiency. Study of 2/4-, 4/6-, and 6/8-mesh charcoal (Columbia type SXC, available from National Carbon Co., Cleveland, Ohio) at a superficial air velocity of 170 fpm yielded efficiencies of 99.63, 99.89, and 99.99+% respectively. Moisture contained in the air stream and adsorbed on the charcoal was not found to interfere with iodine adsorption. Once iodine is adsorbed on charcoal it seems to be firmly held. Air flow in one test was continued for 250 hr, and no downstream transport of iodine could be detected. A typical iodine distribution for a charcoal adsorber is given in Fig. 18.9.

#### Silver-Plated Copper Ribbon

Three tests were made using silver-plated copper ribbon, an iodine collector developed and studied by the Harvard University Air Cleaning Laboratories.<sup>10</sup> The ribbon was 25 × 2 mils thick, woven into a mesh configuration, and plated with

<sup>10</sup>L. Silverman *et al.*, paper presented at the Sixth AEC Air Cleaning Conference, Idaho Falls, Idaho (July 1959).

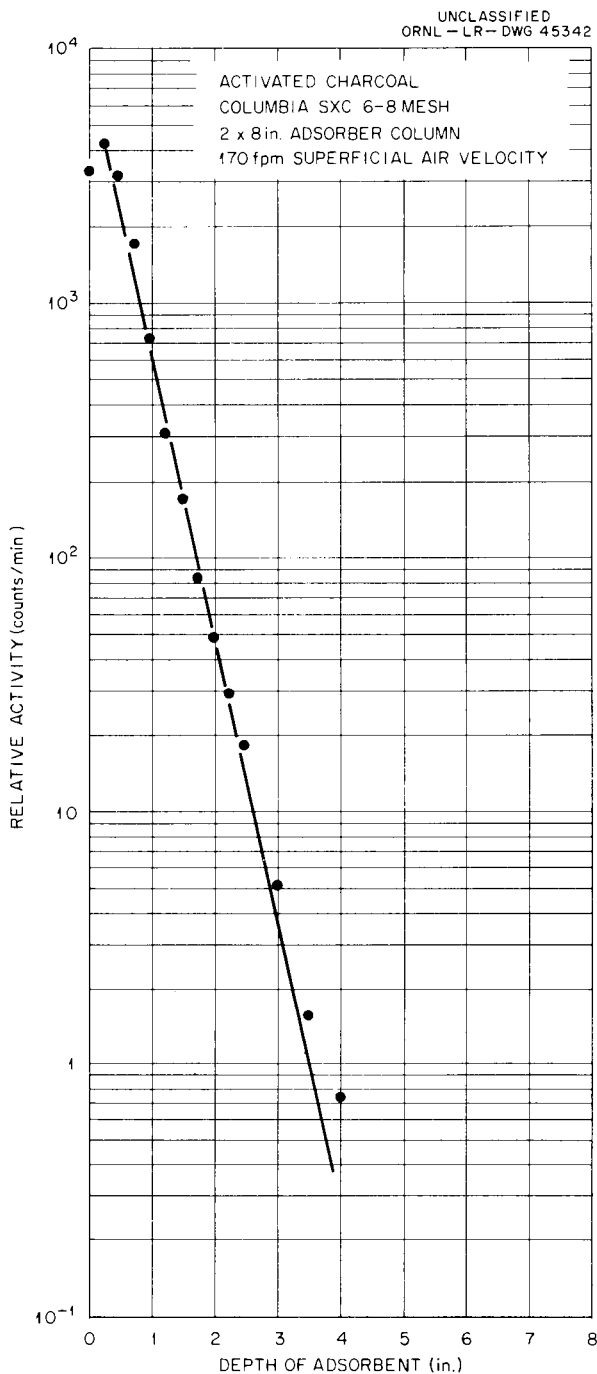


Fig. 18.9. Distribution of  $I^{131}$  Radioactivity in Charcoal Column.

silver equal to 5% by weight (available from Metal Textile Co., Roselle, N.J.). Test conditions were similar to those of the charcoal study. The column contained the mesh compressed to a density of

25 lb/ft<sup>3</sup>. The iodine adsorption efficiency of the system was found to be 92%, with an iodine distribution as shown in Fig. 18.10. A break is noted in the distribution curve at a depth of approximately 4 in., indicating that the efficiency beyond this depth is much lower than at the entrance. The last two tests were run under the same conditions as before except that an additional particle filter was added to the air supply system. The adsorption efficiency was increased to 98 and 99%, and the break in the curve was modified, indicating strongly that particulate matter in the

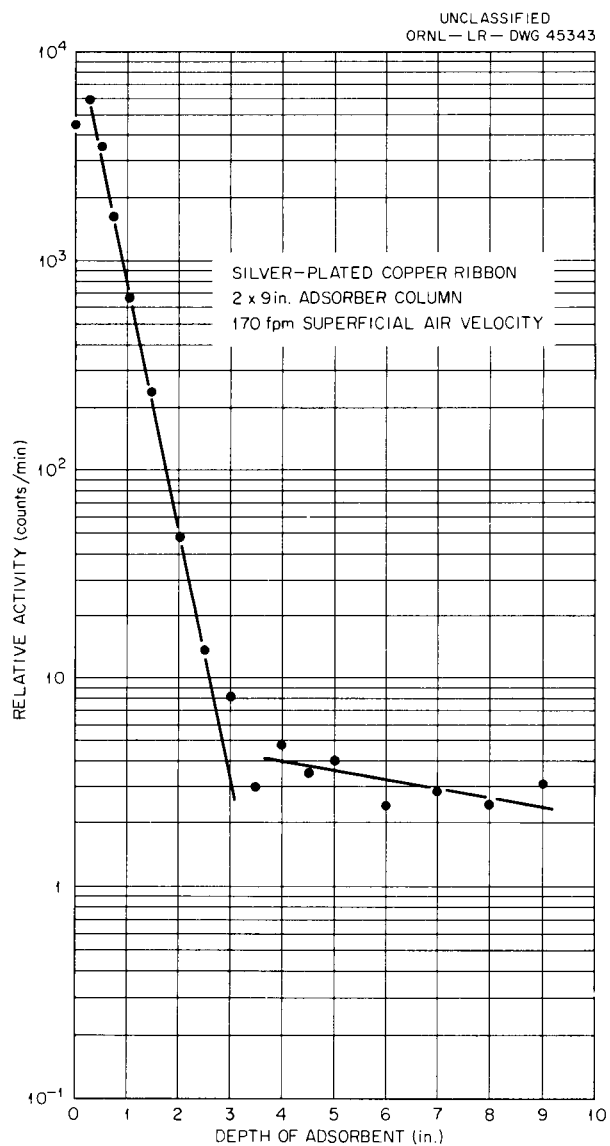


Fig. 18.10. Distribution of  $I^{131}$  Radioactivity in Silver-Plated Copper Ribbon Column.

air may have been responsible for the transport of iodine through the ribbon.

One test employing new copper ribbon was made under similar conditions, and an iodine efficiency of 98.5% was obtained. Copper ribbon and silver-plated copper ribbon have comparable iodine collection properties at room temperature, but at elevated temperatures silver-plated copper ribbon is superior.

#### Comparison of Charcoal and Silver-Copper Ribbon

The choice of using activated charcoal or silver-plated copper ribbon for iodine adsorption will depend upon the application. Each material is subject to shortcomings under various conditions. Charcoal is a more efficient adsorbent, but pressure drop through the charcoal mass may be important in some applications. Silver-plated copper ribbon, while being less efficient, exhibits an almost insignificant pressure drop. On the basis of decontamination efficiency alone, 6/8-mesh charcoal is superior to the other adsorbents tested. In Fig. 18.11 the various mesh sizes of charcoal and silver-copper ribbon are compared, based upon decontamination factor as a function of depth of adsorbent. The decontamination factor is defined as the amount of radioiodine found in the adsorber column divided by the amount which passed through and was collected downstream. The multitude of lines for 6/8-mesh charcoal represent tests under the various conditions of superficial air velocity, moisture content, and duration of air flow. In an attempt to relate pressure drop, superficial air velocity, and decontamination efficiency, a plot was made of the decontamination factor as a function of pressure drop divided by superficial air velocity. This information is contained in Fig. 18.12. The curve for 6/8-mesh charcoal represents one interpretation for consolidating the data presented for this adsorbent in Fig. 18.11. Although some of the curves are based on limited data, tentative conclusions can be drawn regarding the relative merits of the silver-copper ribbon and several mesh sizes of charcoal for application at air velocities in the range 150–200 fpm. From the standpoint of pressure drop, silver-copper ribbon is superior to charcoal for desired decontamination factors up to 100. Between factors of 100 to 300, 2/4- or 4/6-mesh charcoal is more suitable; from 300 to 1000, 4/6-mesh charcoal is the choice; above 1000, 6/8-mesh charcoal is preferable.

The application of charcoal may be limited by its tendency toward rapid oxidation at high temperatures in gas streams containing oxygen. The oxidation rate of the charcoal is the limiting factor, since the adsorption of iodine vapor on charcoal is rather insensitive to moderate temperature increases. Heating of the charcoal can occur from both the beta decay of adsorbed radioiodine and the heat content of the gas containing the iodine. Silver-plated copper ribbon gains in efficiency as the temperature increases but reaches a maximum near 300°C, and at higher temperatures the collected iodine is released.<sup>10</sup> One fact worthy of note is that once exposed to high temperatures in air the silver-copper ribbon exhibits a reduced efficiency on cooling to room temperature. The efficiency of silver-copper ribbon is sensitive to iodine concentration in the gas stream. At low concentrations, for example,  $10^{-3}$  mg/ft<sup>3</sup>, the efficiency may drop to as low as 90%, compared with 98–99% when the iodine concentration is much higher. Charcoal has not exhibited this sensitivity and has a high efficiency over a wide concentration range. This study has been reported in more detail elsewhere.<sup>11</sup>

#### APPLICATIONS TO REACTOR SYSTEMS

##### Fission Gas Adsorption System for the NS "Savannah"

The proposed system was reviewed in the light of our experience in this field. Very briefly, the pertinent features of the system are as follows: hydrogen, containing nitrogen and oxygen at low concentrations and possibly containing fission gases, flows through one of two Deoxo units where the oxygen is to react with some of the hydrogen; then, after moisture removal and cooling, the gas passes through one of three charcoal traps at –280°F, the purpose of which is to remove and retain fission gases.

The results of the review suggested that the following points be given additional consideration: (1) the pressure rise which would occur due to the desorption of hydrogen and nitrogen adsorbed at –280°F on isolating the charcoal trap and warming it to ambient temperature; (2) the

<sup>11</sup>R. E. Adams and W. E. Browning, *Removal of Radioiodine from Air Streams by Activated Charcoal*, ORNL-2872 (Mar. 17, 1960).

UNCLASSIFIED  
ORNL-LR-DWG 45346

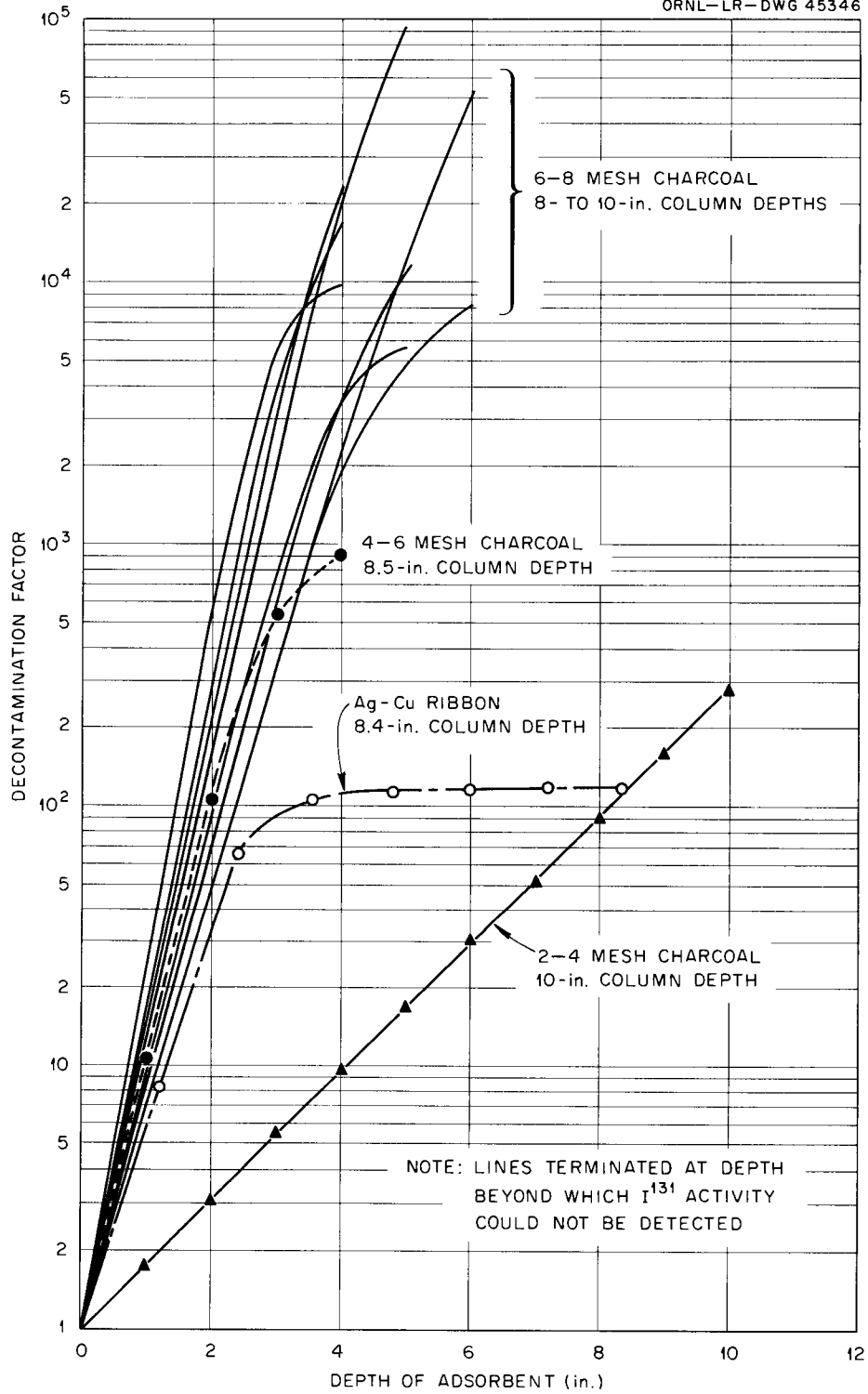


Fig. 18.11. Iodine Decontamination Factor as a Function of Adsorbent Depth.

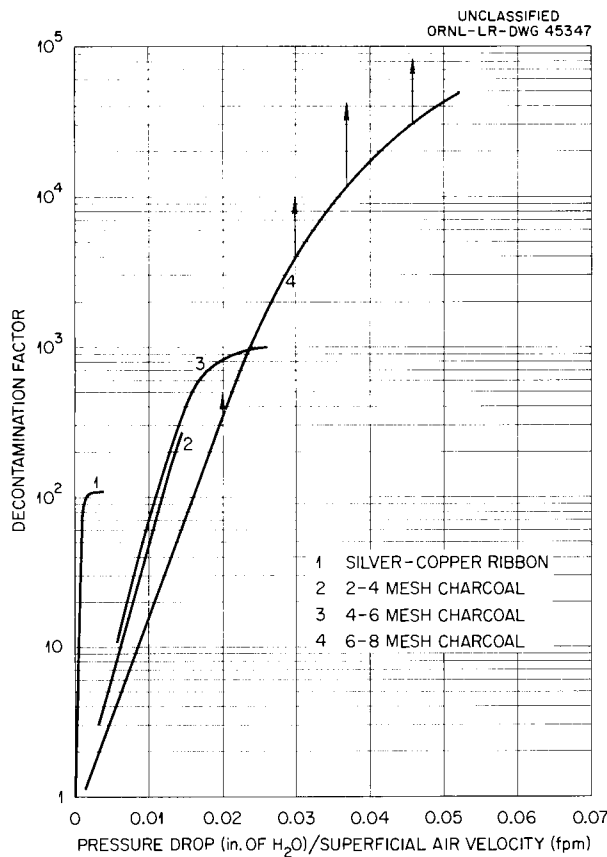


Fig. 18.12. Iodine Decontamination as a Function of Pressure Drop Divided by Superficial Air Velocity.

maximum concentration of oxygen permissible in gas exiting from Deoxo units so that oxygen adsorption on charcoal would not be excessive; and (3) retention of fission gases by the charcoal traps in the presence of hydrogen and nitrogen.

#### Iodine Adsorption System at the Puerto Rico Nuclear Center (PRNC)

The results of the iodine adsorption study were utilized in selecting an adsorbent to be used in the emergency ventilation system of the building housing the 5-Mw swimming-pool reactor at PRNC. In the event of a reactor accident, building air will be diverted from the normal exhaust system and passed through the emergency system, which will contain absolute filters for the removal of particulate matter and activated charcoal for iodine vapor adsorption.

In a system of this size, the pressure drop through the charcoal is important. It can be reduced by decreasing the depth of adsorbent and increasing the face area exposed to air flow. This also reduces the superficial air velocity through the charcoal. A commercial activated-charcoal canister (available from the Connor Engineering Corp., Danbury, Conn., or the Charles E. Manning Co., Pittsburgh, Penn.) is available which contains the charcoal between two concentric cylinders, having perforated walls. The pressure drop through one canister at an air flow of 25 cfm is equal to 0.15 in. of water. Canisters of this type, containing 1.5 lb of  $\frac{6}{14}$ -mesh charcoal and having a charcoal depth of 0.75 in., were tested for iodine vapor adsorption at their rated capacity of 25 cfm. A single canister was found to have an iodine adsorption efficiency of 99.99%.

A single stage of these canisters was proposed for iodine vapor adsorption in the emergency exhaust system of the reactor building at PRNC.

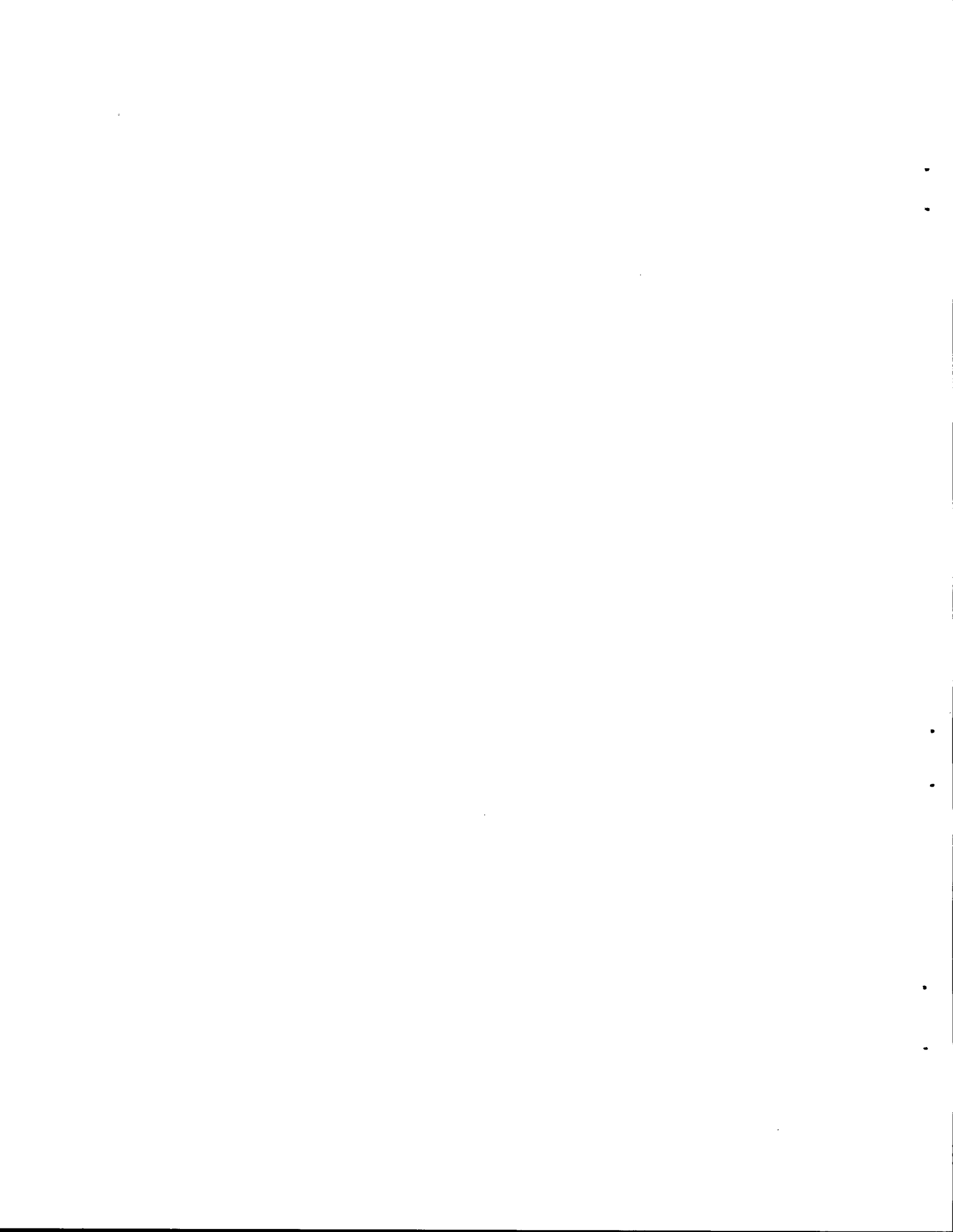
#### Fission Gas-Iodine Vapor Adsorption Systems for In-Pile Experiments

Assistance has been given to several experimental programs in the design and evaluation of off-gas systems connected with in-pile experimentation.<sup>12-14</sup> These systems include provisions for either preventing gross release of gaseous fission products in the event of experiment failure or for continuous processing of off-gas during operation of the experiment. The reports evaluate the performance of the adsorbents both in terms of amounts of fission gases penetrating the system and the probable radiation hazard to personnel resulting from discharge of the fission gases to the atmosphere.

<sup>12</sup>R. E. Adams and W. E. Browning, *Evaluation of the Iodine Vapor-Fission Gas Adsorption Traps for ORR-705 Capsule Experiment, GCPR Capsule Irradiation Program*, ORNL CF-58-12-10 (Dec. 23, 1958).

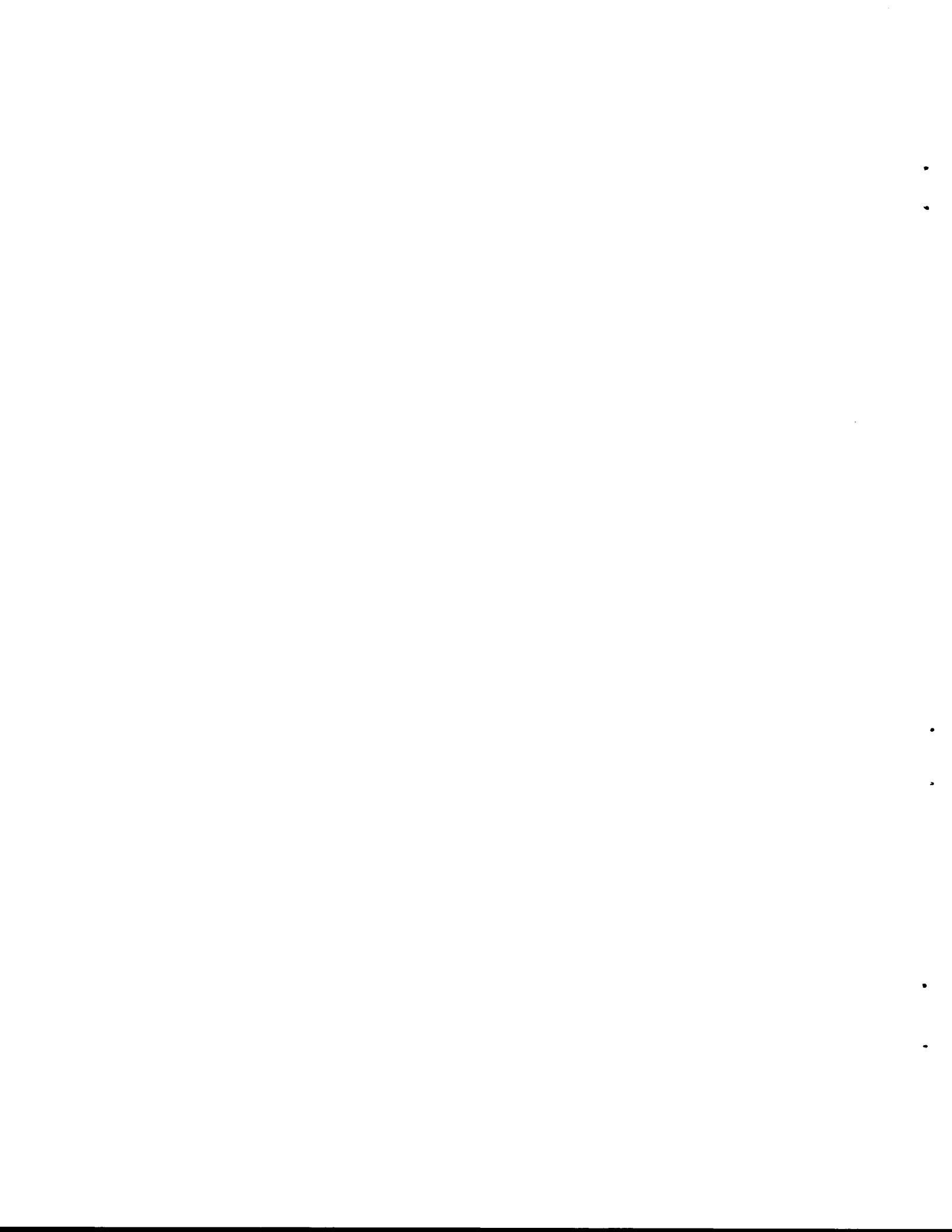
<sup>13</sup>R. E. Adams and W. E. Browning, *Estimate of Hazard Produced by Accidental Release of Gaseous Fission Products from an ORR Fused Salt Capsule Experiment*, ORNL CF-59-4-96 (Apr. 24, 1959).

<sup>14</sup>R. E. Adams and W. E. Browning, *Evaluation of Activated Charcoal Fission Gas Adsorbents Designed for the GC-ORR Loop Experiment Number 1*, ORNL CF-60-1-24 (Jan. 14, 1960).



Part IV

PREPARATION OF REACTOR-GRADE MATERIALS



## 19. PREPARATION OF OXYGEN-FREE YTTRIUM

G. J. Nessel

J. Truitt

J. E. Eorgan

Yttrium metal has properties which make it of potential value, in spite of its high price, in special reactor applications. However, fabricability of this material deteriorates markedly as the oxygen content of the metal increases. Since yttrium metal is quite reactive and since  $Y_2O_3$  is a very stable chemical compound, preparation and handling of oxygen-free yttrium poses difficult problems. These problems are enhanced by the high melting point of pure yttrium (ca.  $1600^\circ C$ ) and by its corrosivity toward virtually all container metals at this temperature.

It seemed likely that elimination of oxygen from the raw materials for the reduction process could be facilitated if these materials could be processed in liquid form and then transferred as liquids to the reduction assembly under an atmosphere of inert gas. Accordingly, an attempt was made to adapt the techniques and equipment for processing and handling of molten fluoride fuels and liquid metals for this purpose.

Yttrium trifluoride can be reduced to yttrium metal by metallic calcium or lithium at elevated temperatures; if the metal is to be readily recovered from the slag, however, both phases must be molten at reduction temperatures. An alloy of yttrium with about 20 at. % Mg melts below  $1000^\circ C$  and is a convenient reduction product; the magnesium can be removed by vacuum distillation before consolidation of the yttrium product by vacuum arc-melting or the equivalent.

Yttrium fluoride can be prepared by precipitation from aqueous solution or by hydrofluorination of  $Y_2O_3$  at elevated temperatures. It is difficult to dry the aqueous preparation without appreciable hydrolysis, and it is difficult to carry the gas-solid reaction to completion. Therefore an attempt

was made to prepare oxygen-free, yttrium-bearing fluoride salts by hydrofluorination in the liquid state.

A preliminary examination of phase behavior in the system revealed that mixtures containing 58.3 mole % LiF, 23.1 mole %  $YF_3$ , and 18.6 mole %  $MgF_2$  could be melted below  $800^\circ C$ . These mixtures could be reduced with metallic Li<sup>0</sup> to produce the low-melting Y-Mg alloy and essentially pure LiF; both phases melt below  $1000^\circ C$ , so phase separation and metal recovery should be easy and complete.

Experiments with 5 lb of the mixture in equipment of copper-lined stainless steel revealed that the oxygen concentration in the salt (measured by the gaseous oxygen evolved upon treatment of samples of the material with  $BrF_3$ ) could be brought to about 200 ppm. Experiments in larger-scale equipment, however, seldom produced material with less than 500 ppm of oxygen. A modification of the apparatus was fabricated which would permit use of a dilute mixture of  $F_2$  in the HF to ensure the absence of water in the HF feed stream. The project ended before this assembly could be tested; it is not, accordingly, known whether the 200 ppm of  $O^{--}$  in the LiF- $YF_3$ - $MgF_2$  preparations represents an equilibrium with the HF feed.

The over-all process was tested through the reduction, magnesium and lithium removal, and yttrium compaction steps in a joint program with the Metallurgy Division. Although some success could be claimed for each processing step, no significant amount of yttrium was produced bearing less than 1000 ppm of oxygen. The program was terminated after a relatively few complete experiments because of demonstration of a successful process elsewhere.

## 20. PREPARATION OF INORGANIC FLUORIDES

B. J. Sturm

## SYNTHESIS OF FLUORIDES OF CHROMIUM

Various fluorides of chromium were synthesized and their properties studied. Interest in these compounds was stimulated by the investigation of the corrosion of chromium alloy containers by molten fluoride mixtures proposed as nuclear reactor fuels.

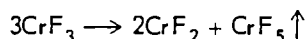
## Ammonium Hexafluorochromate(III)

Anhydrous  $(\text{NH}_4)_3\text{CrF}_6$  was conveniently prepared by reacting  $(\text{NH}_4)_2\text{Cr}_2\text{O}_7$  or  $\text{CrO}_3$  (ref 1) with molten  $\text{NH}_4\text{HF}_2$ . Ammonium hexafluorochromate(III), when so prepared, was free from moisture, and therefore useful for preparing other chromium fluorides by high-temperature reactions. The compounds that have been prepared from  $(\text{NH}_4)_3\text{CrF}_6$  are  $\text{CrF}_3$ ,  $\text{CrF}_2$ , chromium(II,III) fluoride, and various hexafluorochromates.

## Chromous Fluoride

The difficulty of avoiding mixed products on treating chromium metal or  $\text{CrCl}_2$  with HF or  $\text{CrF}_3$  with  $\text{H}_2$  led to the development of new methods of preparing anhydrous  $\text{CrF}_2$ . Among the reactions studied were (1) pyrolysis of  $(\text{NH}_4)_3\text{CrF}_6$ , (2) disproportionation of  $\text{CrF}_3$ , (3) reduction of  $\text{CrCl}_3$  with molten  $\text{SnF}_2$ , and (4) oxidation of chromium metal with molten fluorides of noble metals.

On prolonged heating at  $1100^\circ\text{C}$ ,  $\text{CrF}_3$  was found to disproportionate as follows:<sup>2</sup>



Ammonium hexafluorochromate(III) also gave  $\text{CrF}_2$  under the same conditions. Because of the influence of geometry of the charge and time of reaction, disproportionation and pyrolysis were applicable only for small batches of  $\text{CrF}_2$ . A product contaminated with chloride resulted from the reaction<sup>3</sup>



Lead fluoride,  $\text{CuF}_2$ ,  $\text{CdF}_2$ , and  $\text{BiF}_3$  all oxidized  $\text{Cr}^0$  to  $\text{CrF}_2$ , but the reaction with  $\text{SnF}_2$  was the most convenient method of preparing a pure product.<sup>2,4</sup> A good separation of molten  $\text{Sn}^0$  from  $\text{CrF}_2$  was readily obtained at  $1100^\circ\text{C}$  in impervious graphite.

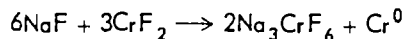
Chromous fluoride of natural isotopic composition was radioactively labeled for use as a tracer by irradiating in the ORNL Graphite Reactor. Natural chromium contains 4.4%  $\text{Cr}^{50}$  which is converted into radioactive  $\text{Cr}^{51}$ . Irradiation for one week yielded a product with an activity of 10 mc/g.

## Chromium(II,III) Fluoride

A new compound,  $\text{CrF}_{2.4}$ , was found in  $\text{CrF}_2$  preparations when the hydrogenation or disproportionation of  $\text{CrF}_3$  was incomplete.<sup>2</sup> It was also made by oxidizing  $\text{CrF}_2$  with HF or  $\text{SnF}_2$  and by fusing a mixture of  $\text{CrF}_2$  and  $\text{CrF}_3$  in a platinum capsule. On the basis of the visual spectrum and other supporting evidence the formula  $\text{Cr}_3^{II}(\text{Cr}^{III}\text{F}_6)_2$  was tentatively assigned to the compound.

## Disproportionation of Chromous Fluoride

If a mixture of equal moles of  $\text{CrF}_2$  and NaF is rapidly fused and quenched a new compound  $\text{NaCrF}_3$  is formed; however, if the molten mixture is cooled slowly or NaF is in excess the disproportionation reaction occurs:



## STANNOUS FLUORIDE AS A PREPARATIVE REAGENT

Stannous fluoride, a useful reagent for the synthesis of  $\text{CrF}_2$ , has also been used to prepare other fluorides and fluocomplexes.

Molten  $\text{SnF}_2$  reacted with the metals Mn, Zn, Al, Fe, V, and U to yield, respectively,  $\text{MnF}_2$ ,  $\text{ZnF}_2$ ,  $\text{AlF}_3$ ,  $\text{FeF}_2$ ,  $\text{VF}_3$ , and  $\text{UF}_4$  (ref 5). The  $\text{MnF}_2$  and  $\text{ZnF}_2$ , so prepared, were pure, as the

<sup>1</sup>MSR Quar. Prog. Rep. Oct. 31, 1959, ORNL-2890, p 68.

<sup>2</sup>MSR Quar. Prog. Rep. Jan. 31, 1959, ORNL-2684, p 113-14.

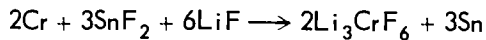
<sup>3</sup>B. J. Sturm, MSR Quar. Prog. Rep. June 30, 1958, ORNL-2551, p 101.

<sup>4</sup>B. J. Sturm, MSR Quar. Prog. Rep. Oct. 31, 1958, ORNL-2626, p 107.

<sup>5</sup>MSR Quar. Prog. Rep. Jan. 31, 1959, ORNL-2684, p 112-13.

resulting fused salt and tin layers were well defined and easily separated.

Fusion of  $\text{SnF}_2$  with half the molar quantity of  $\text{CrF}_2$  forms a phase, presumably  $\text{Sn}_3^{\text{II}}(\text{Cr}^{\text{III}}\text{F}_6)_2$ , which decomposes at  $1000^\circ\text{C}$  to yield  $\text{CrF}_3$  (ref 6). Chromium metal reacted with a molten mixture of  $\text{SnF}_2$  and  $\text{LiF}$  to form  $\text{Li}_3\text{CrF}_6$  (ref 7):



The corresponding treatment of vanadium metal gave a product with an x-ray diffraction pattern slightly shifted from that of  $\text{Li}_3\text{CrF}_6$  and so presumably was  $\text{Li}_3\text{VF}_6$ .

Molten  $\text{SnF}_2$  reacted with  $\text{CuF}_2$ ,  $\text{BiF}_3$ , and  $\text{SbF}_3$  to give, respectively, the free metals Cu, Bi, and Sb (ref 7). The other product of the reaction, presumably  $\text{SnF}_4$ , did not melt at any temperature up to  $500^\circ\text{C}$ . These reactions are surprising as published estimated thermodynamic data<sup>8</sup> shows considerable free energy against their occurring.

#### REACTIONS OF AMMONIUM BIFLUORIDE

Molten  $\text{NH}_4\text{HF}_2$  has served as a reactant for preparing both simple and complex fluorides.

Most metal oxides are attacked by molten  $\text{NH}_4\text{HF}_2$ . Powdered  $\text{Fe}_2\text{O}_3$ ,  $\text{Y}_2\text{O}_3$ ,  $\text{V}_2\text{O}_3$ , and activated  $\text{Al}_2\text{O}_3$  are converted into the corresponding hexafluometallates(III);  $\text{CeO}_2$  is similarly attacked to form, presumably,  $(\text{NH}_4)_3\text{CeF}_6$ . Thermal decomposition of these complexes at  $400$  to  $600^\circ\text{C}$  forms  $\text{FeF}_2$ ,  $\text{YF}_3$ ,  $\text{VF}_3$ ,  $\text{AlF}_3$ , and  $\text{CeF}_3$ ,

respectively.<sup>9</sup> Commercial  $\text{Cr}_2\text{O}_3$  and  $\text{NiO}$  are very resistant to attack by molten  $\text{NH}_4\text{HF}_2$ . Magnesium and beryllium oxides are converted into  $\text{NH}_4\text{MgF}_3$  and  $(\text{NH}_4)_2\text{BeF}_4$ , respectively, which thermally decompose into  $\text{MgF}_2$  and  $\text{BeF}_2$ . Ammonium bifluoride can convert  $\text{ZrO}_2$  into either  $\text{ZrF}_4$  or  $\text{ZrOF}_2$  depending on mode of treatment. Commercial " $\text{Co}_2\text{O}_3$ " reacts slowly with  $\text{NH}_4\text{HF}_2$  to form what seems to be  $\text{NH}_4\text{CoF}_3$ . The oxides  $\text{GeO}$ ,  $\text{UO}_2$ , and  $\text{ThO}_2$  seem to react completely with molten  $\text{NH}_4\text{HF}_2$ , but the products have not yet been identified.

Hydrated  $\text{LiOH}$ , enriched in isotope 7, was converted into anhydrous  $\text{LiF}$  by heating with  $\text{NH}_4\text{HF}_2$ .

The metals Fe, Al, and Cr react with  $\text{NH}_4\text{HF}_2$  to form the respective hexafluometallates(III), but the reaction of chromium is too slow to provide a practical method of preparing  $(\text{NH}_4)_3\text{CrF}_6$ .

The  $\text{SnF}_2$ - $\text{NH}_4\text{HF}_2$  system was investigated to find a solvent useful for reprocessing nuclear reactor fuels. In the range 0 to 40 mole %  $\text{SnF}_2$  the liquidus temperatures were below  $150^\circ\text{C}$  (ref 10). Decomposition, evolving gases, interfered with the study of the system at the temperatures needed to melt compositions of greater than 40%  $\text{SnF}_2$ . As a result of the evolution of gases a composition resulted which melted at  $240^\circ\text{C}$ . The solidified material gave a simple x-ray pattern and a chemical analysis approximating  $\text{NH}_4\text{F} \cdot 4\text{SnF}_2$ . The same phase resulted from the fusion of  $\text{NH}_4\text{SnF}_3$  made from aqueous solution.

<sup>6</sup>MSR Quar. Prog. Rep. Apr. 30, 1959, ORNL-2723, p 94.

<sup>7</sup>MSR Quar. Prog. Rep. July 31, 1959, ORNL-2799, p 94.

<sup>8</sup>A. Glassner, *The Thermochemical Properties of the Oxides, Fluorides, and Chlorides to  $2500^\circ\text{K}$* , ANL-5750 (1957).

<sup>9</sup>MSR Quar. Prog. Rep. Apr. 30, 1959, ORNL-2723, p 93-94; ANP Semiann. Prog. Rep. Mar. 31, 1959, ORNL-2711, p 47-48; MSR Quar. Prog. Rep. Oct. 31, 1959, ORNL-2890, p 68.

<sup>10</sup>MSR Quar. Prog. Rep. Apr. 30, 1959, ORNL-2723, p 78.

## 21. PREPARATION AND PROPERTIES OF INORGANIC OXIDES

## HIGH-TEMPERATURE OXIDE SYSTEMS

H. A. Friedman      R. E. Thoma  
C. F. Weaver

Investigations of the phase relationships of several oxide systems which are relevant to current ORNL efforts pertaining to the  $\text{ThO}_2\text{-UO}_2$  fuel cycle and of  $\text{UO}_2$  as a high-temperature thermoelectric material are in the beginning stages. Although there exist a large number of reports concerning the phase equilibria in the uranium-oxygen system and in the uranium-thorium-oxygen system, few of these define satisfactorily the methods for determining the two phase composition limits or for assigning precise compositions of the materials in combinations. Efforts are proceeding in order to determine the inherent precision and accuracy available in the chemical methods for ascertaining the oxygen/uranium ratios in uranium oxides and to relate these methods with the optical and x-ray diffraction methods for determining these ratios in uranium oxides and in  $\text{UO}_2\text{-ThO}_2$  solid solutions. Optical methods are being established for accurate and rapid determination of solid-solution compositions and in estimating the degree of completion of oxide solid-state reactions. Optical properties of several oxides which are significant as nuclear reactor materials have been measured recently and are reported here for the first time (Table 21.1).

Optical Properties of  $\text{UO}_2\text{-ThO}_2$  Solid Solutions

Several investigators have reported<sup>1</sup> that equilibrium solids in the system  $\text{UO}_2\text{-ThO}_2$  are members of a continuous solid-solution series which obeys Vegard's rule. Measurements of the unit-cell parameters of these solid solutions at the laboratory are in accordance with this statement. Preliminary studies of  $\text{UO}_2\text{-ThO}_2$  solid solutions prepared by firing these materials at  $1650^\circ\text{C}$  in  $\text{H}_2$  for 2 hr (ref 2) indicate that the refractive indices vary as a function of composition. The color of the solid solution ranges from dark red ( $\text{UO}_2$ ) to yellow to colorless ( $\text{ThO}_2$ ). The refractive index range from 2.11 to 2.36 should permit an optical determination of a given member of the solid-solution series to within 0.5 mole % if the refractive indices are nearly linear functions of composition and if the refractive indices of 10- to 100- $\mu$  crystallites may be measured to four significant figures. Reports by other investigators<sup>3</sup> and preliminary results in this laboratory indicate that such precision may be obtained.

<sup>1</sup>W. A. Lamberton, M. H. Mueller, and F. H. Gunzel, Jr., *J. Am. Ceram. Soc.* **36**, 399 (1953).

<sup>2</sup>Prepared by C. E. Curtis, Ceramics Laboratory, Metallurgy Division, ORNL.

<sup>3</sup>H. E. Merwin and E. S. Larsen, Jr., *Am. J. Sci.* **184**(4), 42 (1912).

Table 21.1. Optical Properties of Several Oxides

Compound	Optical Character	Refractive Index
$\text{Y}_2\text{O}_3$	Isotropic, colorless	$1.865 \pm 0.005$ in tungsten light
$\text{U}_3\text{O}_8$	Birefringent, brownish-green, nearly opaque	$2.22 \pm 0.02$ in 6500-Å light
$\text{ThO}_2$	Isotropic, colorless	$2.11 \pm 0.02$ in 6500-Å light <sup>o</sup> ,**
$\text{UO}_2$	Isotropic, red	$2.36 \pm 0.02^{**}$
$\text{MoO}_3$	Biaxial, optic angle very large, parallel extinction, colorless	$N_\alpha = 2.15 \pm 0.02^{**}$ $N_\gamma = 2.23 \pm 0.02^{**}$

<sup>o</sup>A value of 2.20 reported in bulletin No. 118 of the National Research Council is probably that of a member of the  $\text{UO}_2\text{-ThO}_2$  solid-solution series.

\*\*These measurements are precise to three significant figures. Calibration difficulties, at present, indicate that the accuracy may not be this good. Consequently, large errors are assigned in this table. Attempts are in progress to improve both the precision and accuracy of these values.

**PREPARATION OF HIGH-PURITY  
BERYLLIUM OXIDE**

B. J. Sturm

A study of procedures for preparing pure beryllium oxide was initiated as a part of a program for developing improved beryllia ceramics for fuel elements. Very pure beryllium oxide with good sintering characteristics has been obtained by G.E. by the calcination of pure hydrated beryllium oxalate.<sup>4</sup> Oxalic acid is fused with the purest commercial  $\text{Be}(\text{OH})_2$ , and the pure beryllium oxalate is obtained by recrystallization from a filtered aqueous solution. One aim of the beryllium oxide research is the introduction of known quantities of selected impurities in order to evaluate their effects on sintering. Additives are desired which facilitate sintering, retard grain growth during sintering, or increase the resistance of the material to corrosion at high temperatures; however, the addition must not adversely affect the durability or nuclear properties.

Kilograms of  $\text{BeO}$  were prepared by the G-E procedure and modifications thereof. The procedure was simplified by eliminating the melting and casting of the  $\text{H}_2\text{C}_2\text{O}_4\text{-Be}(\text{OH})_2$  composition.<sup>5</sup> This was done by adding initially the water that would be necessary for the eventual aqueous crystallization of the beryllium oxalate.

---

<sup>4</sup>B. J. Sturm, *Beryllium Oxide Conference*, ORNL CF-58-10-74 (Oct. 22, 1958).

<sup>5</sup>ANP *Semiann. Prog. Rep. Oct. 31, 1959*, ORNL-2840, p 64.

<sup>6</sup>ANP *Semiann. Prog. Rep. Mar. 31, 1959*, ORNL-2711, p 50.

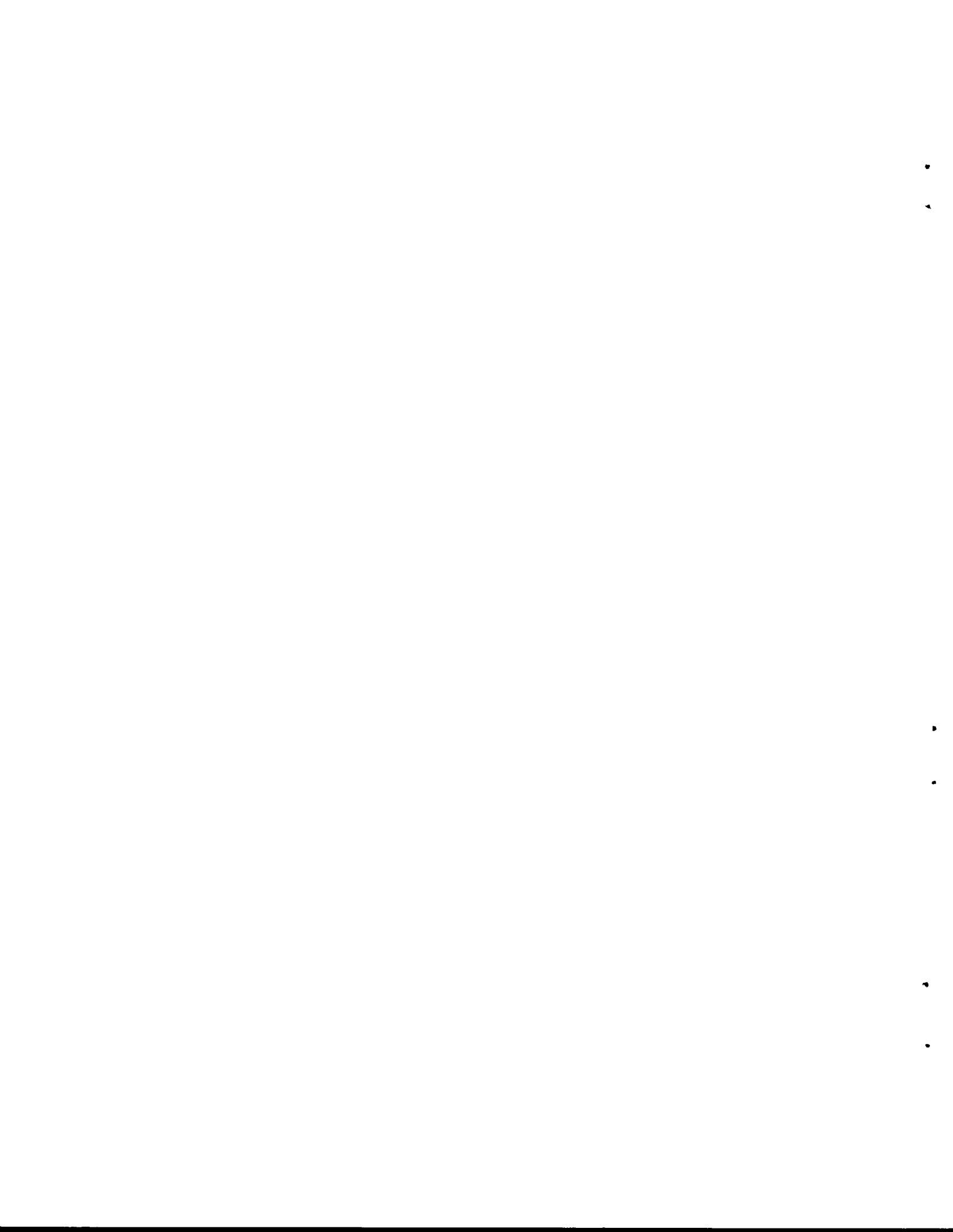
The use of plastic apparatus helped to avoid contamination by the constituents of glass.<sup>6</sup>

The size of the crystals of the beryllium oxalate which is being calcined seems to influence the sintering characteristics of the resulting  $\text{BeO}$ . When a hot, concentrated solution of beryllium oxalate is cooled rapidly while being stirred vigorously, a "fondant" is obtained which consists of a suspension of very small crystals of hydrated beryllium oxalate. An estimated 90% of the crystals were 0.01 to 0.03 mm in diameter when the "fondant" was prepared in a silver container cooled with ice. Crystals obtained by the G-E process are about ten times this size.

Beryllium oxalate as crystallized by cooling an aqueous solution is the trihydrate. Drying this material in an oven formed the monohydrate, the x-ray diffraction pattern of which was determined.<sup>6</sup> The precipitate obtained by boiling aqueous beryllium oxalate was the monohydrate. The  $\text{BeC}_2\text{O}_4\cdot\text{H}_2\text{O}$ , so precipitated, seems to have improved sintering properties.

Beryllium oxide which sintered well generally contained over 100 ppm each of Ca and Si. To evaluate the effects of additions of Si, DuPont's aqueous colloidal silica was added to a hot beryllium oxalate solution just before cooling to obtain crystals.<sup>5</sup> To evaluate Ca additions,  $\text{Ca}(\text{OH})_2$  was added to the  $\text{Be}(\text{OH})_2$  starting material; however, as Ca tends to concentrate in the mother liquor, the product may not have been uniform.

Those oxides which differ most in acidity or basicity from  $\text{BeO}$  are the additives most likely to be effective in cutting down the activity, and correspondingly the volatility of  $\text{BeO}$  in water vapor. A very acid oxide,  $\text{ZrO}_2$ , has been incorporated into  $\text{BeO}$  by adding  $\text{Zr}(\text{OH})_4$  to the starting materials of the oxalate process.<sup>5</sup>



## PUBLICATIONS

R. E. Adams, W. E. Browning, and R. D. Ackley, "Containment of Radioactive Fission Gases by Dynamic Adsorption," *Ind. Eng. Chem.* **51**, 1467 (1959).

C. F. Baes, Jr., and H. T. Baker, "The Extraction of Iron(III) from Acid Perchlorate Solutions by Di(2-Ethyl-hexyl)-Phosphoric Acid in *n*-Octane," *J. Phys. Chem.* **64**, 89 (1960).

J. H. Baldwin, C. E. Higgins, and B. A. Soldano, "The Distribution of Monovalent Electrolytes Between Water and TBP," *J. Phys. Chem.* **63**, 118 (1959).

M. Blander, F. F. Blankenship, and R. F. Newton, "The Thermodynamics of Dilute Solutions of  $\text{AgNO}_3$  and  $\text{KCl}$  in Molten  $\text{KNO}_3$ , from Electromotive Force Measurements. I. Experimental," *J. Phys. Chem.* **63**, 1259 (1959).

M. Blander, "The Thermodynamics of Dilute Solutions of  $\text{AgNO}_3$  and  $\text{KCl}$  in Molten  $\text{KNO}_3$  from Electromotive Force Measurements. II. A Quasi-Lattice Model," *J. Phys. Chem.* **63**, 1262 (1959).

M. Blander, W. R. Grimes, N. V. Smith, and G. M. Watson, "Solubility of Noble Gases in Molten Fluorides. II. In the  $\text{LiF-NaF-KF}$  Eutectic Mixture," *J. Phys. Chem.* **63**, 1164 (1959).

M. Blander and J. Braunstein, "A Quasi-Lattice Model of Molten Reciprocal Salt Systems," *Ann. N.Y. Acad. Sci.* **79**(Art. 11), 838-52 (1960).

J. Braunstein and M. Blander, "The Thermodynamics of Dilute Solutions of  $\text{AgNO}_3$  and  $\text{KCl}$  in Molten  $\text{KNO}_3$  from Electromotive Force Measurements. III. Temperature Variations of the Activity Coefficients," *J. Phys. Chem.* **64**, 10 (1960).

W. E. Browning, "Removal of Fission Product Activity from Gases, Parts I and II," *Nuclear Safety* **1**(3,4) (1960).

H. A. Friedman, "Analysis of Lithium Metal, Hydride, and Hydroxide for Nickel, Copper, Silicon, Iron, Chromium, Aluminum and Hydroxide," *Anal. Chem.* **32**, 137 (1960).

H. A. Friedman, "Modifications of Quenching Techniques for Phase Equilibrium Studies," *J. Am. Ceram. Soc.* **42**, 284 (1959).

W. R. Grimes, N. V. Smith, and G. M. Watson, "Solubility of Noble Gases in Molten Fluorides. I. In Mixtures of  $\text{NaF-ZrF}_4\text{-UF}_4$  (50-46-4 mole %)," *J. Phys. Chem.* **62**, 862 (1958).

W. R. Grimes, F. F. Blankenship, G. W. Keilholtz, H. F. Poppendiek, and M. T. Robinson, "Chemical Aspects of Molten Fluoride Reactors," *U.N. Intern. Conf. Peaceful Uses Atomic Energy, 2nd, Geneva, 1958* **28**, 99-111 (1958).

W. R. Grimes, D. R. Cuneo, F. F. Blankenship, G. W. Keilholtz, H. F. Poppendiek, and M. T. Robinson, "Chemical Aspects of Molten-Fluoride-Salt Reactor Fuels," p 569 in *Fluid Fuel Reactors* (ed. by J. A. Lane, H. G. MacPherson, and F. Maslan), Addison-Wesley, Reading, Mass., 1958.

W. R. Grimes, J. H. Shaffer, N. V. Smith, R. A. Strehlow, W. T. Ward, and G. M. Watson, "High-Temperature Processing of Molten Fluoride Nuclear Reactor Fuels," *Chem. Eng. Progr. Symposium Ser. No.* **55**(27), p 65-70 (1959).

L. A. Harris, G. D. White, and R. E. Thoma, "X-ray Analyses of the Solid Phases in the System  $\text{LiF-ThF}_4$ ," *J. Phys. Chem.* **63**, 1974 (1959).

C. E. Higgins, W. H. Baldwin, and B. A. Soldano, "Effects of Electrolytes and Temperature on the Solubility of Tributyl Phosphate in Water," *J. Phys. Chem.* **63**, 113 (1959).

G. W. Keilholtz, J. G. Morgan, and W. E. Browning, "The Effect of Radiation on Corrosion of Structural Material by Molten Fluorides," *Nuclear Sci. and Eng.* **5**(1), 15-20 (1959).

REACTOR CHEMISTRY PROGRESS REPORT

W. L. Marshall, F. J. Loprest, and C. H. Secoy, "The Equilibrium  $\text{Li}_2\text{CO}_3(s) + \text{CO}_2 + \text{H}_2\text{O} \rightleftharpoons 2\text{Li}^+ + 2\text{HCO}_3^-$  at High Temperature and Pressure," *J. Am. Chem. Soc.* **80**, 5646 (1958).

M. B. Panish, F. F. Newton, W. R. Grimes, and F. F. Blankenship, "Activities in the Chromium-Nickel System," *J. Phys. Chem.* **62**, 980 (1958).

M. B. Panish, F. F. Blankenship, W. R. Grimes, and R. F. Newton, "Thermodynamic Properties of Molten and Solid Solutions of Silver Chloride and Sodium Chloride," *J. Phys. Chem.* **62**, 1325 (1958).

M. B. Panish, R. F. Newton, W. R. Grimes, and F. F. Blankenship, "Thermodynamic Properties of Molten and Solid Solutions of Silver Chloride and Lithium Chloride," *J. Phys. Chem.* **63**, 668 (1959).

J. H. Shaffer, W. R. Grimes, and G. M. Watson, "Solubility of Hydrogen Fluoride in Molten Fluorides. I. In Mixtures of  $\text{NaF-ZrF}_4$ ," *J. Phys. Chem.* **63**, 1999 (1959).

J. E. Ricci, *Guide to the Phase Diagrams of the Fluoride Systems*, ORNL-2396 (Nov. 19, 1958).

R. E. Thoma, H. Insley, B. S. Landau, H. A. Friedman, and W. R. Grimes, "Phase Equilibria in the Alkali Fluoride-Uranium Tetrafluoride Fused Salt Systems. II. The Systems  $\text{KF-UF}_4$  and  $\text{RbF-UF}_4$ ," *J. Am. Ceram. Soc.* **41**, 538 (1958).

R. E. Thoma, H. Insley, B. S. Landau, H. A. Friedman, and W. R. Grimes, "Phase Equilibria in the Alkali Fluoride-Uranium Tetrafluoride Fused Salt Systems. III. The System  $\text{NaF-LiF-UF}_4$ ," *J. Am. Ceram. Soc.* **42**, 21 (1959).

R. E. Thoma, H. Insley, B. S. Landau, H. A. Friedman, and W. R. Grimes, "Phase Equilibria in the Fused Salt Systems  $\text{LiF-ThF}_4$  and  $\text{NaF-ThF}_4$ ," *J. Phys. Chem.* **63**, 1266 (1959).

R. E. Thoma (ed.), *Phase Diagrams of Nuclear Reactor Materials*, ORNL-2548 (Nov. 2, 1959).

W. T. Ward, R. A. Strehlow, W. R. Grimes, and G. M. Watson, *Solubility Relations Among Rare-Earth Fluorides in Selected Molten Fluoride Solvents*, ORNL-2749 (Oct. 13, 1959).

C. F. Weaver, R. E. Thoma, H. Insley, and H. A. Friedman, *Phase Equilibria in the Systems  $\text{UF}_4\text{-ThF}_4$  and  $\text{LiF-UF}_4\text{-ThF}_4$* , ORNL-2719 (Aug. 14, 1959).

## PAPERS PRESENTED AT SCIENTIFIC AND TECHNICAL MEETINGS

R. D. Ackley, R. E. Adams,\* and W. E. Browning, "The Disposal of Radioactive Fission Gases by Adsorption," Sixth AEC Air Cleaning Seminar, Idaho Falls, Idaho, July 7-9, 1959.

R. E. Adams,\* W. E. Browning, and R. D. Ackley, "Dynamic Adsorption of Fission Product Gases from Circulating Fuel Nuclear Reactors," American Chemical Society, Boston, April 5-10, 1959.

C. J. Barton, "Phase Relationships in the System LiF-PuF<sub>3</sub>," American Chemical Society, Boston, April 5-10, 1959.

C. J. Barton, "Solubility of PuF<sub>3</sub> in Fused Alkali Fluoride-Beryllium Fluoride Mixtures," American Chemical Society, Boston, April 5-10, 1959.

M. Blander,\* F. F. Blankenship, and R. F. Newton, "The Thermodynamics of Dilute Solutions of AgNO<sub>3</sub> and KCl in Molten KNO<sub>3</sub> from Electromotive Force Measurements. II. Discussion and Theory," American Chemical Society, Chicago, September 7-12, 1958.

M. Blander\* and J. Braunstein, "The Thermodynamics of Dilute Solutions of AgNO<sub>3</sub> and KCl in Molten KNO<sub>3</sub> from Electromotive Force Measurements. II. Temperature Variations of the Activity Coefficients," American Chemical Society, Boston, April 5-10, 1959.

M. Blander, "Some Specific Applications of Fundamental Physical Chemistry to Reactor Problems," University of Maine Sigma Xi Meeting, April 16, 1959.

M. Blander, "A Quasi-Lattice Model of Molten Salts," University of Maine Chemistry Department Seminar, April 17, 1959.

M. Blander\* and J. Braunstein, "A Quasi-Lattice Model of Molten Reciprocal Salt Systems," Symposium of New York Academy of Sciences, New York, April 13, 1959.

M. Blander, "A Quasi-Lattice Model of Molten Salts," Gordon Research Conference, Meriden, New Hampshire, August 31-September 4, 1959.

M. Blander, "A Quasi-Lattice Model of Molten Salts," Duke University Chemistry Department Seminar, October 30, 1959.

M. Blander, "A Quasi-Lattice Model of Molten Salts," Pennsylvania State University Chemistry Department Seminar, November 12, 1959.

J. Braunstein\* and M. Blander, "The Heat of Solution of AgCl in Molten KNO<sub>3</sub>," American Chemical Society, Boston, April 5-10, 1959.

J. Braunstein,\* R. M. Lindgren, and M. Blander, "The Thermodynamics of Dilute Solutions of Silver Nitrate and Potassium Chloride in Molten Potassium Nitrate from EMF Measurements. The Activity Coefficient of Potassium Chloride," American Chemical Society, Atlantic City, September 13-18, 1959.

W. E. Browning, Jr.,\* R. E. Adams, and R. D. Ackley, "Removal of Fission Product Gases from Reactor Off-Gas Streams by Adsorption," American Nuclear Society, Detroit, December 1958.

S. Cantor, "Freezing Point Depressions in Sodium Fluoride," Gordon Research Conference, Meriden, New Hampshire, August 31-September 4, 1959.

R. B. Evans,\* R. J. Sheil, W. R. Grimes, and G. M. Watson, "Diffusion of Chromium in Inconel Exposed to Molten Salts," American Chemical Society, Chicago, September 7-12, 1958.

L. O. Gilpatrick,\* C. S. Patterson, and B. A. Soldano, "Osmotic Behavior of Aqueous Solutions at 100°C," American Chemical Society Southern Regional Meeting, Richmond, November 5-7, 1959.

---

\*Denotes speaker.

## REACTOR CHEMISTRY PROGRESS REPORT

W. R. Grimes,\* F. F. Blankenship, G. W. Keilholtz, H. F. Poppendiek, and M. T. Robinson, "Chemical Aspects of Molten Fluoride Reactors," Second United Nations International Conference on the Peaceful Uses of Atomic Energy, Geneva, Switzerland, September 1-13, 1958.

D. G. Hill,\* M. Blander, and J. Braunstein, "Activity Coefficients in Molten Salts from Electromotive Force Measurements. The System  $\text{AgNO}_3\text{-NaCl-NaNO}_3$ ," American Chemical Society Southeastern Regional Meeting, Richmond, November 5-7, 1959.

S. Langer\* and F. F. Blankenship, "The Vapor Pressure of Uranium Tetrafluoride," American Society, Boston, April 5-10, 1959.

H. F. McDuffie, "Homogeneous Catalysis," ORINS Lecture, Birmingham-Southern College, January 21, 1959; Loyola University, March 18, 1959; Tulane University, March 19, 1959; University of Oklahoma, April 15, 1959; Vanderbilt University, April 16, 1959.

W. L. Marshall, "Aqueous Solubility Equilibria, 200-374°C," American Chemical Society, Boston, April 5-10, 1959.

W. L. Marshall,\* F. J. Loprest, and C. H. Secoy, "The Equilibrium  $\text{Li}_2\text{CO}_3(s) + \text{CO}_2 + \text{H}_2\text{O} \rightleftharpoons 2\text{Li}^+ + 2\text{HCO}_3^-$  at High Temperature and Pressure," American Chemical Society, Chicago, September 7-12, 1958.

G. J. Nessel\* and W. R. Grimes, "Production and Handling of Molten Fluorides for Use as Reactor Fuels," American Institute of Chemical Engineers, Cincinnati, December 1958.

W. T. Rainey, "Utilization of Radioisotopes in the Textile Industry," Symposium, Georgia Institute of Technology, May 1959.

R. A. Strehlow,\* W. R. Grimes, J. H. Shaffer, N. V. Smith, W. T. Ward, and G. M. Watson, "High Temperature Processing of Molten Fluoride Nuclear Reactor Fuels," American Institute of Chemical Engineers, Cincinnati, December 1958.

B. A. Soldano, "The Introduction of a Statistical Length to Aqueous Solution Problems," South Carolina Academy of Science, Columbia, South Carolina, March 28, 1959.

B. J. Sturm, "Synthesis of Chromium(II) and Chromium(II,III) Fluorides," American Chemical Society, Atlantic City, September 13-18, 1959.

R. E. Thoma,\* H. Insley, B. S. Landau, H. A. Friedman, and W. R. Grimes, "Phase Equilibria in the Fused Salt Systems  $\text{LiF-ThF}_4$  and  $\text{NaF-ThF}_4$ ," American Chemical Society, Chicago, September 7-12, 1958.

R. E. Thoma, "Selections of Fuels for Molten Salt Reactors," U.S. Army Research and Development Unit 3252, Oak Ridge, November 18, 1959.

R. E. Thoma,\* H. Insley, H. A. Friedman, and C. F. Weaver, "Phase Equilibria in the Systems  $\text{BeF}_2\text{-ThF}_4$  and  $\text{LiF-BeF}_2\text{-ThF}_4$ ," American Chemical Society, Atlantic City, September 13-18, 1959.

W. T. Ward, R. A. Strehlow,\* W. R. Grimes, and G. M. Watson, "Solubility Relations of Rare Earth Fluorides in Various Molten  $\text{NaF-ZrF}_4$  ( $-\text{UF}_4$ ) Solvents," American Chemical Society, Chicago, September 7-12, 1958.

G. M. Watson, "Molten Fluorides as High Temperature Solvents," Gordon Research Conference on Inorganic Chemistry, August 20, 1958.

G. M. Watson, "Molten Fluorides as High Temperature Solvents," ORINS Lecture, Ohio University, November 1958; Tennessee Polytechnic Institute, February 12, 1959; Georgia Institute of Technology, February 1959.

---

\*Denotes speaker.

M. Blander, G. M. Watson,\* W. R. Grimes, and N. V. Smith, "Solubility of Noble Gases in Molten Fluorides. II. In the LiF-NaF-KF Mixture," American Chemical Society, Boston, April 5-10, 1959.

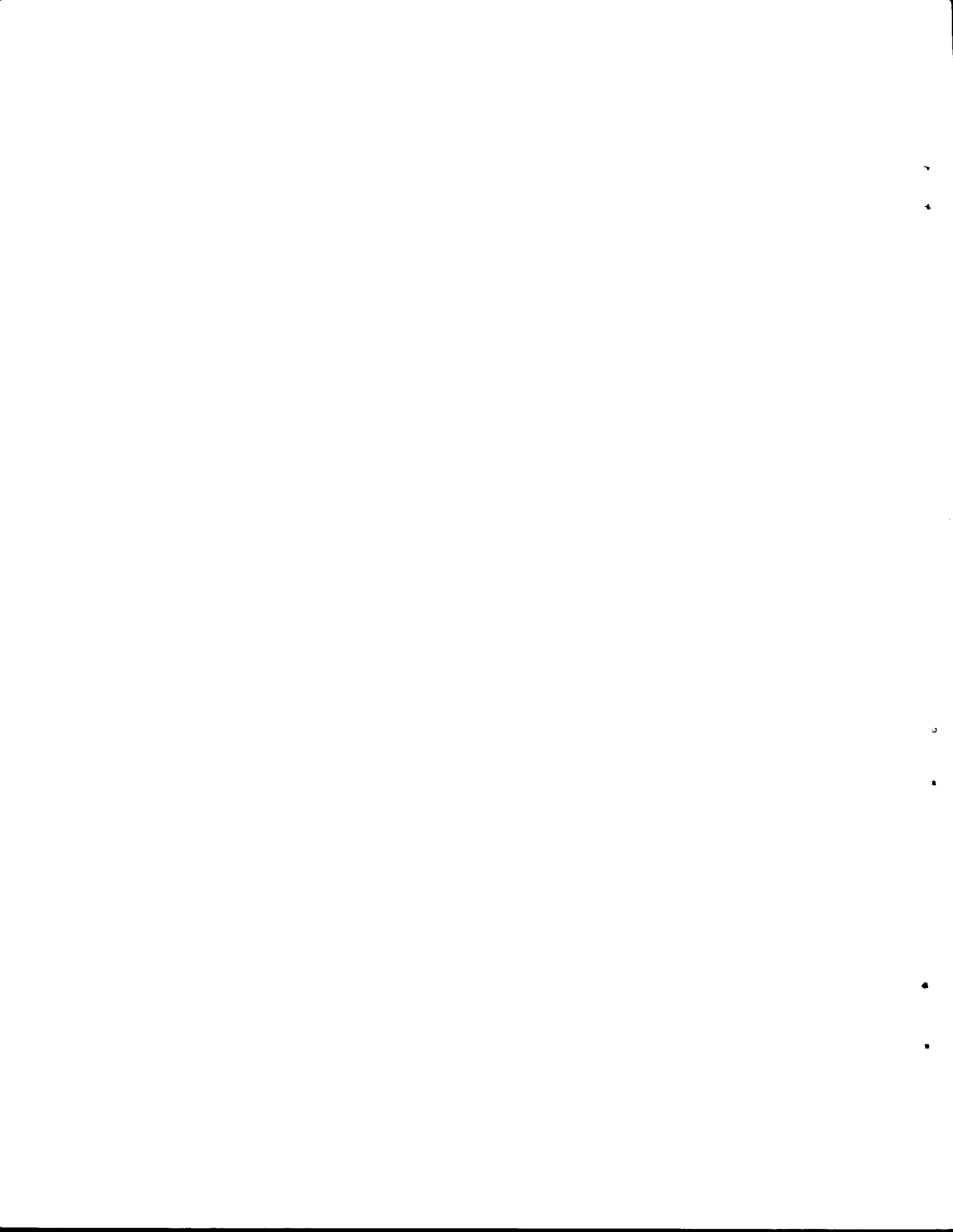
G. M. Watson, "Studies of the Chemistry of Fission Products in Molten Salt Power Reactor Systems," ORINS Lecture, Loyola University, November 10, 1959; Texas A and M College, November 12, 1959.

W. J. Watt\* and M. Blander, "The Thermodynamics of the Molten Salt System  $\text{KNO}_3\text{-AgNO}_3\text{-K}_2\text{SO}_4$  from Electromotive Force Measurements," American Chemical Society, Boston, April 5-10, 1959.

C. F. Weaver,\* R. E. Thoma, H. Insley, and H. A. Friedman, "Phase Equilibria in the Systems  $\text{UF}_4\text{-ThF}_4$  and  $\text{LiF-UF}_4\text{-ThF}_4$ ," American Ceramic Society, Chicago, May 1959.

---

\*Denotes speaker.



INTERNAL DISTRIBUTION

1. C. E. Center
2. A. M. Weinberg
3. L. B. Emlet (K-25)
4. J. P. Murray (Y-12)
5. J. A. Swartout
6. G. E. Boyd
7. R. A. Charpie
8. W. H. Jordan
9. A. H. Snell
10. C. E. Winters
11. R. B. Briggs
12. F. R. Bruce
13. J. A. Lane
14. H. G. MacPherson
15. S. C. Lind
16. P. R. Bell
17. D. S. Billington
18. E. P. Blizard
19. C. J. Borkowski
20. J. A. Cox
21. F. L. Culler
22. J. L. Fowler
23. J. H. Frye, Jr.
24. J. H. Gillette
25. W. R. Grimes
26. A. Hollaender
27. M. T. Kelley
28. T. A. Lincoln
29. R. S. Livingston
30. K. Z. Morgan
31. M. L. Nelson
32. M. E. Ramsey
33. A. F. Rupp
34. H. E. Seagren
35. E. D. Shipley
36. E. H. Taylor
37. C. P. Keim
38. R. S. Cockreham
39. P. M. Reyling
40. M. J. Skinner
41. G. C. Williams
42. J. M. Googin (Y-12)
43. A. L. Boch
44. E. G. Bohlmann
45. M. A. Bredig
46. J. E. Cunningham
47. J. H. Crawford, Jr.
48. A. P. Fraas
49. C. S. Harrill
50. R. N. Lyon
51. W. D. Manly
52. H. F. McDuffie
53. A. J. Miller
54. E. O. Wollan
55. C. D. Susano
56. E. Guth
57. C. F. Baes
58. C. J. Barton
59. R. L. Bennett
60. M. Blander
61. F. F. Blankenship
62. W. E. Browning
63. S. Cantor
64. D. R. Cuneo
65. J. E. Eorgan
66. R. B. Evans
67. E. U. Franck
68. G. W. Keilholtz
69. M. J. Kelly
70. W. L. Marshall
71. R. E. Moore
72. R. F. Newton
73. L. G. Overholser
74. W. T. Rainey
75. J. H. Shaffer
76. M. D. Silverman
77. B. A. Soldano
78. A. R. Saunders
79. R. A. Strehlow
80. R. E. Thoma
81. G. C. Warlick
82. G. M. Watson
83. J. C. White
84. E. V. Jones
85. H. Insley
86. L. G. Alexander
87. S. E. Beall
88. E. S. Bettis
89. W. R. Gall
90. J. C. Griess
91. G. H. Jenks
92. B. W. Kinyon
93. W. B. McDonald
94. I. Spiewak

- |                       |   |
|-----------------------|---|
| 95. W. B. Cottrell    | 129. G. M. Adamson  |
| 96. H. N. Culver      | 130. J. R. Coobs  |
| 97. R. B. Korsmeyer   | 131. J. H. DeVan  |
| 98. E. C. Miller      | 132. L. M. Doney  |
| 99. H. C. McCurdy     | 133. D. A. Douglas  |
| 100. A. M. Perry      | 134. T. Hikido  |
| 101. G. Samuels       | 135. E. E. Hoffman  |
| 102. H. W. Savage     | 136. P. Patriarca   |
| 103. D. B. Trauger    | 137. G. P. Smith  |
| 104. R. Baldock       | 138. A. Taboada   |
| 105. W. H. Baldwin    | 139. R. E. Blanco   |
| 106. A. R. Brosi      | 140. J. C. Bresee   |
| 107. A. H. Busey      | 141. K. B. Brown  |
| 108. G. H. Cartledge  | 142. G. I. Cathers  |
| 109. C. J. Collins    | 143. W. K. Eister   |
| 110. J. S. Drury      | 144. H. E. Goeller  |
| 111. C. J. Hochanadel | 145. D. E. Ferguson   |
| 112. J. S. Johnson    | 146. C. H. Secoy  |
| 113. K. A. Kraus      | 147. M. E. Whatley  |
| 114. H. A. Levy       | 148. P. H. Emmett (consultant)                                  |
| 115. R. Livingston    | 149. D. G. Hill (consultant)                                    |
| 116. G. D. O'Kelley   | 150. C. E. Larson (consultant)                                  |
| 117. S. W. Peterson   | 151. J. E. Ricci (consultant)                                   |
| 118. G. W. Parker     | 152. E. P. Wigner (consultant)                                  |
| 119. G. A. Ropp       | 153. Biology Library  |
| 120. R. W. Stoughton  | 154. Health Physics Library                                     |
| 121. J. W. Cleland    | 155. Reactor Experimental<br>Engineering Library                |
| 122. J. G. Morgan     | 156-158. Central Research Library                               |
| 123. W. W. Parkinson  | 159-178. Laboratory Records Department                          |
| 124. O. Sisman        | 179. Laboratory Records, ORNL R. C.                             |
| 125. P. S. Baker      | 180. ORNL Y-12 Technical Library,<br>Document Reference Section |
| 126. E. E. Beauchamp  |   |
| 127. E. Lamb          |   |
| 128. L. O. Love       |   |

#### *EXTERNAL DISTRIBUTION*

- 181. Division of Research and Development, AEC, Washington
- 182. Division of Research and Development, AEC, ORO
- 183. Division of Reactor Development, AEC, Washington
- 184. Division of Reactor Development, AEC, ORO
- 185-741. Given distribution as shown in TID-4500 (15th ed.) under Chemistry-General category (75 copies - OTS)